

Optical Waves in Crystals

**Propagation and Control
of Laser Radiation**

**AMNON YARIV
POCHI YEH**

Optical Waves in Crystals

Propagation and Control of
Laser Radiation

AMNON YARIV

California Institute of Technology

POCHI YEH

Rockwell International Science Center

A Wiley-Interscience Publication

John Wiley & Sons

New York / Chichester / Brisbane / Toronto / Singapore

A NOTE TO THE READER

This book has been electronically reproduced from digital information stored at John Wiley & Sons, Inc. We are pleased that the use of this new technology will enable us to keep works of enduring scholarly value in print as long as there is a reasonable demand for them. The content of this book is identical to previous printings.

Copyright © 1984 by John Wiley & Sons, Inc.

All rights reserved. Published simultaneously in Canada.

Reproduction or translation of any part of this work beyond that permitted by Section 107 or 108 of the 1976 United States Copyright Act without the permission of the copyright owner is unlawful. Requests for permission or further information should be addressed to the Permissions Department, John Wiley & Sons, Inc.

Library of Congress Cataloging in Publication Data:

Yariv, Amnon.

Optical waves in crystals.

(Wiley series in pure and applied optics, ISSN 0277-2493)

“A Wiley-Interscience publication.”

Includes bibliographies and index.

1. Laser beams. 2. Crystal optics. I. Yeh, Pochi, 1948- II. Title. III. Series.

TA1677.Y37 1983 621.36 83-6892

ISBN 0-471-09142-1

Printed in the United States of America

Preface

This book, intended as a text for a course in electro-optics for electrical-engineering or applied-physics students, has two primary objectives: to present a clear physical picture of the propagation of laser radiation in various optical media and to teach the reader how to analyze and design electro-optical devices.

Only through a study of the electromagnetic propagation can the characteristics of an optical device be appreciated and its limitation be understood. This characterization allows us to exploit the device as an element to manipulate the laser radiation. The emphasis is therefore on the fundamental principles. An effort is made to bridge the gap between theory and practice through the use of numerical examples based on real situations. Only classical electrodynamics is used in dealing with the coherent interaction of laser radiation with various optical media. The optical properties of these media are described by such material parameters as dielectric tensors, gyration tensors, electro-optic coefficients, photo-elastic constants, and non-linear susceptibilities. A very wide range of topics is included, as may be seen from the Contents.

In writing this book we have assumed that the student has been introduced to Maxwell's equations in an intermediate course in electricity and magnetism. It is further expected that the student has some mathematical background in Fourier integrals, matrix algebra, and differential equations.

In the summer of 1982, the preliminary version of the manuscript was used as the text of a graduate course in modern optics which P. Yeh taught at the Taiwan University. He wishes to thank his colleagues and students at the University for countless helpful remarks and discussions. Special mention must be made of Professor K. P. Wang of the Taiwan University, who gave him the opportunity and encouragement to teach such a course. His thanks are also extended to Dr. Monte Khoshnevisan and Dr. Chun-Ching Shih for reading and commenting on the manuscript, and to Dr. Hidehiko Kuwamoto, Dr. Emilio Sovero, and Mark Ewbank for many helpful discussions.

We are grateful to Carmen Byrne and Ruth Stratton for their patient and competent typing of the manuscript. We also wish to thank Phyllis Foraker and Helen Coogan for their help in obtaining copyright permission and in preparing the references. P. Yeh wishes to acknowledge the support of the Rockwell International Science Center, as well as the constant encouragement of Dr. Joseph T. Longo and Dr. John M. Tracy.

AMNON YARIV
POCHI YEH

Pasadena, California
Thousand Oaks, California
May 1983

Contents

Chapter 1. Electromagnetic Fields	1
1.1. Maxwell's Equations and Boundary Conditions	1
1.2. Poynting's Theorem and Conservation Laws	5
1.3. Complex-Function Formalism	6
1.4. Wave Equations and Monochromatic Plane Waves	8
1.5. Propagation of a Laser Pulse; Group Velocity	13
Problems	18
References and Suggested Reading	21
Chapter 2. Propagation of Laser Beams	22
2.1. Scalar Wave Equation	22
2.2. Gaussian Beams in a Homogeneous Medium	25
2.3. Fundamental Gaussian Beam in a Lenslike Medium—The <i>ABCD</i> Law	29
2.4. High-Order Gaussian Beam Modes in a Homogeneous Medium	37
2.5. Gaussian Beam Modes in Quadratic-Index Media	38
Problems	50
References	53
Chapter 3. Polarization of Light Waves	54
3.1. The Concept of Polarization	54
3.2. Polarization of Monochromatic Plane Waves	55
3.3. Complex-Number Representation	61
3.4. Jones-Vector Representation	62
Problems	64
References and Suggested Reading	68

Chapter 4.	Electromagnetic Propagation in Anisotropic Media	69
4.1.	The Dielectric Tensor of an Anisotropic Medium	69
4.2.	Plane-Wave Propagation in Anisotropic Media	71
4.3.	The Index Ellipsoid	77
4.4.	Phase Velocity, Group Velocity, and Energy Velocity	79
4.5.	Classification of Anisotropic Media (Crystals)	82
4.6.	Light Propagation in Uniaxial Crystals	84
4.7.	Double Refraction at a Boundary	88
4.8.	Light Propagation in Biaxial Crystals	89
4.9.	Optical Activity	94
4.10.	Faraday Rotation	103
4.11.	Coupled-Mode Analysis of Wave Propagation in Anisotropic Media	104
4.12.	Equation of Motion for the Polarization State	110
	Problems	113
	References	120
Chapter 5.	Jones Calculus and its Application to Birefringent Optical Systems	121
5.1.	Jones Matrix Formulation	121
5.2.	Intensity Transmission	127
5.3.	Polarization Interference Filters	131
5.4.	Light Propagation in Twisted Anisotropic Media	143
5.5.	The Problem of Fresnel Reflection and Phase Shift	147
	Problems	148
	References	154
Chapter 6.	Electromagnetic Propagation in Periodic Media	155
6.1.	Periodic Media	155
6.2.	Periodic Layered Media	165
6.3.	Bragg Reflection	174
6.4.	Coupled-Mode Theory	177
6.5.	Coupled-Mode Theory of Šolc Filters	189
6.6.	Coupled-Mode Theory of Bragg Reflectors	194
6.7.	Phase Velocity, Group Velocity, and Energy Velocity	201
6.8.	Form Birefringence	205

6.9.	Electromagnetic Surface Waves	209
	Problems	214
	References	219
Chapter 7.	Electro-optics	220
7.1.	The Electro-optic Effect	220
7.2.	Linear Electro-optic Effect	223
7.3.	Electro-optic Modulation	238
7.4.	Wave Propagation in Electro-optic Crystals	245
7.5.	Quadratic Electro-optic Effect	256
7.6.	Physical Properties of Electro-optic Coefficients	264
7.7.	Electro-optic Effects in Liquid Crystals	266
	Problems	270
	References	275
Chapter 8.	Electro-optic Devices	276
8.1.	Electro-optic Light Modulators	276
8.2.	Electro-optic Fabry-Perot Modulators	288
8.3.	Some Design Considerations	293
8.4.	Bistable Electro-optic Devices	298
8.5.	Electro-optic Frequency Shifting and Pulse Compression	303
8.6.	Electro-optic Beam Deflectors	309
	Problems	312
	References	316
Chapter 9.	Acousto-optics	318
9.1.	The Photoelastic Effect	318
9.2.	Basic Concepts of Acousto-optic Interactions	329
9.3.	Particle Picture of Acousto-optic Interactions	332
9.4.	Bragg Diffraction in an Anisotropic Medium	333
9.5.	Coupled-Mode Analysis of Bragg Diffraction	337
9.6.	Raman-Nath Diffraction	354
9.7.	Surface Acousto-optics	358
	Problems	363
	References and Suggested Reading	365

Chapter 10. Acousto-optic Devices	366
10.1. Acousto-optic Modulators	366
10.2. Acousto-optic Deflectors	379
10.3. Acousto-optic Tunable Filters (AOTF)	387
10.4. Acousto-optic Spectrum Analyzers	396
10.5. Acousto-optic Signal Correlators	398
Problems	401
References	404
Chapter 11. Guided Waves and Integrated Optics	405
11.1. General Properties of Dielectric Waveguides	405
11.2. TE and TM Modes in an Asymmetric Waveguide	416
11.3. Dielectric Perturbation and Mode Coupling	425
11.4. Periodic Waveguide—Bragg Reflection	429
11.5. Codirectional Coupling in a Periodic Waveguide	436
11.6. Distributed-Feedback Lasers	439
11.7. Electro-optic Modulation and Mode Coupling	447
11.8. Directional Coupling	459
11.9. Frequency Multiplexers	469
11.10. Other Planar Waveguides	473
11.11. Leaky Dielectric Waveguide	482
11.12. Electromagnetic Surface Waves (Surface Plasmons)	489
Problems	495
References	502
Chapter 12. Nonlinear Optics	504
12.1. Introduction	504
12.2. Second-Order Nonlinear Phenomena—General Methodology	505
12.3. Electromagnetic Formulation of Nonlinear Interaction	516
12.4. Optical Second-Harmonic Generation	518
12.5. Second-Harmonic Generation with a Depleted Input	526
12.6. Second-Harmonic Generation with Gaussian Beams	528
12.7. Parametric Amplification	531
12.8. Parametric Oscillation	533

CONTENTS	xi
12.9. Frequency Tuning in Parametric Oscillation	538
12.10. Frequency Upconversion	542
Problems	545
References	547
Chapter 13. Phase-Conjugate Optics	549
13.1. Introduction	549
13.2. Propagation through a Distorting Medium	549
13.3. Image Transmission in Fibers	551
13.4. Theory of Phase Conjugation by Four-Wave Mixing	553
Author Index	569
Subject Index	573

1

Electromagnetic Fields

The ideal laser emits coherent electromagnetic radiation which can be described by its electric and magnetic field vectors. The propagation of this radiation field is governed by Maxwell's equations. It is thus important to familiarize ourselves at the outset with some of the basic properties of electromagnetic fields.

In this introductory chapter we review and derive some basic relations involving classical electromagnetic fields. Starting with Maxwell's equations and the material equations, we obtain expressions for the energy density and the energy flow of an electromagnetic field. We also derive the Poynting theorem, the conservation laws, and the wave equations. We consider in some detail the propagation of monochromatic plane waves and some of their important properties. Finally, we discuss the concepts of phase velocity and group velocity of a wave packet propagating in a dispersive medium.

1.1. MAXWELL'S EQUATIONS AND BOUNDARY CONDITIONS

1.1.1. Maxwell's Equations

An electromagnetic field in space is described classically by two field vectors, \mathbf{E} and \mathbf{H} , called the electric vector and the magnetic vector, respectively. To include the effect of the field on matter, it is necessary to introduce a second set of vectors, \mathbf{D} and \mathbf{B} , called the electric displacement and the magnetic induction, respectively. These vectors are related by Maxwell's equations (in MKS units):

$$\nabla \times \mathbf{E} + \frac{\partial \mathbf{B}}{\partial t} = 0, \quad (1.1-1)$$

$$\nabla \times \mathbf{H} - \frac{\partial \mathbf{D}}{\partial t} = \mathbf{J}, \quad (1.1-2)$$

$$\nabla \cdot \mathbf{D} = \rho, \quad (1.1-3)$$

$$\nabla \cdot \mathbf{B} = 0, \quad (1.1-4)$$

where \mathbf{J} is the electric current density (amperes per square meter) and ρ is the electric charge density (coulombs per cubic meter).

These four equations are the basic laws of electricity and magnetism in their differential forms. Equation (1.1-1) is the differential form of Faraday's law of induction, which describes the creation of an induced electric field due to a time-varying magnetic flux. Equation (1.1-2) is the differential form of the generalized Ampère law, which describes the creation of an induced magnetic field due to charge flow. Equation (1.1-3) is the differential form of Coulomb's law, which describes the relation between the electric-field distribution and the charge distribution. Equation (1.1-4) may be regarded as a statement of the absence of free magnetic monopoles.

The Maxwell equations (1.1-1), (1.1-2), (1.1-3), and (1.1-4) fully describe the propagation of electromagnetic radiation in any medium.

The charge density ρ and the current density \mathbf{J} may be regarded as the sources of the electromagnetic radiation. In many areas of optics one often deals with the propagation of electromagnetic radiation in regions far from the sources, where both ρ and \mathbf{J} are zero. All the cases considered in this book fall within this category.

The Maxwell equations form a set of coupled partial differential equations involving the four basic quantities of the electromagnetic field, \mathbf{E} , \mathbf{H} , \mathbf{D} , and \mathbf{B} . To allow a unique determination of the field vectors from a given distribution of currents and charges, these equations must be supplemented by relations that describe the effect of the electromagnetic field on material media. These relations are known as constitutive equations (or material equations) and are given by

$$\mathbf{D} = \epsilon \mathbf{E} = \epsilon_0 \mathbf{E} + \mathbf{P}, \quad (1.1-5)$$

$$\mathbf{B} = \mu \mathbf{H} = \mu_0 \mathbf{H} + \mathbf{M}, \quad (1.1-6)$$

where the constitutive parameters ϵ and μ are tensors of rank 2 and are known as the dielectric tensor (or permittivity tensor) and permeability tensor, respectively; \mathbf{P} and \mathbf{M} are the electric and magnetic polarizations, respectively; and ϵ_0 and μ_0 are the permittivity and permeability of vacuum, respectively. If the material medium is isotropic, these tensors reduce to scalars. In many cases the quantities ϵ and μ can be assumed to be independent of the field strengths. However, if the fields are sufficiently strong, such as those obtained, for example, by focusing a laser beam or applying a strong dc electric field to an electro-optic crystal, then the dependence of these quantities on \mathbf{E} and \mathbf{H} must be considered. These nonlinear optical effects will be considered in Chapter 7 and in Chapter 12.

1.1.2. Boundary Conditions

Maxwell's equations can be solved in regions of space where both ϵ and μ are continuous. In optics, one often deals with situations in which the physical properties (characterized by ϵ and μ) change abruptly across one or more smooth surfaces. The field vectors \mathbf{E} , \mathbf{H} , \mathbf{D} , and \mathbf{B} at a point on one side of a smooth surface between two media, 1 and 2, are related to the field vectors at the neighboring point on the opposite side of the interface by boundary conditions that can be derived directly from Maxwell's equations.

Consider now a very short cylinder drawn about a boundary surface, as in Fig. 1.1(a), such that the end faces of the cylinder are in region 1 and 2 and are parallel to the surface of discontinuity. The height of the cylinder is infinitesimal, such that the end faces are arbitrarily close to the boundary surface. An application of the Gauss divergence theorem

$$\int \nabla \cdot \mathbf{F} dV = \int \mathbf{F} \cdot d\mathbf{S} \quad (1.1-7)$$

to both sides of Eqs. (1.1-3) and (1.1-4) yields

$$\begin{aligned} \mathbf{n} \cdot (\mathbf{B}_2 - \mathbf{B}_1) &= 0, \\ \mathbf{n} \cdot (\mathbf{D}_2 - \mathbf{D}_1) &= \sigma, \end{aligned} \quad (1.1-8a)$$

where \mathbf{n} is the unit normal to the surface directed from medium 1 into

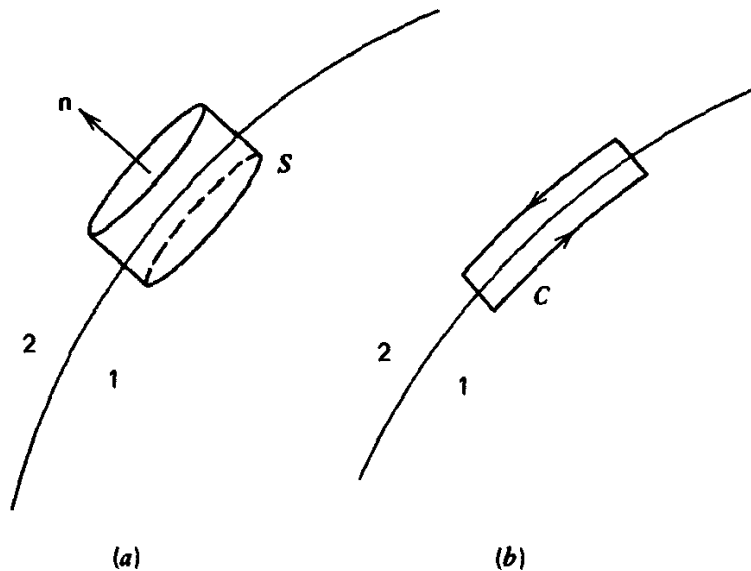


Figure 1.1. (a) A short cylinder about the interface between two media. S is the surface of this cylinder. (b) A narrow rectangle about the interface between two media. C is the boundary of this rectangle.

medium 2, σ is the surface charge density (coulombs per square meter), and the subscripts refer to values at the surface in the two media. The boundary conditions (1.1-8a) are often written as

$$\begin{aligned} B_{2n} &= B_{1n}, \\ D_{2n} - D_{1n} &= \sigma, \end{aligned} \tag{1.1-8b}$$

where $B_{2n} = \mathbf{B}_2 \cdot \mathbf{n}$, $B_{1n} = \mathbf{B}_1 \cdot \mathbf{n}$, $D_{2n} = \mathbf{D}_2 \cdot \mathbf{n}$, and $D_{1n} = \mathbf{D}_1 \cdot \mathbf{n}$. In other words, the normal component of the magnetic induction \mathbf{B} is always continuous, and the difference between the normal components of the electric displacement \mathbf{D} is equal in magnitude to the surface charge density σ .

Next, consider a small, narrow, rectangular circuit loop around a section of the boundary surface, as in Fig. 1.1(b), such that the long sides of the rectangle are in regions 1 and 2 and parallel to the surface of discontinuity. The width of this rectangle is infinitesimal, so that the two long sides are arbitrarily close to the boundary. An application of the Stokes's theorem

$$\int \nabla \times \mathbf{F} \cdot d\mathbf{S} = \int \mathbf{F} \cdot d\mathbf{l} \tag{1.1-9}$$

to both sides of Eqs. (1.1-1) and (1.1-2) yields

$$\begin{aligned} \mathbf{n} \times (\mathbf{E}_2 - \mathbf{E}_1) &= 0, \\ \mathbf{n} \times (\mathbf{H}_2 - \mathbf{H}_1) &= \mathbf{K}, \end{aligned} \tag{1.1-10a}$$

where \mathbf{K} is the surface current density (amperes per meter). Again, the boundary conditions for the electric and magnetic field vectors (1.1-10a) are often written as

$$\begin{aligned} \mathbf{E}_{2t} &= \mathbf{E}_{1t}, \\ \mathbf{H}_{2t} - \mathbf{H}_{1t} &= \mathbf{K}, \end{aligned} \tag{1.1-10b}$$

where the subscript t means the tangential component of the field vector. (Note: The components of these field vectors tangential to the boundary surface are still vectors in the plane tangent to the surface.) In other words, the tangential component of the electric field vector \mathbf{E} is always continuous at the boundary surface, and the difference between the tangential components of the magnetic field vector \mathbf{H} is equal to the surface current density \mathbf{K} .

In many areas of optics, one often deals with situations in which the surface charge density σ and the surface current density \mathbf{K} both vanish. It follows that, in such a case, the tangential components of \mathbf{E} and \mathbf{H} and the normal components of \mathbf{D} and \mathbf{B} are continuous across the interface separating media 1 and 2. These boundary conditions are important in solving many wave propagation problems in optics, such as in guided-wave optics and wave propagation in layered media.

1.2. POYNTING'S THEOREM AND CONSERVATION LAWS

Conservation of energy for electromagnetic fields requires that the time rate of change of electromagnetic energy contained within a certain volume, plus the time rate of energy flowing out through the boundary surfaces of the volume, be equal to the negative of the total work done by the fields on the sources within the volume. For a point charge q , the rate of work done by an external electromagnetic field is $q\mathbf{v} \cdot \mathbf{E}$, where \mathbf{v} is the velocity of the charge. The magnetic field does no work on the point charge, since the magnetic force is always perpendicular to the velocity. In the case of a distributed charge and current, the rate of work done by the fields per unit volume is $\mathbf{J} \cdot \mathbf{E}$. A continuity equation which describes this balance of energy exists. We will now derive this equation starting from the Maxwell equations. By using Eq. (1.1-2), we can express the rate of work done per unit volume by the electromagnetic fields as

$$\mathbf{J} \cdot \mathbf{E} = \mathbf{E} \cdot (\nabla \times \mathbf{H}) - \mathbf{E} \cdot \frac{\partial \mathbf{D}}{\partial t}. \quad (1.2-1)$$

If we now employ the vector identity

$$\nabla \cdot (\mathbf{E} \times \mathbf{H}) = \mathbf{H} \cdot (\nabla \times \mathbf{E}) - \mathbf{E} \cdot (\nabla \times \mathbf{H}) \quad (1.2-2)$$

and use Eq. (1.1-1), the right-hand side of (1.2-1) becomes

$$\mathbf{J} \cdot \mathbf{E} = -\nabla \cdot (\mathbf{E} \times \mathbf{H}) - \mathbf{H} \cdot \frac{\partial \mathbf{B}}{\partial t} - \mathbf{E} \cdot \frac{\partial \mathbf{D}}{\partial t}. \quad (1.2-3)$$

If we now further assume that the material medium involved is linear in its electromagnetic properties (i.e., ϵ and μ are independent of the field strengths), Eq. (1.2-3) can be written

$$\frac{\partial U}{\partial t} + \nabla \cdot \mathbf{S} = -\mathbf{J} \cdot \mathbf{E}, \quad (1.2-4)$$

where U and \mathbf{S} are defined as

$$U = \frac{1}{2}(\mathbf{E} \cdot \mathbf{D} + \mathbf{B} \cdot \mathbf{H}), \quad (1.2-5)$$

$$\mathbf{S} = \mathbf{E} \times \mathbf{H}. \quad (1.2-6)$$

The scalar U represents the energy density of the electromagnetic fields and has the dimensions of joules per cubic meter. The vector \mathbf{S} , representing the energy flow, is called the Poynting vector and has the dimensions of joules per square meter per second. It is consistent to view $|\mathbf{S}|$ as the power per unit area (watts per square meter) carried by the field in the direction of \mathbf{S} . The quantity $\nabla \cdot \mathbf{S}$ thus represents the net electromagnetic power flowing out of a unit volume. Equation (1.2-4) is known as the continuity equation or the conservation of energy (Poynting's theorem). The conservation laws for the linear momentum of the electromagnetic fields can be obtained in a similar way. This is left as a problem for the student (Problem 1.4).

1.3. COMPLEX-FUNCTION FORMALISM

In optics, we generally deal with steady-state sinusoidal time-varying fields, for example, laser radiation. It is convenient to represent each field vector as a complex function. As an example, consider some component of the field vectors:

$$a(t) = |A|\cos(\omega t + \alpha), \quad (1.3-1)$$

where ω is the angular frequency and α is the phase. If we define a complex amplitude of $a(t)$ by

$$A = |A|e^{i\alpha}, \quad (1.3-2)$$

Eq. (1.3-1) can be written as

$$a(t) = \text{Re}[Ae^{i\omega t}]. \quad (1.3-3)$$

We will often represent $a(t)$ by

$$a(t) = Ae^{i\omega t} \quad (1.3-4)$$

instead of by Eq. (1.3-1) or (1.3-3). This, of course, is not strictly correct; when it happens, it is always understood that what is meant (e.g.) by Eq. (1.3-4) is the real part of $Ae^{i\omega t}$. In most situations, representation of field

vectors with the complex form (1.3-4) poses no problems insofar as linear mathematical operations, such as differentiation, integration, and summation, are concerned. The exceptions are cases that involve the product (or powers) of field vectors, such as the energy density and Poynting vector. In these cases, one must use the real form of the physical quantities.

As an example, consider the product of two sinusoidal functions $a(t)$ and $b(t)$, where

$$\begin{aligned} a(t) &= |A|\cos(\omega t + \alpha) \\ &= \operatorname{Re}[Ae^{i\omega t}] \end{aligned} \quad (1.3-5)$$

and

$$\begin{aligned} b(t) &= |B|\cos(\omega t + \beta) \\ &= \operatorname{Re}[Be^{i\omega t}] \end{aligned} \quad (1.3-6)$$

with $A = |A|e^{i\alpha}$ and $B = |B|e^{i\beta}$. Using the real functions, we get

$$a(t)b(t) = \frac{1}{2}|AB|[\cos(2\omega t + \alpha + \beta) + \cos(\alpha - \beta)]. \quad (1.3-7)$$

But if we were to evaluate the product $a(t)b(t)$ with the complex form of the functions, we would get

$$a(t)b(t) = ABe^{i2\omega t} = |AB|e^{i(2\omega t + \alpha + \beta)}. \quad (1.3-8)$$

A comparison of the last result with Eq. (1.3-7) shows that the time-independent (dc) term $\frac{1}{2}|AB|\cos(\alpha - \beta)$ is missing, and thus the use of the complex form led to an error. It is generally true that the product of the real parts of two complex numbers is not equal to the real part of the product of these two complex numbers. In other words, if x and y are two arbitrary complex numbers, the following is generally true:

$$\operatorname{Re}[x]\operatorname{Re}[y] \neq \operatorname{Re}[xy]. \quad (1.3-9)$$

1.3.1. Time-Averaging of Sinusoidal Products

In optical fields, the field vectors are rapidly varying functions of time. For example, the period of a time-varying field with a wavelength of $\lambda = 1 \mu\text{m}$ (one micrometer) is $T = \lambda/c = 0.33 \times 10^{-14}$ s. One often considers the time-averaged values rather than the instantaneous values of many physical quantities such as the Poynting vector and the energy density. It is fre-

quently necessary to find the time average of the product of two sinusoidal functions of the same frequency,

$$\langle a(t)b(t) \rangle = \frac{1}{T} \int_0^T |A| \cos(\omega t + \alpha) |B| \cos(\omega t + \beta) dt, \quad (1.3-10)$$

where $a(t)$ and $b(t)$ are given by Eqs. (1.3-5) and (1.3-6) and the bracket denotes the time averaging; $T = 2\pi/\omega$ is the period of oscillation. Since the integral in Eq. (1.3-10) is periodic in T , the averaging can be performed over a time T . By using Eq. (1.3-7), we obtain directly

$$\langle a(t)b(t) \rangle = \frac{1}{2} |AB| \cos(\alpha - \beta), \quad (1.3-11)$$

since the average over T of the term involving $\cos(2\omega t + \alpha + \beta)$ is zero. This last result can be written in terms of the complex amplitudes A and B , defined immediately following Eq. (1.3-6), as

$$\langle a(t)b(t) \rangle = \frac{1}{2} \text{Re}[AB^*] \quad (1.3-12)$$

or in terms of the analytic form of $a(t)$ and $b(t)$ directly as

$$\langle \text{Re}[a(t)] \text{Re}[b(t)] \rangle = \frac{1}{2} \text{Re}[a(t)b^*(t)], \quad (1.3-13)$$

where the asterisk indicates the complex conjugate. The time dependence on the right-hand side of Eq. (1.3-13) disappears, because both $a(t)$ and $b(t)$ have the same sinusoidal time dependence $e^{i\omega t}$. These two results, (1.3-12) and (1.3-13), are important and will find frequent use throughout the book.

By using complex-function formalism for the field vectors \mathbf{E} , \mathbf{H} , \mathbf{D} , and \mathbf{B} , the time-averaged Poynting vector (1.2-6) and the energy density (1.2-5) for sinusoidally varying fields are given by

$$\mathbf{S} = \frac{1}{2} \text{Re}[\mathbf{E} \times \mathbf{H}^*] \quad (1.3-14)$$

and

$$U = \frac{1}{4} \text{Re}[\mathbf{E} \cdot \mathbf{D}^* + \mathbf{B} \cdot \mathbf{H}^*] \quad (1.3-15)$$

respectively.

1.4. WAVE EQUATIONS AND MONOCHROMATIC PLANE WAVES

The Maxwell equations described in Section 1.1 are a set of coupled partial differential equations. These can be manipulated to yield differential equations which each of the field vectors must satisfy separately. We limit our

attention to regions where both the charge density ρ and the current density \mathbf{J} vanish. We also assume in this section that the medium is isotropic, so that ϵ and μ are scalars.

If we use the constitutive relation (1.1-6) for \mathbf{B} in Eq. (1.1-1), divide both sides by μ , and apply the curl operator, we obtain

$$\nabla \times \left(\frac{1}{\mu} \nabla \times \mathbf{E} \right) + \frac{\partial}{\partial t} \nabla \times \mathbf{H} = 0. \quad (1.4-1)$$

If we now differentiate Eq. (1.1-2) with respect to time, combine it with Eq. (1.4-1), and use the material equation (1.1-5), we obtain

$$\nabla \times \left(\frac{1}{\mu} \nabla \times \mathbf{E} \right) + \epsilon \frac{\partial^2 \mathbf{E}}{\partial t^2} = 0. \quad (1.4-2)$$

We now employ the vector identities

$$\nabla \times \left(\frac{1}{\mu} \nabla \times \mathbf{E} \right) = \frac{1}{\mu} \nabla \times (\nabla \times \mathbf{E}) + \left(\nabla \frac{1}{\mu} \right) \times (\nabla \times \mathbf{E}) \quad (1.4-3)$$

and

$$\nabla \times (\nabla \times \mathbf{E}) = \nabla(\nabla \cdot \mathbf{E}) - \nabla^2 \mathbf{E}, \quad (1.4-4)$$

and Eq. (1.4-2) becomes

$$\nabla^2 \mathbf{E} - \mu \epsilon \frac{\partial^2 \mathbf{E}}{\partial t^2} + (\nabla \log \mu) \times (\nabla \times \mathbf{E}) - \nabla(\nabla \cdot \mathbf{E}) = 0. \quad (1.4-5)$$

By substituting for \mathbf{D} from Eq. (1.1-5) into Eq. (1.1-3) and applying the vector identity

$$\nabla \cdot (\epsilon \mathbf{E}) = \epsilon \nabla \cdot \mathbf{E} + \mathbf{E} \cdot \nabla \epsilon, \quad (1.4-6)$$

we obtain from Eq. (1.4-5)

$$\nabla^2 \mathbf{E} - \mu \epsilon \frac{\partial^2 \mathbf{E}}{\partial t^2} + (\nabla \log \mu) \times (\nabla \times \mathbf{E}) + \nabla(\mathbf{E} \cdot \nabla \log \epsilon) = 0. \quad (1.4-7)$$

This is the wave equation for the field vector \mathbf{E} . The wave equation for the

magnetic field vector \mathbf{H} can be obtained in a similar way and is given by

$$\nabla^2 \mathbf{H} - \mu \epsilon \frac{\partial^2 \mathbf{H}}{\partial t^2} + (\nabla \log \epsilon) \times (\nabla \times \mathbf{H}) + \nabla(\mathbf{H} \cdot \nabla \log \mu) = 0. \quad (1.4-8)$$

Inside a homogeneous and isotropic medium, the gradient of the logarithm of ϵ and μ vanishes, and the wave equations (1.4-7) and (1.4-8) reduce to

$$\nabla^2 \mathbf{E} - \mu \epsilon \frac{\partial^2 \mathbf{E}}{\partial t^2} = 0, \quad \nabla^2 \mathbf{H} - \mu \epsilon \frac{\partial^2 \mathbf{H}}{\partial t^2} = 0. \quad (1.4-9)$$

These are the standard electromagnetic wave equations. They are satisfied by the well-known plane wave*

$$\psi = e^{i(\omega t - \mathbf{k} \cdot \mathbf{r})}, \quad (1.4-10)$$

where the angular frequency ω and the magnitude of the wave vector, \mathbf{k} , are related by

$$|\mathbf{k}| = \omega \sqrt{\mu \epsilon}, \quad (1.4-11)$$

and ψ can be any Cartesian component of \mathbf{E} and \mathbf{H} .

If an observer were to travel in such a way as always to observe the same field value, his position $\mathbf{r}(t)$ would have to satisfy

$$\omega t - \mathbf{k} \cdot \mathbf{r} = \text{constant}, \quad (1.4-12)$$

where the constant is arbitrary and determines the field value “seen” by the observer. Equation (1.4-12) determines a plane normal to the wave vector \mathbf{k} at any instant t . This plane is called a surface of constant phase. It is easily seen that the surface of constant phase travels in the direction of \mathbf{k} with a velocity whose magnitude is

$$v = \frac{\omega}{k}. \quad (1.4-13)$$

This is the phase velocity of the wave. If the wave is frozen in time, the

*This is not the only solution of these equations. Another form of the solution, the so-called “Gaussian beam,” will be discussed in Chapter 2.

separation between two neighboring field peaks, that is, the wavelength, is seen to be

$$\lambda = \frac{2\pi}{k} = 2\pi \frac{v}{\omega}. \quad (1.4-14)$$

The value of the phase velocity is a characteristic of the medium and can be expressed in terms of the dielectric constant ϵ and the magnetic permeability μ . From Eqs. (1.4-13) and (1.4-11), we obtain

$$v = \frac{1}{\sqrt{\mu\epsilon}}. \quad (1.4-15)$$

The phase velocity of electromagnetic radiation in vacuum is

$$c = \frac{1}{\sqrt{\mu_0\epsilon_0}} = 2.997930 \times 10^8 \text{ m/s},$$

whereas in material media it has the value

$$v = \frac{c}{n},$$

where $n = \sqrt{\mu\epsilon/\mu_0\epsilon_0}$ is the index of refraction of the medium. Table 1.1 lists the index of refraction of some common optical materials. We must keep in mind, however, that ϵ and therefore n of a nonmagnetic material ($\mu = \mu_0$) are functions of the frequency. The variation of n with frequency gives rise to the well-known phenomenon of dispersion in optics. In a dispersive medium, the phase velocity of light waves depends on the frequency.

We now turn our attention to the vector nature of the electromagnetic field and the requirement of satisfying Maxwell's equations. Using the complex-function formalism, we write the electromagnetic fields of the plane wave in the form

$$\mathbf{E} = \mathbf{u}_1 E_0 e^{i(\omega t - \mathbf{k} \cdot \mathbf{r})}, \quad (1.4-16)$$

$$\mathbf{H} = \mathbf{u}_2 H_0 e^{i(\omega t - \mathbf{k} \cdot \mathbf{r})}, \quad (1.4-17)$$

where \mathbf{u}_1 and \mathbf{u}_2 are two constant unit vectors, and E_0 and H_0 are complex amplitudes that are constant in space and time. In a homogeneous charge-free medium, the divergence Maxwell equations are $\nabla \cdot \mathbf{E} = 0$ and $\nabla \cdot \mathbf{H} = 0$.

Table 1.1. Index of Refraction of Some Optical Materials^a

Material	Index of Refraction	Material	Index of Refraction
AgCl	2.05	InAs at 10.6 μm	3.42
As-S glass	2.61	InP at 10.6 μm	3.05
BaF ₂	1.47	InSb at 10.6 μm	3.95
Bi ₄ Ge ₃ O ₁₂	2.09	KBr	1.56
CaF ₂	1.43	KCl	1.49
CdF ₂	1.43	KI	1.66
CdS	2.47	LiF	1.39
CdSe at 1 μm	2.55	MgF ₂	1.37
CdTe at 10.6 μm	2.69	MgO	1.74
CsBr	1.69	NaCl	1.54
CsI	1.78	NaF	1.32
CuBr	2.10	PbF ₂	1.76
CuCl	1.96	Sapphire	1.77
CuI	2.32	Si at 10.6 μm	3.42
Diamond	2.41	SiC	2.64
Fused silica (SiO ₂)	1.46	SrTiO ₃	2.38
GaAs at 10.6 μm	3.34	TiO ₂	2.20
GaP at 10.6 μm	2.90	β -ZnS	2.35
GaSb at 10.6 μm	3.84	ZnSe at 10.6 μm	2.39
Ge at 10.6 μm	4.00	ZnTe	2.98

^aAt 25°C, $\lambda = 6328 \text{ \AA}$, unless otherwise specified.

= 0, which when applied to Eqs. (1.4-16) and (1.4-17) result in

$$\mathbf{u}_1 \cdot \mathbf{k} = \mathbf{u}_2 \cdot \mathbf{k} = 0. \quad (1.4-18)$$

This means that \mathbf{E} and \mathbf{H} are both perpendicular to the direction of propagation. Such a wave is called a transverse wave. The transversality condition (1.4-18) holds for all four field vectors for plane-wave propagation in homogeneous and isotropic media. In a general anisotropic medium, only the field vectors \mathbf{D} and \mathbf{B} of a plane wave are perpendicular to the direction of propagation.

The curl Maxwell's equations provide further restrictions on the field vectors. These are obtained by substituting Eqs. (1.4-16) and (1.4-17) into Eq. (1.1-1) and are given by

$$\mathbf{u}_2 = \frac{\mathbf{k} \times \mathbf{u}_1}{|\mathbf{k}|} \quad (1.4-19)$$

and

$$H_0 = \frac{E_0}{\eta}, \quad \eta = \sqrt{\frac{\mu}{\epsilon}}. \quad (1.4-20)$$

This shows that the triad ($\mathbf{u}_1, \mathbf{u}_2, \mathbf{k}$) forms a set of orthogonal vectors and that \mathbf{E} and \mathbf{H} are in phase and in constant ratio, provided ϵ and μ are real. The quantity in Eq. (1.4-20) has the dimensions of resistance and is called the impedance of space. In vacuum, $\eta_0 = \sqrt{\mu_0/\epsilon_0} = 377$ ohms.

The plane wave we have just described is a transverse wave propagating in the direction \mathbf{k} . It represents a time-averaged flux of energy given, according to Poynting's theorem (1.3-14), by

$$\mathbf{S} = \frac{|E_0|^2 \mathbf{u}_3}{2\eta} = \frac{\mathbf{k}}{2\omega\mu} |E_0|^2, \quad (1.4-21)$$

where \mathbf{u}_3 is a unit vector in the direction of \mathbf{k} . The time-averaged energy density is

$$U = \frac{1}{2}\epsilon|E_0|^2. \quad (1.4-22)$$

1.5. PROPAGATION OF A LASER PULSE; GROUP VELOCITY

In the previous section we discussed the plane-wave solutions to Maxwell's equations and studied some basic properties. Only monochromatic waves with a definite frequency and wave number were treated. Laser radiation operating in a continuous-wave (CW) operation may be considered monochromatic and can often be represented by a plane wave. However, many important applications of lasers involve pulse operation. In the pulsed mode, the energy can be concentrated into extremely short times, thereby increasing the peak power. This is of key importance in numerous industrial applications such as machining and welding with lasers, as well as in scientific applications. In the latter category, the use of extremely short pulses makes it possible to probe very short-lived ($< 10^{-12}$ s) transient phenomena.

The finite duration of a laser pulse results in a finite spread of frequencies or, equivalently, wavelengths. Laser-pulse propagation in a linear medium can be described in terms of the propagation of an appropriate linear superposition of plane waves with different frequencies, since Maxwell's equations are linear. However, there are new features associated with

laser-pulse propagation in a dispersive medium, i.e., a medium where the phase velocity depends on the frequency. As a result, different frequency components of the wave propagate with different speeds and tend to change phase with respect to one another. This usually leads to a spreading of the laser pulse as it propagates in a dispersive medium. Also, the velocity of energy flow of a laser pulse propagating in a dispersive medium may differ greatly from the phase velocity. This is a subtle subject and requires careful investigation.

These effects on the propagation of a laser pulse due to dispersion can be described by representing the pulse as a sum of many plane-wave solutions of Maxwell's equations. In the limit, we will replace the summation by an integral. For the sake of clarity in introducing the basic concepts, we will only consider the case of one-dimensional scalar waves. The scalar amplitude $\psi(z, t)$ can be thought of as one of the components of the electromagnetic field vectors. If $A(k)$ denotes the amplitude of the plane-wave component with wave number k , the pulse $\psi(z, t)$ can be written

$$\psi(z, t) = \int_{-\infty}^{\infty} A(k) e^{i(\omega(k)t - kz)} dk. \quad (1.5-1)$$

This integral satisfies Maxwell's equation, since the integrand is a basic plane-wave solution to the same equations. Note that if we view $\psi(z, t)$ at some instant of time, say $t = 0$, then $A(k)$ is formally the Fourier transform of $\psi(z, 0)$. We will then refer to $|A(k)|^2$ as the Fourier spectrum of the field $\psi(z, t)$. The relation between ω and k (called the dispersion relation) is given by (1.4-11) for the electromagnetic field. In an isotropic medium, the dispersion properties cannot depend on the direction of propagation; therefore ω must be an even function of k : $\omega(-k) = \omega(k)$. Here, we further assume that both k and $\omega(k)$ are real. A typical pulse and its Fourier spectrum are shown in Fig. 1.2.

A laser pulse is usually characterized by its center frequency ω_0 (or its corresponding wave number k_0), and the frequency spread $\Delta\omega$ around ω_0 (or the corresponding spread in wave number, Δk). Typically, $A(k)$ is sharply peaked around k_0 (i.e., $\Delta k \ll k_0$). To study the evolution of such a pulse in time, we expand $\omega(k)$ around the value k_0 in terms of a Taylor series:

$$\omega(k) = \omega_0 + \left(\frac{d\omega}{dk} \right)_0 (k - k_0) + \cdots, \quad (1.5-2)$$

and then substitute for ω from Eq. (1.5-2) into (1.5-1). Thus Eq. (1.5-1) can

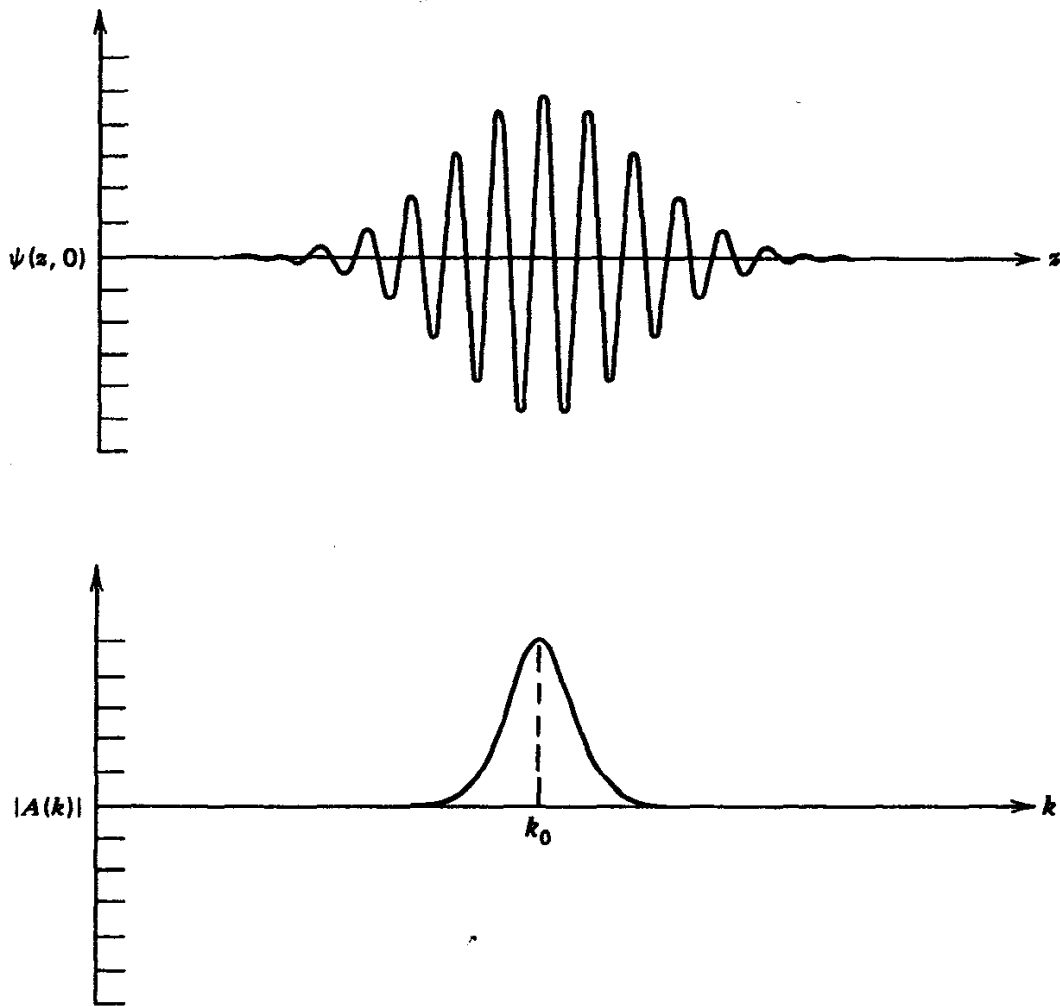


Figure 1.2. A laser pulse of finite extent and its Fourier spectrum in wave- number (k) space.

be written

$$\psi(z, t) = e^{i(\omega_0 t - k_0 z)} \int_{-\infty}^{\infty} A(k) \exp \left\{ i \left[\left(\frac{d\omega}{dk} \right)_0 t - z \right] (k - k_0) \right\} dk, \quad (1.5-3)$$

where we neglect the higher-order terms in $k - k_0$. The integral in Eq. (1.5-3) is a function of the composite variable $[z - (d\omega/dk)_0 t]$ only and is called the envelope function $E[z - (d\omega/dk)_0 t]$. Thus the amplitude of the pulse can be written

$$\psi(z, t) = e^{i(\omega_0 t - k_0 z)} E \left[z - \left(\frac{d\omega}{dk} \right)_0 t \right]. \quad (1.5-4)$$

This shows that, apart from an overall phase factor, the laser pulse travels

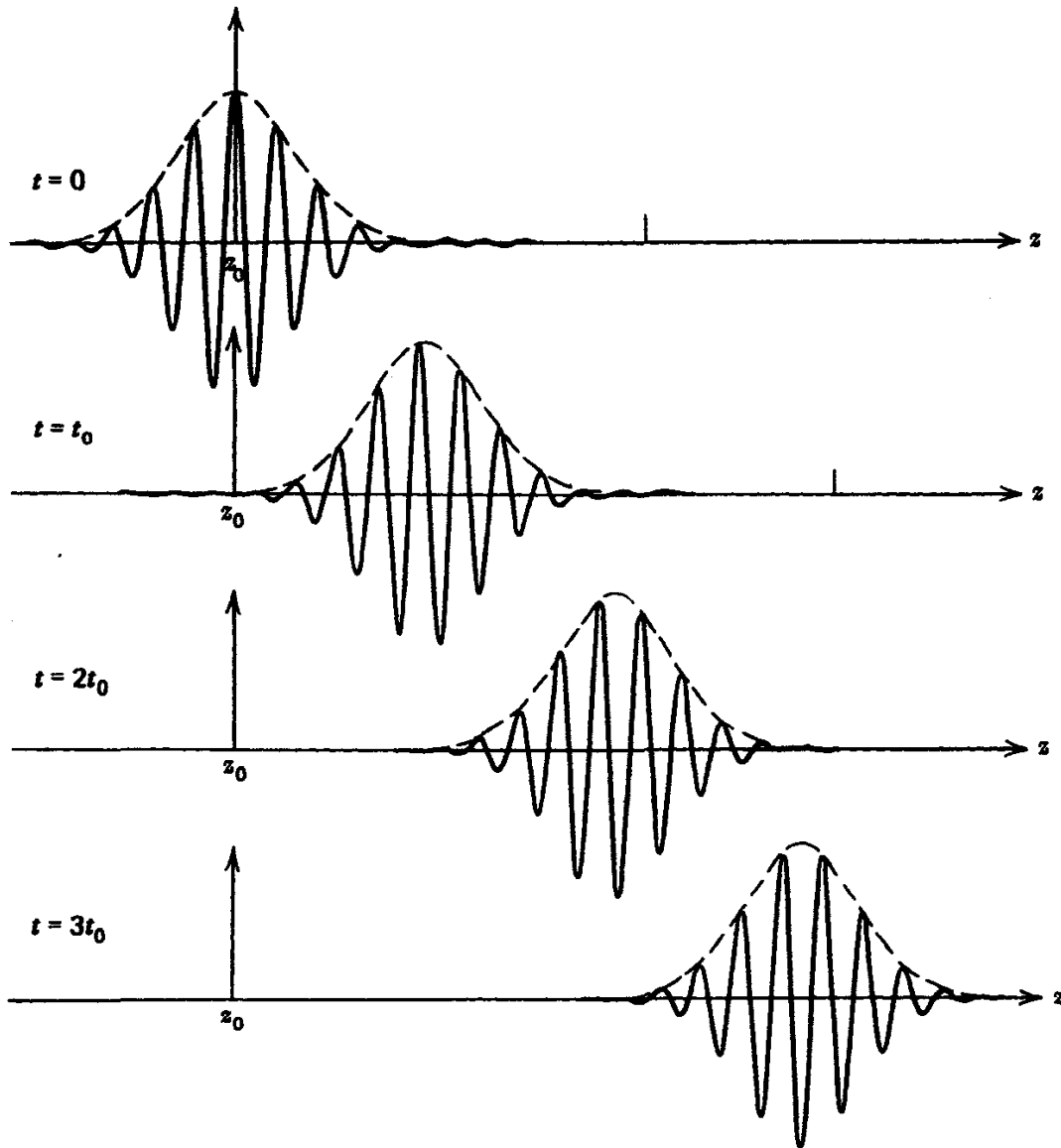


Figure 1.3. Schematic plot of the field amplitude, illustrating the propagation of the wave packet in the regime where Eq. (1.5-2) is valid and the pulse shape remains undistorted.

along undistorted in shape (see Fig. 1.3), with a velocity

$$v_g = \left(\frac{d\omega}{dk} \right)_0, \quad (1.5-5)$$

which is called the group velocity of the pulse. This approximation is legitimate only when the distribution $A(k)$ is sharply peaked at k_0 and the frequency ω is a smoothly varying function of k around k_0 . If the electromagnetic energy density of a laser pulse is associated with the absolute square of the amplitude, it is obvious that in this approximation the group

velocity represents the transport of energy (see Problem 1.7). We note that in the case of a pulse, the phase and group velocities are, in general, different, that is, $(d\omega/dk)_0 \neq \omega_0/k_0$. The phase velocity, which is usually greater than the group velocity, has the same significance as in the case of a plane wave. It is the velocity needed to stay on top of a given wave crest or valley.

In optics, the dispersion of a material medium is usually described by the index of refraction, $n(\omega)$, as a function of frequency (or wavelength), and the relation between ω and k is given by

$$k = n(\omega) \frac{\omega}{c}, \quad (1.5-6)$$

where c is the velocity of light in vacuum. The phase velocity is

$$v_p = \frac{c}{n(\omega)} \quad (1.5-7)$$

and is greater or smaller than c depending on whether $n(\omega)$ is smaller or larger than unity. From Eqs. (1.5-5) and (1.5-6), the group velocity is given by

$$v_g = \frac{c}{n + \omega(dn/d\omega)}. \quad (1.5-8)$$

For normal dispersion, $dn/d\omega > 0$, the group velocity is less than the phase velocity. In regions of anomalous dispersion, however, $dn/d\omega$ can become large and negative. Then the group velocity differs greatly from the phase velocity and sometimes becomes larger than c . The latter case occurs only when $dn/d\omega$ is very negative, which is equivalent to a rapid variation of ω as a function of k , thus making the approximation illegitimate. Therefore, there is no violation of the theory of special relativity.

We have seen that a laser pulse propagating in a dispersive medium will remain undistorted in shape provided the approximation (1.5-2) holds. In the event that the next higher-order term $\frac{1}{2}(d^2\omega/dk^2)_0(k - k_0)^2$ cannot be neglected, the pulse shape will no longer remain unchanged and will, in general, spread as the pulse travels. The spreading of the pulse can be accounted for by noting that the group velocity v_g may not be the same for each frequency component of the laser pulse (group-velocity dispersion). If Δk is the spectral spread of the pulse, the group-velocity spread is of the

order of

$$\Delta v_g \sim \left(\frac{d^2 \omega}{dk^2} \right)_0 \Delta k. \quad (1.5-9)$$

As the pulse propagates, one expects a spread in position of the order of $\Delta v_g t$. The issue of pulse spreading is considered again in Section 2.5 and Problem 1.9.

PROBLEMS

- 1.1. Conservation of charge requires that the charge density at any point in space be related to the current density in that neighborhood by a continuity equation

$$\frac{\partial \rho}{\partial t} + \nabla \cdot \mathbf{J} = 0.$$

Derive this equation from Maxwell's equation.

- 1.2. Derive the boundary conditions for the normal components of \mathbf{B} and \mathbf{D} , Eq. (1.1-8), by using an application of Gauss's divergence theorem to Maxwell's equations.
- 1.3. Derive the boundary conditions which apply to the tangential components of \mathbf{E} and \mathbf{H} , Eq. (1.1-10), by using an application of Stokes's theorem to Maxwell's equations.
- 1.4. The electromagnetic-field momentum density and Maxwell's stress tensor are given respectively by

$$\mathbf{P} = \mu \epsilon (\mathbf{E} \times \mathbf{H}),$$

$$T_{ij} = \epsilon E_i E_j + \mu H_i H_j - \frac{1}{2} \delta_{ij} (\epsilon E^2 + \mu H^2).$$

Derive the hydrodynamical equation of motion

$$\frac{\partial \mathbf{P}}{\partial t} = \nabla \cdot \mathbf{T} - \mathbf{F},$$

where \mathbf{F} is the Lorentz force exerted on a distribution of charges and

currents by the electromagnetic field,

$$\mathbf{F} = \rho \mathbf{E} + \mathbf{J} \times \mathbf{B}.$$

In a source-free region, the time rate of change of the field momentum density is equal to the force which is exerted by Maxwell's stresses on the region considered.

- 1.5. If the magnetic monopole exists, the static magnetic field produced by the magnetic charges obeys the following equation:

$$\nabla \cdot \mathbf{B} = \rho_m,$$

where ρ_m is the magnetic charge density.

- (a) Show that the magnetic field produced by a point charge m in vacuum is

$$\mathbf{H} = \frac{m}{4\pi\mu_0 r^3} \mathbf{r},$$

where \mathbf{r} is measured from the magnetic point charge.

- (b) Consider the electromagnetic field produced by a combination of an electric point charge e located at $(0, 0, \frac{1}{2}d)$ and a magnetic point charge m located at $(0, 0, -\frac{1}{2}d)$. If the angular-momentum density of the field is given by

$$\mathbf{L} = \mathbf{r} \times \mathbf{P}$$

where \mathbf{P} is the linear momentum density given in Problem 1.4, find the total angular momentum of the field by integrating \mathbf{L} over space. Answer: $-(em/4\pi)\hat{\mathbf{z}}$. Note that the angular momentum is independent of the separation d .

- (c) Let the origin of the coordinate system be on the magnetic point charge, so that the electric charge is located at $(0, 0, d)$. Move the electric charge e from $(0, 0, d)$ to $(0, 0, -d)$ on a semicircular path. Find the torque required and then integrate the torque with respect to the time. Show that the angular momentum required to move the electric charge is $-em/2\pi$. This method offers an easier way to calculate the angular momentum than does the direct approach in (b).
- 1.6. Equations (1.5-3) and (1.5-4) are approximate descriptions of a laser pulse. These equations become exact in a dispersionless medium.

Given a distribution in wave number $A(k)$, an envelope function $E(\xi)$ can be obtained by carrying out the integral in Eq. (1.5-3). For each of the forms $A(k)$ below, calculate the envelope function $E(\xi)$, plot $|A(k)|^2$ and $|E(\xi)|^2$, evaluate the standard deviations from the means, Δk and $\Delta \xi$, and test the Heisenberg uncertainty relation $\Delta k \Delta \xi \geq \frac{1}{2}$.

- (a) $A(k) = A(k_0)\exp[-(k - k_0)^2/4q^2]$. This spectral distribution corresponds to a Gaussian pulse and is the minimum wave packet, i.e., $\Delta k \Delta \xi = \frac{1}{2}$.
- (b) $A(k) = A(k_0)\exp(-|k - k_0|/2q)$. This spectral distribution corresponds to a Lorentzian pulse.
- (c) $A(k) = A(k_0)\sin[(k - k_0)/q]/[(k - k_0)/q]$. This spectral distribution corresponds to a square-wave pulse.

- 1.7. A one-dimensional laser pulse is centered at frequency ω_0 and the corresponding wave number k_0 with an envelope function $E(z - v_g t)$ for the electric field:

$$E_x = E(z - v_g t) e^{i(\omega_0 t - k_0 z)}.$$

Find the envelope for the magnetic field H_y , and calculate the Poynting power.

- 1.8. The dispersion in a certain material is described by its index of refraction as a function of frequency,

$$n(\omega) = n_0 - \frac{\Gamma(\omega - \omega_0)}{\Gamma^2 + (\omega - \omega_0)^2}.$$

Find the group velocity v_g for a pulse propagating in this medium.

- 1.9. The envelope of a laser pulse will remain undistorted in shape provided the second-order and higher-order terms in the expansion (1.5-2) of $\omega(k)$ around k_0 can be neglected. Now consider the case when the second-order term is not small and cannot be neglected, but higher-order terms can:

$$\omega(k) = \omega_0 + \left(\frac{d\omega}{dk}\right)_0 (k - k_0) + \frac{1}{2} \left(\frac{d^2\omega}{dk^2}\right)_0 (k - k_0)^2.$$

Find the envelope function of a pulse with the spectral distribution $A(k)$ given in Problem 1.6(a), and find the width of the envelope as a

function of time t . The following integral may be useful:

$$\int_{-\infty}^{\infty} e^{-(\alpha x^2 + \beta x)} dx = \sqrt{\frac{\pi}{\alpha}} e^{\beta^2/4\alpha},$$

where the real part of α must be positive.

- 1.10. If the index of refraction is expressed as a function of wavelength λ , show that the group velocity (1.5-8) can be written

$$v_g = \frac{c}{n - \lambda(dn/d\lambda)}.$$

- 1.11. Show that the Taylor expansion coefficient $\frac{1}{2}(d^2\omega/dk^2)$ is proportional to the group-velocity dispersion, and show that

$$\frac{dv_g}{d\lambda} = v_g^2 \left(\frac{\lambda}{c} \right) \frac{d^2n}{d\lambda^2}.$$

- 1.12. Let $\mathbf{E} = \mathbf{E}_0(\mathbf{r})e^{i\omega t}$, $\mathbf{H} = \mathbf{H}_0(\mathbf{r})e^{i\omega t}$ be solutions to Maxwell's equations.
- (a) Show that \mathbf{E}^* and \mathbf{H}^* also satisfy Maxwell's equations. Note that \mathbf{E}^* , \mathbf{H}^* and \mathbf{E} , \mathbf{H} are in fact the same field, since only the real parts have physical meaning.
- (b) Show that the conjugate waves

$$\mathbf{E}^c = \mathbf{E}_0^*(\mathbf{r})e^{i\omega t},$$

$$\mathbf{H}^c = \mathbf{H}_0^*(\mathbf{r})e^{i\omega t}$$

also satisfy the wave equation provided the medium is lossless (i.e., ϵ and μ are the real tensors).

REFERENCES AND SUGGESTED READING

1. M. Born and E. Wolf, *Principles of Optics*, MacMillan, New York, 1964.
2. J. D. Jackson, *Classical Electrodynamics*, Wiley, New York, 1962.
3. L. D. Landau and E. M. Lifshitz, *Electrodynamics of Continuous Media*, Addison-Wesley, Reading, Mass., 1965.

2

Propagation of Laser Beams

Our main concern in this book is the propagation and control of laser beams. A typical two-reflector laser oscillator and its output beam is sketched in Fig. 2.1. Unlike the infinite plane waves described in Chapter 1, the laser output beam is of finite extent in the transverse direction and spreads with the distance z . Understanding of the propagation characteristics of such beams is of paramount importance to anyone contemplating the study and/or the application of laser phenomena. Although this topic has been treated in many texts, it is included in this book for the purpose of completeness and easy reference.

2.1. SCALAR WAVE EQUATION

A laser beam is coherent electromagnetic radiation. The propagation must therefore obey Maxwell's equations. The field vectors \mathbf{E} and \mathbf{H} which describe the propagation of a laser beam satisfy the vector wave equations (1.4-7) and (1.4-8). If we restrict our attention to beams that have small angular divergence and to media whose refractive index does not vary appreciably in the transverse direction, the vector wave equations can be reduced to a scalar wave equation [1]. In fact, the scalar wave equation can be obtained from (1.4-7) and (1.4-8) by assuming that the fractional change of both the dielectric permittivity ϵ and the magnetic permeability μ in one wavelength is small. In this case Eq. (1.4-7) or (1.4-8) reduces to

$$\nabla^2 \Psi - \frac{n^2}{c^2} \frac{\partial^2 \Psi}{\partial t^2} = 0, \quad (2.1-1)$$

where Ψ can be any Cartesian component of \mathbf{E} and \mathbf{H} , and $n = c\sqrt{\mu\epsilon}$ is the index of refraction. A laser beam is highly monochromatic radiation; therefore it is legitimate to assume that the field quantities vary as $\Psi(x, y, z, t) = \text{Re}[E(x, y, z)e^{i\omega t}]$. The scalar wave equation (2.1-1) be-

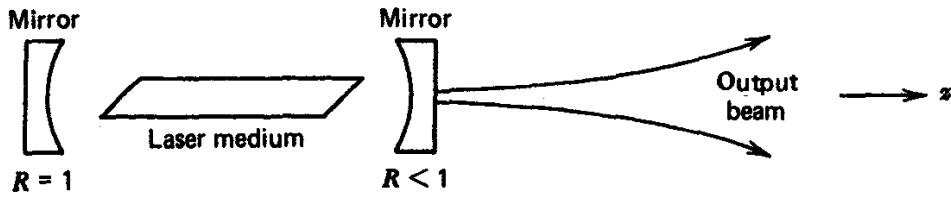


Figure 2.1. A typical laser oscillator and its output beam.

comes

$$\nabla^2 E + K^2 E = 0, \quad (2.1-2)$$

where

$$K^2 = \left(\frac{\omega}{c}\right)^2 n^2(\mathbf{r}), \quad (2.1-3)$$

thus allowing for a possible dependence of n on position \mathbf{r} . Equation (2.1-2) is known as the Helmholtz equation. The most widely encountered type of laser beam in optics is one where the intensity distribution at planes normal to the propagation direction is Gaussian. The medium in which the laser beam will propagate often possesses a cylindrical symmetry with respect to the beam axis. In particular we will consider a lenslike medium whose index of refraction $n = \sqrt{\mu\epsilon/\mu_0\epsilon_0}$ varies according to

$$n^2(\mathbf{r}) = n_o^2 \left(1 - \frac{k_2 r^2}{k}\right), \quad (2.1-4)$$

where k_2 is a constant characteristic of the medium, n_o is the refractive index at the axis of symmetry, r is the distance from the axis, and k is the wave number $k = 2\pi n_o/\lambda$. Since the phase delay of a wave propagating through a section dz of a medium with an index of refraction n is $(2\pi dz/\lambda)n$, it follows directly that a thin slab of the medium described by Eq. (2.1-4) will act as a thin lens, introducing a phase shift proportional to r^2 .

We limit our derivation to the case described by Eq. (2.1-4). The $K^2(r)$ term in the scalar Helmholtz equation (2.1-2) is thus given by

$$K^2(r) = k^2 - k k_2 r^2. \quad (2.1-5)$$

Furthermore, we assume a solution whose transverse dependence is on r

$= \sqrt{x^2 + y^2}$ only, so that in (2.1-2) we can replace ∇^2 by

$$\nabla^2 = \nabla_t^2 + \frac{\partial^2}{\partial z^2} = \frac{\partial^2}{\partial r^2} + \frac{1}{r} \frac{\partial}{\partial r} + \frac{\partial^2}{\partial z^2}. \quad (2.1-6)$$

In other words, we will now look for cylindrically symmetric solutions of the scalar Helmholtz equation (2.1-2).

The kind of propagation we are considering is that of a nearly plane wave in which the flow of energy is predominantly along a single (for example, z) direction, so that we may use the scalar-wave approximation. Taking E as

$$E = \psi(x, y, z) e^{-ikz}, \quad (2.1-7)$$

we obtain from Eqs. (2.1-2) and (2.1-5) in a few simple steps

$$\nabla_t^2 \psi - 2ik\psi' - kk_2 r^2 \psi = 0, \quad (2.1-8)$$

where $\psi' \equiv \partial\psi/\partial z$, and where we assume that the variation of the field amplitude is slow enough that $\partial^2\psi/\partial z^2$ is very small compared with either $k\psi'$ or $k^2\psi$.

Since we are looking for a beam amplitude with cylindrical symmetry, it is convenient to introduce two complex functions $P(z)$ and $q(z)$ such that ψ is in the form of

$$\psi = \exp\left[-i\left(P(z) + \frac{k}{2q(z)} r^2\right)\right]. \quad (2.1-9)$$

We now substitute ψ into Eq. (2.1-8) and after using Eq. (2.1-6) obtain

$$-\left(\frac{k}{q}\right)^2 r^2 - 2i\left(\frac{k}{q}\right) - k^2 r^2 \left(\frac{1}{q}\right)' - 2kP' - kk_2 r^2 = 0, \quad (2.1-10)$$

where the prime indicates differentiation with respect to z . If Eq. (2.1-10) is to hold for all r , the coefficients of the different powers of r must be equal to zero. This leads to

$$\left(\frac{1}{q}\right)^2 + \left(\frac{1}{q}\right)' + \frac{k_2}{k} = 0, \quad P' = -\frac{i}{q}. \quad (2.1-11)$$

The scalar wave equation (2.1-2) is thus reduced to (2.1-11) for the case of cylindrically symmetric beam modes in a lenslike medium.

2.2. GAUSSIAN BEAMS IN A HOMOGENEOUS MEDIUM

If the propagation medium is homogeneous, we can, according to Eq. (2.1-5), put $k_2 = 0$, and Eq. (2.1-11) becomes

$$\frac{1}{q^2} + \left(\frac{1}{q}\right)' = 0, \quad P' = -\frac{i}{q}, \quad (2.2-1)$$

where we recall that the prime indicates a differentiation with respect to z . Introducing the function $u(z)$ by the relation

$$\frac{1}{q} = \frac{1}{u} \frac{du}{dz}, \quad (2.2-2)$$

we obtain directly from Eq. (2.2-1)

$$\frac{d^2u}{dz^2} = 0,$$

so that

$$\frac{du}{dz} = a, \quad u = az + b,$$

or, using Eq. (2.2-2),

$$\frac{1}{q(z)} = \frac{a}{az + b}, \quad (2.2-3)$$

where a and b are arbitrary constants. Equation (2.2-3) may be rewritten in the form

$$q = z + q_0, \quad (2.2-4)$$

where q_0 is a constant complex number [$q_0 = q(0) = b/a$]. The other complex function $P(z)$ can be obtained from Eqs. (2.2-1) and (2.2-4):

$$P' = -\frac{i}{q} = -\frac{i}{z + q_0}, \quad (2.2-5)$$

so that, upon integration, one obtains

$$P(z) = -i \ln \left(1 + \frac{z}{q_0} \right), \quad (2.2-6)$$

where the arbitrary constant of integration is chosen as zero.*

Combining Eqs. (2.2-4) and (2.2-6) in Eq. (2.1-9), we obtain the following cylindrically symmetric solution of the scalar wave equation:

$$\psi = \exp \left\{ -i \left[-i \ln \left(1 + \frac{z}{q_0} \right) + \frac{k}{2(q_0 + z)} r^2 \right] \right\}. \quad (2.2-7)$$

We recall that q_0 is an arbitrary complex constant. It is obvious from the form of Eq. (2.2-7) that a physically realizable solution ψ whose value approaches zero as $r \rightarrow \infty$ results from a choice of an imaginary q_0 . We now reexpress q_0 in terms of a new constant ω_0 :

$$q_0 = i \frac{\pi \omega_0^2 n}{\lambda}, \quad \lambda = \frac{2\pi n}{k} \quad (2.2-8)$$

where n is the same as n_o in a homogeneous medium. With this last substitution, let us consider, one at a time, the two factors in Eq. (2.2-7). The first one becomes

$$\exp \left[-\ln \left(1 - i \frac{\lambda z}{\pi \omega_0^2 n} \right) \right] = \frac{1}{\sqrt{1 + (\lambda z / \pi \omega_0^2 n)^2}} \exp \left[i \tan^{-1} \left(\frac{\lambda z}{\pi \omega_0^2 n} \right) \right], \quad (2.2-9)$$

where we have used $\ln(a + ib) = \ln \sqrt{a^2 + b^2} + i \tan^{-1}(b/a)$. Substituting Eq. (2.2-8) in the second term of Eq. (2.2-7) and separating the exponent into its real and imaginary parts, we obtain

$$\exp \left[\frac{-ikr^2}{2(q_0 + z)} \right] = \exp \left\{ \frac{-r^2}{\omega_0^2 \left[1 + (\lambda z / \pi \omega_0^2 n)^2 \right]} - \frac{ikr^2}{2z \left[1 + (\pi \omega_0^2 n / \lambda z)^2 \right]} \right\}. \quad (2.2-10)$$

*The integration constant will only modify the phase of the field solution (2.1-7). This is equivalent to a mere shift of the time origin.

If we define the parameters

$$\omega^2(z) = \omega_0^2 \left[1 + \left(\frac{\lambda z}{\pi \omega_0^2 n} \right)^2 \right] = \omega_0^2 \left(1 + \frac{z^2}{z_0^2} \right), \quad (2.2-11)$$

$$R = z \left[1 + \left(\frac{\pi \omega_0^2 n}{\lambda z} \right)^2 \right] = z \left(1 + \frac{z_0^2}{z^2} \right), \quad (2.2-12)$$

so that

$$\frac{1}{q(z)} = \frac{1}{z + i(\pi \omega_0^2 n / \lambda)} = \frac{1}{R(z)} - i \frac{\lambda}{\pi \omega^2(z) n} \quad (2.2-13)$$

and

$$\eta(z) = \tan^{-1} \left(\frac{\lambda z}{\pi \omega_0^2 n} \right) = \tan^{-1} \left(\frac{z}{z_0} \right) \quad (2.2-14)$$

with

$$z_0 \equiv \frac{\pi \omega_0^2 n}{\lambda},$$

then we can combine Eqs. (2.2-9) and (2.2-10) in Eq. (2.2-7) and, recalling that $E(x, y, z) = \psi(x, y, z)e^{-ikz}$, obtain

$$\begin{aligned} E(x, y, z) &= E_0 \frac{\omega_0}{\omega(z)} \exp \left\{ -i[kz - \eta(z)] - i \frac{kr^2}{2q(z)} \right\} \\ &= E_0 \frac{\omega_0}{\omega(z)} \exp \left\{ -i[kz - \eta(z)] - r^2 \left(\frac{1}{\omega^2(z)} + \frac{ik}{2R(z)} \right) \right\}, \end{aligned} \quad (2.2-15)$$

where we recall that $k = 2\pi n/\lambda$. This is our basic result. We refer to it as the fundamental Gaussian-beam solution, since we have excluded the more complicated solutions of Eq. (2.1-2) (that is, those with azimuthal variation) by limiting ourselves to transverse dependence involving $r = (x^2 + y^2)^{1/2}$ only. These higher-order modes will be discussed separately.

From Eq. (2.2-15) the parameter $\omega(z)$, which evolves according to Eq. (2.2-11), is the distance r at which the field amplitude is down by a factor

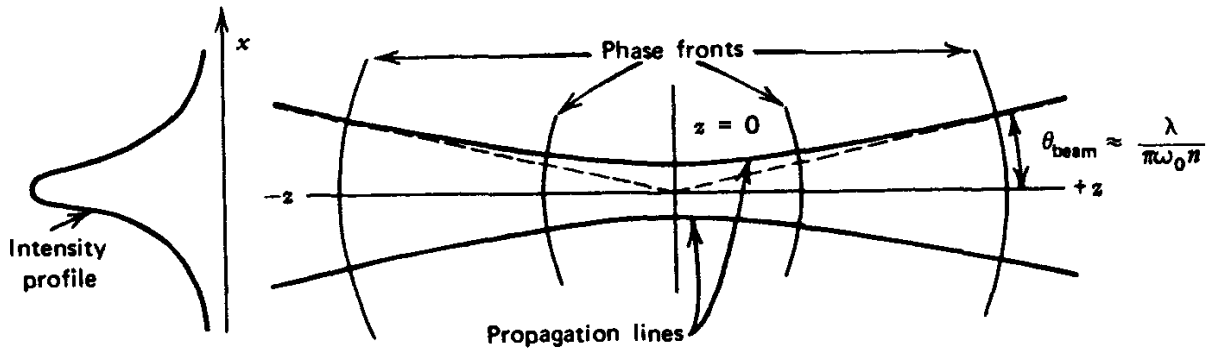


Figure 2.2. Propagating Gaussian beam.

$1/e$ compared to its value on the axis. We will consequently refer to it as the beam “spot size.” The parameter ω_0 is the minimum spot size. It is the beam spot size at the plane $z = 0$. The parameter R in Eq. (2.2-15) is the radius of curvature of the very nearly spherical wavefronts* at z . We can verify this statement by deriving the radius of curvature of the constant-phase surfaces (wavefronts) or, more simply, by considering the form of a spherical wave emitted by a point radiator placed at $z = 0$. It is given by

$$\begin{aligned}
 E &\propto \frac{1}{R} e^{-ikR} = \frac{1}{R} \exp\left(-ik\sqrt{x^2 + y^2 + z^2}\right) \\
 &\approx \frac{1}{R} \exp\left\{-ikz - ik\left(\frac{x^2 + y^2}{2R}\right)\right\}, \quad x^2 + y^2 \ll z^2 \quad (2.2-16)
 \end{aligned}$$

where we have expanded the square root in the region where $z^2 \gg x^2 + y^2$ and taken z equal to R , the radius of curvature of the spherical wave. Comparing Eq. (2.2-15) with Eq. (2.2-16), we identify R as the radius of curvature of the Gaussian beam. The convention regarding the sign of $R(z)$ is that it is negative if the center of curvature occurs at $z' > z$ and positive for $z' < z$.

The form of the fundamental Gaussian beam, according to Eq. (2.2-15), is uniquely determined once its minimum spot size ω_0 and its location—that is, the plane $z = 0$ —are specified. The spot size ω and radius of curvature R at any plane z are then found from Eqs. (2.2-11) and (2.2-12). Some of these characteristics are displayed in Fig. 2-2. The hyperbolae shown in this figure correspond to the ray direction and are intersections of planes that include

*Actually, it follows from (2.2-15) that, with the exception of the immediate vicinity of the plane $z = 0$, the wavefronts are parabolic since they are defined by $k[z + (r^2/2R)] = \text{const.}$ For $r^2 \ll z^2$, the distinction between parabolic and spherical surfaces is not important.

the z axis and the hyperboloids

$$x^2 + y^2 = \text{const } \omega^2(z). \quad (2.2-17)$$

These hyperbolae correspond to the local direction of energy propagation. The spherical surfaces shown have radii of curvature given by Eq. (2.2-12). For large z , the hyperboloids $x^2 + y^2 = \omega^2$ are asymptotic to the cone

$$r = \sqrt{x^2 + y^2} = \frac{\lambda}{\pi\omega_0 n} z, \quad (2.2-18)$$

whose half apex angle, which we take as a measure of the angular beam spread, is

$$\begin{aligned} \theta_{\text{beam}} &= \tan^{-1} \left(\frac{\lambda}{\pi\omega_0 n} \right) \\ &\approx \frac{\lambda}{\pi\omega_0 n} \quad \text{for } \theta_{\text{beam}} \ll \pi. \end{aligned} \quad (2.2-19)$$

This last result is a rigorous manifestation of wave diffraction, according to which a wave that is confined in the transverse direction to an aperture of radius ω_0 will spread (diffract) in the far field ($z \gg \pi\omega_0^2 n/\lambda$) according to Eq. (2.2-19).

2.3. FUNDAMENTAL GAUSSIAN BEAM IN A LENS LIKE MEDIUM—THE *ABCD* LAW

The Gaussian beam (2.2-15) derived in the last section is a solution to the wave equation (2.1-2) in a homogeneous medium ($k_2 = 0$). There are many situations in which the index of refraction of the medium obeys the quadratic variation, as in Eq. (2.1-4) with $k_2 \neq 0$. For example, the index of refraction $n(r)$ of a graded-index fiber (see Fig. 2-5 below) is approximately given by Eq. (2.1-4). Another example of importance is the propagation of a Gaussian beam in a Kerr medium [11]. In the latter case, the quadratic index variation is induced by the intensity distribution of the laser beam itself. Wave propagation in these media can be described by two different methods. In the eigenmode approach, an arbitrary wave can be represented by a linear superposition of eigenmodes which have unique propagation constants and transverse field distributions (see Section 2.5). In the Gaussian-beam approach, the wave propagation at each point z is assumed to

obey Eq. (2.1-9) with beam parameters P and q evolved according to Eq. (2.1-11). The latter approach is more transparent and will be discussed in this section.

We now return to the general case of a lenslike medium, so that $k_2 \neq 0$. The functions P and q of Eq. (2.1-9) obey, according to Eq. (2.1-11),

$$\left(\frac{1}{q}\right)^2 + \left(\frac{1}{q}\right)' + \frac{k_2}{k} = 0, \quad P' = -\frac{i}{q}. \quad (2.3-1)$$

If we introduce the function u defined by

$$\frac{1}{q} = \frac{u'}{u}, \quad (2.3-2)$$

we obtain from Eq. (2.3-1)

$$u'' + u\left(\frac{k_2}{k}\right) = 0, \quad (2.3-3)$$

so that

$$u(z) = a \sin \sqrt{\frac{k_2}{k}} z + b \cos \sqrt{\frac{k_2}{k}} z, \quad (2.3-4)$$

$$u'(z) = a \sqrt{\frac{k_2}{k}} \cos \sqrt{\frac{k_2}{k}} z - b \sqrt{\frac{k_2}{k}} \sin \sqrt{\frac{k_2}{k}} z,$$

where a and b are arbitrary constants and the prime indicates differentiation with respect to z .

Using Eqs. (2.3-4) and (2.3-2) and expressing the result in terms of an input value $q(0) \equiv q_0$ gives the following result for the complex beam radius $q(z)$:

$$q(z) = \frac{q_0 \cos \alpha_2 z + \alpha_2^{-1} \sin \alpha_2 z}{-q_0 \alpha_2 \sin \alpha_2 z + \cos \alpha_2 z} \quad (2.3-5)$$

with α_2 defined as

$$\alpha_2 \equiv \left(\frac{k_2}{k}\right)^{1/2}.$$

The relation (2.3-5) between the input beam parameter q_0 and the output beam parameter q is known in geometrical theory of optical images as the collinear relationship [2].

The physical significance of $q(z)$ in this case can be extracted from Eq. (2.1-9). We expand the part of the field amplitude $\psi(r, z)$ that involves r . The result is

$$\psi \propto e^{-ikr^2/2q(z)}. \quad (2.3-6)$$

If we express the real and imaginary parts of $q(z)$ by means of

$$\frac{1}{q(z)} = \frac{1}{R(z)} - i \frac{\lambda}{\pi n \omega^2(z)}, \quad (2.3-7)$$

we obtain

$$\psi \propto \exp \left[\frac{-r^2}{\omega^2(z)} - i \frac{kr^2}{2R(z)} \right], \quad (2.3-8)$$

so that $\omega(z)$ is the beam spot size and R the radius of curvature of the wavefront, as in the case of a homogeneous medium, which is described by Eq. (2.2-15). For the special case of a homogeneous medium ($k_2 = 0$), Eq. (2.3-5) reduces to Eq. (2.2-4).

2.3.1. Rays in Lenslike Media

The propagation of optical beams can be adequately described by Maxwell's equation, or by the scalar wave equation (2.1-1) under the appropriate conditions. In Eq. (2.1-1), the refractive index n is a property of the medium and, in general, can be a function of position in space. If n is a constant, Eq. (2.1-1) is satisfied by a plane-wave solution (1.4-10). When n is a function of position, the plane wave is no longer a solution. If n varies slowly with position, we may look for a solution resembling the plane wave as closely as possible, i.e.,

$$\Psi = A(\mathbf{r}) e^{i[\omega t - \phi(\mathbf{r})]}. \quad (2.3-9)$$

The quantities $A(\mathbf{r})$ and $\phi(\mathbf{r})$ are functions of position to be determined, and are both considered to be real. $A(\mathbf{r})$ therefore is a measure of the amplitude of the wave. If n were constant, $\phi(\mathbf{r})$ would reduce to $\mathbf{k} \cdot \mathbf{r}$, and in consequence it is called the phase of the wave; it is also frequently referred

to as the eikonal. If we now substitute Eq. (2.3-9) for Ψ into the wave equation (2.1-1), and use the assumption that the fractional variation of n over distances of the order of a wavelength is negligible, the scalar wave equation reduces to the simple form

$$(\nabla\phi)^2 = \left(\frac{2\pi}{\lambda}n\right)^2. \quad (2.3-10)$$

For the case of homogeneous media, an integration of Eq. (2.3-10) yields $\phi(\mathbf{r}) = \mathbf{k} \cdot \mathbf{r}$ with $k = 2\pi n/\lambda$. The derivation of Eq. (2.3-10) is left as an exercise (Problem 2.5). Equation (2.3-10) is known as the eikonal equation of geometrical optics. The surfaces of constant ϕ determined by this equation are surfaces of constant optical phase and thus define the wavefronts. The light rays have been defined as the orthogonal trajectories to the wavefronts $\phi(\mathbf{r}) = \text{const}$ and hence are also determined by Eq. (2.3-10). If \mathbf{r} is a position vector of a typical point on a ray trajectory and s the length of the ray measured from a fixed point on it, then $d\mathbf{r}/ds$ is a unit vector in the direction of $\nabla\phi$ which is normal to the wavefronts. Thus if we take the square root of Eq. (2.3-10), we obtain

$$\frac{2\pi}{\lambda}n \frac{d\mathbf{r}}{ds} = \nabla\phi. \quad (2.3-11)$$

This equation specifies the rays by means of the eikonal $\phi(\mathbf{r})$. Conversely, the eikonal $\phi(\mathbf{r})$ can be expressed as a ray integral

$$\phi(\mathbf{r}) = \frac{2\pi}{\lambda} \int n ds,$$

where the integration is carried along a ray trajectory. A differential equation which describes the ray propagation directly in terms of the refractive index function $n(\mathbf{r})$ can be derived from Eqs. (2.3-10) and (2.3-11) and is given by

$$\frac{d}{ds} \left(n \frac{d\mathbf{r}}{ds} \right) = \nabla n. \quad (2.3-12)$$

For paraxial rays (i.e., rays making very small angles with the z axis) we may replace d/ds by d/dz . For the case of lenslike medium described by

Eq. (2.1-4), the ray equation becomes

$$\frac{d^2 r}{dz^2} + \frac{k_2}{k} r = 0. \quad (2.3-13)$$

We notice that this equation is identical to Eq. (2.3-3). This means that in the paraxial limit the spatial evolution of the complex beam parameter q and the ray parameter $r/(dr/dz)$ in a lenslike medium are the same. In other words, the transformation law of the ray parameter can also be applied to the complex beam parameter q . If we represent a ray at any position z as a column matrix

$$\begin{pmatrix} r \\ r' \end{pmatrix}, \quad r' = \frac{dr}{dz},$$

we can derive from Eq. (2.3-13) a ray matrix for a lenslike medium or a special case of a lenslike medium such that

$$\begin{pmatrix} r \\ r' \end{pmatrix}_2 = \begin{pmatrix} A & B \\ C & D \end{pmatrix} \begin{pmatrix} r \\ r' \end{pmatrix}_1, \quad (2.3-14)$$

where $r' \equiv dr/dz$ and the subscripts 1 and 2 refer to positions z_1 and z_2 , respectively. Table 2.1 lists the ray matrices for some common optical elements and media. Equation (2.3-14) can also be written as

$$(r/r')_2 = \frac{A(r/r')_1 + B}{C(r/r')_1 + D}. \quad (2.3-15)$$

2.3.2. Transformation of Gaussian Beam—The *ABCD* Law

We have derived above the transformation law of a Gaussian beam (2.3-5) and a ray (2.3-15) propagating through a lenslike medium that is characterized by k_2 . We have also shown that the beam parameter q and the ray parameter r/r' obey the same transformation law. That is, the transformation of the complex beam parameter q can be described as

$$q_2 = \frac{Aq_1 + B}{Cq_1 + D}, \quad (2.3-16)$$

where A, B, C, D are the elements of the ray matrix which relate the ray at a plane $z = z_2$ to the ray at a plane $z = z_1$ [Eq. (2.3-14)]. It follows immediately that the propagation through, or reflection from, any of the

Table 2.1 Ray Matrices for Some Common Optical Elements and Media

(1) Straight section: length d		$\begin{bmatrix} 1 & d \\ 0 & 1 \end{bmatrix}$
(2) Thin lens: focal length f ($f > 0$, converging; $f < 0$, diverging)		$\begin{bmatrix} 1 & 0 \\ -\frac{1}{f} & 1 \end{bmatrix}$
(3) Dielectric interface: refractive indices n_1, n_2		$\begin{bmatrix} 1 & 0 \\ 0 & \frac{n_1}{n_2} \end{bmatrix}$
(4) Spherical dielectric interface: radius R		$\begin{bmatrix} 1 & 0 \\ \frac{n_2 - n_1}{n_2 R} & \frac{n_1}{n_2} \end{bmatrix}$
(5) Spherical mirror: radius of curvature R		$\begin{bmatrix} 1 & 0 \\ -\frac{2}{R} & 1 \end{bmatrix}$
(6) Medium with a quadratic index profile		$\begin{bmatrix} \cos\left(\sqrt{\frac{k_2}{k}} l\right) & \sqrt{\frac{k}{k_2}} \sin\left(\sqrt{\frac{k_2}{k}} l\right) \\ -\sqrt{\frac{k_2}{k}} \sin\left(\sqrt{\frac{k_2}{k}} l\right) & \cos\left(\sqrt{\frac{k_2}{k}} l\right) \end{bmatrix}$

elements shown in Table 2.1 also obeys Eq. (2.3-16), since these elements can all be viewed as special cases of a lenslike medium. For future reference we note that by applying Eq. (2.3-16) to a thin lens of focal length f , we obtain from Eq. (2.3-16) and Table 2.1, line (2),

$$\frac{1}{q_2} = \frac{1}{q_1} - \frac{1}{f}, \quad (2.3-17)$$

so that, using Eq. (2.3-17), we have

$$\begin{aligned} \omega_2 &= \omega_1, \\ \frac{1}{R_2} &= \frac{1}{R_1} - \frac{1}{f}, \end{aligned} \quad (2.3-18)$$

where $\omega_{1,2}$ are the beam spot sizes and $R_{1,2}$ are the radii of curvature. These results apply, as well, to reflection from a mirror with a radius of curvature R if we replace f by $R/2$.

Consider next the propagation of a Gaussian beam through two lenslike media that are adjacent to each other. The ray matrix describing the first one is (A_1, B_1, C_1, D_1) , while that of the second one is (A_2, B_2, C_2, D_2) . Taking the input beam parameter as q_1 and the output beam parameter as q_3 , we have, from Eq. (2.3-16),

$$q_2 = \frac{A_1 q_1 + B_1}{C_1 q_1 + D_1}$$

for the beam parameter at the output of medium 1, and

$$q_3 = \frac{A_2 q_2 + B_2}{C_2 q_2 + D_2}.$$

Combining the last two equations, we have

$$q_3 = \frac{A_T q_1 + B_T}{C_T q_1 + D_T}, \quad (2.3-19)$$

where (A_T, B_T, C_T, D_T) are elements of the ray matrix relating the output plane (3) to the input plane (1), that is,

$$\begin{pmatrix} A_T & B_T \\ C_T & D_T \end{pmatrix} = \begin{pmatrix} A_2 & B_2 \\ C_2 & D_2 \end{pmatrix} \begin{pmatrix} A_1 & B_1 \\ C_1 & D_1 \end{pmatrix}. \quad (2.3-20)$$

It follows by induction that Eq. (2.3-19) applies to the propagation of a Gaussian beam through an arbitrary number of lenslike media and elements. The matrix (A_T, B_T, C_T, D_T) is the ordered product of the matrices characterizing the individual members of the chain.

The great utility of the $ABCD$ law is that it enables us to trace the Gaussian-beam parameter $q(z)$ through a complicated sequence of lenslike elements. The beam radius $R(z)$ and spot size $\omega(z)$ at any plane z can be recovered through the use of (2.3-7). The application of this method will be made clear by the following example.

2.3.3. Example—Gaussian-beam Focusing

As an illustration of the application of the $ABCD$ law, we consider the case of a Gaussian beam that is incident at its waist on a thin lens of focal length f , as shown in Fig. 2.3. We will find the location of the waist of the output beam and the beam radius at that point.

At the input plane 1 we have $\omega = \omega_1$, $R_1 = \infty$, so that

$$\frac{1}{q_1} = \frac{1}{R_1} - i \frac{\lambda}{\pi \omega_1^2 n} = -i \frac{\lambda}{\pi \omega_1^2 n}.$$

Using Eq. (2.3-17) leads to

$$\begin{aligned} \frac{1}{q_2} &= \frac{1}{q_1} - \frac{1}{f} = -\frac{1}{f} - i \frac{\lambda}{\pi \omega_1^2 n}, \\ q_2 &= \frac{1}{-1/f - i(\lambda/\pi \omega_1^2 n)} = \frac{-a + ib}{a^2 + b^2}, \\ a &\equiv \frac{1}{f}, \quad b \equiv \frac{\lambda}{\pi \omega_1^2 n}. \end{aligned}$$

At plane 3 we obtain, using Eq. (2.2-4),

$$\begin{aligned} q_3 &= q_2 + l = \frac{-a}{a^2 + b^2} + \frac{ib}{a^2 + b^2} + l \\ \frac{1}{q_3} &= \frac{1}{R_3} - i \frac{\lambda}{\pi \omega_3^2 n} \\ &= \frac{\left(-\frac{a}{a^2 + b^2} + l\right) - i \frac{b}{a^2 + b^2}}{\left(-\frac{a}{a^2 + b^2} + l\right)^2 + \frac{b^2}{(a^2 + b^2)^2}}. \end{aligned}$$

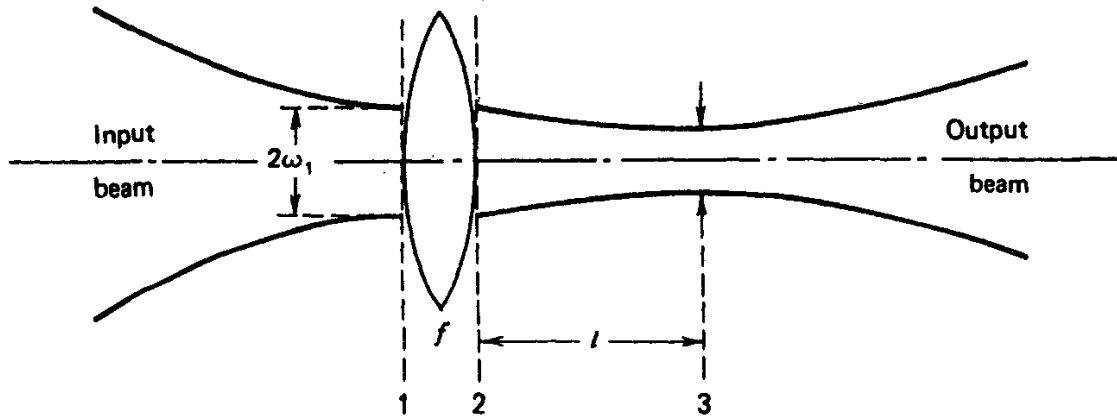


Figure 2.3. Focusing of a Gaussian beam.

Since plane 3, according to the statement of the problem, corresponds to the output beam waist, $R_3 = \infty$. Using this fact in the last equation leads to

$$l = \frac{a}{a^2 + b^2} = \frac{f}{1 + (\lambda f / \pi \omega_1^2 n)^2} = \frac{f}{1 + (f/z_1)^2} \quad (2.3-21)$$

as the location of the new waist, and to

$$\frac{\omega_3}{\omega_1} = \frac{f \lambda / \pi \omega_1^2 n}{\sqrt{1 + (f \lambda / \pi \omega_1^2 n)^2}} = \frac{f/z_1}{\sqrt{1 + (f/z_1)^2}} \quad (2.3-22)$$

for the output beam waist. The confocal beam parameter

$$z_1 \equiv \frac{\pi \omega_1^2 n}{\lambda}$$

is, according to Eq. (2.2-11), the distance from the waist in which the input beam spot size increases by $\sqrt{2}$ and is a convenient measure of the convergence of the input beam. The smaller z_1 , the "stronger" the convergence.

2.4. HIGH-ORDER GAUSSIAN BEAM MODES IN A HOMOGENEOUS MEDIUM

The Gaussian mode treated up to this point has a field variation that depends only on the axial distance z and the distance r from the axis. If we do not impose the condition $\partial/\partial\phi = 0$ [where ϕ is the azimuthal angle in a

cylindrical coordinate system (r, ϕ, z) and if we take $k_2 = 0$, the wave equation (2.1-2) has solutions in the form of [3]

$$\begin{aligned}
 E_{l,m}(x, y, z) &= E_o \frac{\omega_o}{\omega(z)} H_l \left(\sqrt{2} \frac{x}{\omega(z)} \right) H_m \left(\sqrt{2} \frac{y}{\omega(z)} \right) \\
 &\quad \times \exp \left[-ik \frac{x^2 + y^2}{2q(z)} - ikz + i(l + m + 1)\eta \right] \\
 &= E_o \frac{\omega_o}{\omega(z)} H_l \left(\sqrt{2} \frac{x}{\omega(z)} \right) H_m \left(\sqrt{2} \frac{y}{\omega(z)} \right) \\
 &\quad \times \exp \left[-\frac{x^2 + y^2}{\omega^2(z)} - \frac{ik(x^2 + y^2)}{2R(z)} - ikz + i(l + m + 1)\eta \right]
 \end{aligned} \tag{2.4-1}$$

where H_l is the Hermite polynomial of order l , and $\omega(z)$, $R(z)$, $q(z)$, and η are defined as in Eqs. (2.2-11)–(2.2-14).

We note for future reference that the phase shift on the axis is

$$\begin{aligned}
 \eta &= kz - (l + m + 1) \tan^{-1} \left(\frac{z}{z_o} \right) \\
 z_o &= \frac{\pi \omega_o^2 n}{\lambda}.
 \end{aligned} \tag{2.4-2}$$

The transverse variation of the electric field along x (or y) is seen to be of the form $H_l(\xi) \exp(-\xi^2/2)$, where $\xi = \sqrt{2}x/\omega$. This function has been studied extensively, since it also corresponds to the quantum-mechanical wave function $u_l(\xi)$ of the harmonic oscillator [4]. Some low-order functions normalized to represent the same amount of total beam power are shown in Fig. 2-4.

2.5. GAUSSIAN BEAM MODES IN QUADRATIC-INDEX MEDIA

In Section 2.3 we treated the propagation of a circularly symmetric Gaussian beam in lenslike media by solving for the complex beam parameter q as a function of z . Now we adopt the eigenmode approach and derive the normal modes of propagation in media whose index of refraction can be

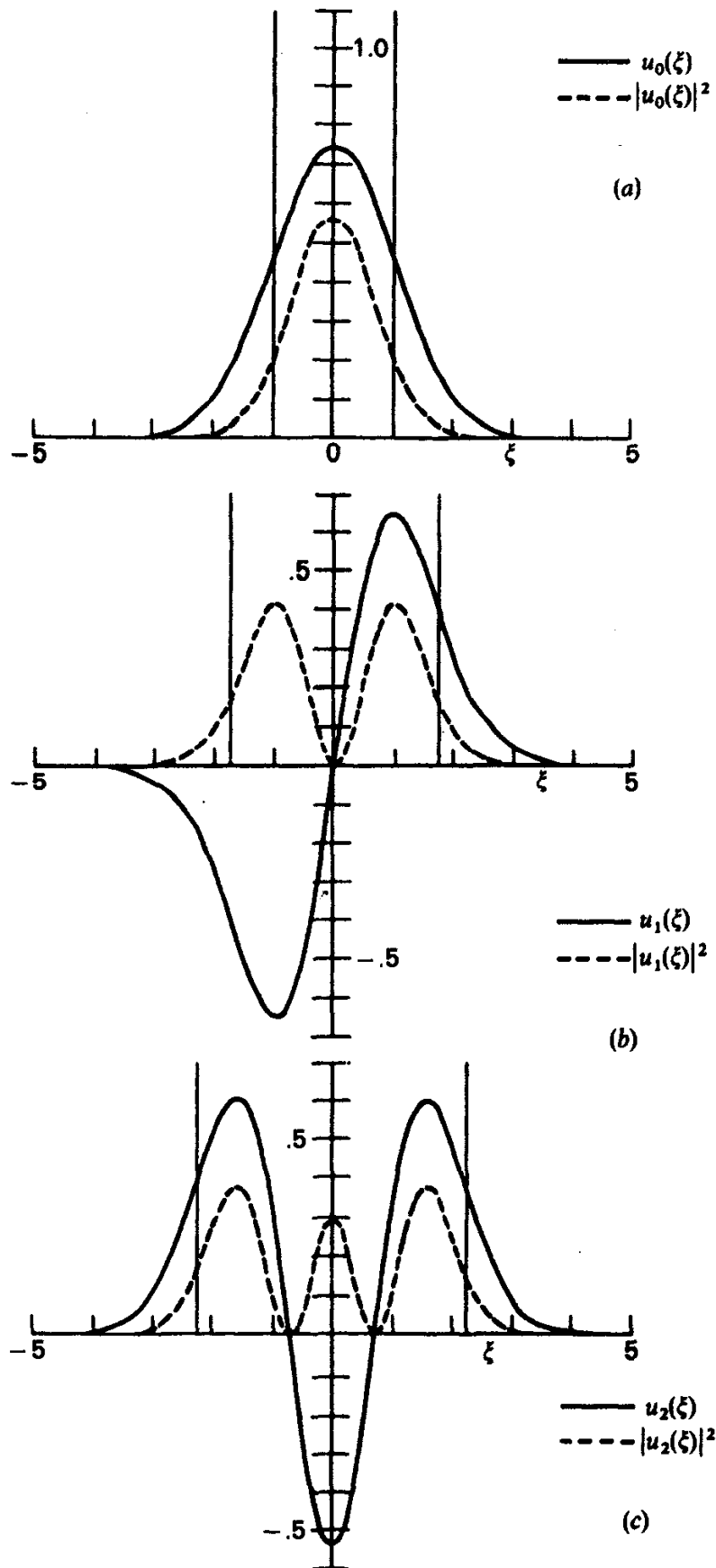


Figure 2.4. Hermite Gaussian functions $u_l(\xi) = (\pi^{1/2} l! 2^l)^{-1/2} H_l(\xi) e^{-\xi^2/2}$ corresponding to higher-order beam solutions (2.4-1). The curves are normalized so as to represent a fixed amount of total beam power in all the modes: $\int_{-\infty}^{\infty} u_l^2(\xi) d\xi = 1$. The solid curves are the functions $u_l(\xi)$ for $l = 0, 1, 2, 3$, and 10. The dashed curves are $u_l^2(\xi)$.

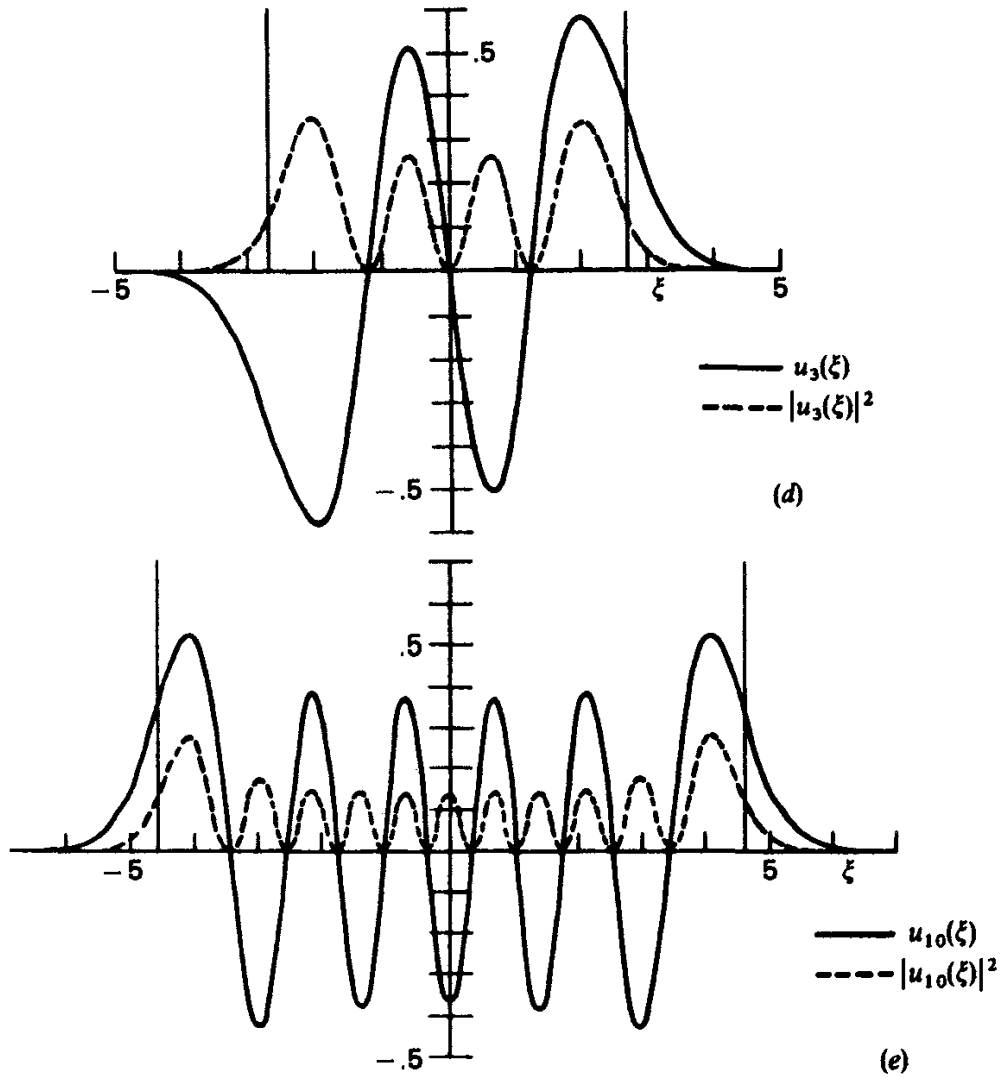


Figure 2.4. (Continued)

described by

$$n^2(r) = n_o^2 \left(1 - \frac{n_2}{n_o} r^2 \right), \quad r^2 = x^2 + y^2, \quad (2.5-1a)$$

which is consistent with Eq. (2.1-4) if we put $k_2 = 2\pi n_2/\lambda$.

The scalar wave equation (2.1-2) takes the form

$$\nabla^2 + k^2 \left(1 - \frac{n_2}{n_o} r^2 \right) E = 0, \quad (2.5-1b)$$

where

$$E(x, y, z) = \psi(x, y) \exp(-i\beta z).$$

Taking $\psi(x, y) = f(x)g(y)$, the wave equation (2.5-1b) becomes

$$\frac{1}{f} \frac{\partial^2 f}{\partial x^2} + \frac{1}{g} \frac{\partial^2 g}{\partial y^2} + k^2 - k^2 \frac{n_2}{n_o} (x^2 + y^2) - \beta^2 = 0. \quad (2.5-2)$$

Since Eq. (2.5-2) is the sum of a y -dependent part and an x -dependent part, it follows that

$$\frac{1}{f} \frac{d^2 f}{dx^2} + \left(k^2 - \beta^2 - k^2 \frac{n_2}{n_o} x^2 \right) = C, \quad (2.5-3)$$

$$\frac{1}{g} \frac{d^2 g}{dy^2} - k^2 \frac{n_2}{n_o} y^2 = -C, \quad (2.5-4)$$

where C is some constant. Consider first Eq. (2.5-4). Defining a variable ξ by

$$\xi = \alpha y, \quad \alpha \equiv k^{1/2} \left(\frac{n_2}{n_o} \right)^{1/4}, \quad (2.5-5)$$

Eq. (2.5-4) becomes

$$\frac{d^2 g}{d\xi^2} + \left(\frac{C}{\alpha^2} - \xi^2 \right) g = 0. \quad (2.5-6)$$

This is a well-known differential equation and is identical to the Schrödinger equation of the harmonic oscillator [5]. The eigenvalue C/α^2 must satisfy

$$\frac{C}{\alpha^2} = (2m + 1), \quad m = 1, 2, 3, \dots \quad (2.5-7)$$

The solution corresponding to a given integer m is

$$g_m(\xi) = H_m(\xi) e^{-\xi^2/2}, \quad (2.5-8)$$

where H_m is the Hermite polynomial of order m .

We now repeat the procedure with Eq. (2.5-3). Substituting

$$\zeta = \alpha x$$

it becomes

$$\frac{d^2 f}{d\xi^2} + \left(\frac{k^2 - \beta^2 - C}{\alpha^2} - \xi^2 \right) f = 0,$$

so that, as in Eq. (2.5-7),

$$\frac{k^2 - \beta^2 - C}{\alpha^2} = (2l + 1), \quad l = 1, 2, 3, \dots, \quad (2.5-9)$$

and

$$f_l(\xi) = H_l(\xi) e^{-\xi^2/2}. \quad (2.5-10)$$

The total solution for ψ is thus

$$\psi(x, y) = H_l\left(\frac{\sqrt{2}x}{\omega}\right) H_m\left(\frac{\sqrt{2}y}{\omega}\right) e^{-(x^2+y^2)/\omega^2}$$

where the “spot size” ω is, according to (2.5-5)

$$\omega = \frac{\sqrt{2}}{\alpha} = \sqrt{\frac{2}{k}} \left(\frac{n_o}{n_2}\right)^{1/4} = \sqrt{\frac{\lambda}{\pi}} \left(\frac{1}{n_o n_2}\right)^{1/4}. \quad (2.5-11)$$

The total (complex) field is

$$\begin{aligned} E_{l,m}(x, y, z) &= \psi_{l,m}(x, y) e^{-i\beta_{l,m}z} \\ &= E_0 H_l\left(\sqrt{2} \frac{x}{\omega}\right) H_m\left(\sqrt{2} \frac{y}{\omega}\right) \exp\left(-\frac{x^2 + y^2}{\omega^2}\right) \exp(-i\beta_{l,m}z). \end{aligned} \quad (2.5-12)$$

The propagation constant $\beta_{l,m}$ of the (l, m) mode is obtained from Eqs. (2.5-7) and (2.5-9):

$$\beta_{l,m} = k \left[1 - \frac{2}{k} \sqrt{\frac{n_2}{n_o}} (l + m + 1) \right]^{1/2}. \quad (2.5-13)$$

Two features of the mode solutions are noteworthy:

1. Unlike the homogeneous-medium solution ($n_2 = 0$), the mode “spot size” ω is independent of z . This can be explained by the focusing action

of the index variation ($n_2 > 0$), which counteracts the natural tendency of a confined beam to diffract (spread). In the case of an index of refraction which increases with r ($n_2 < 0$), it follows from Eqs. (2.5-11) and (2.5-12) that $\omega^2 < 0$ and no confined solutions exist. The index profile in this case leads to defocusing, thus reinforcing the diffraction of the beam.

2. The dependence of β on the mode indices l, m causes the different modes to have phase velocities $v_{l,m} = \omega/\beta_{l,m}$ as well as group velocities $(v_g)_{l,m} = d\omega/d\beta_{l,m}$ which depend on l and m .

Let us consider the modal dispersion (that is, the dependence on l and m) of the group velocity of mode l, m :

$$(v_g)_{l,m} = \frac{d\omega}{d\beta_{l,m}}. \quad (2.5-14)$$

If the index variation is small, so that

$$\frac{1}{k} \sqrt{\frac{n_2}{n_o}} (l + m + 1) \ll 1 \quad (2.5-15)$$

we can approximate Eq. (2.5-13) as

$$\beta_{l,m} \approx k - \sqrt{\frac{n_2}{n_o}} (l + m + 1) - \frac{n_2}{2kn_o} (l + m + 1)^2, \quad (2.5-16)$$

so that, according to Eq. (2.5-14),

$$(v_g)_{l,m} = \frac{\frac{c}{n_o}}{1 + \frac{n_2/n_o}{2k^2} (l + m + 1)^2}. \quad (2.5-17)$$

The effect of the group-velocity dispersion on pulse propagation is considered next.

2.5.1. Pulse Spreading in Quadratic-Index Glass Fibers

Glass fibers with quadratic index profiles (2.5-1a) are excellent channels for optical communication systems [6, 7]. The information is coded onto trains of optical pulses, and the channel information capacity is thus fundamen-

tally limited by the number of pulses that can be transmitted per unit time [8, 9].

There are two ways in which the group velocity dispersion limits the pulse repetition rate of the quadratic index channel.

Modal Dispersion. If the optical pulses fed into the input end of the fiber excite a large number of modes (this will be the case if the input light is strongly focused, so that the "rays" subtend a large angle), then each mode will travel with a group velocity $(v_g)_{l,m}$, as given by Eq. (2.5-17). If all the modes from $(0,0)$ to (l_{\max}, m_{\max}) are excited, the output pulse at $z = L$ will broaden to

$$\Delta\tau \approx L \left[\frac{1}{(v_g)_{l_{\max}, m_{\max}}} - \frac{1}{(v_g)_{0,0}} \right]. \quad (2.5-18)$$

We can use (2.5-17) and the condition $(n_2/n_o)(l+m+1)^2/2k^2 \ll 1$ to obtain

$$\Delta\tau = \frac{n_o L}{c} \frac{n_2}{2n_o k^2} (l_{\max} + m_{\max} + 1)^2. \quad (2.5-19)$$

The maximum number of pulses per second that can be transmitted without serious overlap of adjacent output pulse is thus $f_{\max} \sim 1/\Delta\tau$. The achievement of high-data-rate transmission will consequently require single-mode excitation. This can be achieved by the use of coherent single-mode laser excitation [7-9].

Numerical Example. Consider a 1-km-long quadratic-index fiber with $n_o = 1.5$, $n_2 = 5.1 \times 10^3 \text{ cm}^{-2}$. Let the input optical pulses at $\lambda = 1 \mu\text{m}$ excite the modes up to $l_{\max} = m_{\max} = 30$. Substitution in Eq. (2.5-19) gives

$$\Delta\tau = 3.6 \times 10^{-9} \text{ s}$$

and $f_{\max} \sim (\Delta\tau)^{-1} = 2.8 \times 10^8$ pulses per second for the maximum pulse rate.

Group-Velocity Dispersion. As noted above, the pulse spreading (2.5-19) due to multimode excitation can be eliminated by single-mode (say l, m) propagation. In this case, pulse spreading would still result from the dependence of $(v_g)_{l,m}$ on frequency. This spreading can be explained by the fact that an optical pulse has a spectral width $\Delta\omega$ which will spread in a

distance L by (see Problem 1.9)

$$\Delta\tau = 2L \frac{d}{d\omega} \left(\frac{1}{v_g} \right) \Delta\omega = \frac{2L}{v_g^2} \left(\frac{dv_g}{d\omega} \right) \Delta\omega. \quad (2.5-20)$$

If the pulse is derived from a coherent continuous source with a negligible spectral width, then the pulse spectral width is related to the pulse duration τ by $\Delta\omega \sim 2/\tau$, and Eq. (2.5-20) becomes

$$\Delta\tau = \frac{4L}{v_g^2 \tau} \left(\frac{dv_g}{d\omega} \right) \quad (2.5-21)$$

If the source bandwidth $\Delta\omega$, exceeds τ^{-1} , then we need to replace $\Delta\omega$ in Eq. (2.5-20) by $\Delta\omega_s$. The pulse spreading is thus caused by the dependence of group velocity on ω —group-velocity dispersion.

In order to check our semi-intuitive derivation of Eq. (2.5-21), and also as an instructive exercise in the mathematics of dispersive propagation, we will consider, in what follows, the problem of an optical pulse with a Gaussian envelope propagating in a dispersive channel.

The input pulse is taken as

$$\begin{aligned} E(z=0, t) &= e^{-\alpha t^2} e^{i\omega_0 t} \\ &= e^{i\omega_0 t} \int_{-\infty}^{\infty} F(\Omega) e^{i\Omega t} d\Omega, \end{aligned} \quad (2.5-22)$$

where $F(\Omega)$, the Fourier transform of the envelope $e^{-\alpha t^2}$, is

$$F(\Omega) = \sqrt{\frac{1}{4\pi\alpha}} e^{-\Omega^2/4\alpha}. \quad (2.5-23)$$

Notice that the frequency spectrum is a Gaussian distribution peaked at ω_0 . The field at a distance z is obtained by multiplying each frequency component ($\omega_0 + \Omega$) in Eq. (2.5-22) by $\exp[-i\beta(\omega_0 + \Omega)z]$. If we expand $\beta(\omega_0 + \Omega)$ near ω_0 as

$$\beta(\omega_0 + \Omega) = \beta(\omega_0) + \left. \frac{d\beta}{d\omega} \right|_{\omega_0} \Omega + \frac{1}{2} \left(\frac{d^2\beta}{d\omega^2} \right) \Omega^2 + \dots,$$

we obtain

$$E(z, t) = e^{i(\omega_0 t - \beta_0 z)} \int_{-\infty}^{\infty} d\Omega F(\Omega) \exp\left\{i\left[\Omega t - \frac{\Omega z}{v_g} - \frac{1}{2} \frac{d}{d\omega} \left(\frac{1}{v_g}\right) \Omega^2 z\right]\right\}, \quad (2.5-24)$$

where

$$\beta_0 \equiv \beta(\omega_0), \quad \frac{d\beta}{d\omega} = \frac{1}{v_g} = \frac{1}{\text{group velocity}}.$$

The field envelope is given by the integral in Eq. (2.5-24),

$$\begin{aligned} \epsilon(z, t) &= \int_{-\infty}^{\infty} d\Omega F(\Omega) \exp\left\{i\Omega \left[\left(t - \frac{z}{v_g}\right) - \frac{1}{2} \frac{d}{d\omega} \left(\frac{1}{v_g}\right) \Omega z \right]\right\} \\ &= \int_{-\infty}^{\infty} d\Omega F(\Omega) \exp\left\{i\Omega \left[\left(t - \frac{z}{v_g}\right) - a\Omega z \right]\right\}, \end{aligned} \quad (2.5-25)$$

where

$$a \equiv \frac{1}{2} \frac{d}{d\omega} \left(\frac{1}{v_g}\right) = -\frac{1}{2v_g^2} \frac{dv_g}{d\omega}.$$

After substituting for $F(\Omega)$ from Eq. (2.5-23), the last equation becomes

$$\epsilon(z, t) = \sqrt{\frac{1}{4\pi\alpha}} \int_{-\infty}^{\infty} \exp\left\{-\left[\Omega^2 \left(\frac{1}{4\alpha} + iaz\right) + i\left(t - \frac{z}{v_g}\right)\Omega\right]\right\} d\Omega.$$

Carrying out the integration yields (see Problem 1.9)

$$\epsilon(z, t) = \frac{1}{\sqrt{1 + i4a\alpha z}} \exp\left[-\frac{(t - z/v_g)^2}{1/\alpha + 16a^2 z^2 \alpha}\right] \exp\left[i\frac{4az(t - z/v_g)^2}{1/\alpha^2 + 16a^2 z^2}\right]. \quad (2.5-26)$$

The pulse duration τ at z is taken as the separation between the two times when the square of the pulse-envelope amplitude is half its peak value, that

is,

$$\tau(z) = \sqrt{2 \ln 2} \sqrt{\frac{1}{\alpha} + 16a^2 z^2 \alpha}. \quad (2.5-27)$$

The initial pulse width, defined as the full width at half maximum intensity, is given by

$$\tau_0 = \left(\frac{2 \ln 2}{\alpha} \right)^{1/2}. \quad (2.5-28)$$

The pulse width after propagating a distance L can thus be expressed as

$$\tau(L) = \tau_0 \sqrt{1 + \left(\frac{8aL \ln 2}{\tau_0^2} \right)^2}. \quad (2.5-29)$$

At large distances such that $aL \gg \tau_0^2$ we obtain

$$\tau(L) \sim \frac{(8 \ln 2) aL}{\tau_0}. \quad (2.5-30)$$

If we use the definition of the factor a [see line following Eq. (2.5-25)], the last expression becomes

$$\tau(L) = \frac{4 \ln 2}{v_g^2} \frac{dv_g}{d\omega} \frac{L}{\tau_0}, \quad (2.5-31)$$

which, within a factor of $\ln 2$, is in agreement with Eq. (2.5-21).

The group-velocity dispersion is often characterized by $D \equiv L^{-1} dT/d\lambda$, where T is the pulse transmission time through a length L of the fiber. This definition is related to the second derivative of β with respect to ω as

$$D = -\frac{2\pi c}{\lambda^2} \left(\frac{d^2\beta}{d\omega^2} \right) \quad (2.5-32)$$

and is related to the parameter a used above by

$$D = -\frac{4\pi c}{\lambda^2} a. \quad (2.5-33)$$

With this new definition, the pulse-width expression (2.5-29) can be written as

$$\tau(L) = \tau_0 \sqrt{1 + \left(\frac{2 \ln 2}{\pi c} \frac{DL\lambda^2}{\tau_0^2} \right)^2}. \quad (2.5-34)$$

If DL is in picoseconds per nanometer, λ is in micrometers, and τ is in picoseconds, this amounts to

$$\tau(L) = \tau_0 \sqrt{1 + \left(\frac{1.47 DL\lambda^2}{\tau_0^2} \right)^2}. \quad (2.5-35)$$

The group-velocity dispersion (i.e., the dependence of v_g on ω), which according to Eq. (2.5-31) leads to pulse broadening, is due to two mechanisms:

1. v_g depends on ω according to Eq. (2.5-17), since $k = \omega n/c$.
2. v_g depends implicitly on ω through the dependence of the material index of refraction n on ω . We thus write $dv_g/d\omega = \partial v_g/\partial\omega + (\partial v_g/\partial n) dn/d\omega$ and obtain from Eq. (2.5-20)

$$\Delta\tau = \frac{2L}{c} \left| \frac{n_o n_2}{ck^3} (l + m + 1)^2 - \frac{dn}{d\omega} \right| \Delta\omega, \quad (2.5-36)$$

where in the second term we have assumed $(n_2/2k^2 n_o)(l + m + 1)^2 \ll 1$. In most fibers the pulse spreading is dominated by the material dispersion term $dn/d\omega$.

The actual index variation in a parabolic-index $\text{SiO}_2\text{-B}_2\text{O}_3$ fiber with a value of $n_2 \approx 5 \times 10^3 \text{ cm}^{-2}$ is shown in Fig. 2.5. The broadening of an optical pulse after a propagation distance of $\approx 2.5 \text{ km}$ is illustrated by Fig. 2.6. The input optical pulse excites a large number of (l, m) modes, and the broadening is of the type described by Eq. (2.5-19). The data are reproduced from [8], which also describes the important influence of intermode mixing on pulse broadening.

GRADED-INDEX: $\text{SiO}_2\text{-B}_2\text{O}_3$

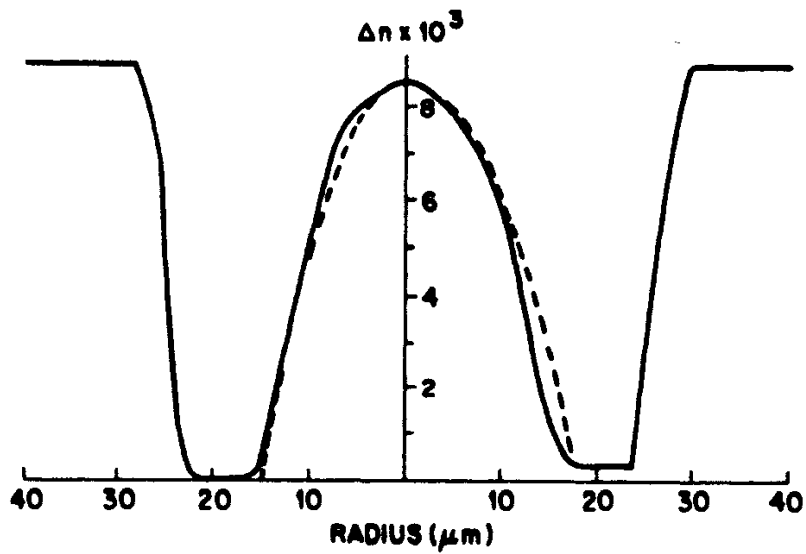


Figure 2.5. Graded-refractive-index profile across the core of a $\text{SiO}_2\text{-B}_2\text{O}_3$ fiber. The dashed lines describe quadratic profiles. (After [8].)

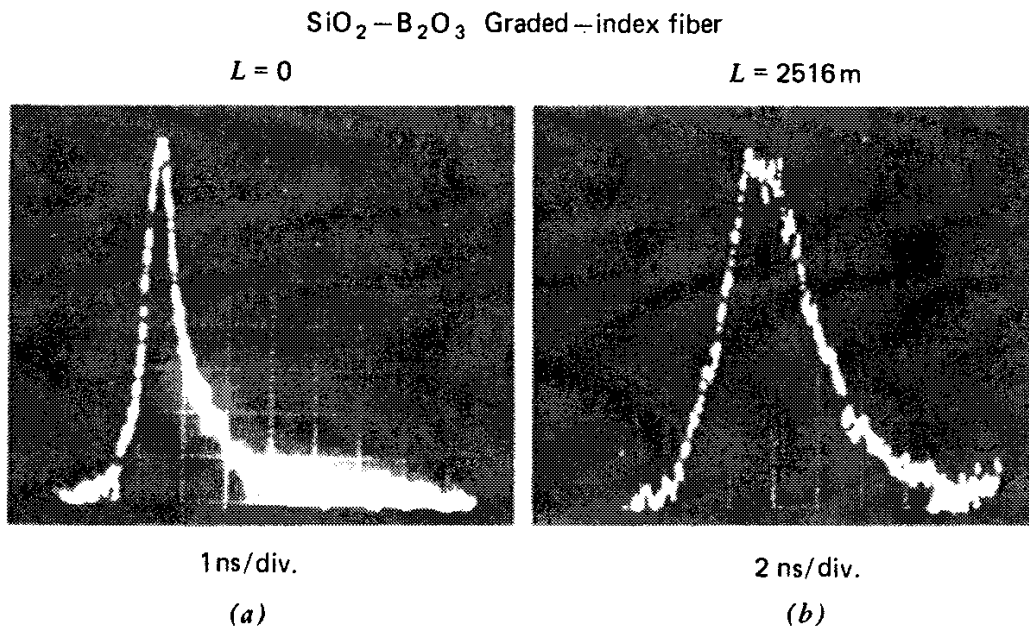


Figure 2.6. (a) Pulse shape at the input of the quadratic-index fiber of Fig. 2.5. (b) The output pulse after propagation through 2516 m (note the change in the time scales). (After [8].)

If we combine Eq. (2.5-26) with Eq. (2.5-24), we find that the total field at z is

$$\begin{aligned}
 E(z, t) &= \varepsilon(z, t) e^{i(\omega_0 t - \beta_0 z)} \\
 &= \frac{e^{-i\beta_0 z}}{\sqrt{1 + i4a\alpha z}} \exp \left\{ i \left[\omega_0 t + \frac{4az(t - z/v_g)^2}{\alpha^{-2} + 16a^2 z^2} \right] \right. \\
 &\quad \left. - \frac{(t - z/v_g)^2}{1/\alpha + 16a^2 z^2 \alpha} \right\}. \quad (2.5-37)
 \end{aligned}$$

The oscillation phase is thus

$$\Phi(z, t) = \omega_0 t + \frac{4az(t - z/v_g)^2}{\alpha^{-2} + 16a^2 z^2} - \beta_0 z. \quad (2.5-38)$$

The local "frequency" of $\omega(z, t)$ is then

$$\omega(z, t) = \frac{\partial \Phi}{\partial t} = \omega_0 + \frac{8az(t - z/v_g)}{\alpha^{-2} + 16a^2 z^2} \quad (2.5-39)$$

and consists of the original frequency ω_0 plus a linear frequency sweep (chirp) which is proportional to the group-velocity dispersion term a . The chirp can be understood intuitively by the fact that, due to group-velocity dispersion, different frequencies travel with different (group) velocity. According to Eq. (2.5-35), the broadening ratio $\tau(L)/\tau_0$ for a given laser pulse will be small (i.e., ~ 1) provided the group dispersion-length product DL is much smaller than $(\tau_0/\lambda)^2$. It is, of course, desirable to transmit the light pulse at the condition where the group-velocity dispersion is zero ($D = 0$). This may happen in optical fibers when the frequency dispersion and the material dispersion cancel each other at some wavelength. Recently, a nearly distortionless propagation of 5-ps (5×10^{-12} -s), Fourier-transform-limited pulses, in two fused-silica, single-mode fibers of 0.76- and 2.5-km length, respectively, has been demonstrated at $\lambda = 1.30\text{-}\mu\text{m}$ where the group-velocity dispersion is zero (or almost zero) [10]. Figure 2.7 shows the measured pulse broadening.

PROBLEMS

- 2.1. Gaussian-beam transformation by a lens. Consider the passage of a Gaussian beam through a thin lens with a focal length f . Assume the light beam is propagating to the right. Let the incident-beam waist be

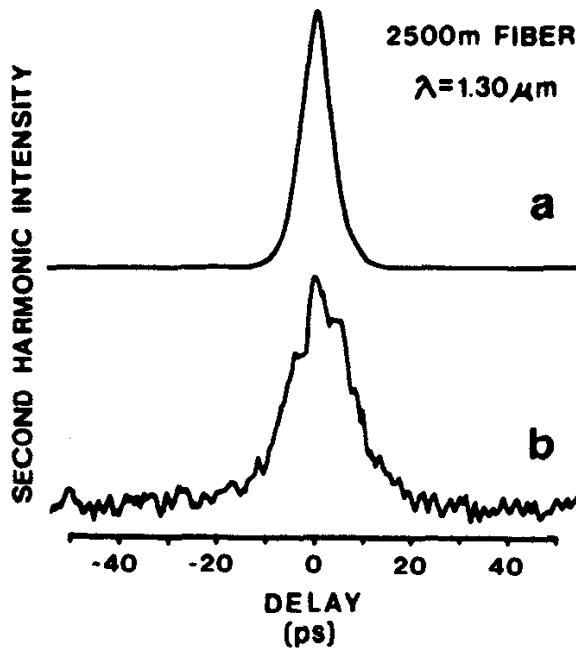


Figure 2.7. Pulse broadening in 2.5-km-long fiber resulting from linear dispersion [10]: (a) input pulse, (b) output pulse.

at a distance d_1 from the lens, with a beam spot size of ω_1 at the waist. Show that the spot size of the transmitted beam at its waist is given by

$$\frac{1}{\omega_2^2} = \frac{1}{\omega_1^2} \left(1 - \frac{d_1}{f}\right)^2 + \frac{1}{f^2} \left(\frac{\pi\omega_1}{\lambda}\right)^2$$

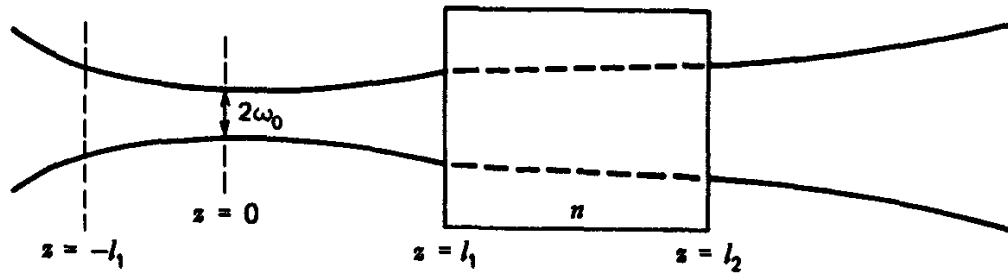
and that the beam waist is at a distance d_2 from the lens with

$$d_2 - f = (d_1 - f) \frac{f^2}{(d_1 - f)^2 + (\pi\omega_1^2/\lambda)^2}$$

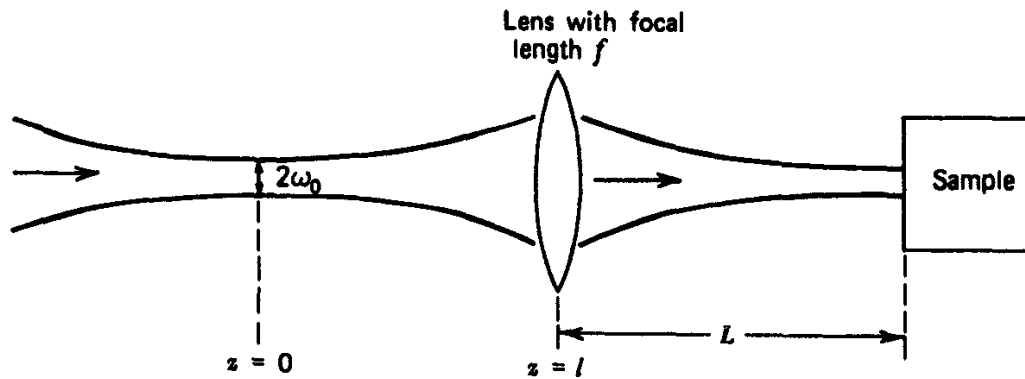
Also show that

$$\frac{\omega_2^2}{\omega_1^2} = \frac{d_2 - f}{d_1 - f}$$

- 2.2. (a) Assume a Gaussian beam incident normally on a solid prism with an index of refraction n as shown. What is the far-field diffraction angle of the output beam?
- (b) Assume that the prism is moved to the left until its input face is at $z = -l_1$. What is the new beam waist and what is its location? (Assume that the crystal is long enough that the beam waist is inside the crystal.)



- 2.3. A Gaussian beam with a wavelength λ is incident on a lens placed at $z = l$ as shown. Calculate the lens focal length f so that the output beam has a waist at the front surface of the sample crystal. Show that (given l and L) two solutions exist. Sketch the beam behavior for each of these solutions.



- 2.4. Find the beam spot size and the maximum number of pulses per second that can be carried by an optical beam ($\lambda = 1 \mu\text{m}$) propagating in a quadratic-index glass fiber with $n = 1.5$, $n_2 = 5 \times 10^2 \text{ cm}^{-2}$ (a) in the case of a single-mode excitation $l = m = 0$; (b) in the case where all the modes with $l, m \leq 5$ are excited. Using dispersion data (in versus ω) of any typical commercial glass and compare the relative contributions of modal and material dispersion to pulse broadening.
- 2.5. Substitute Eq. (2.3-9) for Ψ in the wave equation (2.1-1) and show that

$$\nabla^2 A - A(\nabla\phi)^2 + \left(\frac{2\pi}{\lambda}n\right)^2 A = 0$$

and

$$A\nabla^2\phi + 2\nabla A \cdot \nabla\phi = 0.$$

Show that if $A(\mathbf{r})$ varies slowly as a function of space, $\nabla^2 A$ can be neglected and the first equation reduces to Eq. (2.3-10).

REFERENCES

1. J. A. Arnaud, "Hamiltonian theory of beam mode propagation," in *Progress in Optics XI*, E. Wolf, Ed., North-Holland, Amsterdam, 1973.
2. P. Drude, *Theory of Optics*, Longmans, Green and Co., New York, 1933.
3. D. Marcuse, *Light Transmission Optics*, Van Nostrand, Princeton, N.J., 1972.
4. A. Yariv, *Quantum Electronics*, 2nd Ed., Wiley, New York, 1975, Section 2.2.
5. H. Kogelnik and W. Rigrod, "Visual display of isolated optical resonator modes," *Proc. IRE* **50**, 220 (1962).
6. S. Kawakami and J. Nishizawa, "An optical waveguide with the optimum distribution of the refractive index with reference to waveform distortion," *IEEE Trans. Microwave Theory and Technique* **MTT-16**, 10, 814 (1968).
7. S. E. Miller, E. A. J. Marcatili, and T. Li, "Research toward optical fiber transmission systems," *Proc. IEEE* **61**, 1703 (1973).
8. L. G. Cohen and H. M. Presby, "Shuttle pulse measurement of pulse spreading in a low loss graded index fiber," *Appl. Opt.* **14**, 1361 (1975).
9. L. G. Cohen and S. D. Personick, "Length dependence of pulse dispersion in a long multimode optical fiber," *Appl. Opt.* **14**, 1250 (1975).
10. D. M. Bloom, L. F. Mollenauer, Chirion Lin, D. W. Taylor, and A. M. DelGaudio, "Direct demonstration of distortionless picosecond-pulse propagation in kilometer-length optical fibers," *Opt. Lett.* **4**, 297 (1979).
11. A. Yariv and P. Yeh, "The application of Gaussian beam formalism to optical propagation in nonlinear media," *Opt. Comm.* **27**, 295 (1978).

3

Polarization of Light Waves

The field quantities \mathbf{E} and \mathbf{H} that describe light waves are vectors. In the previous chapter, when we discussed Gaussian-beam propagation, we used the scalar-wave approximation and were not concerned with the direction of oscillation of the electric field vector, except to note that the electric vector lies in a plane perpendicular to the direction of propagation. Many cases involving the propagation of light waves depend crucially on the direction of oscillation of the electric field. In fact, throughout most of the book, we deal almost exclusively with the propagation and control of polarized light. In this chapter we describe many aspects of polarized light and discuss many of the techniques used to study its propagation.

3.1. THE CONCEPT OF POLARIZATION

Light waves are electromagnetic fields and require the four basic field vectors \mathbf{E} , \mathbf{H} , \mathbf{D} , and \mathbf{B} for their complete description. The electric field vector \mathbf{E} is chosen to define the state of polarization of the light waves. This choice is convenient because, in most optical media, physical interactions with the wave involve the electric field. The main reason for studying the polarization of light waves is that in many substances (anisotropic media) the index of refraction depends on the direction of oscillation of the electric field vector \mathbf{E} . This phenomenon can be explained in terms of the motion of electrons which are driven by the electric field of the light waves. To illustrate this point, assume that the anisotropic material consists of non-spherical, needle-like molecules, and suppose that these molecules are all aligned with their long axes parallel to one another. Consider an electromagnetic wave passing through this substance. Because of the structure of the molecule, the electrons in the substance are pushed further from their equilibrium positions by electric fields that are parallel to the axes of the molecules than by those at right angles to the molecular axes. We thus expect a larger induced electronic polarization in the first case than in the second.

There are many other physical phenomena which are only associated with polarized light waves. Before we study these optical phenomena, it is important to understand in detail the characteristics of polarized waves. We start by reviewing the polarization states of monochromatic plane waves.

3.2. POLARIZATION OF MONOCHROMATIC PLANE WAVES

The polarization of light waves is specified by the electric field vector $\mathbf{E}(\mathbf{r}, t)$ at a fixed point in space, \mathbf{r} , at time t . The time variation of the electric field vector \mathbf{E} of a monochromatic wave is exactly sinusoidal, that is, the electric field must oscillate at a definite frequency. If we assume that the light is propagating in the z direction, the electric field vector will lie on the xy plane. Since the x component and the y component of the field vector can oscillate independently at a definite frequency, one must first consider the effect produced by the vector addition of these two oscillating orthogonal components. The problem of superposing two independent oscillations at right angles to each other and with the same frequency is well known and is completely analogous to the classical motion of a two-dimensional harmonic oscillator. The general motion of the oscillator is an ellipse, which corresponds to oscillations in which the x and y components are not in phase. There are, of course, many special cases which are of great importance in optics. We start with a discussion of the general properties of elliptic polarization and follow with a consideration of some special cases.

In the complex-function representation, the electric field vector of a monochromatic plane wave propagating in the z direction is given by

$$\mathbf{E}(z, t) = \text{Re}[\mathbf{A}e^{i(\omega t - kz)}], \quad (3.2-1)$$

where \mathbf{A} is a complex vector which lies in the xy plane. We now consider the nature of the curve which the end point of the electric field vector \mathbf{E} describes at a typical point in space. This curve is the time-evolution locus of the points whose coordinates (E_x, E_y) are

$$\begin{aligned} E_x &= A_x \cos(\omega t - kz + \delta_x), \\ E_y &= A_y \cos(\omega t - kz + \delta_y), \end{aligned} \quad (3.2-2)$$

where we have defined the complex vector \mathbf{A} as

$$\mathbf{A} = \hat{x}A_x e^{i\delta_x} + \hat{y}A_y e^{i\delta_y}, \quad (3.2-3)$$

where A_x and A_y are positive numbers, \hat{x} and \hat{y} are unit vectors. The curve described by the end point of the electric vector as time evolves can be obtained by eliminating $\omega t - kz$ between the equations (3.2-2). After several steps of elementary algebra, we obtain

$$\left(\frac{E_x}{A_x}\right)^2 + \left(\frac{E_y}{A_y}\right)^2 - 2\frac{\cos \delta}{A_x A_y} E_x E_y = \sin^2 \delta, \quad (3.2-4)$$

where

$$\delta = \delta_y - \delta_x. \quad (3.2-5)$$

All the phase angles are defined in the range $-\pi < \delta \leq \pi$.

Equation (3.2-4) is the equation of a conic. From (3.2-2) it is obvious that this conic is confined in a rectangular region with sides parallel to the coordinate axes and whose lengths are $2A_x$ and $2A_y$. Therefore, the curve must be an ellipse. The wave (3.2-1) is then said to be elliptically polarized. A complete description of an elliptical polarization includes the orientation of the ellipse with respect to the coordinate axes, the shape, and the sense of revolution of \mathbf{E} . In general, the principal axes of the ellipse are not in the x and y directions. By using a transformation (rotation) of the coordinate system, we are able to diagonalize Eq. (3.2-4). Let x' and y' be a new set of axes along the principal axes of the ellipse. Then the equation of the ellipse in this new coordinate system becomes

$$\left(\frac{E_{x'}}{a}\right)^2 + \left(\frac{E_{y'}}{b}\right)^2 = 1, \quad (3.2-6)$$

where a and b are the principal axes of the ellipse, and $E_{x'}$ and $E_{y'}$ are the components of the electric field vector in this principal coordinate system.

Let ϕ ($0 \leq \phi < \pi$) be the angle between the direction of the major axis x' and the x axis (see Fig. 3.1) Then the lengths of the principal axes are given by

$$a^2 = A_x^2 \cos^2 \phi + A_y^2 \sin^2 \phi + 2A_x A_y \cos \delta \cos \phi \sin \phi \quad (3.2-7)$$

$$b^2 = A_x^2 \sin^2 \phi + A_y^2 \cos^2 \phi - 2A_x A_y \cos \delta \cos \phi \sin \phi.$$

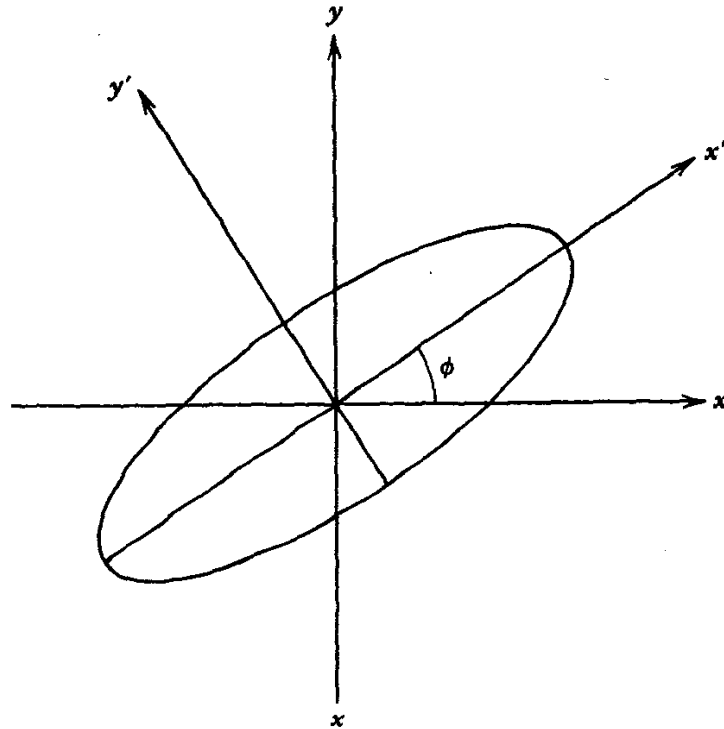


Figure 3.1. A typical polarization ellipse.

The angle ϕ can be expressed in terms of A_x , A_y , and $\cos \delta$ as

$$\tan 2\phi = \frac{2A_x A_y}{A_x^2 - A_y^2} \cos \delta. \quad (3.2-8)$$

The sense of revolution of an elliptical polarization is determined by the sign of $\sin \delta$. The end point of the electric vector will revolve in a clockwise direction if $\sin \delta > 0$ and in a counterclockwise direction if $\sin \delta < 0$. Figure 3.2 illustrates how the polarization ellipse changes with varying phase difference δ .

Before discussing some special cases of polarization, it is important to familiarize ourselves with the terminology. Light is linearly polarized when the tip of the electric field vector \mathbf{E} moves along a straight line. When it describes an ellipse, the light is elliptically polarized. When it describes a circle, the light is circularly polarized. If the end point of the electric field vector is seen to move in a counterclockwise direction by an observer facing the approaching wave, the field is said to possess right-handed polarization. Figure 3.2 also illustrates the sense of revolution of the ellipse. Our convention for labeling right-hand and left-hand polarization is consistent with the terminology of modern physics in which a photon with a right-hand circular polarization has a positive angular momentum along the direction

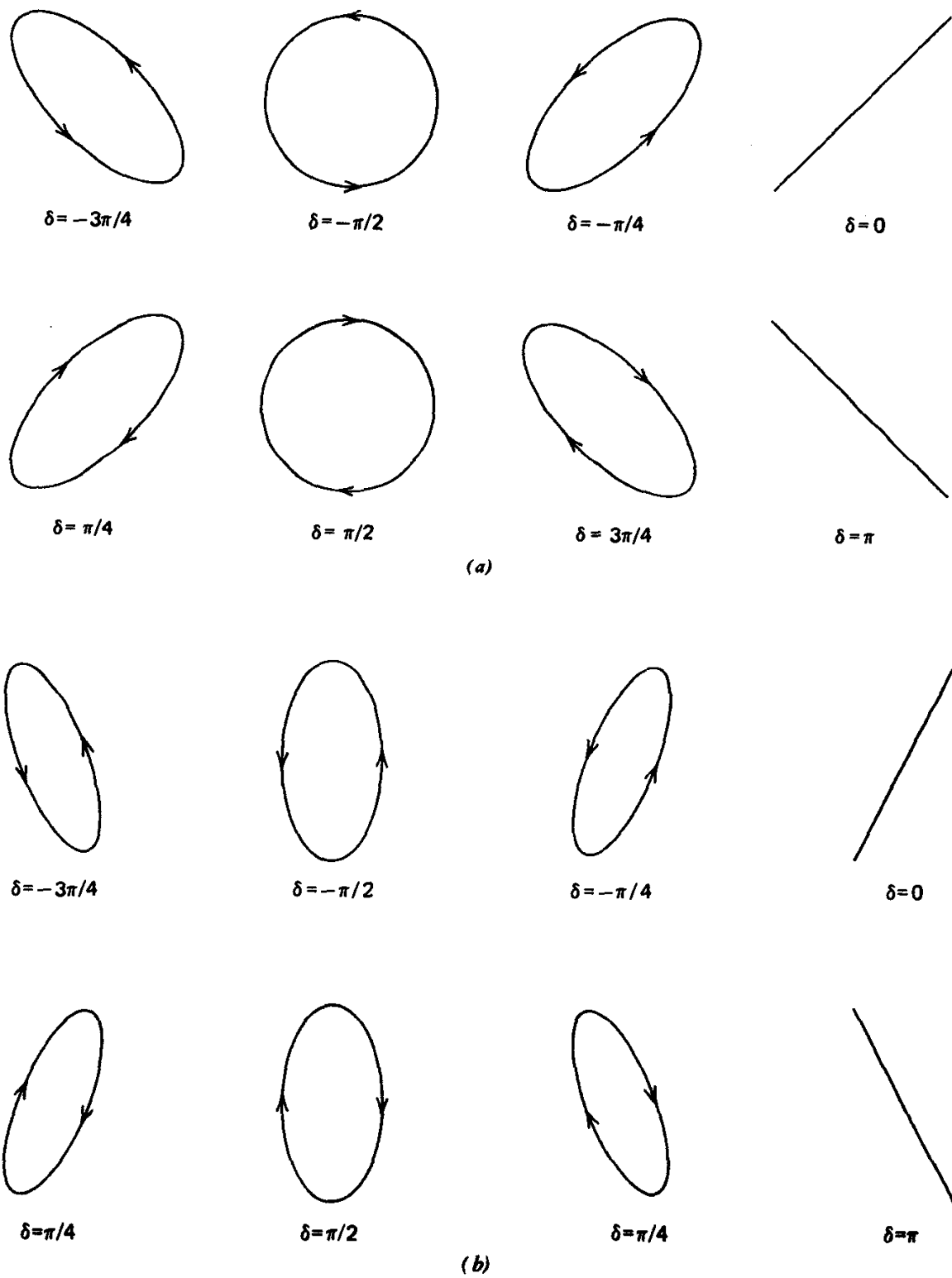
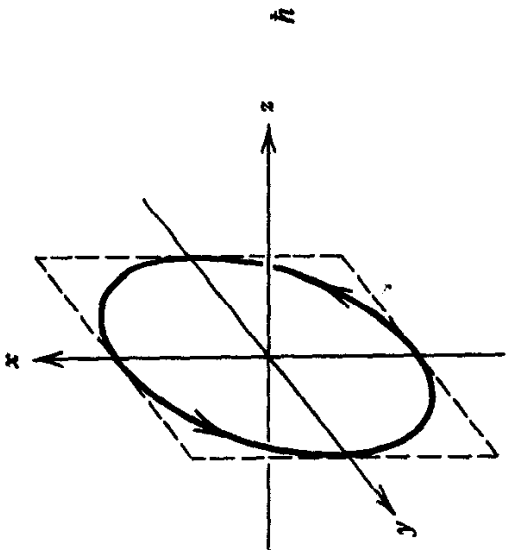
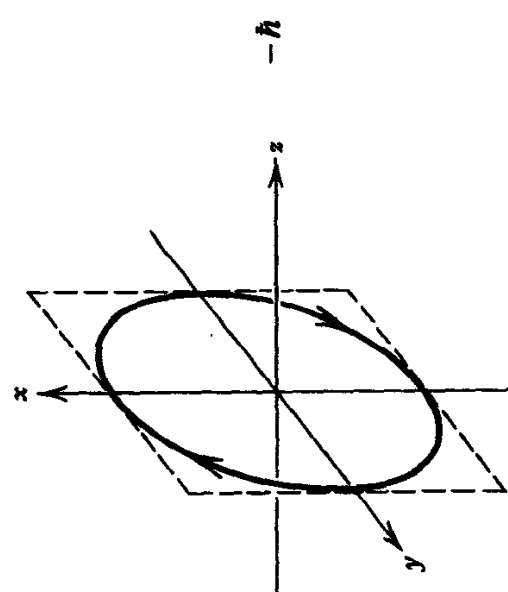


Figure 3.2. Polarization ellipses at various phase angles δ , where: (a) $E_x = \cos(\omega t - kz)$, $E_y = \cos(\omega t - kz + \delta)$; (b) $E_x = \frac{1}{2} \cos(\omega t - kz)$, $E_y = \cos(\omega t - kz + \delta)$.

Table 3.1. Relations between Angular Momentum and Handedness of Circularly Polarized Light

Field of a single photon ($\hbar\omega$)	L_z	Helicity	Handedness
$\left. \begin{aligned} E_x &= A \cos(\omega t - kz) \\ E_y &= A \cos(\omega t - kz - \frac{1}{2}\pi) \end{aligned} \right\}$ 	\hbar	\hbar	Right-handed
$\left. \begin{aligned} E_x &= A \cos(\omega t - kz) \\ E_y &= A \cos(\omega t - kz + \frac{1}{2}\pi) \end{aligned} \right\}$ 	$-\hbar$	$-\hbar$	Left-handed
		$k > 0$	Right-handed
		$k < 0$	Left-handed
		$k > 0$	Left-handed
		$k < 0$	Right-handed

of propagation (see Table 3.1 and Problem 3.4). However, some optics books adopt the opposite convention.

3.2.1. Linear and Circular Polarizations

Two special cases are of significant importance, namely, when the polarization ellipse degenerates into a straight line or a circle. According to Eq. (3.2-4) the ellipse will reduce to a straight line when

$$\delta = \delta_y - \delta_x = m\pi \quad (m = 0, 1). \quad (3.2-9)$$

Here we recall that all the phase angles are defined to be in the range $-\pi < \delta \leq \pi$. In this case, the ratio of the components of the electric field vector is a constant

$$\frac{E_y}{E_x} = (-1)^m \frac{A_y}{A_x} \quad (3.2-10)$$

and the light is linearly polarized.

The other special case of importance is that of a circularly polarized wave. According to Eqs. (3.2-4) and (3.2-7) the ellipse will reduce to a circle when

$$\delta = \delta_y - \delta_x = \pm \frac{1}{2}\pi \quad (3.2-11)$$

and

$$A_y = A_x. \quad (3.2-12)$$

According to our convention, the light is right-hand circularly polarized when $\delta = -\frac{1}{2}\pi$, which corresponds to a counter-clockwise rotation of the electric field vector, and left-hand circularly polarized when $\delta = \frac{1}{2}\pi$, which corresponds to a clockwise rotation of the electric field vector (see Table 3.1).

The ellipticity of a polarization ellipse is defined as

$$e = \pm \frac{b}{a}, \quad (3.2-13)$$

where a and b are the lengths of the principal axes. The ellipticity is taken as positive when the rotation of the electric field vector is right-handed and negative otherwise.

3.3. COMPLEX-NUMBER REPRESENTATION

From the discussion in the previous section we found how the polarization state of a light wave can be described in terms of the amplitudes and the phase angles of the x and y components of the electric field vector. In fact, all the information about the polarization of a wave is contained in the complex amplitude A of the plane wave (3.2-1). Therefore, a complex number χ defined as

$$\chi = e^{i\delta} \tan \psi = \frac{A_y}{A_x} e^{i(\delta_y - \delta_x)} \quad (3.3-1)$$

is sufficient to describe the polarization states. The angle ψ is defined to be between 0 and $\pi/2$. A complete description of the ellipse of polarization, which includes the orientation, sense of revolution, and ellipticity [see Eq. (3.2-13)], can be expressed in terms of δ and ψ . Figure 3.3 illustrates various different polarization states in the complex plane. It can be seen from the figure that all the right-handed elliptical polarization states are in the lower half of the plane, whereas the left-handed elliptical polarization states are in the upper half of the plane. The origin corresponds to a linear polarization state with direction of oscillation parallel to the x axis. Thus, each point on

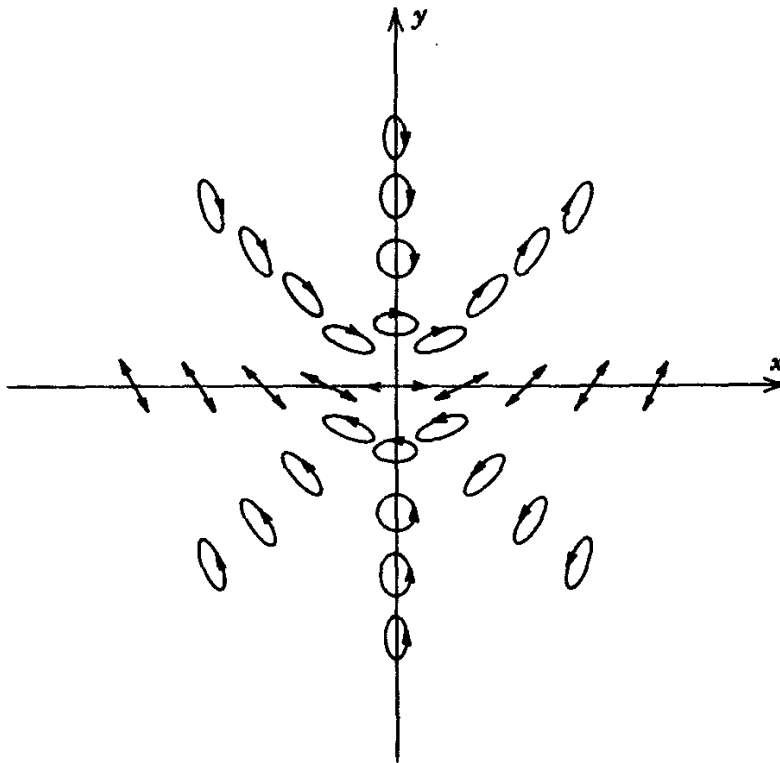


Figure 3.3. Each point of the complex plane is associated with a polarization state.

the complex plane represents a unique polarization state. Each point on the x axis represents a linearly polarized state with different azimuth angles of oscillation. Only two points $(0, \pm 1)$ correspond to circular polarization. Each point of the rest of the complex plane corresponds to a unique elliptical polarization state.

The inclination angle ϕ and the ellipticity angle θ ($\theta \equiv \tan^{-1}e$) of the polarization ellipse correspond to a given complex number χ and are given by

$$\tan 2\phi = \frac{2 \operatorname{Re}[\chi]}{1 - |\chi|^2} \quad (3.3-2)$$

and

$$\sin 2\theta = -\frac{2 \operatorname{Im}[\chi]}{1 + |\chi|^2}. \quad (3.3-3)$$

3.4. JONES-VECTOR REPRESENTATION

The Jones vector, introduced in 1941 by R. C. Jones [1], describes efficiently the polarization state of a plane wave. In this representation, the plane wave (3.2-1) is expressed in terms of its complex amplitudes as a column vector

$$\mathbf{J} = \begin{pmatrix} A_x e^{i\delta_x} \\ A_y e^{i\delta_y} \end{pmatrix}. \quad (3.4-1)$$

Notice that the Jones vector is a complex vector, that is, its elements are complex numbers. \mathbf{J} is not a vector in the real physical space; rather it is a vector in an abstract mathematical space. To obtain, as an example, the real x component of the electric field, we must perform the operation $E_x(t) = \operatorname{Re}[J_x e^{i\omega t}] = \operatorname{Re}[A_x e^{i(\omega t + \delta_x)}]$.

The Jones vector contains complete information about the amplitudes and the phases of the electric-field-vector components. It thus specifies the wave uniquely. If we are only interested in the polarization state of the wave, it is convenient to use the normalized Jones vector which satisfies the condition that

$$\mathbf{J}^* \cdot \mathbf{J} = 1 \quad (3.4-2)$$

where the asterisk (*) denotes complex conjugation. Thus, a linearly polarized light wave with the electric field vector oscillating along a given

direction can be represented by the Jones vector

$$\begin{pmatrix} \cos \psi \\ \sin \psi \end{pmatrix}, \quad (3.4-3)$$

where ψ is the azimuth angle of the oscillation direction with respect to the x axis. The state of polarization which is orthogonal to the state represented by Eq. (3.4-3) can be obtained by the substitution of ψ by $\psi + \frac{1}{2}\pi$, leading to a Jones vector

$$\begin{pmatrix} -\sin \psi \\ \cos \psi \end{pmatrix}. \quad (3.4-4)$$

For special case when $\psi = 0$ represents linearly polarized waves whose electric field vector oscillates along the coordinate axes, the Jones vectors are given by

$$\hat{\mathbf{x}} = \begin{pmatrix} 1 \\ 0 \end{pmatrix}, \quad \hat{\mathbf{y}} = \begin{pmatrix} 0 \\ 1 \end{pmatrix}. \quad (3.4-5)$$

Jones vectors for the right- and left-hand circularly polarized light waves are given by

$$\hat{\mathbf{R}} = \frac{1}{\sqrt{2}} \begin{pmatrix} 1 \\ -i \end{pmatrix}, \quad (3.4-6)$$

$$\hat{\mathbf{L}} = \frac{1}{\sqrt{2}} \begin{pmatrix} 1 \\ i \end{pmatrix}. \quad (3.4-7)$$

These two circular polarizations are mutually orthogonal in the sense that

$$\hat{\mathbf{R}}^* \cdot \hat{\mathbf{L}} = 0. \quad (3.4-8)$$

Since the Jones vector is a column matrix of rank 2, any pair of orthogonal Jones vectors can be used as a basis of the mathematical space spanned by all the Jones vectors. Any polarization can be represented as a superposition of two mutually orthogonal polarizations $\hat{\mathbf{x}}$ and $\hat{\mathbf{y}}$, or $\hat{\mathbf{R}}$ and $\hat{\mathbf{L}}$. In particular, we can resolve the basic linear polarization $\hat{\mathbf{x}}$ and $\hat{\mathbf{y}}$ into two circular

polarizations $\hat{\mathbf{R}}$ and $\hat{\mathbf{L}}$ and vice versa. These relations are given by

$$\hat{\mathbf{R}} = \frac{1}{\sqrt{2}}(\hat{\mathbf{x}} - i\hat{\mathbf{y}}), \quad (3.4-9)$$

$$\hat{\mathbf{L}} = \frac{1}{\sqrt{2}}(\hat{\mathbf{x}} + i\hat{\mathbf{y}}), \quad (3.4-10)$$

$$\hat{\mathbf{x}} = \frac{1}{\sqrt{2}}(\hat{\mathbf{R}} + \hat{\mathbf{L}}), \quad (3.4-11)$$

$$\hat{\mathbf{y}} = \frac{i}{\sqrt{2}}(\hat{\mathbf{R}} - \hat{\mathbf{L}}). \quad (3.4-12)$$

Circular polarizations are seen to consist of linear oscillations along the x and y directions with equal amplitude $1/\sqrt{2}$, but with a phase difference of $\frac{1}{2}\pi$. Similarly, a linear polarization can be viewed as a superposition of two oppositely sensed circular polarizations.

We have so far discussed only the Jones vectors of some simple special cases of polarization. It is easy to show that a general elliptic polarization can be represented by the following Jones vector:

$$\mathbf{J}(\psi, \delta) = \begin{pmatrix} \cos \psi \\ e^{i\delta} \sin \psi \end{pmatrix}. \quad (3.4-13)$$





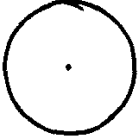
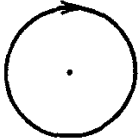

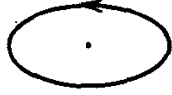
This Jones vector represents the same polarization state as the one represented by the complex number $\chi = e^{i\delta} \tan \psi$. Table 3.2 shows the Jones vectors of some typical polarization states.

The most important application of Jones vectors is in conjunction with the Jones calculus. This is a powerful technique used for studying the propagation of plane waves with arbitrary states of polarizations through an arbitrary sequence of birefringent elements and polarizers. This topic will be considered in some detail in Chapter 5.

PROBLEMS

- 3.1. Derive Eq. (3.2-4).
- 3.2. Derive Eqs. (3.2-7) and (3.2-8).
- 3.3. Show that the end point of the electric vector of an elliptically polarized light will revolve in a clockwise direction if $\sin \delta > 0$ and in a counterclockwise direction if $\sin \delta < 0$.

Table 3.2. Jones Vectors of Some Typical Polarization States

Polarization Ellipse	Jones Vector
	$\begin{pmatrix} 1 \\ 0 \end{pmatrix}$
	$\begin{pmatrix} 0 \\ 1 \end{pmatrix}$
	$\frac{1}{\sqrt{2}} \begin{pmatrix} 1 \\ 1 \end{pmatrix}$
	$\frac{1}{\sqrt{2}} \begin{pmatrix} 1 \\ -1 \end{pmatrix}$
	$\frac{1}{\sqrt{2}} \begin{pmatrix} 1 \\ -i \end{pmatrix}$
	$\frac{1}{\sqrt{2}} \begin{pmatrix} 1 \\ i \end{pmatrix}$
	$\frac{1}{\sqrt{5}} \begin{pmatrix} 1 \\ 2i \end{pmatrix}$
	$\frac{1}{\sqrt{5}} \begin{pmatrix} 2 \\ -i \end{pmatrix}$

- 3.4. (a) A right-hand circularly polarized wave ($\sin \delta < 0$) propagating in the z direction has a finite extent in the x and y directions. Assuming that the amplitude modulation is slowly varying (the wave is many wavelengths broad), show that the electric and magnetic fields are given approximately by

$$\mathbf{E}(x, y, z, t) \approx E_0(x, y)(\hat{x} - i\hat{y}) + \frac{-i}{k} \left(\frac{\partial E_0}{\partial x} - i \frac{\partial E_0}{\partial y} \right) \hat{z} e^{i(\omega t - kz)},$$

$$\mathbf{H}(x, y, z, t) \approx i \frac{k}{\omega \mu} \mathbf{E}(x, y, z, t).$$

- (b) Calculate the time-averaged component of angular momentum along the direction of propagation ($+z$). Show that this component of the angular momentum is \hbar provided the energy of the wave is normalized to $\hbar\omega$. This shows that a right-hand circularly polarized photon carries a positive angular momentum \hbar along the direction of its momentum vector (helicity).
- (c) Show that the transverse components of the angular momentum vanish.
- 3.5. *Orthogonal polarization states.*
- (a) Find a polarization state which is orthogonal to the polarization state

$$\mathbf{J}(\psi, \delta) = \begin{pmatrix} \cos \psi \\ e^{i\delta} \sin \psi \end{pmatrix}.$$

Answer:

$$\begin{pmatrix} \sin \psi \\ e^{i(\pi + \delta)} \cos \psi \end{pmatrix}.$$

- (b) Show that the major axes of the ellipses of two mutually orthogonal polarization states are perpendicular to each other and the senses of revolution are opposite.
- 3.6. (a) An elliptically polarized beam propagating in the z direction has a finite extent in the x and y directions:

$$\mathbf{E}(x, y, z, t) \approx E_0(x, y)(\alpha\hat{x} + \beta\hat{y})e^{i(\omega t - kz)}$$

where $\alpha = \cos \psi$, $\beta = \sin \psi e^{i\delta}$. Show that the electric field must have a component in the z direction [see Problem 3.4(a)], and derive the expressions for the electric field and the magnetic field.

- (b) Calculate the z component of the angular momentum, assuming that the total energy of the wave is $\hbar\omega$. Answer: $L_z = -\hbar \sin 2\psi \sin \delta$.
- (c) Decompose elliptically polarized light into a linear superposition of right-hand and left-hand polarized states $\hat{\mathbf{R}}$ and $\hat{\mathbf{L}}$, i.e., if \mathbf{J} is the Jones vector of the polarization state in (a), find r and l such that

$$\mathbf{J} = r\hat{\mathbf{R}} + l\hat{\mathbf{L}}.$$

- (d) If r and l are the probability amplitudes that the photon is right-hand and left-hand circularly polarized, respectively, show that the angular momentum can be obtained by evaluating $|r|^2 - |l|^2$:

$$L_z = \hbar(|r|^2 - |l|^2).$$

- (e) Express the angular momentum in terms of the ellipticity angle θ .

3.7. Derive Eqs. (3.3-2) and (3.3-3).

3.8. *Orthogonal polarization states.* Consider two monochromatic plane waves of the form

$$\mathbf{E}_a(z, t) = \text{Re}[\mathbf{A}e^{i(\omega t - kz)}],$$

$$\mathbf{E}_b(z, t) = \text{Re}[\mathbf{B}e^{i(\omega t - kz)}].$$

The polarization states of these two waves are orthogonal, that is, $\mathbf{A}^* \cdot \mathbf{B} = 0$.

- (a) Let δ_a, δ_b be the phase angles defined in Eq. (3.2-2). Show that

$$\delta_a - \delta_b = \pm\pi.$$

- (b) Since δ_a, δ_b are all in the range $-\pi < \delta \leq \pi$, show that

$$\delta_a \delta_b \leq 0.$$

- (c) Let χ_a, χ_b be the complex numbers representing the polarization states of these two waves. Show that

$$\chi_a^* \chi_b = -1.$$

- (d) Show that the major axes of the polarization ellipses are mutually orthogonal and the ellipticities are of the same magnitude with opposite signs.

REFERENCES AND SUGGESTED READING

1. W. A. Shurcliff, *Polarized Light*, Harvard University Press, Cambridge, 1966.
2. M. Born and E. Wolf, *Principles of Optics*, MacMillan, New York, 1964.
3. R. M. A. Azzam and N. M. Bashara, *Ellipsometry and Polarized Light*, North-Holland, Amsterdam, 1977.
4. E. E. Wahlstrom, *Optical Crystallography*, Wiley, New York, 1969.

4

Electromagnetic Propagation in Anisotropic Media

There are many materials whose optical properties depend on the direction of propagation as well as polarization of the light waves. These optically anisotropic materials include crystals such as calcite, quartz, and KDP, as well as liquid crystals. They exhibit many peculiar optical phenomena, including double refraction, optical rotation, polarization effects, conical refraction, and electro-optical and acousto-optical effects. Many optical devices are made of anisotropic crystals, for example, prism polarizers, sheet polarizers, and birefringent filters. Anisotropic nonlinear materials are also used for phase-matched second-harmonic generation. A thorough understanding of light propagation in anisotropic media is thus important if these phenomena are to be used for practical applications. The present chapter is devoted entirely to the study of the propagation of electromagnetic radiation in these media.

4.1. THE DIELECTRIC TENSOR OF AN ANISOTROPIC MEDIUM

In an isotropic medium, the induced polarization is always parallel to the electric field and is related to it by a scalar factor (the susceptibility) that is independent of the direction along which the field is applied. This is no longer true in anisotropic media, except for certain particular directions. Since the crystal is made up of a regular periodic array of atoms (or molecules) with certain symmetry, we may expect that the induced polarization will depend, both in its magnitude and direction, on the direction of applied field. Instead of a simple scalar relation linking \mathbf{P} and \mathbf{E} , we have

$$\begin{aligned}P_x &= \epsilon_0(\chi_{11}E_x + \chi_{12}E_y + \chi_{13}E_z), \\P_y &= \epsilon_0(\chi_{21}E_x + \chi_{22}E_y + \chi_{23}E_z), \\P_z &= \epsilon_0(\chi_{31}E_x + \chi_{32}E_y + \chi_{33}E_z),\end{aligned}\tag{4.1-1}$$

where the capital letters denote the complex amplitudes of the corresponding time-harmonic quantities. The 3×3 array of the coefficients χ_{ij} is called the electric susceptibility tensor. The magnitudes of the χ_{ij} depend, of course, on the choice of the x , y , and z axes relative to the crystal structure. It is always possible to choose x , y , and z in such a way that the off-diagonal elements vanish, leaving

$$\begin{aligned} P_x &= \epsilon_0 \chi_{11} E_x, \\ P_y &= \epsilon_0 \chi_{22} E_y, \\ P_z &= \epsilon_0 \chi_{33} E_z. \end{aligned} \quad (4.1-2)$$

These directions are called the principal dielectric axes of the crystal.

We can, instead of using Eq. (4.1-1), describe the dielectric response of the crystal by means of the dielectric permittivity tensor ϵ_{ij} , defined by

$$\begin{aligned} D_x &= \epsilon_{11} E_x + \epsilon_{12} E_y + \epsilon_{13} E_z, \\ D_y &= \epsilon_{21} E_x + \epsilon_{22} E_y + \epsilon_{23} E_z, \\ D_z &= \epsilon_{31} E_x + \epsilon_{32} E_y + \epsilon_{33} E_z. \end{aligned} \quad (4.1-3)$$

From Eq. (4.1-1) and the relation

$$\mathbf{D} = \epsilon_0 \mathbf{E} + \mathbf{P} \quad (4.1-4)$$

we have

$$\epsilon_{ij} = \epsilon_0 (1 + \chi_{ij}). \quad (4.1-5)$$

These nine quantities $\epsilon_{11}, \epsilon_{12}, \dots$ are constants of the medium and constitute the dielectric tensor, Equation (4.1-3) is often written in tensor notation as

$$D_i = \epsilon_{ij} E_j \quad (4.1-6)$$

where the convention of summation over repeated indices is observed.

In the greater part of this chapter we assume that the medium is homogeneous, nonabsorbing, and magnetically isotropic. The energy density of the stored electric field in the anisotropic medium is

$$U_e = \frac{1}{2} \mathbf{E} \cdot \mathbf{D} = \frac{1}{2} E_i \epsilon_{ij} E_j. \quad (4.1-7)$$

When we differentiate Eq. (4.1-7) with respect to time, we obtain

$$\dot{U}_e = \frac{1}{2} \epsilon_{ij} (\dot{E}_i E_j + E_i \dot{E}_j). \quad (4.1-8)$$

According to the derivation of Poynting's theorem in Section 1.2, the net power flow into a unit volume in a lossless medium is

$$-\nabla \cdot (\mathbf{E} \times \mathbf{H}) = \mathbf{E} \cdot \dot{\mathbf{D}} + \mathbf{H} \cdot \dot{\mathbf{B}}, \quad (4.1-9)$$

which, by using Eq. (4.1.6) for \mathbf{D} , can be written as

$$-\nabla \cdot (\mathbf{E} \times \mathbf{H}) = E_i \epsilon_{ij} \dot{E}_j + \mathbf{H} \cdot \dot{\mathbf{B}}. \quad (4.1-10)$$

Since the Poynting vector corresponds to the energy flux in the medium, the first term on the right side of Eq. (4.1-10) must be equal to \dot{U}_e . Therefore, we have the following equation:

$$\frac{1}{2} \epsilon_{ij} (\dot{E}_i E_j + E_i \dot{E}_j) = \epsilon_{ij} E_i \dot{E}_j. \quad (4.1-11)$$

It follows immediately from Eq. (4.1-11) that

$$\epsilon_{ij} = \epsilon_{ji}. \quad (4.1-12)$$

This means that the dielectric tensor is symmetric and has, in general, only six independent elements. This symmetry is a direct consequence of the definition (4.1-6) and the assumption that ϵ is a real dielectric tensor. In the event that a lossless medium is described by a complex dielectric tensor (e.g., optical activity—see Section 4.9), a similar derivation shows that

$$\epsilon_{ij} = \epsilon_{ji}^*. \quad (4.1-13)$$

In other words, the conservation of electromagnetic field energy requires that the dielectric tensor be Hermitian. In the special case when the dielectric tensor becomes real, the Hermitian property (4.1-13) reduces to a symmetric property (4.1-12).

4.2. PLANE-WAVE PROPAGATION IN ANISOTROPIC MEDIA

In an anisotropic medium such as a crystal, the phase velocity of light depends on its state of polarization as well as its direction of propagation. Because of the anisotropy, the polarization state of a plane wave may vary

as it propagates through the crystal. However, given a direction of propagation in the medium, there exist, in general, two eigenwaves with well-defined eigen-phase-velocities and polarization directions. A light wave with polarization parallel to one of these directions will remain in the same polarization state as it propagates through the anisotropic medium. These eigenpolarizations, as well as the corresponding eigen-phase-velocities (or, equivalently eigenindices of refraction), can be determined from Eqs. (1.1-1) and (1.1-2) and the dielectric tensor.

To derive these results, we assume a monochromatic plane wave of angular frequency ω propagating in the anisotropic medium with an electric field

$$\mathbf{E} \exp[i(\omega t - \mathbf{k} \cdot \mathbf{r})] \quad (4.2-1)$$

and a magnetic field

$$\mathbf{H} \exp[i(\omega t - \mathbf{k} \cdot \mathbf{r})], \quad (4.2-2)$$

where \mathbf{k} is the wave vector $\mathbf{k} = (\omega/c)n\mathbf{s}$ with \mathbf{s} a unit vector in the direction of propagation. n is the refractive index to be determined. Substitution for \mathbf{E} and \mathbf{H} from Eqs. (4.2-1) and (4.2-2), respectively, into Maxwell's equations (1.1-1) and (1.1-2) gives

$$\mathbf{k} \times \mathbf{E} = \omega\mu\mathbf{H}, \quad (4.2-3)$$

$$\mathbf{k} \times \mathbf{H} = -\omega\epsilon\mathbf{E}. \quad (4.2-4)$$

By eliminating \mathbf{H} from Eqs. (4.2-3) and (4.2-4), we obtain

$$\mathbf{k} \times (\mathbf{k} \times \mathbf{E}) + \omega^2\mu\epsilon\mathbf{E} = 0. \quad (4.2-5)$$

In the principal coordinate system, the dielectric tensor ϵ is given by

$$\epsilon = \begin{pmatrix} \epsilon_x & 0 & 0 \\ 0 & \epsilon_y & 0 \\ 0 & 0 & \epsilon_z \end{pmatrix}. \quad (4.2-6)$$

Equation (4.2-5) can be written as

$$\begin{pmatrix} \omega^2\mu\epsilon_x - k_y^2 - k_z^2 & k_x k_y & k_x k_z \\ k_y k_x & \omega^2\mu\epsilon_y - k_x^2 - k_z^2 & k_y k_z \\ k_z k_x & k_z k_y & \omega^2\mu\epsilon_z - k_x^2 - k_y^2 \end{pmatrix} \begin{pmatrix} E_x \\ E_y \\ E_z \end{pmatrix} = 0. \quad (4.2-7)$$

For nontrivial solutions to exist, the determinant of the matrix in Eq. (4.2-7) must vanish. This leads to a relation between ω and \mathbf{k} ,

$$\det \begin{vmatrix} \omega^2\mu\epsilon_x - k_y^2 - k_z^2 & k_x k_y & k_x k_z \\ k_y k_x & \omega^2\mu\epsilon_y - k_x^2 - k_z^2 & k_y k_z \\ k_z k_x & k_z k_y & \omega^2\mu\epsilon_z - k_x^2 - k_y^2 \end{vmatrix} = 0. \quad (4.2-8)$$

The above equation can be represented by a three-dimensional surface in \mathbf{k} space (momentum space). This surface is known as the normal surface and consists of two shells, which, in general, have four points in common (see Fig. 4.1). The two lines that go through the origin and these points are known as the optic axes. Figure 4.1 shows one of the optic axes. Given a direction of propagation, there are in general two k values which are the intersections of the direction of propagation and the normal surface. These two k values correspond to two different phase velocities (ω/k) of the waves propagating along the chosen direction. The directions of the electric field vector associated with these propagations can also be obtained from Eq. (4.2-7) and are given by

$$\begin{pmatrix} \frac{k_x}{k^2 - \omega^2\mu\epsilon_x} \\ \frac{k_y}{k^2 - \omega^2\mu\epsilon_y} \\ \frac{k_z}{k^2 - \omega^2\mu\epsilon_z} \end{pmatrix}. \quad (4.2-9)$$

It will be shown in Section 4.3 that the two phase velocities always correspond to two mutually orthogonal polarizations (for displacement vector \mathbf{D}) (see also Problem 4.1).

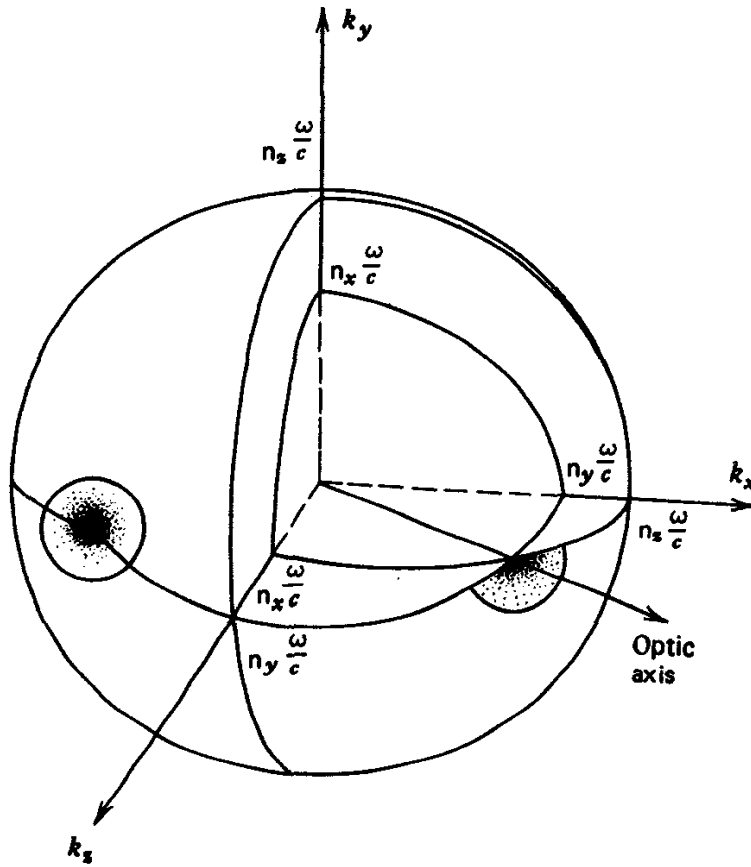


Figure 4.1. The normal surface.

For propagation in the direction of the optic axes, there is only one value of k and, consequently, only one phase velocity. There are, however, two independent directions of polarization.

Equations (4.2-8) and (4.2-9) are often written in terms of the direction cosines of the wave vector. By using the relation $\mathbf{k} = (\omega/c)\mathbf{ns}$ for the plane wave given by Eq. (4.2-1), Eqs. (4.2-8) and (4.2-9) can be written as

$$\frac{s_x^2}{n^2 - \epsilon_x/\epsilon_0} + \frac{s_y^2}{n^2 - \epsilon_y/\epsilon_0} + \frac{s_z^2}{n^2 - \epsilon_z/\epsilon_0} = \frac{1}{n^2} \quad (4.2-10)$$

and

$$\left(\begin{array}{c} \frac{s_x}{n^2 - \epsilon_x/\epsilon_0} \\ \frac{s_y}{n^2 - \epsilon_y/\epsilon_0} \\ \frac{s_z}{n^2 - \epsilon_z/\epsilon_0} \end{array} \right) \quad (4.2-11)$$

respectively.

Equation (4.2-10) is known as Fresnel's equation of wave normals and can be solved for the eigenindices of refraction, and Eq. (4.2-11) gives the directions of polarization. Equation (4.2-10) is a quadratic equation in n^2 . Therefore, for each direction of propagation (set of s_x, s_y, s_z) it yields two solutions for n^2 (Problem 4.2). To complete the solution of the problem, we use the values of n^2 , one at a time, in Eq. (4.2-11). This gives us the polarizations of these waves. It can be seen that in a nonabsorbing medium these eigenwaves are linearly polarized, since all the components are real in (4.2-11). Let \mathbf{E}_1 and \mathbf{E}_2 be the electric field vectors and $\mathbf{D}_1, \mathbf{D}_2$ be the displacement vectors of the linearly polarized eigenwaves associated with n_1^2 and n_2^2 , respectively. Maxwell's equation $\nabla \cdot \mathbf{D} = 0$ implies that $\mathbf{D}_1, \mathbf{D}_2$ are orthogonal to \mathbf{s} . Since $\mathbf{D}_1 \cdot \mathbf{D}_2 = 0$, the three vectors $\mathbf{D}_1, \mathbf{D}_2$, and \mathbf{s} form an orthogonal triad and can be used as a coordinate system for the description of many physical phenomena, including optical activity. Maxwell's equations also imply that \mathbf{D}, \mathbf{E} , and \mathbf{H} are related by

$$\mathbf{D} = -\frac{n}{c}\mathbf{s} \times \mathbf{H} \quad (4.2-12)$$

and

$$\mathbf{H} = \frac{n}{\mu c}\mathbf{s} \times \mathbf{E}. \quad (4.2-13)$$

According to Eqs. (4.2-12) and (4.2-13), \mathbf{D} and \mathbf{H} are both perpendicular to the direction of propagation \mathbf{s} . Consequently, the direction of energy flow as given by the Poynting vector $\mathbf{E} \times \mathbf{H}$ is not, in general, collinear with the direction of propagation \mathbf{s} .

By substituting Eq. (4.2-13) for \mathbf{H} in Eq. (4.2-12) and using the vector identity $\mathbf{A} \times (\mathbf{B} \times \mathbf{C}) = \mathbf{B}(\mathbf{A} \cdot \mathbf{C}) - \mathbf{C}(\mathbf{A} \cdot \mathbf{B})$, we obtain the following expression:

$$\begin{aligned} \mathbf{D} &= -\frac{n^2}{c^2\mu}\mathbf{s} \times (\mathbf{s} \times \mathbf{E}) = \frac{n^2}{c^2\mu}[\mathbf{E} - \mathbf{s}(\mathbf{s} \cdot \mathbf{E})] \\ &= \frac{n^2}{c^2\mu}E_{\text{transverse}}, \end{aligned} \quad (4.2-14)$$

and since $\mathbf{s} \cdot \mathbf{D} = 0$ and $n^2/c^2\mu = n^2\epsilon_0$,

$$D^2 = \frac{n^2}{c^2\mu}\mathbf{E} \cdot \mathbf{D} = n^2\epsilon_0\mathbf{E} \cdot \mathbf{D}. \quad (4.2-15)$$

In other words, \mathbf{D} , \mathbf{E} , and \mathbf{s} all lie in the same plane. It can be shown that these field vectors satisfy the following relations (see Problem 4.1):

$$\begin{aligned}\mathbf{D}_1 \cdot \mathbf{D}_2 &= 0, \\ \mathbf{D}_1 \cdot \mathbf{E}_2 &= 0, \\ \mathbf{D}_2 \cdot \mathbf{E}_1 &= 0, \\ \mathbf{s} \cdot \mathbf{D}_1 &= \mathbf{s} \cdot \mathbf{D}_2 = 0.\end{aligned}\tag{4.2-16}$$

\mathbf{E}_1 and \mathbf{E}_2 are in general not orthogonal. The orthogonality relation of the eigenmodes of propagation is often written as

$$\mathbf{s} \cdot (\mathbf{E}_1 \times \mathbf{H}_2) = 0.\tag{4.2-17}$$

This latter relation shows that the power flow in an anisotropic medium along the direction of propagation is the sum of the power carried by each mode individually.

4.2.1. Orthogonality Properties of the Eigenmodes

We now derive the orthogonality relation (4.2-17) between the two eigenmodes of propagation along a given direction \mathbf{s} . Using Eqs. (4.2-1), (4.2-2) for the field vectors and the Lorentz reciprocity theorem, we obtain

$$\mathbf{s} \cdot (\mathbf{E}_1 \times \mathbf{H}_2) = \mathbf{s} \cdot (\mathbf{E}_2 \times \mathbf{H}_1).\tag{4.2-18}$$

If we substitute Eq. (4.2-13) for \mathbf{H}_1 and \mathbf{H}_2 in Eq. (4.2-18), it becomes

$$\frac{n_2}{\mu c} \mathbf{s} \cdot [\mathbf{E}_1 \times (\mathbf{s} \times \mathbf{E}_2)] = \frac{n_1}{\mu c} \mathbf{s} \cdot [\mathbf{E}_2 \times (\mathbf{s} \times \mathbf{E}_1)].\tag{4.2-19}$$

This equation can be further simplified by using the identity

$$\mathbf{A} \cdot (\mathbf{B} \times \mathbf{C}) = \mathbf{C} \cdot (\mathbf{A} \times \mathbf{B}),$$

and becomes

$$\frac{n_2}{\mu c} (\mathbf{s} \times \mathbf{E}_1) \cdot (\mathbf{s} \times \mathbf{E}_2) = \frac{n_1}{\mu c} (\mathbf{s} \times \mathbf{E}_1) \cdot (\mathbf{s} \times \mathbf{E}_2).\tag{4.2-20}$$

Since this equation must hold for any arbitrary direction of propagation \mathbf{s}

with $n_1 \neq n_2$, it can be satisfied only when both sides vanish. This proves

$$\mathbf{s} \cdot (\mathbf{E}_1 \times \mathbf{H}_2) = \mathbf{s} \cdot (\mathbf{E}_2 \times \mathbf{H}_1) = 0. \quad (4.2-21)$$

To summarize: along an arbitrary direction of propagation \mathbf{s} , there can exist two independent plane-wave, linearly polarized propagation modes. These modes have phase velocities $\pm c/n_1$ and $\pm c/n_2$, where n_1^2 and n_2^2 are the two solutions of Fresnel's equation (4.2-10).

In practice, the indices of refraction n_1 , n_2 and the directions of \mathbf{D} , \mathbf{H} , and \mathbf{E} are found, most often, not by the procedure outlined above but by using the formally equivalent method of the index ellipsoid. This method is discussed in the following section.

4.3. THE INDEX ELLIPSOID

The surfaces of constant energy density U_e in \mathbf{D} space given by Eq. (4.1-7) can be written as

$$\frac{D_x^2}{\epsilon_x} + \frac{D_y^2}{\epsilon_y} + \frac{D_z^2}{\epsilon_z} = 2U_e,$$

where ϵ_x , ϵ_y , and ϵ_z are the principal dielectric constants. If we replace $\mathbf{D}/\sqrt{2U_e}$ by \mathbf{r} and define the principal indices of refraction n_x , n_y , and n_z by $n_i^2 \equiv \epsilon_i/\epsilon_0$ ($i = x, y, z$), the last equation can be written as

$$\frac{x^2}{n_x^2} + \frac{y^2}{n_y^2} + \frac{z^2}{n_z^2} = 1. \quad (4.3-1)$$

This is the equation of a general ellipsoid with major axes parallel to the x , y , and z directions whose respective lengths are $2n_x$, $2n_y$, $2n_z$. The ellipsoid is known as the index ellipsoid or, sometimes, as the optical indicatrix. The index ellipsoid is used mainly to find the two indices of refraction and the two corresponding directions of \mathbf{D} associated with the two independent plane waves that can propagate along an arbitrary direction \mathbf{s} in a crystal. This is done by means of the following prescription: Find the intersection ellipse between a plane through the origin that is normal to the direction of propagation \mathbf{s} and the index ellipsoid (4.3-1). The two axes of the intersection ellipse are equal in length to $2n_1$ and $2n_2$, where n_1 and n_2 are the two indices of refraction, that is, the solutions of (4.2-10). These axes are parallel, respectively, to the directions of the vectors $\mathbf{D}_{1,2}$ of the two allowed solutions (see Fig. 4.2).

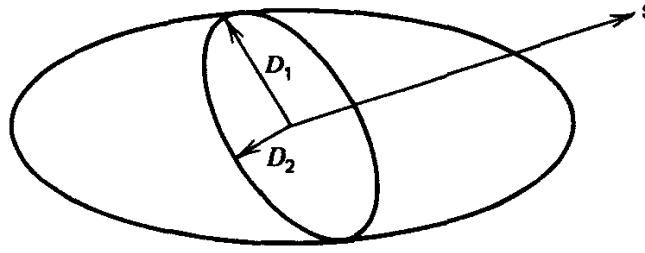


Figure 4.2. Method of the index ellipsoid. The inner ellipse is the intersection of the index ellipsoid with the plane normal to \mathbf{s} .

To show that this procedure is formally equivalent to the method of the last section, we define the impermeability tensor η_{ij} as

$$\eta_{ij} = \epsilon_0 (\epsilon^{-1})_{ij}, \quad (4.3-2)$$

where ϵ^{-1} is the inverse of the dielectric tensor ϵ . By using this definition, the relation between the field vectors \mathbf{E} and \mathbf{D} can be written

$$\mathbf{E} = \frac{1}{\epsilon_0} \boldsymbol{\eta} \mathbf{D}. \quad (4.3-3)$$

Substitution of Eq. (4.3-3) for \mathbf{E} in the wave equation (4.2-5), leads to

$$\mathbf{s} \times [\mathbf{s} \times \boldsymbol{\eta} \mathbf{D}] + \frac{1}{n^2} \mathbf{D} = 0, \quad (4.3-4)$$

where we have used $\mathbf{k} = n(\omega/c)\mathbf{s}$, and \mathbf{s} is a unit vector in the direction of propagation. Since \mathbf{D} is always transverse to the direction of propagation ($\mathbf{s} \cdot \mathbf{D} = 0$), it is convenient to use a new coordinate system with one axis in the direction of propagation of the wave, and denote the two transverse axes by 1 and 2. In this coordinate system the unit vector \mathbf{s} is given by

$$\mathbf{s} = \begin{pmatrix} 0 \\ 0 \\ 1 \end{pmatrix}, \quad (4.3-5)$$

and the wave equation (4.3-4) becomes

$$\begin{pmatrix} \eta_{11} & \eta_{12} & \eta_{13} \\ \eta_{21} & \eta_{22} & \eta_{23} \\ 0 & 0 & 0 \end{pmatrix} \mathbf{D} = \frac{1}{n^2} \mathbf{D}. \quad (4.3-6)$$

Since $\mathbf{s} \cdot \mathbf{D} = 0$, the third component of \mathbf{D} is always zero. We can ignore

η_{13} , η_{23} and define a transverse impermeability tensor η_t as

$$\eta_t = \begin{pmatrix} \eta_{11} & \eta_{12} \\ \eta_{21} & \eta_{22} \end{pmatrix}. \quad (4.3-7)$$

The wave equation then becomes

$$\left(\eta_t - \frac{1}{n^2} \right) \mathbf{D} = 0 \quad (4.3-8)$$

where \mathbf{D} is the displacement field vector.

The polarization vectors of the normal modes are eigenvectors of the transverse impermeability tensor with eigenvalues $1/n^2$. Since η_t is a symmetric 2×2 tensor, there are two orthogonal eigenvectors. These two eigenvectors, \mathbf{D}_1 and \mathbf{D}_2 , correspond to the two normal modes of propagation with refractive indices n_1 and n_2 , respectively.

Let ξ_1 , ξ_2 , ξ_3 be the coordinates of an arbitrary point in the new coordinate system. The index ellipsoid in this coordinate system is expressed by

$$\eta_{\alpha\beta} \xi_\alpha \xi_\beta = 1, \quad (4.3-9)$$

where summation over repeated indices α, β (1, 2, 3) is assumed. The intersection ellipse between a plane ($\xi_3 = 0$) through the origin that is normal to the direction of propagation and the index ellipsoid is obtained by putting $\xi_3 = 0$ in Eq. (4.3-9). Thus we obtain the following equation for the intersection ellipse

$$\eta_{11} \xi_1^2 + \eta_{22} \xi_2^2 + 2\eta_{12} \xi_1 \xi_2 = 1. \quad (4.3-10)$$

The coefficients of this ellipse form the transverse impermeability tensor η_t . The eigenvectors of this 2×2 tensor therefore are along the principal axes of this ellipse. The lengths of the principal axes determine the values of n according to Eq. (4.3-8). This proves the equivalence of the method of the index ellipsoid and the method of the last section.

4.4. PHASE VELOCITY, GROUP VELOCITY, AND ENERGY VELOCITY

The normal surface (surface of constant ω in \mathbf{k} space) described by Eq. (4.2-8) contains information about the phase velocity and the group veloc-

ity. The phase velocity of a plane wave is defined as

$$\mathbf{v}_p = \frac{\omega}{k} \mathbf{s}. \quad (4.4-1)$$

The group velocity for a wave packet is given by

$$\mathbf{v}_g = \nabla_{\mathbf{k}} \omega(\mathbf{k}), \quad (4.4-2)$$

while the velocity of energy flow is defined as

$$\mathbf{v}_e = \frac{\mathbf{S}}{U}, \quad (4.4-3)$$

where \mathbf{S} is the Poynting vector and U is the energy density. The group velocity \mathbf{v}_g , by definition, is a vector perpendicular to the normal surface. We have shown in Section 1.5 that the group velocity represents the velocity of energy flow of the propagation of laser pulses in a dispersive medium. In what follows we will show that the group velocity for a wave packet propagation in an anisotropic medium also represents the transport of energy, that is, $\mathbf{v}_g = \mathbf{v}_e$.

A wave packet can be viewed as a linear superposition of many monochromatic plane waves, each with a definite frequency ω and wave vector \mathbf{k} . Each plane-wave component satisfies the following Maxwell equation in momentum space:

$$\mathbf{k} \times \mathbf{E} = \omega \mu \mathbf{H}, \quad (4.4-4)$$

$$\mathbf{k} \times \mathbf{H} = -\omega \epsilon \mathbf{E}, \quad (4.4-5)$$

where ϵ and μ are assumed to be tensors. These equations may be obtained from Eqs. (1.1-1) and (1.1-2) by assuming $\mathbf{J} = 0$ and an $\exp[i(\omega t - \mathbf{k} \cdot \mathbf{r})]$ dependence for the field vectors.

To prove that \mathbf{v}_e and \mathbf{v}_g are equal, we start from Eqs. (4.4-4) and (4.4-5). Suppose now that \mathbf{k} is changed by an infinitesimal amount $\delta \mathbf{k}$. If $\delta \omega$, $\delta \mathbf{E}$, and $\delta \mathbf{H}$ are the corresponding changes in ω , \mathbf{E} , and \mathbf{H} , we have

$$\delta \mathbf{k} \times \mathbf{E} + \mathbf{k} \times \delta \mathbf{E} = \delta \omega \mu \mathbf{H} + \omega \mu \delta \mathbf{H}, \quad (4.4-6)$$

$$\delta \mathbf{k} \times \mathbf{H} + \mathbf{k} \times \delta \mathbf{H} = -\delta \omega \epsilon \mathbf{E} - \omega \epsilon \delta \mathbf{E}. \quad (4.4-7)$$

Scalar-multiplying Eq. (4.4-6) by \mathbf{H} and Eq. (4.4-7) by \mathbf{E} , and using the vector identity

$$\mathbf{A} \cdot (\mathbf{B} \times \mathbf{C}) = \mathbf{B} \cdot (\mathbf{C} \times \mathbf{A}) = \mathbf{C} \cdot (\mathbf{A} \times \mathbf{B}),$$

we obtain

$$\delta \mathbf{k} \cdot (\mathbf{E} \times \mathbf{H}) + \mathbf{k} \cdot (\delta \mathbf{E} \times \mathbf{H}) = \delta \omega (\mathbf{H} \cdot \boldsymbol{\mu} \mathbf{H}) + \omega (\mathbf{H} \cdot \boldsymbol{\mu} \delta \mathbf{H}) \quad (4.4-8)$$

$$- \delta \mathbf{k} \cdot (\mathbf{E} \times \mathbf{H}) + \mathbf{k} \cdot (\delta \mathbf{H} \times \mathbf{E}) = -\delta \omega (\mathbf{E} \cdot \boldsymbol{\epsilon} \mathbf{E}) - \omega (\mathbf{E} \cdot \boldsymbol{\epsilon} \delta \mathbf{E}). \quad (4.4-9)$$

Subtracting Eq. (4.4-9) from Eq. (4.4-8), we obtain

$$\begin{aligned} 2\delta \mathbf{k} \cdot (\mathbf{E} \times \mathbf{H}) - \delta \omega (\mathbf{E} \cdot \boldsymbol{\epsilon} \mathbf{E} + \mathbf{H} \cdot \boldsymbol{\mu} \mathbf{H}) \\ = \delta \mathbf{H} \cdot (\omega \boldsymbol{\mu} \mathbf{H} - \mathbf{k} \times \mathbf{E}) + \delta \mathbf{E} \cdot (\omega \boldsymbol{\epsilon} \mathbf{E} + \mathbf{k} \times \mathbf{H}), \end{aligned} \quad (4.4-10)$$

where we have used the symmetry properties of the tensors $\boldsymbol{\epsilon}$ and $\boldsymbol{\mu}$:

$$\mathbf{H} \cdot \boldsymbol{\mu} \delta \mathbf{H} = \delta \mathbf{H} \cdot \boldsymbol{\mu} \mathbf{H},$$

$$\mathbf{E} \cdot \boldsymbol{\epsilon} \delta \mathbf{E} = \delta \mathbf{E} \cdot \boldsymbol{\epsilon} \mathbf{E}.$$

The right side of Eq. (4.4-10) vanishes according to Eqs. (4.4-4) and (4.4-5). Thus we have from Eq. (4.4-10)

$$\delta \mathbf{k} \cdot (\mathbf{E} \times \mathbf{H}) = \delta \omega \frac{1}{2} (\mathbf{E} \cdot \boldsymbol{\epsilon} \mathbf{E} + \mathbf{H} \cdot \boldsymbol{\mu} \mathbf{H}). \quad (4.4-11)$$

According to the definition of the energy density (1.2-5) and the Poynting vector (1.2-6), Eq. (4.4-11) can be written

$$\delta \omega = \delta \mathbf{k} \cdot \frac{\mathbf{S}}{U} = \delta \mathbf{k} \cdot \mathbf{v}_e. \quad (4.4-12)$$

From the definition of the group velocity we also have

$$\delta \omega = (\nabla_{\mathbf{k}} \omega) \cdot \delta \mathbf{k} = \delta \mathbf{k} \cdot \mathbf{v}_g. \quad (4.4-13)$$

Since $\delta \mathbf{k}$ is an arbitrary vector, we conclude that

$$\mathbf{v}_g = \mathbf{v}_e. \quad (4.4-14)$$

This equality endows the concept of group velocity as defined by Eq. (4.4-2) with a rigorous meaning.

In the above proof, we assume that \mathbf{E} and \mathbf{H} are real field vectors. If we use the complex representation for the field vectors, we also arrive at Eq. (4.4-14) (see Problem 4.3).

If $\delta\mathbf{k}$ is an infinitesimal vector in the tangent plane of the normal surface, $\delta\omega$ will be zero because the normal surface is a surface of constant ω . From Eq. (4.4-11), we obtain

$$\delta\mathbf{k}' \cdot (\mathbf{E} \times \mathbf{H}) = 0, \quad (4.4-15)$$

where the prime indicates that $\delta\mathbf{k}'$ is in the tangent plane of the normal surface. This result implies that both \mathbf{E} and \mathbf{H} lie in the tangent plane of the normal surface and the Poynting vector $\mathbf{E} \times \mathbf{H}$ is always perpendicular to the normal surface.

4.5. CLASSIFICATION OF ANISOTROPIC MEDIA (CRYSTALS)

We have shown above that the normal surface contains a good deal of information concerning the wave propagation in anisotropic media. The normal surface is uniquely determined by the principal indices of refraction n_x, n_y, n_z . In the general case when the three principal indices n_x, n_y, n_z are all different, there are two optical axes. In this case, the crystal is said to be biaxial. In many optical materials it happens that two of the principal indices are equal, in which case the equation for the normal surface (4.2-8) can be factored according to

$$\left(\frac{k_x^2 + k_y^2}{n_e^2} + \frac{k_z^2}{n_o^2} - \frac{\omega^2}{c^2} \right) \left(\frac{k^2}{n_o^2} - \frac{\omega^2}{c^2} \right) = 0, \quad (4.5-1)$$

where $n_o^2 = \epsilon_x/\epsilon_0 = \epsilon_y/\epsilon_0$, $n_e^2 = \epsilon_z/\epsilon_0$.

The normal surface in this case consists of a sphere and an ellipsoid of revolution. These two sheets of the normal surface touch at two points on the z axis. The z axis is therefore the only optic axis, and the crystal is said to be uniaxial. If all the three principal indices are equal, the two sheets of normal surface degenerate to a single sphere, and the crystal is optically isotropic.

It is obvious that the optical symmetry of the crystals is closely related to the point group of the crystals. For example, in a cubic crystal, the three principal axes are physically equivalent. Therefore, we expect a cubic crystal to be optically isotropic. Table 4.1 lists the optical symmetry of the crystals and the corresponding dielectric tensor.

In a biaxial crystal, the principal coordinate axes are labeled in such a way that the three principal indices are in the following order:

$$n_x < n_y < n_z. \quad (4.5-2)$$

Table 4.1.

Optical Symmetry	Crystal System	Point Groups	Dielectric Tensor	
Isotropic	Cubic	$\bar{4}3m$	$\epsilon = \epsilon_0 \begin{pmatrix} n^2 & 0 & 0 \\ 0 & n^2 & 0 \\ 0 & 0 & n^2 \end{pmatrix}$	
		432		
		m3		
		23		
		m3m		
Uniaxial	Tetragonal	4	$\epsilon = \epsilon_0 \begin{pmatrix} n_o^2 & 0 & 0 \\ 0 & n_o^2 & 0 \\ 0 & 0 & n_e^2 \end{pmatrix}$	
		$\bar{4}$		
		4/m		
		422		
		4mm		
		$\bar{4}2m$		
		4/mmm		
		Hexagonal		6
				$\bar{6}$
				6/m
	622			
	6mm			
	$\bar{6}m2$			
	Trigonal	3		
		$\bar{3}$		
		32		
		3m		
		$\bar{3}m$		
	Biaxial	Triclinic		1
$\bar{1}$				
Monoclinic		2		
		m		
		2/m		
Orthorhombic		222		
		2mm		
		mmm		

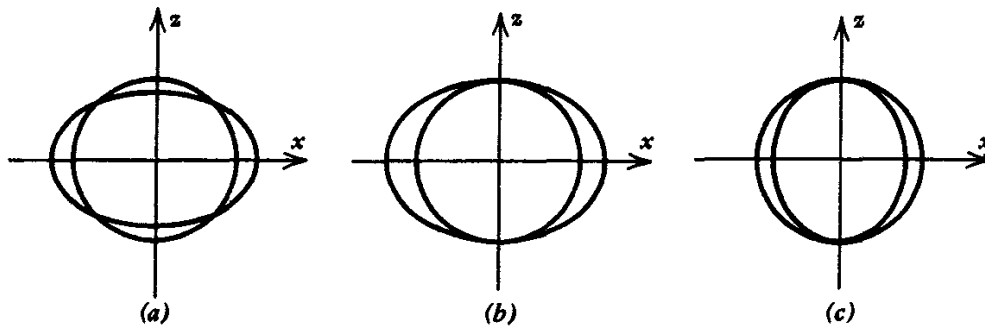


Figure 4.3. Intersection of the normal surface with the xz plane for (a) biaxial crystals, (b) positive uniaxial crystals, (c) negative uniaxial crystals.

In this convention the optical axes lie in the xz plane. The cross section of the normal surfaces with the xz plane is shown in Fig. 4.3(a). In a uniaxial crystal, the index of refraction that corresponds to the two equal elements, $n_o^2 = \epsilon_x/\epsilon_0 = \epsilon_y/\epsilon_0$, is called the ordinary index n_o ; the other index, corresponding to ϵ_z , is called the extraordinary index n_e . If $n_o < n_e$, the crystal is said to be positive, whereas if $n_o > n_e$, it is said to be negative. The intersection of the normal surfaces with the xz plane is again shown in Fig. 4.3(b), (c). The optic axis corresponds to the principal axis, which has a unique index of refraction. Table 4.2 lists some examples of crystals with their indices of refraction.

4.6. LIGHT PROPAGATION IN UNIAXIAL CRYSTALS

Many modern optical devices involve the use of uniaxial crystals. Some common examples are quartz, calcite, and lithium niobate. In these crystals, the equation (4.3-1) of the index ellipsoid simplifies to

$$\frac{x^2}{n_o^2} + \frac{y^2}{n_o^2} + \frac{z^2}{n_e^2} = 1, \quad (4.6-1)$$

where the axis of symmetry has been chosen, following convention, as the z axis.

Figure 4.4 shows the index ellipsoid for a positive uniaxial crystal. The direction of propagation is along s . Since the ellipsoid in this case is invariant under rotation about the z axis, the projection of the s vector on the xy plane is chosen without loss of generality to coincide with the y axis.

According to the prescription given in Section 4.3, we first find the intersection of the plane through the origin that is normal to s with the index ellipsoid. The intersection is an ellipse whose plane is shown in the figure. The length of the semimajor axis OA is equal to the index of

Table 4.2. Refractive Indices of Some Typical Crystals

Isotropic	CdTe	2.69		
	NaCl	1.544		
	Diamond	2.417		
	Fluorite	1.392		
	GaAs	3.40		
Uniaxial:		n_o	n_e	
	positive			
	Ice	1.309	1.310	
	Quartz	1.544	1.553	
	BeO	1.717	1.732	
	Zircon	1.923	1.968	
	Rutile	2.616	2.903	
	ZnS	2.354	2.358	
	negative			
	(NH ₄)H ₂ PO ₄ (ADP)	1.522	1.478	
	Beryl	1.598	1.590	
	KH ₂ PO ₄ (KDP)	1.507	1.467	
	NaNO ₃	1.587	1.336	
	Calcite	1.658	1.486	
	Tourmaline	1.638	1.618	
LiNbO ₃	2.300	2.208		
BaTiO ₃	2.416	2.364		
Proustite	3.019	2.739		
Biaxial		n_x	n_y	n_z
	Gypsum	1.520	1.523	1.530
	Feldspar	1.522	1.526	1.530
	Mica	1.552	1.582	1.588
	Topaz	1.619	1.620	1.627
	NaNO ₂	1.344	1.411	1.651
	SbSI	2.7	3.2	3.8
	YAlO ₃	1.923	1.938	1.947

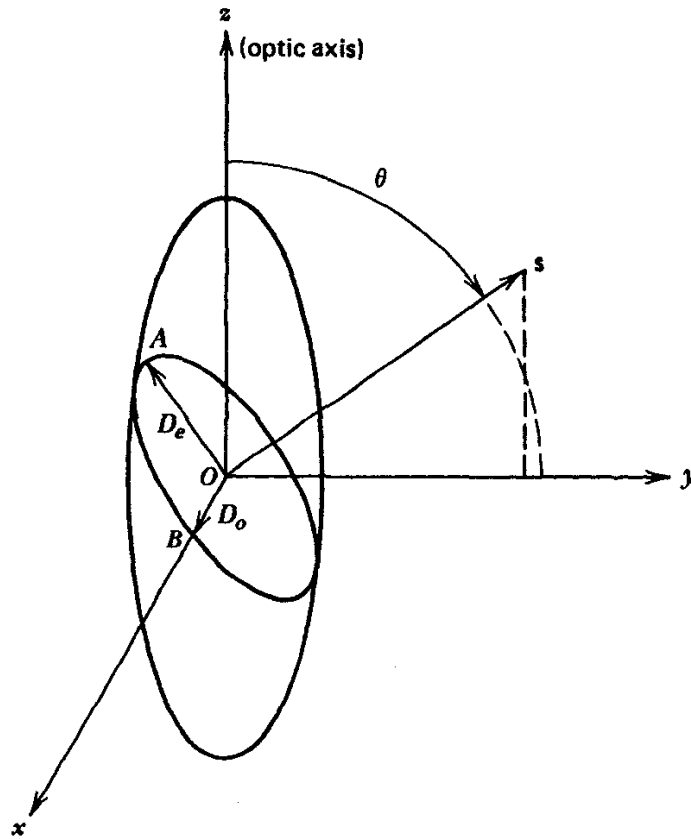


Figure 4.4. The construction for finding the indices of refraction and the polarization of normal modes for a given direction of propagation s . The figure shown is for a uniaxial crystal with $n_x = n_y = n_o$, $n_z = n_e$.

refraction $n_e(\theta)$ of the “extraordinary” ray, whose electric displacement vector $\mathbf{D}_e(\theta)$ is parallel to OA . The “ordinary” ray is polarized (i.e., has its \mathbf{D} vector) along OB , and its index of refraction is equal to n_o .

If we let \mathbf{k} be the wave vector and \mathbf{c} be a unit vector in the direction of the c axis (z axis), the polarizations for these displacement vectors are given by

$$\mathbf{d}_o = \frac{\mathbf{k} \times \mathbf{c}}{|\mathbf{k} \times \mathbf{c}|}, \quad (4.6-2)$$

$$\mathbf{d}_e = \frac{\mathbf{d}_o \times \mathbf{k}}{|\mathbf{d}_o \times \mathbf{k}|} \quad (4.6-3)$$

respectively.

It is clear from Fig. 4.4 that as the angle θ between the optic axis and the direction of propagation s is changed, the direction of polarization of the ordinary ray remains fixed (along the x axis in the figure) and its index of

refraction is always equal to n_o . The direction of \mathbf{D}_e , on the other hand, depends, as shown, on θ . The index of refraction varies from $n_e(\theta) = n_o$ for $\theta = 0^\circ$ to $n_e(\theta) = n_e$ for $\theta = 90^\circ$. The index of refraction $n_e(\theta)$ of the extraordinary ray is equal to OA , which according to Fig. 4.4 is given by

$$\frac{1}{n_e^2(\theta)} = \frac{\cos^2\theta}{n_o^2} + \frac{\sin^2\theta}{n_e^2}. \quad (4.6-4)$$

The indices of refraction for the case of light propagation in a uniaxial crystal can also be determined directly from the normal surfaces (4.5-1). If we substitute $k_z = n(\omega/c)\cos\theta$, $k_x = 0$, $k_y^2 = [(\omega/c)n]^2 - k_z^2$ into Eq. (4.5-1), we obtain, Eq. (4.6-4) from the first factor, and the ordinary refractive index n_o from the second factor. The direction of polarization for the extraordinary electric field is given, from Eq. (4.2-9), by

$$\begin{pmatrix} 0 \\ \frac{\sin\theta}{n_e^2(\theta) - n_o^2} \\ \frac{\cos\theta}{n_e^2(\theta) - n_e^2} \end{pmatrix},$$

where $n_e(\theta)$ is the refractive index for the extraordinary wave (4.6-4). Notice that the electric field vector is, in general, not perpendicular to the propagation vector. The intersection of the yz plane with the normal surfaces for a positive uniaxial crystal ($n_e > n_o$) is shown in Fig. 4.5.

In summary, the propagation of light in a uniaxial crystal in general consists of an ordinary wave and an extraordinary wave. The electric field vector \mathbf{E} (and the displacement vector \mathbf{D}) for the ordinary wave is always

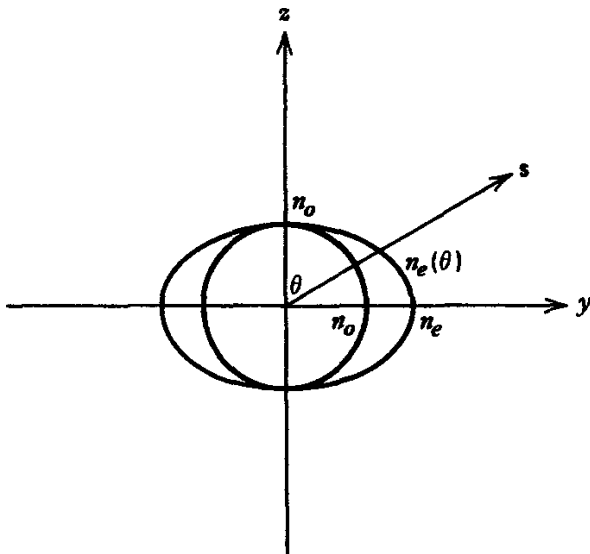


Figure 4.5. The intersection of the sz plane with the normal surface for a positive uniaxial crystal ($n_e > n_o$).

perpendicular to both the c axis and the propagation vector. The phase velocity for the ordinary wave is always c/n_o , regardless of the direction of propagation. The displacement vector \mathbf{D} of the extraordinary wave, is perpendicular to the propagation vector, as is the electric field vector \mathbf{E} of the ordinary wave. The electric field vector \mathbf{E} of the extraordinary wave, however, is in general not perpendicular to the propagation vector. It lies in the plane formed by the propagation vector and the displacement vector. The electric field vectors of these two waves are mutually orthogonal.

4.7. DOUBLE REFRACTION AT A BOUNDARY

Consider a plane wave incident on the surface of an anisotropic crystal. The refracted wave, in general, is a mixture of the two eigenmodes. In a uniaxial crystal, the refracted wave, in general, is a mixture of the ordinary wave and the extraordinary wave. According to the arguments used in connection with reflection and refraction at a plane boundary, the boundary condition requires that all the wave vectors lie in the plane of incidence and that their tangential components along the boundary be the same. This kinematic condition remains true for refraction at a boundary of an anisotropic crystal.

Let \mathbf{k}_0 be the propagation vector of the incident wave, and $\mathbf{k}_1, \mathbf{k}_2$ be the propagation vectors of the refracted waves. Given a prescribed value of the projection of the propagation vector \mathbf{k}_0 on the boundary, the two shells of the normal surface in general yields two propagation vectors, thus giving rise to two refracted waves as shown in Fig. 4.6. The kinematic condition requires that

$$k_0 \sin \theta_0 = k_1 \sin \theta_1 = k_2 \sin \theta_2 \quad (4.7-1)$$

for the refracted waves.

Equation (4.7-1) looks like the Snell's law. However, it is important to remember that k_1, k_2 are not, in general, constant; rather, they vary with the directions of the vectors $\mathbf{k}_1, \mathbf{k}_2$. The algebraic problem of determining θ_1 and θ_2 involves solving a quartic equation. The graphical method is easier and is shown in Fig. 4.6.

In the case of uniaxial crystals, one shell of the normal surface is a sphere. The corresponding wave number k is therefore a constant for all directions of propagation. This wave is the ordinary wave and obeys Snell's law,

$$n_i \sin \theta_0 = n_o \sin \theta_1, \quad (4.7-2)$$

where n_i is the index of refraction of the incident medium and n_o is the ordinary refractive index of the crystal. The other shell of the normal

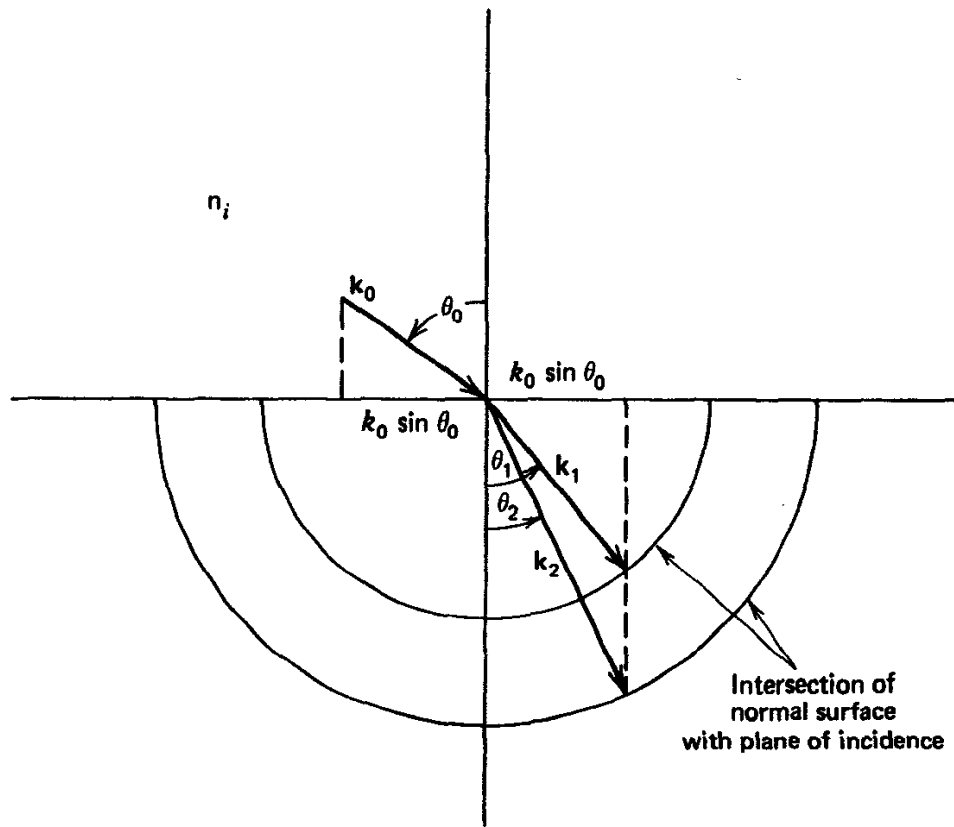


Figure 4.6. Double refraction at a boundary of an anisotropic medium and the graphic method of determining θ_1 and θ_2 .

surface is an ellipsoid of revolution. Therefore, the corresponding wave number k depends on the direction of propagation. This wave is the extraordinary wave. Some examples of double refraction are illustrated in Fig. 4.7.

4.8. LIGHT PROPAGATION IN BIAxIAL CRYSTALS

We now investigate the propagation of electromagnetic radiation in a biaxial crystal. The normal surface [i.e., $\omega(\mathbf{k}) = \text{constant}$] of a typical biaxial crystal is shown in Fig. 4.1. It will help us visualize this surface if we consider first its intersections with the three coordinate planes [see Fig. 4.8(a)]. If we set $k_y = 0$ in Eq. (4.2-8), the equation breaks into two factors, giving

$$\frac{k_x^2 + k_z^2}{n_y^2} = \left(\frac{\omega}{c}\right)^2, \quad (4.8-1)$$

$$\frac{k_x^2}{n_z^2} + \frac{k_z^2}{n_x^2} = \left(\frac{\omega}{c}\right)^2,$$

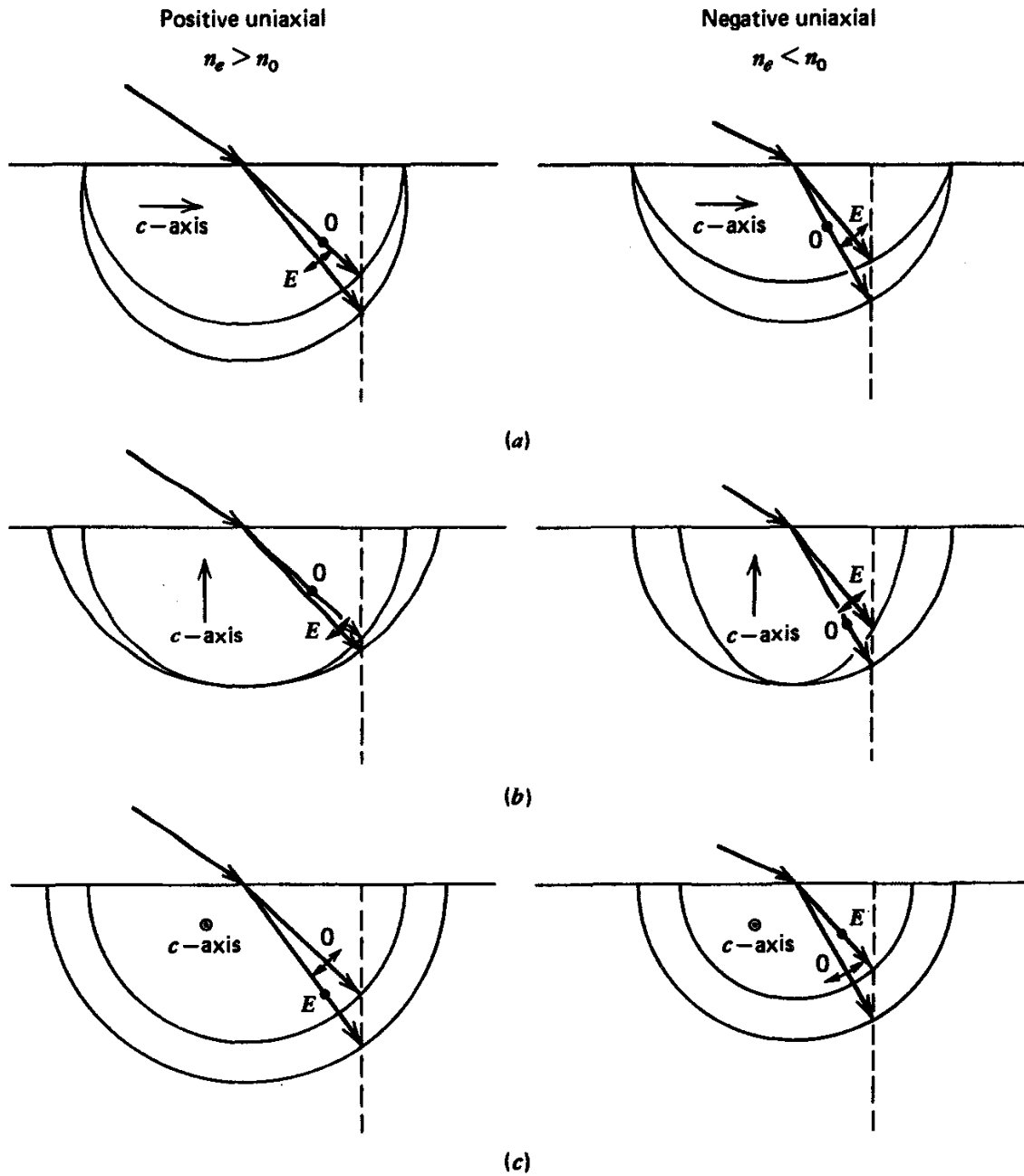


Figure 4.7. Wave vectors for double refraction in uniaxial crystals, with the optic axis (a) parallel to the boundary and parallel to the plane of incidence, (b) perpendicular to the boundary and parallel to the plane of incidence, (c) parallel to the boundary and perpendicular to the plane of incidence. *O* and *E* stand for ordinary and extraordinary rays, respectively.

where n_x , n_y , and n_z are the principal refractive indices. The intersection of the normal surface with the plane $k_y = 0$ consists of a circle with a radius of $n_y\omega/c$ and an ellipse with semiaxes $n_x\omega/c$ and $n_z\omega/c$. The intersection with each of the other two coordinate planes likewise consists of a circle and an ellipse. The circle and the ellipse intersect only in the plane $k_y = 0$, as a result of the choice of the coordinate axes (i.e., $n_x < n_y < n_z$). These four points of intersection define the two optic axes of the crystal.

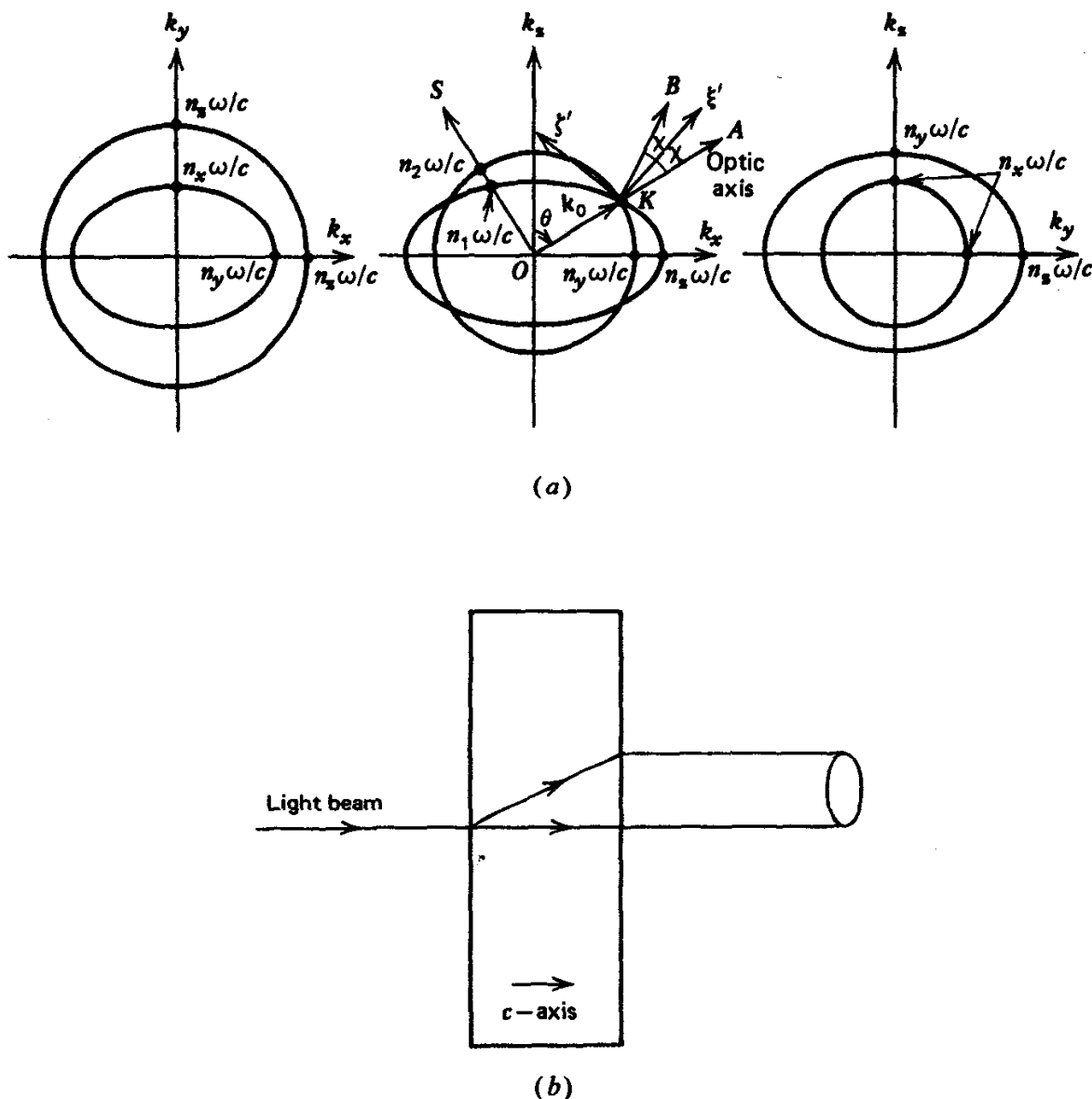


Figure 4.8. (a) Sections of the normal surface of a biaxial crystal. (b) Conical refraction. The biaxial crystal plate is cut in such a way that the plate surfaces are perpendicular to one of the optic axes.

We now consider the wave propagation in the coordinate plane $k_y = 0$. For a general direction of propagation, we draw a line OS along the direction of propagation. There are in general two points of intersection. The distances between the origin O and the points of intersection determine the length of the wave vectors. The modes associated with the circle are polarized perpendicular to the coordinate plane $k_y = 0$, whereas the modes associated with the ellipse are polarized in the plane of the ellipse. Wave propagation in each of the other two coordinate planes is similar except for the propagation along the optic axes. Light propagation in the direction of these optic axes has a unique phase velocity regardless of the state of polarization. The group velocity v_g defined by Eq. (4.4-2)—which represents the flow of electromagnetic energy—is, however, undefined in this direction,

because the two shells of the normal surface degenerate to a point. The refraction phenomena associated with the propagation in this direction are closely related to the nature of the singularity at these points.

If we draw unit normal vectors perpendicular to the normal surface at points in an infinitesimal neighborhood of the singular point, we obtain an infinite number of unit vectors corresponding to the direction of energy flow. These vectors form a surface of a cone. Therefore, we expect that the flow of electromagnetic energy will take the form of a cone. This phenomenon is known as conical refraction.

To study the properties of conical refraction we need to examine the normal surface near the singularity point \mathbf{k}_0 [see Fig. 4.8(a)]. For light propagation in the direction of the optic axis shown in Fig. 4-8(a), the wave vector is given by

$$\mathbf{k}_0 = \hat{x}k_{x0} + \hat{y}k_{y0} + \hat{z}k_{z0} \quad (4.8-2)$$

with

$$\begin{aligned} k_{x0} &= n_y \frac{\omega}{c} \sin \theta, \\ k_{y0} &= 0, \\ k_{z0} &= n_y \frac{\omega}{c} \cos \theta, \end{aligned} \quad (4.8-3)$$

where θ is the angle between the optic axis and the z axis and is given by

$$\tan \theta = \frac{n_z}{n_x} \left(\frac{n_y^2 - n_x^2}{n_z^2 - n_y^2} \right)^{1/2}. \quad (4.8-4)$$

To examine the normal surface near the point \mathbf{k}_0 , we need to perform a Taylor series expansion around this point. Let

$$\begin{aligned} k_x &= k_{x0} + \xi, \\ k_y &= k_{y0} + \eta, \\ k_z &= k_{z0} + \zeta, \end{aligned} \quad (4.8-5)$$

and then substitute them into Eq. (4.2-8). We obtain, after neglecting

higher-order terms in ξ , η , ζ ,

$$4(k_{x0}\xi + k_{z0}\zeta)(n_x^2 k_{x0}\xi + n_z^2 k_{z0}\zeta) + \eta^2(n_y^2 - n_x^2)(n_y^2 - n_z^2) = 0. \quad (4.8-6)$$

This equation of second degree represents a cone whose vertex lies at point \mathbf{k}_0 (i.e., $\xi = \eta = \zeta = 0$). It can be diagonalized by a rotation of the coordinates [see Fig. 4.8(a)] and becomes

$$\zeta'^2 + \frac{1}{1 - \tan^2\chi} \eta^2 = \xi'^2 \cot^2\chi, \quad (4.8-7)$$

where χ is given by

$$\tan^2 2\chi = \frac{(n_z^2 - n_y^2)(n_y^2 - n_x^2)}{n_x^2 n_z^2} \quad (4.8-8)$$

According to (4.8-7), the normal surface near the optic axis is a cone with a vertex at \mathbf{k}_0 . Hence when the wave vector coincides with the optic axis there are an infinite number of directions for energy flows (i.e., an infinite number of \mathbf{v}_g), which lie upon the cone given by

$$\zeta'^2 + (1 - \tan^2\chi) \eta^2 = \xi'^2 \tan^2\chi. \quad (4.8-9)$$

This is an elliptical cone with the ξ' axis as the cone axis and the point \mathbf{k}_0 as the vertex. This cone contains the optic axis OA and intersects any plane which is perpendicular to OA in a circle (see Problem 4.5). The aperture angle of this cone is 2χ in the xz plane [see Fig. 4.8(a)]. Each unit vector originating from the vertex of the cone and lying in the cone represents a direction of energy flow for propagation with wave vector \mathbf{k}_0 . Each such direction corresponds to a linear polarization state. For example, the direction KA represents the energy flow for a y -polarized wave, whereas the direction KB represents the energy flow for waves polarized in the xz plane [see Fig. 4.8(a)].

We now consider a plate of a biaxial crystal (e.g., mica) cut so that its two parallel surfaces are perpendicular to one of the optic axes. If this plate is illuminated by an unpolarized collimated beam of monochromatic light, such as laser light, incident normally on one of its faces, the energy will spread out in the plate in a hollow cone, and on emerging at the other side it will form a hollow cylinder, as shown in Fig. 4.8. Thus, on a screen parallel to the crystal face, we expect to see a bright circular ring.

4.9. OPTICAL ACTIVITY

Certain optical media are found to cause a rotation of the plane of polarization of linearly polarized light passing through them. This phenomenon is known as optical activity and was first observed in quartz. Figure 4.9 illustrates the rotation of the plane of polarization by an optically active medium. The amount of rotation is proportional to the path length of light in the medium. Conventionally, the rotatory power of a medium is given in degrees per centimeter, that is, the specific rotatory power is defined as the amount of rotation per unit length.

The sense of rotation bears a fixed relation to the propagation wave vector of the light, so if the light is made to traverse the medium once in each of two opposite directions, as in the case of reflection from the right end face in Fig. 4.9, the net rotation is zero. A substance is called dextrorotatory or right-handed if the sense of rotation of the plane of polarization is counterclockwise as viewed by an observer facing the approaching light beam. If the sense of rotation is clockwise, the substance is called levorotatory or left-handed. Quartz occurs in both right-handed and left-handed crystalline forms. Many other substances are now known to exhibit optical activity; these include cinnabar, sodium chlorate, turpentine, sugar, strychnine sulfate, tellurium, selenium, and silver thiogallate (AgGaS_2). The specific rotatory powers of some optically active media are given in Table 4.3.

Fresnel first recognized in 1825 that the optical activity arises from circular double refraction, in which the eigenwaves of propagation (i.e., the independent plane-wave solutions of Maxwell's equations) are right and left circularly polarized waves.

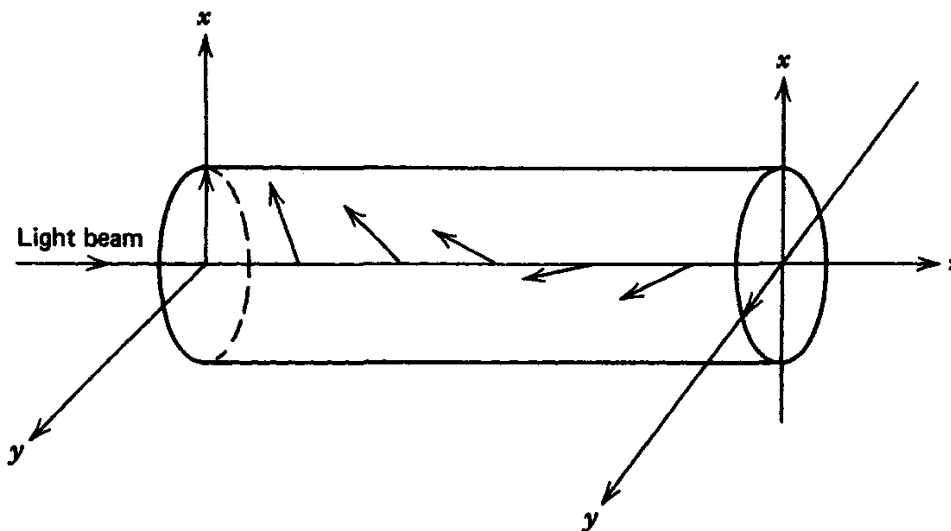


Figure 4.9. Rotation of the plane of polarization by an optically active medium.

Table 4.3. Optical Rotatory Powers

	λ (Å)	ρ (degree/mm)
Quartz	4000	49
	4500	37
	5000	31
	5500	26
	6000	22
	6500	17
AgGaS ₂	4850	950
	4900	700
	4950	600
	5000	500
	5050	430
Se	7500	180
	10000	30
Te	(6 μm)	40
	(10 μm)	15
TeO ₂	3698	587
	4382	271
	5300	143
	6328	87
	10000	30

Let n_r and n_l be the refractive indices associated with these two waves, and assume that the waves are propagating in the $+z$ direction. The displacement vector amplitudes for these two waves are

$$\hat{\mathbf{R}} \exp\left[i\omega\left(t - \frac{zn_r}{c}\right)\right]$$

and

$$\hat{\mathbf{L}} \exp\left[i\omega\left(t - \frac{zn_l}{c}\right)\right],$$

where $\hat{\mathbf{R}}$ and $\hat{\mathbf{L}}$ are unit Jones vectors for the circular polarizations (3.4-9) and (3.4-10), respectively.

If a linearly polarized beam of amplitude D_0 that is polarized along the x direction enters the medium at $z = 0$, it will be represented by the sum of two such waves with amplitudes $D_0/\sqrt{2}$. At distance z in the medium, the resultant will be

$$\frac{D_0}{\sqrt{2}} e^{i\omega t} \{ \hat{\mathbf{R}} e^{-i\omega z n_r/c} + \hat{\mathbf{L}} e^{-i\omega z n_l/c} \}. \quad (4.9-1)$$

This can further be written, if we use Eqs. (3.4-9) and (3.4-10), as

$$D_0 \hat{\mathbf{p}} \exp \left\{ i\omega \left(t - \frac{z(n_r + n_l)}{2c} \right) \right\} \quad (4.9-2)$$

with

$$\hat{\mathbf{p}} = \hat{\mathbf{x}} \cos \left[\frac{\omega(n_l - n_r)}{2c} z \right] + \hat{\mathbf{y}} \sin \left[\frac{\omega(n_l - n_r)}{2c} z \right]. \quad (4.9-3)$$

The polarization of the resultant wave is represented by Eq. (4.9-3). The wave is linearly polarized with its plane of polarization turned in the counter-clockwise sense from x through an angle $\omega z(n_l - n_r)/2c$. Thus the specific rotatory power is given by

$$\rho = \frac{\pi}{\lambda} (n_l - n_r). \quad (4.9-4)$$

The optical rotation is right-handed (counterclockwise) if $n_r < n_l$. Thus the plane of polarization turns in the same sense as the circularly polarized wave which travels with the greater phase velocity.

The specific rotatory power of quartz at $\lambda = 6328 \text{ \AA}$ is $188^\circ/\text{cm}$, giving

$$|n_r - n_l| = 6.6 \times 10^{-5}.$$

It is evident that the rotation of the plane of polarization is an extremely sensitive way of measuring very small amounts of circular double refraction.

The dielectric property of ordinary crystals described by the material equation (4.1-6) does not allow the existence of optical activity. To develop a theory of optical activity we need to generalize the constitutive relations of materials. The electromagnetic theory of optical activity is due mainly to Born and his coworkers and has been well summarized by Condon [3].

According to their theory, the optical activity originates in properties of a molecule represented by a parameter

$$\mathbf{p} = \alpha \mathbf{E} - \beta \dot{\mathbf{H}}, \quad (4.9-5)$$

in which p is the induced dipole moment of the molecule. For a linear molecule it is obvious that $\beta = 0$. A nonvanishing β arises from an intrinsic helical structure in the molecule. When such a helical molecule is in a changing magnetic field, the changing magnetic flux through the molecule sets up an induced current circulating around \mathbf{H} in the sense given by Lenz's law (1.1-1). This induced current will now give rise to a time-varying separation of charges in the direction of \mathbf{H} , thus setting up an electric dipole moment which is represented by the term in β in Eq. (4.9-5). For plane-wave propagation in a homogeneous medium, the material equation for an optically active material can thus be written

$$\mathbf{D} = \epsilon \mathbf{E} + i\epsilon_0 \mathbf{G} \times \mathbf{E} \quad (4.9-6)$$

where ϵ is the dielectric tensor without optical activity, and \mathbf{G} is a vector parallel to the direction of propagation and is called the gyration vector. The vector product $\mathbf{G} \times \mathbf{E}$ can always be represented by the product of an antisymmetric tensor $[G]$ with \mathbf{E} . The matrix elements of $[G]$ are given by

$$\begin{aligned} [G]_{23} &= -[G]_{32} = -G_x, \\ [G]_{31} &= -[G]_{13} = -G_y, \\ [G]_{12} &= -[G]_{21} = -G_z. \end{aligned} \quad (4.9-7)$$

Thus Eq. (4.9-6) becomes

$$\mathbf{D} = (\epsilon + i\epsilon_0 [G])\mathbf{E}. \quad (4.9-8)$$

It is often convenient to define a new dielectric tensor as

$$\epsilon' = \epsilon + i\epsilon_0 [G]. \quad (4.9-9)$$

This new tensor is Hermitian, that is, $\epsilon'_{ij} = \epsilon'^*_{ji}$. We can now substitute ϵ' into Eq. (4.2-5) and solve for the eigenwaves of propagation. Again, let \mathbf{s} be the unit vector in the direction of propagation, so that the gyration vector can be written

$$\mathbf{G} = G\mathbf{s}. \quad (4.9-10)$$

The resulting Fresnel equation for the eigenindices of refraction is given by

$$\begin{aligned} \frac{s_x^2}{n^2 - n_x^2} + \frac{s_y^2}{n^2 - n_y^2} + \frac{s_z^2}{n^2 - n_z^2} - \frac{1}{n^2} \\ = G^2 \frac{s_x^2 n_x^2 + s_y^2 n_y^2 + s_z^2 n_z^2}{n^2 (n^2 - n_x^2)(n^2 - n_y^2)(n^2 - n_z^2)} \end{aligned} \quad (4.9-11)$$

where $n_x, n_y,$ and n_z are the principal refractive indices and s_x, s_y, s_z are the components of \mathbf{s} along the principal dielectric axes. Let n_1^2 and n_2^2 be the roots of the Fresnel equation with $G = 0$. Equation (4.9-11) can be written in terms of n_1^2 and n_2^2 as

$$(n^2 - n_1^2)(n^2 - n_2^2) = G^2. \quad (4.9-12)$$

For propagation along the optic axes we know that $n_1 = n_2 = \bar{n}$, say. Equation (4.9-12) then gives

$$n^2 = \bar{n}^2 \pm G,$$

and since G is small,

$$n = \bar{n} \pm \frac{G}{2\bar{n}}. \quad (4.9-13)$$

These correspond to two circularly polarized waves. From Eq. (4.9-4), the rotatory power is

$$\rho = \frac{\pi G}{\lambda \bar{n}}. \quad (4.9-14)$$

The parameter G in Eq. (4.9-12) varies with the direction of the wave vector and is a quadratic function of the direction cosines s_x, s_y, s_z ; thus we write

$$G = g_{11}s_x^2 + g_{22}s_y^2 + g_{33}s_z^2 + 2g_{12}s_x s_y + 2g_{23}s_y s_z + 2g_{31}s_x s_z, \quad (4.9-15)$$

or

$$G = g_{ij}s_i s_j, \quad i, j = x, y, z, \quad (4.9-16)$$

where g_{ij} are matrix elements of the gyration tensor which describe the optical activity of the crystal.

To study the polarization states of the eigenmodes, it is convenient to use the displacement vector \mathbf{D} , since \mathbf{D} is always perpendicular to the direction of propagation ($\mathbf{D} \cdot \mathbf{s} = 0$). It is also more convenient to use the inverse tensor ϵ^{-1} . The material constitutive relation can now be written

$$\mathbf{E} = \frac{1}{\epsilon'} \mathbf{D} \quad (4.9-17)$$

where ϵ' is given by Eq. (4.9-9). The inverse tensor $1/\epsilon'$ is also a Hermitian tensor. The eigenmodes of propagation can be obtained from the wave equation (4.2-5):

$$n^2 \mathbf{s} \times \left(\mathbf{s} \times \frac{\epsilon_0}{\epsilon'} \right) \mathbf{D} + \mathbf{D} = 0. \quad (4.9-18)$$

Since $[G]$ is small compared with ϵ/ϵ_0 , the inverse tensor can be written

$$\frac{1}{\epsilon'} = \frac{1}{\epsilon} - i\epsilon_0 \frac{1}{\epsilon} [G] \frac{1}{\epsilon}. \quad (4.9-19)$$

Thus Eq. (4.9-18) can be written in terms of the impermeability tensor η ($= \epsilon_0/\epsilon$) as

$$[s][s](\eta - i\eta[G]\eta)\mathbf{D} = -\frac{1}{n^2}\mathbf{D}, \quad (4.9-20)$$

where $[s]$ is the antisymmetrical tensor representation of $\mathbf{s} \times$ and is defined in a similar way to $[G]$ [see (Eq. 4.9-7)]. Let $\mathbf{D}_1, \mathbf{D}_2$ be the normalized eigenmodes of propagation in the absence of optical activity ($G = 0$):

$$\left\{ [s][s]\eta + \frac{1}{n_{1,2}^2} \right\} \mathbf{D}_{1,2} = 0 \quad (4.9-21)$$

and

$$\mathbf{D}_i \cdot \mathbf{D}_j = \delta_{ij}.$$

We will now solve the eigenvalue problem in the coordinate system formed by the triad $(\mathbf{D}_1, \mathbf{D}_2, \mathbf{s})$. In this coordinate system, Eq. (4.9-20) becomes

$$\begin{pmatrix} \frac{1}{n_1^2} & \frac{iG}{n_1^2 n_2^2} \\ -\frac{iG}{n_1^2 n_2^2} & \frac{1}{n_2^2} \end{pmatrix} \mathbf{D} = \frac{1}{n^2} \mathbf{D}. \quad (4.9-22)$$

The refractive indices n of the eigenmodes satisfy the following secular equation:

$$\left(\frac{1}{n_1^2} - \frac{1}{n^2}\right)\left(\frac{1}{n_2^2} - \frac{1}{n^2}\right) = \left(\frac{G}{n_1^2 n_2^2}\right)^2. \quad (4.9-23)$$

The roots of Eq. (4.9-23) are given by

$$\frac{1}{n^2} = \frac{1}{2} \left(\frac{1}{n_1^2} + \frac{1}{n_2^2} \right) \pm \sqrt{\frac{1}{4} \left(\frac{1}{n_1^2} - \frac{1}{n_2^2} \right)^2 + \left(\frac{G}{n_1^2 n_2^2} \right)^2}. \quad (4.9-24)$$

The corresponding polarization states can be represented by the Jones vectors

$$\mathbf{J}_{\pm} = \begin{pmatrix} \frac{1}{2} \left(\frac{1}{n_1^2} - \frac{1}{n_2^2} \right) \pm \sqrt{\frac{1}{4} \left(\frac{1}{n_1^2} - \frac{1}{n_2^2} \right)^2 + \left(\frac{G}{n_1^2 n_2^2} \right)^2} \\ - \frac{iG}{n_1^2 n_2^2} \end{pmatrix}. \quad (4.9-25)$$

These Jones vectors represent two elliptically polarized waves that are orthogonal to each other. Since the first component is real and the second component is pure imaginary, the principal axes of the polarization ellipses are parallel to the "unperturbed" polarizations \mathbf{D}_1 , \mathbf{D}_2 (see Fig. 4.10). The two senses of rotation are opposite to each other. The ellipticity (defined as the ratio of the lengths of the principal axes) of the polarization ellipse is given by

$$e = \frac{-G}{\frac{1}{2}(n_2^2 - n_1^2) \pm \sqrt{\frac{1}{4}(n_2^2 - n_1^2)^2 + G^2}}. \quad (4.9-26)$$

In the case of an isotropic medium ($n_1 = n_2 = \bar{n}$), the refractive indices of the normal modes (4.9-24) become

$$\frac{1}{n^2} = \frac{1}{\bar{n}^2} \pm \frac{G}{\bar{n}^4} = \frac{1}{\bar{n}^2} \left(1 \pm \frac{G}{\bar{n}^2} \right), \quad (4.9-27)$$

which agrees with Eq. (4.9-13). The corresponding polarization states (4.9-25)

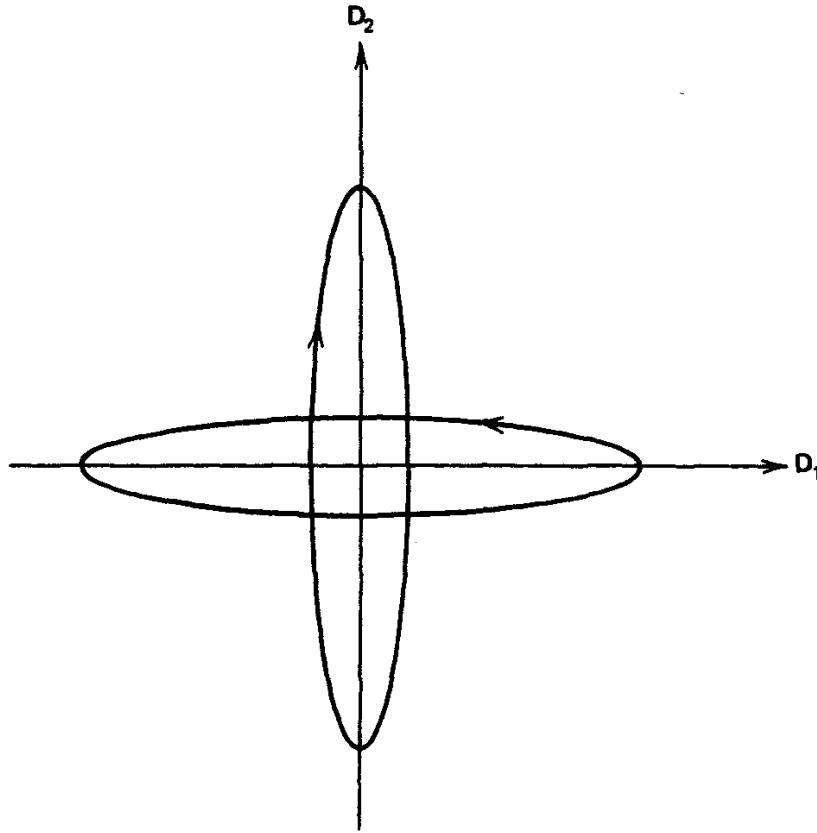


Figure 4.10. Polarization ellipses of the normal modes in the presence of both optical birefringence and rotatory power.

become

$$\mathbf{J}_{\pm} = \begin{pmatrix} \pm 1 \\ -i \end{pmatrix}, \quad (4.9-28)$$

which represent right and left circularly polarized light.

In the case of anisotropic media, G is usually very small compared with $n_2^2 - n_1^2$, and the ellipticity of the polarization ellipse is extremely small (i.e., $e \ll 1$), so that the waves are almost linearly polarized (see Fig. 4.10). As an example, for the propagation of a light beam perpendicular to the optic axes of a quartz crystal at $\lambda = 5100 \text{ \AA}$, the G value according to Szivessy and Munster is 6×10^{-5} , and the ellipticity is 2×10^{-3} [4].

The gyration tensor is symmetric and in general has six independent components. Some components may vanish due to the effect of crystal symmetry. For example, a crystal with a center of symmetry cannot be optically active (see Table 4.4). The arrays of nonvanishing components of the gyration tensors of the different crystal classes are shown in Table 4.4.

Table 4.4. Forms of the Gyration Tensor [g_{ij}]

Centrosymmetric ($\bar{1}$, $2/m$, mmm , $4/m$, $4/mmm$, $\bar{3}$, $\bar{3}m$, $6/m$, $6/mmm$, $m\bar{3}$, $m\bar{3}m$):

$$\begin{pmatrix} 0 & 0 & 0 \\ 0 & 0 & 0 \\ 0 & 0 & 0 \end{pmatrix}$$

Triclinic:

$$\begin{matrix} 1 \\ \begin{pmatrix} g_{11} & g_{12} & g_{13} \\ g_{12} & g_{22} & g_{23} \\ g_{13} & g_{23} & g_{33} \end{pmatrix} \end{matrix}$$

Monoclinic:

$$\begin{matrix} 2 \quad (2 \parallel x_2) & 2 \quad (2 \parallel x_3) \\ \begin{pmatrix} g_{11} & 0 & g_{13} \\ 0 & g_{22} & 0 \\ g_{13} & 0 & g_{33} \end{pmatrix} & \begin{pmatrix} g_{11} & g_{12} & 0 \\ g_{12} & g_{22} & 0 \\ 0 & 0 & g_{33} \end{pmatrix} \\ m \quad (m \perp x_2) & m \quad (m \perp x_3) \\ \begin{pmatrix} 0 & g_{12} & 0 \\ g_{12} & 0 & g_{23} \\ 0 & g_{23} & 0 \end{pmatrix} & \begin{pmatrix} 0 & 0 & g_{13} \\ 0 & 0 & g_{23} \\ g_{13} & g_{23} & 0 \end{pmatrix} \end{matrix}$$

Orthorhombic:

$$\begin{matrix} 222 & 2mm \\ \begin{pmatrix} g_{11} & 0 & 0 \\ 0 & g_{22} & 0 \\ 0 & 0 & g_{33} \end{pmatrix} & \begin{pmatrix} 0 & g_{12} & 0 \\ g_{12} & 0 & 0 \\ 0 & 0 & 0 \end{pmatrix} \end{matrix}$$

Tetragonal:

$$\begin{matrix} 4, 422 & \bar{4} & \bar{4}2m \quad (2 \parallel x_1) \\ \begin{pmatrix} g_{11} & 0 & 0 \\ 0 & g_{11} & 0 \\ 0 & 0 & g_{33} \end{pmatrix} & \begin{pmatrix} g_{11} & g_{12} & 0 \\ g_{12} & -g_{11} & 0 \\ 0 & 0 & 0 \end{pmatrix} & \begin{pmatrix} 0 & g_{12} & 0 \\ g_{12} & 0 & 0 \\ 0 & 0 & 0 \end{pmatrix} \end{matrix}$$

Trigonal and hexagonal:

$$\begin{matrix} 3, 32, 622 \\ \begin{pmatrix} g_{11} & 0 & 0 \\ 0 & g_{11} & 0 \\ 0 & 0 & g_{33} \end{pmatrix} \end{matrix}$$

Cubic:

$$\begin{matrix} 432, 23 \\ \begin{pmatrix} g_{11} & 0 & 0 \\ 0 & g_{11} & 0 \\ 0 & 0 & g_{11} \end{pmatrix} \end{matrix}$$

Table 4.4. (Continued).

 Isotropic (without center of symmetry):

$$\begin{pmatrix} g & 0 & 0 \\ 0 & g & 0 \\ 0 & 0 & g \end{pmatrix}$$

Others (4mm, $\bar{4}3m$, 3m, 6mm, $\bar{6}$, $\bar{6}m2$):

$$\begin{pmatrix} 0 & 0 & 0 \\ 0 & 0 & 0 \\ 0 & 0 & 0 \end{pmatrix}$$

4.10. FARADAY ROTATION

The Faraday effect is a property of transparent substances that causes a rotation of the plane of polarization with distance when the material is placed in a magnetic field, for light propagated along the magnetic field. More accurately, the rotation is proportional to the component of the magnetic field along the direction of propagation of the light. The gyration vector, defined by Eq. (4.9-6), is proportional to the external magnetic field:

$$\mathbf{G} = \gamma \mathbf{B}, \quad (4.10-1)$$

in which γ is the magnetogyration coefficient of the medium. In an optically active medium, the direction of rotation bears a fixed relation to the direction of propagation, so that if a beam of light is reflected back on itself, the net rotation is zero. In the Faraday effect, however, the rotation bears a fixed relation to the magnetic field \mathbf{B} , so that reflection back on itself doubles the rotation. The specific rotation (i.e., rotation per unit length) is often written

$$\rho = VB, \quad (4.10-2)$$

where V is a constant known as the Verdet constant.

The Faraday effect originates from the effect of the static magnetic field on the motion of electrons. In the presence of the electric field of the optical beam, the electrons are displaced from their equilibrium position. This motion coupled with the static magnetic field creates a lateral displacement of electrons due to the Lorentz force $\mathbf{v} \times \mathbf{B}$. As a result, the induced dipole moment involves a term that is proportional to $\mathbf{B} \times \mathbf{E}$. The material relation becomes

$$\mathbf{D} = \epsilon \mathbf{E} + i\epsilon_0 \gamma \mathbf{B} \times \mathbf{E}. \quad (4.10-3)$$

Table 4.5. Values of the Verdet Constant at $\lambda = 5893 \text{ \AA}$

Substance	T (°C)	V (deg/G · mm)
Water	20	2.18×10^{-5}
Fluorite		1.5×10^{-6}
Diamond		2.0×10^{-5}
Glass (crown)	18	2.68×10^{-5}
Glass (flint)		5.28×10^{-5}
Carbon disulfide (CS ₂)	20	7.05×10^{-5}
Phosphorus	33	2.21×10^{-4}
Sodium chloride		6.0×10^{-5}

The factor i accounts for the $\frac{1}{2}\pi$ phase lag between the velocity and the electric field. Faraday rotation has been observed in many solids, liquids, and even gases. A few values of the Verdet constant are given in Table 4.5.

4.11. COUPLED-MODE ANALYSIS OF WAVE PROPAGATION IN ANISOTROPIC MEDIA

The propagation of electromagnetic radiation in anisotropic media has been discussed in Sections 4.2 and 4.3 in terms of normal modes of propagation. These normal modes have well-defined polarization states and phase velocities, and are obtained by diagonalizing the transverse impermeability tensor η_t in Eq. (4.3-8). Any wave propagation in an anisotropic medium can be decomposed into a linear combination of these normal modes with constant amplitudes. Let \mathbf{e}_1 , \mathbf{e}_2 be vectors representing the direction of polarization of the field vector \mathbf{E} of the normal modes, and k_1 , k_2 be the corresponding wave numbers. A general wave propagation in the medium can thus be written

$$\mathbf{E} = A_1 \mathbf{e}_1 e^{i(\omega t - k_1 \zeta)} + A_2 \mathbf{e}_2 e^{i(\omega t - k_2 \zeta)}, \quad (4.11-1)$$

where A_1 , A_2 are constants and ζ is the distance along the direction of propagation \mathbf{s} (i.e., $\zeta = \mathbf{s} \cdot \mathbf{r}$).

Notice that these unit vectors \mathbf{e}_1 , \mathbf{e}_2 are not the same as those of the displacement field vectors and, in general, are not orthogonal to the direction of propagation i.e., $\mathbf{s} \cdot \mathbf{e}_{1,2} \neq 0$. However, \mathbf{e}_1 and \mathbf{e}_2 are almost perpendicular to \mathbf{s} in most crystals with moderate or small birefringence. Along some special direction of propagation, \mathbf{e}_1 , \mathbf{e}_2 are perpendicular to the direction of propagation regardless of the anisotropy of the medium.

In the event that there is an external (or internal) perturbation such as stress, magnetic field, electric field, or even the presence of optical activity, \mathbf{e}_1 and \mathbf{e}_2 are no longer the eigenvectors of propagation. The dielectric permittivity tensor in the presence of these perturbations can be written

$$\boldsymbol{\varepsilon}' = \boldsymbol{\varepsilon} + \Delta\boldsymbol{\varepsilon}, \quad (4.11-2)$$

where $\boldsymbol{\varepsilon}$ is the unperturbed part and $\Delta\boldsymbol{\varepsilon}$ is the change in dielectric permittivity tensor due to the perturbation. Once $\Delta\boldsymbol{\varepsilon}$ is known, the normal modes of propagation for the electric field vector \mathbf{E} can always be found by the method described in Section 4.2.

However, it is sometimes convenient and even advantageous to describe the wave propagation in terms of a linear combination of the unperturbed normal modes, especially when the perturbation is small (i.e., $\Delta\boldsymbol{\varepsilon} \ll \boldsymbol{\varepsilon}$). The mode amplitudes A_1 and A_2 are no longer constants, because $\mathbf{e}_1 e^{i(\omega t - k_1 \zeta)}$ and $\mathbf{e}_2 e^{i(\omega t - k_2 \zeta)}$ are, in general, not the normal modes in the presence of the perturbation $\Delta\boldsymbol{\varepsilon}$. We can however express the total field as

$$\mathbf{E}(\zeta, t) = A_1(\zeta) \mathbf{e}_1 e^{i(\omega t - k_1 \zeta)} + A_2(\zeta) \mathbf{e}_2 e^{i(\omega t - k_2 \zeta)}. \quad (4.11-3)$$

Since \mathbf{e}_1 , \mathbf{e}_2 , k_1 , and k_2 are known from the solution of the unperturbed case (i.e., $\Delta\boldsymbol{\varepsilon} = 0$), the field \mathbf{E} is uniquely specified if $A_1(\zeta)$ and $A_2(\zeta)$ are given. The ζ dependence of A_1 and A_2 is due to the presence of the dielectric perturbation $\Delta\boldsymbol{\varepsilon}$. We will next derive the differential equations for the mode amplitudes.

We start from the wave equation

$$\nabla \times (\nabla \times \mathbf{E}) - \omega^2 \mu (\boldsymbol{\varepsilon} + \Delta\boldsymbol{\varepsilon}) \mathbf{E} = 0. \quad (4.11-4)$$

Since the wave is propagating along the \mathbf{s} direction, the differential operator ∇ can be replaced by $\mathbf{s} \partial / \partial \zeta$. Thus the wave equation (4.11-4) becomes

$$\frac{\partial^2}{\partial \zeta^2} [\mathbf{E} - \mathbf{s}(\mathbf{s} \cdot \mathbf{E})] + \omega^2 \mu (\boldsymbol{\varepsilon} + \Delta\boldsymbol{\varepsilon}) \mathbf{E} = 0 \quad (4.11-5)$$

where we assume that the medium is homogeneous and the field vectors are plane waves. The quantity in the bracket in (4.11-5) is the transverse component of the electric field vector. We will now ignore the longitudinal component of the electric field and assume that $\mathbf{s} \cdot \mathbf{E} = 0$ (i.e., $\mathbf{s} \cdot \mathbf{e}_1 = \mathbf{s} \cdot \mathbf{e}_2 = 0$) and $\mathbf{e}_1 \cdot \mathbf{e}_2 = 0$.

Substituting Eq. (4.11-3) for \mathbf{E} in Eq. (4.11-5) and assuming $\mathbf{e}_1 e^{i(\omega t - k_1 \zeta)}$ and $\mathbf{e}_2 e^{i(\omega t - k_2 \zeta)}$ are eigenmodes of the unperturbed medium, we obtain

$$\begin{aligned} & \left[\frac{d^2 A_1}{d\zeta^2} - 2ik_1 \frac{dA_1}{d\zeta} + \omega^2 \mu \Delta \epsilon A_1 \right] \mathbf{e}_1 e^{i(\omega t - k_1 \zeta)} \\ & + \left[\frac{d^2 A_2}{d\zeta^2} - 2ik_2 \frac{dA_2}{d\zeta} + \omega^2 \mu \Delta \epsilon A_2 \right] \mathbf{e}_2 e^{i(\omega t - k_2 \zeta)} = 0, \end{aligned} \quad (4.11-6)$$

where we have used $k_\alpha^2 \mathbf{e}_\alpha - \omega^2 \mu \epsilon \mathbf{e}_\alpha = 0$, $\alpha = 1, 2$. We now assume that $A_{1,2}$ are slowly varying functions of ζ ,* so that $(d^2 A_\alpha / d\zeta^2) \ll k_\alpha dA_\alpha / d\zeta$ ($\alpha = 1, 2$) and scalar-multiply Eq. (4.11-6) by \mathbf{e}_1 and \mathbf{e}_2 one at a time. This leads to

$$\begin{aligned} \frac{dA_1}{d\zeta} &= -\frac{i\omega^2 \mu}{2k_1} \left[\Delta \epsilon_{11} A_1 + \Delta \epsilon_{12} A_2 e^{-i(k_2 - k_1)\zeta} \right], \\ \frac{dA_2}{d\zeta} &= -\frac{i\omega^2 \mu}{2k_2} \left[\Delta \epsilon_{21} A_1 e^{i(k_2 - k_1)\zeta} + \Delta \epsilon_{22} A_2 \right], \end{aligned} \quad (4.11-7)$$

where we have used the orthonormality of $\mathbf{e}_{1,2}$. The $\Delta \epsilon_{\alpha\beta}$ in Eq. (4.11-7) are the matrix elements of the perturbation tensor $\Delta \epsilon$ expressed in the coordinate system formed by \mathbf{e}_1 , \mathbf{e}_2 , and \mathbf{s} . The coupled-mode equations (4.11-7) can be solved uniquely, given an initial condition on the polarization state of the wave.

As an example in illustrating the use of Eq. (4.11-7), we consider the propagation of electromagnetic radiation in an optically active and birefringent medium. Let the effect of optical activity be a small perturbation $\Delta \epsilon$ given, according to Eq. (4.9-9), by

$$\Delta \epsilon = i\epsilon_0 [G]. \quad (4.11-8)$$

The matrix elements of this perturbation are given by

$$\begin{aligned} \Delta \epsilon_{11} &= \Delta \epsilon_{22} = 0, \\ \Delta \epsilon_{12} &= -i\epsilon_0 G, \\ \Delta \epsilon_{21} &= i\epsilon_0 G. \end{aligned} \quad (4.11-9)$$

*"Slow" means that the fractional change of A in one wavelength is $\ll 1$.

Let $A_1(0)$ and $A_2(0)$ be the mode amplitudes at $\zeta = 0$. The expressions for the mode amplitudes $A_1(\zeta)$ and $A_2(\zeta)$ at a general point ζ are obtained by solving (4.11-7) with $\Delta\epsilon_{\alpha\beta}$ given by (4.11-9). The results are

$$\begin{aligned} A_1(\zeta) &= e^{-\frac{1}{2}i\Delta k\zeta} \left[A_1(0) \left(\cos s\zeta + i\frac{\Delta k}{2s} \sin s\zeta \right) - \frac{\omega}{c} \frac{G}{2n_1s} A_2(0) \sin s\zeta \right], \\ A_2(\zeta) &= e^{\frac{1}{2}i\Delta k\zeta} \left[A_2(0) \left(\cos s\zeta - i\frac{\Delta k}{2s} \sin s\zeta \right) + \frac{\omega}{c} \frac{G}{2n_2s} A_1(0) \sin s\zeta \right], \end{aligned} \quad (4.11-10)$$

where n_1, n_2 are the indices of refraction of modes (i.e., $k_{1,2} = n_{1,2}\omega/c$) and

$$\Delta k = k_2 - k_1 = \frac{\omega}{c} (n_2 - n_1), \quad (4.11-11)$$

$$s^2 = \left(\frac{\Delta k}{2} \right)^2 + \left(\frac{\omega}{c} \right)^2 \frac{G^2}{4n_1n_2}. \quad (4.11-12)$$

Equation (4.11-10) shows how the perturbation $\Delta\epsilon_{12}$ causes energy exchange between modes 1 and 2. We note that when the optical activity disappears ($G = 0$), $\Delta\epsilon_{12}$ vanishes according to Eq. (4.11-9), and we have $A_1(\zeta) = A_1(0)$ and $A_2(\zeta) = A_2(0)$. The polarization state of the wave is therefore a function of position. Let $\chi(0)$ be the complex-number representation of the initial polarization, and $\chi(\zeta)$ be the polarization state at ζ . Then, from Eq. (4.11-10),

$$\chi(\zeta) = \frac{A_2 e^{-ik_2\zeta}}{A_1 e^{-ik_1\zeta}} = \frac{\chi(0) \left(\cos s\zeta - i\frac{\Delta k}{2s} \sin s\zeta \right) + \frac{\omega}{c} \frac{G}{2n_2s} \sin s\zeta}{\cos s\zeta + i\frac{\Delta k}{2s} \sin s\zeta - \chi(0) \frac{\omega}{c} \frac{G}{2n_1s} \sin s\zeta}. \quad (4.11-13)$$

From this expression, we notice that the polarization state is a periodic function of ζ with period π/s . In the special case when $n_2 = n_1$ (i.e., $\Delta k = 0$), the expression (4.11-13) for the polarization state becomes

$$\chi(\zeta) = \frac{\chi(0) \cos \rho\zeta + \sin \rho\zeta}{\cos \rho\zeta - \chi(0) \sin \rho\zeta}, \quad (4.11-14)$$

where $\rho = (\omega/c)G/2n$ is the rotatory power (4.9-14). If the initial polarization state represents a linearly polarized wave at an azimuth angle ψ_0 [i.e., $\chi(0) = \tan \psi_0$], the polarization state at ζ , according to Eq. (4.11-14), is $\chi(\zeta) = \tan(\psi_0 + \rho\zeta)$, which presents a linearly polarized light at an azimuth angle $\psi_0 + \rho\zeta$. In other words, the plane of polarization has been rotated by an angle $\rho\zeta$. This agrees with the discussion in Section 4.9.

We can also derive the normal modes of propagation in the presence of the perturbation using the coupled-mode formalism. In doing this we need to define a Jones vector of the electric field vector to represent the polarization state of the wave as

$$\mathbf{E} = \begin{pmatrix} E_1(\zeta) \\ E_2(\zeta) \end{pmatrix} \equiv \begin{pmatrix} A_1(\zeta) e^{-ik_1\zeta} \\ A_2(\zeta) e^{-ik_2\zeta} \end{pmatrix}.$$

From Eq. (4.11-7) it follows simply that \mathbf{E} obeys the equation

$$\frac{d}{d\zeta} \mathbf{E} = -iK_e \mathbf{E}. \quad (4.11-15)$$

The matrix K_e is called the wave matrix and is given by

$$K_e = \frac{\omega}{c} \begin{pmatrix} n_1 + \frac{1}{2n_1\epsilon_0} \Delta\epsilon_{11} & \frac{1}{2n_1\epsilon_0} \Delta\epsilon_{12} \\ \frac{1}{2n_2\epsilon_0} \Delta\epsilon_{21} & n_2 + \frac{1}{2n_2\epsilon_0} \Delta\epsilon_{22} \end{pmatrix}. \quad (4.11-16)$$

For the case of optical activity, $\Delta\epsilon_{\alpha\beta}$ is given by Eq. (4.11-9) and the wave matrix becomes

$$K_e = \frac{\omega}{c} \begin{pmatrix} n_1 & -\frac{iG}{2n_1} \\ \frac{iG}{2n_2} & n_2 \end{pmatrix} \quad (4.11-17)$$

A normal mode of propagation must, by definition, have a unique propagation constant as well as a unique polarization state. In other words, a normal mode can be written as

$$\mathbf{E} = \mathbf{e} e^{-ik\zeta}. \quad (4.11-18)$$

Substituting Eq. (4.11-18) for \mathbf{E} in Eq. (4.11-15) converts the latter differential equation to algebraic equations which can be written compactly as

$$K_e \mathbf{e} = k \mathbf{e}. \quad (4.11-19)$$

This is a simple eigenvalue equation. It follows that the polarization vectors of the normal modes are the eigenvectors of the wave matrix K_e with the eigenvalues corresponding to the propagation wave numbers. Let $k = (\omega/c)n$, with n to be determined; then the secular equation resulting from Eqs. (4.11-17) and (4.11-19) is

$$\begin{pmatrix} n_1 - n & -\frac{iG}{2n_1} \\ \frac{iG}{2n_2} & n_2 - n \end{pmatrix} = 0, \quad (4.11-20)$$

or equivalently

$$(n_1 - n)(n_2 - n) = \frac{G^2}{4n_1 n_2}. \quad (4.11-21)$$

The roots of Eq. (4.11-21) are the refractive indices of the normal modes and are given by

$$n = \frac{n_1 + n_2}{2} \pm \sqrt{\left(\frac{n_2 - n_1}{2}\right)^2 + \frac{G^2}{4n_1 n_2}}. \quad (4.11-22)$$

The wave numbers of the normal modes are thus given by

$$k = \frac{k_1 + k_2}{2} \pm \sqrt{\left(\frac{\Delta k}{2}\right)^2 + \left(\frac{\omega}{c}\right)^2 \frac{G^2}{4n_1 n_2}}, \quad (4.11-23)$$

where Δk is given by Eq. (4.11-11).

The corresponding eigenvectors for the polarization vectors of the normal modes are obtained by using Eq. (4.11-22) in Eq. (4.11-19):

$$\mathbf{e} = \begin{pmatrix} n_2 - n \\ -\frac{iG}{2n_2} \end{pmatrix}, \quad (4.11-24)$$

where n is given by Eq. (4.11-22). These expressions agree with Eq. (4.9-25), provided $n_2 = n_1$. It is important to realize that the polarization states for electric field vector \mathbf{E} and the displacement vector \mathbf{D} are, in general, different in anisotropic media. The results (4.11-23) and (4.11-24) for the electric field vector are obtained by ignoring its longitudinal component, whereas the results (4.9-24) and (4.9-25) are for the displacement vector \mathbf{D} . In the next section, we will derive an equation of motion for the evolution of the displacement vector \mathbf{D} .

4.12. EQUATION OF MOTION FOR THE POLARIZATION STATE

In the last section, we derived a matrix equation (4.11-15) for the evolution of the electric field vector \mathbf{E} by neglecting the longitudinal component of the electric field. We now will derive an equation of motion for the displacement field vector \mathbf{D} , which is always perpendicular to the direction of propagation. We start from the wave equation (1.4-2) and use Eq. (4.3-3) for \mathbf{E} . Thus, the wave equation becomes

$$\nabla \times (\nabla \times \eta \mathbf{D}) - \left(\frac{\omega}{c}\right)^2 \mathbf{D} = 0. \quad (4.12-1)$$

Since we are studying the polarization state of waves propagating along the \mathbf{s} direction, the differential operator ∇ can be replaced by $\mathbf{s} \partial / \partial \zeta$. This causes the wave equation (4.12-1) to take the form

$$\mathbf{s} \times \left(\mathbf{s} \times \frac{\partial^2}{\partial \zeta^2} \eta \mathbf{D} \right) - \left(\frac{\omega}{c}\right)^2 \mathbf{D} = 0. \quad (4.12-2)$$

We will now use the same coordinate introduced in Section 4.3, in which \mathbf{s} is the direction of the third axis. In this coordinate system, the wave equation becomes

$$\eta_t \frac{\partial^2}{\partial \zeta^2} \mathbf{D} = - \left(\frac{\omega}{c}\right)^2 \mathbf{D}, \quad (4.12-3)$$

where η_t is the 2×2 transverse impermeability tensor defined by Eq. (4.3-7). We now define a 2×2 matrix N such that

$$N^2 \eta_t = 1. \quad (4.12-4)$$

By multiplying Eq. (4.12-3) on the left by N^2 and using Eq. (4.12-4), we

obtain

$$\frac{\partial^2}{\partial \zeta^2} \mathbf{D} = - \left(\frac{\omega}{c} \right)^2 N^2 \mathbf{D}. \quad (4.12-5)$$

This differential equation is equivalent to the following two linear differential equations:

$$\frac{\partial}{\partial \zeta} \mathbf{D} = -i \frac{\omega}{c} N \mathbf{D}, \quad (4.12-6)$$

$$\frac{\partial}{\partial \zeta} \mathbf{D} = i \frac{\omega}{c} N \mathbf{D}. \quad (4.12-7)$$

The matrix N is called the refractive-index matrix and will reduce to the refractive index n for the case of isotropic medium. Since we use the time factor $e^{i\omega t}$, Eq. (4.12-6) corresponds to wave propagation in the $+\zeta$ direction, whereas Eq. (4.12-7) corresponds to the $-\zeta$ direction. Equation (4.12-6) will now be used to describe the evolution of the polarization state in a medium described by a refractive-index matrix N .

We consider the case when there is an external (or internal) perturbation such as stress, magnetic field, electric field, or optical activity. Let 1 and 2 denote the axes of normal-mode propagation in the absence of these perturbations. The dielectric impermeability tensor η_i can be written

$$\eta_i = \begin{pmatrix} \frac{1}{n_1^2} & 0 \\ 0 & \frac{1}{n_2^2} \end{pmatrix} + \Delta\eta, \quad (4.12-8)$$

where $\Delta\eta$ represents the perturbation. If $\Delta\eta$ is small, an explicit expression for N can be obtained directly from the definition and Eq. (4.12-8). The result is

$$N = \begin{pmatrix} n_1 - \frac{1}{2} n_1^3 \Delta\eta_{11} & -\frac{n_1^2 n_2^2}{n_1 + n_2} \Delta\eta_{12} \\ -\frac{n_1^2 n_2^2}{n_1 + n_2} \Delta\eta_{21} & n_2 - \frac{1}{2} n_2^3 \Delta\eta_{22} \end{pmatrix}. \quad (4.12-9)$$

Since η_i is a Hermitian tensor, so is the refractive-index matrix N . Once N is

known, Eq. (4.12-6) can be solved uniquely, provided an initial condition on the polarization state is given. The normal modes of propagation can also be found by diagonalizing the refractive-index matrix in the presence of perturbation.

We will now solve for the normal modes of propagation in an optically active medium. Let $\Delta\eta$ represent the effect of optical activity. According to Eq. (4.9-20), $\Delta\eta$ is given by

$$\Delta\eta = -i\eta[G]\eta. \quad (4.12-10)$$

The matrix elements of $\Delta\eta$ are given by

$$\begin{aligned} \Delta\eta_{11} = \Delta\eta_{22} &= 0, \\ \Delta\eta_{12} &= \frac{iG}{n_1^2 n_2^2}, \\ \Delta\eta_{21} &= -\frac{iG}{n_1^2 n_2^2}. \end{aligned} \quad (4.12-11)$$

The refractive-index matrix N can thus be written

$$N = \begin{pmatrix} n_1 & \frac{-iG}{n_1 + n_2} \\ \frac{iG}{n_1 + n_2} & n_2 \end{pmatrix}. \quad (4.12-12)$$

A normal mode of propagation, by definition, must have a well-defined polarization state and a well-defined wave number. In other words, a normal mode can be written

$$\mathbf{D} = \mathbf{d}e^{-ik\xi}. \quad (4.12-13)$$

We now substitute (4.12-13) for \mathbf{D} into the equation of motion

$$\frac{\partial}{\partial \xi} \mathbf{D} = -i\frac{\omega}{c} N \mathbf{D}, \quad (4.12-14)$$

and it becomes

$$N\mathbf{d} = n\mathbf{d}, \quad (4.12-15)$$

where we have used $k = (\omega/c)n$.

Thus we find that the polarization state \mathbf{d} of a normal mode must be an eigenvector of the refractive-index matrix N . The eigenvalue of the refractive-index matrix gives the refractive index of propagation for the normal modes. The secular equation for n , according to Eqs. (4.12-15) and (4.12-12), is

$$(n - n_1)(n - n_2) = \frac{G^2}{(n_1 + n_2)^2}. \quad (4.12-16)$$

The roots of Eq. (4.12-16) are given by

$$n = \frac{n_1 + n_2}{2} \pm \sqrt{\left(\frac{n_2 - n_1}{2}\right)^2 + \frac{G^2}{(n_1 + n_2)^2}}. \quad (4.12-17)$$

The corresponding Jones vectors for the polarization state of the normal modes are

$$\mathbf{J}_{\pm} = \begin{pmatrix} \frac{n_2 - n_1}{2} \pm \sqrt{\left(\frac{n_2 - n_1}{2}\right)^2 + \frac{G^2}{(n_1 + n_2)^2}} \\ -\frac{iG}{n_1 + n_2} \end{pmatrix}. \quad (4.12-18)$$

This result is identical to the result (4.9-25) obtained in Section 4.9.

PROBLEMS

4.1. *Eigenpolarization.*

- (a) Derive the expression for the eigenpolarization of the electric field vector (4.2-9), (4.2-11).
- (b) Use the relation $\mathbf{D} = \epsilon\mathbf{E}$ and obtain an expression for the corresponding eigenpolarization of the displacement vector \mathbf{D} .
- (c) Let n_1 and n_2 be the solution of the Fresnel equation (4.2-10), and \mathbf{E}_1 , \mathbf{E}_2 , \mathbf{D}_1 , \mathbf{D}_2 the corresponding eigen-field-vectors. Evaluate $\mathbf{E}_1 \cdot \mathbf{E}_2$ and $\mathbf{D}_1 \cdot \mathbf{D}_2$, and show that \mathbf{D}_1 and \mathbf{D}_2 are always mutually orthogonal, whereas \mathbf{E}_1 and \mathbf{E}_2 are only mutually orthogonal in a uniaxial or an isotropic medium.
- (d) Show that $\mathbf{E}_1 \cdot \mathbf{D}_2 = 0$ and $\mathbf{E}_2 \cdot \mathbf{D}_1 = 0$.

4.2. *Fresnel equation.*

- (a) Derive the Fresnel equation (4.2-10) directly from Eq. (4.2-8).
 (b) Show that the Fresnel equation (4.2-10) is a quadratic equation in n^2 , that is,

$$An^4 + Bn^2 + C = 0,$$

and obtain expressions for A , B , and C .

- (c) Show that $B^2 - 4AC > 0$ for the case of pure dielectrics with real and positive ϵ_x , ϵ_y , ϵ_z .
 (d) Derive Eq. (4.5-1) from the equation (4.2-8) for the case of uniaxial crystals.
 (e) Show that in an isotropic medium, Eq. (4.2-8) reduces to

$$k^2 - \frac{\epsilon}{\epsilon_0} \left(\frac{\omega}{c} \right)^2 = 0.$$

4.3. *Energy velocity and group velocity.* In the derivation of the equality (4.4-14) we assume that \mathbf{E} and \mathbf{H} are real field vectors. In fact, Eqs. (4.4-4) and (4.4-5) are for complex field representations. Therefore, the Poynting vector \mathbf{S} and the energy density U must be given by the complex expressions (1.3-14) and (1.3-15). Show that the equality (4.4-14) also holds for complex field amplitudes \mathbf{E} and \mathbf{H} .

4.4. *Group velocity and phase velocity.*

- (a) Derive an expression for the group velocity of the extraordinary wave in a uniaxial crystal as a function of the polar angle θ of the propagation vector.
 (b) Derive an expression for the angle α between the phase velocity and the group velocity. This angle is also the angle between the field vectors \mathbf{E} and \mathbf{D} .
 (c) Show that $\alpha = 0$ when $\theta = 0, \frac{1}{2}\pi$. Find the angle θ at which α is maximized, and obtain an expression for α_{\max} . Calculate this angle α_{\max} for quartz with $n_o = 1.544$, $n_e = 1.553$.
 (d) Show that for $n_o = n_e$ the maximum angular separation α_{\max} occurs at $\theta = 45^\circ$, and show that α_{\max} is proportional to $|n_o - n_e|$.

4.5. *Light propagation in biaxial crystals.* A biaxial crystal is characterized by its three principal indices $n_1 < n_2 < n_3$.

- (a) Show that the intersection of the normal surface with any coordinate plane consists of an ellipse and a circle.

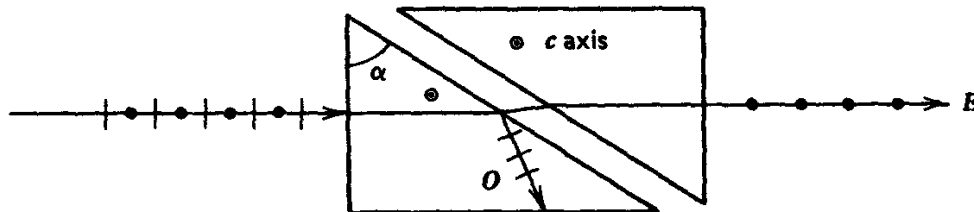
- (b) Show that only the ellipse and the circle in the xz plane intersect. These points of intersection define the optic axes of the crystal.
- (c) Find the points of intersection of the ellipse and the circle in the xz plane, and derive the expression (4.8-4) for the angle between one of the optic axes and the z axis. Show that this angle approaches zero when $n_1 = n_2$. Calculate this angle for mica with $n_1 = 1.552$, $n_2 = 1.582$, and $n_3 = 1.588$.
- (d) The aperture angle of conical refraction can be estimated by the angle between the normal vectors of the ellipse and the circle at the point of intersection. Derive Eq. (4.8-8).
- (e) Show that this cone angle vanishes when $n_1 = n_2$ (or $n_2 = n_3$). Calculate this cone angle for mica.
- (f) Show that a rotation of an angle $\pm\chi$ in the $\xi'\zeta'$ plane will transform the cone (4.8-9) into

$$(\zeta'' \pm \frac{1}{2}\xi'' \tan 2\chi)^2 + \eta^2 = (\frac{1}{2}\xi'' \tan 2\chi)^2$$

The intersection of this cone with the plane $\xi'' = \text{constant}$ is a circle.

4.6. *Prism polarizers.* The phenomenon of double refraction in an anisotropic crystal may be utilized to produce polarized light. Consider a light beam incident on a plane boundary from the inside of a calcite crystal ($n_o = 1.658$, $n_e = 1.486$). Suppose that the c axis of the crystal is normal to the plane of incidence.

- (a) Find the range of the internal angle of incidence such that the ordinary wave is totally reflected. The transmitted wave is thus completely polarized.
- (b) *Glan prism.* Use the basic principle described in (a) to design a calcite Glan prism shown in the following:



Find the range of the apex angle α .

- 4.7. *Quarter-wave plate.* A linearly polarized electromagnetic wave at $\lambda = 6328 \text{ \AA}$ is incident normally at $x = 0$ on the yz face of a quartz crystal plate (x -cut) so that it propagates along the x axis. Suppose the wave is polarized initially so that it has equal components along y and z .

- (a) What is the state of polarization at the plane x where

$$(k_z - k_y)x = \frac{1}{2}\pi$$

Plot the position of the electric field vector in this plane at times $t = 0, \pi/6\omega, \pi/3\omega, \pi/2\omega, 2\pi/3\omega, 5\pi/6\omega$.

- (b) A plate which satisfies the condition in (a) is known as a quarter-wave plate because the difference in the phase shift for the two orthogonal polarization states is a quarter of 2π . Find the thickness of a quartz quarter-wave plate at $\lambda = 6328 \text{ \AA}$.
- (c) *Half-wave Plate.* What is the state of polarization at the plane x , where

$$\frac{2\pi}{\lambda}(n_e - n_o)x = \pi$$

- 4.8. *Dichroic polarizers.* These are materials whose absorption properties and reflection properties are strongly dependent on the direction of vibration of the electric field. If the two absorption coefficients are very different, a thin sheet of the material will be sufficient to transform unpolarized light into a nearly linearly polarized light.

- (a) Let α_1, α_2 be the two absorption coefficients corresponding to two independent polarizations. Derive an expression for the ratio of the two transmitted components as a function of the thickness of the medium.
- (b) Show that, strictly speaking, the normal modes of propagation are no longer linearly polarized in the presence of absorption.

- 4.9. *Hermitian dielectric tensor.* Consider the addition of a small anti-symmetric term in the dielectric tensor, i.e.,

$$D_i = (\epsilon_{ij} - i\gamma_{ij})E_j, \quad (\text{A})$$

where γ_{ij} is the antisymmetric (i.e., $\gamma_{ij} = -\gamma_{ji}$) part, which is not to have an ohmic, dissipative character as in the complex dielectric

constant of a metal. Rather, it is to be conservative, which means that γ_{ij} must not contribute to the electric energy density $U_e = \frac{1}{2}(\mathbf{D} \cdot \mathbf{E})$ as computed from Maxwell's equations.

(a) Evaluate $\mathbf{D} \cdot \mathbf{E}$ and show that

$$\mathbf{D} \cdot \mathbf{E} = \epsilon_{ij} E_i E_j,$$

provided γ_{ij} is an antisymmetric tensor, that is, $\gamma_{ij} = -\gamma_{ji}$.

(b) Show that Eq. (A) can be written

$$D_i = \epsilon_{ij} E_j + i(\boldsymbol{\gamma} \times \mathbf{E})_i$$

where $\boldsymbol{\gamma}$ is a vector with components

$$\gamma_1 = -\gamma_{23} = \gamma_{32},$$

$$\gamma_2 = -\gamma_{31} = \gamma_{13},$$

$$\gamma_3 = -\gamma_{12} = \gamma_{21}.$$

(c) Show that the inverse of a Hermitian tensor is also a Hermitian tensor, and show that

$$E_i = \left\{ \left(\frac{1}{\epsilon} \right)_{ij} - i \left(\frac{1}{\epsilon} \right)_{ik} \gamma_{kl} \left(\frac{1}{\epsilon} \right)_{lj} \right\} D_j. \quad (\text{B})$$

(d) Show that Eq. (B) can be written

$$E_i = \left(\frac{1}{\epsilon} \right)_{ij} D_j - i(\mathbf{A} \times \mathbf{D})_i, \quad (\text{C})$$

and show that the components of the vector \mathbf{A} in the principal coordinate system are given by

$$A_1 = \frac{1}{\epsilon_{11}\epsilon_{22}\epsilon_{33}} \gamma_1 \epsilon_{11},$$

$$A_2 = \frac{1}{\epsilon_{11}\epsilon_{22}\epsilon_{33}} \gamma_2 \epsilon_{22},$$

$$A_3 = \frac{1}{\epsilon_{11}\epsilon_{22}\epsilon_{33}} \gamma_3 \epsilon_{33}.$$

- (e) Show that the wave equation (4.9-18) can be written

$$\mathbf{s} \times \left[\mathbf{s} \times \left(\frac{1}{\epsilon} - i\mathbf{A} \times \right) \mathbf{D} \right] = -\frac{1}{n^2} \mathbf{D}. \quad (\text{D})$$

- (f) Let the vector \mathbf{A} be decomposed into

$$\mathbf{A} = (\mathbf{A} \cdot \mathbf{s})\mathbf{s} + \mathbf{A}_\perp,$$

where \mathbf{A}_\perp is the component of \mathbf{A} perpendicular to the direction of propagation. Show from the wave equation (D) that the optical activity is independent of \mathbf{A}_\perp . In other words, only $\mathbf{A} \cdot \mathbf{s}$ affects the optical rotation.

- (g) In an anisotropic medium the vector \mathbf{A} is given by

$$\mathbf{A} = \alpha \mathbf{s},$$

where α is a symmetric matrix. Show that the optical activity parameter is given by

$$A = \alpha_{ij} s_i s_j.$$

- (h) By following the argument of (g) and assuming that $\mathbf{s} \cdot \mathbf{E} = 0$, show that only the component of \mathbf{G} along the direction of propagation will affect the optical activity. In an anisotropic medium, $\mathbf{G} = g\mathbf{s}$, where g is the gyration tensor. Show that the parameter G in Eq. (4.9-10) is $\mathbf{G} \cdot \mathbf{s}$, and derive Eq. (4.9-15).

4.10. *Displacement eigenmodes.* The wave equation (4.2-5) can be written

$$\mathbf{s} \times \left[\mathbf{s} \times \frac{\epsilon_0}{\epsilon} \mathbf{D} \right] = -\frac{1}{n^2} \mathbf{D},$$

where \mathbf{s} is the unit vector in the direction of propagation. Let $\mathbf{D}_1, \mathbf{D}_2$ be the normalized eigenvectors with eigenvalues $1/n_1^2, 1/n_2^2$, respectively. We assume that ϵ_0/ϵ is a Hermitian tensor.

(a) Show that

$$\left(\frac{\epsilon_0}{\epsilon}\right)_{11} \equiv \mathbf{D}_1^* \cdot \frac{\epsilon_0}{\epsilon} \mathbf{D}_1 \equiv \frac{1}{n_1^2},$$

$$\left(\frac{\epsilon_0}{\epsilon}\right)_{22} \equiv \mathbf{D}_2^* \cdot \frac{\epsilon_0}{\epsilon} \mathbf{D}_2 \equiv \frac{1}{n_2^2},$$

$$\left(\frac{\epsilon_0}{\epsilon}\right)_{12} \equiv \mathbf{D}_1^* \cdot \frac{\epsilon_0}{\epsilon} \mathbf{D}_2 = 0.$$

(b) Show that

$$\mathbf{D}_1^* \cdot \mathbf{D}_2 = 0.$$

4.11. *Displacement eigenmodes in gyrotropic media.* Start from Eq. (4.9-20).

(a) Derive Eqs. (4.9-22) and (4.9-24).

(b) Show that the Jones vectors (4.9-25) satisfy the vector equation (4.9-22).

(c) Show that the Jones vectors (4.9-25) are orthogonal, that is, $\mathbf{J}_+^* \cdot \mathbf{J}_- = 0$.

(d) Let e_{\pm} be the ellipticities of the two eigenmodes. Show that $e_+ e_- = -1$.

4.12. *Conservation of power flow.*

(a) Show that the power flow in the direction of propagation is given by

$$\mathbf{S} \cdot \mathbf{s} = \frac{1}{2} \frac{c}{\epsilon_0} \left[\frac{1}{n_1^3} |\mathbf{D}_1|^2 + \frac{1}{n_2^3} |\mathbf{D}_2|^2 \right],$$

where \mathbf{D}_1 and \mathbf{D}_2 are the amplitudes of the displacement fields of the eigenmodes and n_1, n_2 are the corresponding refractive indices.

(b) Use the relation (4.2-14) to show that

$$\mathbf{S} \cdot \mathbf{s} = \frac{1}{2\mu c} [n_1 |\mathbf{A}_1|^2 + n_2 |\mathbf{A}_2|^2],$$

where $\mathbf{A}_1, \mathbf{A}_2$ are the transverse parts of the electric field vectors.

- (c) Show that the coupled equations (4.11-7) are consistent with the conservation of power flow, i.e.,

$$\frac{d}{d\xi} [n_1|A_1|^2 + n_2|A_2|^2] = 0.$$

- (d) Show that the results (4.11-10) are consistent with (c).

REFERENCES

1. M. Born and E. Wolf, *Principles of Optics*, Pergamon Press, New York, 1965.
2. G. R. Fowles, *Introduction to Modern Optics*, Holt, Rinehart and Winston, New York, 1968.
3. E. U. Condon, "Theories of optical rotatory power," *Rev. Mod. Phys.* **9**, 432 (1937); *Handbook of Physics*, E. U. Condon and H. Odishaw, Eds., (McGraw-Hill, New York, 1958), pp. 6-12.
4. G. Szivessy and C. Munster, "Lattice optics of active crystals," *Ann. Phys. (Leipzig)* **20**, 703-36 (1934).

5

Jones Calculus and its Application to Birefringent Optical Systems

Many sophisticated birefringent optical systems, such as wide-angle electro-optic modulators [1], Lyot filters [2–5] and Šolc filters [6, 7] involve the passage of light through a train of polarizers and retardation plates. The effect of each individual element, either polarizer or retardation plate, on the polarization state of the transmitted light can be easily pictured without the aid of any matrix algebra. However, when an optical system consists of many such elements, each oriented at a different azimuth angle, the calculation of the overall transmission becomes complicated and is greatly facilitated by a systematic approach. The Jones calculus, invented in 1940 by R. C. Jones [8], is a powerful 2×2 -matrix method in which the state of polarization is represented by a two-component vector (see Section 3.4) while each optical element is represented by a 2×2 matrix. The overall matrix for the whole system is obtained by multiplying all the matrices, and the polarization state of the transmitted light is computed by multiplying the vector representing the input beam by the overall matrix. We will first derive the mathematical formulation of the Jones matrix method, and then apply it to some birefringent filters.

5.1. JONES MATRIX FORMULATION

We have shown in the previous chapter that light propagation in a birefringent crystal consists of a linear superposition of two eigenwaves. These eigenwaves have well-defined phase velocities and directions of polarization. The birefringent crystals may be either uniaxial or biaxial. However, most commonly used materials such as calcite and quartz are uniaxial. In a uniaxial crystal, these eigenwaves are the ordinary and the extraordinary wave. The directions of polarization for these eigenwaves are mutually

orthogonal and are called the “slow” and “fast” axes of the crystal for that direction of propagation. Retardation plates are usually cut in such a way that the c axis lies in the plane of the plate surfaces. Thus the propagation direction of normally incident light is perpendicular to the c axis.

Retardation plates (also called wave plates) and phase shifters are polarization-state converters, or transformers. The polarization state of a light beam can be converted to any other polarization state by means of a suitable retardation plate. In formulating the Jones matrix method, we assume that there is no reflection of light from either surface of the plate and the light is totally transmitted through the plate surfaces. In practice, there is reflection, though most retardation plates are coated so as to reduce the surface reflection loss. The Fresnel reflections at the plate surfaces not only decrease the transmitted intensity, but also affect the fine structure of the spectral transmittance because of multiple-reflection interference (see Section 5.5). Referring to Fig. 5.1, we consider an incident light beam with polarization state described by the Jones vector

$$\mathbf{V} = \begin{pmatrix} V_x \\ V_y \end{pmatrix}, \quad (5.1-1)$$

where V_x and V_y are two complex numbers. The x and y axes are fixed laboratory axes. To determine how the light propagates in the retardation

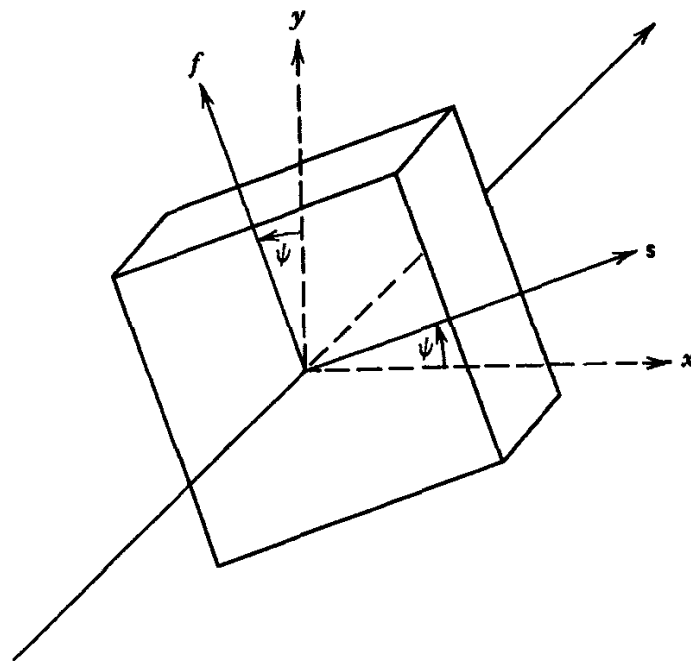


Figure 5.1. A retardation plate with azimuth angle ψ .

plate, we need to decompose the light into a linear combination of the “fast” and “slow” eigenwaves of the crystal. This is done by the coordinate transformation

$$\begin{pmatrix} V_s \\ V_f \end{pmatrix} = \begin{pmatrix} \cos \psi & \sin \psi \\ -\sin \psi & \cos \psi \end{pmatrix} \begin{pmatrix} V_x \\ V_y \end{pmatrix} \equiv R(\psi) \begin{pmatrix} V_x \\ V_y \end{pmatrix}. \quad (5.1-2)$$

V_s is the slow component of the polarization vector V , whereas V_f is the fast component. The “slow” and “fast” axes are fixed in the crystal. These two components are eigenwaves of the retardation plate and will propagate with their own phase velocities and polarizations. Because of the difference in phase velocity, one component is retarded relative to the other. This retardation changes the polarization state of the emerging beam.

Let n_s and n_f be the refractive indices for the “slow” and “fast” components, respectively. The polarization state of the emerging beam in the crystal sf coordinate system is given by

$$\begin{pmatrix} V'_s \\ V'_f \end{pmatrix} = \begin{pmatrix} \exp\left(-in_s \frac{\omega}{c} l\right) & 0 \\ 0 & \exp\left(-in_f \frac{\omega}{c} l\right) \end{pmatrix} \begin{pmatrix} V_s \\ V_f \end{pmatrix} \quad (5.1-3)$$

where l is the thickness of the plate and ω is the frequency of the light beam. The phase retardation is given by the difference of the exponents in (5.1-3) and is equal to

$$\Gamma = (n_s - n_f) \frac{\omega l}{c}. \quad (5.1-4)$$

Notice that the phase retardation Γ is a measure of the relative change in phase, not the absolute change. The birefringence of a typical crystal retardation plate is small, that is, $|n_s - n_f| \ll n_s, n_f$. Consequently, the absolute change in phase caused by the plate may be hundreds of times greater than the phase retardation. Let ϕ be the mean absolute phase change,

$$\phi = \frac{1}{2}(n_s + n_f) \frac{\omega l}{c}. \quad (5.1-5)$$

Then Eq. (5.1-3) can be written in terms of ϕ and Γ as

$$\begin{pmatrix} V'_s \\ V'_f \end{pmatrix} = e^{-i\phi} \begin{pmatrix} e^{-i\Gamma/2} & 0 \\ 0 & e^{i\Gamma/2} \end{pmatrix} \begin{pmatrix} V_s \\ V_f \end{pmatrix}. \quad (5.1-6)$$

The Jones vector of the polarization state of the emerging beam in the xy coordinate is given by transforming back from the crystal sf coordinate system:

$$\begin{pmatrix} V'_x \\ V'_y \end{pmatrix} = \begin{pmatrix} \cos \psi & -\sin \psi \\ \sin \psi & \cos \psi \end{pmatrix} \begin{pmatrix} V'_s \\ V'_f \end{pmatrix}. \quad (5.1-7)$$

By combining Eqs. (5.1-2), (5.1-6), and (5.1-7), we can write the transformation due to the retardation plate as

$$\begin{pmatrix} V'_x \\ V'_y \end{pmatrix} = R(-\psi)W_0R(\psi)\begin{pmatrix} V_x \\ V_y \end{pmatrix}, \quad (5.1-8)$$

where $R(\psi)$ is the rotation matrix and W_0 is the Jones matrix for the retardation plate. These are given, respectively, by

$$R(\psi) = \begin{pmatrix} \cos \psi & \sin \psi \\ -\sin \psi & \cos \psi \end{pmatrix} \quad (5.1-9a)$$

and

$$W_0 = e^{-i\phi} \begin{pmatrix} e^{-i\Gamma/2} & 0 \\ 0 & e^{i\Gamma/2} \end{pmatrix}. \quad (5.1-9b)$$

The phase factor $e^{-i\phi}$ can be neglected if interference effects are not important, or not observable. A retardation plate is characterized by its phase retardation Γ and its azimuth angle ψ , and is represented by the product of three matrices (5.1-8):

$$W = R(-\psi)W_0R(\psi). \quad (5.1-10)$$

Note that the Jones matrix of a wave plate is a unitary matrix, that is,

$$W^\dagger W = 1,$$

where the dagger † means Hermitian conjugate. The passage of a polarized light beam through a wave plate is mathematically described as a unitary transformation. Many physical properties are invariant under unitary transformations; these include the orthogonal relation between the Jones vectors and the magnitude of the Jones vectors. Thus if the polarization states of two beams are mutually orthogonal, they will remain orthogonal after passing through an arbitrary wave plate.

The Jones matrix of an ideal homogeneous linear sheet polarizer oriented with its transmission axis parallel to the laboratory x axis is

$$P_0 = e^{-i\phi} \begin{pmatrix} 1 & 0 \\ 0 & 0 \end{pmatrix}, \quad (5.1-11)$$

where ϕ is the absolute phase accumulated due to the finite optical thickness of the polarizer. The Jones matrix of a polarizer rotated by an angle ψ about z is given by

$$P = R(-\psi)P_0R(\psi). \quad (5.1-12)$$

Thus, if we neglect the absolute phase ϕ , the Jones matrix representations of the polarizers transmitting light with electric field vectors parallel to the x and y axes, respectively, are given by

$$P_x = \begin{pmatrix} 1 & 0 \\ 0 & 0 \end{pmatrix} \quad \text{and} \quad P_y = \begin{pmatrix} 0 & 0 \\ 0 & 1 \end{pmatrix}.$$

To find the effect of a train of retardation plates and polarizers on the polarization state of a polarized light, we write down the Jones vector of the incident beam, and then write down the Jones matrices of the various elements. The Jones vector of the emerging beam is obtained by carrying out the matrix multiplication in sequence.

5.1.1. Example: A Half-Wave Retardation Plate

A half-wave plate has a phase retardation of $\Gamma = \pi$. According, to Eq. (5.1-4) an x -cut* (or y -cut) uniaxial crystal will act as a half-wave plate provided the thickness is $t = \lambda/2(n_e - n_o)$. We will determine the effect of a half-wave plate on the polarization state of a transmitted light beam. The azimuth angle of the wave plate is taken as 45° , and the incident beam as vertically polarized. The Jones vector for the incident beam can be written as

$$\mathbf{V} = \begin{pmatrix} 0 \\ 1 \end{pmatrix}, \quad (5.1-13)$$

and the Jones matrix for the half-wave plate is obtained by using Eqs.

*A crystal plate is called x -cut if its faces are perpendicular to the principal x axis.

(5.1-9) and (5.1-10):

$$W = \frac{1}{\sqrt{2}} \begin{pmatrix} 1 & -1 \\ 1 & 1 \end{pmatrix} \begin{pmatrix} -i & 0 \\ 0 & i \end{pmatrix} \frac{1}{\sqrt{2}} \begin{pmatrix} 1 & 1 \\ -1 & 1 \end{pmatrix} = \begin{pmatrix} 0 & -i \\ -i & 0 \end{pmatrix}. \quad (5.1-14)$$

The Jones vector for the emerging beam is obtained by multiplying Eqs. (5.1-14) and (5.1-13); the result is

$$\mathbf{V}' = \begin{pmatrix} -i \\ 0 \end{pmatrix} = -i \begin{pmatrix} 1 \\ 0 \end{pmatrix}. \quad (5.1-15)$$

This is horizontally polarized light. The effect of the half-wave plate is to rotate the polarization by 90° . It can be shown that for a general azimuth angle ψ , the half-wave plate will rotate the polarization by an angle 2ψ (see Problem 5.1). In other words, linearly polarized light remains linearly polarized, except that the plane of polarization is rotated by an angle of 2ψ .

When the incident light is circularly polarized, a half-wave plate will convert right-hand circularly polarized light into left-hand circularly polarized light and vice versa, regardless of the azimuth angle. The proof is left as an exercise (see Problem 5.1). Figure 5.2 illustrates the effect of a half-wave plate.

5.1.2. Example: A Quarter-Wave Plate

A quarter-wave plate has a phase retardation of $\Gamma = \frac{1}{2}\pi$. If the plate is made of an x -cut (or y -cut) uniaxially anisotropic crystal, the thickness is $t = \lambda/4(n_e - n_o)$ (or odd multiples thereof). Suppose again that the azimuth angle of the plate is $\psi = 45^\circ$ and the incident beam is vertically polarized. The Jones vector for the incident beam is given again by Eq. (5.1-13). The Jones matrix for this quarter-wave plate, according to Eq. (5.1-10), is

$$\begin{aligned} W &= \frac{1}{\sqrt{2}} \begin{pmatrix} 1 & -1 \\ 1 & 1 \end{pmatrix} \begin{pmatrix} e^{-i\pi/4} & 0 \\ 0 & e^{i\pi/4} \end{pmatrix} \frac{1}{\sqrt{2}} \begin{pmatrix} 1 & 1 \\ -1 & 1 \end{pmatrix} \\ &= \frac{1}{\sqrt{2}} \begin{pmatrix} 1 & -i \\ -i & 1 \end{pmatrix}. \end{aligned} \quad (5.1-16)$$

The Jones vector for the emerging beam is obtained by multiplying Eqs. (5.1-16) and (5.1-13) and is given by

$$\mathbf{V}' = \frac{1}{\sqrt{2}} \begin{pmatrix} -i \\ 1 \end{pmatrix} = \frac{-i}{\sqrt{2}} \begin{pmatrix} 1 \\ i \end{pmatrix}. \quad (5.1-17)$$

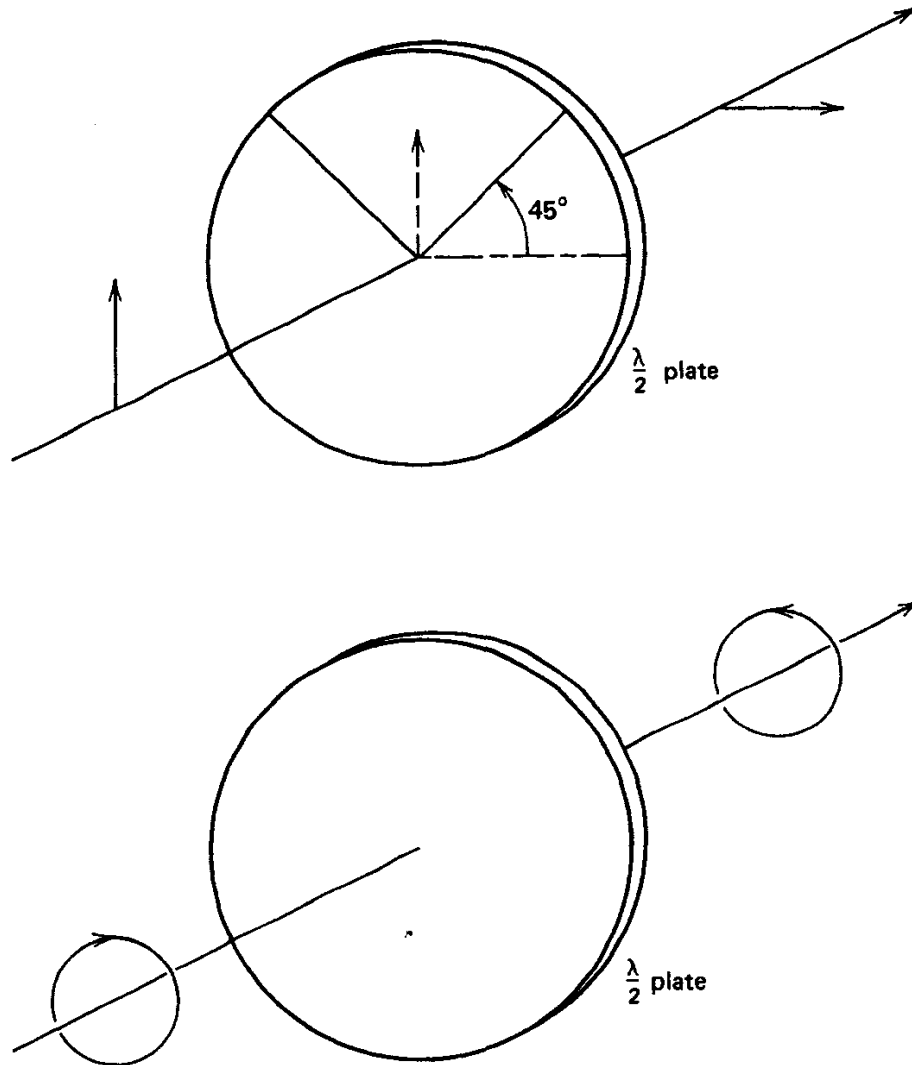


Figure 5.2. The effect of a half-wave plate on the polarization state of a beam.

This is left-hand circularly polarized light. The effect of a 45°-oriented quarter-wave plate is to convert vertically polarized light into left-hand circularly polarized light. If the incident beam is horizontally polarized, the emerging beam will be right-hand circularly polarized. The effect of this quarter-wave plate is illustrated in Fig. 5.3.

5.2. INTENSITY TRANSMISSION

So far our development of the Jones calculus was concerned with the polarization state of the light beam. In many cases, we need to determine the transmitted intensity. A narrowband filter, for example, transmits radiation only in a small spectral regime and rejects (or absorbs) radiation at other wavelengths. To change the intensity of the transmitted beam, an

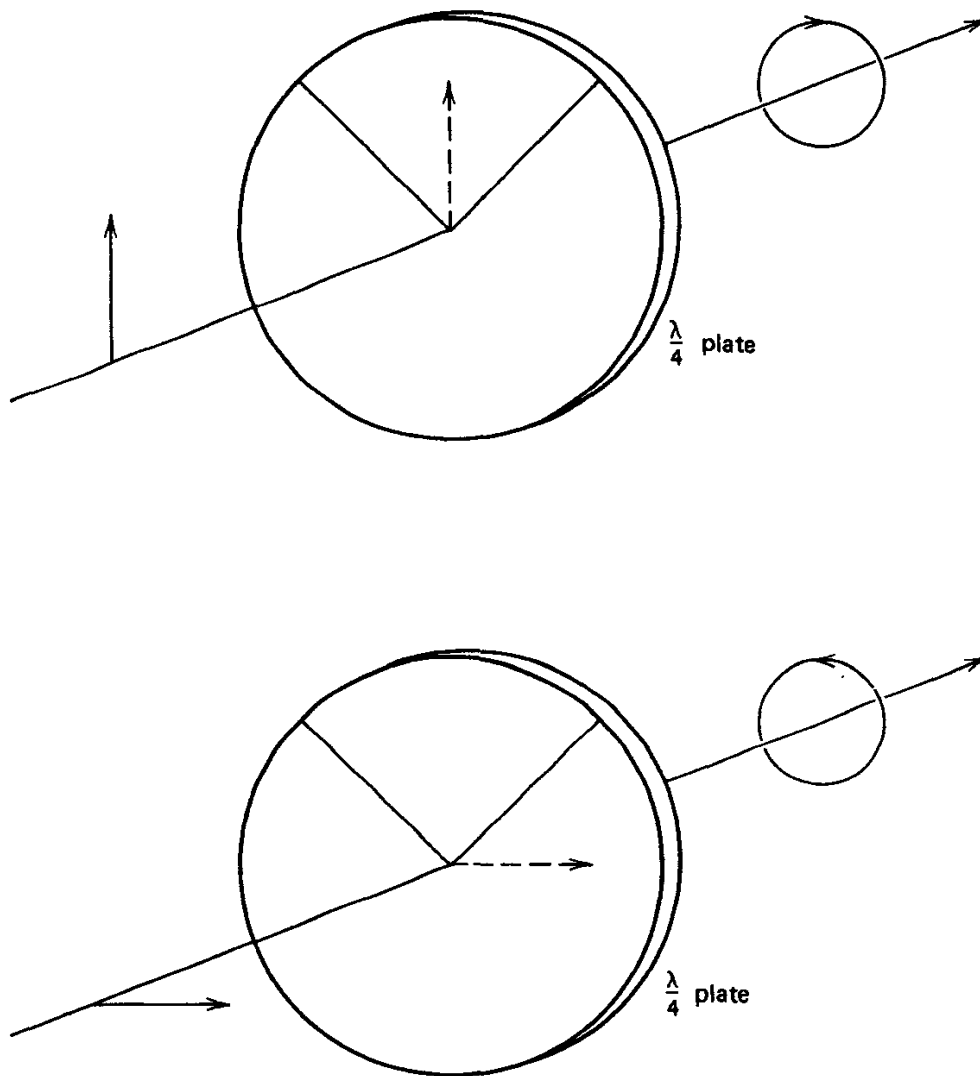


Figure 5.3. The effect of a quarter-wave plate on the polarization state of a linearly polarized beam.

analyzer is usually required. An analyzer is basically a polarizer. It is called an analyzer simply because of its location in the optical system. In most birefringent optical systems, a polarizer is placed in front of the system in order to “prepare” a polarized light. A second polarizer (analyzer) is placed at the output to analyze the polarization state of the emerging beam. Because the phase retardation of each wave plate is wavelength-dependent, the polarization state of the emerging beam depends on the wavelength of the light. A polarizer at the rear will cause the overall transmitted intensity to be wavelength-dependent.

The Jones vector representation of a light beam contains information about not only the polarization state but also the intensity of light. Let us now consider the light beam after it passes through the polarizer. Its electric

vector can be written as a Jones vector

$$\mathbf{E} = \begin{pmatrix} E_x \\ E_y \end{pmatrix}. \quad (5.2-1)$$

The intensity is calculated as follows:

$$I = \mathbf{E}^\dagger \cdot \mathbf{E} = |E_x|^2 + |E_y|^2. \quad (5.2-2)$$

where the dagger indicates the Hermitian conjugate. If the Jones vector of the emerging beam after it passes through the analyzer is written as

$$\mathbf{E}' = \begin{pmatrix} E'_x \\ E'_y \end{pmatrix}, \quad (5.2-3)$$

the transmissivity of the birefringent optical system is calculated as

$$T = \frac{|E'_x|^2 + |E'_y|^2}{|E_x|^2 + |E_y|^2}. \quad (5.2-4)$$

5.2.1. Example: A Birefringent Plate Sandwiched between Parallel Polarizers

Referring to Fig. 5.4, we consider a birefringent plate sandwiched between a pair of parallel polarizers. The plate is oriented so that the “slow” and “fast” axes are at 45° with respect to the polarizer. Let the birefringence be $n_e - n_o$ and the plate thickness be d . The phase retardation is then given by

$$\Gamma = 2\pi(n_e - n_o)\frac{d}{\lambda}, \quad (5.2-5)$$

and the corresponding Jones matrix is, according to Eq. (5.1-10),

$$W = \begin{pmatrix} \cos\frac{1}{2}\Gamma & -i\sin\frac{1}{2}\Gamma \\ -i\sin\frac{1}{2}\Gamma & \cos\frac{1}{2}\Gamma \end{pmatrix}. \quad (5.2-6)$$

Let the incident beam be unpolarized, so that after it passes through the front polarizer, the electric field vector can be represented by the following

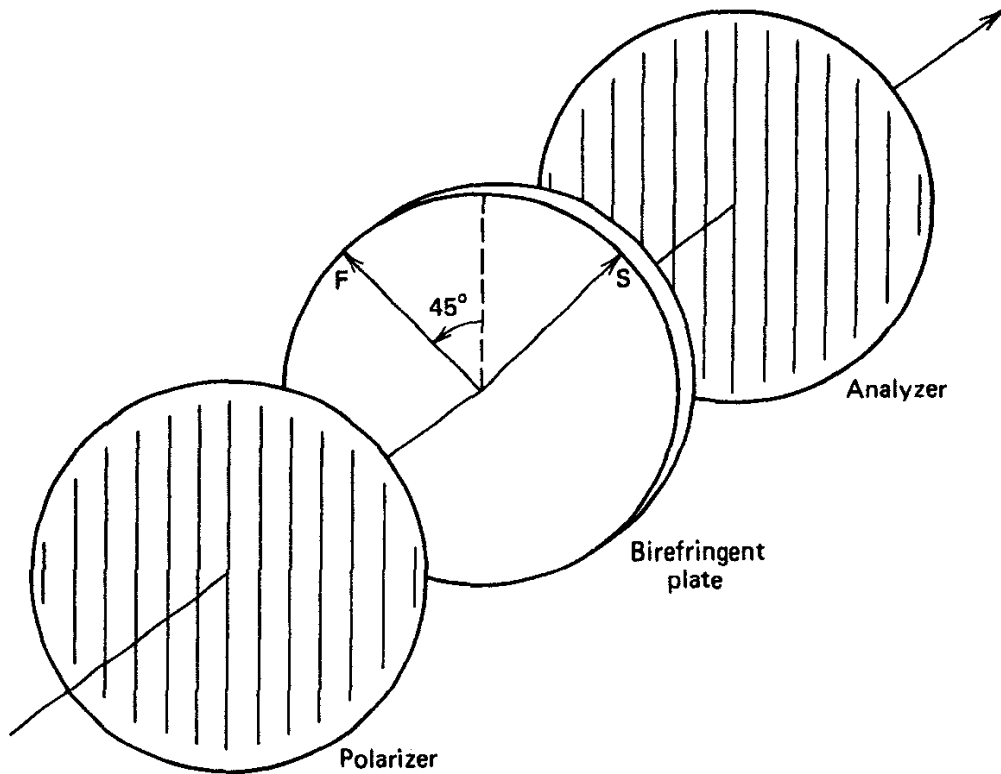


Figure 5.4. A birefringent plate sandwiched between a pair of parallel polarizers.

Jones vector:

$$\frac{1}{\sqrt{2}} \begin{pmatrix} 0 \\ 1 \end{pmatrix}, \quad (5.2-7)$$

where we assume that the intensity of the incident beam is unity and only half of the intensity passes through the polarizer. The Jones vector representation of the electric field vector of the transmitted beam is obtained as follows:

$$\begin{aligned} \mathbf{E}' &= \begin{pmatrix} 0 & 0 \\ 0 & 1 \end{pmatrix} \begin{pmatrix} \cos \frac{1}{2}\Gamma & -i \sin \frac{1}{2}\Gamma \\ -i \sin \frac{1}{2}\Gamma & \cos \frac{1}{2}\Gamma \end{pmatrix} \frac{1}{\sqrt{2}} \begin{pmatrix} 0 \\ 1 \end{pmatrix} \\ &= \frac{1}{\sqrt{2}} \begin{pmatrix} 0 \\ \cos \frac{1}{2}\Gamma \end{pmatrix}. \end{aligned} \quad (5.2-8)$$

The transmitted beam is vertically (y) polarized with an intensity given by

$$I = \frac{1}{2} \cos^2 \frac{1}{2}\Gamma = \frac{1}{2} \cos^2 \left[\frac{\pi(n_e - n_o)d}{\lambda} \right]. \quad (5.2-9)$$

It can be seen from Eq. (5.2-9) that the transmitted intensity is a sinusoidal function of the wave number and peaks at $\lambda = (n_e - n_o)d$, $(n_e - n_o)d/2$, $(n_e - n_o)d/3, \dots$. The wave-number separation between transmission maxima increases with decreasing plate thickness.

5.2.2. Example: A Birefringent Plate Sandwiched between a Pair of Crossed Polarizers

If we rotate the analyzer shown in Fig. 5.4 by 90° , then the input and output polarizers are crossed. The transmitted beam for this case is obtained as follows:

$$\begin{aligned} E' &= \begin{pmatrix} 1 & 0 \\ 0 & 0 \end{pmatrix} \begin{pmatrix} \cos \frac{1}{2}\Gamma & -i \sin \frac{1}{2}\Gamma \\ -i \sin \frac{1}{2}\Gamma & \cos \frac{1}{2}\Gamma \end{pmatrix} \frac{1}{\sqrt{2}} \begin{pmatrix} 0 \\ 1 \end{pmatrix} \\ &= \frac{-i}{\sqrt{2}} \begin{pmatrix} \sin \frac{1}{2}\Gamma \\ 0 \end{pmatrix}. \end{aligned} \quad (5.2-10)$$

The transmitted beam is horizontally (x) polarized with an intensity given by

$$I = \frac{1}{2} \sin^2 \frac{1}{2}\Gamma = \frac{1}{2} \sin^2 \left[\frac{\pi(n_e - n_o)d}{\lambda} \right]. \quad (5.2-11)$$

This is again a sinusoidal function of the wave number. The transmission spectrum consists of a series of maxima at $\lambda = 2(n_e - n_o)d$, $2(n_e - n_o)d/3, \dots$. These wavelengths correspond to phase retardations of π , 3π , $5\pi, \dots$, that is, when the wave plate becomes a half-wave plate or odd integral multiple of a half-wave plate.

5.3. POLARIZATION INTERFERENCE FILTERS

Spectral filters can be based on the interference of polarized light. These filters play an important role in many optical systems where filters of extremely narrow bandwidth with wide angular fields or tuning capability are required. In solar physics, for example, the distribution of hydrogen may be measured by photographing the solar corona in the light of the H_α ($\lambda = 6563 \text{ \AA}$) line. In view of the large amount of light present at neighboring wavelengths, a filter of extremely narrow bandwidth ($\sim 1 \text{ \AA}$) is required if reasonable discrimination is to be attained. Such filters consist of birefrin-

Table 5.1. The Folded Šolc Filter

Element	Azimuth
Front polarizer	0°
Plate 1	ρ
Plate 2	$-\rho$
Plate 3	ρ
\vdots	\vdots
Plate N	$(-1)^{N-1}\rho$
Rear polarizer	90°

gent crystal plates (wave plates) and polarizers. The two basic versions of these birefringent filters are Lyot–Öhman filters [2–5, 12] and Šolc filters [6, 7]. They are based on the interference of polarized light, which requires a phase retardation between the components of the light polarized parallel to the fast and slow axes of the crystal when radiation passes through it. Since the phase retardation introduced by a waveplate is proportional to the birefringence of the crystal, it is desirable to have crystals with large birefringence ($n_e - n_o$) for filter construction. Currently, the most commonly used materials are quartz, calcite, and $(\text{NH}_4)\text{H}_2\text{PO}_4$ (ADP).

The basic principle of the Lyot–Öhman filter is very simple and is outlined in Problem 5.5.

The Jones calculus developed in the previous two sections will now be applied to study the transmission characteristics of the Šolc filters. Šolc filters, named after their inventor [6, 7], are composed of a pile of identical birefringent plates each oriented at a prescribed azimuth angle. The azimuth angle of each plate is measured from the transmission axis of the front polarizer. The whole stack of birefringent plates is placed between a pair of polarizers.

5.3.1. Folded Šolc Filters

There are two basic types of Šolc filters: folded and fan filters. The folded Šolc filter works between crossed polarizers. The azimuth angles of the individual plates are prescribed in Table 5.1. The geometrical arrangement of a six-plate Šolc filter is sketched in Fig. 5-5. As described in Table 5.1, the front polarizer has its transmission axis parallel to the x axis; and the rear polarizer parallel to the y -axis. The overall Jones matrix for these N plates is

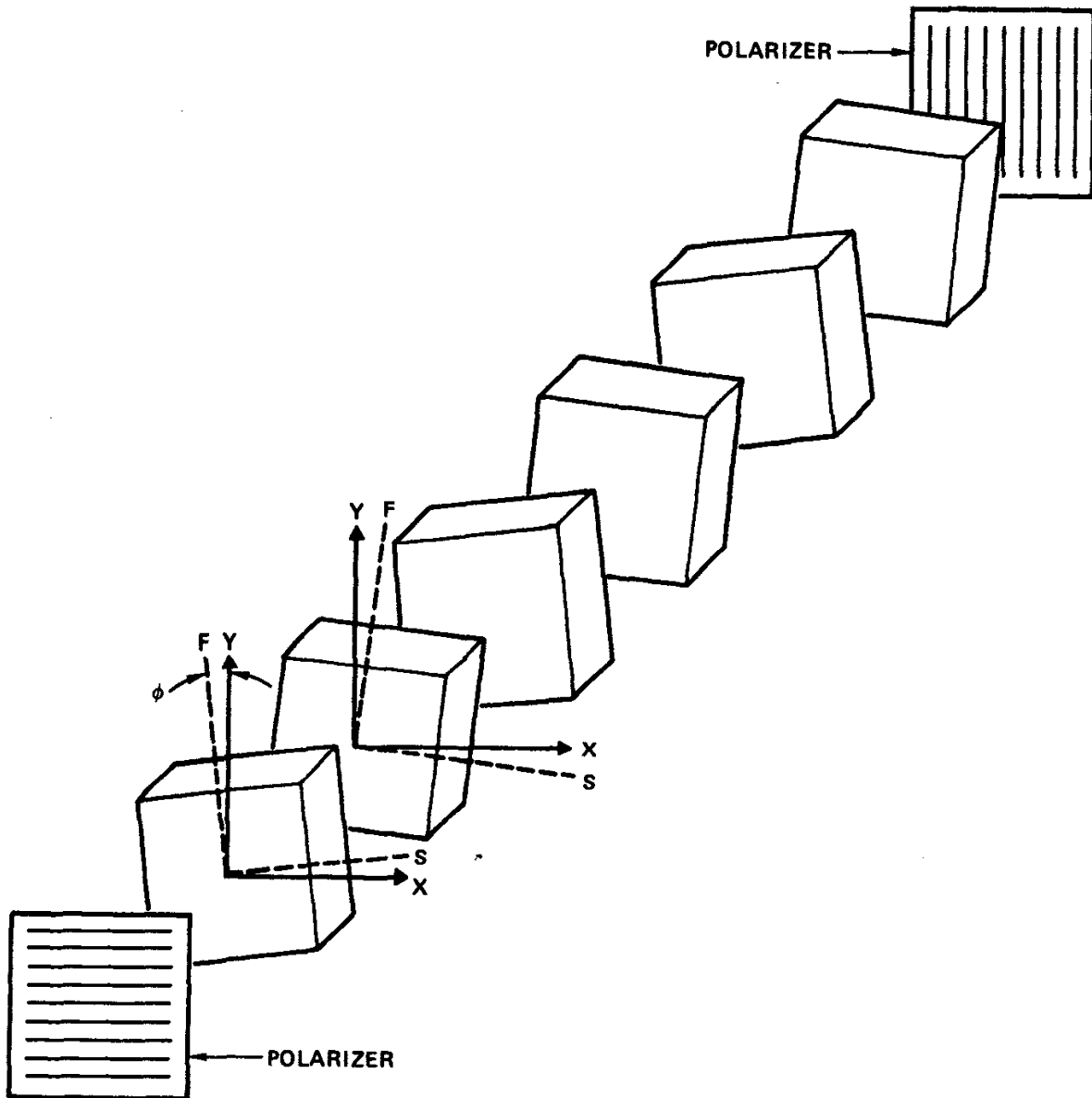


Figure 5.5. A six-stage folded Solc filter.

given by

$$M = [R(\rho)W_0R(-\rho)R(-\rho)W_0R(\rho)]^m, \quad (5.3-1)$$

where we assume that the number of plates is an even number, $N = 2m$. Substituting Eq. (5.1-9) into Eq. (5.3-1) and carrying out the matrix multiplication results in

$$M = \begin{pmatrix} A & B \\ C & D \end{pmatrix}^m \quad (5.3-2)$$

with

$$\begin{aligned}
 A &= (\cos \frac{1}{2}\Gamma - i \cos 2\rho \sin \frac{1}{2}\Gamma)^2 + \sin^2 2\rho \sin^2 \frac{1}{2}\Gamma, \\
 B &= \sin 4\rho \sin^2 \frac{1}{2}\Gamma, \\
 C &= -B, \\
 D &= (\cos \frac{1}{2}\Gamma + i \cos 2\rho \sin \frac{1}{2}\Gamma)^2 + \sin^2 2\rho \sin^2 \frac{1}{2}\Gamma,
 \end{aligned}
 \tag{5.3-3}$$

where Γ is the phase retardation of each plate. Note that this matrix is unimodular (i.e., $AD - BC = 1$), since all the matrices in Eq. (5.3-1) are unimodular. Equation (5.3-2) can be simplified by using Chebyshev's identity [9] to

$$\begin{aligned}
 &\begin{pmatrix} A & B \\ C & D \end{pmatrix}^m \\
 &= \begin{pmatrix} \frac{A \sin mK\Lambda - \sin(m-1)K\Lambda}{\sin K\Lambda} & B \frac{\sin mK\Lambda}{\sin k\Lambda} \\ C \frac{\sin mK\Lambda}{\sin K\Lambda} & \frac{D \sin mK\Lambda - \sin(m-1)K\Lambda}{\sin K\Lambda} \end{pmatrix}
 \end{aligned}
 \tag{5.3-4}$$

with

$$K\Lambda = \cos^{-1}[\frac{1}{2}(A + D)]. \tag{5.3-5}$$

We use the notation $K\Lambda$ for the purpose of comparing this result with that obtained from coupled-mode theory (see Section 6.4).

The incident wave and the emerging wave are related by

$$\begin{pmatrix} E'_x \\ E'_y \end{pmatrix} = P_y M P_x \begin{pmatrix} E_x \\ E_y \end{pmatrix}. \tag{5.3-6}$$

The emerging beam is polarized in the y direction, with a field amplitude given by

$$E'_y = M_{21} E_x \tag{5.3-7}$$

If the incident light is linearly polarized in the x direction, the transmissivity

of this filter is

$$T = |M_{21}|^2. \quad (5.3-8)$$

From Eqs. (5.3-2) and (5.3-3), we obtain

$$T = \left| \sin 4\rho \sin^2 \frac{1}{2} \Gamma \frac{\sin mK\Lambda}{\sin K\Lambda} \right|^2 \quad (5.3-9)$$

with

$$\cos K\Lambda = 1 - 2 \cos^2 2\rho \sin^2 \frac{1}{2} \Gamma. \quad (5.3-10)$$

The transmissivity T is often expressed in terms of a new variable χ , defined by

$$K\Lambda = \pi - 2\chi. \quad (5.3-11)$$

In terms of this new variable χ , the transmissivity is

$$T = \left| \tan 2\rho \cos \chi \frac{\sin N\chi}{\sin \chi} \right|^2 \quad (5.3-12)$$

with

$$\cos \chi = \cos 2\rho \sin \frac{1}{2} \Gamma. \quad (5.3-13)$$

According to Eqs. (5.3-12) and (5.3-13), transmissivity becomes $T = \sin^2 2N\rho$ when the phase retardation of each plate is $\Gamma = \pi, 3\pi, 5\pi, \dots$, that is, when each plate becomes a half-wave plate. This transmissivity is 100% if the azimuth angle ρ is such that

$$\rho = \frac{\pi}{4N}. \quad (5.3-14)$$

The transmission under these conditions can be easily understood if we examine the polarization state after passing through each plate within the Solc filter. We recall that in passing through a half-wave ($\Gamma = \pi, 3\pi, \dots$) plate, the azimuthal angle between the polarization vector and the fast (or slow) axis of the crystal changes sign. Past the front polarizer, the light is linearly polarized in the x direction (azimuth $\psi = 0$). Since the first plate is at the azimuth angle ρ , the emerging beam after passage through the first plate is linearly polarized at $\psi = 2\rho$. The second plate is oriented at the

azimuth angle $-\rho$, making an angle of 3ρ with respect to the polarization direction of light incident on it. The polarization direction at its output face will be rotated by 6ρ and oriented at the azimuth angle -4ρ (see Fig. 5.6). The plates are oriented successively at $+\rho, -\rho, +\rho, -\rho, \dots$, while the polarization direction at the exit of the plates assumes the values $2\rho, -4\rho, 6\rho, -8\rho, \dots$. The final azimuthal angle after N plates is thus $2N\rho$. If this final azimuth angle is 90° (i.e., $2N\rho = \frac{1}{2}\pi$), then the light passes through the rear polarizer without any loss of intensity. Light at other wavelengths, where the plates are not half-wave plates, does not experience a 90° rotation of polarization and suffers loss at the rear polarizer.

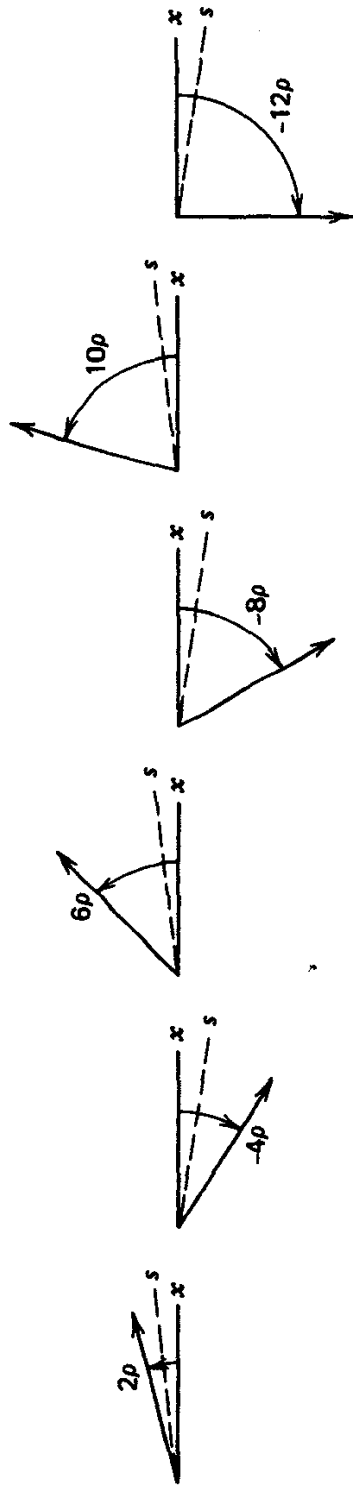
The Šolc filter can also be viewed as a periodic medium as far as wave propagation is concerned. The alternating azimuth angles of the crystal axes constitute a periodic perturbation to the propagation of both eigenwaves. This perturbation couples the fast and slow eigenwaves. Because these waves propagate at different phase velocities, complete exchange of electromagnetic energy is possible only when the perturbation is periodic so as to maintain the relations necessary to cause continuous power transfer from the fast to the slow wave and vice versa. This is the first manifestation of the principle of phase matching by a periodic perturbation, to which we will return in subsequent chapters. The basic physical explanation is as follows: If power is to be transferred gradually with distance from mode A to mode B by a static perturbation, then it is necessary that both waves travel with the same phase velocity. If the phase velocities are not equal, the incident wave A gets progressively out of phase with the wave B into which it couples. This limits the total fraction of power that can be exchanged. This situation can be avoided if the sign of the perturbation is reversed whenever the phase mismatch (between the coupled field and the field into which it couples) is equal to π . This reverses the sign of the coupled power, and thus maintains the proper phase for continuous power transfer. A coupled mode theory of the folded Šolc filter is given in Section 6.5.

The transmission characteristics around the peak and its sidelobes in a Šolc filter are interesting and deserve some investigation. Assume that each plate is characterized by refractive indices n_e and n_o and thickness d . Let λ_ν denote the wavelength at which the phase retardation is $(2\nu + 1)\pi$. The phase retardation at a general wavelength is

$$\Gamma = \frac{2\pi}{\lambda}(n_e - n_o)d. \quad (5.3-15)$$

If λ is slightly away from λ_ν [i.e., $(\lambda - \lambda_\nu) \ll \lambda_\nu$], Γ can be approximately given by

$$\Gamma = (2\nu + 1)\pi + \Delta\Gamma$$



Birefringent plate	1	2	3	4	5	6
Azimuth angle	7.5°	-7.5°	7.5°	-7.5°	7.5°	-7.5°
Polarization azimuth	15°	-30°	45°	-60°	75°	-90°

Figure 5.6. Polarization state within a folded six-stage Solc filter. The dashed lines indicate the directions of the slow axis. The arrows indicate the direction of polarization.

where

$$\Delta\Gamma = -\frac{(2\nu + 1)\pi}{\lambda_\nu}(\lambda - \lambda_\nu). \quad (5.3-16)$$

We assume further that the azimuth angle of the plate obeys the condition (5.3-14), and N is much larger than 1. Under these conditions, the trigonometric functions in Eq. (5.3-13) can be expanded to yield

$$\chi \approx \frac{\pi}{2N} \left[1 + \left(\frac{N\Delta\Gamma}{\pi} \right)^2 \right]^{1/2}. \quad (5.3-17)$$

Substituting χ into Eq. (5.3-12), we obtain

$$T = \left(\frac{\sin\left(\frac{1}{2}\pi\sqrt{1 + (N\Delta\Gamma/\pi)^2}\right)}{\sqrt{1 + (N\Delta\Gamma/\pi)^2}} \right)^2. \quad (5.3-18)$$

This approximate expression for the transmissivity is valid provided $N \gg 1$ and $(\lambda - \lambda_\nu) \ll \lambda_\nu$. From (5.3-18), the full bandwidth at half maximum (FWHM) of the main transmission peak is given approximately by $\Delta\Gamma_{1/2} = 1.60\pi/N$, which in terms of the wavelength is

$$\Delta\lambda_{1/2} \approx 1.60 \left[\frac{\lambda_\nu}{(2\nu + 1)N} \right]. \quad (5.3-19)$$

Thus, to build a narrowband Solc filter with a bandwidth of 1 Å to observe the H_α line ($\lambda_0 = 6563$ Å) requires the number of half-wave ($\nu = 0$) plates be approximately 10^4 . The transmission spectrum consists of a main peak at λ_0 and a series of sidelobes around it. According to Eq. (5.3-18), these secondary maxima occur approximately at

$$\sqrt{1 + \left(\frac{N\Delta\Gamma}{\pi} \right)^2} \approx 2l + 1, \quad l = 1, 2, 3, \dots, \quad (5.3-20)$$

with transmissivity given by

$$T \approx \frac{1}{(2l + 1)^2}. \quad (5.3-21)$$

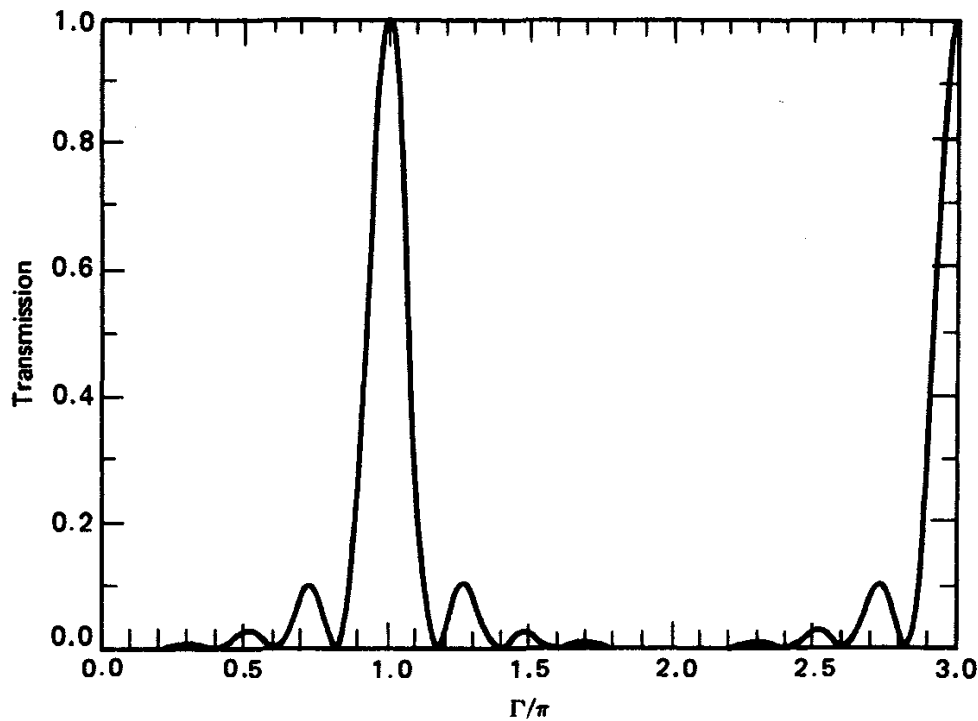


Figure 5.7. A calculated transmission spectrum of a folded Šolc filter.

A calculated transmission spectrum is shown in Fig. 5.7. Notice that the bandwidth is inversely proportional to the total number of plates.

5.3.2. Fan Šolc Filters

A fan Šolc filter also consists of a stack of identical birefringent plates, each oriented at a prescribed azimuth. A brief description of the basic type of fan Šolc filter is given in Table 5.2. The geometrical arrangement is sketched in

Table 5.2. The Fan Šolc Filter

Element	Azimuth
Front polarizer	0°
Plate 1	ρ
Plate 2	3ρ
Plate 3	5ρ
⋮	⋮
Plate N	$(2N - 1)\rho = \frac{1}{2}\pi - \rho$
Rear polarizer	0°

Fig. 5.8. According to the Jones matrix method formulated in the previous section, the overall matrix for these N plates is given by

$$\begin{aligned} M &= R\left(-\frac{1}{2}\pi + \rho\right)W_0R\left(\frac{1}{2}\pi - \rho\right)\cdots \\ &\quad \times R(-5\rho)W_0R(5\rho)R(-3\rho)W_0R(3\rho)R(-\rho)W_0R(\rho) \\ &= R\left(-\frac{1}{2}\pi + \rho\right)[W_0R(2\rho)]^NR(-\rho), \end{aligned} \quad (5.3-22)$$

where we have used the following identity for the rotation matrix:

$$R(\rho_1)R(\rho_2) = R(\rho_1 + \rho_2). \quad (5.3-23)$$

Notice that the last plate always appears first in the product (5.3-22).

By using the Chebyshev identity (5.3-4) and carrying out the matrix multiplication in Eq. (5.3-22), we obtain

$$\begin{aligned} M_{11} &= \sin 2\rho \cos \frac{1}{2}\Gamma \frac{\sin N\chi}{\sin \chi} \\ M_{12} &= -\cos N\chi - i \sin \frac{1}{2}\Gamma \frac{\sin N\chi}{\sin \chi} \\ M_{21} &= \cos N\chi - i \sin \frac{1}{2}\Gamma \frac{\sin N\chi}{\sin \chi} \\ M_{22} &= M_{11} \end{aligned} \quad (5.3-24)$$

with

$$\cos \chi = \cos 2\rho \cos \frac{1}{2}\Gamma. \quad (5.3-25)$$

These are the elements of the overall Jones matrix not including the polarizers.

The incident wave \mathbf{E} and the emerging wave \mathbf{E}' are thus related by

$$\begin{pmatrix} E'_x \\ E'_y \end{pmatrix} = \begin{pmatrix} 1 & 0 \\ 0 & 0 \end{pmatrix} \begin{pmatrix} M_{11} & M_{12} \\ M_{21} & M_{22} \end{pmatrix} \begin{pmatrix} 1 & 0 \\ 0 & 0 \end{pmatrix} \begin{pmatrix} E_x \\ E_y \end{pmatrix}. \quad (5.3-26)$$

The emerging beam is horizontally polarized (x) with amplitude given by

$$E'_x = M_{11}E_x. \quad (5.3-27)$$

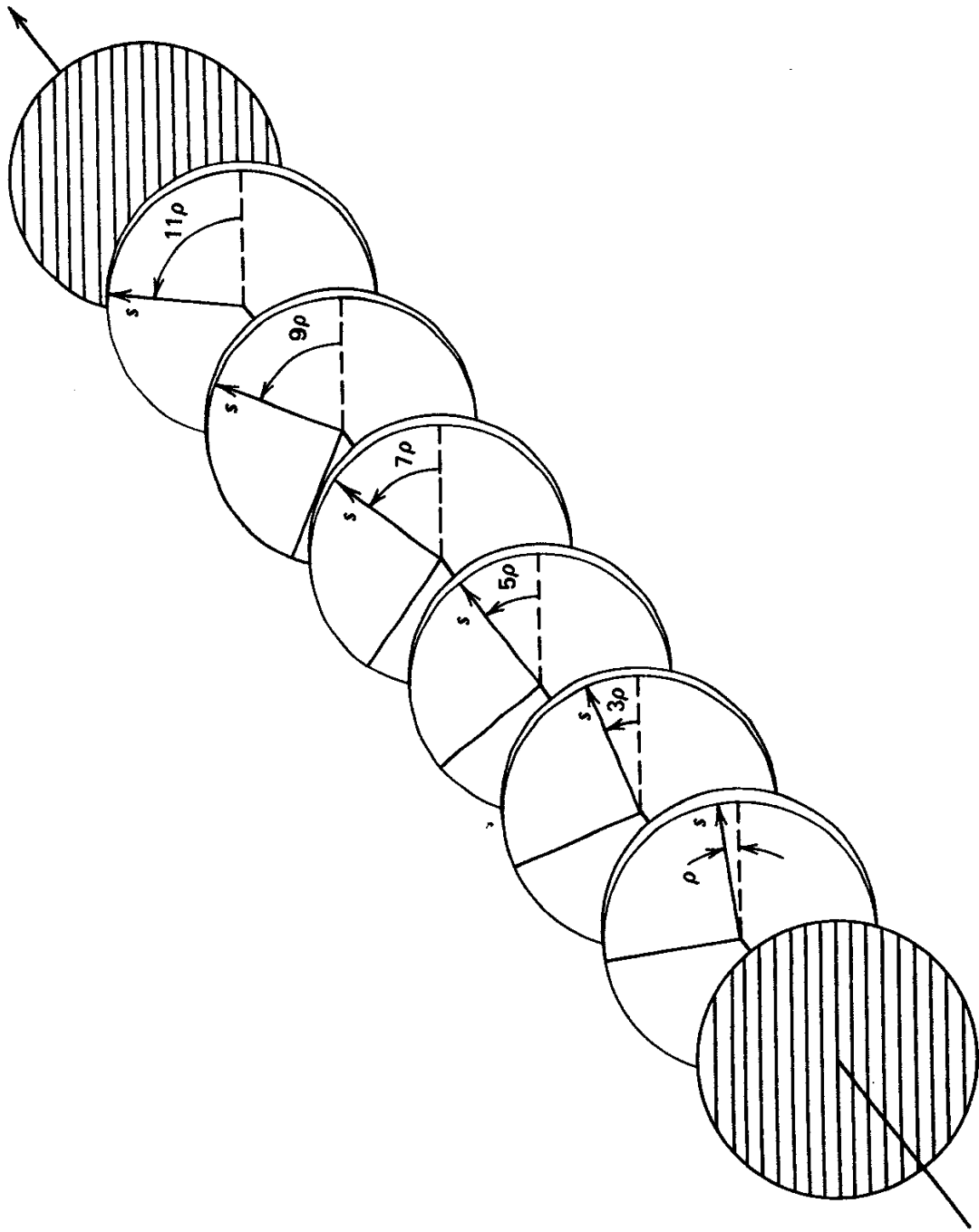


Figure 5.8. A six-stage fan Šolc filter.

If the incident wave is linearly polarized in the x direction, the transmissivity is given by

$$T = |M_{11}|^2. \quad (5.3-28)$$

From Eq. (5.3-24), we have the following expression for the transmissivity:

$$T = \left| \tan 2\rho \cos \chi \frac{\sin N\chi}{\sin \chi} \right|^2 \quad (5.3-29)$$

with

$$\cos \chi = \cos 2\rho \cos \frac{1}{2}\Gamma. \quad (5.3-30)$$

Notice that the transmission formula (5.3-29) is formally identical to Eq. (5.3-12). Maximum transmissivity ($T = 1$) occurs when $\Gamma = 0, 2\pi, 4\pi, \dots$, and $\rho = \pi/4N$. This unity transmission results simply from the fact that at these wavelengths the plates are full-wave plates. The light will remain linearly polarized in the x direction after going through each plate and will suffer no loss at the rear polarizer. Light at other wavelengths, where the plates are not full-wave plates, does not remain linearly polarized in the x direction and suffers loss at the rear polarizer. Let λ_ν be the wavelength at which the phase retardation $\Gamma = 2\nu\pi$. If λ differs slightly from λ_ν (i.e., $\lambda - \lambda_\nu \ll \lambda_\nu$), Γ is given approximately by

$$\Gamma = 2\nu\pi + \Delta\Gamma = 2\nu\pi - \frac{2\nu\pi}{\lambda_\nu}(\lambda - \lambda_\nu), \quad (5.3-31)$$

where $\nu = 1, 2, 3, \dots$. The case $\nu = 0$ occurs only when the birefringence vanishes at some particular wavelength λ_0 . This special case has some important applications in wide-angle narrowband filters and deserves special attention (see Problem 5.8). If we now further assume that N is much larger than 1 and follow the same procedure as in Eq. (5.3-17), we obtain the following approximate expression for the transmissivity:

$$T = \left(\frac{\sin \frac{1}{2}\pi \sqrt{1 + (N\Delta\Gamma/\pi)^2}}{\sqrt{1 + (N\Delta\Gamma/\pi)^2}} \right)^2, \quad (5.3-32)$$

which is identical to Eq. (5.3-18). The FWHM $\Delta\lambda_{1/2}$ of the transmission maxima is again given approximately by

$$\Delta\lambda_{1/2} \approx 1.60 \frac{\lambda_\nu}{2\nu N}, \quad \nu = 1, 2, 3, \dots \quad (5.3-33)$$

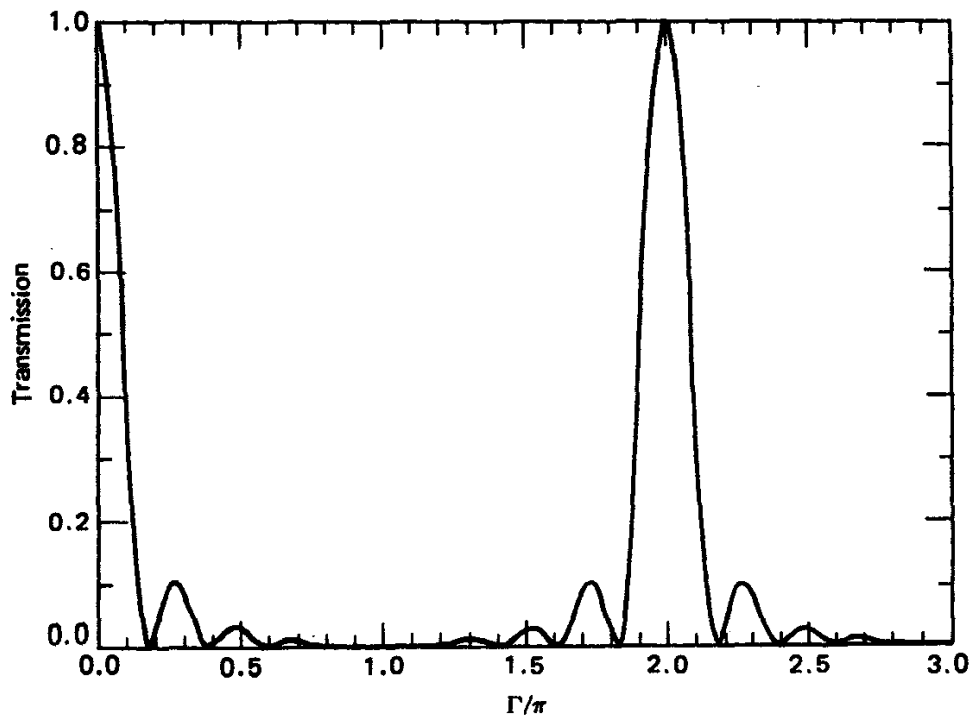


Figure 5.9. A calculated transmission spectrum of a fan Šolc filter.

The transmission spectrum of the fan Šolc filter is identical to that of the folded Šolc filter except that the curves are shifted by $\Gamma = \pi$. In other words, the transmissivity of the fan Šolc filter at a phase retardation Γ is identical to that of the folded Šolc filter at phase retardation $\Gamma + \pi$. This can also be seen from the expression for the transmissivity in Eqs. (5.3-12) and (5.3-29). A calculated transmission spectrum of a fan Šolc filter is shown in Fig. 5.9.

Šolc filters play an important role in many modern optical devices such as electro-optic tunable filters [10, 11] and wide-field-of-view narrowband filters. More information on Šolc filters can be found in [12].

5.4. LIGHT PROPAGATION IN TWISTED ANISOTROPIC MEDIA

In this section the propagation of electromagnetic radiation through a slowly twisting anisotropic medium is described by the Jones calculus. The transmission of light through a twisted nematic liquid crystal is a typical example. This situation is similar to a fan-type Šolc filter structure with the number of plates, N , tending to infinity and the plate thickness tending to zero as $1/N$. In fact, we are going to subdivide the twisted anisotropic medium into N plates and assume that each plate is a wave plate with a

phase retardation and an azimuth angle. The overall Jones matrix can then be obtained by multiplying together all the matrices associated with these plates.

We will limit ourselves to the case when the twisting is linear and the azimuth angle of the axes is

$$\psi(z) = \alpha z, \quad (5.4-1)$$

where z is the distance in the direction of propagation and α is a constant.

Let Γ be the phase retardation of the plate when it is untwisted. In particular, for the case of nematic liquid crystal with c axis parallel to the plate surfaces, Γ is given by

$$\Gamma = \frac{2\pi}{\lambda} (n_e - n_o) l, \quad (5.4-2)$$

where l is the thickness of the plate. The total twist angle is

$$\phi \equiv \psi(l) = \alpha l. \quad (5.4-3)$$

To derive the Jones matrix for such a structure, we need to divide this plate into N equally thick plates. Each plate has a phase retardation of Γ/N . The plates are oriented at azimuth angles $\rho, 2\rho, 3\rho, \dots, (N-1)\rho, N\rho$ with $\rho = \phi/N$. The overall Jones matrix for these N plates is given by

$$M = \prod_{m=1}^N R(-m\rho) W_0 R(m\rho). \quad (5.4-4)$$

It is important to remember that in the above matrix product, $m=1$ appears at the right-hand end. Following the procedure (5.3-23), this matrix can be written

$$M = R(\phi) \left[W_0 R\left(-\frac{\phi}{N}\right) \right]^N, \quad (5.4-5)$$

where

$$W_0 = \begin{pmatrix} e^{-i\Gamma/2N} & 0 \\ 0 & e^{i\Gamma/2N} \end{pmatrix}. \quad (5.4-6)$$

Using Eqs. (5.1-9a) and (5.4-6), we obtain

$$M = R(\phi) \begin{pmatrix} \cos \frac{\phi}{N} e^{-i\Gamma/2N} & -\sin \frac{\phi}{N} e^{-i\Gamma/2N} \\ \sin \frac{\phi}{N} e^{i\Gamma/2N} & \cos \frac{\phi}{N} e^{i\Gamma/2N} \end{pmatrix}^N. \quad (5.4-7)$$

Equation (5.4-7) can be further simplified by using Chebyshev's identity (5.3-4). In the limit when N tends to infinite ($N \rightarrow \infty$), the result is given by (see Problem 5.10)

$$M = R(\phi) \begin{pmatrix} \cos X - i \frac{\Gamma}{2} \frac{\sin X}{X} & -\phi \frac{\sin X}{X} \\ \phi \frac{\sin X}{X} & \cos X + i \frac{\Gamma}{2} \frac{\sin X}{X} \end{pmatrix} \quad (5.4-8)$$

where

$$X = \sqrt{\phi^2 + \left(\frac{\Gamma}{2}\right)^2}. \quad (5.4-9)$$

Here we have an exact expression for the Jones matrix of a linearly twisted anisotropic plate.

Let V be the initial polarization state, the polarization state V' after exiting the plate can be written

$$V' = MV. \quad (5.4-10)$$

5.4.1. Adiabatic Following

It often happens, especially in twisted nematic liquid crystals, that the phase retardation Γ is much larger than the twist angle ϕ . For example, consider a liquid-crystal layer $25 \mu\text{m}$ thick with a twist angle of $\frac{1}{2}\pi$. The birefringence of liquid crystal is typically $n_e - n_o = 0.1$. For wavelength $\lambda = 0.5 \mu\text{m}$, we have $\Gamma/\phi = 20$. This number can be even bigger if the layer is thicker. If we assume $\Gamma \gg \phi$, the overall Jones matrix (5.4-8) becomes

$$M = R(\phi) \begin{pmatrix} e^{-i\Gamma/2} & 0 \\ 0 & e^{i\Gamma/2} \end{pmatrix}. \quad (5.4-11)$$

If the incident light is linearly polarized along either the slow or the fast axis at the entrance plane, then according to Eq. (5.4-11), the light will remain linearly polarized along the "local" slow or fast axis. In a sense, the polarization vector follows the rotation of the local axes, provided the polarization vector is along one of the axes. The operation of the Jones matrix on any polarization vector can be divided into two parts. First, a phase-retardation matrix operates on the Jones vector of the incident wave. For light linearly polarized along one of the principal axes, this matrix only

gives a phase shift to the light beam and leaves the polarization state unchanged. Second, the operation of $R(\phi)$ is to rotate the Jones vector by an angle ϕ . For linearly polarized light, this rotation makes the polarization vector parallel to the principal axes at the exit face of the plate. Thus, if the incident light is polarized along the direction of the normal modes at the input plane ($z = 0$), the polarization vector of the light wave will follow the rotation of principal axes and remain parallel to the local slow (or fast) axis provided the twist rate is small. This is called adiabatic following. This phenomenon has an important application in liquid-crystal light valves. The principle of operation of these light valves is discussed below.

We consider the case of twisted nematic liquid crystal with a quarter turn ($\phi = \frac{1}{2}\pi$). If this layer is placed between a pair of parallel polarizers with their transmission axes (x) parallel to the c axis of the liquid crystal at the entrance plane ($z = 0$), the Jones vector representation of the wave immediately after passage through the first polarizer can be written

$$\begin{pmatrix} 1 \\ 0 \end{pmatrix}. \quad (5.4-12)$$

The rotation matrix $R(\phi)$ in Eq. (5.4-8) can be written

$$R\left(\frac{1}{2}\pi\right) = \begin{pmatrix} 0 & -1 \\ 1 & 0 \end{pmatrix}. \quad (5.4-13)$$

After passing through the liquid crystal, the polarization state of the beam, according to Eqs. (5.4-8), (5.4-12), and (5.4-13), becomes

$$\mathbf{V}' = \begin{pmatrix} \phi \frac{\sin X}{X} \\ \cos X - i \frac{\Gamma}{2} \frac{\sin X}{X} \end{pmatrix}. \quad (5.4-14)$$

The y component will be blocked by the second polarizer. The transmissivity of the whole structure is thus given by

$$T = \frac{\sin^2\left(\frac{1}{2}\pi\sqrt{1 + (\Gamma/\pi)^2}\right)}{1 + (\Gamma/\pi)^2}, \quad (5.4-15)$$

where we have used Eq. (5.4-9) for X and $\phi = \frac{1}{2}\pi$.

For a crystal layer with thickness large enough, the phase retardation is much larger than π (i.e., $\Gamma \gg \pi$). The transmissivity is virtually zero, according to Eq. (5.4-15). This is a result of the adiabatic following. The polarization vector follows the rotation of the axes and therefore is rotated by an angle $\phi = \frac{1}{2}\pi$ equal to the twist angle. Since this direction is orthogonal to the transmission axis of the analyzer, the transmission is zero.

In many twisted liquid crystals, the c axis can be forced to align along a given direction by the application of an electric field (or stress) (see Section 7.7). The application of an electric field along the z direction will destroy this twisted structure (see Section 7.7). This leads to $\Gamma = 0$ and to total transmission of light, according to Eq. (5.4-15). When the electric field is removed, the liquid crystal recovers its twisted structure and the light is extinguished. This is the basic principal of liquid-crystal light valves.

5.5. THE PROBLEM OF FRESNEL REFLECTION AND PHASE SHIFT

In the Jones-calculus formulation, the reflections of light from the surface of the wave plate are neglected. These reflections will normally decrease the throughput of electromagnetic energy. However, if the plate surfaces are optically flat, the interference effect can result in a decrease or increase in the transmissivity, depending on the optical path lengths.

The exact approaches derived from the electromagnetic theory involve the use of a 4×4 -matrix method [13–15]. The light wave of a beam is represented mathematically by a column vector that consists of the complex amplitudes of the incident wave and the reflected wave. Each wave has a slow and a fast component. (The details of this method are beyond the scope of this book; interested readers are referred to the cited references.)

This exact approach gives the exact transmission spectrum of the birefringent filter, because the interference effects due to the reflected waves are accounted for. The practical calculation of the transmission requires a computer. The calculated transmission spectrum of a Šolc Filter (see Fig. 5.10) shows fine structure due to interference. This fine structure should be experimentally observable if the birefringent plates are thin and optically flat. This approach also predicts the existence of a superfine structure that comes from the Fabry–Perot interference fringes of the whole stack of crystals rather than those of the individual plates; however, this superfine structure is beyond the resolution limit of the plotter at the scale shown in Fig. 5.10. The figure also compares the Jones-calculus method, which neglects reflected waves, and the exact 4×4 -matrix method.

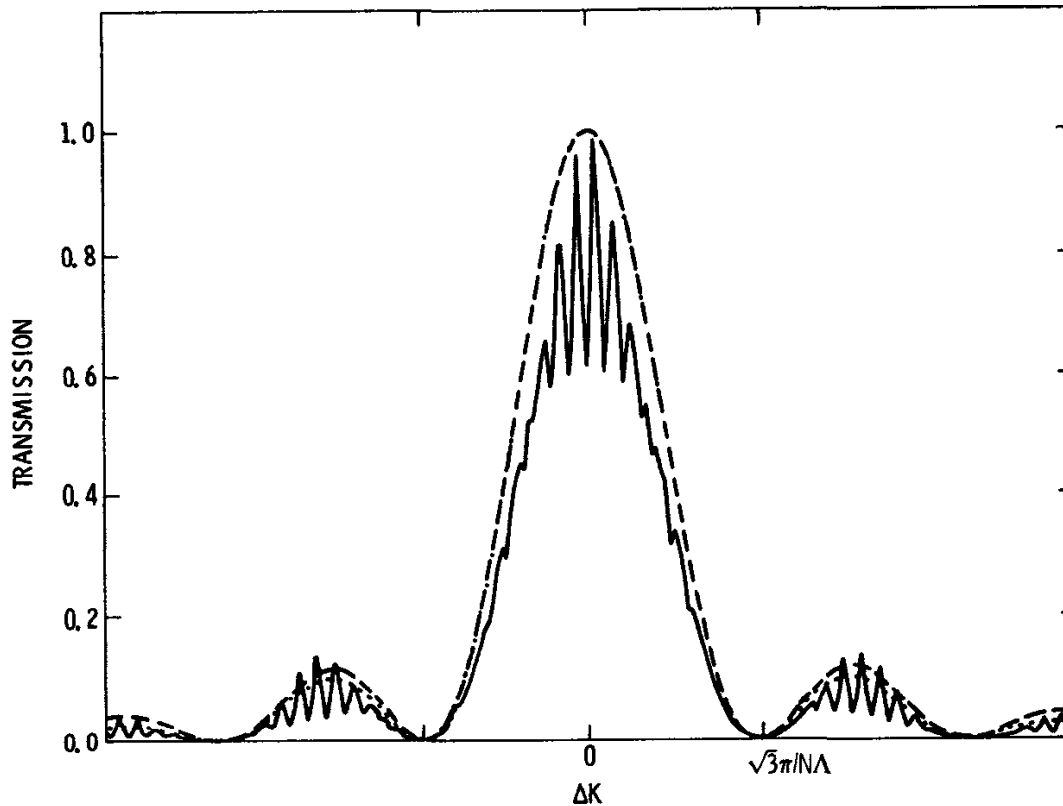


Figure 5.10. Transmission spectrum of a Solc filter: coupled-mode theory (dashed curve) and Jones calculus (dotted curve) with the exact 4×4 -matrix method (solid curve).

PROBLEMS

- 5.1. *Half-wave plate.* A half-wave plate has a phase retardation of $\Gamma = \pi$. Assume that the plate is oriented so that the azimuth angle (i.e., the angle between the x axis and the slow axis of the plate) is ψ .
- Find the polarization state of the transmitted beam, assuming that the incident beam is linearly polarized in the y direction.
 - Show that a half-wave plate will convert right-hand circularly polarized light into left-hand circularly polarized light, and vice versa, regardless of the azimuth angle of the plate.
 - Lithium tantalate (LiTaO_3) is a uniaxial crystal with $n_o = 2.1391$ and $n_e = 2.1432$ at $\lambda = 1 \mu\text{m}$. Find the half-wave-plate thickness at this wavelength, assuming the plate is cut in such a way that the surfaces are perpendicular to the x axis of the principal coordinate (i.e., x -cut).
- 5.2. *Quarter-wave plate.* A quarter-wave plate has a phase retardation of $\Gamma = \frac{1}{2}\pi$. Assume that the plate is oriented in a direction with azimuth angle ψ .
- Find the polarization state of the transmitted beam, assuming that the incident beam is polarized in the y direction.

- (b) If the polarization state resulting from (a) is represented by a complex number on the complex plane, show that the locus of these points as ψ varies from 0 to $\frac{1}{2}\pi$ is a branch of a hyperbola. Obtain the equation of the hyperbola.
- (c) Quartz (α -SiO₂) is a uniaxial crystal with $n_o = 1.53283$ and $n_e = 1.54152$ at $\lambda = 1.1592 \mu\text{m}$. Find the thickness of an x -cut quartz quarter-wave plate at this wavelength.

5.3. *Polarization transformation by a wave plate.* A wave plate is characterized by its phase retardation Γ and azimuth angle ψ .

- (a) Find the polarization state of the emerging beam, assuming that the incident beam is polarized in the x direction.
- (b) Use a complex number to represent the resulting polarization state obtained in (a).
- (c) The polarization state of the incident x -polarized beam is represented by a point at the origin of the complex plane. Show that the transformed polarization state can be anywhere on the complex plane, provided Γ can be varied from 0 to 2π and ψ can be varied from 0 to $\frac{1}{2}\pi$. Physically, this means that any polarization state can be produced from linearly polarized light, provided a proper wave plate is available.
- (d) Show that the locus of these points in the complex plane obtained by rotating a wave plate from $\psi = 0$ to $\psi = \frac{1}{2}\pi$ is a hyperbola. Derive the equation of this hyperbola.
- (e) Show that the Jones matrix W of a wave plate is unitary, that is,

$$W^\dagger W = 1,$$

where the dagger indicates Hermitian conjugation.

- (f) Let V'_1 and V'_2 be the transformed Jones vectors from V_1 and V_2 , respectively. Show that if V_1 and V_2 are orthogonal, so are V'_1 and V'_2 .

5.4. *Polarizers and projection operators.* An ideal polarizer can be considered as a projection operator which acts on the incident polarization state and projects the polarization vector along the transmission axis of the polarizer.

- (a) If we neglect the absolute phase factor in Eq. (5.1-11), show that

$$P_0^2 = P_0 \quad \text{and} \quad P^2 = P.$$

Operators satisfying these conditions are called projection operators in linear algebra.

- (b) Show that if E_1 is the amplitude of the relative field of the electric field, the amplitude of the beam after it passes through the polarizer is given by

$$\mathbf{p}(\mathbf{p} \cdot \mathbf{E}_1),$$

where \mathbf{p} is the unit vector along the transmission axis of the polarizer.

- (c) If the incident beam is vertically polarized (i.e., $\mathbf{E}_1 = \hat{y}E_0$), the polarizer transmission axis is in the x direction (i.e., $\mathbf{p} = \hat{x}$). The transmitted beam has zero amplitude, since $\hat{x} \cdot \hat{y} = 0$. However, if a second polarizer is placed in front of the first polarizer and is oriented at 45° with respect to it, the transmitted amplitude is not zero. Find this amplitude.
- (d) Consider a series of N polarizers with the first one oriented at $\psi_1 = \pi/2N$, the second one at $\psi_2 = 2(\pi/2N)$, the third one at $\psi_3 = 3(\pi/2N), \dots$, and the n th one at $N \cdot (\pi/2N)$. Let the incident beam be horizontally polarized. Show that the transmitted beam is vertically polarized with an amplitude of

$$\left[\cos\left(\frac{\pi}{2N}\right) \right]^N.$$

Evaluate the amplitude for $N = 1, 2, 3, \dots, 10$. Show that in the limit of $N \rightarrow \infty$, the amplitude becomes one. In other words, a series of polarizers oriented like a fan can rotate the polarization of the light without attenuation.

5.5. *Lyot-Öhman filter.* In solar physics, the distribution of hydrogen in the solar corona is measured by photographing at the wavelength of H_α line ($\lambda = 6563 \text{ \AA}$). To enhance the signal-to-noise ratio, a filter of extremely narrow bandwidth ($\sim 1 \text{ \AA}$) is required. The polarization filter devised by Lyot and Öhman consists of a set of birefringent plates separated by parallel polarizers. The plate thicknesses are in geometric progression, that is, $d, 2d, 4d, 8d, \dots$. All the plates are oriented at an azimuth angle of 45° .

- (a) Show that if n_o and n_e are the refractive indices of the plates, the transmissivity of the whole stack of N plates is given by

$$T = \frac{1}{2} \cos^2 x \cos^2 2x \cos^2 4x \cdots \cos^2 2^{N-1} x$$

with

$$x = \frac{\pi d(n_e - n_o)}{\lambda} = \frac{\pi d(n_e - n_o)\nu}{c}.$$

- (b) Show that the transmission can be written

$$T = \frac{1}{2} \left(\frac{\sin 2^N x}{2^N \sin x} \right)^2.$$

- (c) Show that the transmission bandwidth (FWHM) of the whole system is governed by that of the bands of the thickest plate, that is,

$$\Delta\nu_{1/2} \sim \frac{c}{2^N d (n_e - n_o)}$$

and the free spectral range $\Delta\nu$ is governed by that of the bands of the thinnest plate, that is,

$$\Delta\nu \sim \frac{c}{d(n_e - n_o)}.$$

The finesse F of the system, defined as $\Delta\nu/\Delta\nu_{1/2}$, is then

$$F \sim 2^N.$$

- (d) Design a filter with a bandwidth of 1 Å at the H_α line, using quartz as the birefringent material. Assume that $n_o = 1.5416$ and $n_e = 1.5506$ at $\lambda = 6563$ Å. Find the required thickness of the thickest plate.
- (e) Show that according to (b) the bandwidth (FWHM) is given by

$$\Delta\nu_{1/2} = 0.886 \frac{c}{2^N d (n_e - n_o)}.$$

5.6. *Off-axis effect.* A wave plate made of uniaxial crystal with its c axis parallel to the plate surfaces has a phase retardation of $2\pi(n_e - n_o)d/\lambda$ for a normal incident beam. For an off-axis beam, the light will “see” different birefringence because the refractive index for the extraordinary wave is dependent on the direction of the beam. In addition, the path length in the crystal plate is no longer d (see Fig. 5.11).

- (a) Let θ_o , θ_e be the refractive angles for the ordinary and extraordinary waves, respectively. Show that the phase retardation is

$$\Gamma = \frac{2\pi}{\lambda} (n_e \cos \theta_e - n_o \cos \theta_o) d.$$

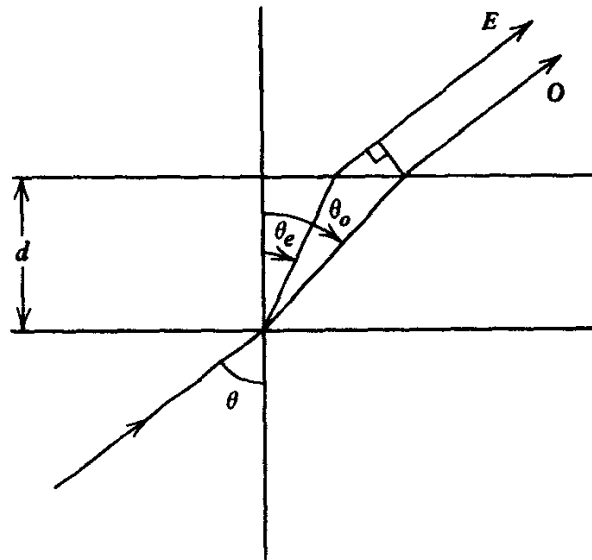


Figure 5.11. Off-axis rays.

- (b) Let θ be the angle of incidence, and ϕ be the angle between the c axis and the tangential component of the wave vector. Show that the phase retardation can be expressed in terms of θ and ϕ as

$$\Gamma = \frac{2\pi}{\lambda} d \left[n_e \sqrt{1 - \frac{\sin^2 \theta \sin^2 \phi}{n_e^2} - \frac{\sin^2 \theta \cos^2 \phi}{n_o^2}} - n_o \sqrt{1 - \frac{\sin^2 \theta}{n_o^2}} \right].$$

- (c) Show that in the case when $\sin^2 \theta$ is much smaller than n_o^2 and n_e^2 , the phase retardation can be written

$$\Gamma = \frac{2\pi}{\lambda} (n_e - n_o) d \left\{ 1 + \sin^2 \theta \left[\frac{\sin^2 \phi}{2n_o n_e} - \frac{\cos^2 \phi}{2n_o^2} \right] \right\}.$$

- (d) According to the result in (c), a Lyot-Öhman filter with a passband of λ_0 at normal incidence will have a passband of $\lambda_0 \pm \Delta\lambda$ for off-axis light. Show that with $n_{\text{eff}}^2 = n_o^2 \approx n_e^2$, $\Delta\lambda$ is given by

$$\Delta\lambda = \frac{\lambda \sin^2 \theta}{2n_{\text{eff}}^2}.$$

- (e) Show that a narrowband Lyot-Öhman filter has a limited aperture of

$$\theta \approx \pm n_o \left(\frac{\Delta\lambda_{1/2}}{\lambda} \right)^{1/2},$$

where we assume $n_e - n_o \ll n_o$.

- 5.7. *Solc filters.* The transmissivity near a transmission peak can be written as

$$T = \frac{\sin^2 \frac{1}{2} \pi \sqrt{1 + x^2}}{1 + x^2}$$

with

$$x = N\Delta\Gamma/\pi.$$

- (a) Show that $T = 0.5$ at $x = 0.8$, and derive the expression (5.3-19) for the FWHM.
- (b) Find the wavelengths for which the transmissivity vanishes.
- (c) Find the peak transmissivity of the sidelobes.
- (d) Estimate the integrated transmissivity over all the sidelobes and compare it with the area under the main peak.
- 5.8. *Iso-index Lyot-Öhman filters.* Consider a Lyot-Öhman filter (Problem 5.5) made of iso-index crystals (i.e., crystals with $n_e = n_o$ at certain wavelength λ_c).
- (a) Derive an expression for the bandwidth (FWHM) as a function of the plate thickness and the rate of change α of the birefringence.
- (b) Derive an expression for the free spectral range as a function of α and the plate thickness d .
- (c) Design an iso-index Lyot-Öhman filter using CdS at 5245 Å with a bandwidth of 0.1 Å and a free spectral range of at least 10 Å.
- (d) Explain why the total thickness required for a given bandwidth $\Delta\lambda_{1/2}$ is usually smaller than in the conventional Lyot-Öhman filter made of quartz or calcite. Show that this is true only when α satisfies

$$\alpha > \left| \frac{n_e - n_o}{\lambda} \right|,$$

where n_e, n_o are the refractive indices of calcite or quartz.

- 5.9. *Field of view of iso-index filters.* Use the result obtained in Problem 5.6(c) to study the field of view of the iso-index Lyot–Öhman filter.
- Show that the passband is independent of the angle of incidence.
 - Derive an expression for the bandwidth for off-axis light as a function of θ and ϕ .
 - Show that for the most extreme angle of incidence, the bandwidth is increased or decreased by a factor of $(1 \pm 1/2n_o^2)$.
- 5.10. *Twisted nematic liquid crystals.*
- Use Chebyshev's identity (5.3-4) to simplify Eq. (5.4-7).
 - Derive Eq. (5.4-8).

REFERENCES

- E. A. West, "Extending the field of view of KD^*P electro-optic modulators," *Appl. Opt.* **17**, 3010 (1978).
- B. Lyot, "Optical apparatus with wide field using interference of polarized light," *C. R. Acad. Sci. (Paris)* **197**, 1593 (1933).
- B. Lyot, "Filter monochromatique polarisant et ses applications en physique solaire," *Ann. Astrophys.* **7**, 31 (1944).
- Y. Öhman, "A new monochromator," *Nature* **41**, 157, 291 (1938).
- Y. Öhman, "On some new birefringent filter for solar research," *Ark. Astron.* **2**, 165 (1958).
- I. Šolc, *Českoslov. Časopis pro Fysiku* **3**, 366 (1953); *Csek. Cas. Fys.* **4**, 607, 699 (1954); **5**, 114 (1955).
- I. Šolc, "Birefringent chain filters," *J. Opt. Soc. Am.* **55**, 621 (1965).
- R. C. Jones, "New calculus for the treatment of optical systems," *J. Opt. Soc. Am.* **31**, 488 (1941).
- See, for example, P. Yeh, A. Yariv, and C. S. Hong, "Electromagnetic propagation in periodic stratified media. I. General theory," *J. Opt. Soc. Am.* **67**, 423 (1977).
- D. A. Pinnow et al., "An electro-optic tunable filter," *Appl. Phys. Lett.* **34**, 392 (1979).
- H. A. Tarry, "Electrically tunable narrowband optical filter," *Electronics Lett.* **11**, 471 (1975).
- J. W. Evans, *J. Opt. Soc. Am.* "The birefringent filter," **39**, 229 (1949); "Šolc birefringent filter," **48**, 142 (1958).
- P. Yeh, "Electromagnetic propagation in birefringent layered media," *J. Opt. Soc. Am.* **69**, 742 (1979).
- P. Yeh, "Transmission spectrum of a Šolc filter," *Opt. Comm.* **29**, (1979).
- P. Yeh, "Optics of anisotropic layered media: A new 4×4 matrix algebra," *Surface Science* **96**, 41–53 (1980).

6

Electromagnetic Propagation in Periodic Media

The propagation of electromagnetic radiation in periodic media exhibits many interesting and potentially useful phenomena. These include the diffraction of X-rays in crystals, the diffraction of light from the periodic strain variation accompanying a sound wave, and the “forbidden” band of light in periodic layered media. These phenomena are employed in many optical devices such as diffraction gratings, holograms, free-electron lasers, distributed-feedback (DFB) lasers, distributed-Bragg-reflector (DBR) lasers, high-reflectance Bragg mirrors, acousto-optic filters, Šolc filters, and so on. In this chapter we will discuss some general properties of electromagnetic propagation in periodic media and then develop a general theory for propagation in periodic layered media. The theory has a strong formal analogy to the quantum theory of electrons in crystals and thus makes heavy use of the concepts of Bloch waves, forbidden gaps, evanescent waves, and surface waves. Finally, we will discuss the application of the theory to a number of familiar problems, such as the reflectivity of a Bragg reflector, Šolc-filter transmission characteristics, and optical surface waves. In addition, we will also discuss form birefringence and its application to dichroic polarizers. Periodic structures also play an important role in integrated optics, which topic will be taken up in Chapter 11.

6.1. PERIODIC MEDIA

The optical properties of a periodic medium are described by its dielectric and permeability tensors, which, reflecting the translational symmetry of the medium, are periodic function of \mathbf{x} :

$$\epsilon(\mathbf{x}) = \epsilon(\mathbf{x} + \mathbf{a}), \quad \mu(\mathbf{x}) = \mu(\mathbf{x} + \mathbf{a}), \quad (6.1-1)$$

where \mathbf{a} is any arbitrary lattice vector. These equations merely state that the

medium “looks” exactly the same to an observer at \mathbf{x} as at $\mathbf{x} + \mathbf{a}$. In a three-dimensional periodic medium such as crystals, there exist primitive vectors $\mathbf{a}_1, \mathbf{a}_2, \mathbf{a}_3$ which define the periodicity of the lattice, such that the medium remains invariant under translation through any vector \mathbf{a} which is the sum of integral multiples of these vectors.

The propagation of monochromatic (frequency ω) laser radiation in a periodic medium is described by Maxwell’s equations,

$$\nabla \times \mathbf{H} = i\omega\epsilon\mathbf{E}, \quad (6.1-2)$$

$$\nabla \times \mathbf{E} = -i\omega\mu\mathbf{H} \quad (6.1-3)$$

These equations remain the same after we have substituted $\mathbf{x} + \mathbf{a}$ for \mathbf{x} in the operator ∇ and ϵ, μ . The translational symmetry of the medium allows us to take its normal modes as

$$\mathbf{E} = \mathbf{E}_{\mathbf{K}}(\mathbf{x})e^{-i\mathbf{K}\cdot\mathbf{x}}, \quad (6.1-4)$$

$$\mathbf{H} = \mathbf{H}_{\mathbf{K}}(\mathbf{x})e^{-i\mathbf{K}\cdot\mathbf{x}},$$

where $\mathbf{E}_{\mathbf{K}}(\mathbf{x})$ and $\mathbf{H}_{\mathbf{K}}(\mathbf{x})$ are both periodic, that is,

$$\mathbf{E}_{\mathbf{K}}(\mathbf{x}) = \mathbf{E}_{\mathbf{K}}(\mathbf{x} + \mathbf{a}), \quad (6.1-5)$$

$$\mathbf{H}_{\mathbf{K}}(\mathbf{x}) = \mathbf{H}_{\mathbf{K}}(\mathbf{x} + \mathbf{a}).$$

This is known as the Floquet (or Bloch) theorem and will be proved below. The subscript \mathbf{K} indicates that the functions $\mathbf{E}_{\mathbf{K}}$ and $\mathbf{H}_{\mathbf{K}}$ depend on \mathbf{K} , which is known as the Bloch wave vector. A dispersion relation exists between ω and \mathbf{K} ,

$$\omega = \omega(\mathbf{K}). \quad (6.1-6)$$

In the event that the periodicity disappears, the functions $\mathbf{E}_{\mathbf{K}}(\mathbf{x})$ and $\mathbf{H}_{\mathbf{K}}(\mathbf{x})$ become constant and the normal modes become plane waves with the Bloch wave vector equal to the plane-wave propagation vector. Our main task is to determine $\mathbf{E}_{\mathbf{K}}(\mathbf{x})$, $\mathbf{H}_{\mathbf{K}}(\mathbf{x})$, and the dispersion relation $\omega(\mathbf{K})$.

6.1.1. One-Dimensional Periodic Media

In modern optics, one often deals with a one-dimensional periodic medium such that

$$\epsilon(z) = \epsilon(z + l\Lambda) \quad (6.1-7)$$

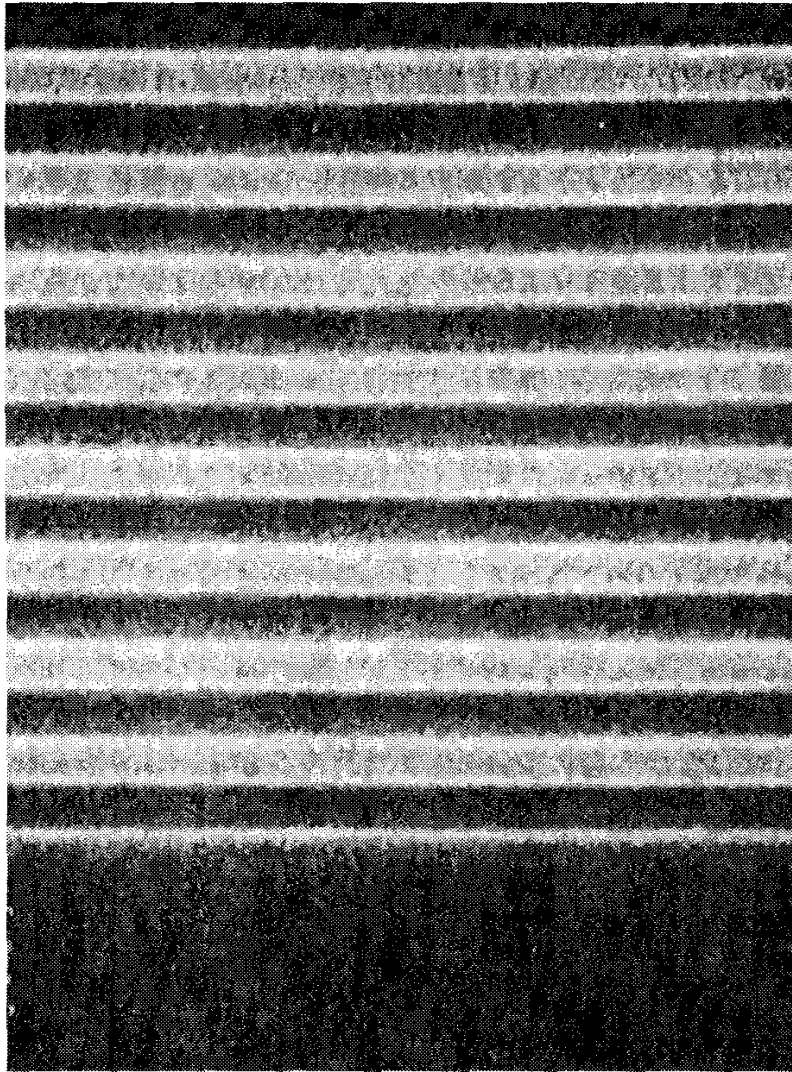


Figure 6.1. A typical periodic layered medium which consists of alternating layers of GaAs and $\text{Al}_x\text{Ga}_{1-x}\text{As}$ grown on a GaAs substrate by molecular-beam epitaxy [7].

where ϵ is the permittivity tensor, Λ is the period, and l is an integer. We will limit the discussion in this chapter to the propagation of laser radiation in one-dimensional periodic, nonmagnetic media. A typical periodic medium made of alternating layers of two transparent materials is shown in Fig. 6.1. Assume that a beam of laser radiation is incident on the periodic layered medium. The light will be reflected and refracted at each interface. Let θ be the angle of incidence. Constructive interference in reflection occurs when the condition

$$m\lambda = 2\Lambda \cos \theta \quad (6.1-8)$$

is satisfied. This is known as the Bragg condition. It can be easily derived by

considering the phase difference between rays reflected from successive lattice planes. Constructive interference occurs when the optical path difference between rays reflected from successive lattice planes contains an integral number of wavelengths. The propagation of electromagnetic radiation in these media obeys the wave equation

$$\nabla \times (\nabla \times \mathbf{E}) - \omega^2 \mu \epsilon \mathbf{E} = 0. \quad (6.1-9)$$

Since the medium is periodic, we can expand the dielectric tensor ϵ in a Fourier series

$$\epsilon(\mathbf{x}) = \sum_{\mathbf{G}} \epsilon_{\mathbf{G}} e^{-i\mathbf{G} \cdot \mathbf{x}}, \quad (6.1-10)$$

where \mathbf{G} runs over all the reciprocal-lattice vectors, including $\mathbf{G} = 0$. In our one-dimensional case

$$\mathbf{G} = l\mathbf{g} = l \frac{2\pi}{\Lambda} \hat{\mathbf{z}}, \quad l = 0, \pm 1, \pm 2, \pm 3, \dots, \quad (6.1-11)$$

and

$$\epsilon(z) = \sum_l \epsilon_l e^{-il(2\pi/\Lambda)z}.$$

The vector \mathbf{G} is known as the reciprocal-lattice vector in solid-state physics and plays a fundamental role in crystal physics. In a one-dimensional periodic medium, \mathbf{g} is parallel to z . The electric field vector in this periodic medium may be expressed in general as a Fourier integral

$$\mathbf{E} = \int d^3k \mathbf{A}(\mathbf{k}) e^{-i\mathbf{k} \cdot \mathbf{x}}. \quad (6.1-12)$$

Substituting Eqs. (6.1-12) and (6.1-10) in Eq. (6.1-9), we obtain

$$\int d^3k \mathbf{k} \times [\mathbf{k} \times \mathbf{A}(\mathbf{k})] e^{-i\mathbf{k} \cdot \mathbf{x}} + \omega^2 \mu \sum_{\mathbf{G}} \int d^3k \epsilon_{\mathbf{G}} \mathbf{A}(\mathbf{k} - \mathbf{G}) e^{-i\mathbf{k} \cdot \mathbf{x}} = 0.$$

This equation is satisfied only when all the coefficients of $e^{-i\mathbf{k} \cdot \mathbf{x}}$ vanish. Thus

$$\mathbf{k} \times [\mathbf{k} \times \mathbf{A}(\mathbf{k})] + \omega^2 \mu \sum_{\mathbf{G}} \epsilon_{\mathbf{G}} \mathbf{A}(\mathbf{k} - \mathbf{G}) = 0 \quad \text{for all } \mathbf{k}, \quad (6.1-13)$$

where the summation is over all the reciprocal-lattice vectors. This is an infinite set of homogeneous equations for the unknown coefficients $\mathbf{A}(\mathbf{k})$. Each equation in the set has a different value of \mathbf{k} . The secular equation which results from setting the determinant of Eq. (6.1-13) equal to zero can be solved in principle for the whole set. However, by inspecting Eq. (6.1-13), we note that not all the coefficients $\mathbf{A}(\mathbf{k})$ are coupled. In fact, only the coefficients of the form $\mathbf{A}(\mathbf{k} - \mathbf{G})$ are coupled. This makes it possible to divide the whole set (6.1-13) into many subsets, each labeled by a wave vector \mathbf{K} and containing equations that involve $\mathbf{A}(\mathbf{K})$ and $\mathbf{A}(\mathbf{K} - \mathbf{G})$ with all the possible \mathbf{G} 's. Each subset can be solved separately. Using this fact in Eq. (6.1-13), the solution of a subset labeled by \mathbf{K} can be written as

$$\begin{aligned}\mathbf{E}_{\mathbf{K}} &= \sum_{\mathbf{G}} \mathbf{A}(\mathbf{K} - \mathbf{G}) e^{-i(\mathbf{K} - \mathbf{G}) \cdot \mathbf{r}} \\ &= e^{-i\mathbf{K} \cdot \mathbf{r}} \sum_{\mathbf{G}} \mathbf{A}(\mathbf{K} - \mathbf{G}) e^{i\mathbf{G} \cdot \mathbf{r}} \\ &= e^{-i\mathbf{K} \cdot \mathbf{r}} \mathbf{E}_{\mathbf{K}}(\mathbf{r}).\end{aligned}\quad (6.1-14)$$

In the one-dimensional case, $\mathbf{G} = l\mathbf{g} = l2\pi\hat{z}/\Lambda$, so that

$$\mathbf{E}_{\mathbf{K}}(\mathbf{r}) = \sum_l \mathbf{A}(\mathbf{K} - l\mathbf{g}) e^{il(2\pi/\Lambda)z} \quad (6.1-15)$$

is periodic in Λ . Equation (6.1-14) is a normal mode of propagation. The most general solution (6.1-12) now becomes a linear superposition of these normal modes. This completes the proof of Eq. (6.1-5).

Given a frequency ω , Eq. (6.1-13) can be used to obtain the \mathbf{K} vector. If the medium is homogeneous in the x and y directions (i.e., ϵ is independent of x and y), then the Bloch mode of the electric vector becomes, according to Eqs. (6.1-14) and (6.1-15),

$$\mathbf{E} = e^{-i(K_x x + K_y y)} e^{-iK_z z} \mathbf{E}_{\mathbf{K}}(z), \quad (6.1-16)$$

where $\mathbf{E}_{\mathbf{K}}(z)$ is a periodic function of z . In this case, given a frequency ω and a set of (K_x, K_y) , K_z can be determined from Eq. (6.1-13). There exist regions of ω where K_z becomes a complex number, so that the Bloch wave (6.1-16) is evanescent. These are the so-called forbidden bands of the periodic medium. Incident radiation under these conditions will be totally reflected. This phenomenon, in the X-ray regime, is known as Bragg reflection. The phenomena and devices based on periodic media are of most interest near or in their forbidden bands, so we will seek in an approximate

solution for the Bloch waves near the Bragg condition. For the sake of simplicity in illustrating the basic idea, we assume in what follows that the wave propagates in the z direction (i.e., $K_x = K_y = 0$) and the field vector is transverse to the propagation vector ($\mathbf{k} \cdot \mathbf{E} = 0$). In addition, we assume that the medium is isotropic, so that the ϵ_l 's are scalar. Thus Eq. (6.1-13) becomes

$$k^2 A(k) - \omega^2 \mu \sum_l \epsilon_l A(k - lg) = 0. \quad (6.1-17)$$

To find the Bloch wave with wave number K (here we drop the subscript z for the sake of simplicity) we need to solve the set of equations (6.1-17) with $k = K, K \pm g, K \pm 2g, \dots$. Since there are again an infinite number of equations involving $A(K), A(K \pm g), A(K \pm 2g), \dots$, an approximation is required to obtain an explicit result. To make the correct approximation, we need to inspect all the terms involved and neglect the small ones. Writing out the first few terms in Eq. (6.1-17) for $k = K$, we obtain

$$K^2 A(K) - \omega^2 \mu \epsilon_0 A(K) - \omega^2 \mu \epsilon_1 A(K - g) - \omega^2 \mu \epsilon_{-1} A(K + g) - \dots = 0, \quad (6.1-18)$$

which can also be written as

$$A(K) = \frac{1}{K^2 - \omega^2 \mu \epsilon_0} [\omega^2 \mu \epsilon_1 A(K - g) + \omega^2 \mu \epsilon_{-1} A(K + g) + \dots]. \quad (6.1-19)$$

Similarly, Eq. (6.1-17) for $k = K - g$ and $k = K + g$ can be written

$$A(K - g) = \frac{1}{(K - g)^2 - \omega^2 \mu \epsilon_0} [\omega^2 \mu \epsilon_1 A(K - 2g) + \omega^2 \mu \epsilon_{-1} A(K) + \dots] \quad (6.1-20)$$

and

$$A(K + g) = \frac{1}{(K + g)^2 - \omega^2 \mu \epsilon_0} [\omega^2 \mu \epsilon_1 A(K) + \omega^2 \mu \epsilon_{-1} A(K + 2g) + \dots] \quad (6.1-21)$$

respectively. An inspection of Eqs. (6.1-19), (6.1-20), and (6.1-21) shows that if

$$|K - g| \approx K \quad (6.1-22)$$

and

$$K^2 \approx \omega^2 \mu \epsilon_0, \quad (6.1-23)$$

the dominant terms are $A(K)$ and $A(K - g)$. Physically, this means that the plane wave components $A(K)$ and $A(K - g)$ are resonantly coupled. Neglecting all other coefficients, the series of equations (6.1-17) for the Bloch wave with wave number K becomes

$$(K^2 - \omega^2 \mu \epsilon_0)A(K) - \omega^2 \mu \epsilon_1 A(K - g) = 0, \quad (6.1-24)$$

$$- \omega^2 \mu \epsilon_{-1} A(K) + [(K - g)^2 - \omega^2 \mu \epsilon_0]A(K - g) = 0. \quad (6.1-25)$$

Notice that ϵ_0 here denotes the zeroth Fourier component of the dielectric tensor, and $\epsilon_{-1} = \epsilon_1^*$ if ϵ is a real dielectric function.

Equations (6.1-24) and (6.1-25) are two coupled linear equations in the field amplitudes $A(K)$ and $A(K - g)$. A nontrivial solution exists only when the determinant vanishes:

$$\begin{vmatrix} K^2 - \omega^2 \mu \epsilon_0 & -\omega^2 \mu \epsilon_1 \\ -\omega^2 \mu \epsilon_{-1} & (K - g)^2 - \omega^2 \mu \epsilon_0 \end{vmatrix} = 0, \quad (6.1-26)$$

or

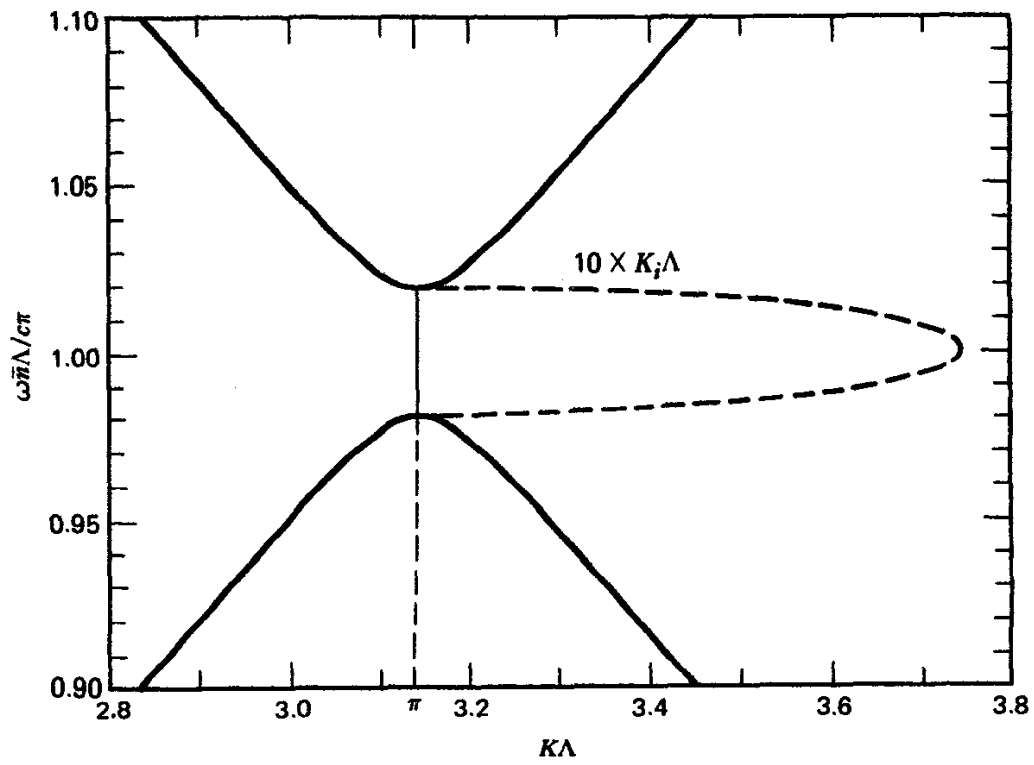
$$(K^2 - \omega^2 \mu \epsilon_0)[(K - g)^2 - \omega^2 \mu \epsilon_0] - (\omega^2 \mu |\epsilon_1|)^2 = 0. \quad (6.1-27)$$

This is an explicit form of the dispersion relation (6.1-6) between ω and K . The Bragg condition (6.1-22) is satisfied at exactly $K = \frac{1}{2}g = \pi/\Lambda$. At this K value, two roots for ω^2 may be obtained from Eq. (6.1-27):

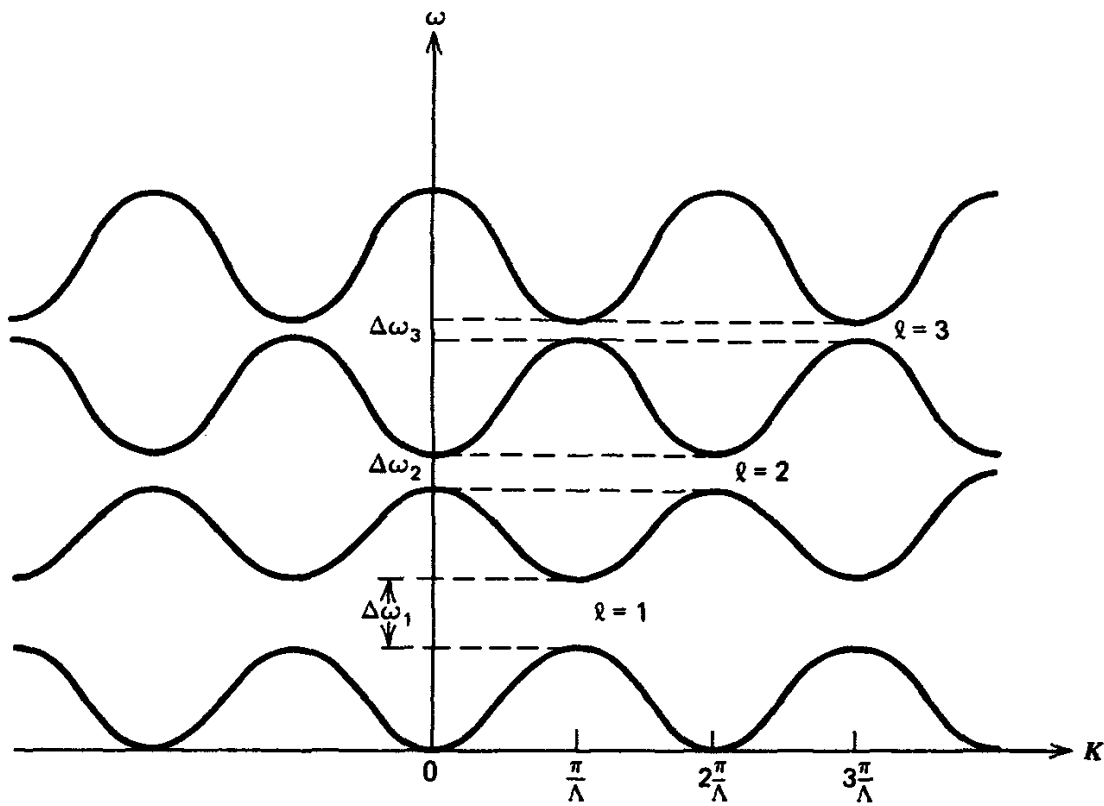
$$\omega_{\pm}^2 = \frac{K^2}{\mu(\epsilon_0 \pm |\epsilon_1|)}. \quad (6.1-28)$$

These are the spectral band edges. At frequencies ω between ω_+ and ω_- , the roots of Eq. (6.1-27) for K are complex, with real part equal to π/Λ . The waves are evanescent, and this spectral regime is referred to as a "forbidden band."

At frequencies ω outside this forbidden band, the roots of Eq. (6.1-27) for K are real and the solutions correspond to propagating waves. The relation



(a)



(b)

Figure 6.2. (a) Dispersion relation near a forbidden band. We notice that K becomes complex when the real part of $K\Lambda$ is π . The dispersion relation is plotted for the periodic structure shown in Fig. 6.3 with $n_1 = 3.2$, $n_2 = 3.4$, $a = b = 0.5\Lambda$. (b) A general dispersion relation $\omega(K)$ showing the fundamental ($l = 1$) and higher-order ($l = 2, 3$) forbidden bands.

(6.1-27) between ω and K is known as the dispersion relation. The dispersion relation (6.1-27) of a typical periodic medium is shown in Fig. 6.2. In a three-dimensional periodic medium, the dispersion relation (6.1-6) corresponds to surfaces of constant frequency in \mathbf{K} space. Forbidden bands of ω can also exist in three-dimensional periodic media. Waves with frequencies in the forbidden bands do not propagate, but are evanescent due to Bragg reflection. This can be easily seen by evaluating the wave number K at the center of the forbidden band when $\omega^2 = (\frac{1}{2}g)^2/\mu\epsilon_0$ [see Eqs. (6.1-22) and (6.1-23)] and $K = \frac{1}{2}g + x$, where $|x| \ll \frac{1}{2}g$. Then Eq. (6.1-27) becomes

$$g^2x^2 + \left(\frac{|\epsilon_1|}{\epsilon_0}\right)^2 \left(\frac{1}{4}g^2\right)^2 = 0. \quad (6.1-29)$$

We neglect the term in x^4 . From Eq. (6.1-29) we obtain the wave number K at the center of the forbidden band:

$$K = \frac{1}{2}g \left(1 \pm i \frac{|\epsilon_1|}{2\epsilon_0}\right). \quad (6.1-30)$$

This wave number is complex and corresponds to an exponentially decaying amplitude. Note that this spatial attenuation is governed essentially by the Fourier expansion coefficient ϵ_1 . The forbidden bandgap is defined as $\Delta\omega_{\text{gap}} = |\omega_+ - \omega_-|$ and is given, according to Eq. (6.1-28), by

$$\Delta\omega_{\text{gap}} = \omega \frac{|\epsilon_1|}{\epsilon_0}. \quad (6.1-31)$$

The bandgap $\Delta\omega_{\text{gap}}$ is proportional to the magnitude of the Fourier expansion coefficient of the dielectric constant. Note from the expressions (6.1-30) and (6.1-31) that the imaginary part of the wave number at the center of the forbidden band is proportional to the fractional bandgap ($\Delta\omega_{\text{gap}}/\omega$) and is given by

$$K_i = \frac{1}{4}g \frac{\Delta\omega_{\text{gap}}}{\omega}, \quad (6.1-32)$$

where we remember that $g = 2\pi/\Lambda$.

In the above derivation, we assumed that the propagation is in the direction of periodic variation of the dielectric constant, that is, along the z axis. For a general direction of propagation (i.e., K_x or $K_y \neq 0$), the dispersion relation is more complicated and is dependent on the polarization state. This will be seen in the next section when we study wave propagation in periodic layered media.

In the derivation of the dispersion relation (6.1-27), we assumed that $|K - g| \approx K$ [Eq. (6.1-22)] and $K^2 \approx \omega^2 \mu \epsilon_0$ [Eq. (6.1-23)], which result in a resonant coupling between the coefficients $A(K)$ and $A(K - g)$. The forbidden band associated with this Bragg condition (6.1-22) is governed by the Fourier expansion coefficient ϵ_l of the dielectric function $\epsilon(z)$. In general, there is a forbidden band associated with each Fourier expansion coefficient ϵ_l of the dielectric function $\epsilon(z)$. To illustrate this, we consider the case when

$$|K - lg| \approx K, \quad l = \pm 1, \pm 2, \dots, \quad (6.1-33)$$

and

$$K^2 \approx \omega^2 \mu \epsilon_0. \quad (6.1-34)$$

An argument identical to that leading to Eqs. (6.1-24) and (6.1-25) will now give

$$(K^2 - \omega^2 \mu \epsilon_0) A(K) - \omega^2 \mu \epsilon_l A(K - lg) = 0, \quad (6.1-35)$$

$$- \omega^2 \mu \epsilon_{-l} A(K) + [(K - lg)^2 - \omega^2 \mu \epsilon_0] A(K - lg) = 0. \quad (6.1-36)$$

This leads to a forbidden band at

$$K = l \frac{g}{2} = l \frac{\pi}{\Lambda}, \quad (6.1-37)$$

which now involves $\epsilon_{-l} = \epsilon_l^*$, so that the bandgap is given by

$$(\Delta\omega_{\text{gap}})_l = \frac{\omega |\epsilon_l|}{\epsilon_0}. \quad (6.1-38)$$

For $l \neq 1$, these bands are referred to as the higher-order forbidden bands, and they occur at higher frequencies because of the conditions (6.1-37) and (6.1-34). In many cases, the Fourier expansion coefficient ϵ_l becomes small as l increases (i.e., $\epsilon_l \rightarrow 0$ as $l \rightarrow \infty$). The corresponding forbidden bands are small, according to Eq. (6.1-38). A general dispersion relation $\omega(K)$ is shown in Fig. 6.2(b).

6.2. PERIODIC LAYERED MEDIA

The simplest periodic medium is one made up of alternating layers of transparent materials with different refractive indices. Recent advances in crystal growth, especially in molecular-beam epitaxy, make it possible to grow periodic layered media with well-controlled periodicities and with layer thicknesses corresponding to a few atomic layers. Wave propagation in periodic layered media has been studied by many workers [1, 2]. Exact solutions of the wave equation can be obtained in this case. We will assume that the materials are nonmagnetic. The simplest periodic layered medium consists of two different materials with a refractive index profile given by

$$n(z) = \begin{cases} n_2, & 0 < z < b, \\ n_1, & b < z < \Lambda, \end{cases} \quad (6.2-1)$$

with

$$n(z) = n(z + \Lambda) \quad (6.2-2)$$

where the z axis is normal to the layer interfaces and Λ is the period. The geometry of the structure is sketched in Fig. 6.3. To solve for the electric field vectors of the Bloch wave, we follow the approach described in [2]. The electric field vector of a general solution of the wave equation can be of the form

$$\mathbf{E}(z) e^{i(\omega t - k_y y)}, \quad (6.2-3)$$

where we have assumed that the plane of propagation is the yz plane; k_y is the y component of the wave propagation vector, which remains constant throughout the medium. The electric field within each homogeneous layer can be expressed as a sum of an incident and a reflected plane wave. The complex amplitudes of these two waves constitute the components of a column vector. The electric field in layer α ($\alpha = 1, 2$) of the n th unit cell can thus be represented by a column vector

$$\begin{pmatrix} a_n^{(\alpha)} \\ b_n^{(\alpha)} \end{pmatrix}, \quad \alpha = 1, 2. \quad (6.2-4)$$

As a result, the electric-field distribution in the same layer can be written

$$E(y, z) = [a_n^{(\alpha)} e^{-ik_{\alpha z}(z - n\Lambda)} + b_n^{(\alpha)} e^{ik_{\alpha z}(z - n\Lambda)}] e^{-ik_y y} \quad (6.2-5)$$

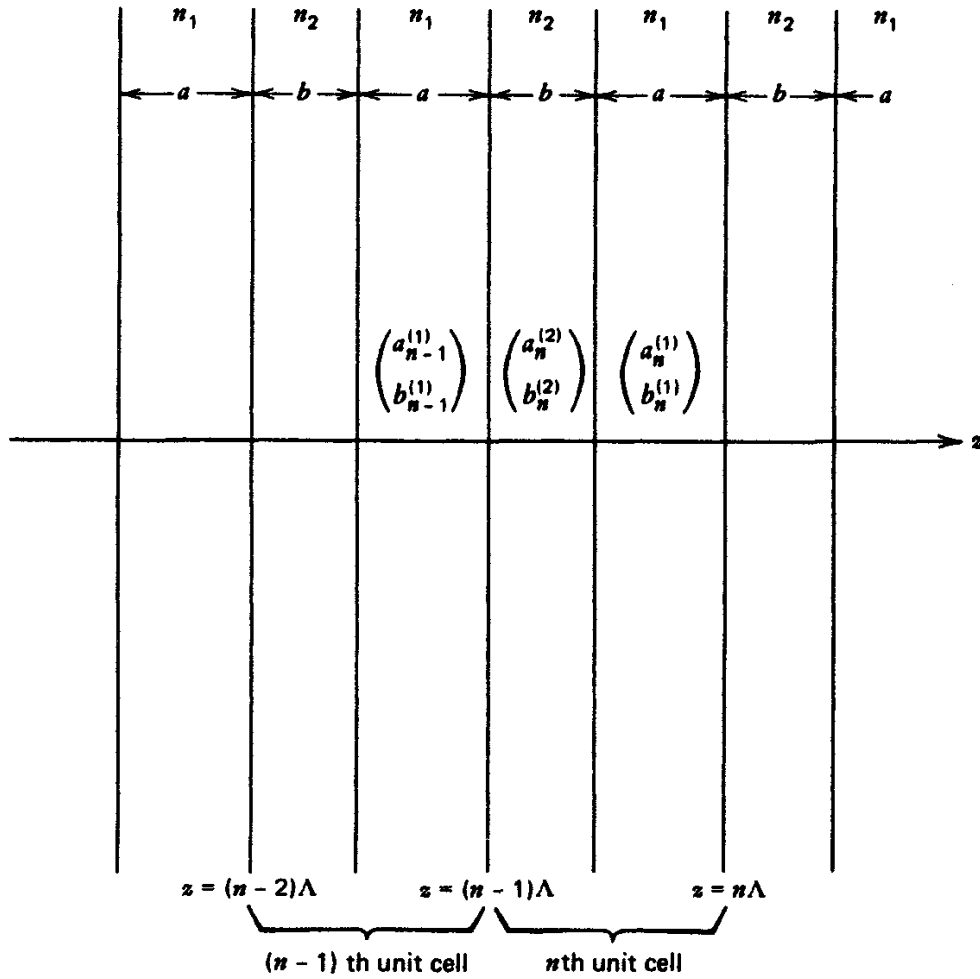


Figure 6.3. A schematic drawing of a periodic layered medium and the plane-wave amplitudes associated with the n th unit cell and its neighboring layers.

with

$$k_{\alpha z} = \left[\left(\frac{n_{\alpha} \omega}{c} \right)^2 - k_y^2 \right]^{1/2}, \quad \alpha = 1, 2. \quad (6.2-6)$$

The column vectors are not independent of each other. They are related through the continuity conditions at the interfaces. As a consequence, only one vector (or two components of different vectors) can be chosen arbitrarily. In the case of TE waves (\mathbf{E} perpendicular to yz plane), imposing the continuity of E_x and H_y ($H_y \propto \partial E_x / \partial z$) at the interfaces (see Fig. 6.3), $z = (n-1)\Lambda$ and $z = (n-1)\Lambda + b$, leads to

$$\begin{aligned} a_{n-1} + b_{n-1} &= e^{ik_{2z}\Lambda} c_n + e^{-ik_{2z}\Lambda} d_n, \\ ik_{1z}(a_{n-1} - b_{n-1}) &= ik_{2z}(e^{ik_{2z}\Lambda} c_n - e^{-ik_{2z}\Lambda} d_n), \\ e^{ik_{2z}a} c_n + e^{-ik_{2z}a} d_n &= e^{ik_{1z}a} a_n + e^{-ik_{1z}a} b_n, \\ ik_{2z}(e^{ik_{2z}a} c_n - e^{-ik_{2z}a} d_n) &= ik_{1z}(e^{ik_{1z}a} a_n - e^{-ik_{1z}a} b_n). \end{aligned} \quad (6.2-7)$$

These four equations can be rewritten as the following two matrix equations:

$$\begin{pmatrix} 1 & 1 \\ 1 & -1 \end{pmatrix} \begin{pmatrix} a_{n-1} \\ b_{n-1} \end{pmatrix} = \begin{pmatrix} e^{ik_{2z}\Lambda} & e^{-ik_{2z}\Lambda} \\ \frac{k_{2z}}{k_{1z}} e^{ik_{2z}\Lambda} & -\frac{k_{2z}}{k_{1z}} e^{-ik_{2z}\Lambda} \end{pmatrix} \begin{pmatrix} c_n \\ d_n \end{pmatrix}, \quad (6.2-8)$$

$$\begin{pmatrix} e^{ik_{2z}a} & e^{-ik_{2z}a} \\ e^{ik_{2z}a} & -e^{-ik_{2z}a} \end{pmatrix} \begin{pmatrix} c_n \\ d_n \end{pmatrix} = \begin{pmatrix} e^{ik_{1z}a} & e^{-ik_{1z}a} \\ \frac{k_{1z}}{k_{2z}} e^{ik_{1z}a} & -\frac{k_{1z}}{k_{2z}} e^{-ik_{1z}a} \end{pmatrix} \begin{pmatrix} a_n \\ b_n \end{pmatrix}, \quad (6.2-9)$$

where we define

$$\begin{aligned} a_n &\equiv a_n^{(1)}, \\ b_n &\equiv b_n^{(1)}, \\ \hat{c}_n &\equiv a_n^{(2)}, \\ d_n &\equiv b_n^{(2)}. \end{aligned} \quad (6.2-10)$$

By eliminating

$$\begin{pmatrix} c_n \\ d_n \end{pmatrix},$$

the matrix equation

$$\begin{pmatrix} a_{n-1} \\ b_{n-1} \end{pmatrix} = \begin{pmatrix} A & B \\ C & D \end{pmatrix} \begin{pmatrix} a_n \\ b_n \end{pmatrix} \quad (6.2-11)$$

is obtained. The matrix elements are

$$A = e^{ik_{1z}a} \left[\cos k_{2z}b + \frac{1}{2}i \left(\frac{k_{2z}}{k_{1z}} + \frac{k_{1z}}{k_{2z}} \right) \sin k_{2z}b \right]$$

$$B = e^{-ik_{1z}a} \left[\frac{1}{2}i \left(\frac{k_{2z}}{k_{1z}} - \frac{k_{1z}}{k_{2z}} \right) \sin k_{2z}b \right]$$

$$C = e^{ik_{1z}a} \left[-\frac{1}{2}i \left(\frac{k_{2z}}{k_{1z}} - \frac{k_{1z}}{k_{2z}} \right) \sin k_{2z}b \right] \quad (6.2-12)$$

$$D = e^{-ik_{1z}a} \left[\cos k_{2z}b - \frac{1}{2}i \left(\frac{k_{2z}}{k_{1z}} + \frac{k_{1z}}{k_{2z}} \right) \sin k_{2z}b \right].$$

The matrix in Eq. (6.2-11) is a unit-cell translation matrix which relates the complex amplitudes of the plane waves in layer 1 of a unit cell to those of the equivalent layer in the next unit cell. Because this matrix relates the field amplitudes of two equivalent layers with the same index of refraction, it is unimodular, that is,

$$AD - BC = 1. \quad (6.2-13)$$

It is important to note that the unit-cell translation matrix which relates the field amplitudes in layer 2 is different from the matrix in Eq. (6.2-12). These matrices, however, possess the same trace. It will be shown later that the trace of a unit-cell translational matrix is directly related to the band structure of the periodic medium.

The matrix elements (A , B , C , D) for TM waves (\mathbf{H} perpendicular to yz plane) are slightly different from those for TE waves. They are given by

$$\begin{aligned} A_{\text{TM}} &= e^{ik_{1z}a} \left[\cos k_{2z}b + \frac{1}{2}i \left(\frac{n_2^2 k_{1z}}{n_1^2 k_{2z}} + \frac{n_1^2 k_{2z}}{n_2^2 k_{1z}} \right) \sin k_{2z}b \right], \\ B_{\text{TM}} &= e^{-ik_{1z}a} \left[\frac{1}{2}i \left(\frac{n_2^2 k_{1z}}{n_1^2 k_{2z}} - \frac{n_1^2 k_{2z}}{n_2^2 k_{1z}} \right) \sin k_{2z}b \right], \\ C_{\text{TM}} &= e^{ik_{1z}a} \left[-\frac{1}{2}i \left(\frac{n_2^2 k_{1z}}{n_1^2 k_{2z}} - \frac{n_1^2 k_{2z}}{n_2^2 k_{1z}} \right) \sin k_{2z}b \right], \\ D_{\text{TM}} &= e^{-ik_{1z}a} \left[\cos k_{2z}b - \frac{1}{2}i \left(\frac{n_2^2 k_{1z}}{n_1^2 k_{2z}} + \frac{n_1^2 k_{2z}}{n_2^2 k_{1z}} \right) \sin k_{2z}b \right]. \end{aligned} \quad (6.2-14)$$

As noted above, only one column vector is independent. We can choose it, for example, as the column vector of layer 1 in the zeroth unit cell. The remaining column vectors of the equivalent layers are related to that of the zeroth unit cell by

$$\begin{pmatrix} a_0 \\ b_0 \end{pmatrix} = \begin{pmatrix} A & B \\ C & D \end{pmatrix}^n \begin{pmatrix} a_n \\ b_n \end{pmatrix}, \quad (6.2-15a)$$

which can be inverted to yield

$$\begin{pmatrix} a_n \\ b_n \end{pmatrix} = \left[\begin{pmatrix} A & B \\ C & D \end{pmatrix}^{-1} \right]^n \begin{pmatrix} a_0 \\ b_0 \end{pmatrix} = \begin{pmatrix} A & B \\ C & D \end{pmatrix}^{-n} \begin{pmatrix} a_0 \\ b_0 \end{pmatrix}. \quad (6.2-15b)$$

By using the identity

$$\begin{pmatrix} A & B \\ C & D \end{pmatrix}^{-1} = \begin{pmatrix} D & -B \\ -C & A \end{pmatrix}$$

for unimodular matrices, Eq. (6.2-15) can be simplified to

$$\begin{pmatrix} a_n \\ b_n \end{pmatrix} = \begin{pmatrix} D & -B \\ -C & A \end{pmatrix}^n \begin{pmatrix} a_0 \\ b_0 \end{pmatrix}. \quad (6.2-16)$$

The column vector for layer 2 of the same unit cell can always be obtained by using Eq. (6.2-9).

6.2.1. Bloch Waves and Band Structures

A periodic layered medium is equivalent to a one-dimensional crystal which is invariant under lattice translations. The lattice-translation operator T is defined by $Tz = z - l\Lambda$, where l is an integer; it follows that

$$T\mathbf{E}(z) = \mathbf{E}(T^{-1}z) = \mathbf{E}(z + l\Lambda). \quad (6.2-17)$$

The $ABCD$ matrix derived above is a representation of the unit-cell translation operator. According to the Bloch theorem derived in Section 6.1, the electric field vector of a normal mode in a periodic layered medium is of the form

$$\mathbf{E} = \mathbf{E}_K(z) e^{-iKz} e^{i(\omega t - k_y y)}, \quad (6.2-18)$$

where $\mathbf{E}_K(z)$ is periodic with period Λ , that is,

$$\mathbf{E}_K(z) = \mathbf{E}_K(z + \Lambda). \quad (6.2-19)$$

The subscript K indicates that the function $\mathbf{E}_K(z)$ depends on K . The constant K is known as the Bloch wave number. The problem at hand is thus that of determining K and $\mathbf{E}_K(z)$ as functions of ω and k_y . (Note that $k_y = K_y$ and the subscript of K_z is dropped for the sake of simplicity in notation.)

In terms of our column-vector representation, and from Eq. (6.2-5), the periodic condition (6.2-19) for the Bloch wave is simply

$$\begin{pmatrix} a_n \\ b_n \end{pmatrix} = e^{-iK\Lambda} \begin{pmatrix} a_{n-1} \\ b_{n-1} \end{pmatrix}. \quad (6.2-20)$$

It follows from Eqs. (6.2-11) and (6.2-20) that the column vector of the Bloch wave satisfies the following eigenvalue equation:

$$\begin{pmatrix} A & B \\ C & D \end{pmatrix} \begin{pmatrix} a_n \\ b_n \end{pmatrix} = e^{iK\Lambda} \begin{pmatrix} a_n \\ b_n \end{pmatrix}. \quad (6.2-21)$$

The phase factor $e^{iK\Lambda}$ is thus the eigenvalue of the translation matrix (A, B, C, D) and satisfies the secular equation

$$\begin{vmatrix} A - e^{iK\Lambda} & B \\ C & D - e^{iK\Lambda} \end{vmatrix} = 0.$$

The solutions are

$$e^{iK\Lambda} = \frac{1}{2}(A + D) \pm \left\{ \left[\frac{1}{2}(A + D) \right]^2 - 1 \right\}^{1/2}. \quad (6.2-22)$$

The eigenvectors corresponding to the eigenvalues are obtained from Eq. (6.2-21) and are

$$\begin{pmatrix} a_0 \\ b_0 \end{pmatrix} = \begin{pmatrix} B \\ e^{iK\Lambda} - A \end{pmatrix} \quad (6.2-23a)$$

times any arbitrary constant. The corresponding column vectors for the n th unit cell are given according to Eq. (6.2-20), by

$$\begin{pmatrix} a_n \\ b_n \end{pmatrix} = e^{-inK\Lambda} \begin{pmatrix} B \\ e^{iK\Lambda} - A \end{pmatrix}. \quad (6.2-23b)$$

The Bloch waves which result from Eq. (6.2-23) can be considered as the eigenvectors of the translation matrix with eigenvalues $e^{iK\Lambda}$ given by Eq. (6.2-22). The two eigenvalues in (6.2-22) are reciprocals of each other, since the translation matrix is unimodular. Equation (6.2-22) gives the dispersion relation between ω , k_y , and K for the Bloch wave function

$$K(k_y, \omega) = \frac{1}{\Lambda} \cos^{-1} \left[\frac{1}{2}(A + D) \right]. \quad (6.2-24)$$

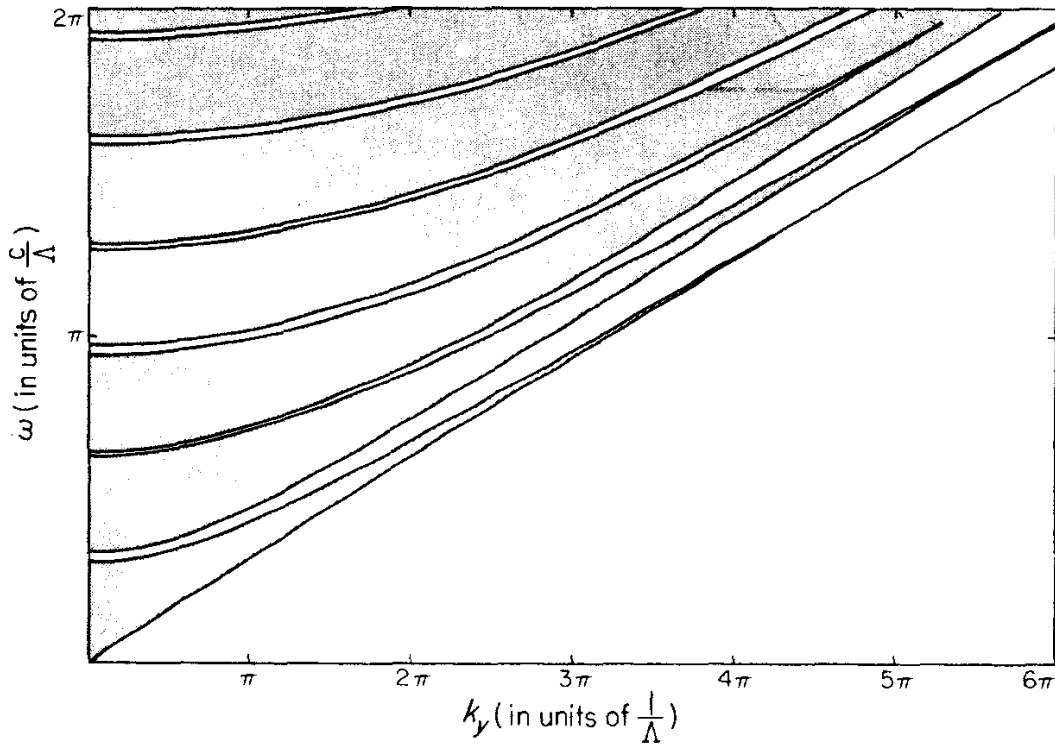


Figure 6.4. TE waves (\mathbf{E} perpendicular to the direction of periodicity): band structure in the ωk_y plane. The dark zones are the allowed bands.

Regimes where $|\frac{1}{2}(A \pm D)| < 1$ correspond to real K and thus to propagating Bloch waves; when $|\frac{1}{2}(A + D)| > 1$, however, $K = m\pi/\Lambda + iK_i$, and so K has an imaginary part K_i and the Bloch wave is evanescent. These regions are the so-called “forbidden” bands of the periodic medium. The band-edge frequencies are those where $|\frac{1}{2}(A + D)| = 1$.

According to Eqs. (6.2-5) and (6.2-23), the final result for the Bloch wave in layer 1 of the n th unit cell is

$$E_K(z)e^{-iKz} = \left[(a_0 e^{-ik_{1z}(z-n\Lambda)} + b_0 e^{ik_{1z}(z-n\Lambda)}) e^{iK(z-n\Lambda)} \right] e^{-iKz}, \quad (6.2-25)$$

where a_0 and b_0 are given by Eq. (6.2-23a). Note that the function inside the square brackets is independent of n and therefore is periodic with period Λ . This completes the solution of the Bloch waves.

The dispersion relation (6.2-24) gives the Bloch wave number K along the z direction for the Bloch wave with frequency ω and y component k_y of the wave vector. It can be represented by a surface in a three-dimensional space (K, k_y, ω) . The intersections of this surface with the planes $K = m\pi/\Lambda$ are curves which represent band edges. The projection of these curves on the

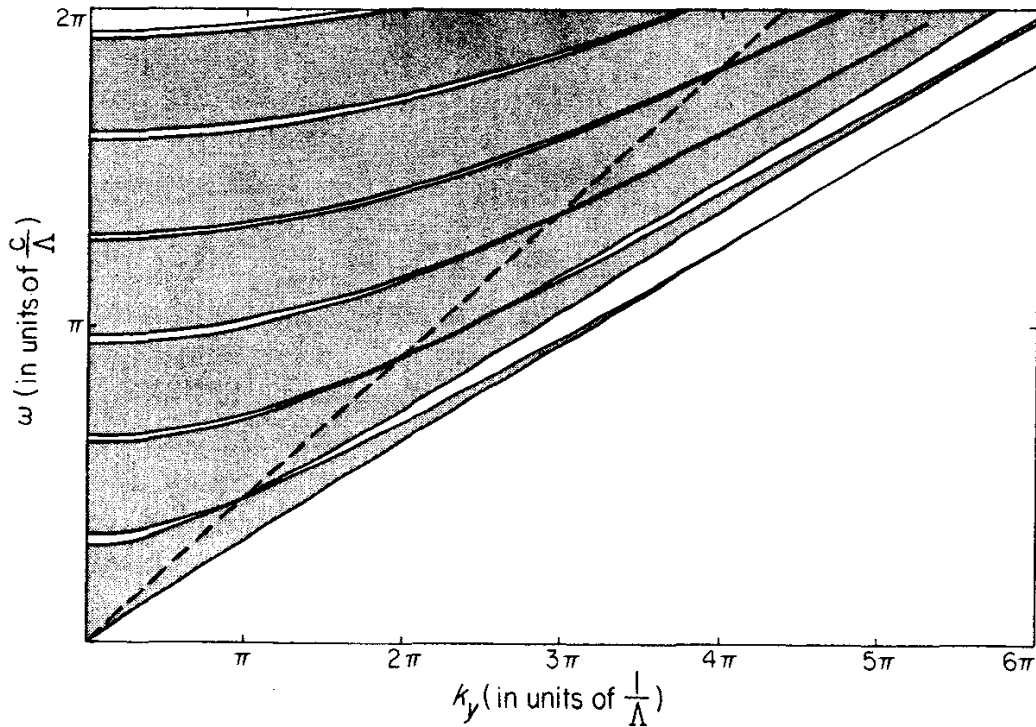


Figure 6.5. TM waves (\mathbf{H} perpendicular to the direction of periodicity): band structure in the ωk_y plane. The dashed line is $k_y = (\omega/c)n_2 \sin \theta_B$. The dark zones are the allowed bands.

$k_y \omega$ plane is shown in Figs. 6.4 and 6.5 for TE and TM waves, respectively. The dark zones are the allowed bands where K is a real number. It is interesting to notice that the TM “forbidden” bands shrink to zero when $k_y = (\omega/c)n_2 \sin \theta_B$ with θ_B the Brewster angle, since at this angle the Fresnel reflection at the interfaces vanishes and the incident and reflected waves are uncoupled. This dispersion relation ω versus K for the special case $k_y = 0$ (i.e., normal incidence) is shown in Fig. 6.6. It can be written as

$$\cos K\Lambda = \cos k_1 a \cos k_2 b - \frac{1}{2} \left(\frac{n_2}{n_1} + \frac{n_1}{n_2} \right) \sin k_1 a \sin k_2 b, \quad (6.2-26)$$

with $k_1 = (\omega/c)n_1$ and $k_2 = (\omega/c)n_2$.

Equation (6.2-26) can be solved approximately for K in the forbidden band. In the first forbidden gap $\text{Re } K = \pi/\Lambda$ we put

$$K\Lambda = \pi \pm ix. \quad (6.2-27)$$

Let ω_0 be the center of the forbidden band such that

$$k_1 a = k_2 b = \frac{1}{2}\pi. \quad (6.2-28)$$

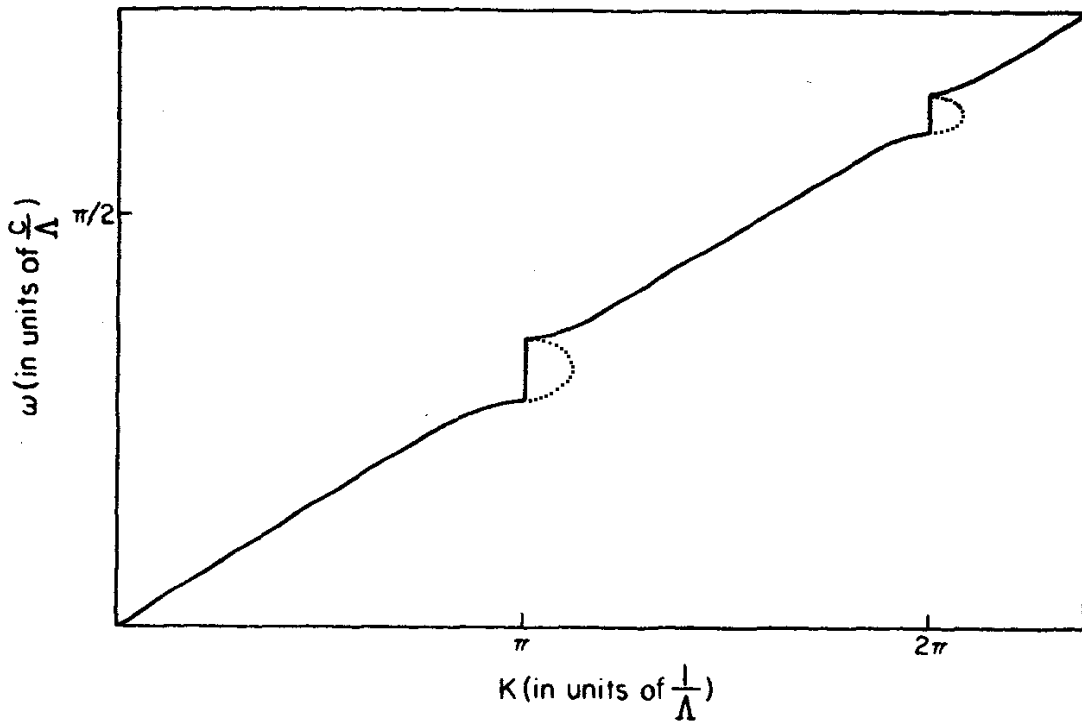


Figure 6.6. The dispersion relation between ω and K when $k_y = 0$ (normal incidence). The dotted curves give the imaginary part of K in arbitrary units.

A structure with this condition is known as a quarter-wave stack. At frequency ω_0 , Eq. (6.2-26) becomes

$$\cos K\Lambda = -\frac{1}{2} \left(\frac{n_1}{n_2} + \frac{n_2}{n_1} \right). \quad (6.2-29)$$

By substituting Eq. (6.2-27) in (6.2-29) and solving for x , we obtain

$$x = \left| \log \frac{n_2}{n_1} \right| \approx 2 \frac{n_2 - n_1}{n_2 + n_1}. \quad (6.2-30)$$

where the approximate equality on the right holds when $|n_2 - n_1| \ll n_{1,2}$. This is the imaginary part of $K\Lambda$ at the center of the forbidden band. Within the forbidden band, x varies from zero at band edges to this maximum value (6.2-30) at ω_0 .

Let y be the normalized frequency deviation from the center of the forbidden band ω_0 , that is,

$$y = \frac{\omega - \omega_0}{c} n_1 a = \frac{\omega - \omega_0}{c} n_2 b. \quad (6.2-31)$$

Substitution of Eqs. (6.2-27) and (6.2-31) in Eq. (6.2-26) leads to

$$\cosh x = \frac{1}{2} \left(\frac{n_2}{n_1} + \frac{n_1}{n_2} \right) \cos^2 y - \sin^2 y. \quad (6.2-32)$$

This is an expression for the imaginary part of $K\Lambda$ in the forbidden band as a function of frequency. The band edges are obtained by setting $x = 0$. The result is

$$y_{\text{edge}} = \pm \frac{n_2 - n_1}{n_2 + n_1}. \quad (6.2-33)$$

The bandgap $\Delta\omega_{\text{gap}}$ in terms of frequency is thus given by

$$\Delta\omega_{\text{gap}} = \omega_0 \frac{4}{\pi} \cdot \frac{|n_2 - n_1|}{n_2 + n_1} \approx \omega_0 \frac{2}{\pi} \cdot \frac{\Delta n}{n}, \quad (6.2-34)$$

whereas the imaginary part of $K\Lambda$ at the center of the forbidden band is

$$(K_i\Lambda)_{\text{max}} = 2 \frac{|n_2 - n_1|}{n_2 + n_1} \approx \frac{\Delta n}{n}, \quad (6.2-35)$$

where $\Delta n = |n_2 - n_1|$ and $n = (n_1 + n_2)/2$. These expressions are consistent with the expressions (6.1-31) and (6.1-32) derived in Section 6.1. As an exercise, the student may want to find the Fourier expansion coefficients of the dielectric constant for the periodic layered medium. The result is

$$\frac{|\epsilon_1|}{\epsilon_0} = \frac{4}{\pi} \frac{|n_2 - n_1|}{n_2 + n_1}. \quad (6.2-36)$$

6.3. BRAGG REFLECTION

Consider a periodic layered medium with N unit cells. The geometry of the structure is sketched in Fig. 6.7. The coefficient of reflection is given by

$$r_N = \left(\frac{b_0}{a_0} \right)_{b_N=0}, \quad (6.3-1)$$

that is, it is the ratio of the complex reflected amplitude b_0 at the input to the incident amplitude a_0 , subject to the boundary condition that to the right of the stack there is no wave incident on it (i.e., $b_N = 0$). From Eq.

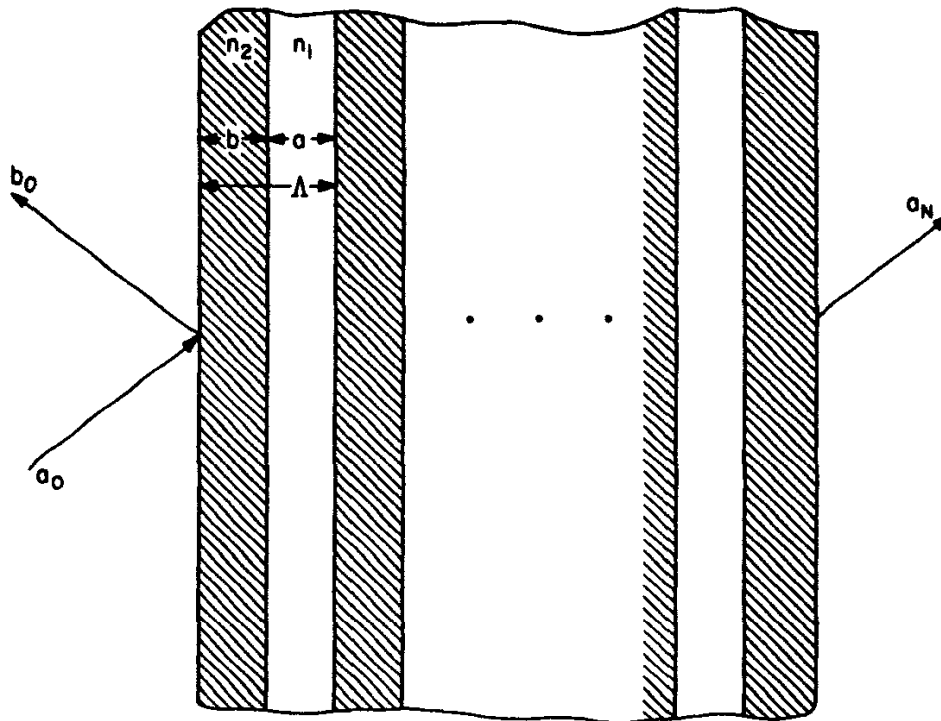


Figure 6.7. The geometry of a typical N -period Bragg reflector.

(6.2-15) we have the following:

$$\begin{pmatrix} a_0 \\ b_0 \end{pmatrix} = \begin{pmatrix} A & B \\ C & D \end{pmatrix}^N \begin{pmatrix} a_N \\ b_N \end{pmatrix}. \quad (6.3-2)$$

The N th power of a unimodular matrix can be simplified by the following matrix identity [see Eq. (5.3-4)]:

$$\begin{pmatrix} A & B \\ C & D \end{pmatrix}^N = \begin{pmatrix} AU_{N-1} - U_{N-2} & BU_{N-1} \\ CU_{N-1} & DU_{N-1} - U_{N-2} \end{pmatrix}, \quad (6.3-3)$$

where

$$U_N = \frac{\sin(N+1)K\Lambda}{\sin K\Lambda} \quad (6.3-4)$$

with K given by Eq. (6.2-24)

The coefficient of reflection is obtained from Eqs. (6.3-1), (6.3-2), and (6.3-3) as

$$r_N = \frac{CU_{N-1}}{AU_{N-1} - U_{N-2}}. \quad (6.3-5)$$

The reflectivity is obtained (Problem 6.10) by taking the absolute square of r_N ,

$$|r_N|^2 = \frac{|C|^2}{|C|^2 + \left(\frac{\sin K\Lambda}{\sin NK\Lambda} \right)^2}. \quad (6.3-6)$$

We have here an analytic expression for the reflectivity of a multilayer reflector. It is important to remember that this reflectivity formula is only valid when the light is incident from a medium with a refractive index n_1 (Problem 6.11). The term $|C|^2$ is directly related to the reflectivity of a single unit cell by

$$|r_1|^2 = \frac{|C|^2}{|C|^2 + 1} \quad (6.3-7)$$

or

$$|C|^2 = \frac{|r_1|^2}{1 - |r_1|^2}. \quad (6.3-8)$$

The $|r_1|^2$ for a typical Bragg reflector is usually much less than one. As a result, $|C|^2$ is roughly equal to $|r_1|^2$. The second term in the denominator of Eq. (6.3-6), for large N , is a fast-varying function of K , or alternatively, of k_y and ω . Therefore, it dominates the structure of the reflectivity spectrum. Between any two “forbidden” bands there are exactly $N - 1$ nodes where the reflectivity vanishes. The peaks of the reflectivity occur at the centers of the “forbidden” bands. There are exactly $N - 2$ side lobes, which are all under the envelope $|C|^2 / [|C|^2 + (\sin K\Lambda)^2]$. At the band edges, $K\Lambda = m\pi$ and the reflectivity is given by

$$|r_N|^2 = \frac{|C|^2}{|C|^2 + (1/N)^2}. \quad (6.3-9)$$

In the “forbidden” gap, $K\Lambda$ is a complex number:

$$K\Lambda = m\pi + iK_i\Lambda, \quad (6.3-10)$$

and the reflectivity formula (6.3-6) becomes

$$|r_N|^2 = \frac{|C|^2}{|C|^2 + \left(\frac{\sinh K_i\Lambda}{\sinh NK_i\Lambda} \right)^2}. \quad (6.3-11)$$

For large N , the second term in the denominator approaches zero exponentially as $e^{-2(N-1)K_1\Lambda}$. It follows that the reflectivity in the forbidden gap is near unity for a Bragg reflector with a substantial number of periods.

TE and TM waves have different band structures and different reflectivities. For TM waves incident at the Brewster angle θ_B , there is no reflected wave regardless of the number of plates N . This is due to the vanishing of the dynamical factor $|C|^2$ at that angle.

The reflectivity for some typical Bragg reflectors as a function of frequency and angle of incidence is shown in Figs. 6.8 and 6.9.

At the center of each forbidden gap, the period of the layered medium is approximately an integral multiple of the light wavelength. The light waves will be highly reflected, since successive reflections from the neighboring interfaces will be in phase with one another and therefore will be constructively superimposed. This situation is analogous to the Bragg reflection of X-rays from crystal planes. This high reflectivity has been demonstrated in a Bragg reflector made of alternating layers of GaAs and $\text{Al}_{0.3}\text{Ga}_{0.7}\text{As}$ grown on a GaAs substrate by molecular-beam epitaxy [see Fig. 6.9(a)]. The measured reflectivity, shown in Fig. 6.9(c), is in good agreement with the theory [3].

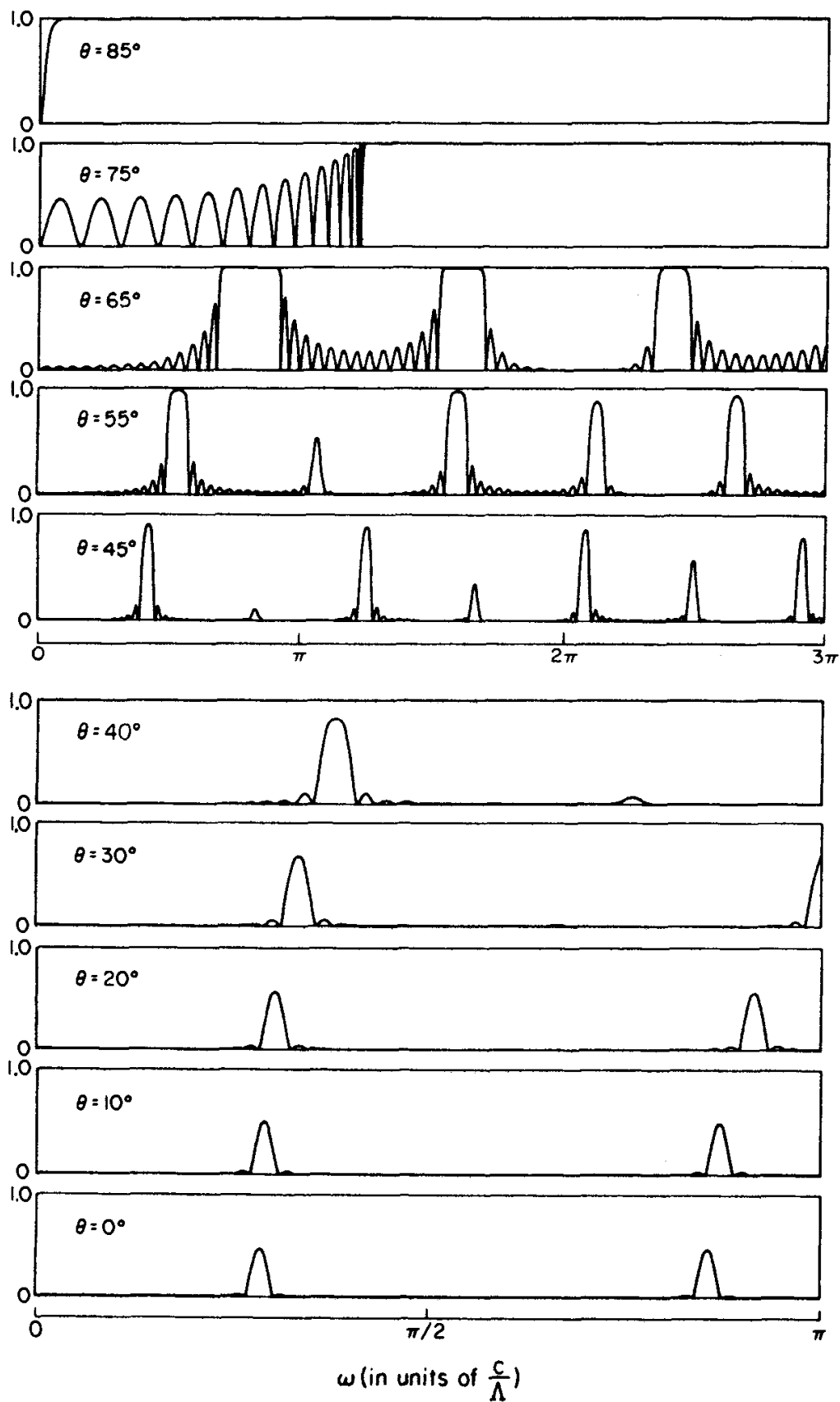
6.4. COUPLED-MODE THEORY

In Section 6.2 we obtained an exact solution for the propagation of electromagnetic radiation in a periodic layered medium. There are, however, many periodic media in which only approximate solutions of the Maxwell's equation can be obtained. Two approaches are generally used. One is the Bloch-wave formalism discussed in Section 6.1. The other is the coupled-mode theory. In the latter theory, the periodic variation of the dielectric tensor is considered as a perturbation that couples the unperturbed normal modes of the structure. In other words, the dielectric tensor as a function of space is written as

$$\epsilon(x, y, z) = \epsilon_0(x, y) + \Delta\epsilon(x, y, z), \quad (6.4-1)$$

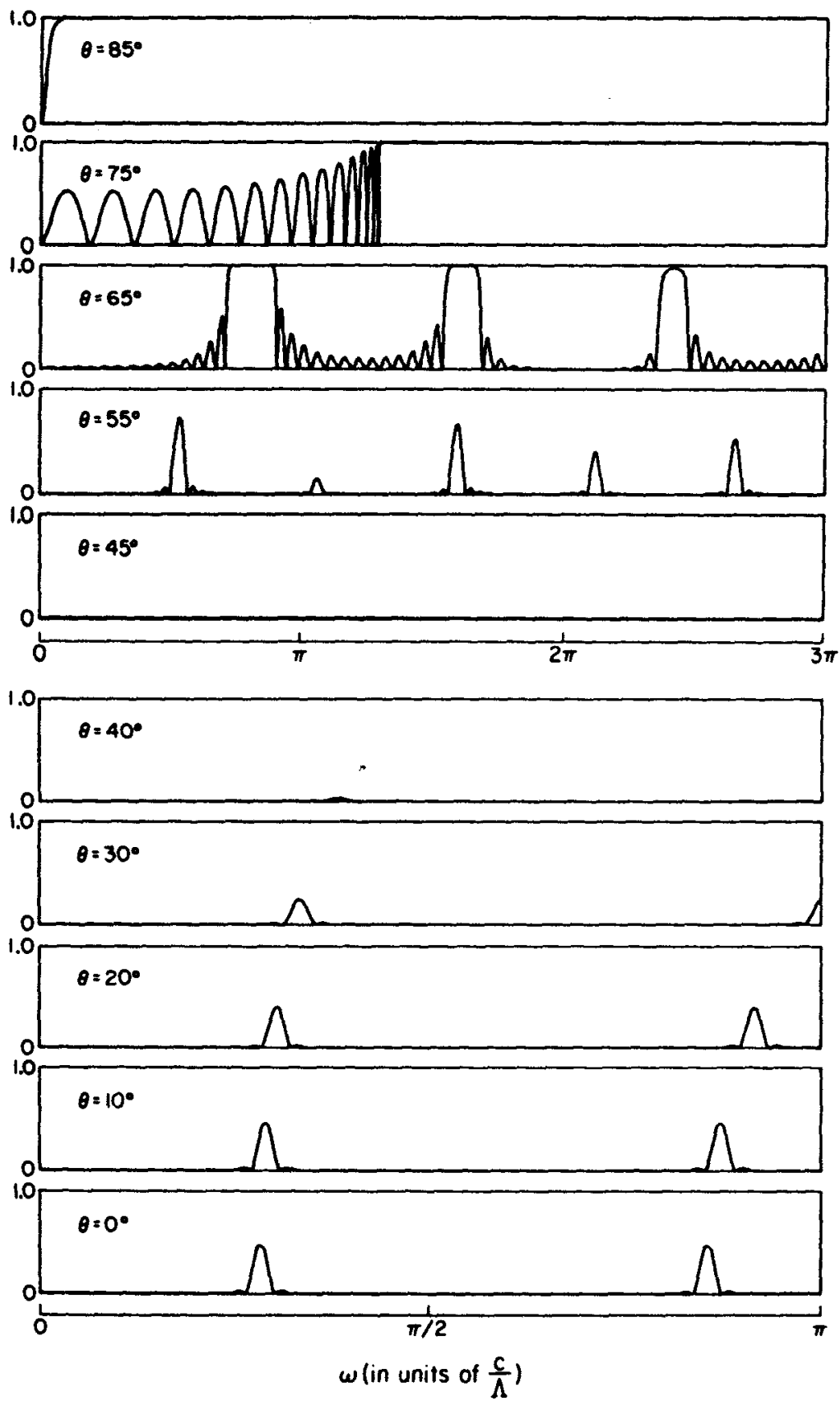
where $\epsilon_0(x, y)$ is the unperturbed part of the dielectric tensor, and $\Delta\epsilon(x, y, z)$ is periodic in the z direction and is the only periodically varying part of the dielectric tensor. If we compare Eq. (6.4-1) with the Fourier expansion of $\epsilon(x, y, z)$ as in Eq. (6.1-10), then $\epsilon_0(x, y)$ is the zeroth component of the series and $\Delta\epsilon(x, y, z)$ contains the rest of the series.

We assume that the normal modes of propagation in the unperturbed dielectric medium described by the dielectric tensor $\epsilon_0(x, y)$ are known.



(a)

Figure 6.8. Reflectivity spectrum of a 15-period Bragg reflector for (a) TE waves and (b) TM waves at various angle of incidence. The indices of refraction of the layers are taken as $n_1 = 3.4$ and $n_2 = 3.6$, and the layer thicknesses are such that $a = b = \frac{1}{2}\Lambda$. The Brewster angle is $\theta_B = 46.6^\circ$.



(b)

Figure 6.8. (Continued)

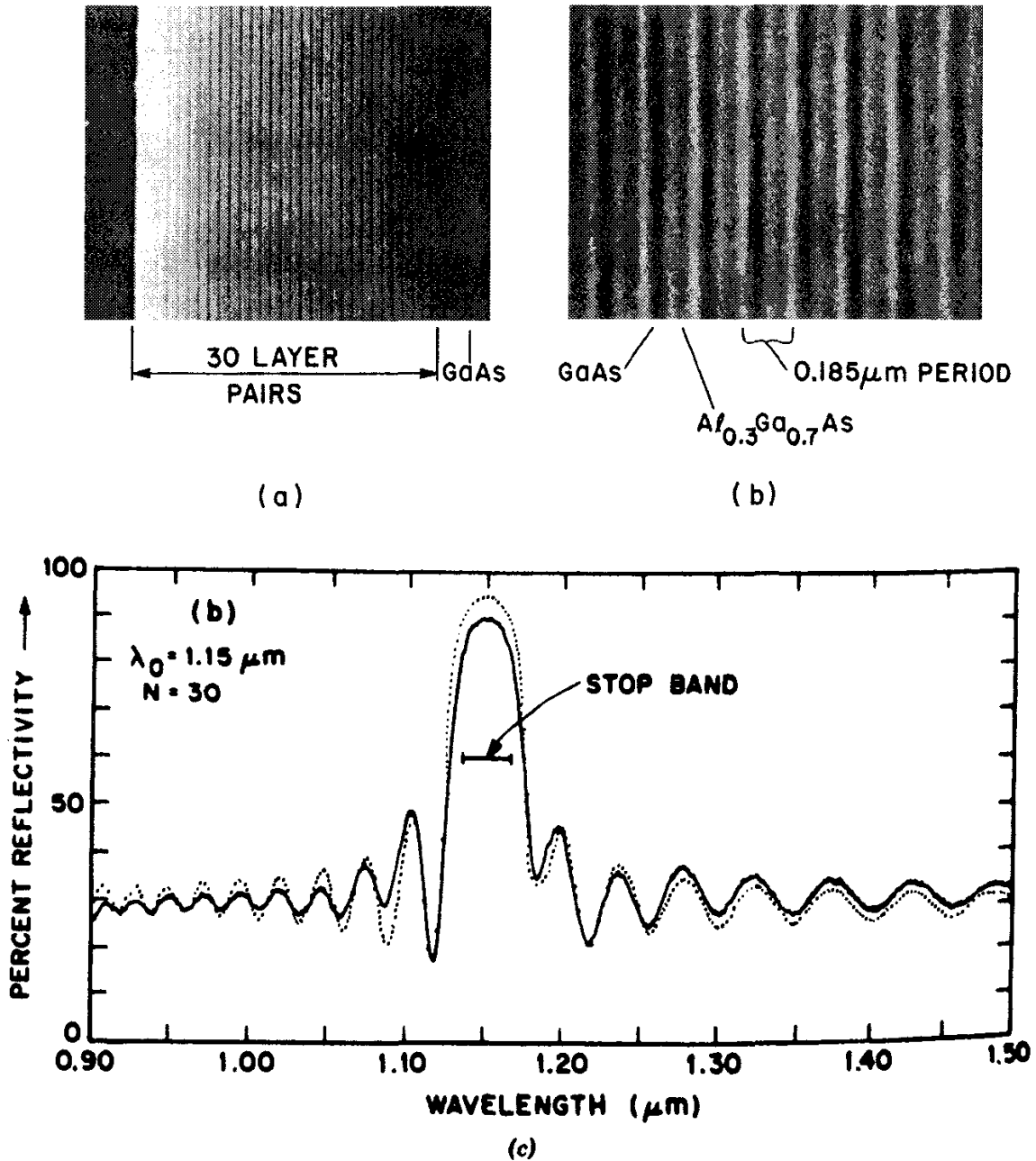


Figure 6.9. (a) Scanning electron micrograph ($11,000\times$) of thirty layer pairs of GaAs (dark color) and $\text{Al}_{0.3}\text{Ga}_{0.7}\text{As}$ (light color) grown on a GaAs substrate. (b) Photograph ($55,000\times$) showing the period $\Lambda = 0.185 \mu\text{m}$. (c) Measured reflectivity spectrum for light incident from air [3].

Since the unperturbed dielectric medium is homogeneous in the z direction [i.e., $\partial\epsilon_0(x, y)/\partial z = 0$], the normal modes can be written in the form

$$\mathbf{E}_m(x, y)e^{i(\omega t - \beta_m z)}, \quad (6.4-2)$$

where the m is the mode subscript, which can be either continuous for unbound modes, such as plane waves, or discrete for confined modes, such

as waveguide modes. These normal modes satisfy

$$\left[\frac{\partial^2}{\partial x^2} + \frac{\partial^2}{\partial y^2} + \omega^2 \mu \epsilon_0(x, y) - \beta_m^2 \right] \mathbf{E}_m(x, y) = 0, \quad (6.4-3)$$

where we assume that $(\nabla \cdot \mathbf{E}) = 0$ and Eq. (6.4-3) is an approximation of the wave equation (1.4-7) (see Section 2.1). If an arbitrary field of frequency ω is excited at $z = 0$, the propagation of this field in the unperturbed medium can always be expressed in terms of a linear combination of normal modes,

$$\mathbf{E} = \sum_m A_m \mathbf{E}_m(x, y) e^{i(\omega t - \beta_m z)}, \quad (6.4-4)$$

where the A_m 's are constants. Such an expansion is possible because these normal modes form a complete set. The modes are usually normalized to a power flow of 1 W in the z direction. Thus the orthogonal relation of the modes can be written (see Section 11.1)

$$\frac{1}{2} \int (\mathbf{E}_l \times \mathbf{H}_k^*)_z dx dy = \delta_{lk}, \quad (6.4-5)$$

where \mathbf{H}_k is the magnetic field associated with the mode \mathbf{E}_k . When $\nabla \cdot \mathbf{E} = 0$ and the modes \mathbf{E}_m satisfy Eq. (6.4-3), this orthogonal relation becomes (see Section 11.1)

$$\int \mathbf{E}_k^*(x, y) \cdot \mathbf{E}_l(x, y) dx dy = \frac{2\omega\mu}{|\beta_k|} \delta_{kl}, \quad (6.4-6)$$

where δ_{kl} is the Kronecker delta for confined modes and the Dirac delta function for unbounded modes. If a single mode is excited at $z = 0$, say $\mathbf{E}_1(x, y) e^{i(\omega t - \beta_1 z)}$, then the electromagnetic wave will remain in this mode throughout the unperturbed medium.

Let us consider next the propagation of an unperturbed mode $\mathbf{E}_1(x, y) e^{i(\omega t - \beta_1 z)}$ in the perturbed medium described by the dielectric tensor $\epsilon_0(x, y) + \Delta\epsilon(x, y, z)$. The presence of the dielectric perturbation $\Delta\epsilon(x, y, z)$ gives rise to a new perturbation polarization

$$\Delta\mathbf{P} = \Delta\epsilon(x, y, z) \mathbf{E}_1(x, y) e^{i(\omega t - \beta_1 z)}.$$

If this polarization wave, acting as a distributed source, can feed energy into (or out of) some other mode $\mathbf{E}_2(x, y) e^{i(\omega t - \beta_2 z)}$, then we say that the dielectric perturbation $\Delta\epsilon(x, y, z)$ couples (i.e., causes energy exchange)

between modes \mathbf{E}_1 and \mathbf{E}_2 . Let us find, next, under what conditions this coupling takes place.

The energy exchange between unperturbed modes due to the dielectric perturbation is analogous to a transition between the eigenstates of an atom under the influence of a time-dependent perturbation. The relevant formalisms are very similar. The mathematical approach is sometimes called the method of variation of constants. The procedure consists of expressing the electric field vector of the electromagnetic wave as an expansion in the normal modes of the unperturbed dielectric structure, where the expansion coefficients evidently depend on z , since for $\Delta\epsilon \neq 0$ the waves $\mathbf{E}_m(x, y)e^{i(\omega t - \beta_m z)}$ are no longer eigenmodes:

$$\mathbf{E} = \sum_m A_m(z) \mathbf{E}_m(x, y) e^{i(\omega t - \beta_m z)}. \quad (6.4-7)$$

Substituting Eq. (6.4-7) into the wave equation

$$\{\nabla^2 + \omega^2 \mu [\epsilon_0(x, y) + \Delta\epsilon(x, y, z)]\} \mathbf{E} = 0 \quad (6.4-8)$$

and using Eq. (6.4-3),

$$\begin{aligned} & \sum_k \left[\frac{d^2}{dz^2} A_k - 2i\beta_k \frac{d}{dz} A_k \right] \mathbf{E}_k(x, y) e^{-i\beta_k z} \\ & = -\omega^2 \mu \sum_l \Delta\epsilon(x, y, z) A_l \mathbf{E}_l(x, y) e^{-i\beta_l z}. \end{aligned} \quad (6.4-9)$$

We now assume further that the dielectric perturbation is “weak,” so that the variation of the mode amplitudes is “slow” and satisfies the condition

$$\left| \frac{d^2}{dz^2} A_k \right| \ll \left| \beta_k \frac{d}{dz} A_k \right|. \quad (6.4-10)$$

This condition is known as parabolic approximation and is often used when the perturbation is small. Thus, neglecting the second derivative in Eq. (6.4-9) leads to

$$\begin{aligned} & -2i \sum_k \beta_k \left(\frac{d}{dz} A_k \right) \mathbf{E}_k(x, y) e^{-i\beta_k z} \\ & = -\omega^2 \mu \sum_l \Delta\epsilon(x, y, z) A_l \mathbf{E}_l(x, y) e^{-i\beta_l z}. \end{aligned} \quad (6.4-11)$$

We next take the scalar product of Eq. (6.4-11) with $\mathbf{E}_k^*(x, y)$ and integrate over all x and y . The result, using the orthogonal property (6.4-6) of the normal modes, is

$$\langle k|k\rangle \frac{d}{dz} A_k(z) = \frac{\omega^2 \mu}{2i\beta_k} \sum_l \langle k|\Delta\epsilon|l\rangle A_l(z) e^{i(\beta_k - \beta_l)z}, \quad (6.4-12)$$

where

$$\langle k|k\rangle \equiv \int \mathbf{E}_k^*(x, y) \cdot \mathbf{E}_k(x, y) dx dy = \frac{2\omega\mu}{|\beta_k|}, \quad (6.4-13)$$

$$\langle k|\Delta\epsilon|l\rangle \equiv \int \mathbf{E}_k^*(x, y) \cdot \Delta\epsilon(x, y, z) \mathbf{E}_l(x, y) dx dy. \quad (6.4-14)$$

Since the dielectric perturbation $\Delta\epsilon(x, y, z)$ is periodic in z , we can expand it as a Fourier series

$$\Delta\epsilon(x, y, z) = \sum_{m \neq 0} \epsilon_m(x, y) \exp\left[-im \frac{2\pi}{\Lambda} z\right] \quad (6.4-15)$$

where the summation is over all m except $m = 0$ because of the definition of $\Delta\epsilon(x, y, z)$ in Eq. (6.4-1).

Substitution of Eqs. (6.4-15), (6.4-14), and (6.4-13) in Eq. (6.4-11) leads to

$$\frac{d}{dz} A_k = -i \frac{\beta_k}{|\beta_k|} \sum_l \sum_m C_{kl}^{(m)} A_l e^{i(\beta_k - \beta_l - m2\pi/\Lambda)z}, \quad (6.4-16)$$

where the coupling coefficient $C_{kl}^{(m)}$ is defined as

$$C_{kl}^{(m)} \equiv \frac{\omega}{4} \langle k|\epsilon_m|l\rangle = \frac{\omega}{4} \int \mathbf{E}_k^*(x, y) \cdot \epsilon_m(x, y) \mathbf{E}_l(x, y) dx dy. \quad (6.4-17)$$

This coefficient $C_{kl}^{(m)}$ reflects the magnitude of coupling between the k th and l th modes due to the m th Fourier component of the dielectric perturbation.

Equation (6.4-16) constitutes a set of coupled linear differential equations. In principle, an infinite number of mode amplitudes are involved. However, in practice, especially near the condition of resonant coupling, only two modes are strongly coupled, and Eq. (6.4-16) reduces to two equations for the two mode amplitudes. By resonant coupling, we mean a

mode coupling at the condition when

$$\beta_k - \beta_l - m \frac{2\pi}{\Lambda} = 0 \quad (6.4-18)$$

for some integer m . This condition is of fundamental importance, and we will refer to it as “longitudinal phase matching” or just as phase matching. This condition is the spatial analogue of the conservation of energy in time-dependent perturbation theory and therefore may be called the conservation of momentum. The resonant coupling can be explained as follows: by examining the coupled equation (6.4-16), we notice that the increment in the field amplitude of the k th mode, dA_k , due to the mode coupling with the l th mode in the region between z and $z + dz$ via the m th Fourier component of the dielectric perturbation is given by

$$dA_k = -i \frac{\beta_k}{|\beta_k|} C_{kl}^{(m)} A_l \exp \left[i \left(\beta_k - \beta_l - m \frac{2\pi}{\Lambda} \right) z \right] dz. \quad (6.4-19)$$

Since the field amplitudes are slowly varying functions of space, we may integrate Eq. (6.4-19) over a distance which is much larger than the period Λ , yet is much smaller than the variation scale of the field amplitudes. This leads to an expression for the net increment of the field amplitude, ΔA_k , due to mode coupling with l th mode over the distance between z and $z + L$ via the m th Fourier component of the dielectric perturbation:

$$\Delta A_k = -i \frac{\beta_k}{|\beta_k|} C_{kl}^{(m)} A_l \int_{L \gg \Lambda} \exp \left[i \left(\beta_k - \beta_l - m \frac{2\pi}{\Lambda} \right) z \right] dz. \quad (6.4-20)$$

From this equation we find that mode coupling between the k th and l th modes is insignificant when the condition (6.4-18) is not satisfied of some integer m , because the integral in Eq. (6.4-20) is nonvanishing only when the exponent is zero, which is exactly the phase-matching condition (6.4-18).

In summary: The propagation of electromagnetic radiation in a periodically perturbed dielectric medium can be described by the method of variation of constants. These mode amplitudes (“constants”) are governed by the coupled-mode equations (6.4-16). For significant mode coupling to take place between modes k and l , two conditions must be satisfied. The first is expressed by Eq. (6.4-18), the kinematical condition. Second, the coupling coefficient, $C_{kl}^{(m)}$, must not vanish. The latter is also called the dynamical condition, since it depends upon characteristics of the waves such as their polarizations and mode profiles.

The general properties of mode coupling described above are of great importance in that they can be used to determine what process can take

place and what kind of perturbation is needed to couple a given pair of normal modes. This point will be demonstrated throughout this chapter by a number of examples.

Equation (6.4-18) is also known as the Bragg condition because of its analogy to X-ray diffraction by crystals. In that case an incident wave, represented by a plane wave with a spatial propagation factor $\exp(-ik_y y - i\beta z)$, is strongly coupled with a reflected wave with a spatial propagation factor $\exp(-ik_y y + i\beta z)$. The constant β is the component of the wave vector perpendicular to the relevant crystal planes. It follows from Eq. (6.4-18) that the spacing Λ of the crystal planes needs to satisfy

$$\beta - (-\beta) = 2\beta = m \frac{2\pi}{\Lambda}, \quad (6.4-21)$$

or, since $\beta = k \cos \theta$, where θ is the angle of incidence,

$$2\Lambda \cos \theta = m\lambda, \quad (6.4-22)$$

where $m = 1, 2, 3, \dots$ is some integer. Equation (6.4-22) is the well-known Bragg condition for X-ray diffraction. As noted above, this condition is necessary but not sufficient. The intensity of diffraction depends upon the Fourier expansion coefficients of the periodic dielectric constant as well as on the polarization of the waves [Eq. (6.4-17)].

6.4.1. Coupled-Mode Equations

Equation (6.4-16) describes the most general case of mode coupling due to a periodic dielectric perturbation. In practice, often only the coupling between two modes is involved. Let the two coupled modes be designated as 1 and 2. Neglecting interaction with any of the other modes, the coupled-mode equations become

$$\frac{d}{dz} A_1 = -i \frac{\beta_1}{|\beta_1|} C_{12}^{(m)} A_2 e^{i\Delta\beta z} \quad (6.4-23)$$

$$\frac{d}{dz} A_2 = -i \frac{\beta_2}{|\beta_2|} C_{21}^{(-m)} A_1 e^{-i\Delta\beta z}$$

where

$$\Delta\beta = \beta_1 - \beta_2 - m \frac{2\pi}{\Lambda} \quad (6.4-24)$$

and $C_{12}^{(m)}$, $C_{21}^{(-m)}$ are the coupling coefficients given by (6.4-17). It can be shown directly from the definition (6.4-17) that

$$C_{12}^{(m)} = [C_{21}^{(-m)}]^* \quad (6.4-25)$$

provided that $\Delta\epsilon(x, y, z)$ is a Hermitian dielectric tensor.

In the event that the dielectric tensor ϵ of Eq. (6.4-1) is a function of z only (i.e., no x, y dependence), the normal modes of the unperturbed medium are plane waves and the Fourier coefficients ϵ_m of the dielectric perturbation are constants. The coupling coefficients for this special case become

$$C_{kl}^{(m)} = \frac{\omega^2 \mu}{2\sqrt{|\beta_k \beta_l|}} \mathbf{p}_k^* \cdot \epsilon_m \mathbf{p}_l, \quad (6.4-26)$$

where \mathbf{p}_k and \mathbf{p}_l are unit polarization vectors of the plane waves.

Notice that the coupling coefficients (6.4-26) depend on the polarization states of the coupled modes as well as on the tensor property of the Fourier expansion coefficient ϵ_m .

The signs of the factors $\beta_1/|\beta_1|$ and $\beta_2/|\beta_2|$ in the coupled equations (6.4-23) are very important and will determine the behavior of the coupling. These signs, of course, depend on the direction of propagation of the coupled modes. The coupling is therefore divided into two categories, codirectional coupling and contradirectional coupling.

6.4.2. Codirectional Coupling

When the coupled modes are propagating in the same direction, say the $+z$ direction, the sign factors $\beta_1/|\beta_1|$ and $\beta_2/|\beta_2|$ are both equal to 1. The coupled equations become

$$\frac{d}{dz} A_1 = -i\kappa A_2 e^{i\Delta\beta z}, \quad (6.4-27)$$

$$\frac{d}{dz} A_2 = -i\kappa^* A_1 e^{-i\Delta\beta z},$$

where

$$\kappa = C_{12}^{(m)}. \quad (6.4-28)$$

Remember that A_1 and A_2 are the complex amplitudes of the normalized modes. Therefore $|A_1|^2$ and $|A_2|^2$ represent the power flow in modes 1 and 2, respectively. The coupled mode equations (6.4-27) are consistent with the conservation of energy, which requires that

$$\frac{d}{dz} \{|A_1|^2 + |A_2|^2\} = 0. \quad (6.4-29)$$

The general solution of Eq. (6.4-27) is obtained by an integration from 0 to z and is given by

$$A_1(z) = e^{i(\Delta\beta/2)z} \left\{ \left[\cos sz - i \frac{\Delta\beta}{2s} \sin sz \right] A_1(0) - i \frac{\kappa}{s} \sin sz A_2(0) \right\}, \quad (6.4-30)$$

$$A_2(z) = e^{-i(\Delta\beta/2)z} \left\{ -i \frac{\kappa^*}{s} \sin sz A_1(0) + \left[\cos sz + i \frac{\Delta\beta}{2s} \sin sz \right] A_2(0) \right\},$$

where

$$s^2 = \kappa^* \kappa + \left(\frac{\Delta\beta}{2} \right)^2, \quad (6.4-31)$$

and $A_1(0)$, $A_2(0)$ are the mode amplitudes at $z = 0$. From Eq. (6.4-30) it can be seen that the fraction of power that is coupled from mode A_2 to A_1 in a distance z , or vice versa, is

$$\frac{|\kappa|^2}{|\kappa|^2 + (\Delta\beta/2)^2} \sin^2 \sqrt{|\kappa|^2 + \left(\frac{\Delta\beta}{2} \right)^2} z. \quad (6.4-32)$$

The maximum fraction of power exchange is $|\kappa|^2 / [|\kappa|^2 + (\Delta\beta/2)^2]$, which becomes small once $\Delta\beta \gg |\kappa|$. A complete exchange of power is only possible when $\Delta\beta = 0$, that is, when phase matching obtains. A typical example of codirectional coupling is the transmission of light in a Šolc filter, which will be described in terms of coupled-mode theory in Section 6.5.

6.4.3. Contradirectional Coupling

When the coupled modes are propagating in opposite directions, say $\beta_1 > 0$ and $\beta_2 < 0$, the sign factors $\beta_1/|\beta_1|$ and $\beta_2/|\beta_2|$ become 1 and -1 ,

respectively. The coupled equations become

$$\begin{aligned}\frac{d}{dz}A_1 &= -i\kappa A_2 e^{i\Delta\beta z}, \\ \frac{d}{dz}A_2 &= i\kappa^* A_1 e^{-i\Delta\beta z},\end{aligned}\tag{6.4-33}$$

where κ is again given by Eq. (6.4-28).

The net power flow in the $+z$ direction for this case is $|A_1|^2 - |A_2|^2$. The coupled mode equations (6.4-33) are again consistent with the conservation of energy, which requires that

$$\frac{d}{dz}\{|A_1|^2 - |A_2|^2\} = 0.\tag{6.4-34}$$

The boundary conditions for contradirectional coupling are usually taken as $A_1 = A(0)$ at $z = 0$ and $A_2 = A_2(L)$ at $z = L$. The general solution is given by

$$\begin{aligned}A_1(z) &= e^{i(\Delta\beta/2)z} \left\{ \frac{s \cosh s(L-z) + i(\Delta\beta/2)\sinh s(L-z)}{s \cosh sL + i(\Delta\beta/2)\sinh sL} A_1(0) \right. \\ &\quad \left. + \frac{-i\kappa e^{i(\Delta\beta/2)L} \sinh sz}{s \cosh sL + i(\Delta\beta/2)\sinh sL} A_2(L) \right\}\end{aligned}\tag{6.4-35}$$

$$\begin{aligned}A_2(z) &= e^{-i(\Delta\beta/2)z} \left\{ \frac{-i\kappa^* \sinh s(L-z)}{s \cosh sL + i(\Delta\beta/2)\sinh sL} A_1(0) \right. \\ &\quad \left. + e^{i(\Delta\beta/2)L} \frac{s \cosh sz + i(\Delta\beta/2)\sinh sz}{s \cosh sL + i(\Delta\beta/2)\sinh sL} A_2(L) \right\}\end{aligned}$$

where

$$s^2 = \kappa^* \kappa - \left(\frac{\Delta\beta}{2} \right)^2.\tag{6.4-36}$$

From the general solution (6.4-35) it can be seen that the power exchange between these two modes in the region between $z = 0$ and $z = L$ is given by

$$\frac{|\kappa|^2 \sinh^2 sL}{s^2 \cosh^2 sL + (\Delta\beta/2)^2 \sinh^2 sL}.\tag{6.4-37}$$

Again we notice that the fractional power exchange decreases as $\Delta\beta$ increases. A complete power exchange for contradirectional coupling, however, only occurs when the phase-matching condition is satisfied ($\Delta\beta = 0$) and L is infinite. This situation is different from that of the codirectional coupling, where the power is exchanged back and forth between the two modes and complete power exchange happens periodically in space provided $\Delta\beta = 0$. The power exchange between the coupled modes is shown in Figs. 6.11 and 6.14 below for codirectional and contradirectional couplings, respectively.

Bragg reflection is a typical example of contradirectional coupling. We will use the coupled-mode theory to treat the optical properties of a Bragg reflector in Section 6.6.

6.5. COUPLED-MODE THEORY OF ŠOLC FILTERS

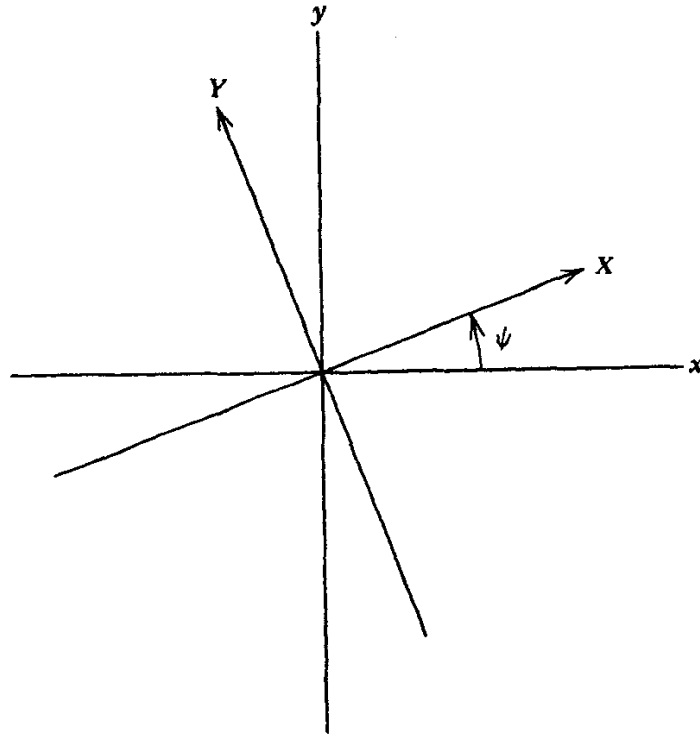
Šolc filters are described in Section 5.3. The transmission characteristics are analyzed by using the Jones-matrix method. This formalism, however, is not very transparent as to the physical mechanism of this structure as a filter. In this section we will use the coupled-mode theory to study the transmission properties of this filter. This, of course, only applies to the folded Šolc filter, which is a periodic structure. The geometry of this filter is sketched in Fig. 5.5 and is described in Table 5.1.

Let n_1 , n_2 , and n_3 be the principal refractive indices of each crystal plate. The propagation z axis coincides with the z axis (c axis) of the crystal and is perpendicular to each plate. The x and y axes are parallel to the transmission direction of the front and rear polarizers, respectively. The dielectric tensor in the principal coordinate of the crystal plates is

$$\epsilon = \epsilon_0 \begin{pmatrix} n_1^2 & 0 & 0 \\ 0 & n_2^2 & 0 \\ 0 & 0 & n_3^2 \end{pmatrix}, \quad (6.5-1)$$

where ϵ_0 is the dielectric constant of the vacuum. Let ψ be the angle between the crystal axes and the xy axes (see Fig. 6.10). The dielectric tensor in the xyz coordinate system is given by

$$\epsilon = \epsilon_0 R(\psi) \begin{pmatrix} n_1^2 & 0 & 0 \\ 0 & n_2^2 & 0 \\ 0 & 0 & n_3^2 \end{pmatrix} R^{-1}(\psi) \quad (6.5-2)$$

Figure 6.10. Azimuth angle ψ .

with

$$R(\psi) = \begin{pmatrix} \cos \psi & -\sin \psi & 0 \\ \sin \psi & \cos \psi & 0 \\ 0 & 0 & 1 \end{pmatrix}, \quad (6.5-3)$$

where R is the rotation matrix, and $R^{-1}(\psi) = R(-\psi)$.

The dielectric tensor (6.5-2) can be decomposed into two parts as

$$\epsilon = \epsilon_0 + \Delta\epsilon, \quad (6.5-4)$$

where ϵ_0 is given by

$$\epsilon_0 = \epsilon_0 \begin{pmatrix} n_1^2 & 0 & 0 \\ 0 & n_2^2 & 0 \\ 0 & 0 & n_3^2 \end{pmatrix} \quad (6.5-5)$$

and $\Delta\epsilon$ is given by

$$\Delta\epsilon = \epsilon_0(n_2^2 - n_1^2) \begin{pmatrix} \sin^2\psi & -\sin\psi\cos\psi & 0 \\ -\sin\psi\cos\psi & -\sin^2\psi & 0 \\ 0 & 0 & 0 \end{pmatrix}. \quad (6.5-6)$$

Since $n_2^2 - n_1^2$ is normally small compared with $n_{1,2}^2$, $\Delta\epsilon$ can be treated as a small dielectric perturbation. The azimuth angle ψ rocks back and forth from ρ to $-\rho$ in the Šolc filter structure. Therefore, the dielectric perturbation $\Delta\epsilon$ is a periodic function of z . The diagonal matrix elements of $\Delta\epsilon$ are, however, constant throughout the filter medium and therefore will not appear in the periodically varying part of the dielectric tensor. These diagonal terms, when included in ϵ_0 [Eq. (6.5-5)], are small compared with $n_{1,2}^2$ and therefore will be neglected. Thus we take (6.5-5) as the unperturbed dielectric tensor and assume that the periodic perturbation is given by

$$\Delta\epsilon = \epsilon_0 \begin{pmatrix} 0 & -\frac{1}{2}(n_2^2 - n_1^2)\sin 2\rho & 0 \\ -\frac{1}{2}(n_2^2 - n_1^2)\sin 2\rho & 0 & 0 \\ 0 & 0 & 0 \end{pmatrix} f(z), \quad (6.5-7)$$

where $f(z)$ is a periodic square wave function of z and is given by

$$f(z) = \begin{cases} 1, & 0 < z < \frac{1}{2}\Lambda, \\ -1, & \frac{1}{2}\Lambda < z < \Lambda. \end{cases} \quad (6.5-8)$$

The period Λ is exactly twice the thickness of a crystal plate.

The normal modes of the unperturbed dielectric medium are linearly polarized plane waves. We will limit ourselves to the propagation of waves in the z direction only. Thus, the normal modes are the x -polarized plane wave e^{-ik_1z} and the y -polarized plane wave e^{-ik_2z} with the respective wave numbers given by

$$k_{1,2} = \frac{\omega}{c} n_{1,2}. \quad (6.5-9)$$

Both codirectional and contradirectional couplings are expected to exist, depending on the spectral regime of interest. The conventional folded Šolc filter is based on the codirectional coupling.

The periodic function $f(z)$ can be written as a Fourier series

$$f(z) = \sum_{m \neq 0} \frac{i(1 - \cos m\pi)}{m\pi} \exp\left[-im\left(\frac{2\pi}{\Lambda}\right)z\right]. \quad (6.5-10)$$

By substituting (6.5-10) in (6.5-7), we obtain the Fourier expansion coefficient ϵ_m of the dielectric perturbation $\Delta\epsilon$,

$$\epsilon_m = \frac{-\epsilon_0}{2} (n_2^2 - n_1^2) \sin 2\rho \begin{pmatrix} 0 & 1 & 0 \\ 1 & 0 & 0 \\ 0 & 0 & 0 \end{pmatrix} \frac{i(1 - \cos m\pi)}{m\pi}. \quad (6.5-11)$$

The coupling constant κ between the normal modes according to Eqs. (6.4-26) and (6.4-28) is thus given by

$$\kappa = -\frac{\omega}{c} \frac{n_2^2 - n_1^2}{4\sqrt{n_1 n_2}} \sin 2\rho \frac{i(1 - \cos m\pi)}{m\pi}. \quad (6.5-12)$$

Notice that the even-order couplings ($m = 2, 4, 6, \dots$) vanish, since $\varepsilon_m = 0$.

To obtain an expression for the transmission characteristics, we recall that the initial condition at $z = 0$ is given by

$$A_1(0) = 1, \quad (6.5-13)$$

$$A_2(0) = 0,$$

where A_1 is the mode amplitude for the polarized normal mode, and A_2 is the mode amplitude for the y -polarized normal mode. The initial condition is determined by the front polarizer, which admits only x -polarized light. The solution of the coupled-mode equation (6.4-27), according to Eqs. (6.4-30) and (6.5-13), is

$$A_1(z) = e^{i(\Delta\beta/2)z} \left[\cos sz - i \frac{\Delta\beta}{2s} \sin sz \right] \quad (6.5-14)$$

$$A_2(z) = e^{-i(\Delta\beta/2)z} (-i\kappa^*) \frac{\sin sz}{s},$$

where s is given by $s^2 = \kappa^* \kappa + (\Delta\beta/2)^2$ [Eq. (6.4-31)] and $\Delta\beta$ is given by

$$\Delta\beta = k_1 - k_2 - m \left(\frac{2\pi}{\Lambda} \right), \quad m = 1, 2, 3, \dots \quad (6.5-15)$$

At the rear polarizer (y -polarized) $z = L$, A_1 is extinguished. The transmission for the y -polarized light is thus given by

$$T = |\kappa|^2 \frac{\sin^2 sL}{s^2}. \quad (6.5-16)$$

From this expression, we find that a 100% conversion of mode energy occurs at

$$\Delta\beta = 0 \quad (6.5-17)$$

and

$$|\kappa|L = \frac{1}{2}\pi, \frac{3}{2}\pi, \frac{5}{2}\pi, \dots, \quad (6.5-18)$$

where L is the length of the filter structure. Notice that complete power exchange occurs periodically in z .

We assume that the filter length satisfies the condition $|\kappa|L = \frac{1}{2}\pi$ [Eq. (6.5-18)], so that complete power conversion occurs only when $\Delta\beta = 0$. The transmission at this condition becomes

$$T = \left(\frac{\sin \frac{1}{2}\pi x}{x} \right)^2, \quad (6.5-19)$$

where

$$x = \left[1 + \left(\frac{\Delta\beta L}{\pi} \right)^2 \right]^{1/2}. \quad (6.5-20)$$

The expression (6.5-19) is identical with Eq. (5.3-18), derived from the Jones calculus. Peak transmission occurs when $\Delta\beta = 0$, which, according to Eq. (6.5-15), corresponds to the case when the crystal plates are half-wave plates (or odd integral multiples thereof). The even Bragg order ($m = 0, 2, 4, \dots$) corresponds to the case when the crystal plates are full-wave plates, which will not change the polarization state of the light, so that coupling cannot exist.

According to Eq. (6.5-16) or (6.5-14), the electromagnetic energy is exchanged between the coupled modes as the waves propagate in the periodic medium. A plot of the mode power for the phase-matched ($\Delta\beta = 0$) and $\Delta\beta \neq 0$ cases is shown in Fig. 6.11.

Contradirectional coupling can also occur in a Šolc periodic medium. This happens when the following Bragg condition is satisfied:

$$k_1 + k_2 - m \frac{2\pi}{\Lambda} = 0. \quad (6.5-21)$$

This reflection of light is different from the conventional Bragg reflection described in Sections 6.3 and 6.6 and is called exchange Bragg reflection. The difference is that a change of polarization occurs simultaneously with the reflection in an exchange Bragg coupling. This coupling involves power exchange between two normal modes with different polarization states as well as different phase velocities. The band structure for this type of coupling is different from the conventional one (direct Bragg coupling). The

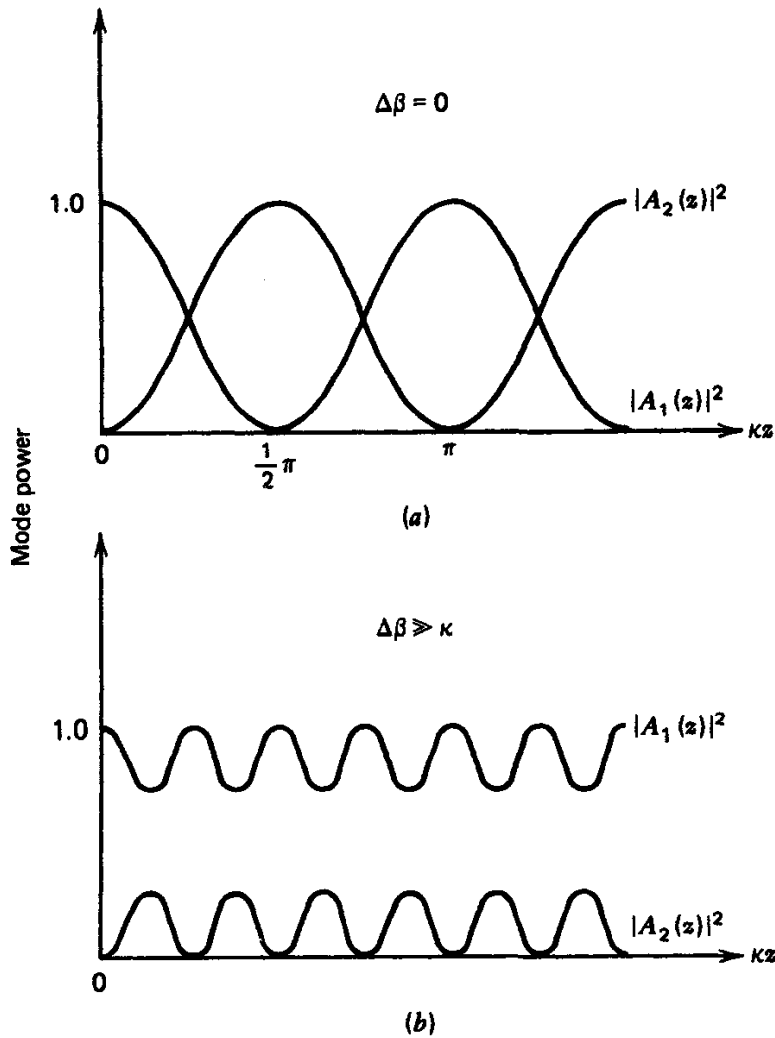


Figure 6.11. Power exchange between two coupled modes in a Solc filter under (a) phase-matched conditions ($\Delta\beta = 0$), (b) $\Delta\beta \neq 0$.

forbidden bands do not necessarily have to be at $K\Lambda = m\pi$. In fact, they can be anywhere in the Brillouin zone [4].

6.6. COUPLED-MODE THEORY OF BRAGG REFLECTORS

The Bragg reflectors described in Section 6.3 will now be analyzed by using the coupled-mode theory. For the sake of simplicity, we will assume that the layer thicknesses are the same and the dielectric constant as a function of z is

$$\varepsilon(z) = \begin{cases} \varepsilon_0 n_2^2, & 0 < z < \frac{1}{2}\Lambda, \\ \varepsilon_0 n_1^2, & \frac{1}{2}\Lambda < z < \Lambda, \end{cases} \quad (6.6-1)$$

with

$$\varepsilon(z) = \varepsilon(z + \Lambda). \quad (6.6-2)$$

This dielectric constant can be decomposed according to Eq. (6.4-1) as

$$\varepsilon(z) = \frac{1}{2}\varepsilon_0(n_1^2 + n_2^2) + \frac{1}{2}\varepsilon_0(n_2^2 - n_1^2)f(z), \quad (6.6-3)$$

where $f(z)$ is a periodic square-wave function (6.5-8).

The normal modes of the unperturbed medium are plane waves $e^{-i\mathbf{k}\cdot\mathbf{r}}$ with wave number given by

$$k^2 = \left(\frac{\omega}{c}\right)^2 \frac{n_1^2 + n_2^2}{2} \equiv \left(\bar{n} \frac{\omega}{c}\right)^2, \quad (6.6-4)$$

where \bar{n} is the (geometrical) averaged refractive index of the medium. These plane waves are divided into TE waves and TM waves according to their polarization states. Since both the perturbed and the unperturbed dielectric constants are scalars, mode coupling between TE waves and TM waves does not exist. Consequently, only coupling between waves of the same polarization state can take place. This is possible only in the contradirectional coupling, because the phase-matching condition for codirectional coupling can never be satisfied [$\Delta\beta = \beta_1 - \beta_2 - m(2\pi/\Lambda) = -m(2\pi/\Lambda) \neq 0$ for finite Λ].

The mode couplings for TE waves and TM waves are similar. The only difference is the coupling constant (6.4-26). Let θ be the angle between the wave vector \mathbf{k} and the z axis, and \mathbf{k}' be the wave vector of the reflected wave (see Fig. 6.12). The coupling constants according to Eqs. (6.4-26), (6.5-10), and (6.6-3) are given by

$$\kappa = \begin{cases} \frac{i(1 - \cos m\pi)}{2m\lambda \cos \theta} \frac{\sqrt{2}(n_2^2 - n_1^2)}{\sqrt{n_2^2 + n_1^2}} & \text{(TE wave),} \\ \frac{i(1 - \cos m\pi)}{2m\lambda \cos \theta} \frac{\sqrt{2}(n_2^2 - n_1^2)}{\sqrt{n_2^2 + n_1^2}} \cos 2\theta & \text{(TM wave).} \end{cases} \quad (6.6-5)$$

Notice that the difference between the two coupling constants is only a directional factor $\cos 2\theta$, which is the cosine of the angle between the polarization vectors of TM waves. According to Eq. (6.6-5), the coupling constant vanishes at $\theta = 45^\circ$ for TM waves. This corresponds to the zero

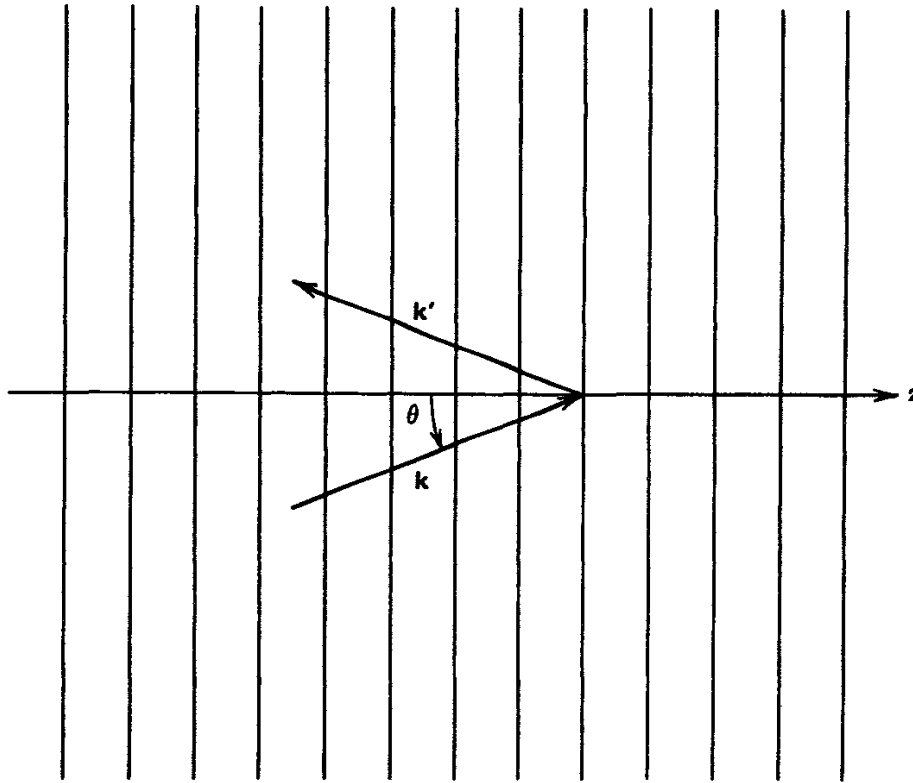


Figure 6.12. Bragg reflection for off-axis light.

reflection of TM waves at the Brewster angle [see Fig. 6.8(b)]. In fact, $\theta_B = \tan^{-1}(n_2/n_1) \approx 45^\circ$ for $n_2 \approx n_1$.

The phase-mismatch factor $\Delta\beta$ is given by

$$\Delta\beta = 2k \cos \theta - m \left(\frac{2\pi}{\Lambda} \right) = 2 \left(\bar{n} \frac{\omega}{c} \right) \cos \theta - m \left(\frac{2\pi}{\Lambda} \right) \quad (6.6-6)$$

where Λ is the period of the layered structure and k is the wave number given by Eq. (6.6-4). According to Eq. (6.6-5), there is no even-order Bragg reflection, since $\kappa = 0$ for $m = 2, 4, 6, \dots$. This corresponds to the case when the thickness of each layer is approximately an integral multiple of half a wavelength, which leads to zero reflection.

To obtain an expression for the reflectivity, we assume that the light is incident at $z = 0$, so that the boundary condition is

$$\begin{aligned} A_1(0) &= 1, \\ A_2(L) &= 0, \end{aligned} \quad (6.6-7)$$

where A_1 is the amplitude of the incident wave and A_2 is the amplitude of the reflected wave. The solution of the coupled equation (6.4-33), according

to Eqs. (6.4-35) and (6.6-7), is given by

$$A_1(z) = e^{i(\Delta\beta/2)z} \frac{s \cosh s(L-z) + i(\Delta\beta/2) \sinh s(L-z)}{s \cosh sL + i(\Delta\beta/2) \sinh sL}, \quad (6.6-8)$$

$$A_2(z) = e^{-i(\Delta\beta/2)z} \frac{-i\kappa^* \sinh s(L-z)}{s \cosh sL + i(\Delta\beta/2) \sinh sL},$$

where s is given [as in Eq. (6.4-36)] by $s^2 = \kappa^* \kappa - (\Delta\beta/2)^2$ and $\Delta\beta$ is given by Eq. (6.6-6).

The reflectivity of the Bragg reflector is defined as

$$R = \left| \frac{A_2(0)}{A_1(0)} \right|^2 \quad (6.6-9)$$

and is given, according to (6.6-8), by

$$R = \frac{\kappa^* \kappa \sinh^2 sL}{s^2 \cosh^2 sL + (\Delta\beta/2)^2 \sinh^2 sL}. \quad (6.6-10)$$

Maximum reflectivity occurs at $\Delta\beta = 0$:

$$R_{\max} = \tanh^2 |\kappa| L. \quad (6.6-11)$$

The calculated reflectivity as a function of $\Delta\beta L$ is plotted in Fig. 6.13. It is seen to be an even function of $\Delta\beta$. Let ω_m be the frequency at which the Bragg condition (6.6-6) is satisfied. Then $\Delta\beta$ can be written

$$\Delta\beta = \frac{2\bar{n}}{c} (\omega - \omega_m) \cos \theta.$$

The spectrum consists of a main peak with a sharp cutoff and a series of sidelobes. The bandwidth of the main peak is given approximately by

$$\Delta\beta = 4|\kappa|, \quad (6.6-12)$$

because at $\Delta\beta = \pm 2|\kappa|$, the parameter s becomes zero and the reflectivity is

$$R = \frac{\kappa^* \kappa L^2}{1 + \kappa^* \kappa L^2}. \quad (6.6-13)$$

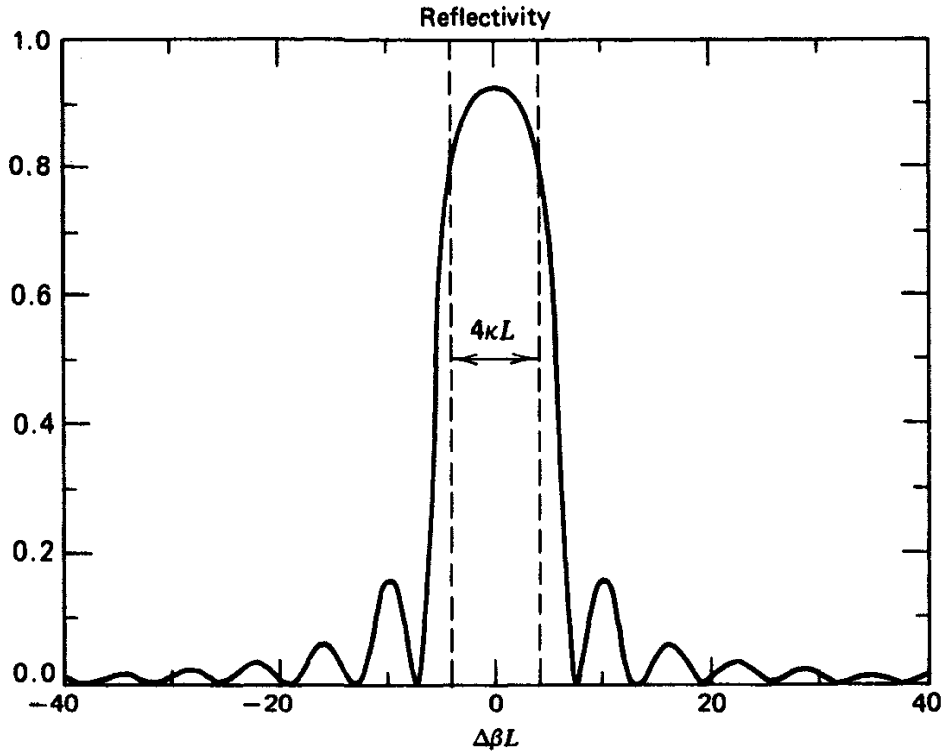


Figure 6.13. The reflectivity of a Bragg reflector calculated by using the coupled-mode theory ($|\kappa|L = 2.0$).

The reflectivity (6.6-13) is usually small because a typical high reflectance requires that $|\kappa|L > 1$ according to Eq. (6.6-11). Therefore Eq. (6.6-12) is a good approximation for the bandwidth. The fractional bandwidth $\Delta\omega/\omega$ is obtained from Eqs. (6.6-6), (6.6-5), and (6.6-12):

$$\frac{\Delta\omega}{\omega} = \left\{ \begin{array}{l} \frac{2}{\pi m \cos^2\theta} \frac{|n_2^2 - n_1^2|}{n_2^2 + n_1^2} \quad (\text{TE}), \\ \frac{2}{\pi m \cos^2\theta} \frac{|n_2^2 - n_1^2|}{n_2^2 + n_1^2} \cos 2\theta \quad (\text{TM}), \end{array} \right\} \quad m = 1, 3, 5, \dots \quad (6.6-14)$$

These expressions are in agreement with Eq. (6.2-34) for the case of normal incidence and $m = 1$, that is, the bandwidth as defined by Eq. (6.6-14) is equal to the size (in units of ω) of the forbidden bandgap. It follows that the frequencies in the forbidden band of a periodic medium which give rise to evanescent waves are strongly reflected if incident on such a medium.

Aside from the main peak at $\Delta\beta = 0$, the reflectivity spectrum also consists of a series of sidelobes on both sides of the main peak. These

sidelobes peak approximately at $sL = i(p + \frac{1}{2})\pi$ ($p = 1, 2, 3, \dots$), which corresponds to $\Delta\beta = \pm 2[\kappa^*\kappa + (p + \frac{1}{2})^2(\pi/L)^2]^{1/2}$. The peak reflectivity of these sidelobes is given, according to Eq. (6.6-10), by

$$R = \frac{|\kappa L|^2}{(p + \frac{1}{2})^2 \pi^2 + |\kappa L|^2}. \quad (6.6-15)$$

These sidelobes become appreciable when $|\kappa L| > \frac{1}{2}\pi$. In fact, the peak reflectivity of first sidelobe reaches 10% when $|\kappa L| = \frac{1}{2}\pi$, at which point the reflectivity of the main peak is only 84%. Zero reflectivity occurs at $sL = iq\pi$ ($q = 1, 2, 3, \dots$), which corresponds to $\Delta\beta = \pm 2[\kappa^*\kappa + (q\pi/L)^2]^{1/2}$.

A plot of the mode powers $|A_1(z)|^2$ and $|A_2(z)|^2$ for this case is shown in Fig. 6.14. For sufficiently large arguments of the hyperbolic-cosine and hyperbolic-sine functions the incident mode power drops off exponentially in the perturbation region. This behavior, however, is due, not to absorption, but to reflection of power into the backward-traveling mode, A_2 , as shown in the figure.

From Eq. (6.6-6) and (6.6-8) we find that the z -dependent part of the wave solutions in the periodic layered medium is an exponential with

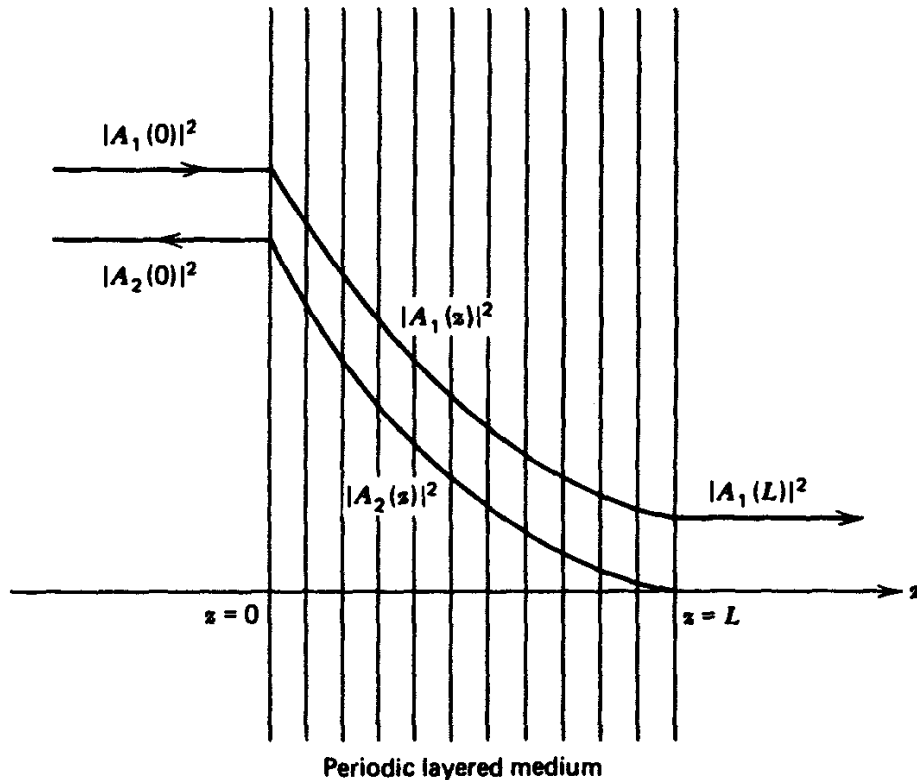


Figure 6.14. Mode powers of the incident mode and the reflected mode in a periodic layered medium when $\Delta\beta = 0$.

propagation constant

$$K = k \cos \theta \pm is = \frac{m\pi}{\Lambda} \pm i\sqrt{\kappa^*\kappa - \left(\frac{\Delta\beta}{2}\right)^2}. \quad (6.6-16)$$

We note that for a range of frequencies such that $|\Delta\beta| < 2|\kappa|$, K has an imaginary part. This is the so-called “forbidden” region, in which the evanescence behavior shown in Fig. 6.14 occurs and which is formally analogous to the energy gap in semiconductors where the periodic crystal potential causes the electron propagation constants to become complex. Note that for each value of m ($m = 1, 2, 3, \dots$) there exists a gap whose center frequency ω_0 satisfies $k \cos \theta = m\pi/\Lambda$. The exceptions are values of m for which κ is zero. Returning to Eq. (6.6-16) and using Eqs. (6.6-4) and (6.6-6), we have

$$K = \frac{m\pi}{\Lambda} \pm i\sqrt{\kappa^*\kappa - \left(\frac{\bar{n}}{c}\right)^2 (\omega - \omega_0)^2 \cos^2 \theta}, \quad (6.6-17)$$

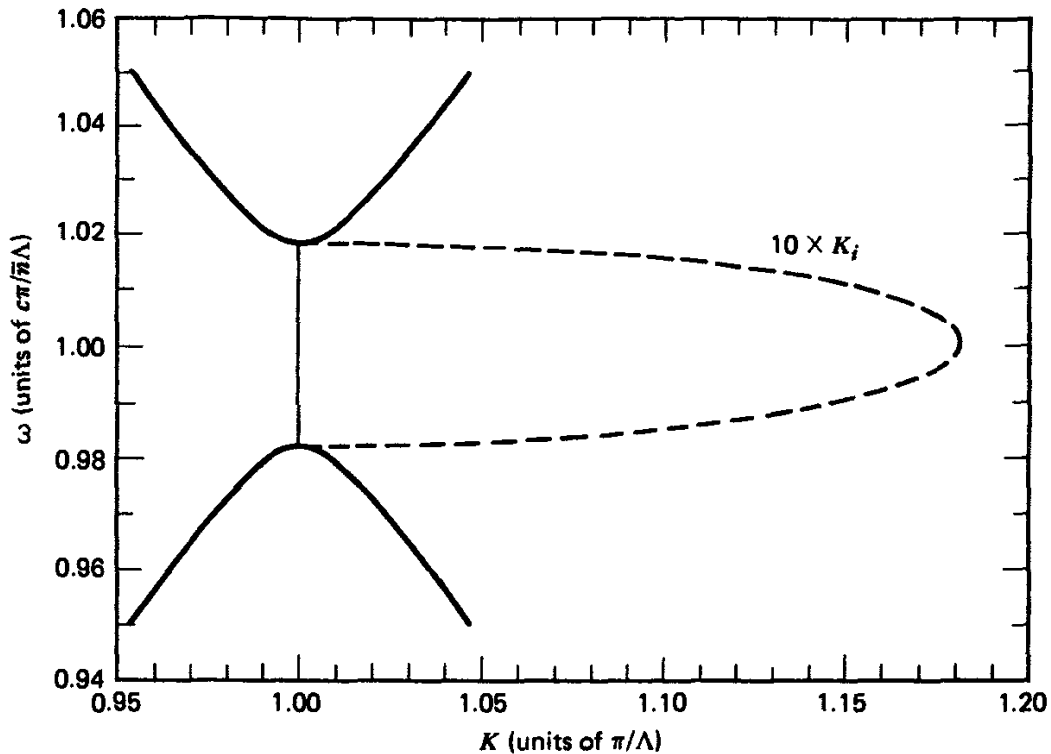


Figure 6.15. Dispersion relation (ω versus K) of a periodic medium with $n_1 = 3.4$, $n_2 = 3.6$, and $a = b = 0.5\Lambda$. The curve is obtained by using either Eq. (6.6-17), which is derived from the coupled-mode theory, or the exact result (6.2-26).

where ω_0 , the midgap frequency, is the value of ω for which $k \cos \theta = m\pi/\Lambda$ (or $\Delta\beta = 0$), and $\bar{n} = [\frac{1}{2}(n_1^2 + n_2^2)]^{1/2}$.

A plot of $\text{Re } K$ and $\text{Im } K$ for $m = 1$ and $\theta = 0$ versus ω , based on Eq. (6.6-17), is shown in Fig. 6.15. We note that the width of the “forbidden” frequency zone is

$$(\Delta\omega)_{\text{gap}} = \frac{2c}{\bar{n}} |\kappa|, \quad (6.6-18)$$

where $|\kappa|$, according to Eq. (6.6-5), is a function of the order m . It follows from Eq. (6.6-16) that

$$(\text{Im } K)_{\text{max}} = |\kappa| = \text{coupling coefficient}. \quad (6.6-19)$$

A short section of a periodic medium thus acts as a high-reflectivity mirror for frequencies near the Bragg value ω_0 .

Figure 6.15 also shows the dispersion relation $\omega(K)$ derived from the Bloch-wave formalism. We note that the coupled-mode theory agrees with the Bloch-wave formalism.

6.7. PHASE VELOCITY, GROUP VELOCITY, AND ENERGY VELOCITY

We have derived some of the important characteristics of electromagnetic propagation in periodic layered media. An explicit expression for the unit-cell translation matrix for the periodic layered medium was obtained. The band structure is derived by diagonalizing the unit-cell translation matrix.

The concepts of phase velocity and group velocity as well as energy velocity in periodic layered media are subtle and require careful examination. The electromagnetic Bloch waves are given by Eq. (6.2-25). The dispersion relation between k_y , K , and ω can be obtained from Eq. (6.2-24). It is important to note that the Bloch wave number K defined by Eq. (6.2-24) is not uniquely defined, in that any integer multiple of $2\pi/\Lambda$ can be added to it. The reduced-Brillouin-zone scheme commonly used in solid-state physics is no longer useful as far as the phase velocity of an electromagnetic Bloch wave is concerned. If $\mathbf{E}_K(z)$ is expanded in a Fourier series

$$\mathbf{E}_K(z) = \sum_l \mathbf{e}_K^{(l)} e^{-il(2\pi/\Lambda)z}, \quad (6.7-1)$$

the Bloch wave can be written as a linear superposition of an infinite

number of partial plane waves, which are the so-called “space harmonics.” From Eqs. (6.2-25) and (6.7-1) we have

$$\mathbf{E} = \sum_l \mathbf{e}_K^{(l)} e^{-i[K+l(2\pi/\Lambda)]z} e^{i(\omega t - k_y y)}, \quad (6.7-2)$$

where $\mathbf{e}_K^{(l)}$ are constant vectors. Thus, the multivalued nature of the Bloch wave number embodies the existence of the whole set of space harmonics. If the periodicity is removed (i.e., $n_1 = n_2$), then the Bloch mode should become a regular plane wave and K should be equal to the z component k_z of the propagation vector.

The principal value of K is determined in such a way that

$$|\mathbf{e}_K^{(0)}| \geq |\mathbf{e}_K^{(l)}| \quad (6.7-3)$$

for all l , or equivalently by choosing K such that the integral

$$\frac{1}{\Lambda} \int_0^\Lambda \mathbf{E}_K(z) dz \equiv \langle \mathbf{E}_K \rangle \quad (6.7-4)$$

has a maximum magnitude. This ensures that when the periodicity is made to vanish, the surviving spatial harmonics is $\mathbf{e}_K^{(0)}$ and $K = k_z$.

Having a proper choice of the Bloch wave number K , we are now in a position to define the phase velocity of a Bloch wave,

$$V_p = \frac{\omega}{(K^2 + k_y^2)^{1/2}}. \quad (6.7-5)$$

If K is complex, we use only its real part.

The phase velocity defined above is, strictly speaking, the phase velocity of the fundamental space harmonic ($l = 0$), which is a plane wave of the form

$$\mathbf{E} = \langle \mathbf{E}_K \rangle e^{i(\omega t - k_y y - Kz)}. \quad (6.7-6)$$

In the long-wavelength regime, where the whole structure behaves as if it were homogeneous, the fundamental space harmonic is the dominant part of the Bloch wave and can be taken as a very good approximation to the whole wave.

The group velocity for a Bloch wave packet propagating in the yz plane is given by

$$\mathbf{V}_g = \left(\frac{\partial \omega}{\partial k_y} \right)_K \hat{\mathbf{y}} + \left(\frac{\partial \omega}{\partial K} \right)_{k_y} \hat{\mathbf{z}}. \quad (6.7-7)$$

In a homogeneous medium, the group velocity represents the velocity of energy flow of a quasimonochromatic wave and is thus parallel to the Poynting vector, which is a constant vector in a homogeneous lossless medium. The Poynting vector of a Bloch wave given by Eq. (6.2-25) is a periodic function of z . The group velocity (6.7-7) of the same wave, however, is a constant vector. The discrepancy is due to the fact that in a periodic medium, the power flow is a periodic function of the space coordinates. We will show, however, that the averaged velocity of energy flow, defined as

$$\mathbf{V}_e = \frac{\frac{1}{\Lambda} \int_0^\Lambda (\text{Poynting vector}) dz}{\frac{1}{\Lambda} \int_0^\Lambda (\text{energy density}) dz}, \quad (6.7-8)$$

is exactly equal to the group velocity as given by Eq. (6.7-7). It is an extremely useful concept, since it makes it possible to consider the propagation of confined finite-aperture beams in a layered medium. The space-averaged Poynting vector and energy density are particularly useful in the long-wavelength regime, where the medium can be considered as quasihomogeneous and anisotropic.

To prove the equality of the energy velocity (6.7-8) and the group velocity (6.7-7) for the case of periodic layered media, we may use the results obtained in Section 6.2 and carry out the integration and differentiation indicated in Eqs. (6.7-8) and (6.7-7), respectively. It is interesting to show that this equality holds in an arbitrary periodic medium, including those with a periodic birefringence, provided the medium is lossless. The electromagnetic susceptibility tensors, reflecting the translational symmetry of the medium, are periodic functions of \mathbf{x} :

$$\epsilon_{ij}(\mathbf{x}) = \epsilon_{ij}(\mathbf{x} + \mathbf{a}), \quad \mu_{ij}(\mathbf{x}) = \mu_{ij}(\mathbf{x} + \mathbf{a}) \quad (6.7-9)$$

where \mathbf{a} is an arbitrary lattice vector. The propagation of the electromagnetic waves is described by Maxwell's equations,

$$\nabla \times \mathbf{H} = i\omega\epsilon\mathbf{E}, \quad (6.7-10)$$

$$\nabla \times \mathbf{E} = -i\omega\mu\mathbf{H}, \quad (6.7-11)$$

where we assume $e^{i\omega t}$ time dependence.

According to the translation symmetry of the medium (and/or the Floquet theorem), Eqs. (6.1-4) and (6.1-5), the waves assume the Bloch

form:

$$\mathbf{E} = \mathbf{E}_{\mathbf{K}}(\mathbf{x})e^{-i\mathbf{K}\cdot\mathbf{x}}, \quad (6.7-12)$$

$$\mathbf{H} = \mathbf{H}_{\mathbf{K}}(\mathbf{x})e^{-i\mathbf{K}\cdot\mathbf{x}}, \quad (6.7-13)$$

where $\mathbf{E}_{\mathbf{K}}(\mathbf{x})$ and $\mathbf{H}_{\mathbf{K}}(\mathbf{x})$ are periodic:

$$\mathbf{E}_{\mathbf{K}}(\mathbf{x}) = \mathbf{E}_{\mathbf{K}}(\mathbf{x} + \mathbf{a}), \quad \mathbf{H}_{\mathbf{K}}(\mathbf{x}) = \mathbf{H}_{\mathbf{K}}(\mathbf{x} + \mathbf{a}). \quad (6.7-14)$$

The subscript \mathbf{K} indicates that the functions $\mathbf{E}_{\mathbf{K}}$ and $\mathbf{H}_{\mathbf{K}}$ depend on \mathbf{K} , which is known as the Bloch wave vector. A dispersion relation exists between \mathbf{K} and ω ,

$$\omega = \omega(\mathbf{K}). \quad (6.7-15)$$

The time-averaged flux of energy in an electromagnetic field is given by

$$\mathbf{S} = \frac{1}{2} \text{Re}[\mathbf{E} \times \mathbf{H}^*]. \quad (6.7-16)$$

The time-averaged electromagnetic energy density is given by

$$U = \frac{1}{4}[\mathbf{E} \cdot \epsilon\mathbf{E}^* + \mathbf{H} \cdot \mu\mathbf{H}^*]. \quad (6.7-17)$$

The electromagnetic-susceptibility tensors are assumed to be real. In the case of a propagating Bloch wave in a periodic structure, \mathbf{S} and U are both periodic functions of space.

We define the energy velocity as

$$\mathbf{V}_e = \frac{\frac{1}{V} \int \mathbf{S} d^3x}{\frac{1}{V} \int U d^3x} \equiv \frac{\langle \mathbf{S} \rangle}{\langle U \rangle} \quad (6.7-18)$$

where the integration is over a unit cell and V is the volume of the cell. By substituting Eqs. (6.7-12) and (6.7-13) into Eqs. (6.7-16) and (6.7-17), we get from Eq. (6.7-18)

$$\mathbf{V}_e = \frac{\langle \frac{1}{2} \text{Re}[\mathbf{E}_{\mathbf{K}} \times \mathbf{H}_{\mathbf{K}}^*] \rangle}{\langle \frac{1}{4}(\mathbf{E}_{\mathbf{K}} \cdot \epsilon\mathbf{E}_{\mathbf{K}}^* + \mathbf{H}_{\mathbf{K}} \cdot \mu\mathbf{H}_{\mathbf{K}}^*) \rangle}, \quad (6.7-19)$$

where the brackets $\langle \rangle$ denote an average over the unit cell.

The group velocity \mathbf{V}_g is defined as

$$\mathbf{V}_g \equiv \nabla_{\mathbf{K}}\omega, \quad (6.7-20)$$

which is a vector perpendicular to the normal surface. If we substitute the Bloch waves (6.7-12) and (6.7-13) into Maxwell's equations (6.7-10) and (6.7-11), we obtain

$$\nabla \times \mathbf{H}_{\mathbf{K}} - i\mathbf{K} \times \mathbf{H}_{\mathbf{K}} = i\omega\epsilon\mathbf{E}_{\mathbf{K}}, \quad (6.7-21)$$

$$\nabla \times \mathbf{E}_{\mathbf{K}} - i\mathbf{K} \times \mathbf{E}_{\mathbf{K}} = -i\omega\mu\mathbf{H}_{\mathbf{K}}. \quad (6.7-22)$$

To prove that \mathbf{V}_e and \mathbf{V}_g are equal, we start from Eqs. (6.7-21) and (6.7-22). Suppose now that \mathbf{K} is changed by an infinitesimal amount $\delta\mathbf{K}$. If $\delta\omega$, $\delta\mathbf{E}_{\mathbf{K}}$, and $\delta\mathbf{H}_{\mathbf{K}}$ are the corresponding changes in ω , $\mathbf{E}_{\mathbf{K}}$, and $\mathbf{H}_{\mathbf{K}}$, respectively, we have, after many algebraic steps (see [4]),

$$\delta\omega = \mathbf{V}_e \cdot \delta\mathbf{K}. \quad (6.7-23a)$$

From the definition of the group velocity we also have

$$\delta\omega = (\nabla_{\mathbf{K}}\omega) \cdot \delta\mathbf{K} = \mathbf{V}_g \cdot \delta\mathbf{K}. \quad (6.7-23b)$$

Since $\delta\mathbf{K}$ is an arbitrary vector, we conclude that

$$\mathbf{V}_e = \mathbf{V}_g. \quad (6.7-24)$$

6.8. FORM BIREFRINGENCE

In the preceding sections we have derived some of the most important characteristics of Bloch waves propagating in a periodic layered medium. An exact expression for the dispersion relation (6.2-24) between K , k_y , and ω was derived. This dispersion relation can be represented by contours of constant frequency in the k_y, K plane, as in Fig. 6.16. It can be seen that these contours are more or less circular with only a slight ellipticity. The origin corresponds to the contour of zero frequency. In the long-wavelength regime ($\lambda \gg \Lambda$), these are similar to the dispersion curves of electromagnetic waves in a negative uniaxial crystal. The birefringence property of a periodic layered medium will now be discussed. These contours become distorted and modified at shorter wavelengths and near the boundaries of the Brillouin zone ($K\Lambda = m\pi$), where the wavelength is comparable to the

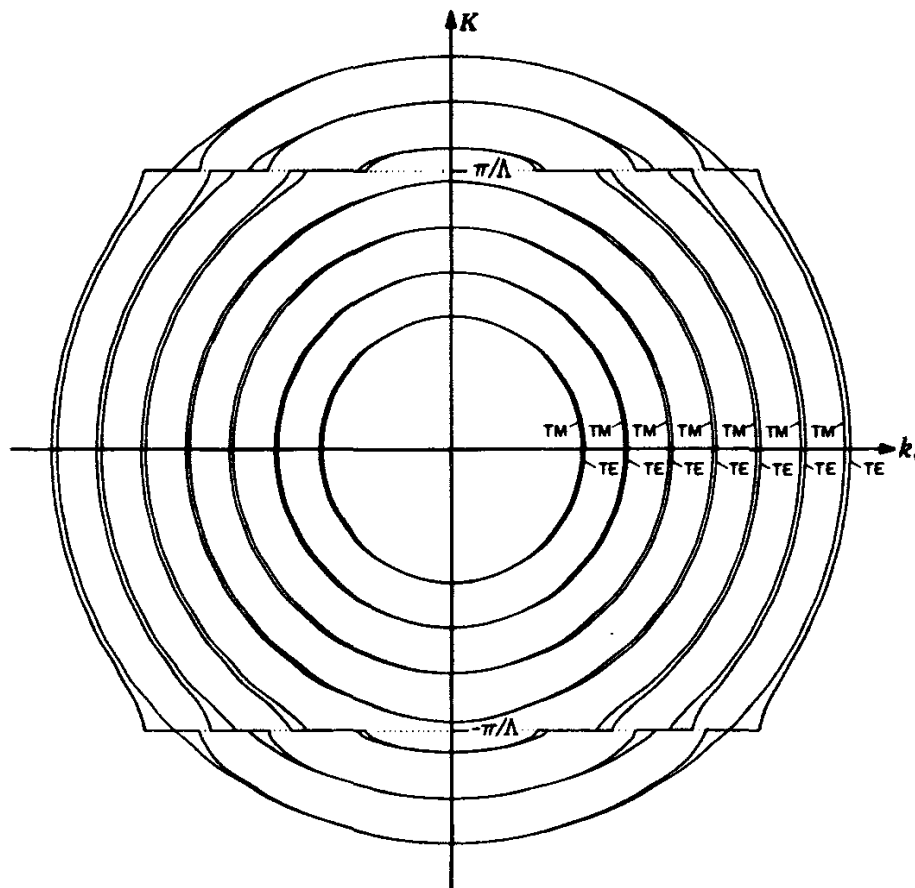


Figure 6.16. Contours of constant frequency in the k_y, K plane.

dimension of a unit cell and the electromagnetic waves interact strongly with the periodic medium.

Let us now consider the propagation of electromagnetic waves in an infinite medium consisting of alternating layers of two different homogeneous and isotropic substances. Although each individual layer is isotropic, the whole structure behaves as an anisotropic medium. TE waves and TM waves are found to propagate with different effective phase velocities, and the periodic medium is birefringent.

If the period Λ is sufficiently small compared to the wavelength, then the whole structure behaves as if it were homogeneous and uniaxially anisotropic. The wave given by Eq. (6.2-25) thus behaves as if it were a plane wave of the form given by Eq. (6.7-6).

In Fig. 6.16 the contours of constant ω are plotted in the Kk_y plane. These are sections of the normal surfaces with the Kk_y plane for various frequencies. It is evident from inspection that at the long-wavelength limit ($\lambda \gg \Lambda$) the dispersion of a layered medium is qualitatively similar to that of a negative uniaxial crystal.

To demonstrate this analogy we take the limit of $k_{1z}a \ll 1$, $k_{2z}b \ll 1$, and $K\Lambda \ll 1$ and expand all the transcendental functions in Eq. (6.2-24). After neglecting higher-order terms, we obtain

$$\frac{K^2}{n_o^2} + \frac{k_y^2}{n_o^2} = \frac{\omega^2}{c^2} \quad (\text{TE}), \quad (6.8-1)$$

$$\frac{K^2}{n_o^2} + \frac{k_y^2}{n_e^2} = \frac{\omega^2}{c^2} \quad (\text{TM}), \quad (6.8-2)$$

with

$$n_o^2 = \frac{a}{\Lambda} n_1^2 + \frac{b}{\Lambda} n_2^2, \quad (6.8-3)$$

$$\frac{1}{n_e^2} = \frac{a}{\Lambda} \frac{1}{n_1^2} + \frac{b}{\Lambda} \frac{1}{n_2^2}. \quad (6.8-4)$$

Equations (6.8-1) and (6.8-2) represent the two shells of the normal surface in the Kk_y plane. One surface (6.8-1) applies to a TE wave and is a sphere, while the TM normal surface (6.8-2) is an ellipsoid of revolution. TE waves thus are formally analogous to the so-called ordinary waves in a uniaxial crystal, while TM waves are the extraordinary waves. The normal surface becomes more complicated at higher frequencies. It consists of two oval surfaces osculating each other at the intersections with the K axis as long as the frequency is below the first forbidden gap. For frequencies higher than the forbidden gap, the oval surfaces break into several sections. The break points occur at

$$K = m \frac{\pi}{\Lambda}, \quad m = \text{integer}, \quad (6.8-5)$$

which is the Bragg condition for the quasi plane wave (6.7-6).

Equations (6.8-3) and (6.8-4) are very important in the optical theory of dichroic polarizers as well as the synthesis of negative uniaxial crystals with prescribed properties. To illustrate this, let us consider a periodic layered medium which consists of alternating metal and dielectric materials. Let n_1 be the complex refractive index of the metal layer, and n_2 be that of the dielectric layer. If the metal is a good conductor, then $|n_1|^2 \gg n_2^2$. Thus, according to Eqs. (6.8-3) and (6.8-4), the ordinary and extraordinary refrac-

tive indices for long-wavelength light ($\lambda \gg \Lambda$) become

$$n_o \approx n_1 \left(\frac{a}{\Lambda} \right)^{1/2}, \quad (6.8-6)$$

$$n_e \approx n_2 \left(\frac{b}{\Lambda} \right)^{-1/2}. \quad (6.8-7)$$

We see that the ordinary refractive index n_o is like that of a metal, and the extraordinary refractive index n_e is like that of a dielectric. Therefore the ordinary wave (TE) will be reflected as if the medium were metallic, and the extraordinary wave (TM) will be transmitted. Physically, the TE waves have their electric field vectors parallel to the layers and induce currents in the metal layers, whereas the TM waves have their electric field vectors perpendicular to the layers. Since the metal layers are separated by dielectric insulating layers, no current flow will be induced.

Form birefringence has been observed in a periodic layered medium consisting of 0.1235- μm -thick AlAs and 0.1062- μm -thick GaAs grown by molecular-beam epitaxy [5]. The measured birefringence ($n_{\text{TE}} - n_{\text{TM}}$) as a function of the wavelength is shown in Fig. 6.17.

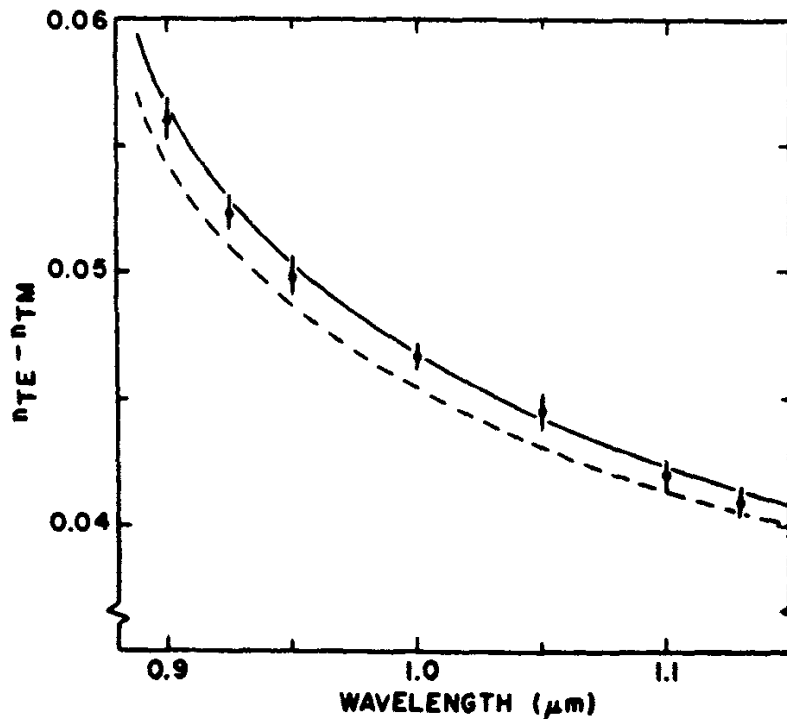


Figure 6.17. Measured form birefringence ($n_{\text{TE}} - n_{\text{TM}}$) of a GaAs-AlAs layered medium. The points give the measured values of the birefringence. The dashed curve is a plot of the birefringence obtained from Eqs. (6.8-3) and (6.8-4). The solid curve is calculated from an expansion (6.2-24) by including the k^2 term for GaAs and $\text{Al}_{0.97}\text{Ga}_{0.03}\text{As}$ [5].

6.9. ELECTROMAGNETIC SURFACE WAVES

It is the purpose of this section to investigate the evanescent Bloch surface waves guided by the boundary of a semiinfinite periodic dielectric layered medium. The surface wave, by definition, is a mode of propagation which is confined to the immediate vicinity of the interface between two semiinfinite systems. For example, the ripple phenomenon in water is a surface wave guided by the interface between air and water. Another interesting kind of surface wave is the electronic surface state, which has been extensively studied in solid-state physics. The electromagnetic surface wave at the interface between a dielectric and a metal will be discussed in Chapter 11. The existence of localized modes ("surface states") near the interface between a layered medium and a homogeneous one was suggested by Kossel [6]. In this section, the band theory of the periodic dielectric medium is employed to study the surface wave with an eigenvalue in the forbidden band.

That such surface waves can exist can be explained as follows: In Section 6.2 we have shown that, at a given frequency, there are regions of k_y for which K is complex and $K = m\pi/\Lambda \pm iK_i$. In the interior of an infinite periodic medium, a wave with exponential intensity variation cannot exist, and we refer to these regions as "forbidden." If the periodic medium is semiinfinite, the exponentially damped solution can be a legitimate solution near the interface, where it can possess a finite amplitude. The field envelope inside the periodic medium decays as $e^{-K_i z}$, where z is the distance from the interface into the periodic medium. It also evanesces exponentially in the semiinfinite homogeneous medium provided $ck_y/\omega > n_a$.

To investigate the properties of the surface modes, consider a semiinfinite periodic multilayer dielectric medium consisting of alternating layers of different indices of refraction. The distribution of the index of refraction is

$$n(y, z) = \begin{cases} n_a, & z \leq 0, \\ n_2, & m\Lambda \leq z < m\Lambda + b, \\ n_1, & m\Lambda + b \leq z < (m+1)\Lambda \end{cases} \quad (6.9-1)$$

$$(m = 0, 1, 2, \dots).$$

The geometry of the structure is sketched in Fig. 6.18. We look for the possibility of confined waves propagating in the positive y direction. Since the structure is semiinfinite, we are only interested in the surface wave as far as guiding is concerned. For the sake of definiteness we consider the case of TE surface modes where the electric field is polarized in the x direction. The

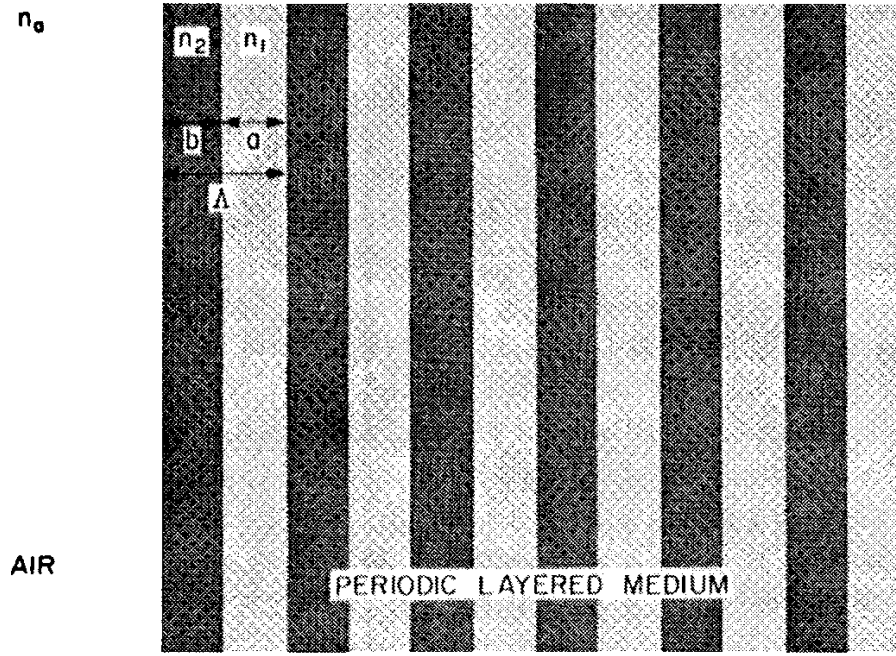


Figure 6.18. A semiinfinite periodic stratified medium.

electric-field distribution (TE) obeys the wave equation (6.4-8). We take the solution in the following form:

$$E(y, z) = \begin{cases} \alpha e^{q_a z} e^{-ik_y y}, & z \leq 0, \\ E_K(z) e^{-iKz} e^{-ik_y y}, & z > 0, \end{cases} \quad (6.9-2)$$

where α is a constant, q_a is given by

$$q_a = \left\{ k_y^2 - \left[\frac{\omega}{c} n_a \right]^2 \right\}^{1/2}, \quad (6.9-3)$$

and $E_K(z) e^{-iKz}$ is the Bloch wave given by Eq. (6.2-25).

For a guided wave to exist, the constant K in Eq. (6.9-2) must be complex, so that the field decays as z goes to infinity. This is possible only when the propagation conditions (i.e., k_y) in the periodic medium correspond to a "forbidden" band. Another condition is that $E(x, y)$ and its derivative $\partial E / \partial z$ must be continuous at the interface $z = 0$ with medium a . By using Eq. (6.9-2) and the explicit form of the Bloch wave (6.2-25) at $n = 0$, the boundary conditions at the interface $z = 0$ become

$$\begin{aligned} \alpha &= a_0 + b_0, \\ q_a \alpha &= -ik_{1z} (a_0 - b_0), \end{aligned} \quad (6.9-4)$$

where a_0 and b_0 are given by Eq. (6.2-23a). By eliminating α from Eq. (6.9-4) and using Eq. (6.2-23a), we obtain the mode condition for the surface waves:

$$q_a = ik_{1z} \frac{A + B - e^{iK\Lambda}}{A - B - e^{iK\Lambda}}, \quad (6.9-5)$$

where A and B are given by Eq. (6.2-12) for TE waves, and $e^{iK\Lambda}$ is given by Eq. (6.2-22). The sign of K is chosen to make its imaginary part negative, so that according to Eq. (6.9-2), the field amplitude decays exponentially as z increases. According to Eqs. (6.2-12), (6.2-24), (6.2-6), and (6.9-3), both sides of Eq. (6.9-5) are functions of k_y for a given ω . Values of k_y satisfying Eq. (6.9-5) for which K is complex correspond to surface waves.

The calculated transverse field distributions $E(0, z)$ of some typical surface waves are shown in Fig. 6.19. It is evident that the energy is more or less concentrated in the first few periods of the semiinfinite periodic medium. It can easily be shown that

$$\frac{\text{energy in the first period}}{\text{energy in the whole semiinfinite periodic structure}} = (1 - e^{-2K_i\Lambda}), \quad (6.9-6)$$

where $K_i > 0$ is the imaginary part of K . Generally speaking, the fundamental surface wave has the highest K_i and hence the highest degree of localization. The fundamental surface wave may happen to be in the zeroth or the first forbidden gap. It depends on the magnitude of the index of refraction n_a . For n_a less than n_1 , which is a case of practical interest (n_a is the index of refraction of air), the fundamental surface wave has a Bloch wave vector in the first forbidden gap.

The field distribution in each period for each mode is similar to that of the distribution in the preceding period, except that the amplitude is reduced by a factor of $(-1)^m e^{-K_i\Lambda}$, where m is the integer corresponding to the m th forbidden gap.

The electromagnetic surface wave has been observed in a periodic layer structure which consists of 12 pairs of alternating layers of 0.5- μm -thick $\text{Al}_{0.2}\text{Ga}_{0.8}\text{As}$ on a GaAs substrate [7, 8]. Under these conditions and at the excitation wavelength of 1.15 μm , the mode condition (6.9-5) predicts that exactly four surface modes can be supported by the structure. Generally speaking, for $n_a < n_1 < n_2$, the maximum number of surface modes at a given ω is m , where $m\pi \leq \text{Re}[K(\omega, k_y = n_a\omega/c)\Lambda] < (m+1)\pi$. The transverse intensity distribution for the fundamental mode is shown in Fig.

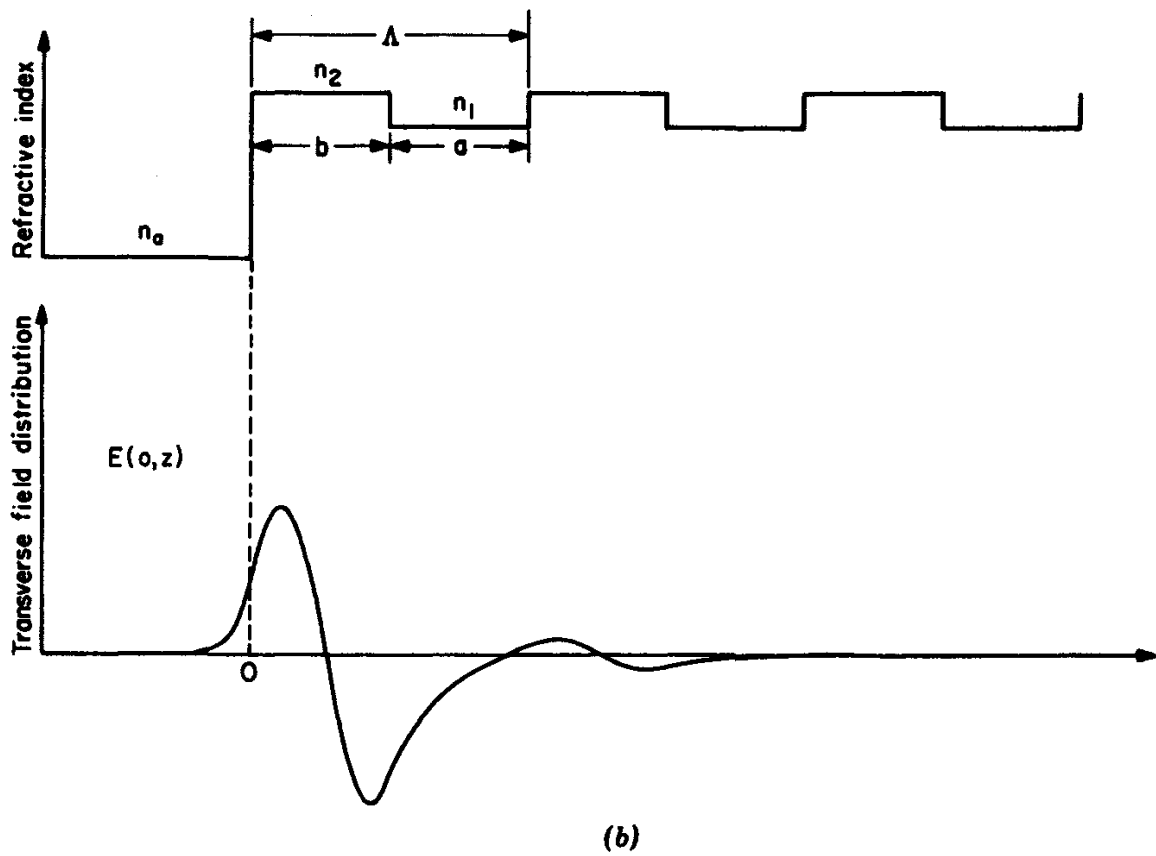
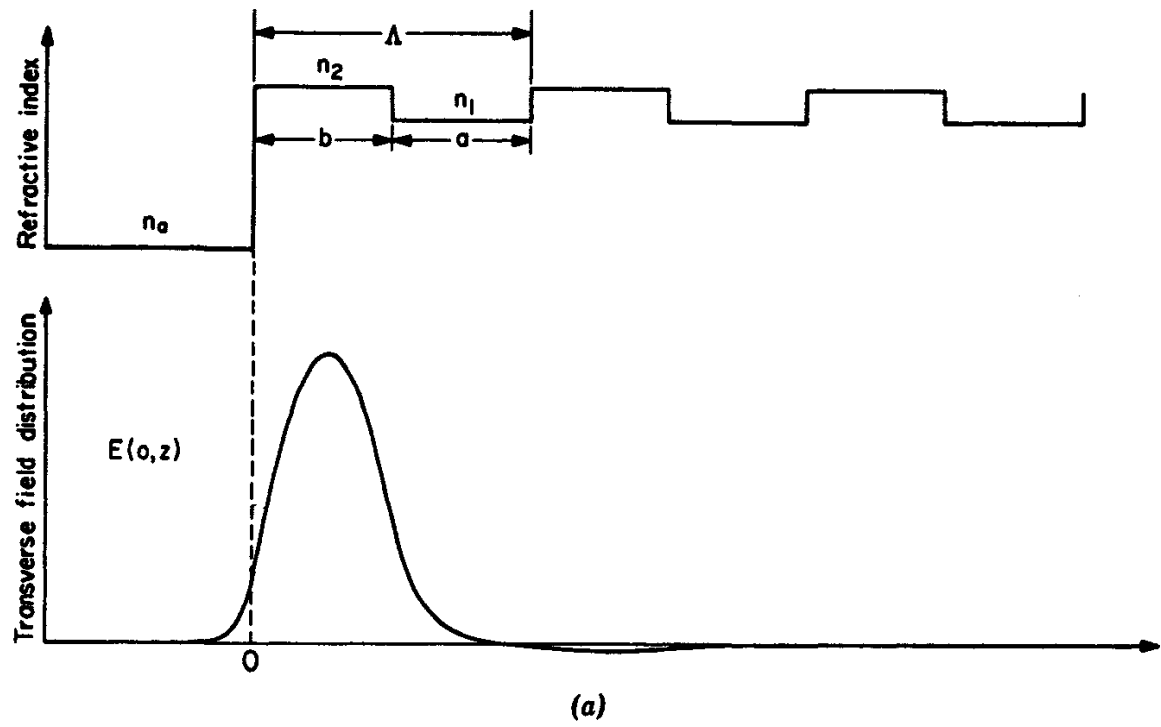


Figure 6.19. Transverse field distributions for typical surface modes guided by the surface of a semiinfinite periodic stratified medium [2]: (a) fundamental mode; (b) higher-order mode.

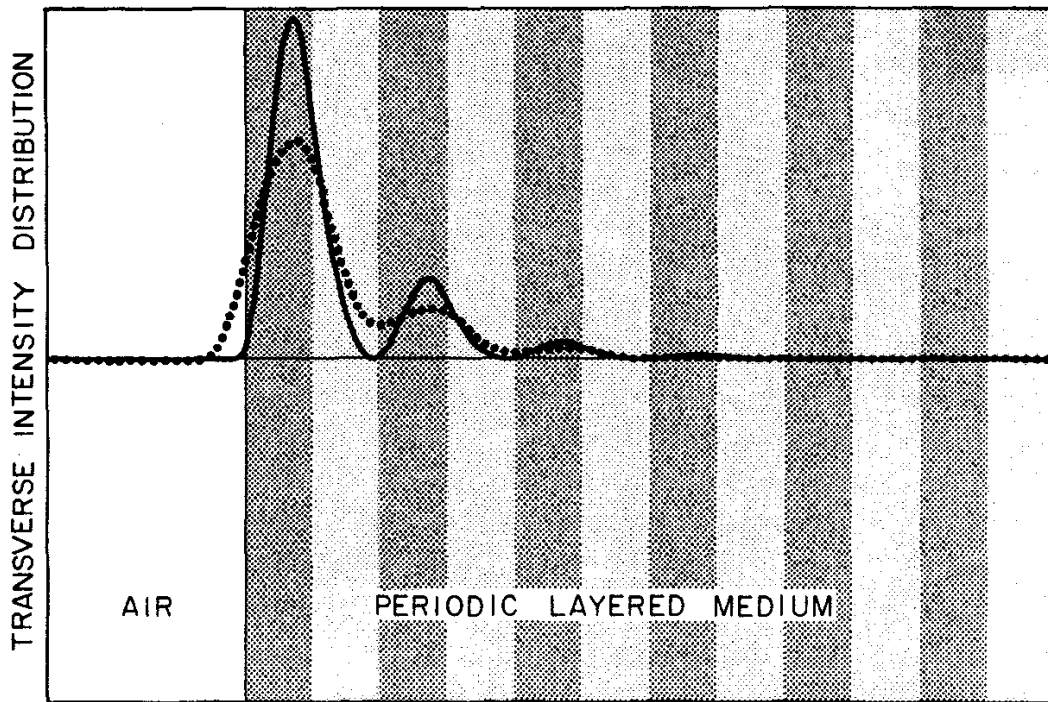


Figure 6.20. The calculated transverse intensity distribution for the fundamental surface mode in a periodic layered medium. The dotted line is the convolved intensity distribution [7].

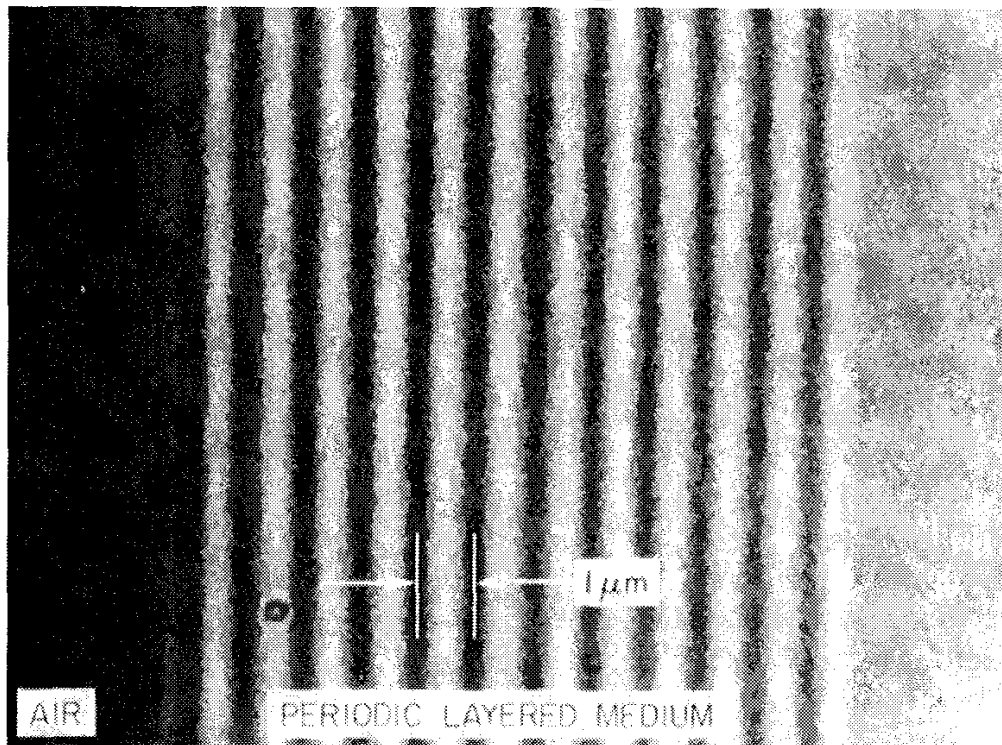


Figure 6.21. A phase-contrast photograph of a cleaved section of a layered medium composed of alternating layers of GaAs and $\text{Al}_{0.2}\text{Ga}_{0.8}\text{As}$ [7].

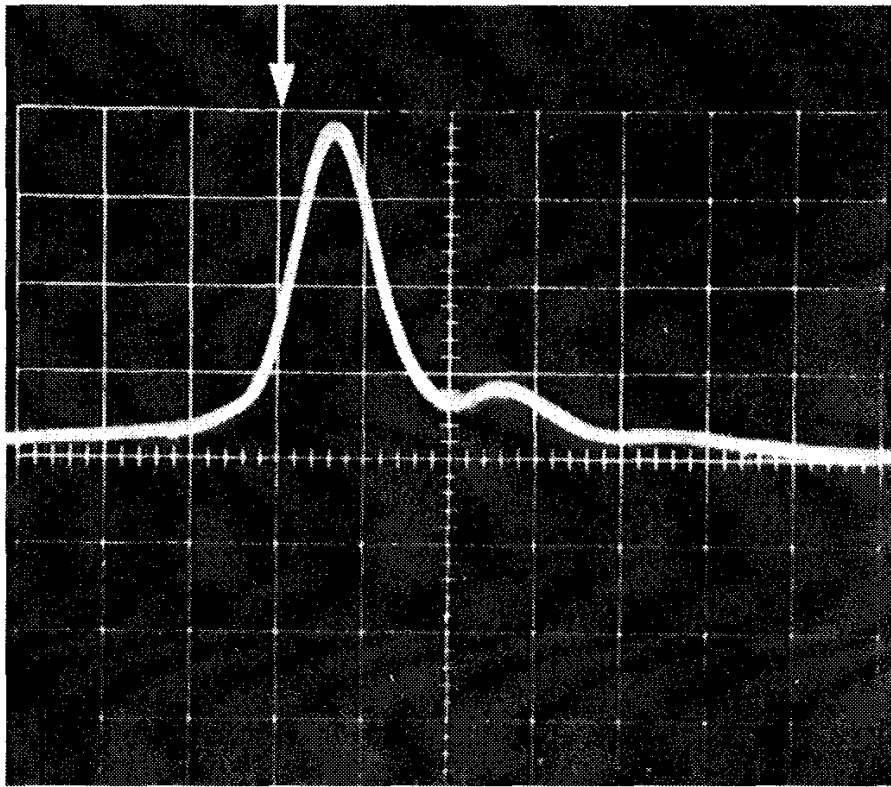


Figure 6.22. Measured transverse intensity distribution of surface waves in a layered medium 15 mm long. The horizontal scale is about $0.5 \mu\text{m}$ per (big) division. The surface of the structure is indicated by an arrow [7].

6.20. The computed Bloch wave number is

$$K\Lambda = \pi + i(7.233 \times 10^{-1}) \quad (6.9-7)$$

at $k_y = 3.357(2\pi/\lambda)$.

A phase-contrast photograph of the structure's cross section is shown in Fig. 6.21. The measured intensity distribution of the fundamental surface wave is shown in Fig. 6.22.

PROBLEMS

6.1. *Forbidden bands of one-dimensional periodic media.* Consider the propagation of electromagnetic radiation in a one-dimensional periodic medium with a dielectric constant

$$\varepsilon(z) = \varepsilon(z + \Lambda).$$

Let z also be the direction of propagation.

- (a) Show that constructive interference in the reflection of light occurs when the Bragg condition

$$\Delta\beta = 2k - \frac{2m\pi}{\Lambda} = 0$$

is satisfied. The above condition can also be written as $|k - mg| = k$. Physically, this means that the space harmonics k and $k - mg$ are resonantly coupled.

- (b) Now assume that the light is incident at an angle θ . Show that the Bragg condition $\Delta\beta = 0$ agrees with Eq. (6.1-8).
 (c) Let ω_0 be the center of the forbidden gap; show that

$$\omega_0^2 = \frac{g^2}{4\mu\epsilon_0},$$

where $g = 2\pi/\Lambda$.

- (d) Let K_i be the imaginary part of the wave number in the forbidden gap, so that

$$K = \frac{1}{2}g + iK_i.$$

Show that the relation between K_i and ω is given by

$$\left(\frac{K_i}{\frac{1}{2}g}\right)^2 + \left(\frac{\omega - \omega_0}{\omega_0}\right)^2 = \left|\frac{\epsilon_1}{2\epsilon_0}\right|^2.$$

Notice that this is an ellipse with a center $\omega = \omega_0$ and $K_i = 0$.

- (e) Derive from (d) that the bandgap is given by

$$\Delta\omega_{\text{gap}} = \left|\frac{\epsilon_1}{\epsilon_0}\right|\omega_0$$

and the maximum value of K_i is given by

$$(K_i)_{\text{max}} = \frac{1}{4}g\left|\frac{\epsilon_1}{\epsilon_0}\right|.$$

- 6.2. *Square-wave medium.* A medium with a square-wave variation of its dielectric constant (or refractive index) as a function of space is called a square-wave medium. In other words, the refractive-index profile of

such a medium is given by

$$n(z) = \begin{cases} n_2, & 0 < z < \frac{1}{2}\Lambda, \\ n_1, & \frac{1}{2}\Lambda < z < \Lambda, \end{cases}$$

with

$$n(z + \Lambda) = n(z).$$

(a) If $f(z)$ is defined as

$$f(z) = \begin{cases} 1, & 0 < z < \frac{1}{2}\Lambda, \\ -1, & \frac{1}{2}\Lambda < z < \Lambda, \end{cases}$$

with $f(z + \Lambda) = f(z)$, show that

$$n^2(z) = \frac{1}{2}(n_2^2 + n_1^2) + \frac{1}{2}(n_2^2 - n_1^2)f(z).$$

(b) Show that the Fourier expansion of $f(z)$ is

$$f(z) = \sum_l \frac{i(1 - \cos l\pi)}{l\pi} \exp\left[-il\frac{2\pi}{\Lambda}z\right].$$

(c) Show that the first forbidden bandgap ($l = 1$) of this medium is given by

$$\frac{\Delta\omega_{\text{gap}}}{\omega_0} = \frac{2\Delta n}{\pi n}.$$

6.3. Matrix elements.

- (a) Derive Eq. (6.2-12).
- (b) Derive Eq. (6.2-14).

6.4. Bloch wave numbers.

- (a) Derive Eq. (6.2-21).
- (b) Derive Eqs. (6.2-22), (6.2-23), and (6.2-24).
- (c) Obtain an explicit expression for $\cos K\Lambda$ from Eqs. (6.2-24), (6.2-12), and (6.2-14) for TE waves and for TM waves.
- (d) Show that at normal incidence ($k_y = 0$) the expressions obtained in (c) reduce to Eq. (6.2-26).

- (e) Show that at the Brewster angle of incidence [$k_y = (\omega/c)n_2 \sin \theta_B$], the Bloch wave number is always real. [Hint: $B = C = 0, AD = 1.$]

6.5. *Quarter-wave stacks.* Consider a periodic layered medium which consists of two alternating dielectric media as described by Eq. (6.2-1).

- (a) Use the expressions obtained in Problem 6.4(c) and show that the maximum of $|\cos K\Lambda|$ occurs when

$$k_{1z}a = \frac{1}{2}\pi, \frac{3}{2}\pi, \frac{5}{2}\pi, \dots$$

and

$$k_{2z}b = \frac{1}{2}\pi, \frac{3}{2}\pi, \frac{5}{2}\pi, \dots$$

A layered structure satisfying these conditions is called a quarter-wave stack.

- (b) Obtain expressions for these maximum values of $\cos K\Lambda$ for both TE and TM waves.
 (c) Show that at normal incidence, these expressions reduce to Eq. (6.2-29).
 (d) Show that the Bloch evanescent wave at normal incidence in a quarter wave stack decays by a factor of n_1/n_2 per period. Take $n_1 < n_2$.

6.6. *Conservation of mode powers.*

- (a) Show that the codirectional coupled equations (6.4-27) are consistent with the conservation of energy (6.4-29).
 (b) Show that the general solution (6.4-30) also obeys the conservation condition (6.4-29).
 (c) Show that the contradirectional coupled equations (6.4-33) are consistent with the conservation of energy (6.4-34).
 (d) Show that the general solution (6.4-35) also agrees with Eq. (6.4-34).

6.7. *Rotation of a crystal plate.* Let ψ be the azimuth angle of a crystal wave plate.

- (a) Show that the dielectric tensor is given by Eqs. (6.5-4) and (6.5-6).
 (b) Show that the dielectric tensor is symmetric.
 (c) Show that the trace of the dielectric tensor is unchanged.
 (d) If ψ is a small angle (i.e., $\psi \ll 1$), show that the dielectric perturbation is only significant in the off-diagonal terms.

6.8. *Šolc filters.*

- (a) Show that Eq. (6.5-19) is equivalent to Eq. (5.3-18).
 (b) Show that the bandwidth of a Šolc filter is inversely proportional to the length of the periodic medium.

6.9. *Bragg reflectors.*

- (a) Derive the expressions for the coupling constants for both TE waves and TM waves [Eq. (6.6-5)].
 (b) Show that the bandwidth of a Bragg reflector is independent of the length L of the medium.
 (c) Show that the reflectivity is finite at $s = 0$ (i.e., $\Delta\beta = 2|\kappa|$).
 (d) Show that the first reflectivity zero occurs at $sL = i\pi$. What is $\Delta\beta$ at this point?

6.10. The transmission coefficient of a Bragg reflector is defined as

$$t_N = \left(\frac{a_N}{a_0} \right)_{b_N=0}.$$

- (a) Show that

$$t_N = \frac{1}{AU_{N-1} - U_{N-2}}.$$

- (b) The transmissivity T is given by

$$T = |t_N|^2.$$

Show that

$$T = \frac{1}{1 + |C|^2 \frac{\sin^2 N K \Lambda}{\sin^2 K \Lambda}}$$

Note that $A^* = D$ and $|C|^2 = |A|^2 - 1$.

- (c) Use $R = 1 - T$ to derive Eq. (6.3-6).

6.11. The reflectivity formula (6.3-6) and the transmissivity formula derived in Problem 6.10 are valid only when the light is incident from the medium with refractive index n_1 . Show that if the light is incident from a medium with refractive index n_a (for air $n_a = 1$), the reflection coefficient is

$$r = \frac{r_{a1} + r_N}{1 + r_{a1} r_N},$$

where r_N is given by Eq. (6.3-5) and r_{a1} is the reflection coefficient for light incident from medium n_a on medium n_1 . For normal incidence

$$r_{a1} = \frac{n_a - n_1}{n_a + n_1}.$$

[Hint: Use Airy's formula* by assuming a layer of refractive index n_1 with an infinitesimal thickness sandwiched between medium n_a and the Bragg reflector.]

REFERENCES

1. See, for example, F. Abeles, "Investigations on the propagation of sinusoidal electromagnetic waves in stratified media. Application to thin films," *Ann. Phys. (Paris)* **5**, 596 (1950); "Investigations on the propagation of sinusoidal electromagnetic waves in stratified media. Application to thin films. II. Thin films," **5**, 706 (1950).
2. P. Yeh, A. Yariv, and C.-S. Hong, "Electromagnetic propagation in periodic stratified media. I. General theory," *J. Opt. Soc. Am.* **67**, 423-437 (1977); A. Yariv and P. Yeh, "II. Birefringence, phase matching, and X-ray lasers," *J. Opt. Soc. Am.* **61**, 438-448 (1977).
3. J. P. van der Ziel and M. Illegems, "Multilayer GaAs-Al_{0.3}Ga_{0.7}As dielectric quarter wave stacks grown by molecular beam epitaxy," *Appl. Opt.* **14**, 2627 (1975).
4. P. Yeh, "Electromagnetic propagation in birefringent layered media," *J. Opt. Soc. Am.* **69**, 742 (1979).
5. J. P. van der Ziel, M. Illegems, and R. M. Mikulyak, "Optical birefringence of thin GaAs-AlAs multilayer films," *Appl. Phys. Lett.* **28**, 735 (1976).
6. D. Kossel, "Analogies between thin-film optics and electron-band theory of solids," *J. Opt. Soc. Am.* **56**, 1434 (1966).
7. P. Yeh, A. Yariv, and A. Y. Cho, "Optical surface waves in periodic layered media," *Appl. Phys. Lett.* **32**, 104 (1978).
8. W. Ng, P. Yeh, P. C. Chen, and A. Yariv, "Optical surface waves in periodic layered medium grown by liquid phase epitaxy," *Appl. Phys. Lett.* **32**, 370 (1978).
9. See, for example, M. Born and E. Wolf, *Principles of Optics*, MacMillan, New York, 1964, p. 62.

*Airy's formula for the reflection and transmission coefficients are [9]

$$r = \frac{r_{12} + r_{23}e^{-2i\phi}}{1 + r_{12}r_{23}e^{-i2\phi}}, \quad t = \frac{t_{12}t_{23}e^{-i\phi}}{1 + r_{12}r_{23}e^{-2i\phi}},$$

where

$$\phi = \frac{2\pi n_2 t \cos \theta_2}{\lambda}.$$

7

Electro-optics

In Chapter 4 we treated the propagation of electromagnetic radiation in anisotropic crystal media. It was shown that the normal modes of propagation can be determined from the index ellipsoid surface. In this chapter we consider the problem of propagation of optical radiation in crystals in the presence of an applied electric field. We find that, in certain types of crystals, the application of an electric field results in a change in both the dimensions and orientation of the index ellipsoid. This is referred to as the electro-optic effect. The electro-optic effect affords a convenient and widely used means of controlling the phase or intensity of the optical radiation. This modulation is used in an ever-expanding number of applications, including the impression of information onto optical beams, optical beam deflection, and spectral tunable filters. Some of these applications will be discussed further in the next chapter.

7.1. THE ELECTRO-OPTIC EFFECT

The propagation of optical radiation in a crystal can be described completely in terms of the impermeability tensor η_{ij} (4.3-2). We recall that $\eta = \epsilon_0 \epsilon^{-1}$. The two directions of polarization as well as the corresponding indices of refraction (i.e., velocity of propagation) of the normal modes are found most easily by using the index ellipsoid (4.3-9). The index ellipsoid assumes its simplest form in the principal coordinate system:

$$\frac{x^2}{n_x^2} + \frac{y^2}{n_y^2} + \frac{z^2}{n_z^2} = 1, \quad (7.1-1)$$

where the directions x , y , and z are the principal axes—that is, the directions in the crystal along which \mathbf{D} and \mathbf{E} are parallel. $1/n_x^2$, $1/n_y^2$, and $1/n_z^2$ are the principal values of the impermeability tensor η_{ij} .

According to the quantum theory of solids, the optical dielectric impermeability tensor depends on the distribution of charges in the crystal. The application of an electric field will result in a redistribution of the bond charges and possibly a slight deformation of the ion lattice. The net result is a change in the optical impermeability tensor. This is known as the electro-optic effect. The electro-optic coefficients are defined traditionally as

$$\begin{aligned}\eta_{ij}(\mathbf{E}) - \eta_{ij}(0) &\equiv \Delta\eta_{ij} = r_{ijk}E_k + s_{ijkl}E_kE_l \\ &= f_{ijk}P_k + g_{ijkl}P_kP_l,\end{aligned}\quad (7.1-2)$$

where \mathbf{E} is the applied electric field and \mathbf{P} is the polarization field vector. The constants r_{ijk} and f_{ijk} are the linear (or Pockels) electro-optic coefficients, and s_{ijkl} and g_{ijkl} are the quadratic (or Kerr) electro-optic coefficients. In the above expansion, terms higher than the quadratic are neglected because these higher-order effects are too small for most applications. The quadratic effect was first discovered by J. Kerr, in 1875, in optically isotropic media such as liquids and glasses. The Kerr electro-optic effect in liquids is associated mostly with the alignment of the anisometric molecules in the presence of an electric field. The substance then behaves optically as if it were a uniaxial crystal in which the electric field defines the optic axis. The linear electro-optic effect was first studied by F. Pockels in 1893.

We will use the electro-optic coefficients r_{ijk} and s_{ijkl} throughout this book. Some authors use f_{ijk} and g_{ijkl} . These coefficients are related by the following equations:

$$f_{ijk} = \frac{r_{ijk}}{\epsilon_k - \epsilon_0}, \quad (7.1-3)$$

$$g_{ijkl} = \frac{s_{ijkl}}{(\epsilon_k - \epsilon_0)(\epsilon_l - \epsilon_0)}, \quad (7.1-4)$$

where ϵ_k, ϵ_l are the principal optical dielectric constants. Thus the index ellipsoid of a crystal in the presence of an applied electric field is given by

$$\eta_{ij}(\mathbf{E})x_ix_j = 1. \quad (7.1-5)$$

When the electric field vanishes, the index ellipsoid reduces to (7.1-1). We have shown in Section 4.1 that the dielectric tensor ϵ_{ij} is a symmetric tensor, provided the medium is lossless and optically inactive. According to the definition (4.3-2) of η_{ij} , we conclude that η_{ij} must also be a symmetric tensor, provided the medium is lossless and optically inactive. Consequently, the indices i and j in Eq. (7.1-2) can be permuted. The quadratic electro-optic

coefficient is given, according to Eq. (7.1-2), by

$$s_{ijkl} = \frac{1}{2} \left(\frac{\partial^2 \eta_{ij}}{\partial E_k \partial E_l} \right)_{E=0}. \quad (7.1-6)$$

Since the order of partial differentiation is immaterial, we find the indices k and l can be permuted. These permutation symmetries are summarized in the following equations:

$$r_{ijk} = r_{jik}, \quad (7.1-7)$$

$$s_{ijkl} = s_{jilk}, \quad (7.1-8)$$

$$s_{ijkl} = s_{ijlk}. \quad (7.1-9)$$

Because of these permutation symmetries, it is convenient to introduce contracted indices to abbreviate the notation. They are defined as

$$\begin{aligned} 1 &= (11), \\ 2 &= (22), \\ 3 &= (33), \\ 4 &= (23) = (32), \\ 5 &= (13) = (31), \\ 6 &= (12) = (21). \end{aligned} \quad (7.1-10)$$

Using these contracted indices, we can write

$$\begin{aligned} r_{1k} &= r_{11k}, \\ r_{2k} &= r_{22k}, \\ r_{3k} &= r_{33k}, \\ r_{4k} &= r_{23k} = r_{32k}, \\ r_{5k} &= r_{13k} = r_{31k}, \\ r_{6k} &= r_{12k} = r_{21k}, \\ k &= 1, 2, 3. \end{aligned} \quad (7.1-11)$$

It is important to remember that the contraction of the indices is just a matter of convenience. These matrix elements (6×3) do not have the usual tensor transformation or multiplication properties. The permutation symmetry reduces the number of independent elements of r_{ijk} from 27 to 18, and the number of elements of s_{ijkl} from 81 to 36.

7.2. THE LINEAR ELECTRO-OPTIC EFFECT

We have mentioned in the last section that the electro-optic effect results from the redistribution of charges due to the application of a dc electric field. It may be expected that the electro-optic effect will depend on the ratio of the applied electric field to the intraatomic electric field binding the charged particles such as electrons and ions. In most practical applications of the electro-optic effect, the applied electric field is small compared with the electric field inside the atom, which is typically of the order of 10^8 V/cm. As a result, the quadratic effect is expected to be small compared to the linear effect and is often neglected when the linear effect is present. However, in crystals with centrosymmetric point groups, the linear electro-optic effect vanishes and the quadratic effect becomes the dominant phenomenon. To prove the last statement consider the effect of spatial inversion on a crystal.

The inversion is performed by transforming the point at r in the crystal with respect to the inversion center, to the position $-r$. Among the 32 point groups listed in Table 7.1, there are eleven crystal systems in which the inversion operation I is a symmetry operation. These crystals are said to be centrosymmetric. Consider now the transformation of the linear electro-optic tensor r_{ijk} under the operation of an inversion:

$$I r_{ijk} = r'_{ijk} = -r_{ijk}. \quad (7.2-1)$$

But because of the inversion symmetry, any tensor property must be invariant under the operation of an inversion; thus

$$r'_{ijk} = r_{ijk}. \quad (7.2-2)$$

Equations (7.2-1) and (7.2-2) can be satisfied simultaneously only if $r_{ijk} = 0$. This proves that the linear electro-optic effect must vanish in centrosymmetric crystals. In fact, all third-rank tensors must vanish in the eleven crystal systems that possess a center of inversion.

Table 7.1. Point Groups [1]

Crystal System	Class Symbol		Elements of Symmetry	Some Representative Crystals
	International	Schoenflies		
Triclinic	1	C_1	E	KIO_3
	$\bar{1}$	C_i	EI	Mica, Al_2SiO_5
Monoclinic	m	C_2	$E\sigma_h$	$PbHPO_4$, $SrTeO_3$, α - Ga_2S_3
	2	C_2	EC_2	KOH
	2/m	C_{2h}	$EC_2I\sigma_h$	AgAuTe ₄ , PbSiO ₃
Orthorhombic	2mm	C_{2v}	$EC_2\sigma'_v\sigma''_v$	$KNbO_3$, SbSI ($T < T_c$)*
	222	D_2	$EC_2C_2''C_2'''$	$KNa(C_4H_4O_6) \cdot 4H_2O$ (Rochelle salt)
	mmm	D_{2h}	$EC_2C_2''C_2'''I\sigma_h\sigma'_v\sigma''_v$	SbSI ($T > T_c$), $CaCl_2$, Al_2BeO_4 (Alexandrite)
Tetragonal	4	C_4	$E2C_4C_2$	γ - Fe_2O_3
	$\bar{4}$	S_4	$E2S_4C_2$	$CdGa_2S_4$, β - Ag_2HgI_4
	4/m	C_{4h}	$E2C_4C_2I2S_4\sigma_h$	$AgIO_4$, NaIO, $KCuF_4$
	4mm	C_{4v}	$E2C_4C_22\sigma'_v2\sigma''_v$	BaTiO ₃ (25°C), KTN ($T < T_c$)
	$\bar{4}2m$	D_{2d}	$EC_2C_2''C_2'''2\sigma'_v2S_4\sigma''_v$	AgGaS ₂ , ADP, KDP
	422	D_4	$E2C_4C_22C_2''2C_2'''$	TeO ₂
4/mmm	D_{4h}	$E2C_4C_22C_2''2C_2'''I2S_4\sigma_h2\sigma'_v2\sigma''_v$	TiO ₂ , GeO ₂	

Trigonal	3	C_3	$E2C_3$	$Pb_5Ge_3O_{11}, B_2O_3$	
	$\bar{3}$	C_{3i}	$E2C_3I2S_3$	S, Ge_3N_4, AsI_3	
	3m	C_{3v}	$E2C_33\sigma_v$	$Ag_3AsS_3, LiNbO_3, LiTaO_3$	
	32	D_3	$E2C_33C_2$	SiO_2 (α -quartz), Te, Se, AlF_3	
	$\bar{3}m$	D_{3d}	$E2C_33C_2I2S_33\sigma_v$	$Al_2O_3, CaCO_3$ (calcite), $NaNO_3$	
	Hexagonal	6	C_6	$E2C_62C_3C_2$	$KLiSO_4$
$\bar{6}$		C_{3h}	$E2C_3\sigma_h2S_6$	Li_2O_2	
6/m		C_{6h}	$E2C_62C_3C_2I2S_32S_6\sigma_v$	$PbSb_2S_4, \beta-Si_3N_4$	
$\bar{6}m2$		D_{3h}	$E2C_33C_2\sigma_h2S_63\sigma_v$	$GaSe, GaS$	
6mm		C_{6v}	$E2C_62C_3C_23\sigma_v3\sigma''$	$CdS, CdSe, ZnO, \alpha-ZnS$	
622		D_6	$E2C_62C_3C_23C_23C_2''$	$CsCuCl_3, BaAl_2O_4$	
6/mmm		D_{6h}	$E2C_62C_3C_23C_23C_2''I2S_32S_6\sigma_h2\sigma_v3\sigma_v''$	$BN, \beta-Al_2O_3, NiAs$	
Cubic		23	T	$E8C_33C_2$	$Bi_{12}GeO_{20}, Bi_{12}SiO_{20}$
		m3	T_h	$E8C_33C_2I8S_33\sigma$	$H_2S, MnSe_2, MgO_2$
		$\bar{4}3m$	T_d	$E8C_33C_26\sigma6S_4$	$CdTe, GaAs, InAs, ZnTe, MgO$
	432	O	$E8C_33C_26C_26C_4$	$LiFe_5O_8$	
	m3m	O_h	$E8C_33C_26C_26C_4I8S_33\sigma6\sigma6S_4$	$BaTiO_3$ ($T > T_c$), KTN ($T > T_c$), $SrTiO_3$, Ge, Si	

* T_c is the Curie temperature (or transition temperature).

By using the contracted indices (7.1-11), the equation of the index ellipsoid in the presence of an electric field can be written

$$\left(\frac{1}{n_x^2} + r_{1k}E_k\right)x^2 + \left(\frac{1}{n_y^2} + r_{2k}E_k\right)y^2 + \left(\frac{1}{n_z^2} + r_{3k}E_k\right)z^2 + 2yzzr_{4k}E_k + 2zxr_{5k}E_k + 2xyr_{6k}E_k = 0 \quad (7.2-3)$$

where E_k ($k = 1, 2, 3$) is a component of the applied electric field and summation over repeated indices k is assumed. Here 1, 2, 3 correspond to the principal dielectric axes x, y, z , and n_x, n_y, n_z are the principal refractive indices. This new ellipsoid (7.2-3) reduces to the unperturbed ellipsoid (7.1-1) when $E_k = 0$. In general, the principal axes of the ellipsoid (7.2-3) do not coincide with the unperturbed axes (x, y, z).

A new set of principal axes can always be found by a coordinate rotation, which is known as the principal-axis transformation of a quadratic form. The dimensions and orientation of the ellipsoid (7.2-3) are, of course, dependent on the direction of the applied field as well as the 18 matrix elements r_{ik} . We have argued above that in crystals possessing an inversion symmetry (centrosymmetric), $r_{ik} = 0$. The form, but not the magnitude, of the tensor r_{ik} can be derived from symmetry considerations, which dictate which of the 18 coefficients r_{ik} are zero, as well as the relationships that exist between the remaining coefficients. In Table 7.2 we give the form of the electro-optic tensor for all the noncentrosymmetric crystal classes. The electro-optic coefficients of some crystals are listed in Table 7.3.

7.2.1. Example: The Electro-optic Effect in KH_2PO_4

Consider the specific example of a crystal of potassium dihydrogen phosphate (KH_2PO_4), also known as KDP. The crystal has a fourfold axis of symmetry, which by strict convention is taken as the z (optic) axis, as well as two mutually orthogonal twofold axes of symmetry that lie in the plane normal to z . These are designated as the x and y axes. The symmetry group of this crystal is $\bar{4}2m$. Using Table 7.2, we write the electro-optic tensor in the form

$$r_{ij} = \begin{pmatrix} 0 & 0 & 0 \\ 0 & 0 & 0 \\ 0 & 0 & 0 \\ r_{41} & 0 & 0 \\ 0 & r_{41} & 0 \\ 0 & 0 & r_{63} \end{pmatrix}, \quad (7.2-4)$$

Table 7.2. Electro-optic Coefficients in Contracted Notation for All Crystal Symmetry Classes^a

Centrosymmetric ($\bar{1}$, $2/m$, mmm , $4/m$, $4/mmm$, $\bar{3}$, $\bar{3}m$, $6/m$, $6/mmm$, $m3$, $m3m$):

$$\begin{pmatrix} 0 & 0 & 0 \\ 0 & 0 & 0 \\ 0 & 0 & 0 \\ 0 & 0 & 0 \\ 0 & 0 & 0 \\ 0 & 0 & 0 \end{pmatrix}$$

Triclinic:

$$\begin{matrix} 1 \\ \begin{pmatrix} r_{11} & r_{12} & r_{13} \\ r_{21} & r_{22} & r_{23} \\ r_{31} & r_{32} & r_{33} \\ r_{41} & r_{42} & r_{43} \\ r_{51} & r_{52} & r_{53} \\ r_{61} & r_{62} & r_{63} \end{pmatrix} \end{matrix}$$

Monoclinic:

$$\begin{matrix} 2 \quad (2 \parallel x_2) & 2 \quad (2 \parallel x_3) \\ \begin{pmatrix} 0 & r_{12} & 0 \\ 0 & r_{22} & 0 \\ 0 & r_{32} & 0 \\ r_{41} & 0 & r_{43} \\ 0 & r_{52} & 0 \\ r_{61} & 0 & r_{63} \end{pmatrix} & \begin{pmatrix} 0 & 0 & r_{13} \\ 0 & 0 & r_{23} \\ 0 & 0 & r_{33} \\ r_{41} & r_{42} & 0 \\ r_{51} & r_{52} & 0 \\ 0 & 0 & r_{63} \end{pmatrix} \\ \\ m \quad (m \perp x_2) & m \quad (m \perp x_3) \\ \begin{pmatrix} r_{11} & 0 & r_{13} \\ r_{21} & 0 & r_{23} \\ r_{31} & 0 & r_{33} \\ 0 & r_{42} & 0 \\ r_{51} & 0 & r_{53} \\ 0 & r_{62} & 0 \end{pmatrix} & \begin{pmatrix} r_{11} & r_{12} & 0 \\ r_{21} & r_{22} & 0 \\ r_{31} & r_{32} & 0 \\ 0 & 0 & r_{43} \\ 0 & 0 & r_{53} \\ r_{61} & r_{62} & 0 \end{pmatrix} \end{matrix}$$

Orthorhombic:

$$\begin{matrix} 222 & 2mm \\ \begin{pmatrix} 0 & 0 & 0 \\ 0 & 0 & 0 \\ 0 & 0 & 0 \\ r_{41} & 0 & 0 \\ 0 & r_{52} & 0 \\ 0 & 0 & r_{63} \end{pmatrix} & \begin{pmatrix} 0 & 0 & r_{13} \\ 0 & 0 & r_{23} \\ 0 & 0 & r_{33} \\ 0 & r_{42} & 0 \\ r_{51} & 0 & 0 \\ 0 & 0 & 0 \end{pmatrix} \end{matrix}$$

Table 7.2. (Continued).

Tetragonal:

$$\begin{array}{ccc}
 4 & & \bar{4} & & 422 \\
 \begin{pmatrix} 0 & 0 & r_{13} \\ 0 & 0 & r_{13} \\ 0 & 0 & r_{33} \\ r_{41} & r_{51} & 0 \\ r_{51} & -r_{41} & 0 \\ 0 & 0 & 0 \end{pmatrix} & & \begin{pmatrix} 0 & 0 & r_{13} \\ 0 & 0 & -r_{13} \\ 0 & 0 & 0 \\ r_{41} & -r_{51} & 0 \\ r_{51} & r_{41} & 0 \\ 0 & 0 & r_{63} \end{pmatrix} & & \begin{pmatrix} 0 & 0 & 0 \\ 0 & 0 & 0 \\ 0 & 0 & 0 \\ r_{41} & 0 & 0 \\ 0 & -r_{41} & 0 \\ 0 & 0 & 0 \end{pmatrix}
 \end{array}$$

$$\begin{array}{cc}
 4mm & \bar{4}2m \quad (2 \parallel x_1) \\
 \begin{pmatrix} 0 & 0 & r_{13} \\ 0 & 0 & r_{13} \\ 0 & 0 & r_{33} \\ 0 & r_{51} & 0 \\ r_{51} & 0 & 0 \\ 0 & 0 & 0 \end{pmatrix} & \begin{pmatrix} 0 & 0 & 0 \\ 0 & 0 & 0 \\ 0 & 0 & 0 \\ r_{41} & 0 & 0 \\ 0 & r_{41} & 0 \\ 0 & 0 & r_{63} \end{pmatrix}
 \end{array}$$

Trigonal:

$$\begin{array}{cc}
 3 & 32 \\
 \begin{pmatrix} r_{11} & -r_{22} & r_{13} \\ -r_{11} & r_{22} & r_{13} \\ 0 & 0 & r_{33} \\ r_{41} & r_{51} & 0 \\ r_{51} & -r_{41} & 0 \\ -r_{22} & -r_{11} & 0 \end{pmatrix} & \begin{pmatrix} r_{11} & 0 & 0 \\ -r_{11} & 0 & 0 \\ 0 & 0 & 0 \\ r_{41} & 0 & 0 \\ 0 & -r_{41} & 0 \\ 0 & -r_{11} & 0 \end{pmatrix}
 \end{array}$$

$$\begin{array}{cc}
 3m \quad (m \perp x_1) & 3m \quad (m \perp x_2) \\
 \begin{pmatrix} 0 & -r_{22} & r_{13} \\ 0 & r_{22} & r_{13} \\ 0 & 0 & r_{33} \\ 0 & r_{51} & 0 \\ r_{51} & 0 & 0 \\ -r_{22} & 0 & 0 \end{pmatrix} & \begin{pmatrix} r_{11} & 0 & r_{13} \\ -r_{11} & 0 & r_{13} \\ 0 & 0 & r_{33} \\ 0 & r_{51} & 0 \\ r_{51} & 0 & 0 \\ 0 & -r_{11} & 0 \end{pmatrix}
 \end{array}$$

Table 7.2. (Continued).

Hexagonal:

$\begin{matrix} 6 \\ \left(\begin{array}{ccc} 0 & 0 & r_{13} \\ 0 & 0 & r_{13} \\ 0 & 0 & r_{33} \\ r_{41} & r_{51} & 0 \\ r_{51} & -r_{41} & 0 \\ 0 & 0 & 0 \end{array} \right) \end{matrix}$	$\begin{matrix} 6mm \\ \left(\begin{array}{ccc} 0 & 0 & r_{13} \\ 0 & 0 & r_{13} \\ 0 & 0 & r_{33} \\ 0 & r_{51} & 0 \\ r_{51} & 0 & 0 \\ 0 & 0 & 0 \end{array} \right) \end{matrix}$	$\begin{matrix} 622 \\ \left(\begin{array}{ccc} 0 & 0 & 0 \\ 0 & 0 & 0 \\ 0 & 0 & 0 \\ r_{41} & 0 & 0 \\ 0 & -r_{41} & 0 \\ 0 & 0 & 0 \end{array} \right) \end{matrix}$
$\begin{matrix} \bar{6} \\ \left(\begin{array}{ccc} r_{11} & -r_{22} & 0 \\ -r_{11} & r_{22} & 0 \\ 0 & 0 & 0 \\ 0 & 0 & 0 \\ 0 & 0 & 0 \\ -r_{22} & -r_{11} & 0 \end{array} \right) \end{matrix}$	$\begin{matrix} \bar{6}m2 \quad (m \perp x_1) \\ \left(\begin{array}{ccc} 0 & -r_{22} & 0 \\ 0 & r_{22} & 0 \\ 0 & 0 & 0 \\ 0 & 0 & 0 \\ 0 & 0 & 0 \\ -r_{22} & 0 & 0 \end{array} \right) \end{matrix}$	$\begin{matrix} \bar{6}m2 \quad (m \perp x_2) \\ \left(\begin{array}{ccc} r_{11} & 0 & 0 \\ -r_{11} & 0 & 0 \\ 0 & 0 & 0 \\ 0 & 0 & 0 \\ 0 & 0 & 0 \\ 0 & -r_{11} & 0 \end{array} \right) \end{matrix}$

Cubic:

$\begin{matrix} \bar{4}3m, 23 \\ \left(\begin{array}{ccc} 0 & 0 & 0 \\ 0 & 0 & 0 \\ 0 & 0 & 0 \\ r_{41} & 0 & 0 \\ 0 & r_{41} & 0 \\ 0 & 0 & r_{41} \end{array} \right) \end{matrix}$	$\begin{matrix} 432 \\ \left(\begin{array}{ccc} 0 & 0 & 0 \\ 0 & 0 & 0 \\ 0 & 0 & 0 \\ 0 & 0 & 0 \\ 0 & 0 & 0 \\ 0 & 0 & 0 \end{array} \right) \end{matrix}$
--	---

^aThe symbol over each matrix is the conventional symmetry-group designation.

so that the only nonvanishing elements are $r_{41} = r_{52}$ and r_{63} . Using Eqs. (7.2-3) and (7.2-4), we obtain the equation of the index ellipsoid in the presence of a field $\mathbf{E}(E_x, E_y, E_z)$ as

$$\frac{x^2}{n_o^2} + \frac{y^2}{n_o^2} + \frac{z^2}{n_e^2} + 2r_{41}E_x yz + 2r_{41}E_y xz + 2r_{63}E_z xy = 1, \quad (7.2-5)$$

where the constants involved in the first three terms do not depend on the field and, since the crystal is uniaxial, are taken as $n_x = n_y = n_o$, $n_z = n_e$. We thus find that the application of an electric field causes the appearance of "mixed" terms in the equation of the index ellipsoid. These are the terms with xv , xz , yz . This means that the major axes of the ellipsoid, with a field

Table 7.3. Linear Electro-optic Coefficients [2]

Substance	Symmetry	Wavelength λ (μm)	Electro-optic Coefficients ^a r_{ik} (10^{-12} m/V)	Index of Refraction n_i	$n^3 r$ (10^{-12} m/V)	Dielectric Constant ^a ϵ_i (ϵ_0)
CdTe	43m	1.0	(T) $r_{41} = 4.5$	$n = 2.84$	103	(S) $\epsilon = 9.4$
		3.39	(T) $r_{41} = 6.8$			
		10.6	(T) $r_{41} = 6.8$	$n = 2.60$	120	
		23.35	(T) $r_{41} = 5.47$	$n = 2.58$	94	
		27.95	(T) $r_{41} = 5.04$	$n = 2.53$	82	
GaAs	43m	0.9	$r_{41} = 1.1$	$n = 3.60$	51	(S) $\epsilon = 13.2$
		1.15	(T) $r_{41} = 1.43$	$n = 3.43$	58	(T) $\epsilon = 12.3$
		3.39	(T) $r_{41} = 1.24$	$n = 3.3$	45	
		10.6	(T) $r_{41} = 1.51$	$n = 3.3$	54	
GaP	43m	0.55-1.3	(T) $r_{41} = -1.0$	$n = 3.66-3.08$		(S) $\epsilon = 10$
		0.633	(S) $r_{41} = -0.97$	$n = 3.32$	35	
		1.15	(S) $r_{41} = -1.10$	$n = 3.10$	33	
		3.39	(S) $r_{41} = -0.97$	$n = 3.02$	27	
β -ZnS (sphalerite)	43m	0.4	(T) $r_{41} = 1.1$	$n = 2.52$	18	(T) $\epsilon = 16$
		0.5	(T) $r_{41} = 1.81$	$n = 2.42$		(S) $\epsilon = 12.5$
		0.6	(T) $r_{41} = 2.1$	$n = 2.36$		
		0.633	(S) $r_{41} = -1.6$	$n = 2.35$		
		3.39	(S) $r_{41} = -1.4$			
ZnSe	43m	0.548	(T) $r_{41} = 2.0$	$n = 2.66$		(T) $\epsilon = 9.1$
		0.633	(S) $r_{41} = 2.0$	$n = 2.60$	35	(S) $\epsilon = 9.1$
		10.6	(T) $r_{41} = 2.2$	$n = 2.39$		
ZnTe	43m	0.589	(T) $r_{41} = 4.51$	$n = 3.06$		(T) $\epsilon = 10.1$
		0.616	(T) $r_{41} = 4.27$	$n = 3.01$		(S) $\epsilon = 10.1$
		0.633	(T) $r_{41} = 4.04$	$n = 2.99$	108	
			(S) $r_{41} = 4.3$			
		0.690	(T) $r_{41} = 3.97$	$n = 2.93$		
3.41	(T) $r_{41} = 4.2$	$n = 2.70$	83			
10.6	(T) $r_{41} = 3.9$	$n = 2.70$	77			

$\text{Bi}_{12}\text{GeO}_{20}$	23	0.666	(T) $r_{41} = 3.22$	$n = 2.54$	53
$\text{Bi}_{12}\text{SiO}_{20}$	23	0.633	$r_{41} = 5.0$	$n = 2.54$	82
CdS	6mm	0.589	(T) $r_{51} = 3.7$	$n_o = 2.501$	(T) $\epsilon_1 = 9.35$
			(T) $r_{51} = 1.6$	$n_c = 2.519$	(T) $\epsilon_3 = 10.33$
			(T) $r_{13} = 3.1$	$n_o = 2.460$	(S) $\epsilon_1 = 9.02$
			(T) $r_{33} = 3.2$	$n_c = 2.477$	(S) $\epsilon_3 = 9.53$
		1.15	(T) $r_{51} = 2.0$	$n_o = 2.320$	
			(T) $r_{13} = 3.5$	$n_c = 2.336$	
			(T) $r_{33} = 2.9$		
			(T) $r_{51} = 2.0$		
		3.39	(T) $r_{13} = 3.5$	$n_o = 2.276$	
			(T) $r_{33} = 2.9$	$n_c = 2.292$	
			(T) $r_{51} = 2.0$		
			(T) $r_c = 6.4'$		
		10.6	(T) $r_{13} = 2.45$	$n_o = 2.226$	
			(T) $r_{33} = 2.75$	$n_c = 2.239$	
			(T) $r_{51} = 1.7$		
			(T) $r_c = 5.2'$		
CdSe	6mm	3.39	(S) $r_{13} = 1.8$	$n_o = 2.452$	(T) $\epsilon_1 = 9.70$
			(T) $r_{33} = 4.3$	$n_c = 2.471$	(T) $\epsilon_3 = 10.65$
ZnO	6mm	0.633	(S) $r_{13} = 1.4$	$n_o = 1.990$	$\epsilon_1 = \epsilon_2 = 8.15$
			(S) $r_{33} = 2.6$	$n_c = 2.006$	$\approx \epsilon_3$
			(S) $r_{13} = 0.96$	$n_o = 1.902$	
			(S) $r_{33} = 1.9$	$n_c = 1.916$	
α -ZnS (wurtzite)	6mm	0.633	(S) $r_{13} = 0.9$	$n_o = 2.347$	(T) $\epsilon_1 = \epsilon_2 = 8.7$
			(S) $r_{33} = 1.8$	$n_c = 2.360$	(S) $\epsilon_1 = 8.7$
$\text{Pb}_{0.814}\text{La}_{0.124}$ ($\text{Ti}_{0.6}\text{Zr}_{0.4}$) O_3 (PLZT)	oom	0.546	$n_o^3 r_{33} - n_o^3 r_{13} = 2320$	$n_o = 2.55$	

Table 7.3. (Continued).

Substance	Symmetry	Wavelength λ (μm)	Electro-optic Coefficients ^a r_{ik} (10^{-12} m/V)	Index of Refraction n_i	n^2 (10^{-12} m/V)	Dielectric Constant ^a ϵ_j (ϵ_0)
LiIO ₃	6	0.633	(S) $r_{13} = 4.1$ (S) $r_{41} = 1.4$	$n_o = 1.8830$ $n_e = 1.7367$		
Ag ₃ AsS ₃	3m	0.633	(S) $n_o^3 r_c = 70$ (S) $n_o^5 r_{22} = 29$	$n_o = 3.019$ $n_c = 2.739$		
LiNbO ₃ ($T_c = 1230^\circ\text{C}$)	3m	0.633	(T) $r_{13} = 9.6$ (T) $r_{22} = 6.8$ (T) $r_{33} = 30.9$ (T) $r_{51} = 32.6$ (T) $r_c = 21.1$	$n_o = 2.286$ $n_c = 2.200$		(T) $\epsilon_1 = \epsilon_2 = 78$ (T) $\epsilon_3 = 32$ (S) $\epsilon_1 = \epsilon_2 = 43$ (S) $\epsilon_3 = 28$
		1.15	(T) $r_{22} = 5.4$ (T) $r_c = 19$	$n_o = 2.229$ $n_c = 2.150$		
		3.39	(T) $r_{22} = 3.1$ (T) $r_c = 18$	$n_o = 2.136$ $n_c = 2.073$		
LiTaO ₃	3m	0.633	(T) $r_{13} = 8.4$ (T) $r_{33} = 30.5$ (T) $r_{22} = -0.2$ (T) $r_c = 22$	$n_o = 2.176$ $n_c = 2.180$		(T) $\epsilon_1 = \epsilon_2 = 51$ (T) $\epsilon_3 = 45$ (S) $\epsilon_1 = \epsilon_2 = 41$ (S) $\epsilon_3 = 43$
		3.39	(S) $r_{33} = 27$ (S) $r_{13} = 4.5$ (S) $r_{51} = 15$ (S) $r_{22} = 0.3$	$n_o = 2.060$ $n_c = 2.065$		
AgGaS ₂	$\bar{4}2m$	0.633	(T) $r_{41} = 4.0$ (T) $r_{63} = 3.0$	$n_o = 2.553$ $n_c = 2.507$		

CsH_2AsO_4 (CDA)	42m	0.55	(T) $r_{41} = 14.8$ (T) $r_{63} = 18.2$	$n_o = 1.572$ $n_c = 1.550$	
KH_2PO_4 (KDP)	42m	0.546	(T) $r_{41} = 8.77$ (T) $r_{63} = 10.3$	$n_o = 1.5115$ $n_c = 1.4698$	(T) $\epsilon_1 = \epsilon_2 = 42$ (T) $\epsilon_3 = 21$
		0.633	(T) $r_{41} = 8$ (T) $r_{63} = 11$	$n_o = 1.5074$ $n_c = 1.4669$	(S) $\epsilon_1 = \epsilon_2 = 44$ (S) $\epsilon_3 = 21$
		3.39	(T) $r_{63} = 9.7$ (T) $n_o^3 r_{63} = 33$		
KD_2PO_4 (KD*P)	42m	0.546	(T) $r_{63} = 26.8$ (T) $r_{41} = 8.8$	$n_o = 1.5079$ $n_c = 1.4683$	(T) $\epsilon_3 = 50$ (S) $\epsilon_1 = \epsilon_2 = 58$
		0.633	(T) $r_{63} = 24.1$	$n_o = 1.502$ $n_c = 1.462$	(S) $\epsilon_3 = 48$
$(\text{NH}_4)\text{H}_2\text{PO}_4$ (ADP)	42m	0.546	(T) $r_{41} = 23.76$ (T) $r_{63} = 8.56$	$n_o = 1.5266$ $n_c = 1.4808$	(T) $\epsilon_1 = \epsilon_2 = 56$ (T) $\epsilon_3 = 15$
		0.633	(T) $r_{41} = 23.41$ (T) $n_o^3 r_{63} = 27.6$	$n_o = 1.5220$ $n_c = 1.4773$	(S) $\epsilon_1 = \epsilon_2 = 58$ (S) $\epsilon_3 = 14$
$(\text{NH}_4)_2\text{D}_2\text{PO}_4$ (AD*P)	42m	0.633	(T) $r_{41} = 40$ (T) $r_{63} = 10$	$n_o = 1.516$ $n_c = 1.475$	
BaTiO_3 ($T_c = 395 \text{ K}$)	4mm	0.546	(T) $r_{51} = 1640$ (T) $r_c = 108$	$n_o = 2.437$ $n_c = 2.365$	(T) $\epsilon_1 = \epsilon_2 = 3600$ (T) $\epsilon_3 = 135$
$\text{KTa}_x\text{Nb}_{1-x}\text{O}_3$ (KTN), $x = 0.35$ ($T_c = 40\text{--}60^\circ\text{C}$)		0.633	(T) $r_{51} = 8000 (T_c - 28)$ (T) $r_c = 500 (T_c - 28)$ (T) $r_{51} = 3000 (T_c - 16)$ (T) $r_c = 700 (T_c - 16)$	$n_o = 2.318$ $n_c = 2.277$ $n_o = 2.318$ $n_c = 2.281$	
$\text{Ba}_{0.25}\text{Sr}_{0.75}\text{Nb}_2\text{O}_6$ ($T_c = 395 \text{ K}$)	4mm	0.633	(T) $r_{13} = 67$ (T) $r_{33} = 1340$	$n_o = 2.3117$ $n_c = 2.2987$	$\epsilon_3 = 3400$ (15 MHz)

Table 7.3. (Continued).

Substance	Symmetry	Wavelength λ (μm)	Electro-optic Coefficients ^a r_{ik} (10^{-12} m/V)	Index of Refraction n_i	$n^3 r$ (10^{-12} m/V)	Dielectric Constant ^a $\epsilon_j (\epsilon_0)$
α -HfO ₃	222	0.633	(T) $r_{41} = 6.6$	$n_1 = 1.8365$ $n_2 = 1.984$ $n_3 = 1.960$		
			(T) $r_{52} = 7.0$			
			(T) $r_{63} = 6.0$			
KNbO ₃	2mm	0.633	(T) $r_{13} = 28$	$n_1 = 2.280$ $n_2 = 2.329$ $n_3 = 2.169$		
			(T) $r_{42} = 380$			
			(T) $r_{51} = 105$			
KIO ₃	1	0.500	$r_{62} = 90$	$n_1 = 1.700$ $n_2 = 1.828$ (5893Å) $n_3 = 1.832$		

^a“(T)” = low frequency from dc through audio range; (S) = high frequency; see Eq. (7.6-3).

$r_{13} = r_{33} - n_1^3 r_{13}/n_e^3$

^b r_{33} and r_{13} are of opposite sign.

applied, are no longer parallel to the x , y , and z crystal axes. It becomes necessary, then, to find the directions of the new axes, and the magnitudes of the respective indices in the presence of \mathbf{E} , so that we may determine the effect of the field on the propagation. To be specific, we choose the direction of the applied field parallel to the z axis, so Eq. (7.2-5) becomes

$$\frac{x^2 + y^2}{n_o^2} + \frac{z^2}{n_e^2} + 2r_{63}E_z xy = 1. \quad (7.2-6)$$

The problem is one of finding a new coordinate system (x' , y' , z') in which the equation of the ellipsoid (7.2-6) contains no mixed terms; that is, it is of the form

$$\frac{x'^2}{n_{x'}^2} + \frac{y'^2}{n_{y'}^2} + \frac{z'^2}{n_{z'}^2} = 1. \quad (7.2-7)$$

x' , y' , and z' are then the directions of the major axes of the ellipsoid in the presence of an external field applied parallel to z . The lengths of the major axes of the ellipsoid are, according to Eq. (7.2-7), $2n_{x'}$, $2n_{y'}$, and $2n_{z'}$, and these will, in general, depend on the applied field.

In the case of Eq. (7.2-6) it is clear by inspection that in order to put it in a diagonal form we need to choose a coordinate system x' , y' , z' , where z' is parallel to z . Because of the symmetry of Eq. (7.2-6) in x and y , the coordinates x' and y' are related to x and y by a 45° rotation as shown in Fig. 7-1. The transformation relations from x , y to x' , y' are thus

$$x = x' \cos 45^\circ - y' \sin 45^\circ,$$

$$y = x' \sin 45^\circ + y' \cos 45^\circ,$$

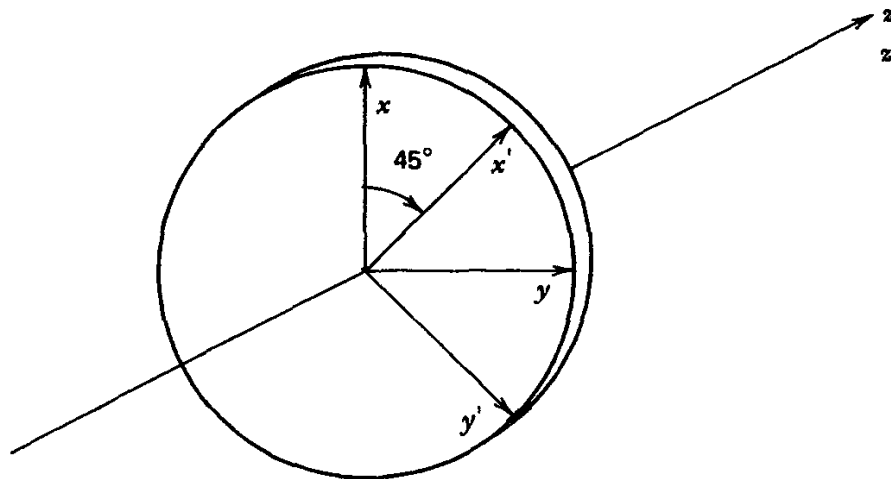


Figure 7.1. The x , y , z axes of $\bar{4}2m$ crystals (such as KH_2PO_4) and the x' , y' , z' axes, where z is the fourfold optic axis and x and y are the twofold symmetry axes.

which, upon substitution in Eq. (7.2-6), yield

$$\left(\frac{1}{n_o^2} + r_{63}E_z\right)x'^2 + \left(\frac{1}{n_o^2} - r_{63}E_z\right)y'^2 + \frac{z^2}{n_e^2} = 1. \quad (7.2-8)$$

This equation shows that x' , y' , and z are indeed the principal axes of the ellipsoid when a field is applied along the z direction. We also see that the length of the x' axis of the ellipsoid is $2n_{x'}$, where

$$\frac{1}{n_{x'}^2} = \frac{1}{n_o^2} + r_{63}E_z,$$

which, assuming $r_{63}E_z \ll n_o^{-2}$ and using the differential relation

$$dn = -\frac{1}{2}n^3 d\left(\frac{1}{n^2}\right),$$

gives

$$n_{x'} = n_o - \frac{1}{2}n_o^3 r_{63}E_z \quad (7.2-9)$$

and, similarly,

$$n_{y'} = n_o + \frac{1}{2}n_o^3 r_{63}E_z, \quad (7.2-10)$$

$$n_z = n_e. \quad (7.2-11)$$

Let us now consider the case when the applied dc electric field is parallel to the x axis, so that Eq. (7.2-5) becomes

$$\frac{x^2}{n_o^2} + \frac{y^2}{n_o^2} + \frac{z^2}{n_e^2} + 2yzt_{41}E_x = 1. \quad (7.2-12)$$

In this case it is clear from inspection of Eq. (7.2-12) that the new principal axis x' will coincide with the x axis, because the "mixed" term involves only y and z . A rotation in the yz plane is therefore required to put it in a diagonal form. Let θ be the angle between the new coordinate $y'z'$ and the old coordinate yz . The transformation from y, z to y', z' is given by

$$\begin{aligned} y &= y'\cos\theta - z'\sin\theta, \\ z &= y'\sin\theta + z'\cos\theta. \end{aligned} \quad (7.2-13)$$

We now substitute Eq. (7.2-13) for y and z in Eq. (7.2-12) and require that the coefficient of the $y'z'$ term vanishes. This yields

$$\frac{x^2}{n_o^2} + \left(\frac{1}{n_o^2} + r_{41} E_x \tan \theta \right) y'^2 + \left(\frac{1}{n_e^2} - r_{41} E_x \tan \theta \right) z'^2 = 1 \quad (7.2-14)$$

with θ given by

$$\tan 2\theta = \frac{2r_{41} E_x}{\frac{1}{n_o^2} - \frac{1}{n_e^2}}. \quad (7.2-15)$$

The new index ellipsoid (7.2-14) has its principal axes rotated at an angle θ about the x axis with respect to the unperturbed principal axes when a field E_x is applied along the x direction. This angle is very small, even for moderately high electric field. For KDP with an applied field of $E_x = 10^6$ V/m, this angle is only 0.04° . According to Eq. (7.2-15), this angle is only significant for materials with $n_o \approx n_e$. In particular, $\theta = 45^\circ$ when $n_o = n_e$. The new principal refractive indices, according to Eq. (7.2-14), are given by

$$n_{x'} = n_o, \quad (7.2-16)$$

$$n_{y'} = n_o - \frac{1}{2} n_o^3 r_{41} E_x \tan \theta, \quad (7.2-17)$$

$$n_{z'} = n_e + \frac{1}{2} n_e^3 r_{41} E_x \tan \theta. \quad (7.2-18)$$

For KDP with a moderate field E_x , θ is small and is almost linearly proportional to $r_{41} E_x$ according to Eq. (7.2-15). Therefore the change in the refractive indices (7.2-17) and (7.2-18) is of second order in E_x .

7.2.2. Example: The Electro-optic Effect in LiNbO_3

The LiNbO_3 crystal has a crystal symmetry of $3m$. The electro-optic coefficients are in the form

$$\begin{pmatrix} 0 & -r_{22} & r_{13} \\ 0 & r_{22} & r_{13} \\ 0 & 0 & r_{33} \\ 0 & r_{51} & 0 \\ r_{51} & 0 & 0 \\ -r_{22} & 0 & 0 \end{pmatrix} \quad (7.2-19)$$

according to Table 7.2. We now consider the case when the electric field is along the c axis of the crystal so that the equation of the index ellipsoid can be written, according to Eq. (7.2-3), as

$$x^2 \left(\frac{1}{n_o^2} + r_{13} E \right) + y^2 \left(\frac{1}{n_o^2} + r_{13} E \right) + z^2 \left(\frac{1}{n_e^2} + r_{33} E \right) = 1, \quad (7.2-20)$$

where n_o and n_e are the ordinary and extraordinary refractive indices, respectively. Since no mixed terms appear in Eq. (7.2-20), the principal axes of the new index ellipsoid remain unchanged. The lengths of the new semiaxes are

$$n_x = n_o - \frac{1}{2} n_o^3 r_{13} E, \quad (7.2-21)$$

$$n_y = n_o - \frac{1}{2} n_o^3 r_{13} E, \quad (7.2-22)$$

$$n_z = n_e - \frac{1}{2} n_e^3 r_{33} E. \quad (7.2-23)$$

Notice that under the influence of the electric field in the direction of c axis, the crystal remains uniaxially anisotropic (see Problem 7.2). If a light beam is propagating along the x axis, the birefringence seen by it is

$$n_z - n_y = (n_e - n_o) - \frac{1}{2} (n_e^3 r_{33} - n_o^3 r_{13}) E. \quad (7.2-24)$$

7.3. ELECTRO-OPTIC MODULATION

We have demonstrated in the previous section that an applied electric field can change the index ellipsoid of certain crystals. We also know that the propagation characteristics of electromagnetic radiation in crystals are governed by the index ellipsoid. We can consequently use the electro-optic effect of these crystals, to manipulate the propagation of light waves, especially their polarization state. As an example, we consider a z -cut KDP plate with an applied electric field \mathbf{E} parallel to z . If we consider propagation of light along the z direction, then, according to Eqs. (7.2-9) and (7.2-10), the birefringence is given by

$$n_{y'} - n_{x'} = n_o^3 r_{63} E_z. \quad (7.3-1)$$

Let d be the thickness of the plate. The phase retardation of this plate is

then given by

$$\Gamma = \frac{\omega}{c} (n_{y'} - n_{x'}) d = \frac{2\pi}{\lambda} n_o^3 r_{63} V, \quad (7.3-2)$$

where V is the voltage applied and is given by $V = E_z d$. We know from the discussion in Chapter 5 that retardation plates are polarization-state converters. Here, we have a plate with a phase retardation proportional to the applied voltage. Consequently, we are able to convert the polarization state of the incident light into a desired polarization state electrically. To illustrate this, let us assume that the incident light is linearly polarized at 45° from the x' axis (see Fig. 7.2). The polarization state at the input plane $z = 0$ can be represented by a Jones vector

$$\frac{1}{\sqrt{2}} \begin{pmatrix} 1 \\ 1 \end{pmatrix}. \quad (7.3-3)$$

The polarization state of the emerging beams at the output plane $z = d$ is given by

$$\frac{1}{\sqrt{2}} \begin{pmatrix} e^{i\Gamma/2} \\ e^{-i\Gamma/2} \end{pmatrix}, \quad (7.3-4)$$

where Γ is given by Eq. (7.3-2).

Figure 7.3 shows the polarization ellipse of the output beam at various values of the phase retardation Γ . The voltage which yields a phase

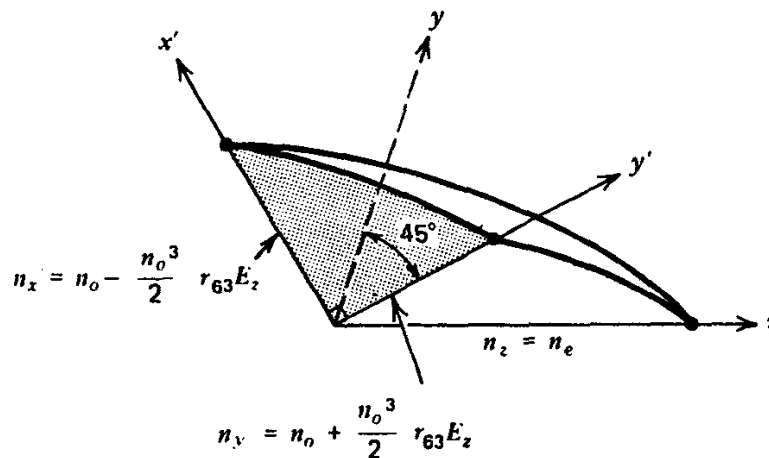


Figure 7.2. A section of the index ellipsoid of KDP, showing the principal dielectric axes x' , y' , and z due to an electric field applied along the z axis. The directions x' and y' are defined by Fig. 7.1.

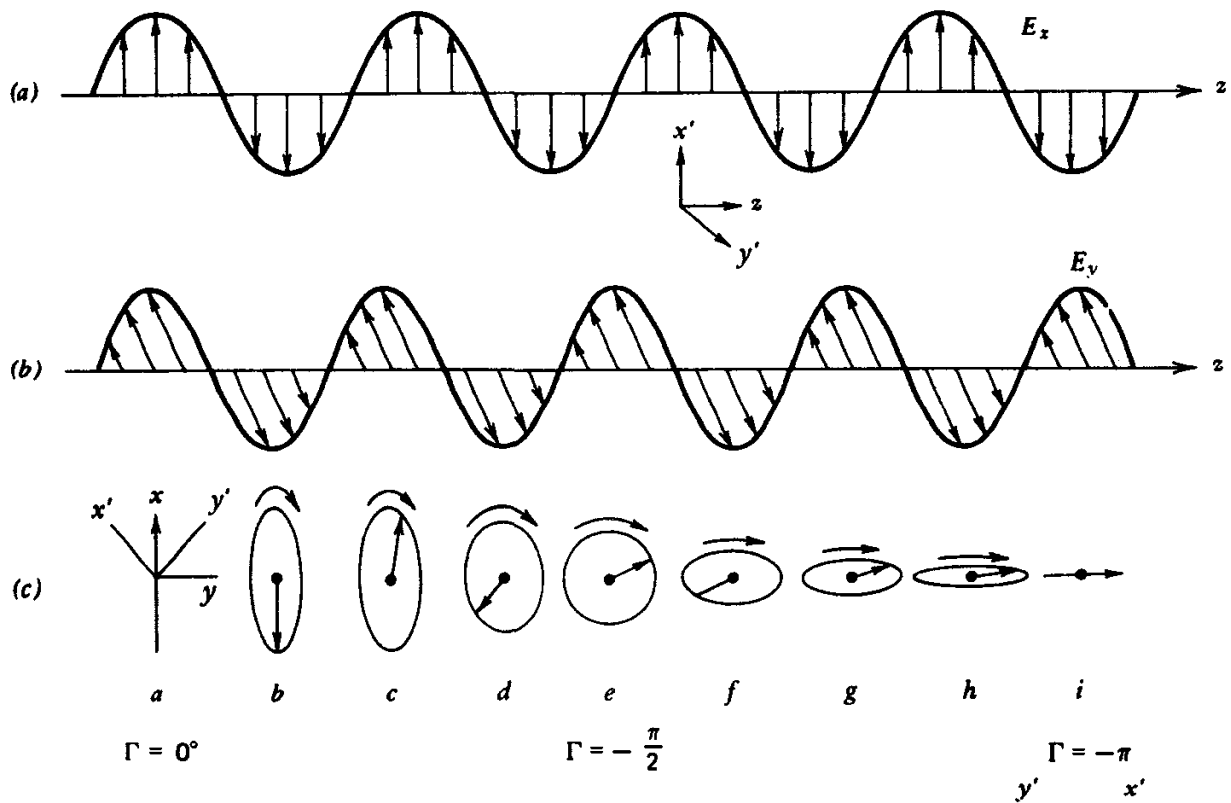


Figure 7.3. An optical field that is linearly polarized along x is incident along the z direction on an electro-optic crystal having its electrically induced principal axes along x' and y' . (This is the case in KH_2PO_4 when an electric field is applied along its z axis.) (a) The component E_x , at some time t as a function of the position z along the crystal. (b) E_y , as a function of z at the same value of t as in (a). (c) Ellipses in the $x'y'$ plane traversed by the tip of the optical electric field at various points (a through i) along the crystal during one optical period. The arrow shows the instantaneous field vector at time t , while the curved arrow gives the sense in which the ellipse is traversed. (d) A plot of the polarization ellipse due to two orthogonal components with a retardation of $\Gamma = \frac{1}{6}\pi$ [i.e., $E_{x'} = \cos \omega t$ and $E_{y'} = \cos(\omega t - \frac{1}{6}\pi)$]. Also shown are the instantaneous field vectors at (1) $\omega t = 0$, (2) $\omega t = 60^\circ$, (3) $\omega t = 120^\circ$, (4) $\omega t = 210^\circ$, and (5) $\omega t = 270^\circ$.

retardation of $\Gamma = \pi$ is known as the “half-wave voltage,” and is given in this case by

$$V_{\pi} = \frac{\lambda}{2n_o^3 r_{63}}, \quad (7.3-5)$$

where λ is the wavelength of light. The half-wave voltage for a z-cut KDP plate at $\lambda = 6328 \text{ \AA}$ is about 9.3 kV. Note that the half-wave voltage is proportional to the wavelength λ and is inversely proportional to the relevant electro-optic coefficient.

7.3.1. Amplitude Modulation

We have just shown that the electrically induced birefringence (7.3-1) causes a wave incident at $z = 0$ with its polarization along x to acquire a y polarization, which grows with voltage at the expense of the x component until at $V = V_{\pi}$ the polarization becomes parallel to y . If, at the output plane $z = d$, one inserts a polarizer at right angles to the input polarization—that is, one that allows E_y to pass—then with the field on, the optical beam passes through unattenuated, whereas with the field off ($\Gamma = 0$), the output beam is blocked off completely by the crossed output polarizer. This control of the optical energy flow serves as the basis of the electro-optic amplitude modulation of light.

A typical arrangement of an electro-optic amplitude modulator is shown in Fig. 7.4. It consists of an electro-optic crystal placed between two crossed polarizers, which are at an angle of 45° to the new principal axes x' and y' . Also included in the optical path is a naturally birefringent crystal that introduces a fixed retardation, so the total retardation Γ is the sum of the retardation due to this crystal and the electrically induced one. In Chapter 5, we showed that the transmission through such a combination for polarized light is

$$T = \sin^2 \frac{\Gamma}{2} = \sin^2 \left(\frac{\pi}{2} \frac{V}{V_{\pi}} \right). \quad (7.3-6)$$

The second equality was obtained by using Eqs. (7.3-2) and (7.3-5). The transmission T versus voltage V is plotted in Fig. 7.5.

The process of amplitude modulation of an optical signal is also illustrated in Fig. 7.5. The modulator is usually biased with a fixed retardation $\Gamma_B = \frac{1}{2}\pi$ to the 50% transmission point. This bias can be achieved by applying a voltage $V = \frac{1}{2}V_{\pi}$ or, more conveniently, by using a naturally

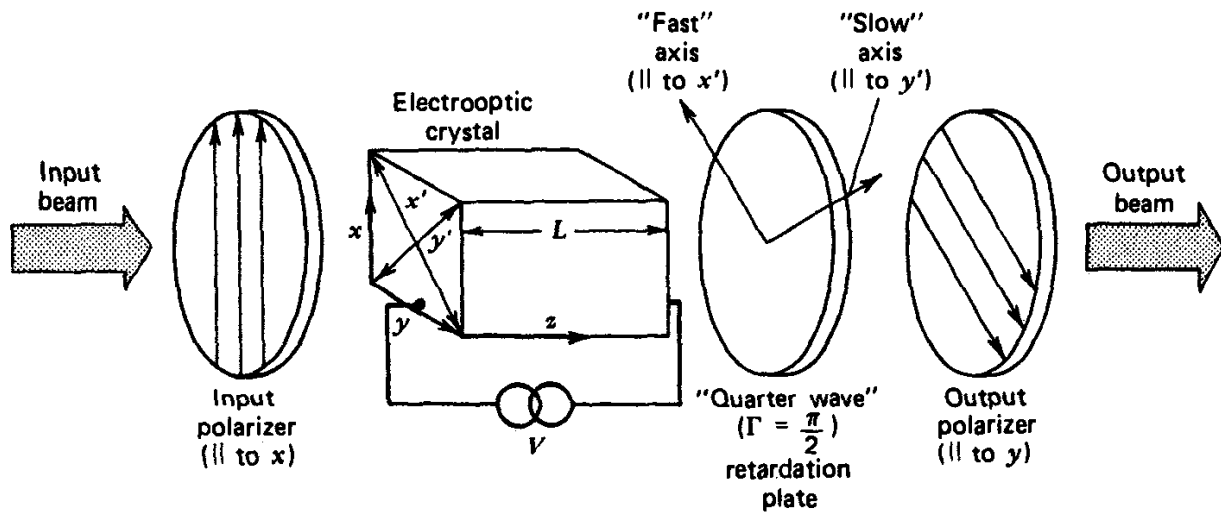


Figure 7.4. A typical electro-optic amplitude modulator. The total retardation Γ is the sum of the fixed retardation bias ($\Gamma_B = \frac{1}{2}\pi$) introduced by the quarter-wave plate and that caused by the electro-optic crystal.

birefringent crystal as in Fig. 7.4 to introduce a phase difference (retardation) of $\frac{1}{2}\pi$ between the x' and y' components. A small sinusoidal modulation voltage will then cause a nearly sinusoidal modulation of the transmitted intensity as shown.

To treat the situation depicted by Fig. 7.5 mathematically, we take

$$\Gamma = \frac{1}{2}\pi + \Gamma_m \sin \omega_m t, \quad (7.3-7)$$

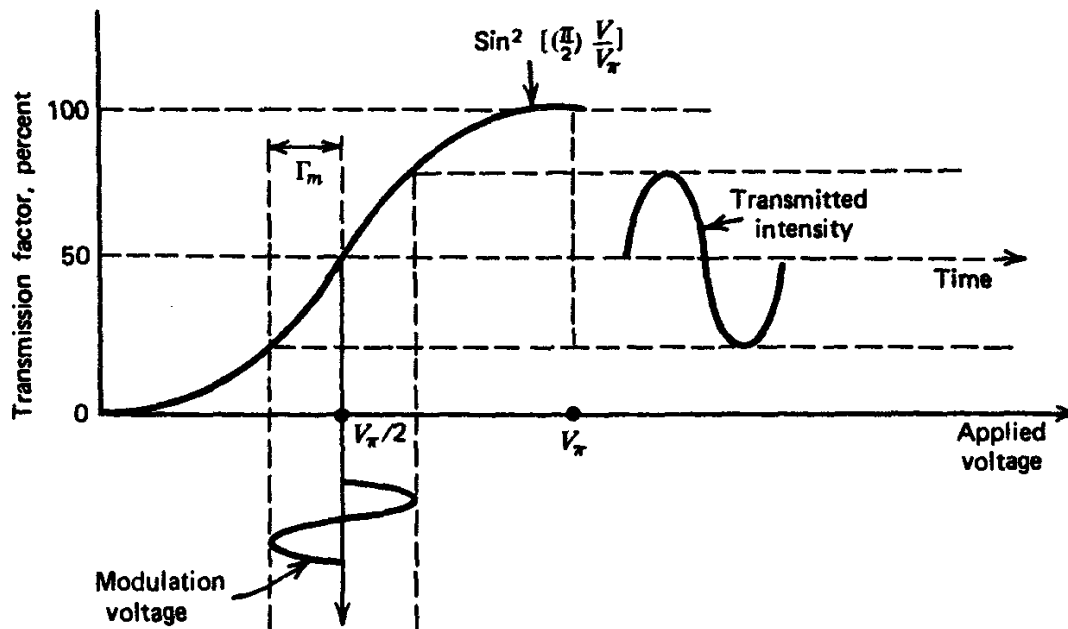


Figure 7.5. Transmission factor of a cross-polarized electro-optic modulator as a function of applied voltage. The modulator is biased to the point $\Gamma = \frac{1}{2}\pi$, which results in a 50% intensity transmission. A small applied sinusoidal voltage modulates the transmitted intensity about the bias point.

where the bias retardation is taken as $\frac{1}{2}\pi$, and Γ_m is related to the amplitude V_m of the modulation voltage $V_m \sin \omega_m t$ by Eq. (7.3-2); thus $\Gamma_m = \pi V_m / V_\pi$. Using Eq. (7.3-6), we obtain

$$\frac{I_0}{I_i} = \sin^2\left(\frac{1}{4}\pi + \frac{1}{2}\Gamma_m \sin \omega_m t\right) \quad (7.3-8)$$

$$= \frac{1}{2}\left[1 + \sin(\Gamma_m \sin \omega_m t)\right], \quad (7.3-9)$$

which, for $\Gamma_m \ll 1$, becomes

$$\frac{I_0}{I_i} \approx \frac{1}{2}(1 + \Gamma_m \sin \omega_m t) \quad (7.3-10)$$

so that the intensity modulation is a linear replica of the modulating voltage $V_m \sin \omega_m t$. If the condition $\Gamma_m \ll 1$ is not fulfilled, it follows from Fig. 7.5 or from Eq. (7.3-9) that the intensity variation is distorted and will contain an appreciable amount of the higher (odd) harmonics.

7.3.2. Phase Modulation of Light

In the preceding section we saw how the modulation of the state of polarization, from linear to elliptic, of an optical beam by means of the electro-optic effect can be converted, using polarizers, to intensity modulation. Here we consider the situation depicted by Fig. 7.6, in which, instead of having equal components along the induced birefringent axes (x' and y' in Fig. 7.4), the incident beam is polarized parallel to one of them— x' , for example. In this case, the application of the electric field along the z direction does not change the state of polarization, but merely changes the output phase by

$$\Delta\phi_{x'} = -\frac{\omega d}{c} \Delta n_{x'}$$

where $d = L$ is the length of the crystal, so that from (7.2-9),

$$\Delta\phi_{x'} = \frac{\omega n_o^3 r_{63}}{2c} E_z d. \quad (7.3-11)$$

If the bias field is sinusoidal and is taken as

$$E_z = E_m \sin \omega_m t, \quad (7.3-12)$$

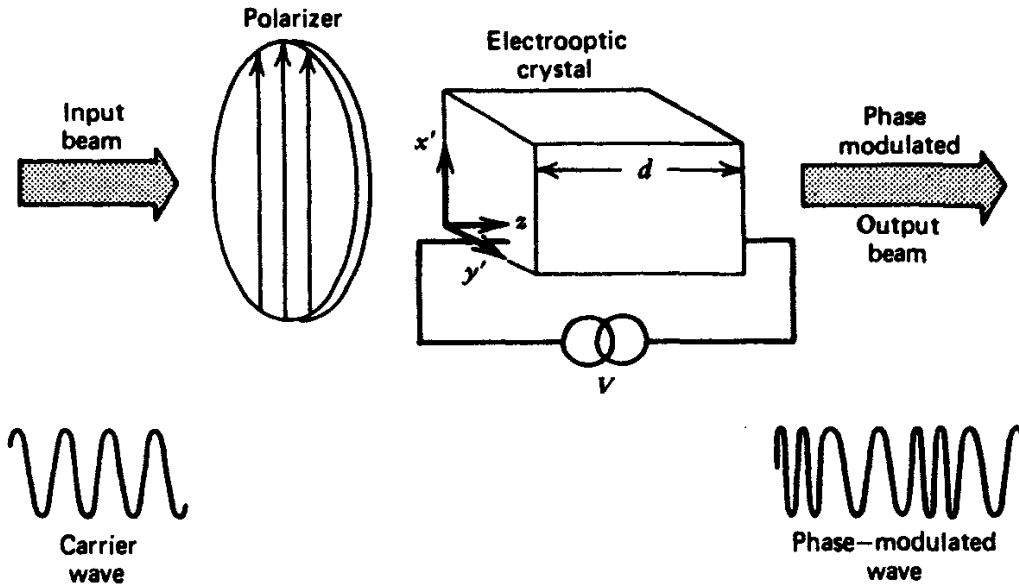


Figure 7.6. An electro-optic phase modulator. The crystal orientation and applied directions are appropriate to KDP. The optical polarization is parallel to an electrically induced principal dielectric axis (x').

then an incident optical field that at the input ($z = 0$) face of the crystal varies as $E_{\text{in}} = A \cos \omega t$ will emerge as

$$E_{\text{out}} = A \cos \left[\omega t - \frac{\omega}{c} \left(n_o - \frac{n_o^3}{2} r_{63} E_m \sin \omega_m t \right) d \right],$$

where d is the length of the crystal. Dropping the constant phase factor, which is of no consequence here, we rewrite the last equation as

$$E_{\text{out}} = A \cos[\omega t + \delta \sin \omega_m t], \quad (7.3-13)$$

where

$$\delta = \frac{\omega n_o^3 r_{63} E_m d}{2c} = \frac{\pi n_o^3 r_{63} E_m d}{\lambda} \quad (7.3-14)$$

is referred to as the phase-modulation index. The optical field is thus phase-modulated with a modulation index δ . If we use the Bessel-function identities

$$\cos(\delta \sin \omega_m t) = J_0(\delta) + 2J_2(\delta) \cos 2\omega_m t + 2J_4(\delta) \cos 4\omega_m t + \dots$$

and

$$\sin(\delta \sin \omega_m t) = 2J_1(\delta) \sin \omega_m t + 2J_3(\delta) \sin 3\omega_m t + \dots,$$

we can rewrite Eq. (7.3-13) as

$$\begin{aligned}
 E_{\text{out}} = A [& J_0(\delta) \cos \omega t + J_1 \cos(\omega + \omega_m)t - J_1(\delta) \cos(\omega - \omega_m)t \\
 & + J_2(\delta) \cos(\omega + 2\omega_m)t + J_2(\delta) \cos(\omega - 2\omega_m)t \\
 & + J_3(\delta) \cos(\omega + 3\omega_m)t - J_3(\delta) \cos(\omega - 3\omega_m)t \\
 & + J_4(\delta) \cos(\omega + 4\omega_m)t + J_4(\delta) \cos(\omega - 4\omega_m)t + \dots],
 \end{aligned}
 \tag{7.3-15}$$

which form gives the distribution of energy in the sidebands as a function of the modulation index δ . We note that, for $\delta = 0$, $J_0(0) = 1$ and $J_n(\delta) = 0$, $n \neq 0$. Another point of interest is that the phase-modulation index δ , as given by Eq. (7.3-14), is one-half the retardation Γ as given by Eq. (7.3-2).

7.4. WAVE PROPAGATION IN ELECTRO-OPTIC CRYSTALS

In the previous discussion of electro-optic modulation we assumed that the phase of an electromagnetic wave exiting from an electro-optic crystal is determined by the instantaneous values of the applied electric field. It is clear that this assumption breaks down when the applied field in the crystal oscillates at sufficiently high frequencies. When that happens, the applied field may change appreciably (even reverse sign several times) during the propagation of light through the crystal and the net retardation (or phase change) may be very small. High-frequency modulations are especially important in high-data-rate optical communication systems where the modulation field may oscillate at the microwave frequencies. To include these high-frequency effects in the electro-optic modulation, we need to consider the problem of light propagation in crystals in the presence of time- and space-varying electric fields.

We start from the equation of motion for the displacement field vector \mathbf{D} in the presence of a perturbation in an anisotropic medium derived in Section 4.12,

$$\left[\frac{\partial}{\partial \xi} + \frac{1}{c} N \frac{\partial}{\partial t} \right] \mathbf{D} = 0
 \tag{7.4-1}$$

where we recall that ζ is the distance in the direction of propagation, c is the velocity of light in vacuum, and N is refractive-index matrix and is given by

$$N = \begin{pmatrix} n_1 - \frac{1}{2}n_1^3\Delta\eta_{11} & -\frac{n_1^2n_2^2}{n_1+n_2}\Delta\eta_{12} \\ -\frac{n_1^2n_2^2}{n_1+n_2}\Delta\eta_{21} & n_2 - \frac{1}{2}n_2^3\Delta\eta_{22} \end{pmatrix}, \quad (7.4-2)$$

where n_1 and n_2 are the indices of refraction of the medium for the propagation of the unperturbed eigenmodes. The $\Delta\eta_{\alpha\beta}$'s are the changes in the dielectric impermeability tensor due to the perturbation. In the case of electro-optic modulation, $\Delta\eta_{\alpha\beta}$ is given, according to the definition (7.1-2), by

$$\Delta\eta_{\alpha\beta} = r'_{\alpha\beta\gamma}E_\gamma, \quad (7.4-3)$$

where summation over the repeated index γ is assumed. We use $r'_{\alpha\beta\gamma}$ to remind ourselves that the coordinate system used in Eqs. (7.4-1) and (7.4-2) is in general different from the principal dielectric axes. Let a_{ij} be the coordinate transformation matrix which rotates the coordinate frame from the principal dielectric axes to the propagation axes ($\mathbf{D}_1, \mathbf{D}_2, \mathbf{s}$). Then the electro-optic coefficients in the new coordinate frame are

$$r'_{\alpha\beta\gamma} = a_{\alpha i}a_{\beta j}a_{\gamma k}r_{ijk}, \quad (7.4-4)$$

where summations over the repeated indices i, j, k are assumed. The n_1, n_2 in Eq. (7.4-2) are the refractive indices for the normal modes of propagation in the absence of perturbation (i.e., $E_\gamma = 0$).

Let $A_1(\zeta, t)$ and $A_2(\zeta, t)$ be the mode amplitudes, so that the displacement field vector can be written

$$\mathbf{D} = A_1(\zeta, t)\mathbf{d}_1e^{i(\omega t - k_1\zeta)} + A_2(\zeta, t)\mathbf{d}_2e^{i(\omega t - k_2\zeta)}, \quad (7.4-5)$$

where \mathbf{d}_1 and \mathbf{d}_2 are the polarization vectors of the normal modes, and k_1, k_2 are the propagation wave numbers given by

$$k_\alpha = \frac{\omega}{c}n_\alpha, \quad \alpha = 1, 2. \quad (7.4-6)$$

Substitution for \mathbf{D} from Eq. (7.4-5) into Eq. (7.4-1) yields

$$\begin{aligned} \left(\frac{\partial}{\partial \xi} + \frac{n_1}{c} \frac{\partial}{\partial t} \right) A_1 &= -i \frac{\omega}{c} \Delta N_{11} A_1 - i \frac{\omega}{c} \Delta N_{12} A_2 e^{i(k_1 - k_2)\xi}, \\ \left(\frac{\partial}{\partial \xi} + \frac{n_2}{c} \frac{\partial}{\partial t} \right) A_2 &= -i \frac{\omega}{c} \Delta N_{22} A_2 - i \frac{\omega}{c} \Delta N_{21} A_1 e^{-i(k_1 - k_2)\xi}, \end{aligned} \quad (7.4-7)$$

where $\Delta N_{\alpha\beta}$ are the matrix element of the perturbation in the refractive-index matrix

$$(\Delta N_{\alpha\beta}) = \begin{pmatrix} -\frac{1}{2}n_1^3 \Delta\eta_{11} & -\frac{n_1^2 n_2^2}{n_1 + n_2} \Delta\eta_{12} \\ -\frac{n_1^2 n_2^2}{n_1 + n_2} \Delta\eta_{21} & -\frac{1}{2}n_2^3 \Delta\eta_{22} \end{pmatrix}. \quad (7.4-8)$$

Equation (7.4-7) is a set of coupled linear partial differential equations for the mode amplitudes. Mode coupling disappears when the off-diagonal matrix element of ΔN_{12} vanishes. This corresponds to the case of pure phase modulation. We will now solve the equation (7.4-7) for the case of pure phase modulation.

7.4.1. Phase Modulation

In this case, the application of the electric field does not couple the unperturbed normal modes, since $\Delta\eta_{12} = \Delta\eta_{21} = 0$. This happens when

$$r'_{12\gamma} E_\gamma = 0. \quad (7.4-9)$$

The equation for the mode amplitudes A_1, A_2 , becomes uncoupled under these conditions and can be solved separately. Let the modulation field be in the form of a traveling wave $\mathbf{E}_m \sin(\omega_m t - k_m \xi)$. The dielectric perturbation in the impermeability tensor is, according to Eq. (7.1-2),

$$\Delta\eta_{\alpha\alpha} = r'_{\alpha\alpha\gamma} E_{m\gamma} \sin(\omega_m t - k_m \xi), \quad \alpha = 1, 2, \quad (7.4-10)$$

where $E_{m\gamma}$ is the γ -component of \mathbf{E}_m . The equation for the mode amplitude can thus be written

$$\left(\frac{\partial}{\partial \xi} + \frac{n}{c} \frac{\partial}{\partial t} \right) A(\xi, t) = i\beta \sin(\omega_m t - k_m \xi) A(\xi, t), \quad (7.4-11)$$

with

$$\beta = \frac{\omega n^3}{2c} r'_{\alpha\alpha\gamma} E_{m\gamma}, \quad \alpha = 1 \text{ or } 2, \quad (7.4-12)$$

where n can be either n_1 or n_2 and A can be either A_1 or A_2 .

Equation (7.4-11) is a first-order linear partial differential equation and can be integrated by introducing the new variables

$$\begin{aligned} u &= \zeta + \frac{c}{n}t, \\ v &= \zeta - \frac{c}{n}t. \end{aligned} \quad (7.4-13)$$

Using

$$\begin{aligned} \frac{\partial}{\partial \zeta} &= \frac{\partial u}{\partial \zeta} \frac{\partial}{\partial u} + \frac{\partial v}{\partial \zeta} \frac{\partial}{\partial v} = \frac{\partial}{\partial u} + \frac{\partial}{\partial v}, \\ \frac{\partial}{\partial t} &= \frac{\partial u}{\partial t} \frac{\partial}{\partial u} + \frac{\partial v}{\partial t} \frac{\partial}{\partial v} = \frac{c}{n} \left(\frac{\partial}{\partial u} - \frac{\partial}{\partial v} \right), \end{aligned}$$

Eq. (7.4-11) becomes

$$2 \frac{\partial}{\partial u} A = i\beta \sin \left[\frac{n\omega_m}{2c} (u - v) - \frac{k_m}{2} (u + v) \right] A. \quad (7.4-14)$$

By treating u and v as independent variables, an integration of (7.4-14) yields

$$A(\zeta, t) = C \left(\zeta - \frac{c}{n}t \right) \exp \left[-i \frac{\beta c}{\omega_m (n - n_m)} \cos(\omega_m t - k_m \zeta) \right], \quad (7.4-15)$$

where C is an arbitrary function and $n_m = ck_m/\omega_m$. The boundary condition at the input ($\zeta = 0$) face of the crystal is

$$A(0, t) = A_0, \quad (7.4-16)$$

where A_0 is an arbitrary constant. This condition requires that the function C be of the form

$$C \left(\zeta - \frac{c}{n}t \right) = A_0 \exp \left[i \frac{\beta c}{\omega_m (n - n_m)} \cos \left(\omega_m t - \frac{n}{c} \omega_m \zeta \right) \right]. \quad (7.4-17)$$

The mode amplitude $A(\zeta, t)$ is then, according to Eq. (7.4-15) and (7.4-17), given by

$$A(\zeta, t) = A_0 \exp \left\{ i \frac{\beta c}{\omega_m (n - n_m)} \right. \\ \left. \times \left[\cos \left(\omega_m t - \frac{\omega_m}{c} n \zeta \right) - \cos \left(\omega_m t - \frac{\omega_m}{c} n_m \zeta \right) \right] \right\}. \quad (7.4-18)$$

By using the trigonometric identity

$$\cos \alpha - \cos \beta = -2 \sin \frac{1}{2}(\alpha + \beta) \sin \frac{1}{2}(\alpha - \beta),$$

the mode amplitude at the output face ($\zeta = L$) of the crystal can be written

$$A(L, t) = A_0 \exp [i \delta \sin(\omega_m t - \phi)], \quad (7.4-19)$$

where

$$\delta = \beta L \frac{\sin \frac{\omega_m}{2c} (n_m - n) L}{\frac{\omega_m}{2c} (n_m - n) L}, \quad (7.4-20)$$

$$\phi = \frac{\omega_m}{2c} (n + n_m) L. \quad (7.4-21)$$

If there is no further perturbation beyond $\zeta = L$, then the displacement field of the emerging beam can be written

$$D(\zeta, t) = A_0 \exp \{ i [\omega t + \delta \sin(\omega_m t - \phi) - k \zeta] \}. \quad (7.4-22)$$

This is a phase-modulated wave with a modulation index δ . The value of δ given by Eq. (7.4-20) for this case is no longer proportional to the length of the crystal, L , and is reduced from its maximum value βL by a factor

$$\frac{\sin \Delta L}{\Delta L},$$

where

$$\Delta = \frac{\omega_m}{2c} (n_m - n) = \frac{\omega_m}{2} \left(\frac{1}{v_m} - \frac{1}{v_0} \right) \quad (7.4-23)$$

in which v_0 and v_m are the phase velocities of the light and modulating wave, respectively. Physically, this reduction factor is due to the mismatch of the phase velocities of the waves. In the event that the light wave and the modulating wave are traveling with the same phase velocities, then the light wave will experience a constant modulating field as it propagates through the electro-optic crystal. The reduction factor in this case is unity, that is, there is no reduction in the modulation index δ . The modulation index is thus linearly proportional to the length of the crystal. In the event when the phase velocities are not equal δ becomes a periodic function of the length of the crystal. A plot of δ versus L is shown in Fig. 7.7. The maximum δ occurs at the condition when

$$\frac{\omega_m}{2c}(n_m - n)L = \frac{\pi}{2}, \quad (7.4-24)$$

with the maximum modulation index, δ_{\max} , given by

$$\delta_{\max} = \frac{\omega}{\omega_m} \frac{n^3}{|n - n_m|} r'_{\alpha\alpha\gamma} E_{m\gamma}. \quad (7.4-25)$$

Example: LiNbO₃ Phase Modulator. Referring to Fig. 7.8, we consider a rectangular LiNbO₃ rod with its input and output planes parallel to the xz

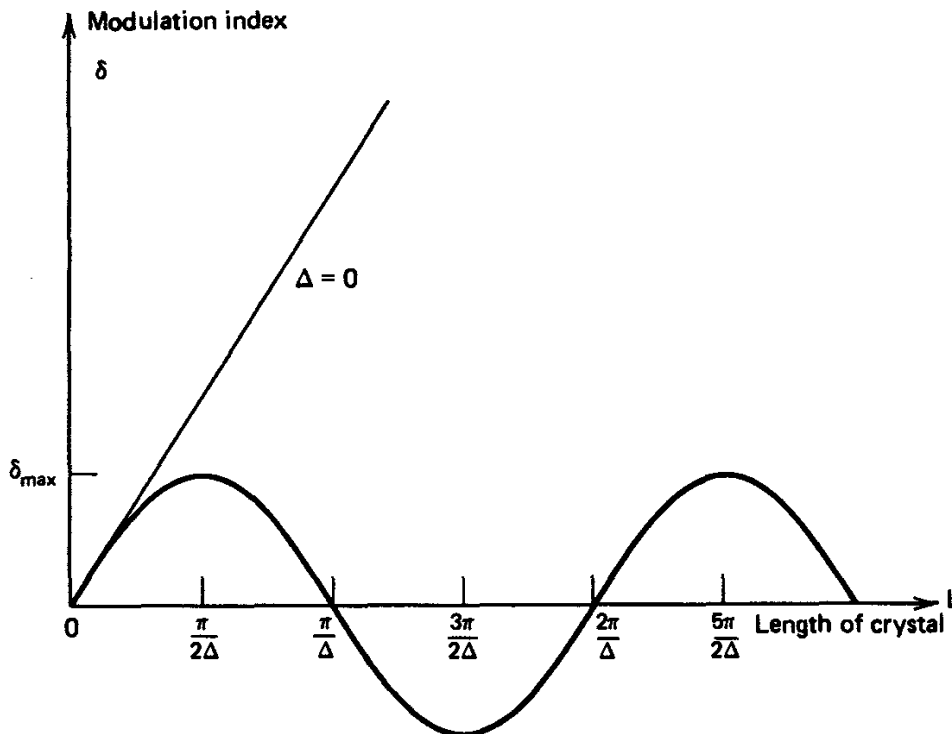


Figure 7.7. The modulation index δ versus the length L of the crystal.

plane of the principal axes. An RF field with an E vector parallel to the z axis is applied to the crystal. Both the RF field and the optical beam are propagating in the y direction. An input polarizer in front of the input plane insures that the light is polarized in the z direction in the crystal. The modulation index δ is given, according to Eqs. (7.2-9), (7.4-12), and (7.4-20), by

$$\delta = \frac{\omega}{2c} n_e^3 r_{33} E_z L \frac{\sin \frac{\omega_m}{2c} (n_m - n_e) L}{\frac{\omega_m}{2c} (n_m - n_e) L},$$

where n_e is the extraordinary index of refraction of the crystal, L is the length of the crystal, and r_{33} is the relevant electro-optic coefficient. Let $\omega_m/2\pi = 6$ GHz, $n_m = 0$, and $n_e = 2.2$; then the maximum modulation occurs at $L = 6.8$ cm according to Eq. (7.4-24). The symmetry group of LiNbO_3 is $3m$. From Table 7.2, it is obvious that the relevant electro-optic coefficient for the structure shown in Fig. 7.8 is r_{33} .

7.4.2. Amplitude Modulation

We now consider the case when the unperturbed normal modes are coupled by the applied electric field. This occurs when the off-diagonal matrix elements of the perturbation in Eq. (7.4-7) are not zero, that is, $\Delta\eta_{12} \neq 0$. In this case, the electromagnetic energy is exchanged between the coupled modes as the wave propagates in the crystal. The magnitudes of the mode amplitudes are therefore functions of space and time. The mode amplitudes

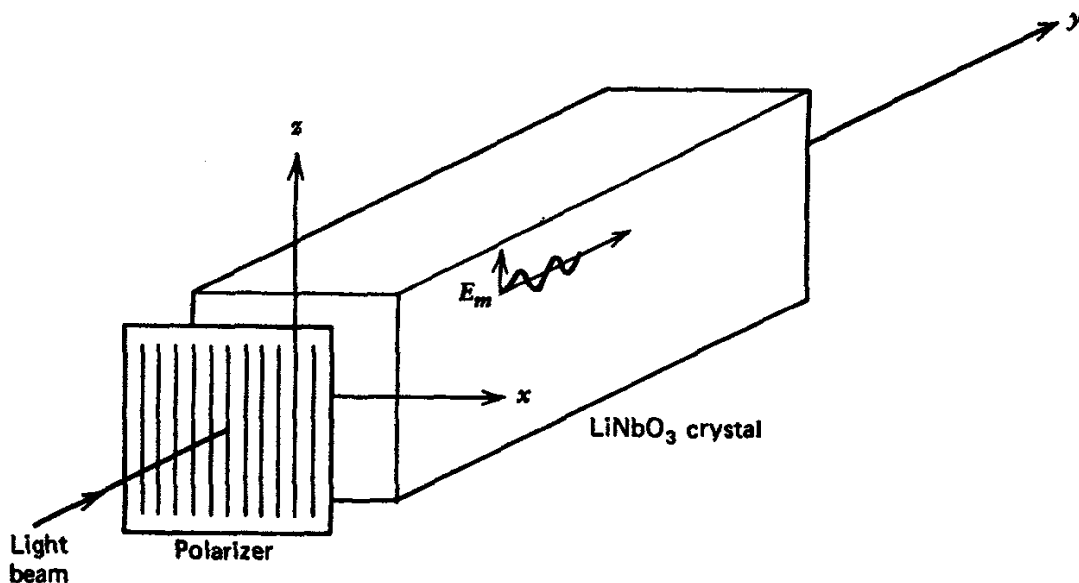


Figure 7.8. A LiNbO_3 rod used as the electro-optic crystal for phase modulation. The modulating RF field is polarized along the z axis and is propagating along the y axis.

satisfy the coupled-mode equation (7.4-7). We will now consider a case of pure amplitude modulation, that is, $\Delta\eta_{11} = \Delta\eta_{22} = 0$. This corresponds to the condition

$$r'_{11\gamma}E_\gamma = r'_{22\gamma}E_\gamma = 0. \quad (7.4-26)$$

Again, we assume that the modulation field is in the form of a traveling wave $E_m \sin(\omega_m t - k_m \xi)$. The dielectric perturbation in the impermeability tensor is, according to Eq. (7.1-2),

$$\Delta\eta_{12} = \Delta\eta_{21} = r'_{12\gamma}E_{m\gamma} \sin(\omega_m t - k_m \xi), \quad (7.4-27)$$

where $E_{m\gamma}$ is the γ component of E_m . The coupled equations for the mode amplitudes can thus be written

$$\begin{aligned} \left(\frac{\partial}{\partial \xi} + \frac{n_1}{c} \frac{\partial}{\partial t} \right) A_1 &= i\kappa \sin(\omega_m t - k_m \xi) A_2 e^{i(k_1 - k_2)\xi}, \\ \left(\frac{\partial}{\partial \xi} + \frac{n_2}{c} \frac{\partial}{\partial t} \right) A_2 &= i\kappa \sin(\omega_m t - k_m \xi) A_1 e^{-i(k_1 - k_2)\xi}, \end{aligned} \quad (7.4-28)$$

where

$$\kappa = \frac{n_1^2 n_2^2}{n_1 + n_2} \frac{\omega}{c} r'_{12\gamma} E_{m\gamma}, \quad (7.4-29)$$

where summation over γ is assumed. In the case when $n_1 = n_2 = n$, the coupled equations become

$$\begin{aligned} \left(\frac{\partial}{\partial \xi} + \frac{n}{c} \frac{\partial}{\partial t} \right) A_1 &= i\kappa \sin(\omega_m t - k_m \xi) A_2, \\ \left(\frac{\partial}{\partial \xi} + \frac{n}{c} \frac{\partial}{\partial t} \right) A_2 &= i\kappa \sin(\omega_m t - k_m \xi) A_1, \end{aligned} \quad (7.4-30)$$

with

$$\kappa = \frac{\omega n^3}{2c} r'_{12\gamma} E_{n\gamma}. \quad (7.4-31)$$

The solutions of the coupled mode equations (7.4-28) for the general case ($n_1 \neq n_2$) are very complicated and will not be discussed here. For the case when $n_1 = n_2 = n$, the general solution of the coupled mode equations is

given by

$$\begin{aligned}
 A_1(\xi, t) &= C_1\left(\xi - \frac{c}{n}t\right)\cos\left[\frac{\kappa c}{\omega_m(n - n_m)}\cos(\omega_m t - k_m \xi)\right] \\
 &\quad + C_2\left(\xi - \frac{c}{n}t\right)\sin\left[\frac{\kappa c}{\omega_m(n - n_m)}\cos(\omega_m t - k_m \xi)\right], \\
 A_2(\xi, t) &= iC_2\left(\xi - \frac{c}{n}t\right)\cos\left[\frac{\kappa c}{\omega_m(n - n_m)}\cos(\omega_m t - k_m \xi)\right] \\
 &\quad - iC_1\left(\xi - \frac{c}{n}t\right)\sin\left[\frac{\kappa c}{\omega_m(n - n_m)}\cos(\omega_m t - k_m \xi)\right],
 \end{aligned}
 \tag{7.4-32}$$

where C_1 and C_2 are arbitrary functions. Let the boundary condition at the input ($\xi = 0$) face of the crystal be

$$A_1(0, t) = A_0, \tag{7.4-33}$$

$$A_2(0, t) = 0.$$

These conditions correspond to the case where the input polarizer is parallel to \mathbf{d}_1 (one of the unperturbed principal axes).

Let $\xi = 0$ in Eq. (7.4-32); then the boundary condition (7.4-33) becomes

$$\begin{aligned}
 C_1\left(-\frac{c}{n}t\right)\cos\left[\frac{\kappa c}{\omega_m(n - n_m)}\cos \omega_m t\right] \\
 + C_2\left(-\frac{c}{n}t\right)\sin\left[\frac{\kappa c}{\omega_m(n - n_m)}\cos \omega_m t\right] = A_0,
 \end{aligned}
 \tag{7.4-34}$$

$$\begin{aligned}
 C_1\left(-\frac{c}{n}t\right)\sin\left[\frac{\kappa c}{\omega_m(n - n_m)}\cos \omega_m t\right] \\
 - C_2\left(-\frac{c}{n}t\right)\cos\left[\frac{\kappa c}{\omega_m(n - n_m)}\cos \omega_m t\right] = 0.
 \end{aligned}$$

This gives

$$\begin{aligned} C_1\left(-\frac{c}{n}t\right) &= A_0 \cos\left[\frac{\kappa c}{\omega_m(n-n_m)} \cos \omega_m t\right], \\ C_2\left(-\frac{c}{n}t\right) &= A_0 \sin\left[\frac{\kappa c}{\omega_m(n-n_m)} \cos \omega_m t\right]. \end{aligned} \quad (7.4-35)$$

Equation (7.4-35) gives the functions C_1 and C_2 at $\zeta = 0$. Since C_1 and C_2 are arbitrary functions of $\zeta - (c/n)t$, they are given by

$$\begin{aligned} C_1\left(\zeta - \frac{c}{n}t\right) &= A_0 \cos\left[\frac{\kappa c}{\omega_m(n-n_m)} \cos\left(\omega_m t - \frac{\omega_m}{c}n\zeta\right)\right], \\ C_2\left(\zeta - \frac{c}{n}t\right) &= A_0 \sin\left[\frac{\kappa c}{\omega_m(n-n_m)} \cos\left(\omega_m t - \frac{\omega_m}{c}n\zeta\right)\right]. \end{aligned} \quad (7.4-36)$$

Substituting Eq. (7.4-36) into Eq. (7.4-32), the mode amplitudes become

$$\begin{aligned} A_1(\zeta, t) &= A_0 \cos\left\{\frac{\kappa c}{\omega_m(n-n_m)} \left[\cos(\omega_m t - k_m \zeta) - \cos\left(\omega_m t - \frac{\omega_m}{c}n\zeta\right)\right]\right\}, \\ A_2(\zeta, t) &= iA_0 \sin\left\{\frac{\kappa c}{\omega_m(n-n_m)} \left[\cos\left(\omega_m t - \frac{\omega_m}{c}n\zeta\right) - \cos(\omega_m t - k_m \zeta)\right]\right\}. \end{aligned} \quad (7.4-37)$$

Using next the trigonometric identity

$$\cos \alpha - \cos \beta = -2 \sin \frac{1}{2}(\alpha + \beta) \sin \frac{1}{2}(\alpha - \beta)$$

and the relation $k_m = (\omega_m/c)n_m$, the mode amplitudes at the output plane ($\zeta = L$) of the crystal become

$$\begin{aligned} A_1(L, t) &= A_0 \cos[\delta \sin(\omega_m t - \phi)], \\ A_2(L, t) &= iA_0 \sin[\delta \sin(\omega_m t - \phi)], \end{aligned} \quad (7.4-38)$$

where

$$\delta = \kappa L \frac{\sin \frac{\omega_m}{2c}(n-n_m)L}{\frac{\omega_m}{2c}(n-n_m)L} \quad (7.4-39)$$

and ϕ is given by Eq. (7.4-21).

Notice that δ in Eq. (7.4-39) is identical to the phase modulation in its dependence on the length of the crystal L . Therefore, all the discussion of the phase-velocity matching for phase modulation can also be applied to amplitude modulation. In particular, maximum modulation occurs at the condition (7.4-24), and the maximum modulation depth is given by

$$\delta_{\max} = \frac{\omega}{\omega_m} \frac{n^3}{|n - n_m|} r'_{12\gamma} E_{m\gamma}. \quad (7.4-40)$$

The results (7.4-38) can also be obtained by taking advantage of the formalism developed for phase modulation in the treatment of the case when $n_1 = n_2$. The incident optical beam is polarized along the unperturbed eigenvector \mathbf{d}_1 . In the presence of the perturbation, the new normal modes for the case $n_1 = n_2$ are polarized in the directions which are 45° from the unperturbed ones (see the first example in Section 7.2). The incident optical wave can be decomposed into a linear combination of the new normal modes,

$$A_0 \mathbf{d}_1 = \frac{1}{\sqrt{2}} A_0 (\mathbf{d}'_1 + \mathbf{d}'_2), \quad (7.4-41)$$

where \mathbf{d}'_1 and \mathbf{d}'_2 are the unit vectors in the directions of polarization of the new normal modes. These components then undergo pure phase modulation, since there will be no coupling between the new normal modes. The optical wave at the output plane ($\zeta = L$) can be written

$$\frac{1}{\sqrt{2}} A_0 \{ \mathbf{d}'_1 e^{i\delta \sin(\omega_m t - \phi)} + \mathbf{d}'_2 e^{-i\delta \sin(\omega_m t - \phi)} \}, \quad (7.4-42)$$

where δ is given by Eq. (7.4-39). This field amplitude can now be decomposed into a linear combination of the unperturbed normal modes. Let A'_1 and A'_2 be the amplitudes for the new normal modes, and A_1, A_2 be the amplitudes for the unperturbed modes. The amplitudes A_1 and A_2 are given by

$$\begin{aligned} A_1 &= \frac{1}{\sqrt{2}} (A'_1 + A'_2) = A_0 \cos[\delta \sin(\omega_m t - \phi)], \\ A_2 &= \frac{1}{\sqrt{2}} (A'_1 - A'_2) = i A_0 \sin[\delta \sin(\omega_m t - \phi)]. \end{aligned} \quad (7.4-43)$$

The result is identical to the previous result (7.4-38), which is obtained directly from the coupled mode equations.

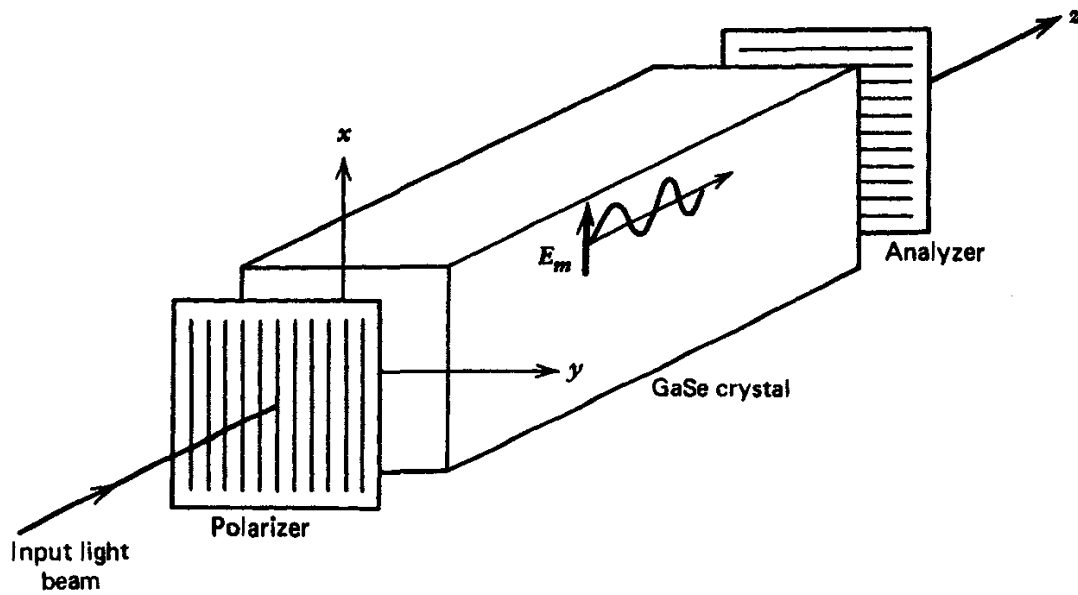


Figure 7.9. A GaSe rod used as the electro-optic crystal for amplitude modulation.

Example: GaSe Amplitude Modulator. Referring to Fig. 7.9, we consider a rectangular GaSe rod with its input and output planes parallel to the xy plane of the principal axes. Both the RF field and the optical beam are propagating along the z axis (c axis) of the crystal. Let the \mathbf{E} vector of the RF field be polarized in the x direction. This crystal is sandwiched between a pair of crossed polarizers. The symmetry group of GaSe is $\bar{6}m2$. Using Table 7.2, we find that $r_{61} = r_{22}$ is the electro-optic coefficient which couples the x and y components of the optical wave. The amplitude-modulation index is thus given, according to (7.4-29) and (7.4-39), by

$$\delta = \frac{\omega}{2c} n_o^3 r_{61} E_x L \frac{\sin \frac{\omega_m}{2c} (n - n_m) L}{\frac{\omega_m}{2c} (n - n_m) L},$$

where n_o is the ordinary refractive index of the crystal ($r_{61} = r_{121} = r_{22}$). Let $\omega_m/2\pi = 6$ GHz, $n_m = 0$, and $n_o = 2.46$; then the maximum modulation, according to Eq. (7.4-40), occurs at $L = 6.1$ cm.

7.5. QUADRATIC ELECTRO-OPTIC EFFECT

The quadratic electro-optic effect is a higher-order effect and is normally neglected when the linear electro-optic effect is present. Unlike the linear electro-optic effect, it exists in a medium with any symmetry. By using

contracted indices (7.1-11), the equation of the index ellipsoid in the presence of an electric field can be written

$$\begin{aligned}
 & x^2 \left(\frac{1}{n_x^2} + s_{11} E_x^2 + s_{12} E_y^2 + s_{13} E_z^2 + 2s_{14} E_y E_z + 2s_{15} E_z E_x + 2s_{16} E_x E_y \right) \\
 & + y^2 \left(\frac{1}{n_y^2} + s_{21} E_x^2 + s_{22} E_y^2 + s_{23} E_z^2 + 2s_{24} E_y E_z + 2s_{25} E_z E_x + 2s_{26} E_x E_y \right) \\
 & + z^2 \left(\frac{1}{n_z^2} + s_{31} E_x^2 + s_{32} E_y^2 + s_{33} E_z^2 + 2s_{34} E_y E_z + 2s_{35} E_z E_x + 2s_{36} E_x E_y \right) \\
 & + 2yz \left(s_{41} E_x^2 + s_{42} E_y^2 + s_{43} E_z^2 + 2s_{44} E_y E_z + 2s_{45} E_z E_x + 2s_{46} E_x E_y \right) \\
 & + 2zx \left(s_{51} E_x^2 + s_{52} E_y^2 + s_{53} E_z^2 + 2s_{54} E_y E_z + 2s_{55} E_z E_x + 2s_{56} E_x E_y \right) \\
 & + 2xy \left(s_{61} E_x^2 + s_{62} E_y^2 + s_{63} E_z^2 + 2s_{64} E_y E_z + 2s_{65} E_z E_x + 2s_{66} E_x E_y \right) = 1.
 \end{aligned} \tag{7.5-1}$$

The coefficients s_{ij} are usually given in the principal coordinate axes. This new ellipsoid (7.5-1) reduces to the unperturbed ellipsoid (7.1-1) when the electric field vanishes. The electric field, in general, changes the dimensions and orientation of the index ellipsoid. This change is dependent upon the direction of the applied electric field as well as the 6×6 matrix elements s_{ij} . The form, but not the magnitude, of the quadratic electro-optic coefficients s_{ij} can be derived from the symmetry considerations, which dictate which of the 36 coefficients are zero, as well as the relationships that exist between the remaining ones. Table 7.4 gives the form of the quadratic electro-optic coefficients for all the crystal classes. The quadratic electro-optic coefficients of some crystals are given in Table 7.5.

7.5.1. Example: Kerr Electro-optic Effect in an Isotropic Medium

When an optically isotropic medium is placed in a static electric field, it becomes birefringent. This effect is associated mostly with the alignment of the molecules in the presence of the field. The medium then behaves optically as if it were a uniaxial medium in which the electric field defines the optic axis. Since the medium is isotropic, we may choose the z axis to be in the direction of the electric field. From Table 7.4 and Eq. (7.5-1), the

Table 7.4. Quadratic Electro-Optic Coefficients in Contracted Notation for All Crystal Symmetry Classes

Triclinic:

$$1, \bar{1}$$

$$\begin{pmatrix} s_{11} & s_{12} & s_{13} & s_{14} & s_{15} & s_{16} \\ s_{21} & s_{22} & s_{23} & s_{24} & s_{25} & s_{26} \\ s_{31} & s_{32} & s_{33} & s_{34} & s_{35} & s_{36} \\ s_{41} & s_{42} & s_{43} & s_{44} & s_{45} & s_{46} \\ s_{51} & s_{52} & s_{53} & s_{54} & s_{55} & s_{56} \\ s_{61} & s_{62} & s_{63} & s_{64} & s_{65} & s_{66} \end{pmatrix}$$

Monoclinic:

$$2, m, 2/m$$

$$\begin{pmatrix} s_{11} & s_{12} & s_{13} & 0 & s_{15} & 0 \\ s_{21} & s_{22} & s_{23} & 0 & s_{25} & 0 \\ s_{31} & s_{32} & s_{33} & 0 & s_{35} & 0 \\ 0 & 0 & 0 & s_{44} & 0 & s_{46} \\ s_{51} & s_{52} & s_{53} & 0 & s_{55} & 0 \\ 0 & 0 & 0 & s_{64} & 0 & s_{66} \end{pmatrix}$$

Orthohombic:

$$2mm, 222, mmm$$

$$\begin{pmatrix} s_{11} & s_{12} & s_{13} & 0 & 0 & 0 \\ s_{21} & s_{22} & s_{23} & 0 & 0 & 0 \\ s_{31} & s_{32} & s_{33} & 0 & 0 & 0 \\ 0 & 0 & 0 & s_{44} & 0 & 0 \\ 0 & 0 & 0 & 0 & s_{55} & 0 \\ 0 & 0 & 0 & 0 & 0 & s_{66} \end{pmatrix}$$

Tetragonal:

$$4, \bar{4}, 4/m$$

$$\begin{pmatrix} s_{11} & s_{12} & s_{13} & 0 & 0 & s_{16} \\ s_{12} & s_{11} & s_{13} & 0 & 0 & -s_{16} \\ s_{31} & s_{31} & s_{33} & 0 & 0 & 0 \\ 0 & 0 & 0 & s_{44} & s_{45} & 0 \\ 0 & 0 & 0 & -s_{45} & s_{44} & 0 \\ s_{61} & -s_{61} & 0 & 0 & 0 & s_{66} \end{pmatrix}$$

$$422, 4mm, \bar{4}2m, 4/mm$$

$$\begin{pmatrix} s_{11} & s_{12} & s_{13} & 0 & 0 & 0 \\ s_{12} & s_{11} & s_{13} & 0 & 0 & 0 \\ s_{31} & s_{31} & s_{33} & 0 & 0 & 0 \\ 0 & 0 & 0 & s_{44} & 0 & 0 \\ 0 & 0 & 0 & 0 & s_{44} & 0 \\ 0 & 0 & 0 & 0 & 0 & s_{66} \end{pmatrix}$$

Table 7.4. (Continued).

Trigonal:

$$\begin{array}{c}
 3, \bar{3} \\
 \left(\begin{array}{cccccc}
 s_{11} & s_{12} & s_{13} & s_{14} & s_{15} & -s_{61} \\
 s_{12} & s_{11} & s_{13} & -s_{14} & -s_{15} & s_{61} \\
 s_{31} & s_{31} & s_{33} & 0 & 0 & 0 \\
 s_{41} & -s_{41} & 0 & s_{44} & s_{45} & -s_{51} \\
 s_{51} & -s_{51} & 0 & -s_{45} & s_{44} & s_{41} \\
 s_{61} & -s_{61} & 0 & -s_{15} & s_{14} & \frac{1}{2}(s_{11} - s_{12})
 \end{array} \right)
 \end{array}$$

$$\begin{array}{c}
 32, 3m, \bar{3}m \\
 \left(\begin{array}{cccccc}
 s_{11} & s_{12} & s_{13} & s_{14} & 0 & 0 \\
 s_{12} & s_{11} & s_{13} & -s_{14} & 0 & 0 \\
 s_{13} & s_{13} & s_{33} & 0 & 0 & 0 \\
 s_{41} & -s_{41} & 0 & s_{44} & 0 & 0 \\
 0 & 0 & 0 & 0 & s_{44} & s_{41} \\
 0 & 0 & 0 & 0 & s_{14} & \frac{1}{2}(s_{11} - s_{12})
 \end{array} \right)
 \end{array}$$

Hexagonal:

$$\begin{array}{c}
 6, \bar{6}, 6/m \\
 \left(\begin{array}{cccccc}
 s_{11} & s_{12} & s_{13} & 0 & 0 & -s_{61} \\
 s_{12} & s_{11} & s_{13} & 0 & 0 & s_{61} \\
 s_{31} & s_{31} & s_{33} & 0 & 0 & 0 \\
 0 & 0 & 0 & s_{44} & s_{45} & 0 \\
 0 & 0 & 0 & -s_{45} & s_{44} & 0 \\
 s_{61} & -s_{61} & 0 & 0 & 0 & \frac{1}{2}(s_{11} - s_{12})
 \end{array} \right)
 \end{array}$$

$$\begin{array}{c}
 622, 6mm, \bar{6}m2, 6/mmm \\
 \left(\begin{array}{cccccc}
 s_{11} & s_{12} & s_{13} & 0 & 0 & 0 \\
 s_{12} & s_{11} & s_{13} & 0 & 0 & 0 \\
 s_{31} & s_{31} & s_{33} & 0 & 0 & 0 \\
 0 & 0 & 0 & s_{44} & 0 & 0 \\
 0 & 0 & 0 & 0 & s_{44} & 0 \\
 0 & 0 & 0 & 0 & 0 & \frac{1}{2}(s_{11} - s_{12})
 \end{array} \right)
 \end{array}$$

Cubic:

$$\begin{array}{c}
 23, m\bar{3} \\
 \left(\begin{array}{cccccc}
 s_{11} & s_{12} & s_{13} & 0 & 0 & 0 \\
 s_{13} & s_{11} & s_{12} & 0 & 0 & 0 \\
 s_{12} & s_{13} & s_{11} & 0 & 0 & 0 \\
 0 & 0 & 0 & s_{44} & 0 & 0 \\
 0 & 0 & 0 & 0 & s_{44} & 0 \\
 0 & 0 & 0 & 0 & 0 & s_{44}
 \end{array} \right)
 \end{array}$$

Table 7.4. (Continued).

432, m3m, $\bar{4}3m$	
	$\begin{pmatrix} s_{11} & s_{12} & s_{12} & 0 & 0 & 0 \\ s_{12} & s_{11} & s_{12} & 0 & 0 & 0 \\ s_{12} & s_{12} & s_{11} & 0 & 0 & 0 \\ 0 & 0 & 0 & s_{44} & 0 & 0 \\ 0 & 0 & 0 & 0 & s_{44} & 0 \\ 0 & 0 & 0 & 0 & 0 & s_{44} \end{pmatrix}$
Isotropic:	$\begin{pmatrix} s_{11} & s_{12} & s_{12} & 0 & 0 & 0 \\ s_{12} & s_{11} & s_{12} & 0 & 0 & 0 \\ s_{12} & s_{12} & s_{11} & 0 & 0 & 0 \\ 0 & 0 & 0 & \frac{1}{2}(s_{11} - s_{12}) & 0 & 0 \\ 0 & 0 & 0 & 0 & \frac{1}{2}(s_{11} - s_{12}) & 0 \\ 0 & 0 & 0 & 0 & 0 & \frac{1}{2}(s_{11} - s_{12}) \end{pmatrix}$

index ellipsoid is then given by

$$x^2 \left(\frac{1}{n^2} + s_{12} E^2 \right) + y^2 \left(\frac{1}{n^2} + s_{12} E^2 \right) + z^2 \left(\frac{1}{n^2} + s_{11} E^2 \right) = 1, \quad (7.5-2)$$

where E is the magnitude of the applied electric field, and we have used $s_{13} = s_{23} = s_{12}$ and $s_{33} = s_{11}$. This index ellipsoid can be written as

$$\frac{x^2 + y^2}{n_o^2} + \frac{z^2}{n_e^2} = 1 \quad (7.5-3)$$

with

$$\begin{aligned} n_o &= n - \frac{1}{2} n^3 s_{12} E^2 \\ n_e &= n - \frac{1}{2} n^3 s_{11} E^2. \end{aligned} \quad (7.5-4)$$

The birefringence ($n_e - n_o$) is given by

$$n_e - n_o = \frac{1}{2} n^3 (s_{12} - s_{11}) E^2, \quad (7.5-5)$$

Table 7.5. Quadratic Electro-optic Coefficients [2]

Substance	Symmetry	Wavelength λ (μm)	Electro-optic Coefficients s_{ij} ($10^{-18} \text{ m}^2/\text{V}^2$)	Index of Refraction n_i	Temperature ^a T ($^{\circ}\text{C}$)
BaTiO ₃ ($T_c = 120^{\circ}\text{C}$)	m3m	0.633 0.500	$s_{11} - s_{12} = 2290$ $n_0^3(s_{11} - s_{12}) = 72,000$ $n_0^3 s_{44} = 44,000$	$n = 2.42$	$T > T_c$ $T \approx T_c$
K(Nb _{0.37} Ta _{0.63})O ₃ KTaO ₃	m3m m3m	0.633 0.633	$s_{11} - s_{12} = 2890$ $s_{11} - s_{12} = 10$	$n = 2.29$ $n = 2.24$	20 -226
SrTiO ₃	m3m	0.633	$s_{11} - s_{12} = 31$ (-126°C) , $s_{44} > 500/n^3$ (-153°C)	$n = 2.38$	
Pb _{0.88} La _{0.08} (Ti _{0.35} Zr _{0.65})O ₃ (PLZT) $T_c = 63^{\circ}\text{C}$	∞ m	0.550	$s_{33} - s_{13} = 26000/n^3$ (63°C)	$n = 2.450$	RT
KH ₂ PO ₄ (KDP)	$\bar{4}2\text{m}$	0.540	$n_e^3(s_{33} - s_{13}) = 31$ $n_o^3(s_{31} - s_{11}) = 13.5$ $n_o^3(s_{12} - s_{11}) = 8.9$ $n_o^3 s_{66} = 3.0$	$n_o = 1.5115^b$ $n_e = 1.4698^b$	RT
(NH ₄)H ₂ PO ₄ (ADP)	$\bar{4}2\text{m}$	0.540	$n_e^3(s_{33} - s_{13}) = 24$ $n_o^3(s_{31} - s_{11}) = 16.5$ $n_o^3(s_{12} - s_{11}) = 5.8$ $n_o^3 s_{66} = 2$	$n_o = 1.5266^b$ $n_e = 1.4808^b$	RT

^aRT = room temperature.

^bAt 0.546 μm .

where n_o is the index of refraction for light polarized at right angles to the electric field \mathbf{E} , and n_e is the index of refraction for light polarized in the direction of \mathbf{E} . Equation (7.5-5) can also be written

$$n_e - n_o = -n^3 s_{44} E^2 \quad (7.5-6)$$

by using the relationship $s_{44} = \frac{1}{2}(s_{11} - s_{12})$ for isotropic media (see Table 7.4). Equations (7.5-5) and (7.5-6) are often written as

$$n_e - n_o = K \lambda E^2, \quad (7.5-6a)$$

where K is the so-called Kerr constant and λ is the vacuum wavelength. Table 7.6 lists the Kerr constants of several materials. The Kerr constant and the quadratic electro-optic coefficients of an isotropic medium are related by

$$s_{44} = -\frac{K\lambda}{n^3}$$

Table 7.6. Kerr Constant of Some Selected Substances

Substance	λ (μm)	n	K (m/V^2)
Benzene	0.546	1.503	4.9×10^{-15}
	0.633	1.496	4.14×10^{-15}
CS_2	0.546	1.633	3.88×10^{-14}
	0.633	1.619	3.18×10^{-14}
	0.694	1.612	2.83×10^{-14}
	1.000	1.596	1.84×10^{-14}
	1.600	1.582	1.11×10^{-14}
CCl_4	0.633	1.456	7.4×10^{-16}
	0.546	1.460	8.6×10^{-16}
Water	0.589		5.1×10^{-14}
Nitrotoluene	0.589		1.37×10^{-12}
Nitrobenzene	0.589		2.44×10^{-12}

7.5.2. Example: Electro-optic Effect in BaTiO₃

Consider the specific example of a crystal of barium titanate (BaTiO₃). This is a ferroelectric crystal with a phase transition temperature of $T_c = 120^\circ\text{C}$. Below the transition temperature ($T < T_c$) the crystal is acentric with point group 4mm, and the linear electro-optic effect is dominant. Above the transition temperature ($T > T_c$), the crystal symmetry becomes m3m (cubic) and the linear electro-optic effect disappears. Let the applied electric field be along a $\langle 110 \rangle$ direction in the crystal:

$$\mathbf{E} = \frac{1}{\sqrt{2}} E(\hat{x} + \hat{y}). \quad (7.5-7)$$

From Table 7.4 and Eq. (7.5-1), the index ellipsoid can be written

$$\begin{aligned} x^2 \left(\frac{1}{n^2} + \frac{1}{2}s_{11}E^2 + \frac{1}{2}s_{12}E^2 \right) + y^2 \left(\frac{1}{n^2} + \frac{1}{2}s_{11}E^2 + \frac{1}{2}s_{12}E^2 \right) \\ + z^2 \left(\frac{1}{n^2} + s_{12}E^2 \right) + 2xys_{44}E^2 = 1. \end{aligned} \quad (7.5-8)$$

Because of the symmetry of Eq. (7.5-8) in x and y , a rotation of 45° in the xy plane can transform it into its diagonal form

$$\frac{x'^2}{n_{x'}^2} + \frac{y'^2}{n_{y'}^2} + \frac{z'^2}{n_{z'}^2} = 1, \quad (7.5-9)$$

where

$$\begin{aligned} \frac{1}{n_{x'}^2} &= \frac{1}{n^2} + \frac{1}{2}(s_{11} + s_{12})E^2 + s_{44}E^2, \\ \frac{1}{n_{y'}^2} &= \frac{1}{n^2} + \frac{1}{2}(s_{11} + s_{12})E^2 - s_{44}E^2, \\ \frac{1}{n_{z'}^2} &= \frac{1}{n^2} + s_{12}E^2. \end{aligned} \quad (7.5-10)$$

Assuming $sE^2 \ll n^{-2}$ and using the differential relation $dn =$

– $\frac{1}{2}n^3 d(1/n^2)$, we obtain

$$\begin{aligned}n_{x'} &= n - \frac{1}{2}n^3 s_{44} E^2 - \frac{1}{4}n^3 (s_{11} + s_{12}) E^2, \\n_{y'} &= n + \frac{1}{2}n^3 s_{44} E^2 - \frac{1}{4}n^3 (s_{11} + s_{12}) E^2, \\n_{z'} &= n - \frac{1}{2}n^3 s_{12} E^2.\end{aligned}\tag{7.5-11}$$

7.6. PHYSICAL PROPERTIES OF ELECTRO-OPTIC COEFFICIENTS

The electro-optic coefficients r_{ijk} and s_{ijkl} defined in Eq. (7.1-2) depend, in general, on the wavelength of light, the modulation frequency, and the temperature of the crystal. These coefficients are related directly to the nonlinear susceptibility tensors $x_{ijk}^{(2)}$, $x_{ijkl}^{(3)}$, and can be calculated by using quantum theory (see Chapter 12 and the references therein). The quantum-mechanical calculation of these electro-optic coefficients is beyond the scope of this book. We will present an elementary theory instead. This theory explains qualitatively the wavelength dependence as well as the modulation-frequency dependence.

Let q and Q be the dynamical variables (e.g., displacements) which describe the electronic and ionic charge distributions, respectively. The optical dielectric impermeability η is a direct function of q and is indirectly dependent on Q , which in turn depends on the temperature T . It is known that the direct ionic contribution to the polarizability of a molecule is very small (smaller by a factor of $\approx \frac{1}{2000}$ than the electronic contribution). In a solid, however, the electronic potential is mainly determined by the ionic charge distribution. Therefore, a change in the ionic charge distribution will result in a corresponding change in the electronic potential, which in turn changes the polarizability of the solid.

A modulating field $E(\omega_m)$ induces two independent changes in the optical impermeability:

$$r = \frac{d\eta}{dE} = \left(\frac{\partial \eta}{\partial q} \right)_Q \frac{\partial q}{\partial E} + \left(\frac{\partial \eta}{\partial Q} \right)_q \frac{\partial Q}{\partial E}.\tag{7.6-1}$$

The first term is purely electronic in origin and is due to the redistribution of electrons caused by the modulating field. If the electrons are represented by a damped harmonic oscillator with resonant frequency ω_0 , the quantities $(\partial \eta / \partial Q)_q$ and $(\partial \eta / \partial q)_Q$ are resonant at frequency ω_0 (typically 10^{14} – 10^{15} Hz). The second term takes account of the change in optical impermeability due to ionic charge redistribution (or lattice deformation) caused by the

applied modulating field, $E(\omega_m)$. If the lattice is represented by a damped harmonic oscillator, the quantity

$$\frac{\partial Q}{\partial E} \approx \frac{e/M}{(\omega_T^2 - \omega_m^2) + 2i\omega_m\Gamma} \quad (7.6-2)$$

is resonant at the lattice frequency ω_T with a linewidth 2Γ . Since the resonant frequency ω_T is usually much smaller than the optical resonance frequency ω_0 (i.e., $\omega_T \ll \omega_0$), the dispersion properties of r can be considered separately. RF dispersion (variation of r versus ω_m) occurs strongly only near the lattice resonant frequency ($\omega_m \approx \omega_T$), and optical dispersion (variation of r versus ω) occurs strongly near the electronic transition frequency ($\omega \approx \omega_0$). Lattice resonances are typically in the neighborhood of 10^{13} Hz, and electronic resonances are near 10^{15} Hz (3000 Å). In electro-optic devices, the modulation frequency ω_m is usually much smaller than the lattice resonance frequency ω_T (i.e., $\omega_m \ll \omega_T$). Therefore, the RF dispersion is very small, except for some materials near their phase transition points where the lattices become "soft" (ω_T becomes small).

Before we examine the experimentally measured electro-optic coefficients, we should know a little bit about how these data are obtained. The most common methods of determining electro-optic coefficients is by measuring the phase changes of the light and the intensities of the sidebands. The phase changes (7.3-11) and the sideband intensities (7.3-15) are all directly related to the relevant electro-optic coefficient. Both methods of measurement are usually carried out under quasielectrostatic conditions, that is, with modulation frequencies well below the fundamental frequencies of the acoustic resonances of the sample. Under these conditions, the crystal is free to deform according to the law of piezoelectricity, and the variation of the strain follows the modulation field; the measured electro-optic coefficient is designated r_{ijk}^T (low frequency). If the frequency of the applied electric field is well above the fundamental frequencies of the acoustic resonances of the same, the crystal does not deform and is virtually clamped (i.e., under constant strain), and the measured electro-optic coefficient is designated r_{ijk}^S (high frequency). The coefficients r_{ijk}^T and r_{ijk}^S have the same symmetry properties and differ by the indirect electro-optic effect as follows:

$$r_{ijk}^T = r_{ijk}^S + p_{ijlm} d_{lmk}, \quad (7.6-3)$$

where p_{ijlm} and d_{lmk} are the elasto-optic and piezoelectric coefficients, respectively. Figure 7.10 illustrates the effect of acoustic resonance and the difference between r_{63}^T and r_{63}^S in KDP and ADP. The wavelength dependence of r_{63}^T for KDP, KD*P, ADP, AD*P, and RDP is shown in Fig. 7.11.

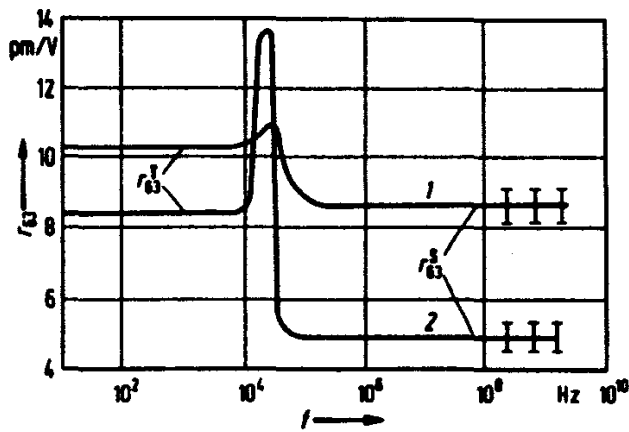


Figure 7.10. The frequency dependence of the linear electro-optic coefficient r_{63} for (1) KDP and (2) ADP, illustrating the effect of elastic resonance and the difference between r_{63}^T and r_{63}^S [3].

The temperature dependence of the electro-optic coefficients has been studied extensively. It is known that in ferroelectrics and other materials that exhibit a phase transition, the electro-optic coefficients may depend strongly on temperature and generally increase approximately in proportion to $(T - T_c)^{-1}$ as the transition temperature T_c is approached (see Fig. 7.12). This phenomenon is explained in terms of the “softening” of a transverse optical-phonon mode [i.e., lowering of ω_T in Eq. (7.6-2)] which leads to a large ionic lattice distortion caused by a small applied electric field.

7.7. ELECTRO-OPTIC EFFECTS IN LIQUID CRYSTALS

Liquid crystals are, by definition, liquids in which an ordered arrangement of molecules exists. They arise under certain conditions in organic substances having sharply anisometric molecules, that is, large elongated (cigar-like) molecules or flat (disc-like) molecules. A direct consequence of the ordering of anisometric molecules is the anisotropy of mechanical, electric,

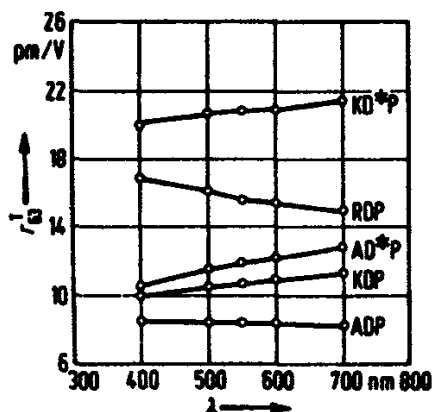


Figure 7.11. The wavelength dependence of r_{63}^T for KDP, KD*P, ADP, AD*P, and RDP [4].

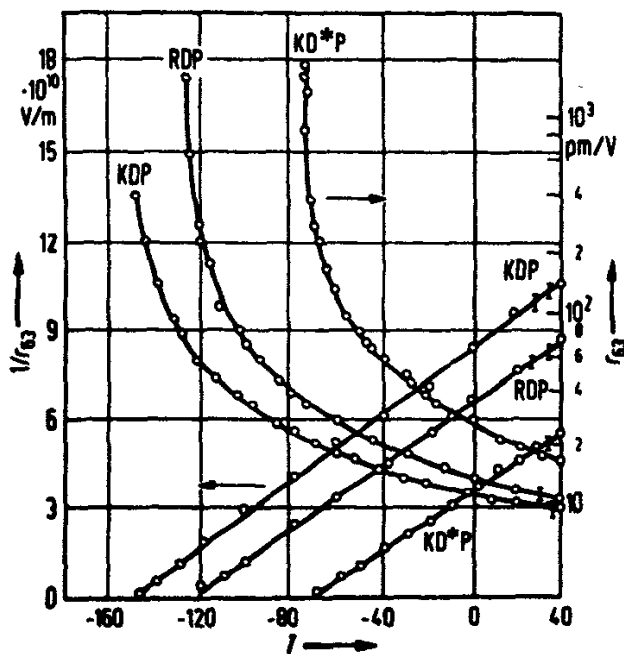


Figure 7.12. The temperature dependence of r_{63} and $1/r_{63}$ for KDP, KD*P, and RDP [5].

magnetic, and optical properties. A good example of such a substance is *p*-methoxybenzylidene-*p'*-*n*-butylaniline (MBBA), which shows a liquid-crystalline phase of the simplest type (nematic) over the temperature range of 21–47°C. There are three phases of liquid crystals, whose structure is shown in Fig. 7.13. Figure 7.13(a) illustrates the nematic phase, in which a long-range orientational order of the axes of the molecules exists, whereas the centers of the molecules are randomly distributed. Figure 7.13(b) illustrates the smectic phase, in which one-dimensional translational order as well as orientational order exist. Figure 7.13(c) illustrates the cholesteric phase, in which an orientational order also exists; however, the molecules are found in rows, with the molecular direction in each row twisted at a well-defined angle. A smectic liquid crystal is closest in structure to solid crystals. It is interesting to note that in substances that form both a nematic and a smectic phase, the sequence of phase changes on rising temperature is: solid crystal → smectic liquid crystal → nematic liquid crystal → isotropic liquid. Although the smectic phase possesses the highest degree of order, it is the nematic and cholesteric phases which have the greatest number of electro-optical applications.

Because of the orientational ordering of the anisometric molecules, the smectic and nematic liquid crystals are uniaxially symmetric, with the optic axis parallel to the axes of the molecules. The optic axis of cholesteric liquid crystals is defined only locally. The anisotropy of the refractive index is

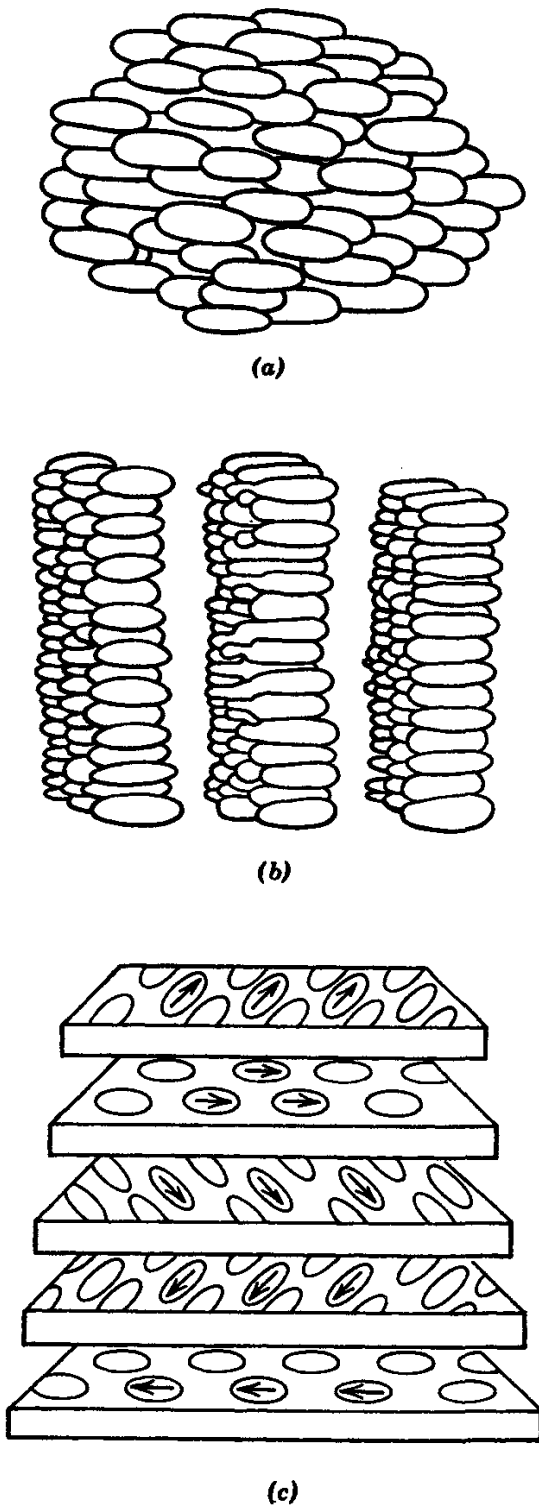


Figure 7.13. The (a) nematic phase; (b) smectic phase; (c) cholesteric phase of liquid crystals.

characterized by $\Delta n = n_e - n_o$. In all known nematic and smectic liquid crystals $\Delta n > 0$. The dielectric anisotropy, $\Delta\epsilon = \epsilon_{\parallel} - \epsilon_{\perp}$, of liquid crystals can be either positive (up to $\approx +15\epsilon_0$) or negative (down to $-2\epsilon_0$); ϵ_{\parallel} and ϵ_{\perp} refer to the dielectric constants for an electric field parallel and perpendicular to the optic axis (also called the director). A positive $\Delta\epsilon$ is characteristic of molecules having a longitudinal dipole moment. It is $\Delta\epsilon$ (its

sign as well as its magnitude) which is most critical in determining how a liquid crystal will respond to an applied electric field.

There are many electro-optical effects in liquid crystals. Most of them involve the switching of their optical properties by an external electric field. It is found that the molecules in the liquid crystal tend to rotate in such a way that the direction of the maximum dielectric constant coincides with the direction of the field. Since the liquid crystal itself is very anisotropic, any change in the structure is easily observed optically. The time constant involved in the reorientation of molecules in the liquid crystal is of the order of 10^{-3} s, depending on the viscosity.

We next discuss, briefly and somewhat qualitatively, various kinds of electro-optic effect in liquid crystals.

7.7.1. Orientational Effect

In a nematic liquid crystal, the optic axis may be reoriented by the application of an electric field. Consider first the case when $\epsilon_{\parallel} > \epsilon_{\perp}$ ($\Delta\epsilon > 0$). The initial orientation of the optic axis is along the z axis. In the presence of an electric field perpendicular to the z axis, the optic axis tends to be reoriented along the direction of the field. Let θ be the angle between the optic axis and the z axis. The extraordinary refractive index seen by a light beam propagating parallel to the electric field is given, according to Eq. (4.6-4), by

$$\frac{1}{n_e^2(\theta)} = \frac{\cos^2\theta}{n_o^2} + \frac{\sin^2\theta}{n_e^2}, \quad (7.7-1)$$

where n_e and n_o are the extraordinary and ordinary refractive indices. The angle θ depends on the field strength. In a strong electric field θ becomes zero and the birefringence $[n_e(\theta) - n_o]$ vanishes. When the field is removed, the angle θ returns to 90° and the birefringence reappears.

In the case when $\epsilon_{\parallel} < \epsilon_{\perp}$ ($\Delta\epsilon < 0$), with an initial orientation of the optic axis along the z axis, the applied electric field must also be along the z axis. The optic axis tends to reorient itself so that it is perpendicular to the applied electric field and is in a definite direction (x or y) defined by the application of an additional perturbation (e.g., a magnetic field or special physicochemical treatment of the electrodes).

Because of these electrically induced reorientation of the optic axis, the phase retardation of a thin layer of properly oriented liquid crystal can be switched from zero to $2\pi(n_e - n_o)l/\lambda$ and back with the application of an electric field. In some cases, the phase retardation can be tuned continuously.

7.7.2. Twist Effect

A thin layer of nematic liquid crystal with its optic axis parallel to the surfaces may be twisted in such a way that the “local” optic axis varies as a function of z . This creates a twisted anisotropic medium. In a linearly twisted nematic crystal, the azimuth angle of the optic axis is a linear function of z :

$$\psi = \alpha z. \quad (7.7-2)$$

The propagation of light in a linearly twisted anisotropic medium has been treated in Section 5.4. It was shown that linearly polarized light with its plane of polarization parallel to one of the local dielectric axes will remain “locked in” with the local dielectric axes as it propagates in the medium, provided the twisting rate α is small [i.e., $\alpha \ll 2\pi(n_e - n_o)/\lambda$]. In other words, the plane of polarization of such linearly polarized light will rotate in the same way as the optic axis does. This has often been misinterpreted as optical rotatory power.

Consider a thin layer of positive ($\Delta\epsilon > 0$) nematic liquid crystal twisted by one-fourth turn (90°), placed between a pair of parallel polarizers, with the transmission axis parallel to the optic axis at the entrance plane. This structure transmits no light unless a field is applied. The electric field tends to set the local optic axis along the field direction (z axis), giving rise to the transmission of light due to the vanishing of birefringence.

There are other electro-optical effects, such as dynamic light scattering, cholesteric–nematic phase transition, and the guest–host effect. The discussion of these effects is beyond the scope of this book. Interested readers are referred to [6].

PROBLEMS

7.1. *Linear electro-optic coefficients and crystal symmetry.* If a_{ij} is a matrix representation of an invariant symmetry operation of a crystal, the transformed electro-optic tensor is

$$r'_{ijk} = a_{il}a_{jm}a_{kn}r_{lmn}.$$

This tensor is identical to the original tensor because of the symmetry, i.e., $r'_{ijk} = r_{ijk}$. This fact can be used to reduce the electro-optic coefficients shown in Table 7.1.

- (a) *Monoclinic 2.* Let z be the axis of the twofold rotation C_2 . The matrix representation of C_2 is

$$a_{ij} = \begin{pmatrix} -1 & 0 & 0 \\ 0 & -1 & 0 \\ 0 & 0 & 1 \end{pmatrix}.$$

Show that

$$r_{ijk} = a_{ii}a_{jj}a_{kk}r_{ijk} = (\pm)r_{ijk}.$$

Thus the electro-optic coefficient r_{ijk} is zero if the indices 1 and 2 appear one or three times—in other words, if the index 3 appears zero or two times. Check this result against Table 7.2.

- (b) *Monoclinic m .* Let xy plane be the plane of mirror symmetry, σ . The matrix representation of σ is

$$a_{ij} = \begin{pmatrix} 1 & 0 & 0 \\ 0 & 1 & 0 \\ 0 & 0 & -1 \end{pmatrix}.$$

Show that again

$$r_{ijk} = a_{ii}a_{jj}a_{kk}r_{ijk} = (\pm)r_{ijk}.$$

Thus the electro-optic coefficient r_{ijk} is zero if the index 3 appears one or three times. Check this result against Table 7.2. Also show that the vanishing components of the electro-optic tensor for the point group m is complementary to that for the point group 2, provided the twofold axis in 2 is perpendicular to the plane of mirror symmetry in m .

- (c) *Orthohombic 222.* The point group 222 has three mutually perpendicular twofold axes x, y, z . Show from the result (a) that the only nonvanishing components of the electro-optic tensor are $r_{123}, r_{231}, r_{312}$.
- (d) *Tetragonal $\bar{4}2m$ (KDP-ADP type).* The point group $\bar{4}2m$ has all the symmetry of 222 plus a twofold rotation-inversion symmetry $2S_4$ and two mirror symmetries. This rotation-inversion symmetry is a rotation of $\frac{1}{2}\pi$ about the z axis followed by an inversion through the origin. Show that the matrix representation of this symmetry operation is

$$a_{ij} = \begin{pmatrix} 0 & -1 & 0 \\ 1 & 0 & 0 \\ 0 & 0 & -1 \end{pmatrix}.$$

Show that $r_{231} = r_{132}$; this proves that $r_{52} = r_{41}$ for $\bar{4}2m$ crystals.

- (e) *Cubic $\bar{4}3m$.* The point group $\bar{4}3m$ has all the symmetries of $\bar{4}2m$ plus threefold symmetries and others. The simplest threefold symmetry operation is $x \rightarrow y$, $y \rightarrow z$, and $z \rightarrow x$, which can be represented by

$$a_{ij} = \begin{pmatrix} 0 & 1 & 0 \\ 0 & 0 & 1 \\ 1 & 0 & 0 \end{pmatrix}.$$

Show that $r_{123} = r_{231} = r_{312}$; this proves that $r_{63} = r_{52} = r_{41}$.

7.2. *Electric-optic effects in uniaxial crystals.* Consider the case of an electric field applied along the c -axis of an electro-optic uniaxial crystal.

- (a) Show that all the hexagonal and trigonal crystals remain uniaxially symmetric, that is, $n_{x'} = n_{y'}$.
- (b) In the tetragonal crystal class, only crystals with point group 4, 422 , $4mm$, or any centrosymmetric one remain uniaxially symmetric.
- (c) Show that crystals with point group $\bar{4}$ or $\bar{4}2m$ become optically biaxial in the presence of an electric field along the c axis. (For $\bar{4}2m$ see example in text.)
- (d) Show that in $\bar{4}$ crystals, the new index ellipsoid is given by

$$x^2 \left(\frac{1}{n_o^2} + r_{13}E \right) + y^2 \left(\frac{1}{n_o^2} - r_{13}E \right) + \frac{z^2}{n_e^2} + 2xyr_{63}E = 1.$$

- (e) Show that the new principal axes are obtained by rotating the old principal axes by an angle θ along the z axis (c axis). This angle θ is independent of the field strength E and is given by

$$\tan 2\theta = \frac{r_{63}}{r_{13}}.$$

- (f) Show that the principal indices of refraction are given by

$$n_{x'} = n_o - \frac{1}{2}n_o^3 r_{13}E - \frac{1}{2}n_o^3 \tan \theta r_{63}E,$$

$$n_{y'} = n_o + \frac{1}{2}n_o^3 r_{13}E + \frac{1}{2}n_o^3 \tan \theta r_{63}E,$$

$$n_{z'} = n_e.$$

- (g) If a light beam is propagating along the z axis, show that the birefringence it sees is

$$n_{y'} - n_{x'} = n_o^3 E \sqrt{r_{13}^2 + r_{63}^2}.$$

- (h) Think of a physical model which explains the destruction of uniaxial symmetry even when the electric field is applied along the axis of symmetry.

7.3. *Electro-optic tunable retardation plate (longitudinal).* Consider a wave plate made of electro-optic crystal with thickness d . If a voltage V is applied across the plate, the phase retardation Γ is proportional to the applied voltage and is electrically tunable. Show that the phase retardation is as follows:

- (a) For an x -cut (or y, z -cut) $\bar{4}3m, 23,$ or cubic crystal plate, (e.g., CdTe, GaAs),

$$\Gamma = \frac{2\pi}{\lambda} n^3 r_{41} V.$$

- (b) For an x -cut $\bar{6}m2$ plate ($m_{\perp} x_2$; e.g., GaSe),

$$\Gamma = \frac{2\pi}{\lambda} [(n_e - n_o) d - \frac{1}{2} n_o^3 r_{11} V].$$

- (c) For a z -cut $\bar{4}2mm$ plate,

$$\Gamma = \frac{2\pi}{\lambda} n_o^3 r_{63} V.$$

- (d) For a z -cut $\bar{4}$ plate,

$$\Gamma = \frac{2\pi}{\lambda} n_o^3 V \sqrt{r_{13}^2 + r_{63}^2}.$$

- (e) For a z -cut $2mm$ plate,

$$\Gamma = \frac{2\pi}{\lambda} [(n_2 - n_1) d - \frac{1}{2} (n_2^3 r_{23} - n_1^3 r_{13}) V].$$

7.4. *Propagation axes in a cubic $\bar{4}3m$ crystal.* Consider the propagation of light in a $\bar{4}3m$ crystal with \mathbf{k} vector in the polar direction (θ, ϕ) . In the system of propagation axes shown in Fig. 7.14, z' coincides with the

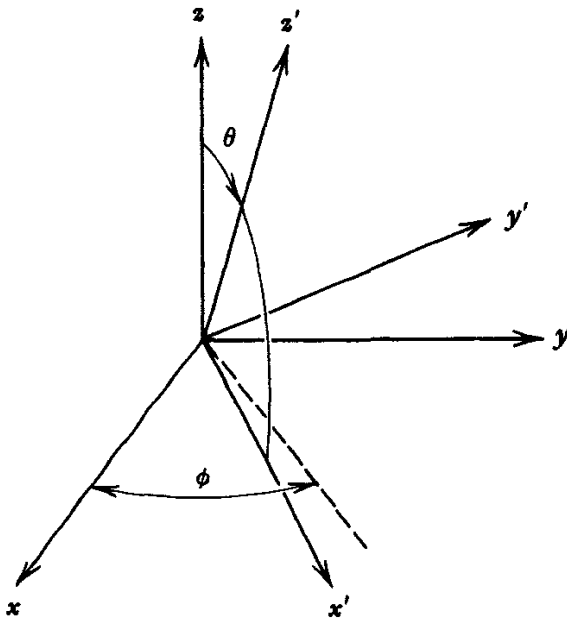


Figure 7.14. Coordinates for Problem 7.4.

direction of propagation, \mathbf{k} , and x' is chosen so that $x'z'$ plane contains the c axis of the crystal (z axis). The y' axis is perpendicular to z' and x' .

- (a) Show that the transformation can be obtained by first a rotation of ϕ around the z axis and then a rotation of θ around the y' axis. Show that the transformation matrix is

$$a_{ij} = \begin{pmatrix} \cos \theta \cos \phi & \cos \theta \sin \phi & \sin \theta \\ -\sin \phi & \cos \phi & 0 \\ -\sin \theta \cos \phi & -\sin \theta \sin \phi & \cos \theta \end{pmatrix}.$$

- (b) Use the transformation formula (7.4-4) for the electro-optic coefficients to show that

$$r'_{123} = \cos 2\theta \cos 2\phi r_{123} \quad (\text{note: } r_{123} = r_{41}),$$

$$r'_{113} = \cos \theta \sin 2\phi (\cos^2 \theta - 2 \sin^2 \theta) r_{123},$$

$$r'_{223} = -\cos \theta \sin 2\phi r_{123}.$$

- (c) Derive expressions for r'_{333} , r'_{313} , r'_{323} .

7.5. *Quadratic electro-optic coefficients of isotropic media.* Show that for isotropic media

$$s_{44} = \frac{1}{2}(s_{11} - s_{12}).$$

- (a) Use a direct coordinate transformation of rotation by 45° around the z axis. The matrix representing the rotation is given by

$$a_{ij} = \begin{pmatrix} \frac{1}{\sqrt{2}} & \frac{1}{\sqrt{2}} & 0 \\ -\frac{1}{\sqrt{2}} & \frac{1}{\sqrt{2}} & 0 \\ 0 & 0 & 1 \end{pmatrix}.$$

Note that $s_{44} = s_{1212}$; use

$$s_{1212} = a_{1i}a_{2j}a_{1k}a_{2l}s_{ijkl}.$$

- (b) Apply an electric field $\mathbf{E} = (1/\sqrt{2})E(\hat{x} + \hat{y})$ and diagonalize the index ellipsoid. Show that the principal indices of refraction are

$$\frac{1}{n_{x'}^2} = \frac{1}{n^2} + \frac{1}{2}(s_{11} + s_{12})E^2 + s_{44}E^2,$$

$$\frac{1}{n_{y'}^2} = \frac{1}{n^2} + \frac{1}{2}(s_{11} + s_{12})E^2 - s_{44}E^2,$$

$$\frac{1}{n_{z'}^2} = \frac{1}{n^2} + s_{12}E^2,$$

where x' is in the direction of the electric field. Use the symmetry requirement that $n_{y'} = n_{z'}$ to derive the result for s_{44} .

REFERENCES

1. S. Bhagavantam, *Crystal Symmetry and Physical Properties*, Academic Press, New York, 1966.
2. W. R. Cook, Jr. and H. Jaffe, Electro-optic Coefficients, Landolt-Bornstein, New Series, K.-H. Hellwege, Ed., Vol. 11, Springer-Verlag, 1979, pp. 552-651.
3. Yu. V. Pisarevskii, G. A. Tregubov, and Yu. V. Shaldin, *Fiz. Tverd. Tela* 7, 661-663 (1965); "The electro-optical properties of $\text{NH}_4\text{H}_2\text{PO}_4$, KH_2PO_4 , and $\text{N}_4(\text{CH}_2)_6$ crystals in UHF fields," *Sov. Phys. Solid State* 7, 530-531 (1965).
4. R. S. Adhav, "Linear electro-optic effects in tetragonal phosphates and arsenates," *J. Opt. Soc. Am.* 59, 414-418 (1969).
5. A. S. Vasilevskaya and A. S. Sonin, *Fiz. Tverd. Tela* 13, 1550-1556 (1971); "Relationship between the dielectric and electro-optical properties of ferroelectric crystals of the potassium dihydrogen phosphate group in the paraelectric phase," *Sov. Phys. Solid State* 13, 1299-1304 (1971).
6. L. M. Blinov, "Electro-optical effects in liquid crystals," *Sov. Phys. Usp.* 17, 658 (1975).

8

Electro-optic Devices

We have discussed in Chapter 7 the electro-optic effects in crystals—the effect of an applied electric field on the propagation of electromagnetic radiation. These effects can be used to build light modulators, spectral tunable filters, electro-optic filters, beam deflectors, and so on. The use of electro-optic modulation offers the possibility of manipulating a laser beam or controlling the signal radiation at high speeds (up to the multigigahertz region), since no mechanical moving parts are involved. In this chapter we will study various device structures and their transmission characteristics and principles of operation. Some important design considerations will also be discussed. Guided-wave electro-optic devices, such as modulators and couplers, will be discussed in Chapter 11.

8.1. ELECTRO-OPTIC LIGHT MODULATORS

We have discussed briefly in Section 7.3 the electro-optic modulation of light in a *z*-cut KDP plate (i.e., plate surface perpendicular to the *c* axis of the crystal). The basic principle involved is that the application of the electric field changes the index ellipsoid. Consequently, the index of refraction of the crystal for the linearly polarized normal modes depends on the field strength. It is clear that the phase shift of these normal modes passing through the crystal depends on the index of refraction. After traversing a distance *L* in the crystal, the change in phase shift due to the applied electric field is typically

$$\Delta\phi = \frac{\pi}{\lambda} n^3 r E L, \quad (8.1-1)$$

where λ is the wavelength of the light, n is the index of refraction, r is the relevant electro-optic coefficient, and E is the applied electric field. If E varies sinusoidally with time, then the phase delay of the wave follows the applied electric field and also varies sinusoidally provided the modulation

frequency is not too high. Thus, the electro-optic effect leads directly to phase modulation of these normal modes. Amplitude modulation can be obtained by combining two normal modes of propagation with two different electro-optically induced phase shifts. Normally, one polarizer is required to prepare linearly polarized light for phase retardation. Amplitude modulation requires an additional polarizer (analyzer) oriented at an appropriate angle to obtain proper interference.

The electro-optic modulation of light waves is also divided into two basic types according to the direction of the applied electric field. If the electric field is parallel to the direction of propagation, the modulation is referred to as longitudinal. If the electric field is perpendicular to the direction of propagation, the modulation is referred to as transverse. These two cases will now be taken up separately.

8.1.1. Longitudinal Electro-optic Modulation

Figure 8.1 shows the geometry of a typical longitudinal electro-optic modulator. This modulator structure offers a large acceptance area with a thin electro-optic crystal plate. The electric field of the modulating field is parallel to the beam path of the light except near the edge of the electrodes. If we limit our consideration to the linear electro-optic effect, the refractive-index change induced by the electric field is proportional to the electric field E . The electrically induced phase change (or phase retardation) for light passing through the crystal plate is thus proportional to EL , which is the applied voltage V regardless of the crystal plate thickness L . Some example of phase changes due to the applied electric field are calculated in the following examples.

z-Cut LiNbO₃ Plate. Consider the case when the electro-optic crystal is a z-cut LiNbO₃ plate. The point group of LiNbO₃ is 3m. According to Table 7.2 and Eq. (7.2-3), the index ellipsoid in the presence of an electric field in the z-direction (i.e., $\mathbf{E} = E\hat{z}$) is

$$x^2 \left(\frac{1}{n_o^2} + r_{13}E \right) + y^2 \left(\frac{1}{n_o^2} + r_{13}E \right) + z^2 \left(\frac{1}{n_e^2} + r_{33}E \right) = 1, \quad (8.1-2)$$

where n_o and n_e are the ordinary and extraordinary refractive indices of the crystal, and r_{13} and r_{33} are the relevant electro-optic coefficients. Since Eq. (8.1-2) contains no mixed terms, the principal indices of refraction are

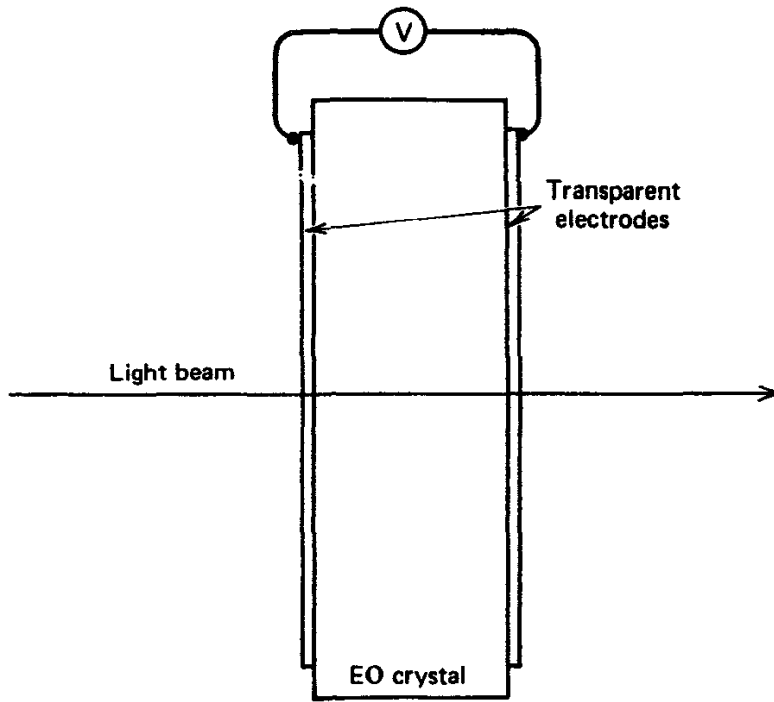


Figure 8.1. Geometry of a typical longitudinal modulator.

given, according to Eq. (8.1-2), by

$$\begin{aligned} n_x &= n_o - \frac{1}{2}n_o^3 r_{13} E, \\ n_y &= n_o - \frac{1}{2}n_o^3 r_{13} E, \\ n_z &= n_e - \frac{1}{2}n_e^3 r_{33} E, \end{aligned} \quad (8.1-3)$$

where we assume that $n^3 r E \ll n$. According to Eq. (8.1-3), $n_x = n_y$, so the crystal remains uniaxial and the c axis remains unchanged. Light propagating along z will experience the same phase change regardless of its polarization state. An unpolarized laser beam can thus be phase modulated with such a modulator structure. The transmitted light beam gains a phase factor of e^{-ikL} , which consists of a zero-field ($E = 0$) phase and an electrically induced phase change

$$kL = \frac{2\pi}{\lambda} n_o L - \frac{\pi}{\lambda} n_o^3 r_{13} V, \quad (8.1-4)$$

where V is the applied voltage. The voltage required to change the phase by

π is called the half-wave voltage for phase modulation, and is given by

$$V_{\pi} = \frac{\lambda}{n_o^3 r_{13}} \quad (\text{PM}). \quad (8.1-5)$$

If the applied voltage is sinusoidal in time and is taken as

$$V = V_m \sin \omega_m t, \quad (8.1-6)$$

the transmitted beam will be phase-modulated and can be expressed as

$$E(z, t) = A \exp[i(\omega t - kz - \phi_0 + \delta \sin \omega_m t)] \quad (8.1-7)$$

where A is the constant amplitude and

$$\delta = \frac{\pi}{\lambda} n_o^3 r_{13} V_m = \pi \frac{V_m}{V_{\pi}}, \quad (8.1-8)$$

and

$$\phi_0 = \frac{2\pi}{\lambda} n_o L.$$

Since no birefringence is induced by the electric field in this device geometry, there is no phase retardation between any two orthogonally polarized waves. No amplitude modulation can be achieved with this configuration unless optical feedback is introduced (see Section 8.2).

Other z -cut uniaxial electro-optic crystal plates behave similarly, except crystals with $\bar{4}2m$ or $\bar{4}$ symmetry, which become biaxial under the influence of an electric field [see Problem 7.2].

z -Cut Cubic Crystal. Consider now the case when the crystal is a z -cut cubic crystal plate. Examples of such crystals are GaAs, CdTe, InAs, and ZnS. The index ellipsoid in the presence of an electric field in the z direction (i.e., $\mathbf{E} = E\hat{z}$) is, according to Table 7.2 and Eq. (7.2-3),

$$\frac{x^2}{n^2} + \frac{y^2}{n^2} + \frac{z^2}{n^2} + 2r_{41}Exy = 1.$$

The applied electric field couples the x -polarized and the y -polarized waves. The principal dielectric axes x and y are rotated around the z axis by 45° because of the electric field in the z -direction. The index ellipsoid in the new principle coordinate system (x' , y' , z') becomes

$$x'^2 \left(\frac{1}{n^2} + r_{41}E \right) + y'^2 \left(\frac{1}{n^2} - r_{41}E \right) + \frac{z'^2}{n^2} = 1. \quad (8.1-9)$$

The principal indices of refraction are given, according to Eq. (8.1-9), by

$$\begin{aligned}n_{x'} &= n - \frac{1}{2}n^3r_{41}E, \\n_{y'} &= n + \frac{1}{2}n^3r_{41}E, \\n_{z'} &= n.\end{aligned}\tag{8.1-10}$$

If the plate is to be used as a phase modulator, the light must be polarized in either the x' or the y' direction. The phase change induced by the applied voltage is given by

$$\Delta\phi = \frac{\pi}{\lambda}n^3r_{41}V,\tag{8.1-11}$$

where V is the modulating voltage ($V = EL$). The half-wave voltage for phase modulation is

$$V_{\pi} = \frac{\lambda}{n^3r_{41}} \quad (\text{PM}).\tag{8.1-12}$$

If the modulating field is sinusoidal in time and is of the form (8.1-6), then the modulation index is

$$\delta = \frac{\pi}{\lambda}n^3r_{41}V_m = \pi\frac{V_m}{V_{\pi}} \quad (\text{PM}).\tag{8.1-13}$$

If the plate is to be used as an amplitude modulator, a front polarizer can be aligned along the x axis so that equal amplitudes of x' mode and y' mode are excited. A phase retardation of $\Gamma = 2\pi(n_{y'} - n_{x'})L/\lambda$ is accumulated in passage through the crystal and is given by

$$\Gamma = \frac{2\pi}{\lambda}n^3r_{41}V.\tag{8.1-14}$$

The half-wave voltage for amplitude modulation is defined as the voltage required to obtain a phase retardation of π and is given by

$$V_{\pi} = \frac{\lambda}{2n^3r_{41}} \quad (\text{AM}).\tag{8.1-15}$$

If the modulation voltage is sinusoidal in time and is taken as in Eq. (8.1-6), and a properly oriented quarter-wave plate is inserted in series with the electro-optic crystal, then the phase retardation becomes

$$\Gamma = \frac{\pi}{2} + \frac{2\pi}{\lambda}n^3r_{41}V_m \sin \omega_m t = \frac{\pi}{2} + \pi\frac{V_m}{V_{\pi}} \sin \omega_m t.\tag{8.1-16}$$

An analyzer at the output, oriented perpendicular to the front polarizer, converts the phase modulation to amplitude modulation. The transmissivity of the whole structure is $T = \sin^2 \frac{1}{2} \Gamma$, where Γ is given by Eq. (8.1-16). If $\pi V_m \ll V\pi$, the transmissivity T is given approximately by

$$T = T_0(1 + \Delta \sin \omega_m t) \quad (8.1-17a)$$

where $T_0 = \frac{1}{2}$ and Δ is given by

$$\Delta = \Gamma_m = \frac{\pi V_m}{V\pi}. \quad (8.1-17b)$$

The quantity Δ is referred to as the modulation depth. An x -cut or z -cut cubic crystal plate would behave exactly the same as the y -cut plate because of the symmetry.

In the above two examples, we see that the modulation index (or modulation depth) is proportional to the applied voltage. The half-wave voltages are proportional to the wavelength of the light and are inversely proportional to the electro-optic coefficient. These voltages at visible-light wavelengths are of the order of several kilovolts. Increasing the plate thickness results in a longer interaction length—at the expense, however, of the electric field strength. There is consequently no net gain in the modulation due to an increase of the plate thickness in the longitudinal modulation. The need to use high voltages becomes very serious for infrared radiation because of the long wavelength of the light (e.g., $10.6 \mu\text{m}$). Longitudinal modulators are used only when large acceptance area and wide field of view are required. It can be shown that the field of view of a longitudinal modulator made of z -cut 43m crystals is almost 2π (see Problem 8.1).

8.1.2. Transverse Electro-optic Modulation

Figure 8.2 shows the geometry of a transverse electro-optic modulator. This structure can provide a long interaction length at a given field strength. The modulating field is transverse to the optical beam path. Limiting ourselves to the linear electro-optic effect, the refractive-index change induced by the electric field is proportional to the field E . The electrically induced phase change (or phase retardation) for light passing through the crystal plate is thus proportional to EL , which can be written as VL/d , with d the separation between the electrodes. We find that the phase change is proportional to the length L of the crystal. This advantage has been used to construct electro-optic modulators for laser beams with low driving voltages. The transverse electro-optic modulation is illustrated in the following examples.

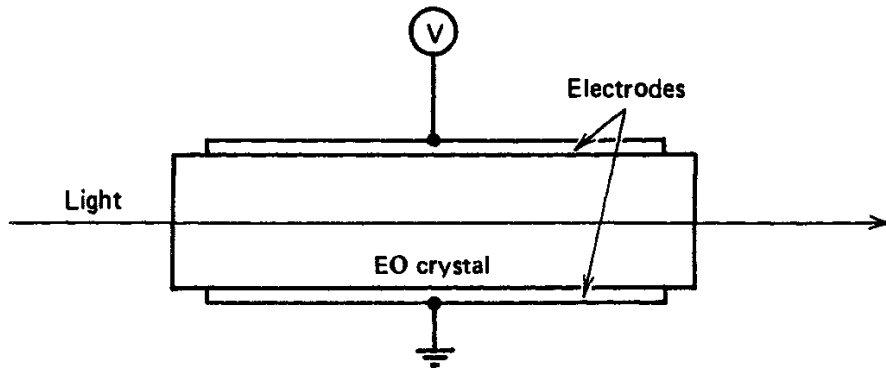


Figure 8.2. Geometry of a transverse electro-optic modulator.

LiTaO₃ Electro-Optic Modulator. Referring to Fig. 8.3, we consider a LiTaO₃ crystal rod with its input and output face perpendicular to the y axis. The side surfaces are perpendicular to the x and z axes, respectively. LiTaO₃ has a 3m point-group symmetry (as does LiNbO₃). Let the modulating electric field be applied in the z -direction, so that the principal refractive indices are given by Eq. (8.1-3). Since the light beam is propagating in the y direction, the birefringence seen by the light beam is

$$n_z - n_x = (n_e - n_o) - \frac{1}{2}(n_e^3 r_{33} - n_o^3 r_{13})E. \quad (8.1-18)$$

It consists of the natural birefringence ($n_e - n_o$) plus an electrically induced birefringence term $\frac{1}{2}(n_e^3 r_{33} - n_o^3 r_{13})E$. The phase retardation for light passing through the crystal rod is thus given by

$$\Gamma = \frac{2\pi}{\lambda}(n_e - n_o)L - \frac{\pi}{\lambda}(n_e^3 r_{33} - n_o^3 r_{13})\frac{L}{d}V, \quad (8.1-19)$$

where V is the applied voltage and d is the separation between the electrodes.

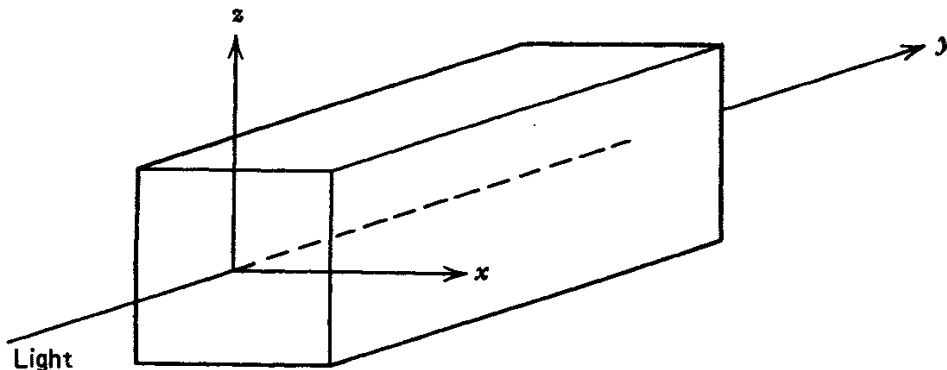


Figure 8.3. A LiTaO₃ electro-optic crystal rod.

If the light is linearly polarized along the z direction, the phase change induced by the applied electric field is

$$\Delta\phi = \frac{\pi}{\lambda} n_e^3 r_{33} \frac{L}{d} V. \quad (8.1-20)$$

Because of the natural birefringence term, an amplitude modulator using LiTaO_3 requires a phase compensator which can be adjusted until the total phase retardation in the absence of the applied voltage is an odd integral multiple of $\frac{1}{2}\pi$. In addition, the input and output faces must be parallel, so that the beam undergoes the same phase retardation throughout the cross section of the beam. The half-wave voltage for this case is

$$V_\pi = \frac{d}{L} \cdot \frac{\lambda}{n_e^3 r_{33} - n_o^3 r_{13}}. \quad (8.1-21)$$

If the applied voltage is sinusoidal in time and is taken as Eq. (8.1-6), the phase retardation can be written

$$\Gamma = \Gamma_0 + \pi \frac{V_m}{V_\pi} \sin \omega_m t = \Gamma_0 + \Gamma_m \sin \omega_m t, \quad (8.1-22)$$

where Γ_0 is the total phase retardation in the absence of applied voltage. The modulation depth, if Γ_0 is an odd multiple of $\frac{1}{2}\pi$, is

$$\Delta = \Gamma_m = \pi \frac{V_m}{V_\pi}. \quad (8.1-23)$$

Notice from Eq. (8.1-21) that the half-wave voltage can be reduced by choosing a longer crystal rod which provides longer interaction region. Light-intensity modulators have been constructed using LiTaO_3 and LiNbO_3 with this geometry at modulation frequencies up to 4 GHz [1].

Electro-Optic Modulators Using Cubic Crystals. Cubic crystals are optically isotropic (no birefringence) and therefore offer a wide field of view in many optical systems. Here we consider the case of crystals of the $\bar{4}3m$ symmetry (zinc blende) group. Examples of this group are InAs, CuCl, GaAs, and CdTe. The last two are used for modulation in the infrared, since they remain transparent beyond 10 μm . These crystals are cubic and have axes of fourfold symmetry along the cube edges (i.e., $\langle 100 \rangle$, $\langle 010 \rangle$, $\langle 001 \rangle$)

directions), and threefold axes of symmetry along the cube diagonals (i.e., $\langle 111 \rangle$, $\langle \bar{1}\bar{1}\bar{1} \rangle$, $\langle 1\bar{1}\bar{1} \rangle$, $\langle 1\bar{1}1 \rangle$ directions).

According to Table 7.2 and Eq. (7.2-3), the index ellipsoid in the presence of the electric field is

$$\frac{x^2 + y^2 + z^2}{n^2} + 2r_{41}(yzE_x + zxE_y + xyE_z) = 1, \quad (8.1-24)$$

where E_x , E_y , and E_z are the components of the field along the crystal axes, and r_{41} is the electro-optic coefficient. In this case, all the three variables (x , y , z) are coupled. The general approach to transform Eq. (8.1-24) into its diagonal form is to solve the following eigenvalue problem:

$$\begin{pmatrix} \frac{1}{n^2} & r_{41}E_z & r_{41}E_y \\ r_{41}E_z & \frac{1}{n^2} & r_{41}E_x \\ r_{41}E_y & r_{41}E_x & \frac{1}{n^2} \end{pmatrix} \mathbf{V} = \frac{1}{n'^2} \mathbf{V}. \quad (8.1-25)$$

The eigenvectors \mathbf{V} are the new principal axes, and the eigenvalues n' are the new principal indices of refraction. To be specific, we consider the case when the electric field is in the $\langle 110 \rangle$ direction. Taking the field magnitude as E , we have

$$E_x = E_y = \frac{1}{\sqrt{2}}E, \quad E_z = 0. \quad (8.1-26)$$

Substitution of Eq. (8.1-26) for E_x , E_y , and E_z into Eq. (8.1-25) leads to the following secular equation:

$$\begin{pmatrix} \frac{1}{n^2} - \frac{1}{n'^2} & 0 & \frac{1}{\sqrt{2}}r_{41}E \\ 0 & \frac{1}{n^2} - \frac{1}{n'^2} & \frac{1}{\sqrt{2}}r_{41}E \\ \frac{1}{\sqrt{2}}r_{41}E & \frac{1}{\sqrt{2}}r_{41}E & \frac{1}{n^2} - \frac{1}{n'^2} \end{pmatrix} = 0. \quad (8.1-27)$$

The roots of this equation are the principal indices of refraction and are

given by

$$\begin{aligned}n_{x'} &= n + \frac{1}{2}n^3r_{41}E, \\n_{y'} &= n - \frac{1}{2}n^3r_{41}E, \\n_{z'} &= n.\end{aligned}\tag{8.1-28}$$

The new principal axes are given by

$$\begin{aligned}x' &= \frac{1}{2}x + \frac{1}{2}y - \frac{1}{\sqrt{2}}z, \\y' &= \frac{1}{2}x + \frac{1}{2}y + \frac{1}{\sqrt{2}}z, \\z' &= \frac{1}{\sqrt{2}}x - \frac{1}{\sqrt{2}}y.\end{aligned}\tag{8.1-29}$$

An amplitude modulator based on the foregoing situation is shown in Fig. 8.4. The phase retardation is

$$\Gamma = \frac{2\pi}{\lambda}n^3r_{41}\left(\frac{L}{d}\right)V.\tag{8.1-30}$$

Table 8.1 summarizes the phase-retardation and electro-optical properties of $\bar{4}3m$ crystals with the field along $\langle 001 \rangle$, $\langle 110 \rangle$, and $\langle 111 \rangle$ directions. It is seen that the maximum achievable phase retardation is given by Eq. (8.1-30). The half-wave voltage is given by

$$V_{\pi} = \frac{d}{L} \cdot \frac{\lambda}{2n^3r_{41}}.\tag{8.1-31}$$

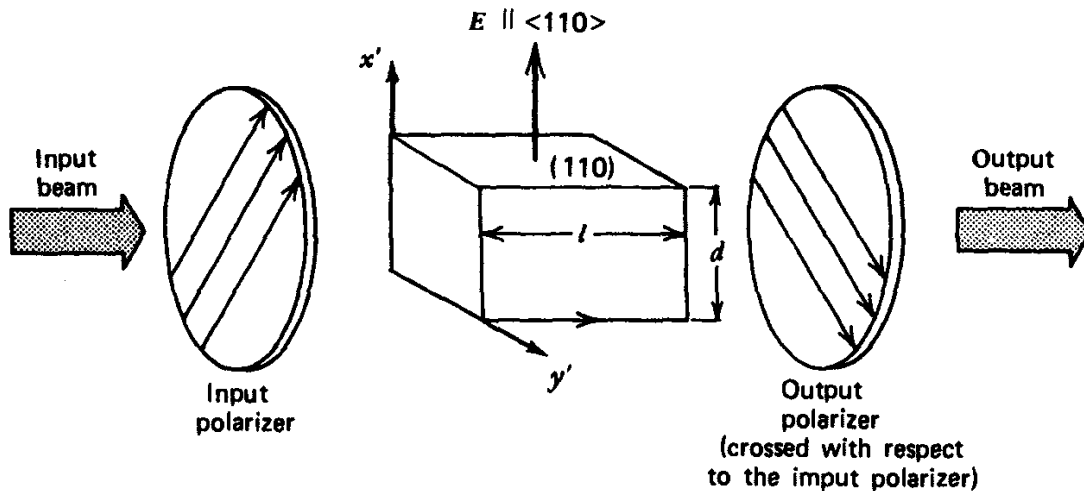
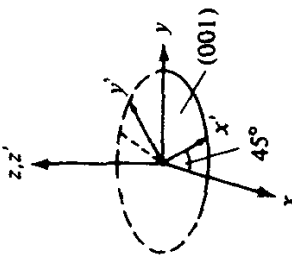
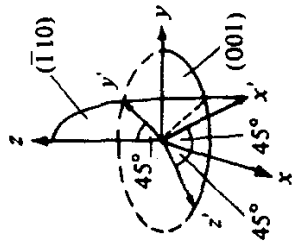
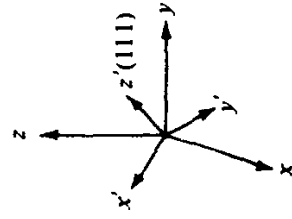


Figure 8.4. A transverse electro-optic modulator using a zinc-blende-type ($\bar{4}3m$) crystal with E parallel to a cube diagonal ($\langle 110 \rangle$ direction).

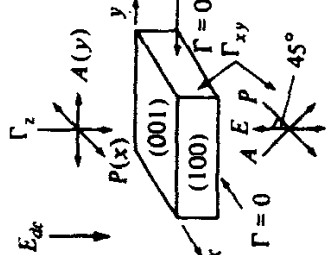
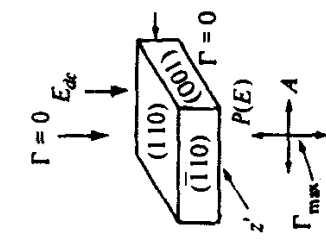
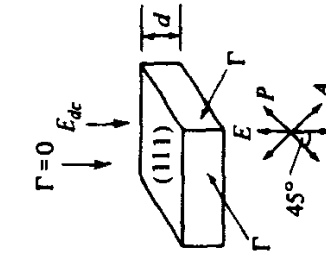
Table 8.1. Electro-optical Properties and Retardation in $\bar{4}3m$ (Zinc-Blende-Structure) Crystals for Three Directions of Applied Field [2]

	$E \perp (001)$ plane $E_x = E_y = 0, E_z = E$	$E \perp (110)$ plane $E_x = E_y = \frac{E}{\sqrt{2}}, E_z = 0$	$E \perp (111)$ plane $E_x = E_y = E_z = \frac{E}{\sqrt{3}}$
Index ellipsoid	$\frac{x^2 + y^2 + z^2}{n_o^2} + 2r_{41}E_{xy} = 1$	$\frac{x^2 + y^2 + z^2}{n_o^2} + \sqrt{2}r_{41}E(yz + zx) = 1$	$\frac{x^2 + y^2 + z^2}{n_o^2} + \frac{2}{\sqrt{3}}r_{41}E(yz + zx + xy) = 1$
n'_x	$n_o + \frac{1}{2}n_o^3r_{41}E$	$n_o + \frac{1}{2}n_o^3r_{41}E$	$n_o + \frac{1}{2\sqrt{3}}n_o^3r_{41}E$
n'_y	$n_o - \frac{1}{2}n_o^3r_{41}E$	$n_o - \frac{1}{2}n_o^3r_{41}E$	$n_o + \frac{1}{2\sqrt{3}}n_o^3r_{41}E$
n'_z	n_o	n_o	$n_o - \frac{1}{\sqrt{3}}n_o^3r_{41}E$

Coordinates
 $x'y'z'$



Directions of optical
 path and axes of
 crossed polarizer



$$\Gamma = \frac{\sqrt{3}\pi L}{\lambda} n_o^3 r_{41} V$$

$$\Gamma_{\max} = \frac{2\pi L}{\lambda} n_o^3 r_{41} V$$

$$\Gamma_z = \frac{2\pi}{\lambda} n_o^3 r_{41} V$$

$$\Gamma_{xy} = \frac{\pi L}{\lambda} n_o^3 r_{41} V$$

Phase retardation
 $\Gamma (V = Ed)$

8.2. ELECTRO-OPTIC FABRY-PEROT MODULATORS

In the above discussion of electro-optic modulators, especially the transverse geometry (Fig. 8.2), we found that the modulation is proportional to the interaction length L . If V_m is the amplitude of the modulating voltage and the modulator is properly biased, the phase-modulation depth (8.1-8) is given by

$$\delta = \pi \frac{V_m}{V_\pi}, \quad (8.2-1)$$

and the amplitude-modulation depth (8.1-23) is given by the simple form

$$\Delta = \pi \frac{V_m}{V_\pi}. \quad (8.2-2)$$

According to Eqs. (8.2-1) and (8.2-2), a large modulation depth requires a small half-wave voltage V_π at a given modulation voltage. In transverse operation this requires a long crystal rod.

In this section we consider the incorporation of the electro-optic crystal in a Fabry-Perot resonator. The effective interaction length of the light beam with the electro-optic crystal is greatly increased because the light is bouncing back and forth within the optical cavity. This will greatly enhance the modulation depth for both phase and amplitude modulations. They will now be discussed in detail.

8.2.1. Amplitude Modulation

Referring to Fig. 8.5, we consider a z -cut LiNbO_3 (or LiTaO_3) thin plate coated with high-reflectivity dielectric mirrors. Transparent electrodes are deposited on the outer surfaces of the whole structure. The transmissivity of the Fabry-Perot cavity is given by [11]

$$T = \frac{(1 - R)^2}{(1 - R)^2 + 4R \sin^2 \phi}, \quad (8.2-3)$$

where R is the mirror reflectivity, and ϕ is the phase shift of light in passage through the medium and is given by

$$\phi = \frac{2\pi}{\lambda} nL \quad (8.2-4)$$

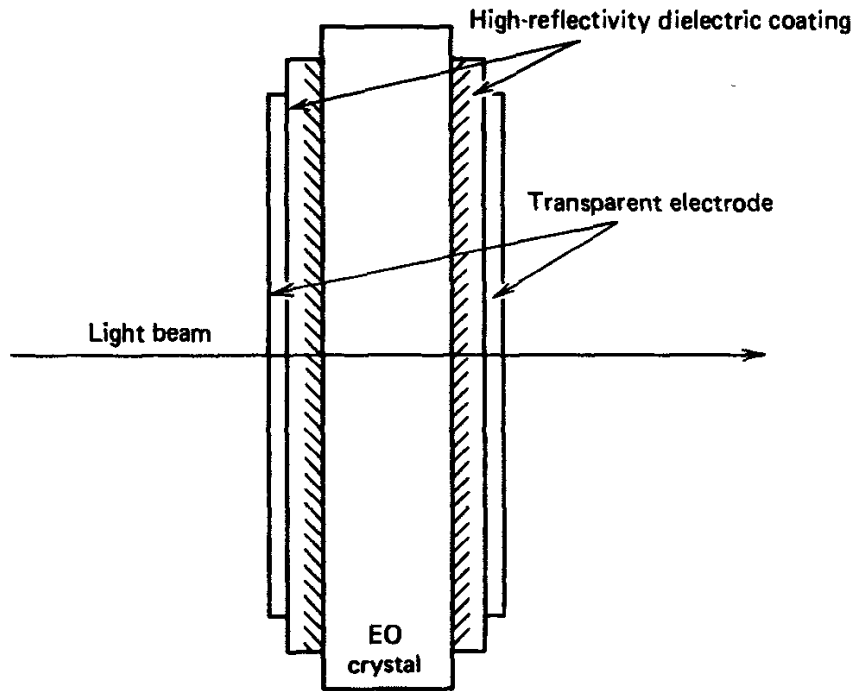


Figure 8.5. An electro-optic Fabry-Perot modulator.

with L the thickness of the plate. The index of refraction n in the presence of an applied electric field is given, according to Eq. (8.1-3), by

$$n = n_o - \frac{1}{2}n_o^3 r_{13} E. \quad (8.2-5)$$

Substituting Eq. (8.2-5) for n in Eq. (8.2-4), we obtain

$$\phi = \frac{2\pi}{\lambda} n_o L - \frac{\pi}{\lambda} n_o^3 r_{13} V, \quad (8.2-6)$$

where V is the applied voltage.

If the incident light beam is monochromatic, the intensity of the transmitted beam is a function of ϕ , which is electrically tunable according to Eq. (8.2-6). In addition, if the Fabry-Perot resonator is properly biased so that the transmission is 50% in the absence of the modulation voltage, the transmitted intensity will be strongly modulated with a relatively small modulating voltage. This situation is illustrated in Fig. 8.6. High modulation depth results from the sharp cutoff of the transmissivity peak, provided the finesse of the cavity is high. In fact, the slope of the transmission curve at the half-transmissivity point, according to Eq. (8.2-3), is

$$\left(\frac{dT}{d\phi} \right)_{1/2} = \frac{F}{\pi}, \quad (8.2-7)$$

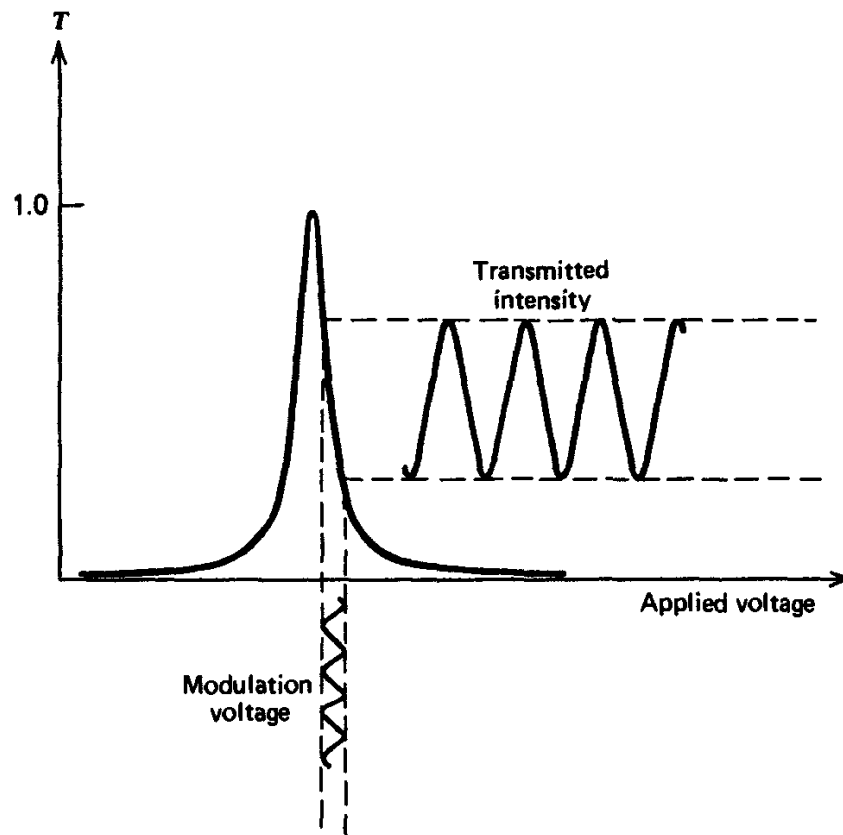


Figure 8.6. Transmission factor of a Fabry-Perot electro-optic modulator as a function of applied voltage. The modulator is biased at half-maximum transmission. A small applied sinusoidal voltage modulates the transmitted intensity about the bias point.

where F is the finesse of the cavity. A Fabry-Perot cavity with a finesse of $F = 30$ is easily achievable. Thus, we see that the slope (8.2-7) can be of the order of 10. In a conventional amplitude modulator (e.g., see Fig. 7.5) this slope is 1. Let the applied voltage be $V = V_m \sin \omega_m t$. The modulation depth of the transmitted beam can then be written, according to Eqs. (8.2-7), (8.1-4), and (8.1-5),

$$\Delta = F \frac{V_m}{V_\pi} \quad (8.2-8)$$

In comparison with (8.2-2) we notice that there is a net gain factor of F/π in the modulation depth provided the voltage V_m/V_π is the same.

8.2.2. Phase Modulation

Although the amplitude-modulated light beam passing through an electro-optic Fabry-Perot modulator is also phase modulated, it is desirable to be

able to have a purely phase-modulated light beam. Figure 8.7 shows an idealized structure for pure phase modulation. This is an asymmetric Fabry-Perot cavity with a rear mirror reflectivity of 100%. The front mirror is a partially reflecting dielectric coating with $R < 1.0$. This is the so-called Gires-Tournois etalon [9]. The reflectivity of the whole stack is obviously 100%, because light cannot pass through the second mirror and the whole stack is lossless. All the electromagnetic energy will be reflected provided the mirror reflectivity remains 100% in the spectral regions of interest. In fact, the reflection coefficient can be written

$$r = e^{i\Phi} = \frac{-\sqrt{R} + e^{-2i\phi}}{1 - \sqrt{R} e^{-2i\phi}}, \quad (8.2-9)$$

where we have taken $r_{12} = -\sqrt{R}$ and $r_{23} = 1$, and ϕ is given by

$$\phi = \frac{2\pi}{\lambda} nL \quad (8.2-10)$$

The phase shift upon reflection, Φ , defined in Eq. (8.2-9), can be expressed

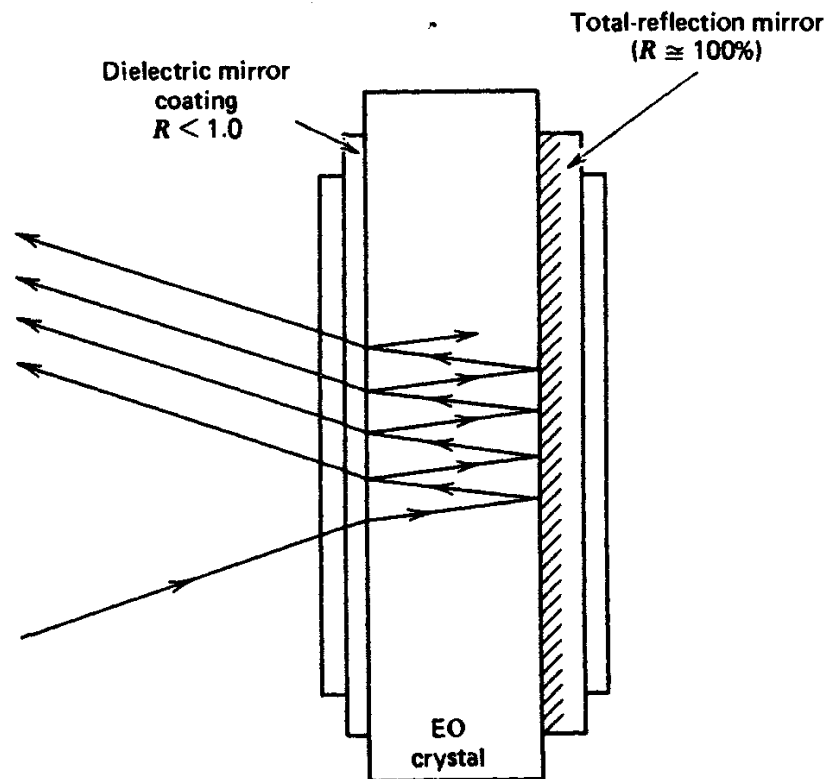


Figure 8.7. An asymmetric Fabry-Perot cavity (Gires-Tournois etalon) as a phase modulator.

in terms of ϕ as

$$\Phi = -2 \tan^{-1} \left(\frac{1 + \sqrt{R}}{1 - \sqrt{R}} \tan \phi \right) \quad (8.2-11)$$

In the limit when the reflectivity of the front mirror vanishes ($R = 0$), this phase Φ is reduced to -2ϕ , which is simply the round-trip optical phase gained by the light beam. When the reflectivity is greater than zero ($R > 0$), the phase Φ is substantially increased because of the multiple reflections in the asymmetric Fabry–Perot cavity (see Fig. 8.7).

In the presence of the electric field the phase shift ϕ is given by Eq. (8.2-6) for the case of a z -cut LiNbO_3 plate:

$$\phi = \frac{2\pi}{\lambda} n_o L - \frac{\pi}{\lambda} n_o^3 r_{13} V. \quad (8.2-6)$$

If, in addition, the electro-optic crystal is properly biased so that in the absence of the modulating voltage the phase $\phi = m\pi$. Thus the phase shift Φ of the reflected beam can be written

$$\Phi = 2 \tan^{-1} \left(\frac{1 + \sqrt{R}}{1 - \sqrt{R}} \tan \pi \frac{V}{V_\pi} \right). \quad (8.2-12)$$

We now assume that the modulation voltage is small, so that the phase modulation is

$$\Delta\Phi = 2\pi \frac{1 + \sqrt{R}}{1 - \sqrt{R}} \cdot \frac{V}{V_\pi}. \quad (8.2-13)$$

We notice that the presence of the front mirror increases the modulation index by a factor of $(1 + \sqrt{R})/(1 - \sqrt{R})$. As an example, if $R = 0.9$, this factor is 38. A plot of Φ versus V/V_m is shown in Fig. 8.8. Equation (8.2-13) is a linear approximation of Eq. (8.2-12).

In the above two examples we found that the optical feedback provided by the Fabry–Perot cavity effectively increases the interaction length and therefore increases the modulation depth at a given voltage. This enhancement, however, is only available for those optical frequencies that fulfill the Fabry–Perot resonance conditions. In other words, the electro-optic crystal must be properly biased. Since the phase bias depends on the wavelength, the cavity may not be properly biased at other wavelengths. Therefore, the presence of the optical cavity decreases the optical bandwidth of the modulator.

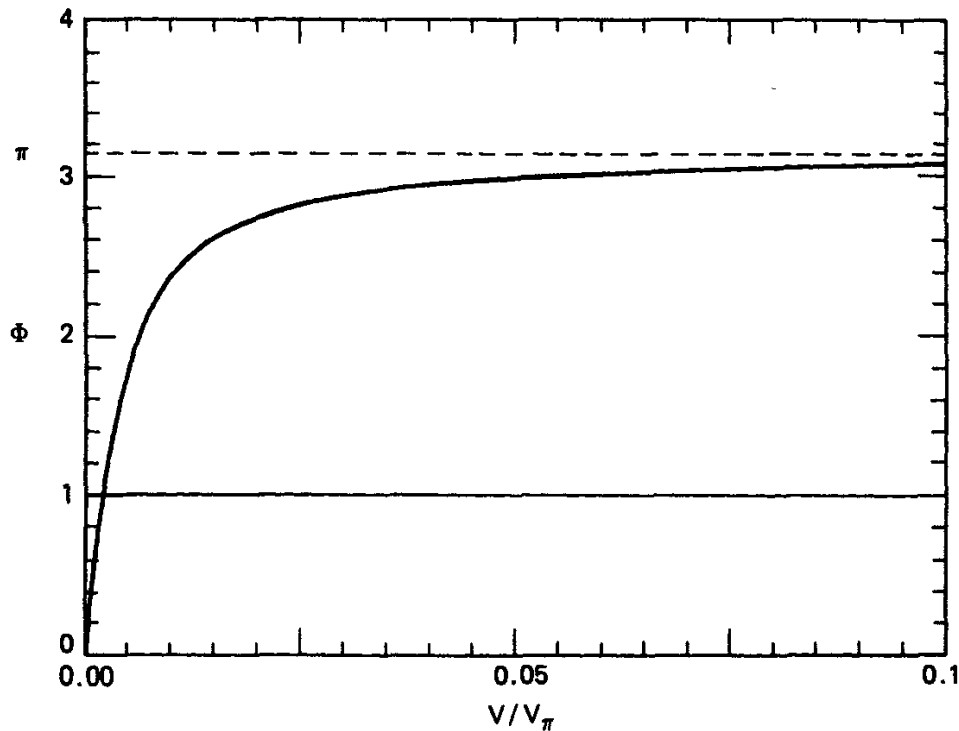


Figure 8.8. Φ versus V for $R = 0.95$.

The use of a passive asymmetric Fabry–Perot resonator in pulse compression will be discussed in Section 8.6.

8.3. SOME DESIGN CONSIDERATIONS

8.3.1. High-Frequency Modulation Considerations

In the examples considered in the two preceding sections, we derived expressions for the retardation caused by electric fields of low frequencies. In many practical situations the modulation signal is at very high frequencies and may occupy a large bandwidth. In this section we consider some of the basic factors limiting the highest usable modulation frequencies in a number of typical experimental situations.

Consider first the situation described by Fig. 8.9. The electro-optic crystal is placed between two electrodes with a modulation field containing frequencies near $\omega_0/2\pi$ applied to them. R_s is the internal resistance of the modulation source, and C represents the parallel-plate capacitance due to the electro-optic crystal. If $R_s > (\omega_0 C)^{-1}$, most of the modulation voltage drop is across R_s and is thus wasted, since it does not contribute to the retardation. This can be remedied by resonating the crystal capacitance with an inductance L , where $\omega_0^2 = (LC)^{-1}$, as shown in Fig. 8.9. In addition, a

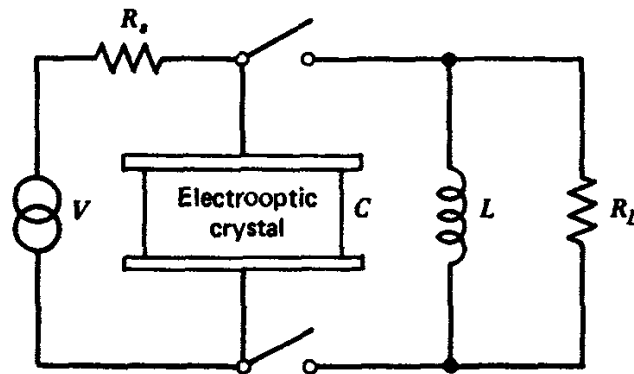


Figure 8.9. Equivalent circuit of an electro-optic modulation crystal in a parallel-plate configuration.

shunting resistance R_L is used so that at $\omega = \omega_0$ the impedance of the parallel RLC circuit is R_L , which is chosen to be larger than R_s , so most of the modulation voltage appears across the crystal. The resonant circuit has a finite bandwidth—that is, its impedance is high only over a frequency interval $\Delta\omega/2\pi \approx 1/(2\pi R_L C)$ (centered on ω_0). Therefore, the maximum modulation bandwidth (the frequency spectrum occupied by the modulation signal) must be less than

$$\frac{\Delta\omega}{2\pi} \approx \frac{1}{2\pi R_L C} \quad (8.3-1)$$

if the modulation field is to be a faithful replica of the modulation signal.

In practice, the size of the modulation bandwidth $\Delta\omega/2\pi$ is dictated by the specific application. In addition, one requires a certain peak retardation Γ_m . Using Eq. (7.3-2) to relate Γ_m to the peak modulation voltage $V_m = (E_z)_m L$, we can show, with the aid of Eq. (8.3-1), that the power $V_m^2/2R_L$ needed in KDP-type crystals to obtain a peak retardation Γ_m is related to the modulation bandwidth $\Delta\nu = \Delta\omega/2\pi$ as

$$P = \frac{\Gamma_m^2 \lambda^2 A \epsilon \Delta\nu}{4\pi L n_o^6 r_{63}^2}, \quad (8.3-2)$$

where L is the length of the optical path in the crystal, A is the cross-sectional area of the crystal normal to L , and ϵ is the dielectric constant at the modulation frequency ω_0 .

8.3.2. Transit-Time Limitations in a Lumped Modulator

Another important high-frequency modulation consideration is the transit-time limitations in a lumped modulator. In the event that the modulating

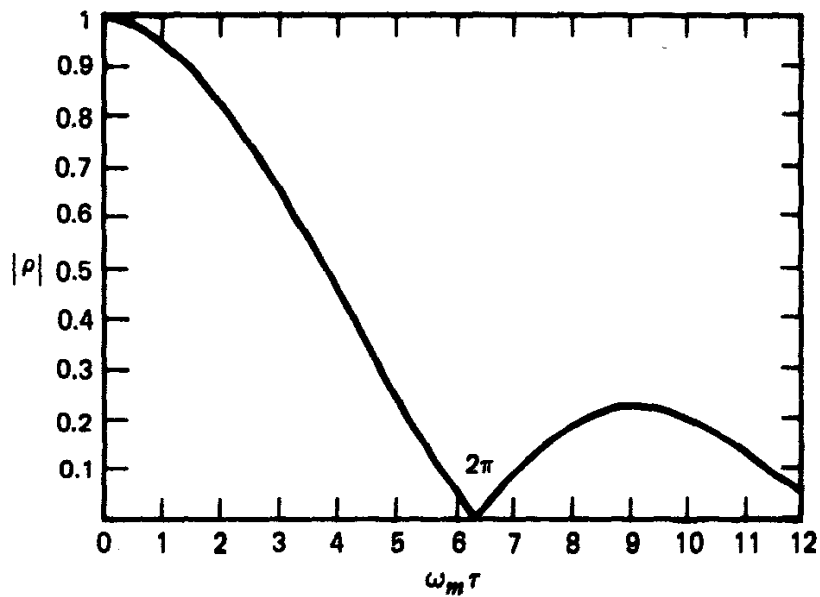


Figure 8.10. Magnitude of the transit-time reduction factor ρ versus $\omega_m t$.

field is a very fast-varying function of time, the optical phase no longer follows the time-varying refractive index adiabatically, especially when the transit time $\tau = nL/c$ is comparable to the period $2\pi/\omega_m$ of the modulating field. This has been discussed in Section 7.4. According to the general result (7.4-23), the reduction in the modulation depth for a lumped modulator ($n_m = 0$) due to the finite transit time is

$$\rho = \frac{\sin \frac{1}{2} \omega_m \tau}{\frac{1}{2} \omega_m \tau}, \quad (8.3-3)$$

where ω_m is the modulation frequency.

For $\rho \approx 1$ (i.e., no reduction), the condition $\omega_m \tau \ll 1$ must be satisfied, that is, the transit time must be small compared to the shortest modulation period. The factor ρ is plotted in Fig. 8.10.

If, somewhat arbitrarily, we take the highest useful modulation frequency as that for which $\omega_m \tau = \pi$ (at this point, according to Fig. 8.10, $\rho = 0.64$), and we use the relation $\tau = Ln/c$, we obtain

$$(\nu_m)_{\max} = \frac{c}{2Ln}, \quad (8.3-4)$$

which using a KDP crystal ($n \approx 1.5$) and a length $L = 2$ cm, yields $(\nu_m)_{\max} = 5 \times 10^9$ Hz.

8.3.3. Traveling-Wave Modulators

One method that can, in principle, overcome the transit-time limitation involves applying the modulation signal in the form of a traveling wave as shown in Fig. 8.11. It has been shown in Section 7.4 that if the optical- and modulation-field phase velocities are equal, a portion of an optical wavefront will experience the same instantaneous modulating electric field, which corresponds to the field it encounters at the entrance face, as it propagates through the crystal, and the transit-time problem discussed above is eliminated. This form of modulation is used mostly in the transverse geometry as discussed in the preceding section, since the RF field in most propagating structures is predominantly transverse.

In general, if there is a phase-velocity mismatch between the modulating wave and the light wave, a reduction factor in the modulation depth is given by Eq. (7.4-23). The maximum useful modulation frequency is taken, as in the treatment leading to Eq. (8.3-4), to be

$$(\nu_m)_{\max} = \frac{c}{2L(n - n_m)}, \quad (8.3-5)$$

which, upon comparison with Eq. (8.3-4), shows an increase in the frequency limit or useful crystal length of $(1 - n_m/n)^{-1}$. We recall that n is the index of refraction of the medium at the frequency of the light beam and n_m is the index of refraction at the modulating frequency.

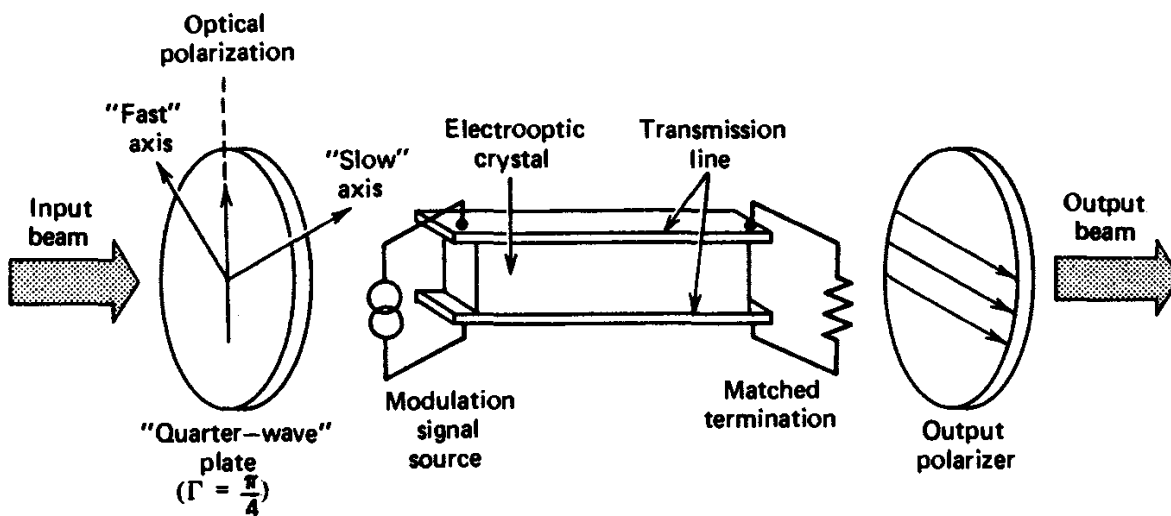


Figure 8.11. A traveling-wave electro-optic modulator.

8.3.4. Geometrical Considerations

In the discussion of the transverse electro-optic modulator, we found that in order to decrease the modulation voltage it is desirable to use a long crystal rod with small transverse dimension (i.e., large L/d). On the other hand, the transverse dimension d must be large enough to accommodate the light beam to be modulated. A light beam with a finite cross section will, in general, diverge as it propagates. Therefore, a crystal rod with a given transverse dimension d has a maximum useful length for electro-optic modulation.

Consider a Gaussian laser beam propagating in the lowest-order transverse mode and passing through an electro-optic crystal rod of length L and diameter d . Given a rod with a fixed length L , it can be shown (see Problem 8.4) that the diameter of the cylinder will be a minimum when the Gaussian beam is focused in such a way that the confocal parameter z_0 equals one-half the length L , and the beam waist is located at the center of the rod. This is illustrated in Fig. 8.12. Under these conditions, the beam diameter is $2\omega_0$ at the waist and $\sqrt{8}\omega_0$ at the input and output plane of the cylinder, where

$$\omega_0^2 = \frac{\lambda L}{2\pi n}, \quad (8.3-6)$$

and ω_0 is called the beam spot size in Section 2.2. In practice, the diameter d is chosen to be larger than $\sqrt{8}\omega_0$ for ease of alignment. In Chapter 11 we will discuss a guided-wave electro-optic modulator in which the light is

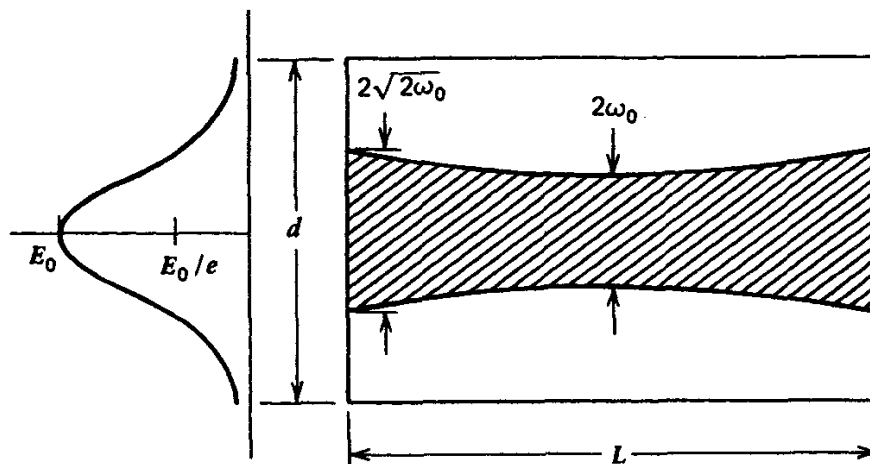


Figure 8.12. A beam of Gaussian cross section passing through a rod of diameter d and length L .

confined to a region with very small ($\sim \lambda$) transverse dimensions. Since the light is in a guided mode, there is no diffraction and the interaction path can be made very long.

8.4. BISTABLE ELECTRO-OPTIC DEVICES

So far we have only discussed optical devices in which the transmitted intensity is always linearly proportional to the input intensity. These devices are called linear optical devices and are characterized by

$$I_o = I_i T(n, \lambda), \quad (8.4-1)$$

where I_o and I_i are output and input beam intensities, respectively, and $T(n, \lambda)$ is the transmissivity, which is a function of the refractive-index distribution n and the wavelength λ . The transmissivity T of a linear device is independent of the input and output beam intensities. This linearity disappears when n depends on either the input intensity I_i or the output intensity, or both. This may occur naturally if the optical medium exhibits nonlinearity, that is,

$$n(z) = n_o(z) + n_2 I(z), \quad (8.4-2)$$

where $I(z)$ is the local beam intensity at z and n_2 is a constant. Or it may happen “artificially” if some optical feedback is provided in an electro-optic crystal. Nonlinear optical devices exhibit many interesting properties. These include differential gain and bistability (hysteresis), which have been seen, for example, in the transmission of a Fabry–Perot interferometer containing Na vapor irradiated by light from a CW dye laser [3]. Bistable devices usually operate in the high-power regime where the medium responds nonlinearly. When the medium nonlinearity is enhanced by resonant electronic transitions, the bandwidth is very small. In the following, we will discuss some “artificially” nonlinear electro-optic devices which have operating characteristics similar to the natural nonlinear optical devices and exhibit all the nonlinear functions, but avoid some of their problems.

8.4.1. Bistable Fabry–Perot Resonator

Referring to Fig. 8.13, we consider a Fabry–Perot resonator containing an electro-optic phase modulator. A small fraction of the transmitted beam is monitored by a detector whose output is proportional to the transmitted light intensity and is amplified and is used to drive the modulator in the

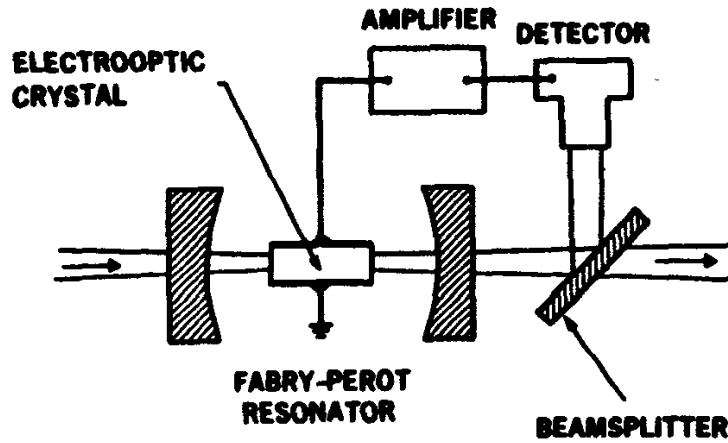


Figure 8.13. Schematic of bistable Fabry-Perot device (after [4, 5]).

resonator. This arrangement simulates a nonlinear-medium effect, since the electro-optically controlled index of refraction is now a function of the light intensity. The transmissivity of this resonator can be written as

$$T = \frac{I_o}{I_i} = \frac{(1 - R)^2}{(1 - R)^2 + 4R \sin^2 \phi} \quad (8.4-3)$$

with

$$\phi = \phi_0 + \alpha I_o, \quad (8.4-4)$$

where ϕ_0 is one-half of the round-trip phase shift of light in the cavity without the feedback servo, and α is a constant. αI_o is the phase change due to the electro-optic crystal driven by a voltage which is proportional to the transmitted intensity I_o . Equation (8.4-3) can also be written

$$I_i = I_o \frac{(1 - R)^2 + 4R \sin^2(\phi_0 + \alpha I_o)}{(1 - R)^2}. \quad (8.4-5)$$

We can plot I_o versus I_i using Eq. (8.4-5) for various values of ϕ_0 and R (see Fig. 8.14). We find that under the appropriate conditions such a device will exhibit bistability, differential gain and optical limiting action.

Notice that for some input-power ranges, the output power is multivalued and is not uniquely determined. The actual output intensity depends on how the input-power value is approached. In other words, the output intensity of the beam at a given input intensity is dependent on the history of the device. This is known as hysteresis. As an example, we examine the I_o

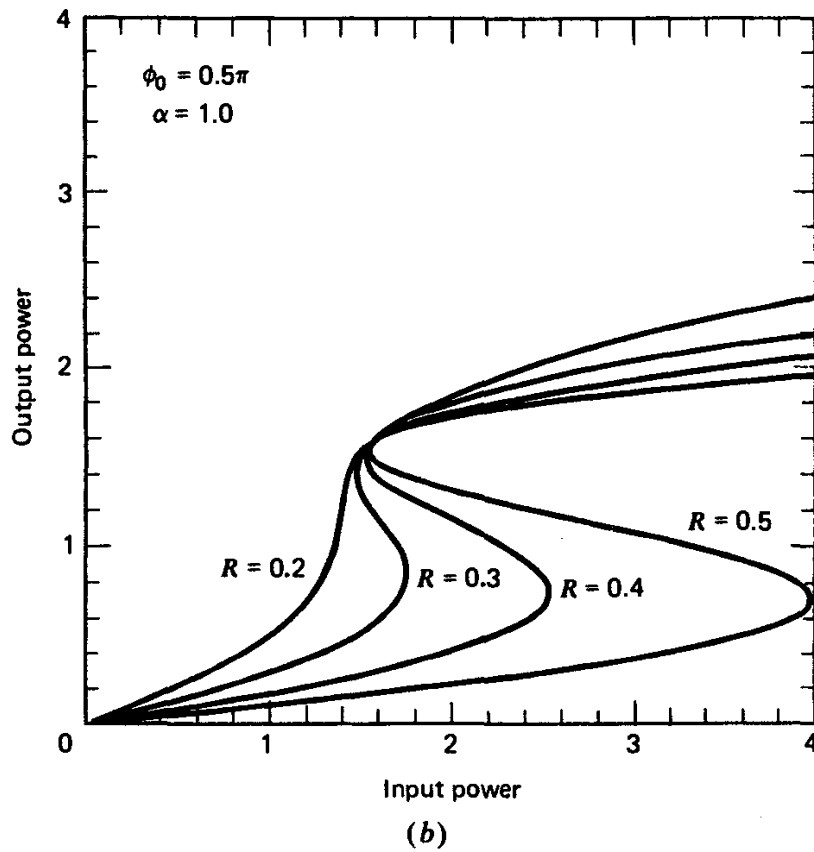
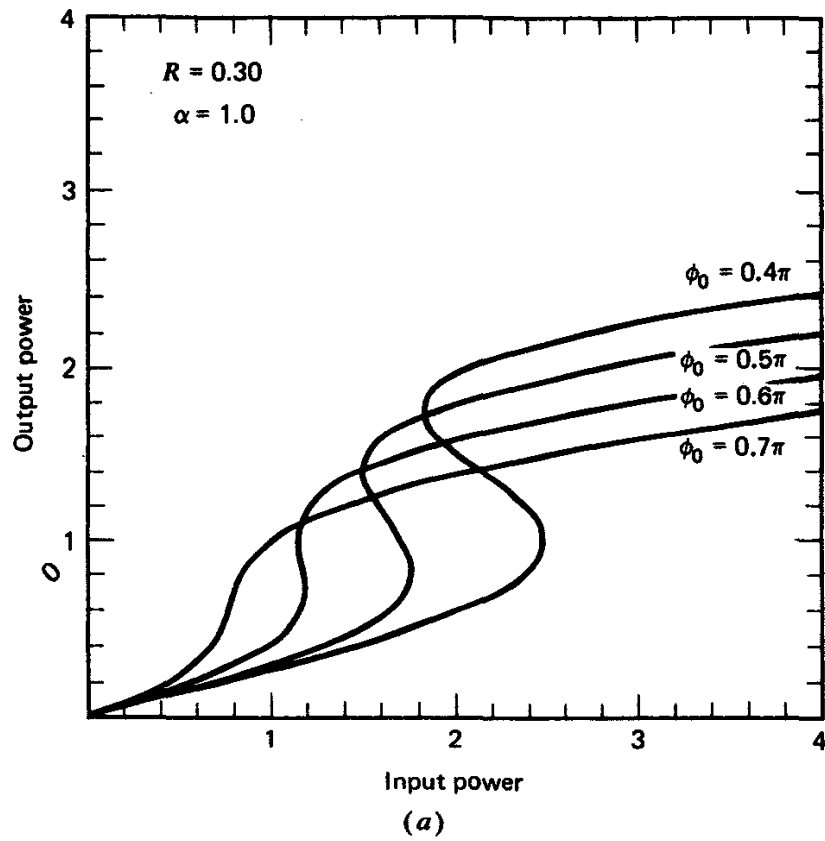


Figure 8.14. Output characteristics of a bistable Fabry-Perot resonator (a) with $R = 0.3$ and various ϕ_0 's; (b) with $\phi_0 = 0.5\pi$, $\alpha = 1$, and various R 's.

versus I_i curve of Fig. 8.15 when the input power is gradually increased from zero. Between the origin and point A , the output power is uniquely defined. As the input power reaches point A , the output power becomes multivalued. If the input power is increased adiabatically as it passes point A , the output power will follow curve AB until the input power reaches B . At point B an infinitesimal increment in the input power will cause the output power to switch abruptly to point C . Beyond point C , any increment in the input power will result in a uniquely determined output. Next consider what happens when the input power is decreased gradually. The output power will follow curve CD until point D . At this point, again an infinitesimal decrease in the input power will cause the output power to switch abruptly to point A . This hysteresis has been observed experimentally in a Fabry-Perot resonator containing a KDP electro-optic modulator using a He-Ne laser at 6328 \AA [4].

The switching between the low-transmissivity and high-transmissivity states can be accomplished either by increasing the input beam power momentarily or by varying the voltage bias to the modulator (note: ϕ_0 depends on the voltage bias). It can be shown that the curve BD represents an unstable state and is not physically realizable. The proof and the switching dynamics are beyond the scope of this book. The curve labeled $\phi_0 = 0.6\pi$ in fig. 8.14(a) is interesting, as it indicates a characteristic that

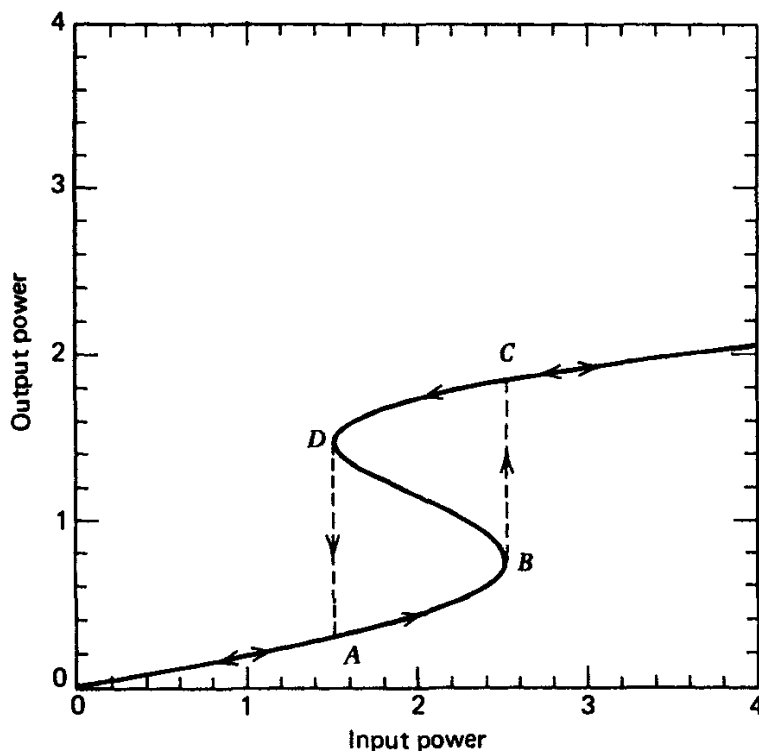


Figure 8.15. Output characteristics for the device shown in Fig. 8.13.

exhibits large differential gain. If the input power is tuned close to the knee of the curve, a small modulation of the input power will result in a large modulation of the output power. There are many other interesting functions of such a device, such as pulse shaping and power limiting (see Problem 8.6).

The bistability of a Fabry–Perot resonator using reflected-light feedback has also been demonstrated [5] (see Problem 8.7).

8.4.2. Bistable Electro-optic Amplitude Modulator

Optical bistability can also be produced with an electro-optic amplitude modulator by application of a feedback signal, proportional to the transmitted intensity, to the modulator crystal. A schematic diagram of this device operation is shown in Fig. 8.16. If the polarizer is oriented at 45° with respect to the principal axes of the crystal in the presence of the modulating field and the analyzer is crossed to the polarizer, the transmissivity of this amplitude modulator is given by Eq. (5.2-11):

$$I_o = I_i \sin^2 \frac{1}{2} \Gamma \quad (8.4-6)$$

where I_i and I_o are the input and output intensity, respectively, and Γ is the phase retardation of the crystal. Because of the feedback signal, the modulating voltage is proportional to the intensity of the transmitted beam. The phase retardation can therefore be written as

$$\frac{1}{2} \Gamma = \phi_0 + \alpha I_o \quad (8.4-7)$$

where α is a proportionality constant and ϕ_0 can be adjusted by a dc bias field applied to the crystal or by putting a Soleil–Babinet compensator in series with the crystal. Figure 8.17 shows plots of Eq. (8.4-6) for various

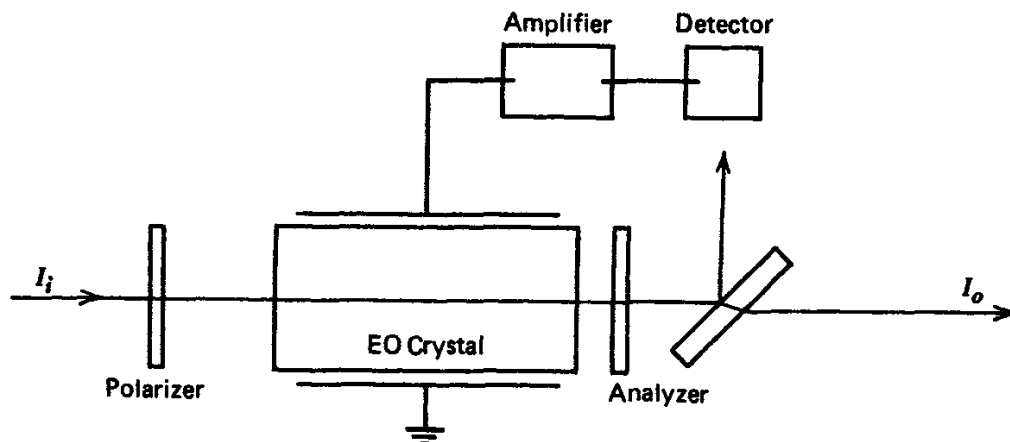


Figure 8.16. Schematic diagrams of a bistable electro-optic amplitude modulator.

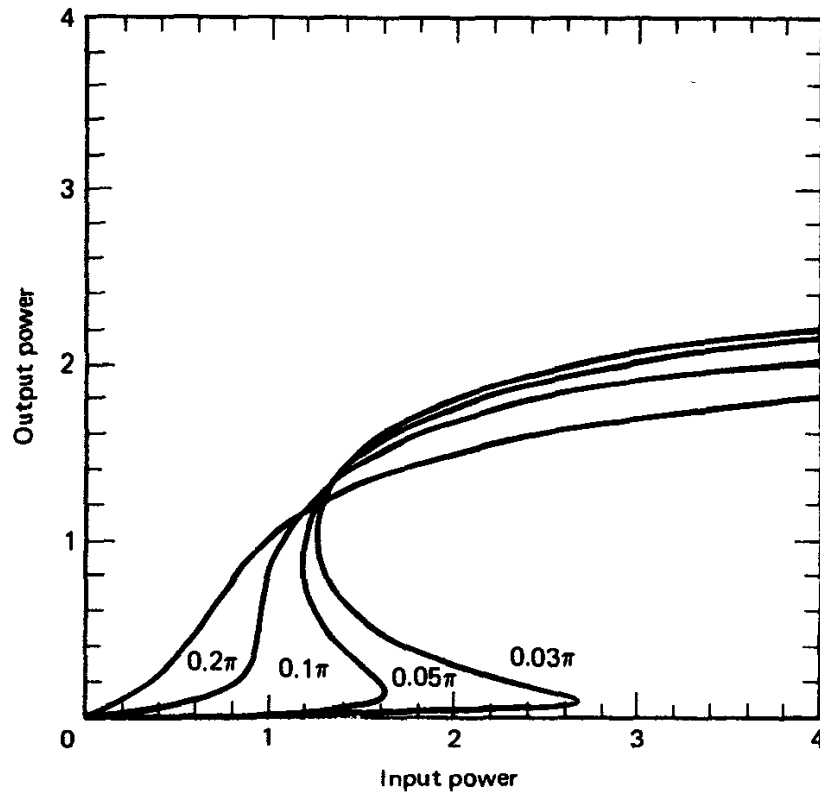


Figure 8.17. Output characteristics of the bistable electro-optic amplitude modulator for various values of ϕ_0 .

values of the parameter ϕ_0 with $\alpha = 1$. These curves exhibit all the nonlinear features of the bistable Fabry–Perot resonator. Optical bistability has been demonstrated using a LiNbO_3 electro-optic modulator [6, 7].

The bistable optical devices discussed above are potentially important in many applications, including optical communications and signal processing. They can function as differential amplifiers, switches, limiters, clippers, and so on.

8.5. ELECTRO-OPTIC FREQUENCY SHIFTING AND PULSE COMPRESSION

In our discussion of phase modulation, the modulating voltage was usually assumed to be sinusoidal in time, so that the index of refraction of the crystal also varies sinusoidally. We now consider a special but interesting case in which the modulating voltage varies linearly with time. As a result of the electro-optic effect, the refractive index of the crystal also varies linearly in time. The phase change of the transmitted beam can thus be written

$$\Delta\phi(t) = \phi_0 + \delta t, \quad (8.5-1)$$

where δ is the proportionality constant. The transmitted beam can thus be represented as

$$E(z, t) = e^{i(\omega_0 t + \delta t + \phi_0) - ikz}. \quad (8.5-2)$$

This is a plane wave with frequency $\omega_0 + \delta$. In other words, the frequency of the transmitted beam is upshifted ($\delta > 0$) because of this modulation. In fact, if we define $\phi(t)$ as the exponent of the plane wave (8.5-2), a generalized frequency can be defined as

$$\omega' = \frac{\partial \phi}{\partial t} = \omega_0 + \delta. \quad (8.5-3)$$

According to Eq. (8.5-3), the generalized frequency of a plane wave is the rate of change of the phase with time.

Let us now consider another special case of interest in which the modulating voltage varies quadratically with time. Again, the refractive index of the crystal follows the voltage and also varies quadratically with time via the electro-optic effect. The phase change of the transmitted beam is now

$$\Delta\phi(t) = \phi_0 - \alpha t^2, \quad (8.5-4)$$

where α is the proportionality constant. The transmitted beam can thus be written

$$E(z) = A(t) e^{i(\omega_0 t - \alpha t^2 + \phi_0) - ikz}. \quad (8.5-5)$$

If we consider $\partial\phi/\partial t$ as the local (or temporal) frequency at time t , then this frequency is given by

$$\omega' = \omega_0 - 2\alpha t. \quad (8.5-6)$$

This is called “chirping.” If a laser pulse passes through such a modulator, then there will be a linear frequency sweep across the pulse. In fact if $\alpha > 0$ and $t = 0$ is the center of the pulse, then the front (leading edge) of the pulse will be upshifted and the rear (tail) of the pulse will be downshifted. This is illustrated in Fig. 8.18.

8.5.1. Pulse Compression

Let us now consider the propagation of a frequency-chirped laser pulse through a dispersive medium. The original laser pulse has a width τ . As a result of the linear chirping, the leading edge of the pulse is upshifted in frequency and the rear of the pulse is downshifted (see Fig. 8-18). If the

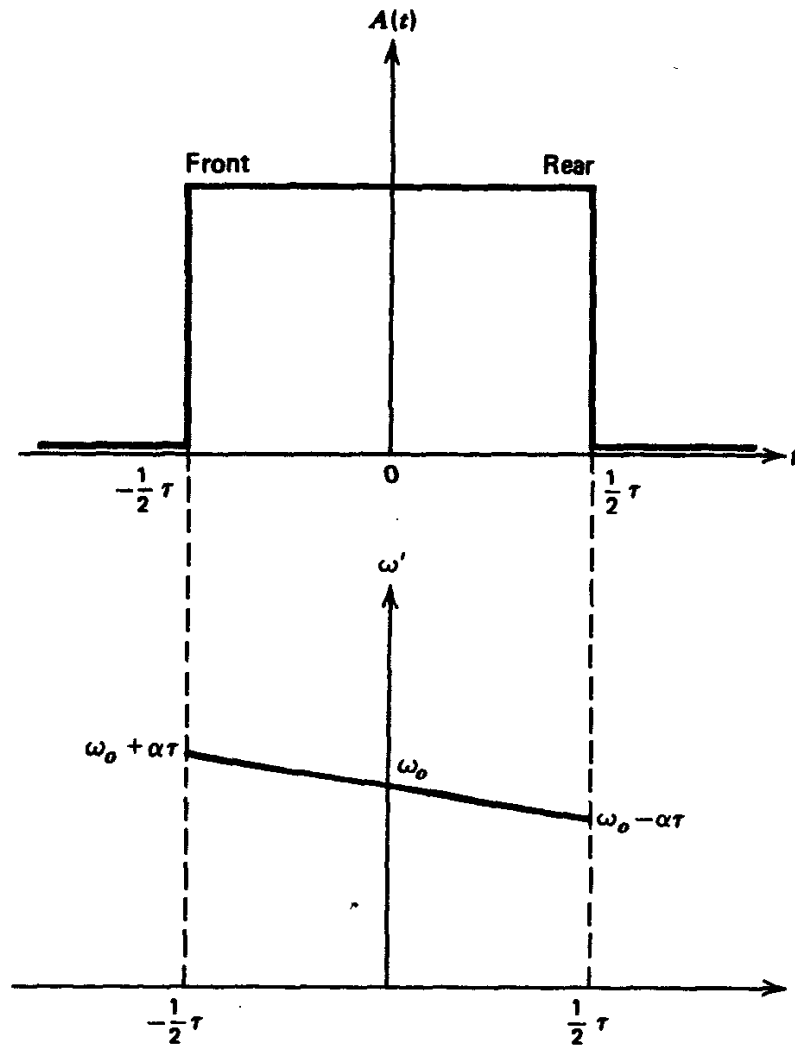


Figure 8.18. Chirping of a laser pulse.

pulse propagates in a medium with a group-velocity dispersion, and if the dispersion is such that the group velocity varies linearly with frequency, then the rear (low-frequency) part of the pulse can catch up with the front (high-frequency) part, and the pulse can be compressed to a minimum width $(2\alpha\tau)^{-1}$, where $2\alpha\tau$ is the magnitude of the frequency sweep.

Let a be the parameter which measures the group-velocity dispersion in the medium:

$$a \equiv \frac{1}{2} \frac{d}{d\omega} \left(\frac{1}{v_g} \right). \quad (8.5-7)$$

This same parameter was used to discuss the pulse spreading in Section 2.5. The condition for pulse compression is that the difference in the time of flight between the front part and the rear part of the laser pulse must be

equal to the original pulse duration, τ . Let T_f and T_r be the times of flight for the front and the rear part of the pulse, respectively. This condition becomes

$$\begin{aligned}\tau &= T_f - T_r = \frac{L}{v_g(\omega + \alpha\tau)} - \frac{L}{v_g(\omega - \alpha\tau)} \\ &= L \frac{d}{d\omega} \left(\frac{1}{v_g} \right) \cdot 2\alpha\tau,\end{aligned}\quad (8.5-8)$$

or equivalently

$$4aL\alpha = 1, \quad (8.5-9)$$

where we have used (8.5-7), and L is the length of the medium. The condition (8.5-9) for the chirping rate α and group-velocity dispersion a must be satisfied for maximum pulse compression.

We will now consider the problem of pulse compression analytically. Let the initial laser pulse be represented by

$$E_1(t) = A(t)e^{i\omega_0 t}, \quad (8.5-10)$$

where $A(t)$ is the envelope of the pulse. After the linear chirping, the laser pulse becomes

$$E_2(t) = A(t)e^{i\omega_0 t - iat^2}. \quad (8.5-11)$$

This frequency chirped pulse next passes through a dispersive medium. To determine the effect of this medium on the pulse, we expand it in a Fourier integral

$$E_2(t) = \int F(\omega) e^{i\omega t} d\omega, \quad (8.5-12)$$

where $F(\omega)$ is the frequency spectrum of the chirped pulse and is given by

$$F(\omega) = \frac{1}{2\pi} \int E_2(t') e^{-i\omega t'} dt'. \quad (8.5-13)$$

After passing through the dispersive medium, each frequency component of the pulse gains a phase of e^{-ikL} , where k is the wave number and is a function of frequency ω . This k can be expanded in a Taylor series as a

function of ω around ω_0 :

$$k(\omega) = k_0 + \left(\frac{dk}{d\omega}\right)_0 (\omega - \omega_0) + \frac{1}{2} \left(\frac{d^2k}{d\omega^2}\right) (\omega - \omega_0)^2, \quad (8.5-14)$$

where k_0 is the wave number for the center frequency, ω_0 , and $(dk/d\omega)_0$ is the reciprocal of the group velocity, v_g^{-1} , at ω_0 . By using the definition (8.5-7) and the definition of the group velocity, Eq. (8.5-14) can be written

$$k(\omega) = k_0 + \left(\frac{1}{v_g}\right)_0 (\omega - \omega_0) + a(\omega - \omega_0)^2. \quad (8.5-15)$$

The transmitted pulse can be written

$$E_2(t) = \int F(\omega) e^{i\omega t - ik(\omega)L} d\omega. \quad (8.5-16)$$

Substitution of Eq. (8.5-15) for $k(\omega)$ in Eq. (8.5-16) leads to

$$E_3(t) = \int F(\omega) e^{i\omega t - ik_0 L - i(\omega - \omega_0)T - ia(\omega - \omega_0)^2 L} d\omega \quad (8.5-17)$$

where $T = L/v_g$ is the time of flight for the center frequency component. We now substitute Eq. (8.5-13) for $F(\omega)$ in Eq. (8.5-17), use Eq. (8.5-11), and then perform the integration over ω . This leads to

$$E_3(t) = \frac{1}{2\pi} \sqrt{\frac{\pi}{iaL}} e^{i(\omega_0 t - k_0 L)} \int A(t') e^{i(t' + T - t)^2 / 4aL - ia t'^2} dt', \quad (8.5-18)$$

where we have used the integral formula

$$\int_{-\infty}^{\infty} e^{-\alpha x^2 - \beta x} dx = \sqrt{\frac{\pi}{\alpha}} \exp\left(\frac{\beta^2}{4\alpha}\right). \quad (8.5-19)$$

If we now define $A_3(t)$ as the envelope of the transmitted pulse such that

$$E_3(t) = A_3(t) e^{i\omega_0 t - ik_0 L}, \quad (8.5-20)$$

then this envelope can be written, according to Eq. (8.5-18),

$$A_3(t) = \frac{1}{\sqrt{4i\pi aL}} \int A(t') e^{i(t' + T - t)^2 / 4aL - ia t'^2} dt'. \quad (8.5-21)$$

We now assume that the original pulse has a Gaussian distribution

$$A(t') = e^{-t'^2/2\tau^2}. \quad (8.5-22)$$

Substituting Eq. (8.5-22) for $A(t')$ in Eq. (8.5-21) and using Eq. (8.5-19), we obtain

$$A_3(t) = (i4aLB)^{-1/2} \exp \left[i \frac{(t-T)^2}{4aL} - \frac{(t-T)^2}{16a^2L^2B} \right] \quad (8.5-23)$$

with

$$B = \frac{1}{2\tau^2} - i \left(\frac{1}{4aL} - \alpha \right). \quad (8.5-24)$$

The pulse width of the transmitted laser pulse, according to Eqs. (8.5-23) and (8.5-24), is

$$\tau_3 = \sqrt{8} aL \left[\left(\frac{1}{2\tau^2} \right)^2 + \left(\frac{1}{4aL} - \alpha \right)^2 \right]^{1/4}. \quad (8.5-25)$$

From the above expression, it is obvious that the pulse width is minimum when $\alpha = 1/4aL$, which is the condition derived by the semiintuitive method (8.5-9). By substituting $aL = 1/4\alpha$ in Eq. (8.5-25), we obtain the expression for the minimum pulse width

$$(\tau_3)_{\min} = \frac{1}{2\alpha\tau}. \quad (8.5-26)$$

The technique mentioned above has been used to compress pulses from 500 ps to 270 ps [8]. It can be shown from Eqs. (8.5-26) and (8.5-9) that the length of the dispersive medium required for maximum compression is

$$L = \frac{\tau\tau_3}{2a}. \quad (8.5-27)$$

This length is proportional to the product of the original pulse width and the final pulse width, and is inversely proportional to the dispersion parameter a . For pulses with width of the order of 100 ps, this length L is impractically long for most dispersive materials. The dispersive element used in [8] was an asymmetric Fabry-Perot cavity which was first proposed

by Gires and Tournois [9]. It can be shown that the phase shift of the light reflected from the asymmetric Fabry–Perot interferometer provides the necessary dispersive properties, provided the cavity length is adjusted properly and the reflectivity of the front mirror is high (see Problem 8.8).

According to the above discussion, it normally takes two steps to compress an optical pulse. The first step involves the broadening of the spectrum. The second step is the propagation of the spectrally broadened pulse through a dispersive medium. A grating pair may be used to substitute for the dispersive medium. Recently, a pulse of 30 fs duration was produced by a similar technique [12]. In this approach, a 70 fs optical pulse is spectrally broadened by propagating through an optical fiber and then compressed to 30 fs by a grating pair. The spectral broadening in passage through the fiber is a result of self-phase modulation due to the Kerr effect and the temporal variation of the optical intensity.

8.6. ELECTRO-OPTIC BEAM DEFLECTION

The electro-optic effect is also used to deflect light beams [10]. The operation of such a beam deflector is shown in Fig. 8.19. Imagine an optical wavefront incident on a crystal in which the optical path length depends on the transverse position x . This could be achieved by having the velocity of propagation—that is, the index of refraction n —depend on x , as in Fig. 8.19. Taking the index variation to be a linear function of x , the upper ray A “sees” an index $n + \Delta n$ and hence traverses the crystal in a time

$$T_A = \frac{L}{c}(n + \Delta n).$$

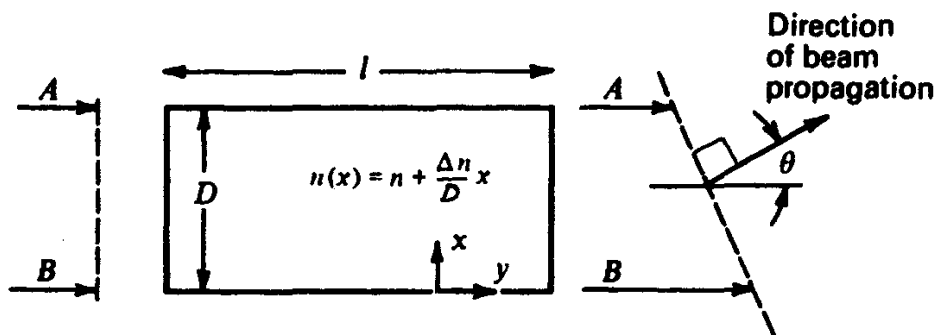


Figure 8.19. Schematic diagram of a beam deflector. The index of refraction varies linearly in the x direction as $n(x) = n_0 + ax$. Ray B “gains” on ray A in passing through the crystal axis, thus causing a tilting of the wavefront by θ .

The lower portion of the wavefront (that is, ray B) “sees” an index n and has a transit time

$$T_B = \frac{L}{c}n.$$

The difference in transit times results in a lag of ray A with respect to B of

$$\Delta y = \frac{c}{n}(T_A - T_B) = L \frac{\Delta n}{n},$$

which corresponds to a deflection of the beam-propagation axis, as measured inside the crystal, at the output face of

$$\theta' = -\frac{\Delta y}{D} = -\frac{L\Delta n}{Dn} = -\frac{L}{n} \frac{dn}{dx}, \quad (8.6-1)$$

where we have replaced $\Delta n/D$ by dn/dx . The external deflection angle θ , measured with respect to the horizontal axis, is related to θ' by Snell's law,

$$\frac{\sin \theta}{\sin \theta'} = n,$$

which, using (8.6-1) and assuming $\sin \theta \approx \theta \ll 1$, yields

$$\theta = \theta'n = -L \frac{\Delta n}{D} = -L \frac{dn}{dx}. \quad (8.6-2)$$

A simple realization of such a deflector using a KH_2PO_4 (KDP) crystal is shown in Fig. 8.20. It consists of two KDP prisms with edges along the x' , y' , and z directions. These are the principal axes of the index ellipsoid when an electric field is applied along the z direction as described in the example of Section 7.2. The two prisms have their z axes opposite to one another, but are otherwise similarly oriented. The electric field is applied parallel to the z direction, and the light propagates in the y' direction with its polarization along x' . For this case, the index of refraction “seen” by ray A , which propagates entirely in the upper prism, is given by Eq. (7.2-9) as

$$n_A = n_o - \frac{n_o^3}{2} r_{63} E_z,$$

while in the lower prism the sign of the electric field with respect to the z axis is reversed, so that

$$n_B = n_o + \frac{n_o^3}{2} r_{63} E_z.$$

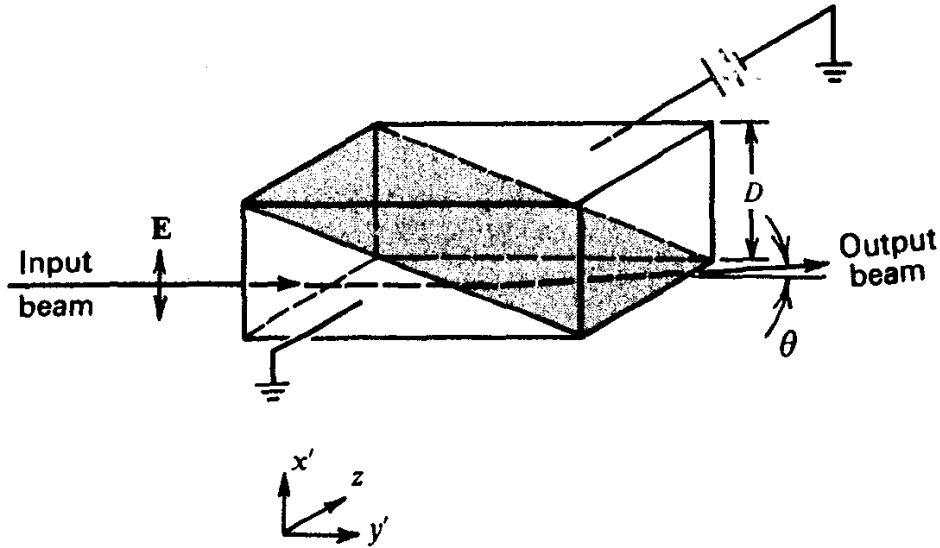


Figure 8.20. Double-prism KDP beam deflector. Upper and lower prisms have their z axes reversed with respect to each other. The deflection field is applied parallel to z .

Using Eq. (8.6-2) with $\Delta n = n_A - n_B$, the deflection angle is given by

$$\theta = \frac{L}{D} n_o^3 r_{63} E_z. \quad (8.6-3)$$

According to Eq. (2.2-19), every optical beam has a finite far-field divergence angle, which we call θ_{beam} . It is clear that a fundamental figure of merit for the deflector is not the angle of deflection θ which can be changed merely by a lens, but the factor N by which θ exceeds θ_{beam} . If one were, as an example, to focus the output beam, then N would correspond to the number of resolvable spots that can be displayed in the focal plane using fields with a magnitude up to E_z .

To get an expression for N , we assume that the crystal is placed astride the "waist" of a Gaussian (fundamental) beam with a spot size ω_0 . According to Eq. (2.2-19) the far-field diffraction angle in air is

$$\theta_{\text{beam}} = \frac{\lambda}{\pi \omega_0}.$$

Such a beam can be passed through a crystal with height $D = 2\omega_0$, so that, by using Eq. (8.6-3), the number of resolvable spots is

$$N = \frac{\theta}{\theta_{\text{beam}}} = \frac{\pi L n_o^3 r_{63}}{2\lambda} E_z. \quad (8.6-4)$$

It follows directly from Eq. (8.6-4), the details being left as a problem, that an electric field that induces a birefringent retardation (in a distance l) $\Delta\Gamma = \pi$ will yield $N \approx 1$. Therefore, fundamentally, the electro-optic extinction of a beam, which according to Eq. (8.6-4) requires $\Gamma = \pi$, is equivalent to a deflection by one spot diameter.

The deflection of an optical beam by diffraction from a sound wave is discussed in Chapter 10.

PROBLEMS

8.1. *Field of view of $\bar{4}3m$ electro-optic modulator.* Consider the electro-optic effect in a crystal with point-group symmetry $\bar{4}3m$ such that in the presence of the electric field along the cubic axis the principal refractive indices are given by

$$n_{x'} = n + \frac{1}{2}n^3 r_{41} E,$$

$$n_{y'} = n - \frac{1}{2}n^3 r_{41} E,$$

$$n_{z'} = n.$$

- (a) Assume that the plate is z' -cut with thickness l . Show that the phase retardation for the normally incident light is

$$\Gamma_0 = \frac{2\pi}{\lambda} n^3 r_{41} E l.$$

- (b) Let the incident light beam propagate along the direction (θ, ϕ) , where θ is the angle of incidence and ϕ is the azimuth angle of incidence. Show that the wave vector of the incident light can be written

$$\mathbf{k} = \frac{2\pi}{\lambda} (\sin \theta \cos \phi \mathbf{x}' + \sin \theta \sin \phi \mathbf{y}' + \cos \theta \mathbf{z}').$$

- (c) Show that the wave vectors for the wave in the crystal can be written

$$\mathbf{k}' = k_{x'} \mathbf{x}' + k_{y'} \mathbf{y}' + k_{z'} \mathbf{z},$$

where

$$k_{x'} = \frac{2\pi}{\lambda} \sin \theta \cos \phi,$$

$$k_{y'} = \frac{2\pi}{\lambda} \sin \theta \sin \phi.$$

- (d) Substitute k_x' , k_y' , and k_z' into Eq. (4.2-8). Show that a quadratic equation of k_z^2 can be obtained. Solve for the roots, and calculate the phase retardation

$$\Gamma = (k_{z'2} - k_{z'1})l.$$

Show that

$$\Gamma = \Gamma_0 \left[1 + \frac{\sin^4 \theta (\cos^2 \phi - \sin^2 \phi)}{4n^2(n^2 - \sin^2 \theta)} \right]^{1/2}.$$

- (e) Show that in the extreme case ($\theta = \frac{1}{2}\pi$, $\phi = 0$ or $\frac{1}{2}\pi$)

$$\Gamma = \Gamma_0 \left[1 + \frac{1}{4n^2(n^2 - 1)} \right]^{1/2}.$$

In the case of GaAs, where $n = 3.4$, the phase retardation for the extreme angle of incidence is different from that of the normal incidence by a factor of 1.0×10^{-3} .

- 8.2. Show that the slope of the Fabry-Perot transmission curve at the half-intensity point is

$$\left(\frac{dT}{d\phi} \right)_{1/2} = \frac{F}{\pi} = \frac{\sqrt{R}}{1 - R}.$$

Evaluate this slope for the case when the mirror reflectivity is 90% (i.e., $R = 0.9$).

- 8.3. *Transit-time limitations.* The reduction factor in the modulation depth for a lumped modulator (8.3-3) can be derived by the following semiintuitive approach.

- (a) If the field E changes appreciably during the transit time $\tau = nl/c$ of light through the crystal, show that the phase retardation can be written

$$\Gamma = \frac{1}{\tau} \Gamma_0 \int_t^{t+\tau} \sin \omega_m t' dt'$$

where Γ_0 is the peak phase retardation at dc ($\omega_m = 0$) and the field is assumed to be sinusoidal (i.e., $E \propto \sin \omega_m t$).

- (b) Evaluate the integral in (a) and show that

$$\Gamma = \Gamma_0 \cdot \frac{\sin \frac{1}{2} \omega_m \tau}{\frac{1}{2} \omega_m \tau} \sin(\omega_m t + \frac{1}{2} \omega_m \tau).$$

8.4. *Gaussian-beam modulation.* Consider the propagation of a Gaussian beam in a crystal rod with a fixed length l .

- Show that from the symmetry point of view the minimum rod diameter occurs when the beam waist is located at the center of the rod.
- Show that when the waist of a beam is located at the center, minimum rod diameter occurs when the confocal beam parameter z_0 equals half the length, l (i.e., $z_0 = \frac{1}{2}l$).
- Find this minimum diameter.

8.5. *Differential gain.* Bistable optical devices often exhibit differential gain. The gain factor g is defined as

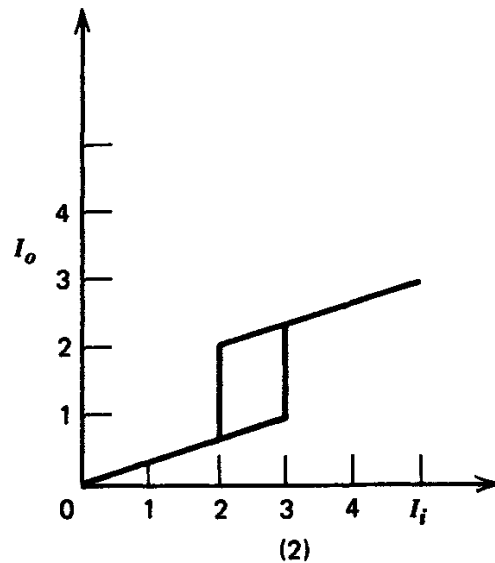
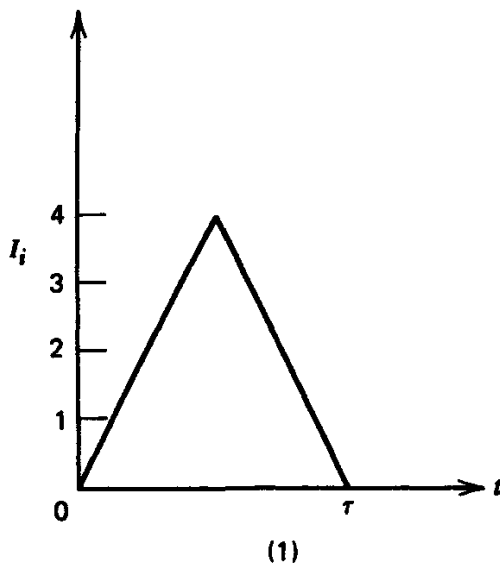
$$g = \frac{dI_o}{dI_i}.$$

- Derive an expression for the differential gain g for the bistable Fabry-Perot resonator. Show that g can be positive or negative or even infinite.
- Derive an expression for the differential gain g for the device shown in Fig. 8.16. Show that infinite gain g occurs when

$$\tan(\phi_0 + \alpha I_o) = 2\alpha I_o.$$

- Explain how this differential gain can be used to build an optical triode.

8.6. *Pulse shaping.* Consider the propagation of a light pulse through a bistable optical device.



- (a) Show that the transmitted pulse shape will be different from that of the input pulse even if there is no dispersion.
- (b) The pulse shaping due to transmission through a bistable optical device can be easily demonstrated by a graphic method. Let the input pulse $I_i(t)$ be represented by curve (1) in the accompanying drawing, and I_o versus I_i be represented by curve (2). Obtain the transmitted pulse graphically.

8.7. *Bistable Fabry-Perot resonator via reflection feedback.*

- (a) Derive a relation between the input power and the transmitted power by assuming

$$\phi = \phi'_0 + \alpha' I_r,$$

where I_r is the reflected intensity and α' , ϕ'_0 are constants.

- (b) If the Fabry-Perot resonator is lossless, I_o can be replaced by $I_i - I_r$. Derive an expression that links I_r and I_i . Show that bistability can exist.
- (c) Try to construct the curve of I_o versus I_i from the curve of I_r versus I_i .

8.8. *Group-velocity dispersion in an asymmetric Fabry-Perot resonator.*

- (a) Let l be the length of a dispersive medium. A plane wave $e^{i(\omega t - kz)}$ propagating through this medium will gain a phase factor of e^{-ikl} . Let $\Phi(\omega) = -k(\omega)l$. Show that the group-velocity dispersion a is related to the dispersion $\Phi(\omega)$ by

$$a = \frac{-1}{2l} \frac{d^2\Phi}{d\omega^2}.$$

- (b) Show that the condition for maximum pulse compression can be written

$$2\alpha \frac{d^2\Phi}{d\omega^2} = -1.$$

- (c) Let τ_1 and τ_3 be the original and final pulse widths, respectively. Show that the condition for maximum pulse compression is

$$\frac{d^2\Phi}{d\omega^2} = -\tau_1\tau_3.$$

- (d) Show that the phase shift Φ in an empty resonator is

$$\Phi = -2 \tan^{-1} \left(\frac{1 + \sqrt{R}}{1 - \sqrt{R}} \tan \frac{\omega}{c} l \right),$$

where l is the length of the cavity and R is the reflectivity of the front mirror.

- (e) Assume that R is a constant (i.e., independent of ω). Show that

$$\frac{d\Phi}{d\omega} = - \frac{2l}{c} \frac{1 + \sqrt{R}}{1 - \sqrt{R}} \cdot \frac{(1 - \sqrt{R})^2}{(1 - \sqrt{R})^2 + 4\sqrt{R} \sin^2(\omega l/c)}.$$

If $d\Phi/d\omega$ is plotted against ω , the curve consists of a series of peaks similar to the Fabry-Perot comb structures with a finesse f given by

$$f = \frac{\pi R^{1/4}}{1 - \sqrt{R}}.$$

- (f) Show that at the half-maximum point of $d\Phi/d\omega$,

$$\left(\frac{d^2\Phi}{d\omega^2} \right)_{1/2} = \pm \frac{2R^{1/4}}{1 - \sqrt{R}} \frac{1 + \sqrt{R}}{1 - \sqrt{R}} \cdot \left(\frac{l}{c} \right)^2,$$

where the sign depends on which side of the peak is evaluated. Thus the condition for maximum pulse compression becomes

$$\frac{2R^{1/4}}{1 - \sqrt{R}} \frac{1 + \sqrt{R}}{1 - \sqrt{R}} \cdot \left(\frac{l}{c} \right)^2 = \tau\tau_3.$$

- (g) Let $\tau = 100$ ps, $\tau_3 = 10$ ps. Find the length of the cavity for $R = 0.5$, $R = 0.9$. Answer: 0.16 cm, 0.0250 cm.

REFERENCES

1. I. P. Kaminow and W. M. Sharpless, "Performance of LiTaO₃ and LiNbO₃ light modulators at 4 GHz," *Appl. Opt.* **6**, 351 (1967).
2. C. S. Namba, "Electro-optical effect of zincblende," *J. Opt. Soc. Am.* **51**, 76 (1961).
3. H. M. Gibbs, "Differential gain and bistability using a sodium-filled Fabry-Perot interferometer," *Phys. Rev. Lett.* **36**, 1135 (1976).

4. P. W. Smith and E. H. Turner, "A bistable Fabry-Perot resonator," *Appl. Phys. Lett.* **30**, 280 (1977).
5. P. W. Smith, E. H. Turner, and B. B. Mumford, "Nonlinear electro-optical Fabry-Perot devices using reflected light feedback," *Opt. Lett.* **2**, 55 (1978).
6. E. Garmire, J. H. Marburger, and S. D. Allen, "Incoherent mirrorless bistable optical devices," *Appl. Phys. Lett.* **32**, 320 (1978).
7. A. Feldman, "Bistable optical systems based on a Pockels cells," *Opt. Lett.* **4**, 115 (1979).
8. M. A. Duguay and J. W. Hansen, "Compression of pulses from a mode-locked He-Ne laser," *Appl. Phys. Lett.* **14**, 14 (1969).
9. F. Gires and P. Tournois, "An interferometer useful for pulse compression of a frequency modulated light pulse," *C. R. Acad. Sci.*, (Paris) **258**, 6112 (June 1964).
10. V. J. Fowler and J. Schlafer, "A survey of laser beam deflection techniques," *Proc. IEEE* **54**, 1437 (1966).
11. See, for example, A. Yariv, "Introduction to optical electronics," (Holt, Rinehart and Winston, New York, 1976).
12. C. V. Shank, R. L. Fork, R. Yen and W. J. Tomlinson, "Compression of femtosecond optical pulses," Conference on lasers and electro-optics (Phoenix, Arizona, April 14-16, 1982).

9

Acousto-optics

Acousto-optics deals with the interaction of optical waves with the acoustic waves in material media. Such an interaction was first predicted by Brillouin in 1922; it was experimentally verified in 1932 by Debye and Sears in the U.S. and by Lucas and Biguard in France. The most interesting phenomenon associated with the interaction of light with sound waves is the diffraction of light by the acoustically perturbed medium. When an acoustic wave propagates in a medium, there is an associated strain field. The strain results in a change in the index of refraction. This is referred to as the photoelastic effect. The strain field is a periodic function of position for a plane acoustic wave. The index of refraction of the medium becomes periodically perturbed, and therefore Bragg coupling takes place in the manner described in Chapter 6. The acousto-optic interaction affords a convenient way of probing the sound field in a solid as well as manipulating the laser radiation. The modulation of light by acousto-optic interaction is used in a number of applications, including light modulators, beam deflectors, signal processors, tunable filters, and spectrum analyzers. Some of these device applications will be discussed in the next chapter.

9.1. THE PHOTOELASTIC EFFECT

The photoelastic effect in a material couples the mechanical strain to the optical index of refraction. This effect occurs in all states of matter and is traditionally described by

$$\Delta\eta_{ij} = \Delta\left(\frac{1}{n^2}\right)_{ij} = p_{ijkl}S_{kl}, \quad (9.1-1)$$

where $\Delta\eta_{ij}$ [or $\Delta(1/n^2)_{ij}$] is the change in the optical impermeability tensor and S_{kl} is the strain tensor. The coefficients p_{ijkl} form the strain-optic tensor. In the expression (9.1-1), higher-order terms involving powers of S_{kl}

are neglected, because these terms are usually small compared with the linear term ($S_{kl} \sim 10^{-5}$ typically). The index ellipsoid of a crystal in the presence of an applied strain field is thus given by

$$(\eta_{ij} + p_{ijkl}S_{kl})x_i x_j = 1. \quad (9.1-2)$$

In the event when the strain field vanishes ($S_{kl} = 0$), the index ellipsoid reduces to Eq. (7.1-1) in the principal coordinate system. Since both η_{ij} and S_{kl} are symmetric tensors, the indices i and j as well as k and l in Eq. (9.1-1) can be permuted. The permutation symmetry of the strain-optic tensor, p_{ijkl} , is identical to that of the quadratic electro-optic tensor s_{ijkl} , (7.1-9) and (7.1-8). It is thus convenient to use the contracted indices to abbreviate the notation. Equation (9.1-1) then becomes

$$\Delta \left(\frac{1}{n^2} \right)_i = p_{ij} S_j, \quad i, j = 1, 2, \dots, 6, \quad (9.1-3)$$

where S_j are the strain components. The equation of the index ellipsoid in the presence of a strain field can now be written

$$\begin{aligned} & x^2 \left(\frac{1}{n_x^2} + p_{11}S_1 + p_{12}S_2 + p_{13}S_3 + p_{14}S_4 + p_{15}S_5 + p_{16}S_6 \right) \\ & + y^2 \left(\frac{1}{n_y^2} + p_{21}S_1 + p_{22}S_2 + p_{23}S_3 + p_{24}S_4 + p_{25}S_5 + p_{26}S_6 \right) \\ & + z^2 \left(\frac{1}{n_z^2} + p_{31}S_1 + p_{32}S_2 + p_{33}S_3 + p_{34}S_4 + p_{35}S_5 + p_{36}S_6 \right) \\ & + 2yz(p_{41}S_1 + p_{42}S_2 + p_{43}S_3 + p_{44}S_4 + p_{45}S_5 + p_{46}S_6) \\ & + 2zx(p_{51}S_1 + p_{52}S_2 + p_{53}S_3 + p_{54}S_4 + p_{55}S_5 + p_{56}S_6) \\ & + 2xy(p_{61}S_1 + p_{62}S_2 + p_{63}S_3 + p_{64}S_4 + p_{65}S_5 + p_{66}S_6) \\ & = 1, \quad (9.1-4) \end{aligned}$$

where n_x , n_y , and n_z are the principal indices of refraction. The strain-optic coefficients p_{ij} are usually defined in the principal coordinate system. The new index ellipsoid in the presence of the strain field is in general different

from the zero-field index ellipsoid. The strain field changes the dimensions as well as the orientation of the index ellipsoid (7.1-1). This change is, of course, dependent upon the applied strain field as well as the strain-optic coefficients p_{ij} according to Eq. (9.1-4). The form, but not the magnitude, of the strain-optic coefficients p_{ij} can be derived from the symmetry of the crystal. This point-group symmetry dictates which of the 36 coefficients are zero, as well as relationships that may exist between the nonvanishing coefficients. Table 9.1 illustrates the forms of the strain-optic coefficients for all classes of crystal symmetry. Notice that these forms are identical to those of the quadratic electro-optic coefficients (see Table 7.4). The measured strain-optic coefficients of some crystals are found in Table 9.2.

9.1.1. Example: The Acousto-optic Effect in Water

Consider the propagation of a sound wave in water. Let the sound wave be a longitudinal wave propagating along the z direction with the particle displacement given by

$$\mathbf{u}(z, t) = A\hat{\mathbf{z}} \cos(\Omega t - Kz),$$

where A is the amplitude of oscillation, Ω is the sound frequency, and K is the wave number. The strain field associated with this sound wave is

$$S_3 = KA \sin(\Omega t - Kz) \equiv S \sin(\Omega t - Kz),$$

where S is defined as KA . Water is an isotropic medium. Thus, according to Table 9.1 and Eq. (9.1-3), the change in the dielectric impermeability is

$$\Delta\eta_{11} = \Delta\left(\frac{1}{n^2}\right)_1 = p_{12}S \sin(\Omega t - Kz),$$

$$\Delta\eta_{22} = \Delta\left(\frac{1}{n^2}\right)_2 = p_{12}S \sin(\Omega t - Kz),$$

$$\Delta\eta_{33} = \Delta\left(\frac{1}{n^2}\right)_3 = p_{11}S \sin(\Omega t - Kz),$$

$$\Delta\eta_{ij} = 0 \quad \text{for } i \neq j.$$

Table 9.1. Forms of the Elasto-optic Coefficients in Contracted Notation for all Classes of Crystal Symmetry

Triclinic (36)† $\begin{pmatrix} P_{11} & P_{12} & P_{13} & P_{14} & P_{15} & P_{16} \\ P_{21} & P_{22} & P_{23} & P_{24} & P_{25} & P_{26} \\ P_{31} & P_{32} & P_{33} & P_{34} & P_{35} & P_{36} \\ P_{41} & P_{42} & P_{43} & P_{44} & P_{45} & P_{46} \\ P_{51} & P_{52} & P_{53} & P_{54} & P_{55} & P_{56} \\ P_{61} & P_{62} & P_{63} & P_{64} & P_{65} & P_{66} \end{pmatrix}$					
Monoclinic (20)			Orthorhombic (12)		
$\begin{pmatrix} P_{11} & P_{12} & P_{13} & 0 & P_{15} & 0 \\ P_{21} & P_{22} & P_{23} & 0 & P_{25} & 0 \\ P_{31} & P_{32} & P_{33} & 0 & P_{35} & 0 \\ 0 & 0 & 0 & P_{44} & 0 & P_{46} \\ P_{51} & P_{52} & P_{53} & 0 & P_{55} & 0 \\ 0 & 0 & 0 & P_{64} & 0 & P_{66} \end{pmatrix}$			$\begin{pmatrix} P_{11} & P_{12} & P_{13} & 0 & 0 & 0 \\ P_{21} & P_{22} & P_{23} & 0 & 0 & 0 \\ P_{31} & P_{32} & P_{33} & 0 & 0 & 0 \\ 0 & 0 & 0 & P_{44} & 0 & 0 \\ 0 & 0 & 0 & 0 & P_{55} & 0 \\ 0 & 0 & 0 & 0 & 0 & P_{66} \end{pmatrix}$		
Tetragonal (10) classes $4, \bar{4}, 4/m$			Tetragonal (7) classes $4mm, 422, 4/mmm$		
$\begin{pmatrix} P_{11} & P_{12} & P_{13} & 0 & 0 & P_{16} \\ P_{12} & P_{11} & P_{13} & 0 & 0 & -P_{16} \\ P_{31} & P_{31} & P_{33} & 0 & 0 & 0 \\ 0 & 0 & 0 & P_{44} & P_{45} & 0 \\ 0 & 0 & 0 & -P_{45} & P_{44} & 0 \\ P_{61} & -P_{61} & 0 & 0 & 0 & P_{66} \end{pmatrix}$			$\begin{pmatrix} P_{11} & P_{12} & P_{13} & 0 & 0 & 0 \\ P_{12} & P_{11} & P_{13} & 0 & 0 & 0 \\ P_{31} & P_{31} & P_{33} & 0 & 0 & 0 \\ 0 & 0 & 0 & P_{44} & 0 & 0 \\ 0 & 0 & 0 & 0 & P_{44} & 0 \\ 0 & 0 & 0 & 0 & 0 & P_{66} \end{pmatrix}$		
Trigonal (12) classes $3, \bar{3}$					
$\begin{pmatrix} P_{11} & P_{12} & P_{13} & P_{14} & P_{15} & P_{16} \\ P_{12} & P_{11} & P_{13} & -P_{14} & -P_{15} & -P_{16} \\ P_{31} & P_{31} & P_{33} & 0 & 0 & 0 \\ P_{41} & -P_{41} & 0 & P_{44} & P_{45} & -P_{51} \\ P_{51} & -P_{51} & 0 & -P_{45} & P_{44} & P_{41} \\ -P_{16} & P_{16} & 0 & -P_{15} & P_{14} & \frac{1}{2}(P_{11} - P_{12}) \end{pmatrix}$					

Table 9.1. (Continued).

Trigonal (8)

classes $3m, 32, \bar{3}m$

$$\begin{pmatrix} p_{11} & p_{12} & p_{13} & p_{14} & 0 & 0 \\ p_{12} & p_{11} & p_{13} & -p_{14} & 0 & 0 \\ p_{13} & p_{13} & p_{33} & 0 & 0 & 0 \\ p_{41} & -p_{41} & 0 & p_{44} & 0 & 0 \\ 0 & 0 & 0 & 0 & p_{44} & p_{41} \\ 0 & 0 & 0 & 0 & p_{14} & \frac{1}{2}(p_{11} - p_{12}) \end{pmatrix}$$

Hexagonal (8)

classes $6, \bar{6}, 6/m$

$$\begin{pmatrix} p_{11} & p_{12} & p_{13} & 0 & 0 & p_{16} \\ p_{12} & p_{11} & p_{13} & 0 & 0 & -p_{16} \\ p_{31} & p_{31} & p_{33} & 0 & 0 & 0 \\ 0 & 0 & 0 & p_{44} & p_{45} & 0 \\ 0 & 0 & 0 & -p_{45} & p_{44} & 0 \\ -p_{16} & p_{16} & 0 & 0 & 0 & \frac{1}{2}(p_{11} - p_{12}) \end{pmatrix}$$

Hexagonal (6)

classes $\bar{6}m2, 6mm, 622, 6/mmm$

$$\begin{pmatrix} p_{11} & p_{12} & p_{13} & 0 & 0 & 0 \\ p_{12} & p_{11} & p_{13} & 0 & 0 & 0 \\ p_{31} & p_{31} & p_{33} & 0 & 0 & 0 \\ 0 & 0 & 0 & p_{44} & 0 & 0 \\ 0 & 0 & 0 & 0 & p_{44} & 0 \\ 0 & 0 & 0 & 0 & 0 & \frac{1}{2}(p_{11} - p_{12}) \end{pmatrix}$$

Cubic (4)

classes $23, m\bar{3}$

$$\begin{pmatrix} p_{11} & p_{12} & p_{21} & 0 & 0 & 0 \\ p_{21} & p_{11} & p_{12} & 0 & 0 & 0 \\ p_{12} & p_{21} & p_{11} & 0 & 0 & 0 \\ 0 & 0 & 0 & p_{44} & 0 & 0 \\ 0 & 0 & 0 & 0 & p_{44} & 0 \\ 0 & 0 & 0 & 0 & 0 & p_{44} \end{pmatrix}$$

Cubic (3)

classes $\bar{4}3m, 432, m\bar{3}m$

$$\begin{pmatrix} p_{11} & p_{12} & p_{12} & 0 & 0 & 0 \\ p_{12} & p_{11} & p_{12} & 0 & 0 & 0 \\ p_{12} & p_{12} & p_{11} & 0 & 0 & 0 \\ 0 & 0 & 0 & p_{44} & 0 & 0 \\ 0 & 0 & 0 & 0 & p_{44} & 0 \\ 0 & 0 & 0 & 0 & 0 & p_{44} \end{pmatrix}$$

Table 9.1. (Continued).

Isotropic (2)						
p_{11}	p_{12}	p_{12}	0	0	0	0
p_{12}	p_{11}	p_{12}	0	0	0	0
p_{12}	p_{12}	p_{11}	0	0	0	0
0	0	0	$\frac{1}{2}(p_{11} - p_{12})$	0	0	0
0	0	0	0	$\frac{1}{2}(p_{11} - p_{12})$	0	0
0	0	0	0	0	0	$\frac{1}{2}(p_{11} - p_{12})$

† The number inside the parentheses indicates the number of independent coefficients.

The new index ellipsoid is given by Eq. (9.1-4) and can now be written

$$\begin{aligned}
 &x^2 \left[\frac{1}{n^2} + p_{12} S \sin(\Omega t - Kz) \right] + y^2 \left[\frac{1}{n^2} + p_{12} S \sin(\Omega t - Kz) \right] \\
 &+ z^2 \left[\frac{1}{n^2} + p_{11} S \sin(\Omega t - Kz) \right] = 0.
 \end{aligned}$$

Since no mixed terms are involved, the principal axes remain unchanged.

The new principal indices of refraction are thus given by

$$n_x = n - \frac{1}{2} n^3 p_{12} S \sin(\Omega t - Kz),$$

$$n_y = n - \frac{1}{2} n^3 p_{12} S \sin(\Omega t - Kz),$$

$$n_z = n - \frac{1}{2} n^3 p_{11} S \sin(\Omega t - Kz),$$

where p_{11}, p_{12} are the strain-optic coefficients and n is the index of refraction of water. We notice that in the presence of the sound wave, the water becomes a periodic medium which is equivalent to a volume grating with a grating constant $2\pi/K = \Lambda$.

Table 9.2. Strain-Optic Coefficients^a [1]

(a) Isotropic System						
Substance	Wavelength		P_{11}	P_{12}	P_{44}	$P_{11} - P_{12}$
	λ (μm)	λ (μm)				
Fused silica (SiO_2)	0.63		0.121	0.270		
As_2S_3 glass	1.15		0.308	0.299		
Water	0.63		± 0.31	± 0.31		
$\text{Ge}_{33}\text{Se}_{55}\text{As}_{12}$ (glass)	1.06		± 0.21	± 0.21		
Lucite	0.63		± 0.30	± 0.28		
Polystyrene	0.63		± 0.30	± 0.31		
(b) Cubic System: Classes $\bar{4}3m$, 432, and $m\bar{3}m$						
Substance	Wavelength		P_{11}	P_{12}	P_{44}	$P_{11} - P_{12}$
	λ (μm)	λ (μm)				
CdTe	10.60		-0.152	-0.017	-0.057	-0.135
GaAs	1.15		-0.165	-0.140	-0.072	-0.025
GaP	0.633		-0.151	-0.082	-0.074	-0.069
Ge	2.0-2.2		-0.063	-0.0535	-0.074	-0.0095
	10.60		0.27	0.235	0.125	
NaCl	0.55-0.65		0.115	0.159	-0.011	-0.042

NaF	0.633	0.08	0.20	-0.03	-0.12
	0.589			-0.021	-0.10
Si	1.15	-0.101	0.0094		-0.110
	3.39	-0.094	0.017	-0.051	-0.111
$Y_3Fe_5O_{12}$	1.15	± 0.025	± 0.073	± 0.041	
$Y_3Al_5O_{12}$	0.633	-0.029	0.0091	-0.0615	-0.038
KRS5	0.633	± 0.18	± 0.27	± 0.15	
KRS6	0.633	± 0.28	± 0.25	± 0.14	
β -ZnS	0.546			-0.044	
	0.589			-0.137	
	0.633	0.091	-0.01	0.075	010

Table 9.2. (Continued).

(c) Hexagonal System: Classes 6m2, 6mm, 622, and 6/mm

Substance	Wavelength λ (μm)		P_{11}	P_{12}	P_{13}	P_{31}	P_{33}	P_{44}
CdS	0.633	-0.142	-0.066	-0.057	-0.041	-0.20	± 0.054	
	10.60	0.104		0.011				
SnO	0.633	± 0.222	± 0.099	-0.111	± 0.088	-0.235	-0.0585	
α -ZnS (wurtzite)	0.633	-0.115	0.017	0.025	0.0271	-0.13	-0.0627	

(d) Trigonal System: Classes 3m, 32, and $\bar{3}m$

Substance	Wavelength λ (μm)		P_{11}	P_{12}	P_{13}	P_{14}	P_{31}	P_{33}	P_{41}	P_{44}
Al_2O_3	0.644	-0.23	-0.03	0.02	0.00	-0.04	-0.20	0.01	-0.10	
LiNbO_3	0.633	-0.026	0.090	0.133	-0.075	0.179	0.071	-0.151	0.146	
LiTaO_3	0.633	-0.081	0.081	0.093	-0.026	0.089	-0.044	-0.085	0.028	
SiO_2 (quartz)	0.589	0.16	0.27	0.27	-0.030	0.29	0.10	-0.047	-0.079	
Ag_3AsS_3 (proustite)	0.633	± 0.10	± 0.19	± 0.22		± 0.24	± 0.20			
	1.15	± 0.056	± 0.082	± 0.068		± 0.103	± 0.100		± 0.01	

(e) Tetragonal System: Classes 4mm, $\bar{4}2m$, 422, and 4/mmm

Substance	Wavelength λ (μm)					
	p_{11}	p_{12}	p_{13}	p_{31}	p_{33}	p_{66}
$(\text{NH}_4)\text{H}_2\text{PO}_4$ (ADP)	0.589	0.277	0.169	0.197	0.167	-0.091
	0.633	0.243	0.208	0.188	0.228	
MgF_2	$p_{11} - p_{12} = 0.892, p_{11} - p_{31} = 0.0695, p_{33} - p_{13} = 0.1128$					
KH_2PO_4 (KDP)	0.589	0.287	0.174	0.241	0.122	-0.064
	0.633	0.254	0.233	0.221	0.212	-0.0552
$\text{Sr}_x\text{Ba}_{1-x}\text{Nb}_2\text{O}_6$ $x = 0.75$ $x = 0.5$	0.63	0.16	0.08	0.11	0.47	
	0.633	0.06	0.17	0.09	0.23	
TeO_2	0.633	0.0074	0.340	0.0905	0.240	-0.0463
TiO_2 (rutile)	0.514	-0.001	0.113	-0.167	-0.064	-0.066
	0.633	-0.011	0.172	-0.168	-0.0965	± 0.072

(f) Tetragonal System: Classes 4, $\bar{4}$, and 4/m

Substance	Wavelength λ (μm)					
	p_{11}	p_{12}	p_{13}	p_{16}	p_{33}	p_{66}
PbMoO_4	0.633	0.24	0.24	0.0255	0.017	
		0.175	0.300			
		0.067	-0.01			
		0.013	0.05			
CdMoO_4	0.633	0.12	0.10	0.13		
		0.11	0.18			

9.1.2. Example: The Acousto-optic Effect in Germanium

Consider the propagation of a sound wave along the $\langle 001 \rangle$ direction (z axis). Let the wave be a shear wave polarized in the $\langle 010 \rangle$ direction (y axis) with the particle displacement given by

$$\mathbf{u}(z, t) = \hat{y}A \cos(\Omega t - kz),$$

where \hat{y} is a unit vector along the $\langle 010 \rangle$ direction. The strain field associated with this shear wave is

$$S_4 = KA \sin(\Omega t - Kz) \equiv S \sin(\Omega t - Kz),$$

where S is again defined as KA . The germanium crystal is cubic with point-group symmetry $m3m$. The photo-elastic coefficients are of the form, according to Table 9.1,

$$(p_{ij}) = \begin{pmatrix} p_{11} & p_{12} & p_{12} & 0 & 0 & 0 \\ p_{12} & p_{11} & p_{12} & 0 & 0 & 0 \\ p_{12} & p_{12} & p_{11} & 0 & 0 & 0 \\ 0 & 0 & 0 & p_{44} & 0 & 0 \\ 0 & 0 & 0 & 0 & p_{44} & 0 \\ 0 & 0 & 0 & 0 & 0 & p_{44} \end{pmatrix}.$$

Thus, according to Eq. (9.1-3), the change in the dielectric impermeability tensor is

$$\Delta\eta_{23} = \Delta\eta_{32} = p_{44}S \sin(\Omega t - Kz)$$

and all the other components are zero. The index ellipsoid (9.1-4) thus becomes

$$\frac{1}{n^2}(x^2 + y^2 + z^2) + 2yzp_{44}S \sin(\Omega t - Kz) = 1.$$

This equation is similar to (7.2-12) with $n_o = n_e = n$. The new principal axes are obtained by rotating the old principal axes around the x axis by 45° . The principal refractive indices are thus given by

$$n_{x'} = n,$$

$$n_{y'} = n - \frac{1}{2}n^3 p_{44}S \sin(\Omega t - Kz),$$

$$n_{z'} = n + \frac{1}{2}n^3 p_{44}S \sin(\Omega t - Kz).$$

Again, an optical volume grating is created by the shear acoustic wave via the strain–optic effect. This optical grating travels at speed $v = \Omega/K$.

9.2. BASIC CONCEPTS OF ACOUSTO-OPTIC INTERACTIONS

We now consider the propagation of a monochromatic plane light wave in a medium in which an acoustic wave is excited and the optical impermeability is periodically modulated. As shown in the examples in Section 9.1, the acoustic wave causes a change in the index of refraction of the medium. The medium becomes periodic with a period equal to that of the acoustic wavelength. This periodic perturbation is a function of both space and time. If the acoustic wave is a traveling wave, so is the periodic perturbation, which moves at a velocity equal to the sound velocity (typically a few times 10^3 m/s). Since the velocity of sound is some five orders of magnitude smaller than that of light ($c = 3 \times 10^8$ m/s), the periodic perturbation caused by the sound wave is essentially stationary. The problem reduces to one of electromagnetic propagation in a periodic medium, which is discussed in Chapter 6. As an example to illustrate the acousto-optic interaction, we consider the propagation of a light beam in water. The sound wave induces a change in the refractive indices due to the strain–optic effect. Let z be the axis in the direction of propagation of the sound wave, and the yz coordinate plane be parallel to the plane of incidence. If the light beam is linearly polarized in the x direction (TE wave), the index of refraction for this mode is, according to the example in Section 9.1.1,

$$n_x = n - \frac{1}{2}n^3 p_{12} S \sin(\Omega t - Kz), \quad (9.2-1)$$

where $\Omega/K = v$. Figure 9.1 illustrates this sinusoidal variation of the index of refraction.

If the transverse dimension of the acoustic wave is infinite, the kinematic boundary condition requires that the reflected beam lie in the plane of incidence (yz plane) with an angle of reflection equal to the angle of incidence θ (see Fig. 9.2). According to the coupled-mode theory discussed in Section 6.4, strong reflection of light occurs when

$$2k \sin \theta = mK = m \cdot \frac{2\pi}{\Lambda}, \quad (9.2-2)$$

where k is the wavenumber of the light beam ($k = n2\pi/\lambda$) and m is an integer. The integer m corresponds to the m th Fourier component of the dielectric perturbation. For the case of a pure sinusoidal acoustic wave, the

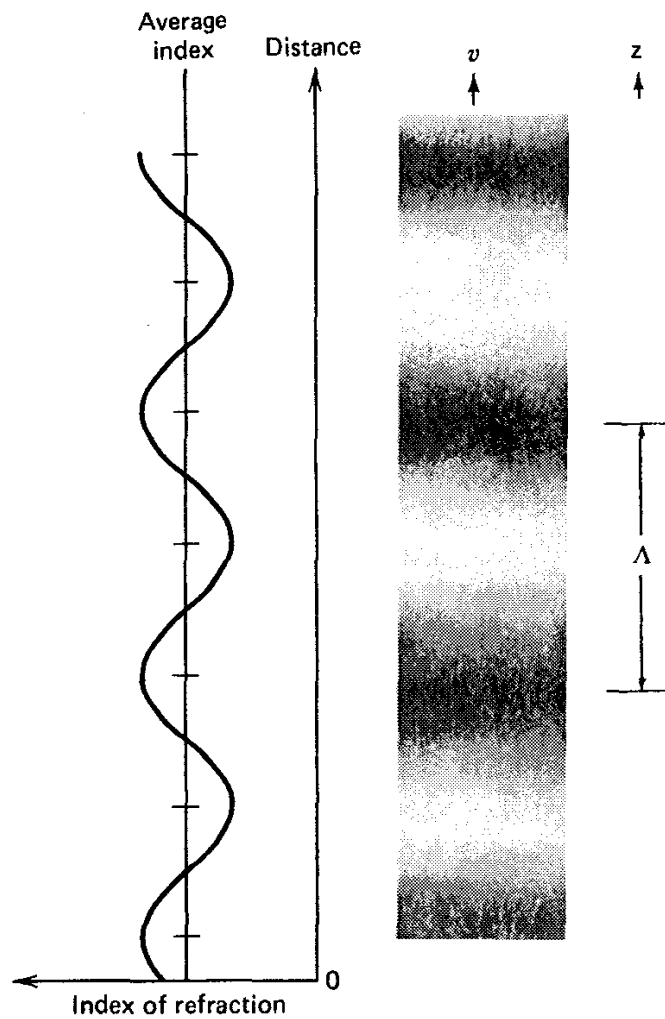


Figure 9.1. Traveling sound wave “frozen” at some instant of time. It consists of alternating regions of compression (dark) and rarefaction (white), which travel at the sound velocity v . Also shown is the instantaneous spatial variation of the index of refraction that accompanies the sound wave.

Fourier components with $m \geq 2$ are all vanishing. Therefore, the resonant reflection of light from an acoustic wave occurs at

$$2k \sin \theta = K. \quad (9.2-3)$$

By using $K = 2\pi/\Lambda$ and $k = n2\pi/\lambda$, this equation becomes

$$2\Lambda \sin \theta = \frac{\lambda}{n}. \quad (9.2-4)$$

The diffraction of light that satisfies Eq. (9.2-4) is known as Bragg diffraction after a similar law applying in X-ray diffraction from crystals. To

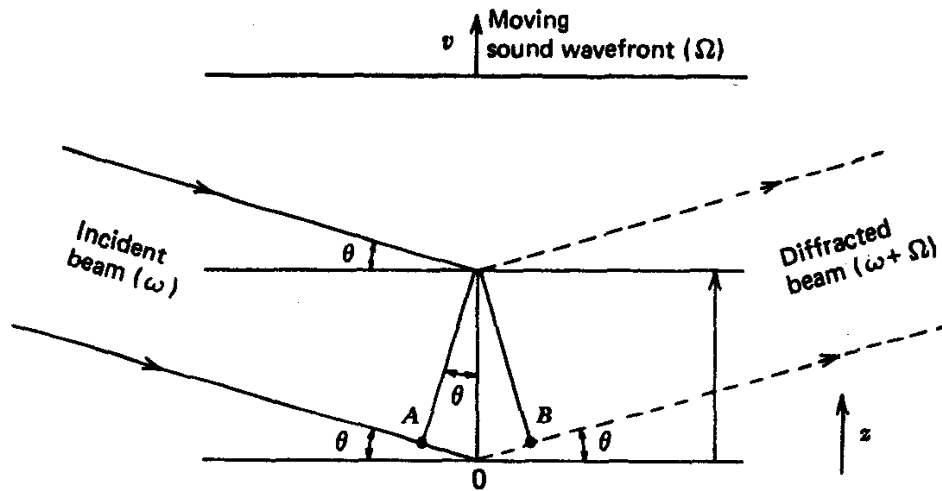


Figure 9.2. The reflections from two equivalent planes in the sound beam (that is, planes separated by the sound wavelength Λ), which add up in phase along the direction θ if the optical path difference $AO + OB$ is equal to one optical wavelength.

get an idea of the order of magnitude of the angle θ , consider the case of diffraction of light with $\lambda = 0.5 \mu\text{m}$ from a 500-MHz sound wave. Taking the sound velocity from Table 9.3 as $v = 1.5 \times 10^3 \text{ m/s}$, we have $\Lambda = 3 \times 10^{-6} \text{ m}$ and, from Eq. (9.2-4),

$$\theta \approx 6 \times 10^{-2} \text{ rad} \approx 3.6^\circ.$$

The Bragg diffraction condition (9.2-4) is derived by assuming that the periodic perturbation is fixed relative to the light beam. The effect of the displacement can be derived by considering the Doppler shift undergone by an optical beam incident on a mirror moving at the sound velocity v at an angle satisfying the Bragg condition (9.2-4). The formula for the Doppler frequency shift of a wave reflected from a moving object is

$$\Delta\omega = 2\omega \frac{v_{\parallel}}{c/n},$$

where ω is the optical frequency and v_{\parallel} is the projection of the object velocity vector along the wave propagation direction. From Fig. 9.2 we have $v_{\parallel} = v \sin \theta$, and thus

$$\Delta\omega = 2\omega \frac{v \sin \theta}{c/n}. \quad (9.2-5)$$

Using Eq. (9.2-4) for $\sin \theta$, we obtain

$$\Delta\omega \equiv \frac{2\pi v}{\Lambda} = \Omega, \quad (9.2-6)$$

and therefore the frequency of the reflected light beam is upshifted by Ω .

If the direction of propagation of the sound beam is reversed so that, in Fig. 9.2, the sound recedes from the optical beam, the Doppler shift changes sign and the diffracted beam has a frequency $\omega - \Omega$.

9.3. PARTICLE PICTURE OF ACOUSTO-OPTIC INTERACTIONS

Many of the features of the diffraction of light by sound can be deduced if we take advantage of the dual particle-wave nature of light and of sound. According to this picture, a light beam with a propagation vector \mathbf{k} and frequency ω can be considered to consist of a stream of particles (photons) with momentum $\hbar\mathbf{k}$ and energy $\hbar\omega$. The sound wave, likewise, can be thought of as made up of particles (phonons) with momentum $\hbar\mathbf{K}$ and energy $\hbar\Omega$. The diffraction of light by an approaching sound beam, illustrated in Fig. 9.2, can be described as a sum of single collisions, each of which involves the annihilation of one incident photon at ω and one phonon and simultaneous creation of a new (diffracted) photon at a frequency $\omega' = \omega + \Omega$, which propagates along the direction of the scattered beam. The conservation of momentum requires that the momentum $\hbar(\mathbf{k} + \mathbf{K})$ of the colliding particles be equal to the momentum $\hbar\mathbf{k}'$ of the scattered photon, so that

$$\mathbf{k}' = \mathbf{k} + \mathbf{K}. \quad (9.3-1)$$

The conservation of energy takes the form

$$\omega' = \omega + \Omega. \quad (9.3-2)$$

Thus the diffracted beam is shifted in frequency by an amount equal to the sound frequency. Since the interaction involves the annihilation of a phonon, conservation of energy implies that the shift in frequency is such that $\omega' > \omega$ and the phonon energy is added to that of the annihilated photon to form a new photon. From this argument it follows that if the direction of the sound beam in Fig. 9.2 were reversed, so that it was receding from the incident optical wave, the scattering process could be considered as one in which a new photon (diffracted photon) and a new phonon are generated while the incident photon is annihilated. In this case, the conservation-of-energy principle yields

$$\omega' = \omega - \Omega.$$

The relation between the sign of the frequency change and the sound propagation direction is consistent with the Doppler-shift arguments discussed at the end of last section.

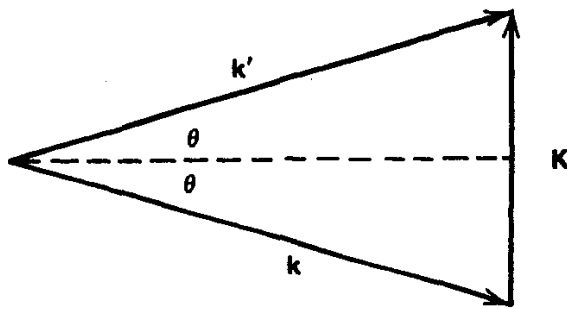


Figure 9.3. The momentum-conservation relation (9.3-1) used to derive the Bragg condition $2\Lambda \sin \theta = \lambda/n$ for an optical beam that is diffracted by an approaching sound wave. θ is the angle between the incident or diffracted beam and the acoustic wavefront.

The conservation-of-momentum condition (9.3-1) is equivalent to the Bragg condition (9.2-3). To show why this is true, consider Fig. 9.3. Since the sound frequencies of interest are below 10^{10} Hz and those of the optical beam are usually above 10^{13} Hz, we have

$$\omega' \approx \omega, \quad \text{so} \quad |\mathbf{k}'| \approx |\mathbf{k}|$$

and the magnitude of the two optical wave vectors is taken as k . The magnitude of the sound wave vector is thus

$$K = 2k \sin \theta \quad (9.3-3)$$

which is identical to Eq. (9.2-3).

9.4. BRAGG DIFFRACTION IN AN ANISOTROPIC MEDIUM

We have seen in the last section that the diffraction of light by sound waves can be pictured as an interaction process with three particles: the incident photon, the acoustic phonon and the diffracted photon. The conservation of momentum requires that the three momentum vectors associated with these three particles form a triangle. In an isotropic medium, the refractive index associated with a light beam is independent of the direction of propagation, and therefore $|\mathbf{k}'|$ is always nearly the same as $|\mathbf{k}|$. Thus the triangle is isosceles, and its resolution leads to the Bragg diffraction condition (9.2-3) or (9.3-3).

In an anisotropic medium, the refractive index associated with a light beam is, in general, dependent on the direction of propagation. Since the diffracted light beam, in general, propagates in a different direction from the incident beam, the magnitudes of the wave vectors are no longer nearly the same. In some cases, there may even be a change of the polarization state between the incident and the diffracted beam. Let n' and n be the

refractive indices associated with the diffracted and the incident beam, respectively. The triangle formed by k' , k , and K has sides equal, respectively, to $n'\omega'/c$, $n\omega/c$, and K . Since n' and n are, in general, different, the triangle is not isosceles even if we neglect the small differences between ω and ω' . Let θ and θ' be the angles between the light beams and the wavefront of the sound wave (Fig. 9.4). The Bragg diffraction conditions are obtained from the triangle in Fig. 9.4 and are given by

$$2k \sin \theta = K - \frac{k'^2 - k^2}{K} \quad (9.4-1)$$

and

$$2k' \sin \theta' = K + \frac{k'^2 - k^2}{K}, \quad (9.4-2)$$

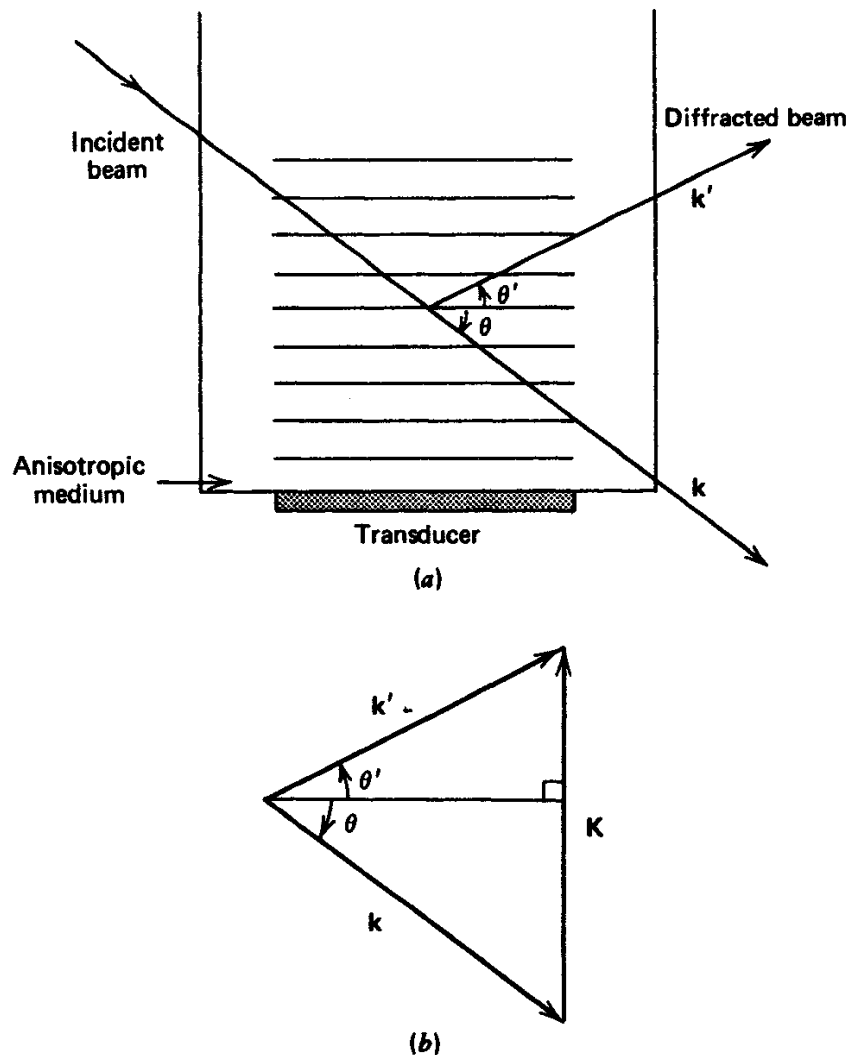


Figure 9.4. Bragg diffraction in an anisotropic medium: (a) diffraction of a light beam from a sound wave; (b) conservation of momentum.

or equivalently,

$$2\Lambda \sin \theta = \frac{\lambda}{n} - \frac{\Lambda^2}{n\lambda} (n'^2 - n^2) \quad (9.4-3)$$

and

$$2\Lambda \sin \theta' = \frac{\lambda}{n'} + \frac{\Lambda^2}{n'\lambda} (n'^2 - n^2). \quad (9.4-4)$$

For $n' = n$, the Bragg diffraction condition (9.2-3) is obtained again when $\theta' = \theta$. To illustrate the effect of anisotropy, we consider a special case of Bragg diffraction in a uniaxial crystal (e.g., LiNbO_3). We assume that both the light beams and the acoustic beam propagate in a plane perpendicular to the optic axis (c axis) of the crystal. The incident light beam is linearly polarized parallel to the c axis, so that it propagates in the extraordinary mode of the crystal with a refractive index n_e . The diffracted light beam is assumed to be linearly polarized perpendicular to the c axis and is in the ordinary mode of the crystal with a refractive index n_o (see Fig. 9.5). The angles of incidence and diffraction for the beams are, according to Eqs.

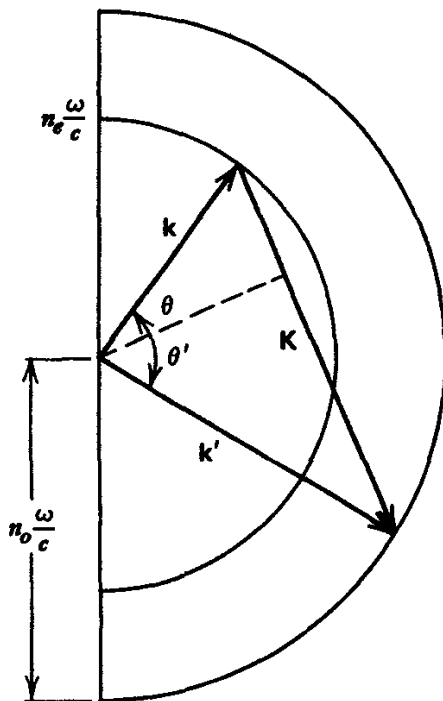


Figure 9.5. Bragg diffraction in a negative uniaxial crystal (e.g., LiNbO_3). All the three momentum vectors k , k' , and K are in a plane perpendicular to the c axis. The incident beam is an extraordinary wave, while the diffracted beam is an ordinary wave.

(9.4-3) and (9.4-4),

$$\sin \theta = \frac{1}{2n_e} \left[\frac{\lambda}{\Lambda} - \frac{\Lambda}{\lambda} (n_o^2 - n_e^2) \right] \quad (9.4-5)$$

and

$$\sin \theta' = \frac{1}{2n_o} \left[\frac{\lambda}{\Lambda} + \frac{\Lambda}{\lambda} (n_o^2 - n_e^2) \right]. \quad (9.4-6)$$

Thus the angle of incidence θ and the angle of diffraction θ' are both functions of λ/Λ for a given crystal when n_o and n_e are fixed. For $\lambda/\Lambda = |n_o \pm n_e|$, $|\theta'| = |\theta| = 90^\circ$, the vectors \mathbf{k} , \mathbf{k}' , and \mathbf{K} are collinear. Bragg diffraction is only possible when $|n_o - n_e| \leq \lambda/\Lambda \leq |n_o + n_e|$, and the angles θ' and θ are real. In the regimes when $\lambda/\Lambda < |n_o - n_e|$ or $\lambda/\Lambda > |n_o + n_e|$, $\sin \theta'$ and $\sin \theta$ become greater than one and the diffraction is impossible. Figure 9.6 shows the dependence of θ and θ' on λ/Λ for a typical uniaxial crystal. The point $\lambda/\Lambda = |n_o - n_e|$ corresponds to a codirectional collinear Bragg coupling such as that of a Šolc filter (see Section 6.5).

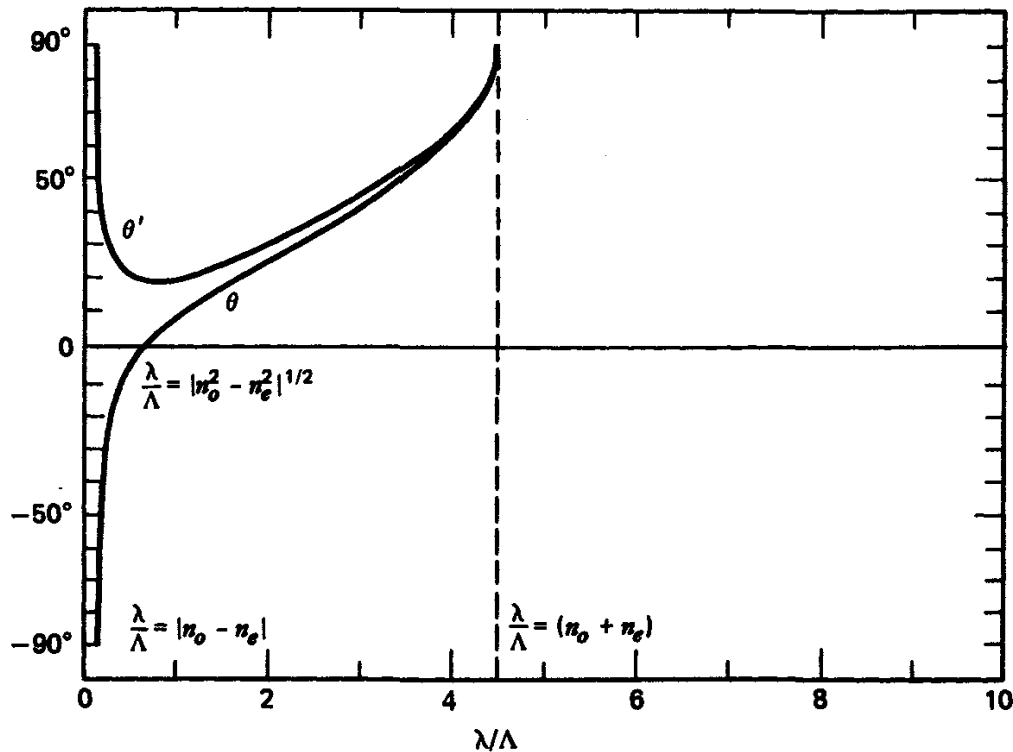


Figure 9.6. Angle of incidence (θ) and of diffraction (θ') as a function of the ratio of the light and sound wavelengths in a LiNbO_3 crystal, where we take $n = 2.2$ and $n' = 2.3$.

9.5. COUPLED-MODE ANALYSIS OF BRAGG DIFFRACTION

In the last section we derived the kinematic properties of the Bragg diffraction, that is, conservation of energy and momentum. These conservation laws lead to the Bragg diffraction condition which determines the angle of the incident and the diffracted light beam. In order to answer questions such as the intensities and the polarization state of the diffracted beam, we need to solve the electromagnetic problem. The coupled-mode formalism derived in Chapter 6 will now be employed to study the Bragg diffraction of light by sound waves. In doing so, we assume that the acoustic wave is a plane wave of infinite extent, so that higher diffraction orders (see next section) are missing, and the only two waves coupled by the sound are the incident wave at ω and a diffracted wave at $\omega + \Omega$ or $\omega - \Omega$, depending on the direction of propagation of the sound relative to the incident optical beam.

According to the discussion in Section 9.1, the sound wave causes a traveling modulation of the optical dielectric impermeability given by

$$\Delta\eta_{ij} = \Delta\left(\frac{\epsilon_0}{\epsilon}\right)_{ij} = p_{ijkl}S_{kl}\cos(\Omega t - Kz), \quad (9.5-1)$$

where S_{kl} is the amplitude of the strain field associated with the sound, and z is in the direction of propagation. The p_{ijkl} are the photoelastic coefficients. Summation over the repeated indices k, l is assumed. This modulation in the impermeability tensor $\Delta\eta_{ij}$ corresponds to a traveling modulation of the dielectric tensor given by

$$\Delta\epsilon(z, t) = 2\epsilon_1\cos(\Omega t - Kz) \equiv \Delta\epsilon\cos(\Omega t - Kz), \quad (9.5-2)$$

where ϵ_1 is also a tensor and is given by

$$\epsilon_1 = -\frac{\epsilon(pS)\epsilon}{2\epsilon_0} \quad (9.5-3)$$

and (pS) is the matrix with elements $p_{ijkl}S_{kl}$. The factor 2 is inserted in Eq. (9.5-2) for convenience, so that ϵ_1 is the first (and the only) Fourier component of the dielectric perturbation $\Delta\epsilon$ [see Eq. (6.4-15)]. Under the appropriate conditions and according to the results obtained in Chapter 6, this periodic dielectric perturbation will couple two modes of propagation: the incident wave and the diffracted wave.

Let the total electric field be taken as

$$\mathbf{E} = A_1 \mathbf{E}_1 e^{i(\omega_1 t - \mathbf{k}_1 \cdot \mathbf{r})} + A_2 \mathbf{E}_2 e^{i(\omega_2 t - \mathbf{k}_2 \cdot \mathbf{r})}, \quad (9.5-4)$$

where \mathbf{k}_1 and \mathbf{k}_2 are the propagation wave vectors of the incident and diffracted light waves, respectively. ω_1 and ω_2 are the corresponding frequencies of the light waves. \mathbf{E}_1 and \mathbf{E}_2 are the modes of propagation, which are constant in a homogeneous medium. A_1 and A_2 are the mode amplitudes. In the presence of the dielectric perturbation $\Delta\epsilon$ (9.5-2), the two modes are coupled and the mode amplitudes A_1 and A_2 are functions of position. The time dependence is neglected, since Ω is much smaller compared with $\omega_{1,2}$ and the dielectric perturbation $\Delta\epsilon$ (9.5-2) is practically stationary. Let the plane of incidence (i.e., the plane formed by \mathbf{k}_1, \mathbf{K}) be the xz plane. The conservation of momentum requires that \mathbf{k}_2 must also lie in this plane. The electric field can thus be written

$$\mathbf{E} = A_1 \mathbf{E}_1 e^{i(\omega_1 t - \alpha_1 x - \beta_1 z)} + A_2 \mathbf{E}_2 e^{i(\omega_2 t - \alpha_2 x - \beta_2 z)}, \quad (9.5-5)$$

where $\beta_{1,2}$ are the z components of the wave vectors \mathbf{k}_1 and \mathbf{k}_2 , respectively, and $\alpha_{1,2}$ are the components of these wave vectors parallel to the wavefront of the acoustic wave. The mode amplitudes A_1 and A_2 are in general functions of both x and z . However, there are a number of cases in which the interaction configuration requires that the mode amplitudes A_1 and A_2 be functions of either x or z only. The acousto-optic interaction is thus divided into two interaction configurations, which are illustrated in Fig. 9.7. For low sound frequencies the bounded column configuration shown in Fig. 9.7(a) is most common; for very high frequencies the plane wave of finite length shown in Fig. 9.7(b) often applies. In the small-angle Bragg-diffraction configuration [Fig. 9.7(a)], the mode amplitudes A_1 and A_2 are functions of x as required by the boundary conditions. In the large-angle Bragg-diffraction configuration [Fig. 9.7(b)], the mode amplitudes A_1 and A_2 are functions of z only. In either case, the electric field \mathbf{E} (9.5-5) must satisfy the following wave equation:

$$(\nabla^2 + \omega^2 \mu \epsilon + \omega^2 \mu \Delta\epsilon) \mathbf{E} = 0 \quad (9.5-6)$$

where ϵ is the dielectric tensor of the medium in the absence of the sound wave and $\Delta\epsilon$ is the dielectric perturbation (9.5-2) due to the sound. Both $\mathbf{E}_1 \exp[i(\omega_1 t - \alpha_1 x - \beta_1 z)]$ and $\mathbf{E}_2 \exp[i(\omega_2 t - \alpha_2 x - \beta_2 z)]$ are solutions of Eq. (9.5-6) when $\Delta\epsilon = 0$. Substitution of Eq. (9.5-5) for \mathbf{E} in Eq. (9.5-6)

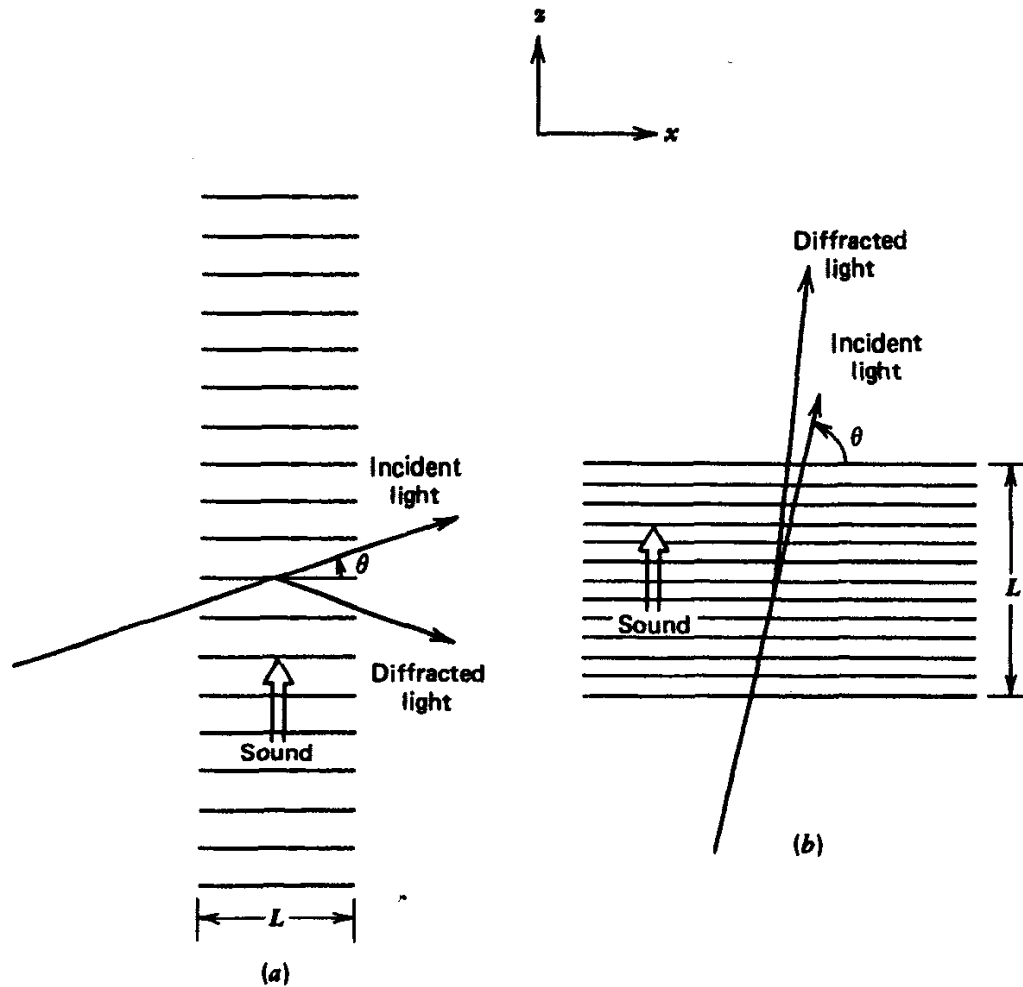


Figure 9.7. Two common interaction configurations: (a) Small-Bragg-angle diffraction; (b) Large-Bragg-angle diffraction.

leads to

$$\sum_{m=1,2} \left\{ \left[\frac{\partial^2}{\partial z^2} + \frac{\partial^2}{\partial x^2} - 2i\beta_m \frac{\partial}{\partial z} - 2i\alpha_m \frac{\partial}{\partial x} \right] A_m \right\} \mathbf{E}_m e^{i(\omega_m t - \alpha_m x - \beta_m z)}$$

$$= -\omega^2 \mu \sum_{l=1,2} \Delta \epsilon A_l \mathbf{E}_l e^{i(\omega_l t - \alpha_l x - \beta_l z)} \quad (9.5-7)$$

The second derivatives $\partial^2 A / \partial z^2$ and $\partial^2 A / \partial x^2$ are often neglected, since the acousto-optic perturbation is normally small ($\Delta \epsilon / \epsilon_0 \sim 10^{-5}$), and the differential equation (9.5-7) is dominated by the first derivatives. However, even the first-order differential equation is difficult to solve in a two-dimensional case (i.e., in x and z). We will therefore limit our derivation to the

two common cases shown in Fig. 9.7, when the differential equation becomes one-dimensional.

9.5.1. Small-Angle Bragg Diffraction

When the angle between the direction of propagation of the light beam and the acoustic wavefront is small, the interaction length L is the width of the acoustic beam. Consequently, the mode amplitudes A_1 and A_2 are functions of x only, because x measures the depth of penetration in this interaction configuration [see Fig. 9.7(a)]. We will normalize the mode vectors \mathbf{E}_1 and \mathbf{E}_2 in such a way that

$$\mathbf{E}_i = \left(\frac{2\mu\omega_i}{\alpha_i} \right)^{1/2} \mathbf{p}_i, \quad i = 1, 2, \quad (9.5-8)$$

where \mathbf{p}_i are the unit vectors representing the polarization states of the modes, and α_i are the x components of the wave vectors. This normalization is consistent with Eq. (6.4-6), so that each mode represents a power flow of 1 W/m² in the x direction for the case of an isotropic medium [see Eq. (1.4-2)]. The coupled equation (9.5-7) for this case becomes

$$\begin{aligned} & -2i\alpha_1 \frac{dA_1}{dx} \mathbf{E}_1 e^{i(\omega_1 t - \alpha_1 x - \beta_1 z)} - 2i\alpha_2 \frac{dA_2}{dx} \mathbf{E}_2 e^{i(\omega_2 t - \alpha_2 x - \beta_2 z)} \\ & = -\omega^2 \mu (\epsilon_1 e^{i(\Omega t - Kz)} + \epsilon_1 e^{-i(\Omega t - Kz)}) \\ & \times (A_1 \mathbf{E}_1 e^{i(\omega_1 t - \alpha_1 x - \beta_1 z)} + A_2 \mathbf{E}_2 e^{i(\omega_2 t - \alpha_2 x - \beta_2 z)}) \end{aligned} \quad (9.5-9)$$

where we have substituted Eq. (9.5-2) for $\Delta\epsilon$ in Eq. (9.5-7).

By scalar-multiplying Eq. (9.5-9) with $\mathbf{E}_l^* e^{-i(\omega_l t - \alpha_l x - \beta_l z)}$, $l = 1, 2$, one at a time and integrating over z and t , we obtain the following set of coupled equations:

$$\begin{aligned} \frac{dA_1}{dx} &= -i\kappa_{12} A_2 e^{i\Delta\alpha x}, \\ \frac{dA_2}{dx} &= -i\kappa_{12}^* A_1 e^{-i\Delta\alpha x}, \end{aligned} \quad (9.5-10)$$

where κ_{12} is the coupling constant and is given by

$$\kappa_{12} = \frac{\omega^2 \mu}{2\sqrt{\alpha_1 \alpha_2}} \mathbf{p}_1^* \cdot \epsilon_1 \mathbf{p}_2 \quad (9.5-11)$$

provided the following conditions are satisfied:

$$\beta_2 = \beta_1 \pm K \quad (9.5-12)$$

and

$$\omega_2 = \omega_1 \pm \Omega. \quad (9.5-13)$$

The coupled equations are not valid when either one of the above conditions is not satisfied. The quantity $\Delta\alpha$ is the momentum mismatch in the x direction and is given by

$$\Delta\alpha = \alpha_1 - \alpha_2. \quad (9.5-14)$$

These two components, α_1 and α_2 , are assumed to be positive. For the case of an isotropic medium, the Bragg condition (9.5-12) can be satisfied when $\beta_1 = -\beta_2 = -k \sin \theta_B = -\frac{1}{2}K$, in which case a phonon is absorbed, or $\beta_1 = -\beta_2 = k \sin \theta_B = \frac{1}{2}K$ when the emission of a phonon takes place. At this Bragg angle of incidence

$$\theta_B = \sin^{-1}\left(\frac{K}{2k}\right) = \sin^{-1}\left(\frac{\lambda}{2\Lambda}\right), \quad (9.5-15)$$

the momentum mismatch $\Delta\alpha$ vanishes ($\Delta\alpha = 0$), the x axis bisects the angle between \mathbf{k}_1 and \mathbf{k}_2 , and the coupled equations become

$$\begin{aligned} \frac{dA_1}{dx} &= -i\kappa_{12}A_2, \\ \frac{dA_2}{dx} &= -i\kappa_{12}^*A_1. \end{aligned} \quad (9.5-16)$$

The solutions to Eq. (9.5-16) are, according to Eq. (6.4-30),

$$\begin{aligned} A_1(x) &= A_1(0)\cos \kappa x - i\frac{\kappa_{12}}{\kappa}A_2(0)\sin \kappa x, \\ A_2(x) &= A_2(0)\cos \kappa x - i\frac{\kappa_{12}^*}{\kappa}A_1(0)\sin \kappa x, \end{aligned}$$

where κ is the magnitude of κ_{12} ,

$$\kappa = |\kappa_{12}|. \quad (9.5-17)$$

In the special case of a single wave incident at $x = 0$ [i.e., $A_2(0) = 0$], the solutions become

$$\begin{aligned} A_1(x) &= A_1(0)\cos \kappa x, \\ A_2(x) &= -i\frac{\kappa_2^*}{\kappa}A_1(0)\sin \kappa x. \end{aligned} \quad (9.5-18)$$

We note that

$$|A_1(x)|^2 + |A_2(x)|^2 = |A_1(0)|^2, \quad (9.5-19)$$

so that the total mode power carried by both light waves is conserved.

If the interaction distance L between the two beams is such that $\kappa L = \frac{1}{2}\pi$, the total power of the incident beam is transferred into the diffracted beam. Since this process is used in a large number of technological and scientific applications, it may be worthwhile to gain some appreciation for the diffraction efficiencies using known acoustic media and conveniently available acoustic power levels.

The fraction of the power of the incident beam transferred in a distance L into the diffracted beam is given, using Eq. (9.5-18), by

$$\frac{I_{\text{diffracted}}}{I_{\text{incident}}} = \frac{|A_2(L)|^2}{|A_1(0)|^2} = \sin^2 \kappa L, \quad (9.5-20)$$

where κ is given, according to Eqs. (9.5-17), (9.5-11), and (9.5-2), by

$$\kappa = \frac{\omega^2 \mu}{4\alpha} |\mathbf{p}_1^* \cdot \Delta \epsilon \mathbf{p}_2|. \quad (9.5-21)$$

At the Bragg condition (9.5-12), we have $|\beta_1| = |\beta_2| = k \sin \theta = \frac{1}{2}K$ and $\alpha = k \cos \theta_B = (\omega/c)n \cos \theta_B$, and the coupling constant κ can be written

$$\kappa = \frac{\omega \mu c}{4n \cos \theta_B} |\mathbf{p}_1^* \cdot \Delta \epsilon \mathbf{p}_2|, \quad (9.5-22)$$

where we recall that $\Delta \epsilon$ is the change in dielectric constant due to the acoustic wave, and $\mathbf{p}_{1,2}$ are the unit vectors representing the polarization states of the incident and diffracted waves, respectively. By using Eqs. (9.5-3) and (9.5-2), the coupling constant κ can also be expressed in terms of

the strain components and the photoelastic coefficients as

$$\kappa = \frac{\omega}{4nc \cos \theta_B} |\mathbf{p}_1^* \cdot \epsilon' (pS) \epsilon' \mathbf{p}_2|, \quad (9.5-23)$$

where

$$\epsilon' = \frac{\epsilon}{\epsilon_0} \quad (9.5-24)$$

and (pS) is the matrix formed by the elements $p_{ijkl} S_{kl}$. For the case of an isotropic medium, $\epsilon' = n^2$ and Eq. (9.5-23) becomes

$$\kappa = \frac{\omega n^3}{4c \cos \theta_B} |\mathbf{p}_1^* \cdot (pS) \mathbf{p}_2|. \quad (9.5-25)$$

Since the strain component S is directly related to the Poynting power flow or the acoustic intensity I_{acoustic} of the sound, it is convenient to express the diffraction efficiency (9.5-20) in terms of I_{acoustic} . For this purpose, the coupling constant is written formally as

$$\kappa = \frac{\omega n^3}{4c} \bar{p} \bar{S}, \quad (9.5-26)$$

where \bar{p} is the effective photoelastic coefficient and \bar{S} is the effective strain component; while the acoustic intensity is written formally as

$$I_{\text{acoustic}} = \frac{1}{2} \rho v^3 \bar{S}^2, \quad (9.5-27)$$

where v is the phase velocity and ρ is the mass density. Since the strain amplitude \bar{S} in Eq. (9.5-26) is proportional to the square root of the acoustic intensity I_{acoustic} according to Eq. (9.5-27), it is convenient to define a diffraction figure of merit as

$$M = \frac{n^6 \bar{p}^2}{\rho v^3}, \quad (9.5-28)$$

so that Eq. (9.5-20) becomes

$$\frac{I_{\text{diffracted}}}{I_{\text{incident}}} = \sin^2 \left(\frac{\pi L}{\sqrt{2} \lambda} \sqrt{M I_{\text{acoustic}}} \right). \quad (9.5-29)$$

The diffraction figure of merit M defined in Eq. (9.5-28) is a parameter which measures the diffraction efficiencies of acousto-optic materials at a given acoustic power level. This parameter M is not uniquely defined for a given material, because it depends on the interaction configuration, the direction of propagation, and the polarization states of the waves.

Taking water as an example, we assume that both the incident and the diffracted light waves are polarized parallel to the plane of incidence (xz plane). The relevant photoelastic coefficient is p_{12} according to the example in Section 9.1. Taking an optical wavelength of $\lambda = 0.6328 \mu\text{m}$ and the constants (from Table 9.3)

$$\begin{aligned} n &= 1.33, \\ \bar{p} &= 0.31, \\ v &= 1.5 \times 10^3 \text{ m/s}, \\ \rho &= 1000 \text{ kg/m}^3, \end{aligned}$$

Eq. (9.5-29) gives

$$\left(\frac{I_{\text{diffracted}}}{I_{\text{incident}}} \right)_{\text{H}_2\text{O}, 0.6328 \mu\text{m}} = \sin^2 \left(1.4 L \sqrt{I_{\text{acoustic}}} \right). \quad (9.5-30)$$

For other materials and at other wavelengths we can combine the last two equations to obtain a convenient working formula

$$\frac{I_{\text{diffracted}}}{I_{\text{incident}}} = \sin^2 \left(1.4 \frac{0.6328}{\lambda (\mu\text{m})} L \sqrt{M_w I_{\text{acoustic}}} \right) \quad (9.5-31)$$

where $M_w = M_{\text{material}}/M_{\text{H}_2\text{O}}$ is the diffraction figure of merit of the material relative to water. Values of M and M_w for some common materials are listed in Tables 9.3 and 9.4.

According to Eq. (9.5-29), at small diffraction efficiencies, the diffracted light intensity is proportional to the acoustic intensity. This fact is used in acoustic modulation of optical radiation. The information signal is used to modulate the intensity of the acoustic beam. This modulation is then transferred, according to Eq. (9.5-29) as intensity modulation onto the diffracted optical beam.

Numerical Example—Scattering in Lead Molybdate. Calculate the fraction of 0.633- μm light which is diffracted under Bragg conditions from a

Table 9.3. Properties of Some Materials Commonly Used in the Diffraction of Light by Sound^a

Material	$\rho \times 10^{-3}$ (kg/m ³)	v (km/s)	n	\bar{p}	M_w
Water	1.0	1.5	1.33	0.31	1.0
Extra-dense flint glass	6.3	3.1	1.92	0.25	0.12
Fused quartz (SiO ₂)	2.2	5.97	1.46	0.20	0.006
Polystyrene	1.06	2.35	1.59	0.31	0.8
KRS-5	7.4	2.11	2.60	0.21	1.6
Lithium niobate (LiNbO ₃)	4.7	7.40	2.25	0.15	0.012
Lithium fluoride (LiF)	2.6	6.00	1.39	0.13	0.001
Rutile (TiO ₂)	4.26	10.30	2.60	0.05	0.001
Sapphire (Al ₂ O ₃)	4.0	11.00	1.76	0.17	0.001
Lead molybdate (PbMO ₄)	6.95	3.75	2.30	0.28	0.22
Alpha iodic acid (HIO ₃)	4.63	2.44	1.90	0.41	0.5
Tellurium dioxide (TeO ₂) (slow shear wave)	5.99	0.617	2.35	0.09	5.0

^a ρ is the density, v the velocity of sound, n the index of refraction, \bar{p} the effective photoelastic constant as defined by Eq. (9.5-26), and M_w the relative diffraction constant defined below Eq. (9.5-31). (After [2], copyright ©1967, IEEE.)

^b Slow shear wave.

sound wave in PbMoO₄ with the following characteristics

$$\text{acoustic power} = 1 \text{ W},$$

$$\text{acoustic beam cross section} = 1 \text{ mm} \times 1 \text{ mm},$$

$$L = \text{optical path in acoustic beam} = 1 \text{ mm},$$

$$M_w \text{ (from Table 9.3)} = 0.22.$$

Substituting these data into Eq. (9.5-31) yields

$$\frac{I_{\text{diffracted}}}{I_{\text{incident}}} \approx 40\%.$$

Let us now consider the situation when the angle of incidence is slightly deviated from the Bragg angle:

$$\theta_B = \sin^{-1} \left(\frac{K}{2k} \right) = \sin^{-1} \left(\frac{\lambda}{2\Lambda} \right). \quad (9.5-32)$$

Table 9.4. Properties of Materials Commonly Used in Acousto-optic Interactions^a

Material	λ (μm)	n	ρ (g/cm^3)	Acoustic Wave Polarization and Direction	v (10^3 m/s)	Opt. Wave Polarization and Direction ^b	$M = n^6 p^2 / \rho v^3$ in Units of 10^{-15}c
Fused quartz	0.63	1.46	2.2	Long.	5.95	\perp	1.51
Fused quartz	0.63			Trans.	3.76	\parallel or \perp	0.467
GaP	0.63	3.31	4.13	Long. in [110]	6.32	\parallel	44.6
GaP	0.63			Trans. in [100]	4.13	\parallel or \perp in [010]	24.1
GaAs	1.15	3.37	5.34	Long. in [110]	5.15	\parallel	104
GaAs	1.15			Trans. in [100]	3.32	\parallel or \perp in [010]	46.3
TiO ₂	0.63	2.58	4.6	Long. in [11-20]	7.86	\perp in [001]	3.93
LiNbO ₃	0.63	2.20	4.7	Long. in [11-20]	6.57	(b)	6.99
YAG	0.63	1.83	4.2	Long. in [100]	8.53	\parallel	0.012
YAG	0.63			Long. in [110]	8.60	\perp	0.073
YIG	1.15	2.22	5.17	Long. in [100]	7.21	\perp	0.33
LiTaO ₃	0.63	2.18	7.45	Long. in [001]	6.19	\parallel	1.37
As ₂ S ₃	0.63	2.61	3.20	Long.	2.6	\perp	433
As ₂ S ₃	1.15	2.46		Long.		\parallel	347
SF-4	0.63	1.616	3.59	Long.	3.63	\perp	4.51
β -ZnS	0.63	2.35	4.10	Long. in [110]	5.51	\parallel in [001]	3.41
β -ZnS	0.63			Trans. in [110]	2.165	\parallel or \perp in [001]	0.57
α -Al ₂ O ₃	0.63	1.76	4.0	Long. in [001]	11.15	\parallel in [11-20]	0.34
CdS	0.63	2.44	4.82	Long. in [11-20]	4.17	\parallel	12.1
ADP	0.63	1.58	1.803	Long. in [100]	6.15	\parallel in [010]	2.78
ADP	0.63			Trans. in [100]	1.83	\parallel or in [001]	6.43
KDP	0.63	1.51	2.34	Long. in [100]	5.50	\parallel in [010]	1.91
KDP	0.63			Trans. in [100]		\parallel or \perp in [001]	3.83
H ₂ O	0.63	1.33	1.0	Long.	1.5	\parallel	160
Te	10.6	4.8	6.24	Long. in [11-20]	2.2	\parallel in [0001]	4400
PbMoO ₄	0.63	2.4		Long. \parallel c axis	3.75	\parallel or \perp	73

^aAfter [3].

^bThe optical-beam direction actually differs from that indicated by the magnitude of the Bragg angle. The polarization is defined as parallel or perpendicular to the scattering plane formed by the acoustic and optical \mathbf{k} vectors.

^cFigure of merit defined by Eq. (9.5-28), in MKS units.

Let the incident angle θ_1 be written

$$\theta_1 = \theta_B + \Delta\theta, \quad (9.5-33)$$

where $\Delta\theta$ is a small angle. The Bragg condition (9.5-12) requires that

$$\theta_2 = \theta_B - \Delta\theta. \quad (9.5-34)$$

Therefore, $\Delta\alpha$ (9.5-14) becomes

$$\Delta\alpha = 2k \Delta\theta \sin \theta_B = K \Delta\theta. \quad (9.5-35)$$

Since $\Delta\alpha$ is not zero, the solution to Eq. (9.5-10), subject to the boundary condition $A_2(0) = 0$, is given, according to Eq. (6.4-30), by

$$A_1(x) = e^{i\frac{1}{2}\Delta\alpha x} A_1(0) \left[\cos sx - i \frac{\Delta\alpha}{2s} \sin sx \right], \quad (9.5-36)$$

$$A_2(x) = -ie^{-i\frac{1}{2}\Delta\alpha x} A_1(0) \frac{\kappa_{12}^*}{s} \sin sx,$$

where

$$s^2 = \kappa^2 + \left(\frac{1}{2}\Delta\alpha\right)^2 = \kappa^2 + \left(\frac{1}{2}K \Delta\theta\right)^2. \quad (9.5-37)$$

Inspection of Eq. (9.5-36) reveals that the power transfer, or diffraction efficiency, can never be complete and is given by

$$\frac{I_d}{I_i} = \frac{\kappa^2}{\kappa^2 + \left(\frac{1}{2}K \Delta\theta\right)^2} \left[\sin^2 \kappa L \sqrt{1 + \left(\frac{K \Delta\theta}{2\kappa}\right)^2} \right]. \quad (9.5-38)$$

The maximum diffraction efficiency is $\kappa^2/[\kappa^2 + (K \Delta\theta/2\kappa)^2]$, which becomes small when $K \Delta\theta \gg \kappa$. This angular deviation $\Delta\theta$ can be due to either the misalignment of the laser beam or the distortion of the acoustic wavefront due to the finite size of the transducer. The latter connection can be used to describe the angular plane-wave spectrum of a transducer with width L . Thus, if the power of the diffracted light beam is measured and plotted as a function of $\Delta\theta$, the radiation pattern of the transducer will be traced out.

9.5.2. Large-Angle Bragg Diffraction

We now consider the acousto-optic interaction configuration shown in Fig. 9.7(b). The wave-propagation analysis in this case is relatively simple because the medium is homogeneous in both x and y directions. The

boundary condition requires that $\alpha_2 = \alpha_1$ in Eq. (9.5-5), and the mode amplitudes A_1 and A_2 are functions of z only. Thus, the electric field can be written

$$\mathbf{E} = [A_1(z)\mathbf{E}_1 e^{i(\omega_1 t - \beta_1 z)} + A_2(z)\mathbf{E}_2 e^{i(\omega_2 t - \beta_2 z)}] e^{-i\alpha x}, \quad (9.5-39)$$

where β_1 and β_2 are the z components of the wave vectors and α is the component of the wave vectors parallel to the wavefronts of the sound. In terms of the particle picture, the component of the wave vectors transverse to the sound-wave propagation will remain unchanged, due to the conservation of momentum.

The mode vectors \mathbf{E}_1 and \mathbf{E}_2 are now normalized so that

$$\mathbf{E}_i = \left(\frac{2\mu\omega_i}{|\beta_i|} \right)^{1/2} \mathbf{p}_i, \quad i = 1, 2, \quad (9.5-40)$$

where \mathbf{p}_i are the unit vectors describing the polarization states of the modes. This normalization is consistent with Eq. (6.4-6), so that each mode represents a power flow of 1 W/m^2 in the z direction for the case of an isotropic medium [see Eq. (1.4-21)]. By following the procedure described in Section 6.4, a set of coupled equations is obtained:

$$\frac{d}{dz} A_1 = -i \frac{\beta_1}{|\beta_2|} \kappa_{12} A_2 e^{i\Delta\beta z}, \quad (9.5-41)$$

$$\frac{d}{dz} A_2 = -i \frac{\beta_2}{|\beta_2|} \kappa_{12}^* A_1 e^{-i\Delta\beta z},$$

where

$$\Delta\beta = \beta_1 - \beta_2 \pm K \quad (9.5-42)$$

and

$$\kappa_{12} = \frac{\omega^2 \mu}{2\sqrt{|\beta_1 \beta_2|}} \mathbf{p}_1^* \cdot \boldsymbol{\varepsilon}_1 \mathbf{p}_2. \quad (9.5-43)$$

The sign in front of K in Eq. (9.5-42) is determined by whether a phonon is absorbed (+ sign, $\omega_2 = \omega_1 + \Omega$) or emitted (- sign, $\omega_2 = \omega_1 - \Omega$). Since $\omega_2 \approx \omega_1$, the ω in Eq. (9.5-43) is taken as the common value of the frequency of the light. An inspection of Eq. (9.5-41) reveals that a prerequisite for continuous cumulative interaction between the incident field and

the diffracted field is that

$$\beta_2 = \beta_1 \pm K. \quad (9.5-44)$$

Otherwise, it follows from Eq. (9.5-41) that contributions to A_2 (as an example) from different path elements do not add in phase and no sustained spatial growth of A_2 is possible.

Equation (9.5-44) is the general Bragg condition for many types of Bragg diffraction. The Bragg condition (9.2-3) is a special case when $\beta_2 = -\beta_1 = k \sin \theta$ for the absorption of a phonon (approaching sound wave; K, β_1 are different in sign) or $\beta_1 = -\beta_2 = k \sin \theta$ for the emission of a phonon (receding sound wave; K, β_1 have the same sign). The Bragg condition (9.5-44) also corresponds to the conservation of momentum for codirectional coupling in an acousto-optic tunable filter (see next chapter), which cannot be described by Eq. (9.2-3). The nature of the coupling between the two modes depends on the direction of propagation relative to the z direction. The solutions to the coupled equations (9.5-41) are next discussed separately in the two categories: codirectional light coupling and contradirectional light coupling.

Codirectional Light Coupling ($\beta_1 \beta_2 > 0$). In codirectional coupling between the two waves, the diffracted (A_2) and the incident (A_1) waves are both propagating in the same direction [either both $+z$ or $-z$; see Fig. 9.8(a)]. These two waves are coupled, and their propagation characteristics are described by Eq. (9.5-41), which now becomes

$$\frac{d}{dz} A_1 = -i\kappa_{12} A_2 e^{i\Delta\beta z}, \quad (9.5-45)$$

$$\frac{d}{dz} A_2 = -i\kappa_{12}^* A_1 e^{-i\Delta\beta z},$$

where $\Delta\beta$ is given by (9.5-42) and κ_{12} is given by (9.5-43). Let $\theta_{1,2}$ be the angles between the wave vectors $k_{1,2}$ and the acoustic wavefront, and use Eqs. (9.5-2) and (9.5-3). We then obtain

$$\kappa_{12} = \frac{\omega \mathbf{p}_1^* \cdot \epsilon'(pS) \epsilon' \mathbf{p}_2}{4c |n_1 n_2 \sin \theta_1 \sin \theta_2|^{1/2}}, \quad (9.5-46)$$

where $n_{1,2}$ are the indices of refraction associated with the waves, $\mathbf{p}_{1,2}$ are the polarization states, and S is the strain tensor.

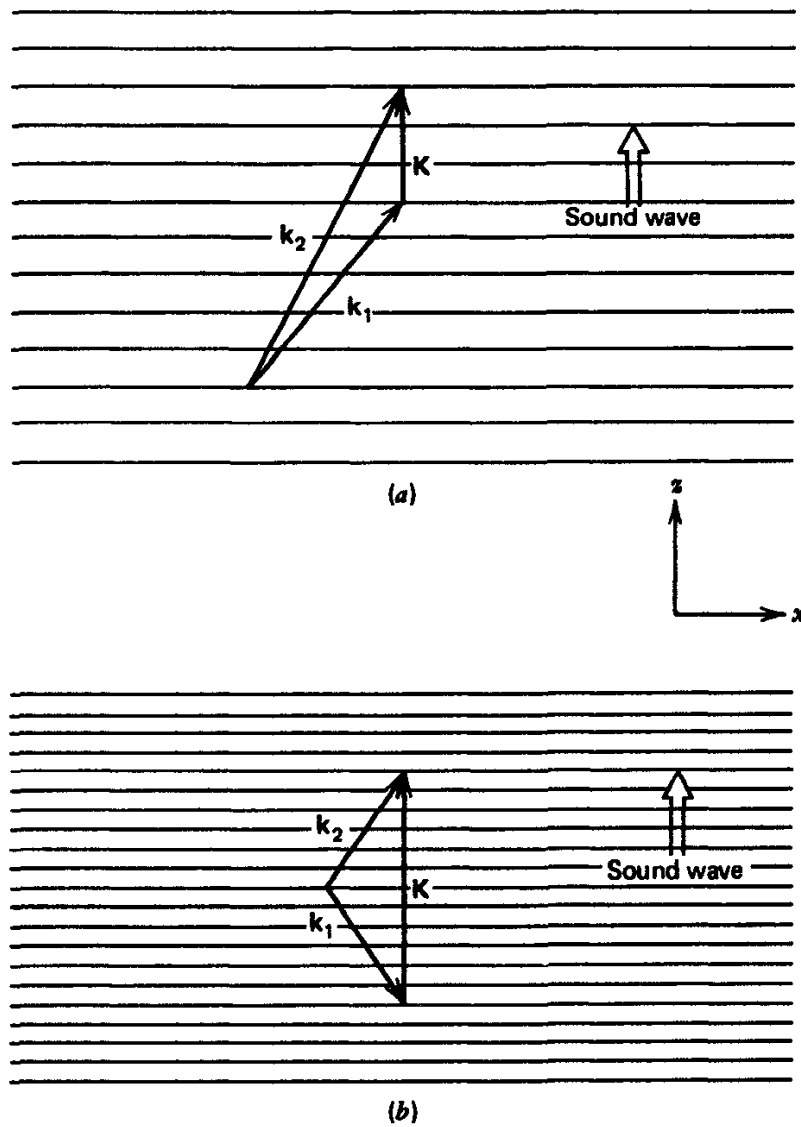


Figure 9.8. (a) Codirectional coupling ($\beta_1\beta_2 > 0$). (b) Contradirectional coupling ($\beta_1\beta_2 < 0$).

The general solutions of Eq. (9.5-45) are given by Eq. (6.4-30). For the case of a single incident wave at $z = 0$, the boundary conditions are $A_1(0) = \text{const}$ and $A_2(0) = 0$. The solution to these conditions is

$$A_1(z) = A_1(0) e^{i\frac{1}{2}\Delta\beta z} \left[\cos sz - i \frac{\Delta\beta}{2s} \sin sz \right] \quad (9.5-47)$$

$$A_2(z) = -iA_1(0) e^{-i\frac{1}{2}\Delta\beta z} \frac{\kappa_{12}^*}{s} \sin sz$$

where

$$s^2 = |\kappa_{12}|^2 + \left(\frac{1}{2}\Delta\beta\right)^2. \quad (9.5-48)$$

Inspection of this solution reveals that the power transfer between the two modes is maximum when $\Delta\beta = 0$. The fraction of power transferred in an interaction distance L is given by

$$T = \frac{|A_2(L)|^2}{|A_1(0)|^2} = \frac{|\kappa_{12}|^2}{|\kappa_{12}|^2 + (\frac{1}{2}\Delta\beta)^2} \sin^2 sL. \quad (9.5-49)$$

This is exactly the transmission of a Šolc filter as discussed in Section 6.5. The dependence of the fraction of power conversion on the phase mismatch $\Delta\beta$ can be used to make a filter which is tunable through the acoustic frequency. To illustrate this, we consider the following example.

Example: Collinear Acousto-optic Interaction in LiNbO₃. We consider the case when an acoustic shear wave and the incident light beam are propagating collinearly down the y axis of the LiNbO₃ crystal, along which the acousto-optic interaction takes place. We take the incident light beam to be an extraordinary wave, polarized along the z (or c) axis of the crystal. The diffracted beam will be an ordinary wave, polarized along the x axis of the crystal. The acoustic wave that is necessary to accomplish this Bragg coupling is a shear wave polarized along the x axis of the crystal. The amplitude of the strain field is thus given by

$$S = \begin{pmatrix} 0 \\ 0 \\ 0 \\ 0 \\ 0 \\ S_6 \end{pmatrix}. \quad (9.5-50)$$

According to the form of the photoelastic tensor shown in Table 9.1, the change in the optical impermeability tensor is

$$\Delta\eta = (pS) = \begin{pmatrix} 0 & \frac{1}{2}(p_{11} - p_{12})S_6 & p_{41}S_6 \\ \frac{1}{2}(p_{11} - p_{12})S_6 & 0 & 0 \\ p_{41}S_6 & 0 & 0 \end{pmatrix}. \quad (9.5-51)$$

The polarization states of the incident and diffracted beams are represented

by

$$\mathbf{p}_1 = \begin{pmatrix} 0 \\ 0 \\ 1 \end{pmatrix}, \quad \mathbf{p}_2 = \begin{pmatrix} 1 \\ 0 \\ 0 \end{pmatrix} \quad (9.5-52)$$

respectively. The dielectric permittivity tensor ϵ' is

$$\epsilon' = \begin{pmatrix} n_o^2 & 0 & 0 \\ 0 & n_o^2 & 0 \\ 0 & 0 & n_e^2 \end{pmatrix} \quad (9.5-53)$$

where n_o , n_e are the refractive indices of the crystal. We now take $n_1 = n_e$, $n_2 = n_o$, and $\theta_1 = \theta_2 = \frac{1}{2}\pi$ in Eq. (9.5-46). Thus, the coupling constant κ_{12} becomes, after using Eqs. (9.5-51), (9.5-52), and (9.5-53),

$$\kappa_{12} = -\frac{\omega(n_o n_e)^{3/2} p_{41} S_6}{4c}. \quad (9.5-54)$$

According to Eq. (9.5-49), it is clear that maximum power conversion, $\sin^2 sL$, will be attained when $\Delta\beta = 0$, or

$$\frac{2\pi}{\lambda}(n_o - n_e) = \frac{2\pi}{\Lambda}. \quad (9.5-55)$$

A 100% power conversion requires that

$$|\kappa_{12}|L = \frac{1}{2}\pi, \quad (9.5-56)$$

where L is the interaction length. The strain amplitude S_6 is directly related to the acoustic intensity by (see Problem 9.1)

$$I_{\text{acoustic}} = \frac{1}{2}\rho v^3 |S_6|^2. \quad (9.5-57)$$

For a 10-cm-long crystal of LiNbO_3 at a central wavelength of $\lambda = 6328 \text{ \AA}$, we have $p_{41} = -0.151$ from Table 9.2(d). Take $n_o = 2.29$, $n_e = 2.20$, $\rho = 4640 \text{ kg/m}^3$, and $v = 4.0 \times 10^3 \text{ m/s}$; a 100% power conversion requires an acoustic power density of 0.2 W/cm^2 according to Eqs. (9.5-56), (9.5-57), and (9.5-54). The acoustic frequency required, according to Eq. (9.5-55), is 0.57 GHz.

Contradirectional Light Coupling ($\beta_1 \beta_2 < 0$). In this coupling, the z components of the two waves are different in sign [see Fig. 9.8(b)]. The coupled

equations (9.5-41), therefore, become

$$\begin{aligned}\frac{d}{dz}A_1 &= i\kappa_{12}A_2e^{i\Delta\beta z} \\ \frac{d}{dz}A_2 &= -i\kappa_{12}^*A_1e^{-i\Delta\beta z}\end{aligned}\quad (9.5-58)$$

where $\Delta\beta$ is given by Eq. (9.5-42) and κ_{12} is given by Eq. (9.5-43) or (9.5-46). In deriving Eq. (9.5-58) from Eq. (9.5-41) we assume that $\beta_1 < 0$ and $\beta_2 > 0$, which corresponds to the interaction configuration shown in Fig. 9.8(b). The general solutions of Eq. (9.5-58) are given by Eq. (6.4-35) with $\kappa = -\kappa_{12}$. For the case of a single wave incident at $z = 0$, the boundary condition is $A_2(L) = 0$. The solution then becomes

$$\begin{aligned}A_1(z) &= A_1(0)e^{i\frac{1}{2}\Delta\beta z} \left[\frac{s \cosh s(L-z) + i\frac{1}{2}\Delta\beta \sinh s(L-z)}{s \cosh sL + i\frac{1}{2}\Delta\beta \sinh sL} \right] \\ A_2(z) &= A_1(0)e^{-i\frac{1}{2}\Delta\beta z} \left[\frac{i\kappa_{12}^* \sinh s(L-z)}{s \cosh sL + i\frac{1}{2}\Delta\beta \sinh sL} \right]\end{aligned}\quad (9.5-59)$$

where

$$s^2 = |\kappa_{12}|^2 - \left(\frac{1}{2}\Delta\beta\right)^2. \quad (9.5-60)$$

Again, the solution Eq. (9.5-59) reveals that maximum coupling of power back to E_2 mode occurs at $\Delta\beta = 0$. The fraction of power transferred in an interaction distance L is given by

$$R = \left| \frac{A_2(0)}{A_1(0)} \right|^2 = \frac{|\kappa_{12}|^2 \sinh^2 sL}{s^2 \cosh^2 sL + \left(\frac{1}{2}\Delta\beta\right)^2 \sinh^2 sL}. \quad (9.5-61)$$

The expression is exactly the same as the reflectivity of a Bragg reflector [Eq. (6.6-10)]. The coupling characteristics of contradirectional acousto-optic interaction are in fact identical to those of the Bragg reflector, except that the refractive-index modulation induced by the acoustic wave is a traveling one. Since the velocity of sound is negligibly small compared with that of light, the periodic perturbation caused by the sound is essentially stationary. Therefore, all the results obtained in Section 6.6 for Bragg reflectors can be applied to the contradirectional acousto-optic interaction.

Example: Contradirectional Collinear Acousto-optic Coupling in LiNbO₃. Consider the Bragg reflection of light in a LiNbO₃ crystal. All the geometry,

the polarization states, and the direction of propagation are exactly the same as those of the previous example, except that the diffracted wave is propagating backward. The phase-matching condition (Bragg condition) $\Delta\beta = 0$ requires that

$$\frac{2\pi}{\lambda}(n_o + n_e) = \frac{2\pi}{\Lambda}, \quad (9.5-62)$$

where Λ is the wavelength of the sound. At $\lambda = 6328 \text{ \AA}$ with a sound velocity of $v = 4.0 \times 10^3 \text{ m/s}$, the acoustic frequency required is 28 GHz, which is too lossy to propagate in most solids. Therefore, large-angle contradirectional acousto-optic interactions are not practical in device applications.

In addition to the high frequency required, the fraction of power reflected at the condition $\kappa_{12}L = \frac{1}{2}\pi$ is only $R = \tanh^2 \frac{1}{2}\pi = 0.84$.

Contradirectional coupling, however, is strongly enhanced if the angles $\theta_{1,2}$ between the wave vectors $\mathbf{k}_{1,2}$ and the acoustic wavefront are small. The coupling constant κ_{12} (9.5-46) at small angles $\theta_{1,2}$ becomes large. The acoustic frequency is also decreased by a similar factor of $\sin \theta$ because the Bragg condition (9.5-62) becomes

$$\frac{2\pi}{\lambda}(n_1 \sin \theta_1 + n_2 \sin \theta_2) = \frac{2\pi}{\Lambda} = \frac{\Omega}{v}. \quad (9.5-63)$$

In fact, this is the Bragg coupling discussed in connection with the small-angle interaction (Section 9.5.1). According to Eq. (9.5-63), the acoustic frequency Ω becomes small when $\theta_{1,2}$ are small.

9.6. RAMAN-NATH DIFFRACTION

We have thus far treated the diffraction of light by an acoustic plane wave of infinite extent. In the particle picture, a plane wave of infinite extent is represented by a particle (phonon) with a well-defined momentum and energy. The Bragg diffraction is viewed as a sum of single collisions each involving the absorption or emission of a phonon by a photon. This fundamental process can occur only when both energy and momentum are conserved. Since the acoustic frequency is much smaller than the optical frequencies, the conservation of energy and momentum requires that the wave vectors of the photons and the phonon form an isosceles triangle (see Fig. 9.3). In this Bragg diffraction, the incident wave at the Bragg angle, $\theta_B = \sin^{-1}(\lambda/2n\Lambda)$, is diffracted by absorbing a phonon. Can the diffracted

wave absorb another phonon and get scattered at a larger angle? The answer is no for the case of an acoustic plane wave of infinite extent, because the conservation of energy and momentum cannot be satisfied simultaneously. This is illustrated in Fig. 9.9(b). Wave vector 0 represents the incident wave at the Bragg angle θ_B . Wave vector 1 represents the diffracted wave that results from the absorption of a phonon. To absorb another phonon with the same phonon wave vector \mathbf{K} , the momentum conservation cannot be satisfied [Fig. 9.9(b)]. Also shown in the same figure [9.9(a)] are multiple or successive three-particle interaction processes which involve the absorption of phonons with slightly different wave vectors. In the latter case, both the energy and momentum are conserved. Thus, we conclude that multiple scattering processes cannot occur when the acoustic wave vector is uniquely defined, which corresponds to a plane wave of infinite extent. Multiple scattering processes can occur only when there is an angular distribution of the acoustic wave vectors \mathbf{K} . The latter corresponds to the case when the acoustic wave is a beam of finite extent.

Let us now investigate qualitatively the criterion for multiple scattering. Inspection of Fig. 9.9(a) reveals that multiple scattering will occur if the angular distribution of the acoustic wave vector \mathbf{K} is large compared to the Bragg angle θ_B . Let L be the beamwidth of the acoustic wave; the angle of spreading of the beam in the far-field region is

$$\Phi \approx \frac{\Lambda}{L}, \quad (9.6-1)$$

where Λ is the wavelength of the sound. According to Eq. (9.2-4), the Bragg

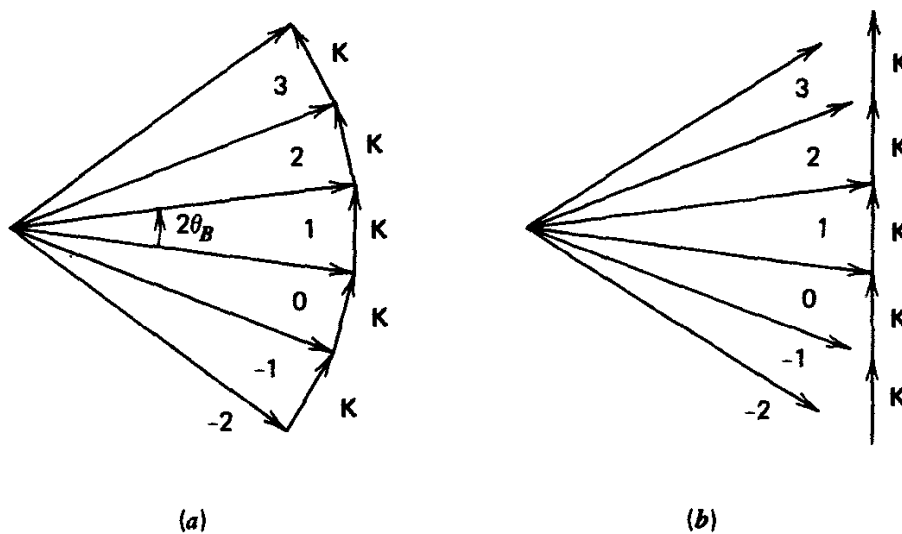


Figure 9.9. Wave vector diagrams for multiple scattering. (a) Multiple scatterings are allowed when the acoustic wave vector has an angular distribution. (b) Multiple scatterings are forbidden when the acoustic wave vector is well defined.

angle is given approximately by

$$\theta_B = \frac{\lambda}{2n\Lambda}. \quad (9.6-2)$$

It is customary to distinguish between the two regimes of diffraction by defining a dimensionless parameter Q :

$$Q = \frac{2\pi\lambda L}{n\Lambda^2} = \frac{4\pi\theta_B}{\Phi}. \quad (9.6-3)$$

One defines the regime $Q > 1$ as the Bragg regime of optical diffraction. In this regime, multiple scattering is not permitted and only one order of diffraction of light is produced. Conversely, one defines the regime $Q < 1$ as the Raman–Nath regime of optical diffraction. In this regime, the angular spread of the acoustic beam is much larger than the Bragg angle θ_B , and therefore many orders of diffraction can be observed. The initial light beam of angular frequency ω is split, after interacting with the acoustic wave, into several beams corresponding to different orders of diffraction. These orders are distinguished by the numbers $0, \pm 1, \pm 2, \pm 3, \dots, \pm m$ which correspond to frequencies $\omega, \omega \pm \Omega, \omega \pm 2\Omega, \dots, \omega \pm m\Omega$ and wave vectors $\mathbf{k}, \mathbf{k} \pm \mathbf{K}, \mathbf{k} \pm 2\mathbf{K}, \dots, \mathbf{k} \pm m\mathbf{K}$. Beam 0 is the extension of the incident beam, beam $+m$ corresponds to the absorption of m phonons, and beam $-m$ corresponds to the emission of m phonons.

To evaluate the diffraction efficiencies associated with each diffraction order, we consider a thin-sheet region in a medium in which an acoustic wave induces a traveling-wave modulation in the index of refraction given by

$$\Delta n(x, y, z, t) = \begin{cases} \Delta n_o \sin(\Omega t - \mathbf{K} \cdot \mathbf{r}), & 0 < z < L, \\ 0 & \text{otherwise.} \end{cases} \quad (9.6-4)$$

For the sake of simplicity in illustrating the basic ideas, we assume that the medium is isotropic and Δn is a scalar. An incident optical wave is represented by

$$\mathbf{E} = \mathbf{E}_0 \exp[i(\omega t - \mathbf{k} \cdot \mathbf{r})]. \quad (9.6-5)$$

This wave is incident onto the thin sheet of sound wave at $z = 0$. In the Raman–Nath regime ($Q < 1$), the interaction length L is small enough so that this periodically perturbed sheet ($0 < z < L$) acts as a phase grating. In other words, the transmission of light through the perturbed region $0 < z <$

L only affects the phase of the plane wave. Thus, the transmitted wave can be written

$$\mathbf{E}_t = \mathbf{E}_0 \exp[-i\phi + i(\omega t - \mathbf{k} \cdot \mathbf{r})], \quad (9.6-6)$$

where ϕ is the phase shift result from passing through the perturbed region and can be written

$$\phi = \int \frac{\omega}{c} \Delta n \, ds. \quad (9.6-7)$$

Here the integral is over the ray path within the region $0 < z < L$. Let θ be the angle of incidence (i.e., the angle between the \mathbf{k} vector and the sound column, which is parallel to the z axis); the path length in the perturbed region is $L/\cos \theta$. If L is small enough, the integral (9.6-7) can simply be written

$$\phi = \frac{\omega}{c} \Delta n_o \frac{L}{\cos \theta} \sin(\Omega t - \mathbf{K} \cdot \mathbf{r}). \quad (9.6-8)$$

Substitution of Eq. (9.6-8) for ϕ in Eq. (9.6-6) leads to

$$\mathbf{E}_t = \mathbf{E}_0 \exp[i(\omega t - \mathbf{k} \cdot \mathbf{r}) - i\delta \sin(\Omega t - \mathbf{K} \cdot \mathbf{r})], \quad (9.6-9)$$

where δ is given by

$$\delta = \frac{\omega L \Delta n_o}{c \cos \theta} = \frac{2\pi L \Delta n_o}{\lambda \cos \theta} \quad (9.6-10)$$

and is referred to as the modulation index. We note that the transmitted field (9.6-9) is phase-modulated. By using the identity for Bessel functions

$$e^{-i\delta \sin x} = \sum_{m=-\infty}^{\infty} J_m(\delta) e^{-imx}, \quad (9.6-11)$$

the transmitted field (9.6-9) can be written

$$\mathbf{E}_t = \mathbf{E}_0 \sum_{m=-\infty}^{\infty} J_m(\delta) \exp[i(\omega - m\Omega)t - i(\mathbf{k} - m\mathbf{K}) \cdot \mathbf{r}]. \quad (9.6-12)$$

According to this equation, the transmitted field is a linear superposition of plane waves with frequencies $\omega - m\Omega$ and wave vectors $\mathbf{k} - m\mathbf{K}$ which are precisely the $-m$ th-order diffracted beam discussed above. The amplitude

of the $-m$ th-order diffracted beam is $J_m(\delta)$. The diffraction efficiency for the m th-order Raman-Nath diffraction is thus given by

$$\eta_m = J_m^2(\delta) = J_m^2\left(\frac{2\pi L \Delta n_o}{\lambda \cos \theta}\right). \quad (9.6-13)$$

In the absence of the modulation ($\Delta n_o = 0$), all the light energy is found in the $m = 0$ order, that is, $\eta_o = 1$ and $\eta_m = 0$ for $m \neq 0$. The diffraction efficiency of the order $m = \pm 1$ is maximum when the modulation index δ is 1.85. The zeroth order is completely quenched when $\delta = 2.4$, since $J_0(2.4) = 0$. Using the identity

$$\sum_{m=-\infty}^{\infty} J_m^2(\delta) = J_0^2(0) = 1, \quad (9.6-14)$$

it follows that

$$\sum_{m=-\infty}^{\infty} \eta_m = 1. \quad (9.6-15)$$

In other words, the sum of the intensities of all the diffracted orders must be equal to the intensity of the incident beam so that the energy is conserved.

9.7. SURFACE ACOUSTO-OPTICS

So far we have limited the discussion to the interaction of light with a bulk acoustic wave in a material medium. The bulk acoustic wave induces a volume phase grating in a photo-elastic medium. The light is then diffracted by the medium via the periodic perturbation in the refractive index. Surface acoustic waves (e.g., Rayleigh waves) propagate on a free surface of a semiinfinite substrate, with the acoustic energy concentrating in a surface layer of the order of one acoustic wavelength. The presence of a surface acoustic wave also changes the optical properties of the substrate. In 1967 Ippen [4] reported the first experimental observation of light diffraction by Rayleigh waves in quartz. The diffraction of light can be produced for two different reasons:

1. The free surface along which the surface wave propagates shows periodic undulations; this traveling periodic corrugation acts as a surface grating and diffracts light.
2. If the substrate is made of photoelastic medium, the strain field associated with the surface acoustic wave will induce periodic variations in the

refractive index; this periodic dielectric perturbation also acts as a surface grating and also diffracts light. However, the effective interaction length is of the order of an acoustic wavelength Λ , and the observed effects are small [5, 6] in comparison to those caused by surface undulations.

We now consider the diffraction of light by the surface undulation caused by the surface acoustic wave. Again, we assume that the surface undulation is stationary, since the acoustic frequency is much smaller than the optical frequency. Let K be the wave number of the acoustic wave ($K = 2\pi/\Lambda$). The profile of the surface undulation can be described by

$$x' = f(z') = a \sin Kz', \quad (9.7-1)$$

where a is the amplitude of the surface undulation and is typically of the order of $10^{-3}\Lambda$. This surface undulation provides a very small perturbation to the surface at $x' = 0$. The diffraction of light can now be described by using the elementary Huygens principle. Each point of the surface acts as a secondary source driven by the light incident on the surface. Most of the light which encounters such a surface is reflected or refracted according to the Fresnel's law, because a is so small ($a \sim 10^{-3}\Lambda$).

The coordinate is chosen so that the x axis is normal to the free surface of the substrate, and the acoustic surface wave is propagating in the z direction (see Fig. 9.10). Let θ , θ_r , and θ_t be the angles of the direction of the incident, reflected, and transmitted light beams, respectively, measured from the x axis. The wave vectors of the reflected and transmitted light beams are given, respectively, by

$$\mathbf{k}_r = k(\cos \theta_r \hat{\mathbf{x}} + \sin \theta_r \hat{\mathbf{z}}), \quad (9.7-2)$$

$$\mathbf{k}_t = nk(-\cos \theta_t \hat{\mathbf{x}} + \sin \theta_t \hat{\mathbf{z}}),$$

where k is the wave number of the incident light ($k = 2\pi/\lambda$) and n is the index of refraction of the medium. Let E_0 be the amplitude of the incident plane wave. The field at the surface of the medium is given by

$$E = E_0 \exp[-ik(-\cos \theta x' + \sin \theta z')], \quad (9.7-3)$$

which, on scattering from the surface, forms a distributed source.

Each point (x', z') on the surface will scatter some of the radiation out of the incident beam. The contribution of the surface element dz' at point P to the amplitude of the reflected wave at far field involves a phase factor of

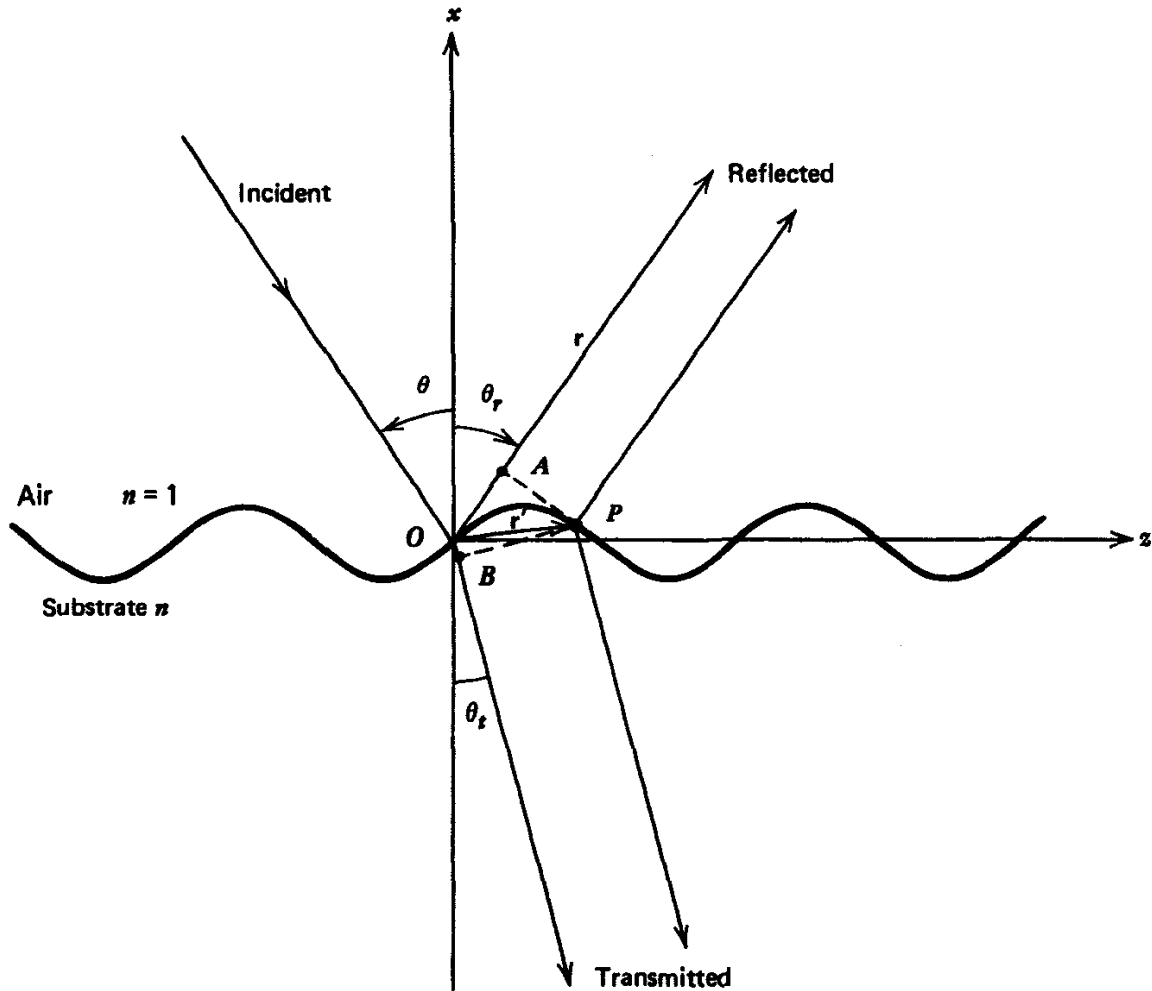


Figure 9.10. Coordinates for light diffraction by an acoustic surface wave.

$e^{i\mathbf{k}_r \cdot \mathbf{r}'}$ relative to the contribution from the origin O (see Fig. 9.10). Here \mathbf{k}_r is the wave vector of the reflected wave and \mathbf{r}' is the vector OP . We now assume that the surface-undulation amplitude a is much smaller than the wavelength of light (i.e., $ka \ll 1$), so that the contributions from each point of the surface are weighted equally. Thus the amplitude of the reflected wave at far field is proportional to

$$\int E e^{i\mathbf{k}_r \cdot \mathbf{r}'} e^{-i\mathbf{k}_r \cdot \mathbf{r}} dz' d\beta, \quad (9.7-4)$$

where \mathbf{r} is the position of a general point of observation and $\beta = k \sin \theta_r$ is the z component of the wave vector \mathbf{k}_r . The z' integration (9.7-4) is over the surface $x' = a \sin Kz'$ from $-\infty$ to $+\infty$, and the integration over β is also from $-\infty$ to $+\infty$. By using Eqs. (9.7-2) and (9.7-3), the reflected wave can

be written

$$E_r = CE_0 \int e^{ikx'(\cos \theta + \cos \theta_r) - i(k \sin \theta - \beta)z' - ik_r \cdot r} dz' d\beta, \quad (9.7-5)$$

where we have used $\beta = k \sin \theta_r$, C is a proportionality constant, and x' is given by Eq. (9.7-1). We now substitute Eq. (9.7-1) for x' in Eq. (9.7-5) and use the following identity for Bessel functions:

$$e^{i\alpha \sin \phi} = \sum_{l=-\infty}^{\infty} J_l(\alpha) e^{il\phi}. \quad (9.7-6)$$

Equation (9.7-5) becomes

$$E_r = CE_0 \int \sum_{l=-\infty}^{\infty} J_l(\alpha) e^{ilKz' - i(k \sin \theta - \beta)z' - ik_r \cdot r} dz' d\beta, \quad (9.7-7)$$

where

$$\alpha = ka(\cos \theta + \cos \theta_r). \quad (9.7-8)$$

By carrying out the integration over z' in Eq. (9.7-7), the amplitude of the reflected wave becomes

$$E_r = CE_0 \sum_{l=-\infty}^{\infty} \int J_l(\alpha) 2\pi \delta(\beta + lK - k \sin \theta) e^{-ik_r \cdot r} d\beta, \quad (9.7-9)$$

where δ is the Dirac delta function. By using Eq. (9.7-2) and carrying out the integration over β , Eq. (9.7-9) can be written

$$E_r = 2\pi CE_0 \sum_{l=-\infty}^{\infty} J_l(\alpha) e^{-ik \cos \theta_r x - i(k \sin \theta - lK)z}, \quad (9.7-10)$$

where θ_r is given by

$$k(\sin \theta_r - \sin \theta) = -lK. \quad (9.7-11)$$

The condition (9.7-11) is the conservation of momentum, which also determines the angles of diffraction θ_r for various orders $l = 0, \pm 1, \pm 2, \dots$. It can also be written as

$$\sin \theta_r = \sin \theta - \frac{l\lambda}{\Lambda}. \quad (9.7-12)$$

In practice, the acoustic wavelength Λ is usually much larger than the optical wavelength λ ; the angle θ_r can be approximated by

$$\theta_r = \theta + \Delta\theta = \theta - \frac{l\lambda}{\Lambda \cos \theta} \quad (9.7-13)$$

provided that l is not too large, where $\Delta\theta = \theta_r - \theta$ is the angle between the directions of the diffracted and the reflected beam. Since $\theta_r \approx \theta$, α in Eq. (9.7-8) can be written $\alpha \approx 2ka \cos \theta$. Thus the amplitude of the reflected wave (9.7-10) can be written

$$E_r = 2\pi C E_0 \sum_{l=-\infty}^{\infty} J_l(2ka \cos \theta) e^{-ik \cos \theta x - i(k \sin \theta - lK)z}. \quad (9.7-14)$$

The proportionality constant C can be determined by considering the limiting case when the surface undulation disappears ($a = 0$). When this happens, the amplitude of the reflected wave is simply rE_0 . Here r is the Fresnel reflection coefficient. By setting $a = 0$ in Eq. (9.7-10), the amplitude E_r becomes

$$E_r = 2\pi C E_0 e^{-ik \cos \theta x - ik \sin \theta z}. \quad (9.7-15)$$

Therefore, the constant C is simply $r/2\pi$. The amplitude E_r of the reflected wave can thus be written

$$\begin{aligned} E_r &= rE_0 \sum_{l=-\infty}^{\infty} J_l(2ka \cos \theta) e^{-ik \cos \theta x - i(k \sin \theta - lK)z} \\ &= rE_0 \sum_{l=-\infty}^{\infty} J_l(2ka \cos \theta) e^{-i(\mathbf{k} - lK\hat{z}) \cdot \mathbf{r}}, \end{aligned} \quad (9.7-16)$$

where r is the Fresnel reflection coefficient and l is the diffraction order. Here we have an expression for the reflected wave which consists of a linear superposition of plane wave components with wave vectors $\mathbf{k} - lK\hat{z}$. Each l corresponds to a diffracted beam. Each diffraction beam is propagating in a direction θ_r given by Eq. (9.7-11) or (9.7-12) with an amplitude of $rE_0 J_l(2ka \cos \theta)$. The diffraction efficiency defined as the fraction of power diffracted is thus

$$\eta_l = |r|^2 J_l^2(2ka \cos \theta). \quad (9.7-17)$$

Using similar arguments, the amplitude of the transmitted wave can be written as

$$E_t = C' E_0 \int e^{ikx'(\cos \theta - n \cos \theta_t) - i(k \sin \theta - \beta)z' - ik_t \cdot r} dz' d\beta, \quad (9.7-18)$$

where $\beta = nk \sin \theta_t$. The result can be obtained in a similar way and is given by

$$E_t = tE_0 \sum_{l=-\infty}^{\infty} J_l(ka \cos \theta - nka \cos \theta_t) e^{in k \cos \theta_t x - i(k \sin \theta - lK)z} \quad (9.7-19)$$

and

$$nk \sin \theta_t - k \sin \theta = -lK. \quad (9.7-20)$$

According to Eq. (9.7-19), the transmitted wave also consists of many diffracted beams. Each diffracted beam is propagating in the direction θ_t given by Eq. (9.7-20). The diffraction efficiencies for the transmitted wave are thus given by

$$\eta_l = \frac{n \cos \theta_t}{\cos \theta} |t|^2 J_l^2(ka \cos \theta - nka \cos \theta_t), \quad (9.7-21)$$

where t is the Fresnel transmission coefficient and the factor $(n \cos \theta_t)/\cos \theta$ corrects for the difference in the velocity of light in the two media.

The above derivation for the intensity of the diffracted beams is based on the scalar diffraction theory and is valid only when $ka \ll 1$. For typical acoustic surface waves, the amplitude of undulation is of the order of 10^{-3} μm or less, making $ka \sim 10^{-3}$ for optical diffraction. The scalar approximation for the diffraction amplitudes derived above is thus very good. In fact, the results (9.7-17) and (9.7-21) agree with the conservation of energy if we recall that $|r|^2 + (n \cos \theta_t |t|^2)/\cos \theta = 1$ and use Eq. (9.6-14).

PROBLEMS

9.1. *Acousto-optical effect in LiNbO₃.* We consider the propagation of an x -polarized shear wave in the y direction of a LiNbO₃ crystal. Let the particle displacement be represented by

$$u(y, t) = \hat{x} u_0 \exp[i(\Omega t - Ky)].$$

- (a) Derive an expression of the strain field associated with this shear wave.

- (b) The point-group symmetry of LiNbO_3 is $3m$. Use Table 9.1 and obtain an expression for the change in the optical dielectric impermeability tensor $\Delta\eta_{ij}$ induced by the strain field.

- 9.2. Bragg's law for diffraction of X-rays in crystals is [7]

$$2d \sin \theta = m \frac{\lambda}{n}, \quad m = 1, 2, 3, \dots,$$

where d is the distance between equivalent atomic planes, θ is the angle of incidence, and λ/n is the wavelength of the diffracted radiation. Bragg diffraction of light from sound [see Eq. (9.2-4)] takes place when

$$2\Lambda \sin \theta = \frac{\lambda}{n}.$$

Thus, if we compare it with the X-ray result and take $\Lambda = d$, only the case of $m = 1$ is allowed. Explain the difference. Why don't we get light diffracted along directions θ corresponding to $m = 2, 3, \dots$? [Hint: The diffraction of X-rays can be assumed to take place at discrete atomic planes, which can be idealized as infinitely thin sheets, whereas the sound wave is continuous in z ; see Fig. 9.2.]

- 9.3. What happens in Bragg diffraction of light from a standing sound wave? Describe the frequency shifts and direction of diffraction.
- 9.4. *Surface acousto-optics.* Consider the propagation of a surface wave along the free surface of a photoelastic medium. Let the surface undulation be

$$x = a \sin Kz.$$

- (a) Ignore the photoelastic effect and assume that the surface undulation acts like a phase grating. Show that the modulation index is

$$\phi_1 = k(n - 1)2a$$

for normal incident light.

- (b) Show that the strain field associated with the surface wave has an amplitude of the order of

$$S \approx Ka.$$

- (c) Ignore the surface undulation and consider only the phase grating induced by this strain field. Assume that the strain field is

only confined in a region of $1/K$ from the surface. Show that the modulation index is

$$\phi_2 = \frac{1}{2} n^3 k p S / K.$$

(d) Use $S = Ka$ from (b) and show that

$$\phi_2 = \frac{1}{2} n^3 k p a \quad \text{and} \quad \frac{\phi_2}{\phi_1} = \frac{n^3 p}{4(n-1)}.$$

(e) Evaluate this number ϕ_2/ϕ_1 for quartz, germanium, and LiNbO_3 . Show that the diffraction due to the surface undulation is usually stronger than that of the refractive-index modulation for surface acoustic waves.

REFERENCES AND SUGGESTED READING

1. K. -H. Hellwege, *Landolt-Bornstein*, Vol. 11, Springer-Verlag, 1979.
2. See, for example, Robert Adler, "Interaction between light and sound," *IEEE Spectrum* **4**, 42 (May 1967).
3. R. W. Dixon, "Photoelastic properties of selected materials and their relevance for applications to acoustic light modulators and scanners," *J. Appl. Phys.* **38**, 5149 (1967).
4. E. I. Gordon, *Proc. IEEE* "A review of acousto-optical deflection and modulation devices," **54**, 1391 (1967).
5. E. Salzmann and D. Weismann, "Optical detection of Rayleigh waves," *J. Appl. Phys.* **40**, 3408 (1969).
6. E. P. Ippen, *Proc. IEEE* "Diffraction of light by surface acoustic waves," **55**, 248 (1967).
7. C. Kittel, *Introduction to Solid State Physics*, 3d Ed., Wiley, New York, 1967, p. 38.
8. R. W. Damon, W. T. Maloney, and D. H. McMachon, "Interaction of light with ultrasound; Phenomena and applications," in *Physical Acoustics*, W. P. Mason, Ed., Vol. VII, Academic Press, New York 1970.
9. A. Korpel, "Acousto-optics," in *Applied Solid State Science*, R. Wolfe, Ed., Vol. 3, Academic Press, New York 1972.
10. E. G. Lean, "Interaction of light and acoustic surface waves," in *Progress in Optics*, Vol. XI, E. Wolf, Ed., North-Holland, Amsterdam 1973.
11. J. Sapriel, *Acousto-optics*, Wiley, New York, 1979.

10

Acousto-optic Devices

The interaction of light beams with a sound wave in a photoelastic medium is shown in Chapter 9 to exhibit many interesting effects. These effects (e.g., Bragg diffraction) can be used to build light modulators, beam deflectors, tunable filters, spectral analyzers, and signal processors. The use of acousto-optic interactions offers the possibility of manipulating a laser beam or processing signal radiation at high speed, since no mechanical moving parts are involved. This property is very similar to that of the electro-optic modulation, except that in the acousto-optic interaction an RF field is required instead of a dc field. Recent advances in the acousto-optic device applications have resulted principally from the availability of lasers, which produce intense, coherent light beams; from the development of efficient broadband transducers which generate elastic waves up to microwave frequencies; and from the discovery of materials that have excellent elastic and optical properties. In this chapter we will study various device applications which utilize Bragg diffraction. The transmission characteristics, diffraction efficiencies, operation bandwidth, and other design considerations will be discussed.

10.1. ACOUSTO-OPTIC MODULATORS

The acousto-optic interaction can be used to construct a variety of light modulators. Both amplitude modulation and frequency translation can be achieved. The modulator can operate in either the Raman-Nath regime or the Bragg regime. The first acousto-optic modulator [1,2] operated in the Raman-Nath regime at frequencies below 10 MHz. Figure 10.1 illustrates the principle of operation. According to the discussions in Chapter 9, the amplitude of the first-order diffracted wave is proportional to $J_1(k\Delta nL)$. Here $k\Delta nL$ is the modulation index and is proportional to the acoustic field amplitude. If the RF sound carrier is modulated with the information-bearing

ing signal, the diffracted light will also be modulated with the same signal. In this operation the zeroth-order light must be blocked by a suitably located stop. The modulation is reasonably linear provided the modulation index $k\Delta nL$ is less than 2.4 [see Section 9.6]. The disadvantage of operating in the Raman–Nath regime is the small interaction length permitted by the criterion $2\pi\lambda L/n\Lambda^2 < 1$. At high RF frequencies (small Λ), the maximum allowable length L is too small for practical application (see Problem 10.1), because of the excessive acoustic power required. This causes the Raman–Nath light modulators to be limited to low-frequency operation and consequently to possess limited bandwidths.

In this section, modulators operating in the Bragg regime ($2\pi\lambda L/n\Lambda^2 > 1$) will be emphasized, since only high-frequency modulators can give the very wide bandwidths which are of interest. From Eq. (9.5-29) it is seen that

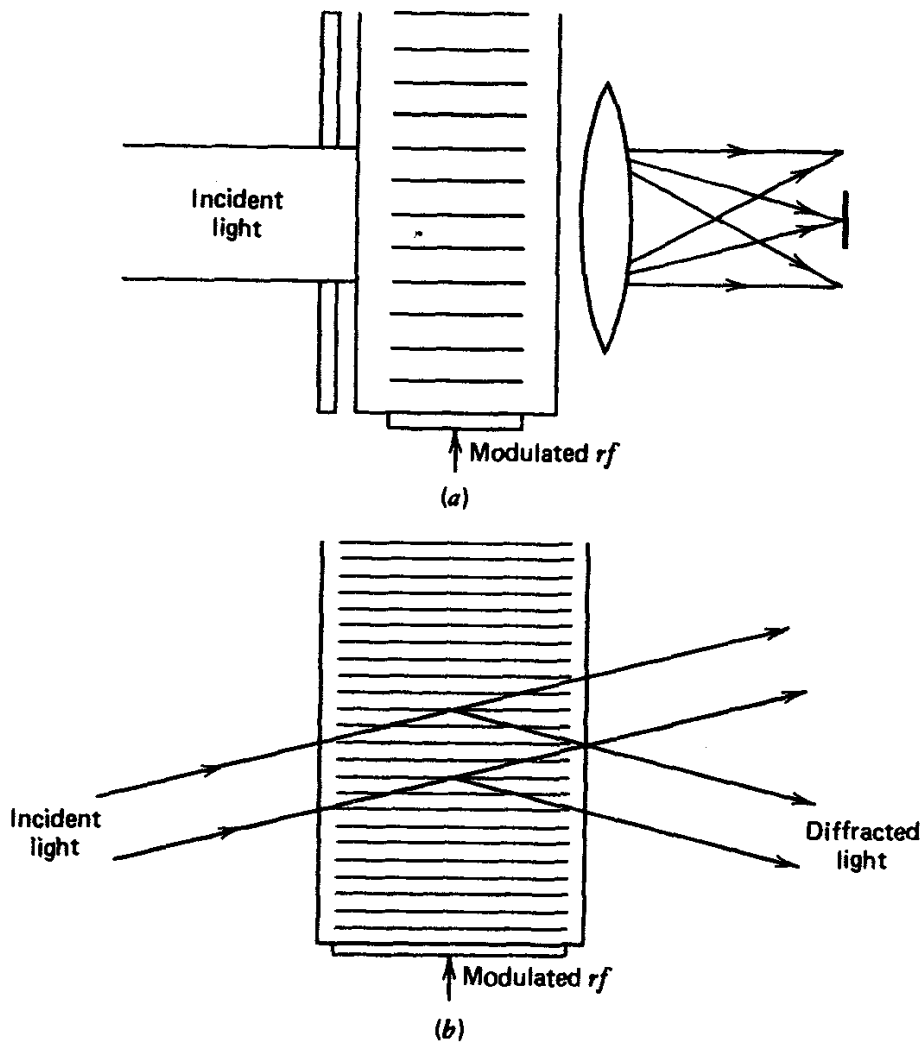


Figure 10.1. Acousto-optic light modulators: (a) Raman–Nath regime; (b) Bragg regime.

the fraction of light diffracted is

$$\eta = \frac{I_{\text{diffracted}}}{I_{\text{incident}}} = \sin^2 \left(\frac{\pi L}{\lambda \sqrt{2} \cos \theta_B} \sqrt{M I_a} \right), \quad (10.1-1)$$

where L is the length of interaction, λ is the wavelength of light, θ_B is the Bragg angle, I_a is the acoustic intensity, and M is the figure of merit of the material. For small acoustic power levels, the diffraction efficiency η increases monotonically with the acoustic intensity:

$$\eta \approx \frac{\pi^2 L^2}{2 \lambda^2 \cos^2 \theta_B} M I_a. \quad (10.1-2)$$

Therefore, if the acoustic intensity is modulated, so is the diffracted light-beam intensity. Thus acousto-optic Bragg diffraction offers a way of imprinting information on the optical beam. The Bragg diffraction, of course, occurs with acceptable efficiency only when the directions of incident and diffracted light are approximately symmetrical with respect to the acoustic wavefronts. The angle of incidence and diffraction is then known as the Bragg angle θ_B and is given by

$$\theta_B = \sin^{-1} \frac{\lambda}{2n\Lambda} = \sin^{-1} \frac{\lambda f}{2nv}, \quad (10.1-3a)$$

where n is the index of refraction of the medium, v is the phase velocity of sound, and f is the sound frequency. In practice, the Bragg angle θ_B is small, so Eq. (10.1-3a) can be written as

$$\theta_B = \frac{\lambda}{2n\Lambda} = \frac{\lambda f}{2nv}. \quad (10.1-3b)$$

For small Bragg angle θ_B , the angle of deflection $2\theta_B$ is linearly proportional to the sound frequency. This is the basic principle of operation of an acousto-optic beam deflector (see Section 10.2). In what follows, we will discuss some important parameters of the modulators such as bandwidth and efficiency.

10.1.1. Bandwidth

A modulated acoustic wave is usually characterized by its center frequency f_0 and bandwidth Δf (i.e., modulation bandwidth). The attainable modula-

tion bandwidth Δf of an acousto-optic modulator is determined mainly by the angular spread of the light beam, as will be seen in the following discussion. For infinitely wide beams of sound and light, the wave vectors are well defined. Therefore, for a given angle of incidence and the corresponding angle of diffraction, the Bragg condition (10.1-3) can only be satisfied at one acoustic frequency (zero bandwidth, $\Delta f = 0$). In practice one is constrained to use finite beams of sound and light, which result in finite angular beam spread. The finite angular distribution of the wave vectors allows the Bragg diffraction to occur over a range of acoustic frequencies (finite bandwidth). By differentiating Eq. (10.1-3a), one obtains the bandwidth

$$\Delta f = \frac{2nv \cos \theta}{\lambda} \Delta \theta, \quad (10.1-4)$$

where $\Delta \theta$ is the variation of the angle of incidence and diffraction due to the angular spread of the beams of sound and light. This $\Delta \theta$ is the change in the Bragg angle required to satisfy the Bragg conditions when the acoustic frequency is changed by Δf . Let $\delta \theta$ be the angular spread of the light wave vectors, and $\delta \phi$ be the angular spread of the sound wave vectors. These beam divergence angles are related to the wavelength and the beam width, and are given approximately, for the diffraction limited beams, by

$$\delta \theta = \frac{2\lambda}{\pi n \omega_0}, \quad \delta \phi = \frac{\Lambda}{L}, \quad (10.1-5)$$

where ω_0 is the spot size of the laser beam at the waist, and n is the index of refraction of the medium. It is obvious that the angle of incidence (angle between the light wave vector \mathbf{k} and the sound wave vector \mathbf{K}) now covers a range of

$$\Delta \theta = \delta \theta + \delta \phi. \quad (10.1-6)$$

Let us now investigate the Bragg diffraction of a finite light beam from a modulated acoustic beam of finite width L . The diverging beams can be represented by plane waves with wave vectors lying within the angular spread. For each angular component of the light beam, the Bragg condition can be satisfied over a range of acoustic frequencies corresponding to the allowed values of \mathbf{K} within $\delta \phi$. At each acoustic frequency, a different plane-wave component with a different direction of \mathbf{K} is responsible for the diffraction. The diffracted light beam corresponding to this fixed angle of incident light has an angular spread of $2\delta \phi$. Each direction corresponds to a

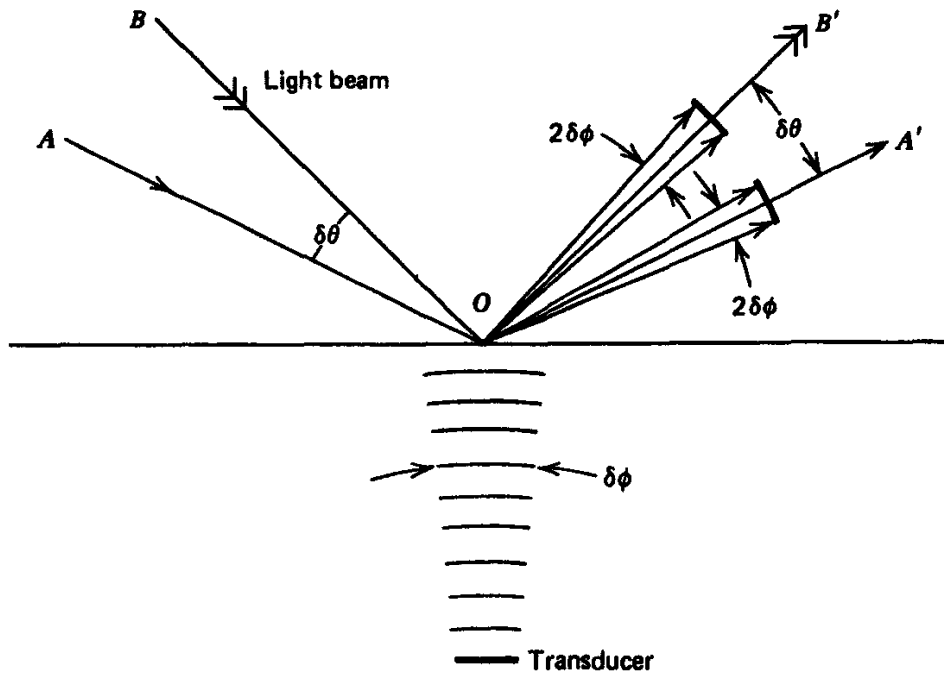


Figure 10.2. Bragg diffraction of a finite light beam from a modulated acoustic beam of finite width. The angular spreads of the beams are $\delta\theta$ and $\delta\phi$, respectively, for the light and sound.

different frequency shift. Figure 10.2 illustrates the angular spreading of light beams for the two extreme angular components. In order to recover the intensity modulation of the diffracted light beam, it is necessary that the spectrally shifted components of the diffracted light be mixed in a square-law detector. Therefore, it is desirable that the two extreme diffracted lights (OA' and OB' in Fig. 10.2) have some angular overlap. This requires that $\delta\phi \approx \delta\theta$. Taking $\delta\theta = \delta\phi = \lambda/\pi n \omega_0$ gives the modulating bandwidth

$$(\Delta f)_m = \frac{1}{2} \Delta f = \frac{2v}{\pi \omega_0} \cos \theta, \quad (10.1-7)$$

which is roughly equal to the reciprocal of the acoustic transit time across the optical beam. According to this expression, the bandwidth of an acousto-optic modulator is inversely proportional to the beam diameter of the light. A large modulation bandwidth Δf can be obtained by using beams with small width. However, when the beam divergence angle $\delta\theta$ becomes too big, the diffracted light beam will have some overlap with the undiffracted beam. This may degrade the operation of the modulator. Therefore, the maximum fractional bandwidth of an acousto-optic modulator is usually determined by the condition that the diffracted light beam does not interfere with the undifferentiated beam, which requires that $\Delta\theta < \theta_B$. Thus, from Eqs.

(10.1-3) and (10.1-4), and using $\Delta\theta = \theta_B$, we obtain

$$\frac{(\Delta f)_m}{f} \approx \frac{\Delta f}{2f} < \frac{1}{2}. \quad (10.1-8)$$

Thus the maximum modulation bandwidth is approximately one-half of the acoustic frequency. Therefore, large modulation bandwidths are only available with high-frequency Bragg diffraction.

10.1.2. Efficiency

Another important parameter of an acousto-optic modulator is the diffraction efficiency, that is, the fraction of incident light energy diffracted. According to Eq. (10.1-1), the acoustic intensity I_a required for 100% modulation (i.e., total conversion of the incident light) is given by

$$I_a = \frac{\lambda^2 \cos^2 \theta_B}{2ML^2}, \quad (10.1-9)$$

where M is the figure of merit defined in Eq. (9.5-28) and λ is the wavelength of the light. Notice that the acoustic intensity required is proportional to λ^2 . Let h be the height of the transducer. The acoustic power required, P_a , is

$$P_a = hLI_a = \frac{\lambda^2 \cos^2 \theta_B}{2M} \left(\frac{h}{L} \right). \quad (10.1-10)$$

According to Eq. (10.1-10), it is desirable to have a small aspect ratio (h/L) for efficient operation of a modulator. For small diffraction efficiency ($\eta \ll 1$), Eq. (10.1-1) can be written approximately as

$$\eta = \frac{I_{\text{diffracted}}}{I_{\text{incident}}} = \frac{\pi^2 L^2}{2\lambda^2 \cos^2 \theta_B} MI_a, \quad (10.1-11)$$

or, using $I_a = P_a/hL$,

$$\eta = \frac{\pi^2}{2\lambda^2 \cos^2 \theta_B} \left(\frac{L}{h} \right) MP_a. \quad (10.1-12)$$

The figure of merit M is often written as M_2 in Eq. (10.1-12) for the purpose of introducing other useful figures of merit. The M_2 defined in Eq. (9.5-28)

is often formally written as

$$M_2 = \frac{n^6 p^2}{\rho v^3}. \quad (10.1-13)$$

A more useful figure of merit should include the modulator bandwidth, which is often an important design parameter. According to Eq. (10.1-12), the diffraction efficiency η increases linearly with the acoustic beam width L . However, the angular spread of the acoustic beam, $\delta\phi$, is proportional to L^{-1} according to Eq. (10.1-5). A small $\delta\phi$ means a small modulation bandwidth, according to Eq. (10.1-4) and the requirement that $\delta\phi \approx \delta\theta = \frac{1}{2}\Delta\theta$. Taking $\delta\phi = \Lambda/2L$ and using Eqs. (10.1-6), (10.1-5), and (10.1-4), the bandwidth can be written

$$\Delta f = \frac{2nv\Lambda}{\lambda L} \cos \theta_B, \quad (10.1-14)$$

where Λ is the acoustic wavelength and θ_B is the Bragg angle. A quantity introduced by Gordon [3], which is independent of the modulator width L , is

$$2\eta f_0 \Delta f = \left(\frac{n^7 p^2}{\rho v} \right) \frac{2\pi^2}{\lambda^3 \cos \theta_B} \left(\frac{P_a}{h} \right), \quad (10.1-15)$$

where f_0 is the center acoustic frequency ($f_0 = v/\Lambda$). The factor

$$M_1 = \frac{n^7 p^2}{\rho v} \quad (10.1-16)$$

provides a useful figure of merit for materials to be used in modulators (and deflectors).

Another quantity, introduced by Dixon [4], which is independent of the acoustic and optical beam dimensions is

$$\eta f_0 = \left(\frac{n^7 p^2}{\rho v^2} \right) \frac{\pi^2}{2\lambda^3 \cos^2 \theta_B} P_a, \quad (10.1-17)$$

where we have taken $\Lambda/L = 2\lambda/\pi n\omega_0$ (i.e., $\delta\phi = \delta\theta$) and used $h = \frac{1}{2}\pi\omega_0$. The third figure of merit is

$$M_3 = \frac{n^7 p^2}{\rho v^2}. \quad (10.1-18)$$

The figures of merit M_1 , M_2 , and M_3 defined above all have their significances in the device operation. For small modulation efficiency, M_2 is proportional to the efficiency η . If we take into account the bandwidth Δf of modulation, then we have to consider the figure of merit M_1 , which is proportional to $2\eta f_0 \Delta f$. Values of M_1 , M_2 , and M_3 for a number of materials are given in Table 10.1. These parameters, although written formally in terms of n , p , ρ , v , depend on the interaction configurations and the polarization states of the waves. As will be seen in Section 10.2, these parameters are also applicable to acousto-optic beam deflectors.

10.1.3. Birefringent Acousto-optic Modulators

In the above derivation of the bandwidth, we assumed that the incident and diffracted light waves were of equal wave vector. This is not necessarily true in birefringent materials. As described in the last chapter, the Bragg condition for acousto-optic interaction in anisotropic media is modified if the incident and the diffracted light beams possess different phase velocities. The modulation bandwidth of a birefringent acousto-optic modulator may be different from that of the isotropic case. To illustrate this, we consider the following two examples:

Example: Noncollinear Acousto-optic Modulation in a Uniaxial Crystal. We consider the acousto-optic interaction in a uniaxial crystal (e.g., LiNbO_3) in which the plane of scattering is perpendicular to the c axis. The interaction configuration is shown in Fig. 10.3(a). We assume that the crystal is negatively uniaxial ($n_e < n_o$). The incident light is linearly polarized along the c axis so that it propagates in the extraordinary mode of the crystal with a phase velocity of c/n_e . The diffracted light is assumed to be linearly polarized in the scattering plane (xy plane), and is in the ordinary mode of the crystal with a phase velocity c/n_o . The angles of incidence and diffraction are given by Eqs. (9.4-5) and (9.4-6) and are plotted in Fig. 9.5 as functions of $\lambda/\Lambda = \lambda f/v$. It can be seen from Fig. 9.6 that the angle of diffraction θ' is nearly constant over a broad range of acoustic frequencies, while the angle of incidence varies near $\theta = 0^\circ$. In fact, according to Eqs. (9.4-5) and (9.4-6), the rate of variation of the diffraction angle θ' with λ/Λ vanishes when $\theta = 0$ (i.e., $\partial\theta'/\partial f = 0$, when $\theta = 0$). This corresponds to the interaction configuration shown in Fig. 10.3a. The acoustic frequency responsible for this scattering configuration is given, according to Eq. (9.4-5) with $\theta = 0$, by

$$f_0 = \frac{v}{\lambda} \sqrt{n_o^2 - n_e^2} \approx \frac{v}{\lambda} \sqrt{2n_o \Delta n} \quad (10.1-19)$$

Table 10.1. Properties of Acousto-optic Materials^a

Material	λ (μm)	n	ρ (g/cm^3)	Acoustic-Wave Polarization and Direction	v (10^3 m/sec)	Optical-Wave ^b Polarization and Direction	Figures of Merit		
							$M_1 =$ $n^7 p^2 / \rho v$	$M_2 =$ $n^6 p^2 / \rho v^3$	$M_3 =$ $n^7 p^2 / \rho v^2$
Fused quartz	0.63	1.46	2.2	Long. Trans.	5.95 3.76	\perp \parallel or \perp	7.89×10^{-8} 0.963	1.51×10^{-15} 0.467	1.29×10^{-11} 0.0256
GaP	0.63	3.31	4.13	Long. in [110] Trans. in [100]	6.32 4.13	\parallel \parallel or \perp in [010]	590 137	44.6 24.1	93.5 33.1
GaAs	1.15	3.37	5.34	Long. in [110] Trans. in [100]	5.15 3.32	\parallel \parallel or \perp in [010]	925 155	104 46.3	179 49.2
TiO ₂	0.63	2.58	4.6	Long. in [11 $\bar{2}$ 0]	7.86	\perp in [001]	62.5	3.93	7.97
LiNbO ₃	0.63	2.20	4.7	Long. in [11 $\bar{2}$ 0]	6.57	\parallel	66.5	6.99	10.1
YAG	0.63	1.83	4.2	Long. in [100] Long. in [110]	8.53 8.60	\parallel \perp	0.16 0.98	0.012 0.073	0.019 0.114
YIG	1.15	2.22	5.17	Long. in [100]	7.21	\perp	3.94	0.33	0.53
LiTaO ₃	0.63	2.18	7.45	Long. in [001]	6.19	\parallel	11.4	1.37	1.84
As ₂ S ₃	0.63	2.61	3.20	Long. Long.	2.6 3.63	\perp \parallel	762 619	433 347	293 236
SF-4	0.63	1.616	3.59	Long.	5.51	\perp	1.83	1.51	3.97
β -ZnS	0.63	2.35	4.10	Long. in [110] Trans. in [110]	2.165	\parallel in [001] \parallel or \perp in [001]	24.3 10.6	3.41 0.57	4.41 4.9
α -Al ₂ O ₃	0.63	1.76	4.0	Long. in [001]	11.15	\parallel in [11 $\bar{2}$ 0]	7.32	0.34	0.66
CdS	0.63	2.44	4.82	Long. in [11 $\bar{2}$ 0]	4.17	\parallel	51.8	12.1	12.4
ADP	0.63	1.58	1.803	Long. in [100] Trans. in [100]	6.15 1.83	\parallel in [010] \parallel or \perp in [001]	16.0 3.34	2.78 6.43	2.62 1.83
KDP	0.63	1.51	2.34	Long. in [100] Trans. in [100]	5.50	\parallel in [010] \parallel or \perp in [001]	8.72 1.57	1.91 3.83	1.45 0.95
H ₂ O	0.63	1.33	1.0	Long.	1.5	\parallel	4.36	160	29.1
Te	10.6	4.8	6.24	Long. in [11 $\bar{2}$ 0]	2.2	\parallel in [0001]	10,200	4400	4640

TeO ₂	0.63	5.99	Long. in [100]	2.98	[100] in [010]	0.097	0.048
			Long. in [100]		[001] in [010]	22.9	10.6
			Long. in [001]	4.26	[100] in [010]	142	34.5
			Long. in [001]		[001] in [010]	113	25.6
			[010] in [100]	3.04	Arb. in [001]	3.70	1.76
			Long. in [110]	4.21	[110] in $\bar{1}10$	323	0.802
			Long. in [110]		[001] in $\bar{1}10$	16.2	3.77
			Long. in [101]	3.64	[010] in $\bar{1}01$	101	33.4
			Long. in [010]	2.98	[101] in $\bar{1}01$	42.6	20.4
			$\bar{1}10$ in [110]	0.617	Arb. in 001	68.6	793
PbMoO ₄			$\bar{1}01$ in [101]	2.08	[100] in [010]	76.4	77
	0.63	6.95	Long. in [100]	3.98	[001] in [010]		7.5
			Long. in [100]	3.98	[100] in [010]		24
			Long. in [100]	3.98	[010] in [001]		24
			[100] in [010]	2.20*	[100] in [001]		12.8
			[100] in [001]	1.99			
			Long. in [001]	3.75	[100] in [010]		35.6
			Long. in [001]	3.75	[001] in [010]		35.6
			Long. in [001]	3.75	[100] in [010]		43.4
			Long. in [001]	3.75	[100] in [010]		56.1
Bi ₁₂ GeO ₂₀ (BGO)	0.63	2.55	Long. in [110]	3.42	Arb. pol. ^c	29.5	9.91
	0.63		Long. in [100]	3.83	Arb. pol. ^c	33.8	9.02
	0.63	2.30	Long. in [001]		[001] pol.	26.8	38.6
		2.31	Long. in [100]		[100] pol.	26.9	2.66
		2.27	Long. in [001]		[001] pol.	59.3	8.62
		2.31	Long. in [001]		[100] pol.	36.4	5.19
			Long.	2.5			246
		4.0	Long.	3.80	⊥		10
		4.8	Long.				8
		6.3	Long.	3.10	⊥		16
Ge ₃₃ As ₁₂ Se ₅₅ glass	1.06		Long.				
	0.63		Long.				
Clear lead glass	0.63	1.72	Long.				
Yellow lead glass	0.63	1.96	Long.				
			Long.				

Table 10.1. (Continued).

Lucite	0.63	1.55	1.18	Long.	2.68	⊥	50
			Long.			∥	56
Polystyrene	0.63	1.59	1.06	Long.	2.35	⊥	127
			Long.			∥	113
KRS-5	0.63	2.6	7.37	Long.	2.11	⊥	180
			Long.			∥	254
PbNO ₃	0.63	1.78	4.7	Long.	2.62	⊥	26
			Long.			∥	16
<i>m</i> -Xylene	0.63	1.50	0.86	Long.	1.30	⊥ or ∥	40

^aFrom [5].

^bThe symbols ∥ and ⊥ refer to polarization directions parallel or perpendicular to the plane of light and sound propagation vectors.

^cDue to the strong optical activity of BGO and BSO the diffracted beam intensity is independent of polarization.

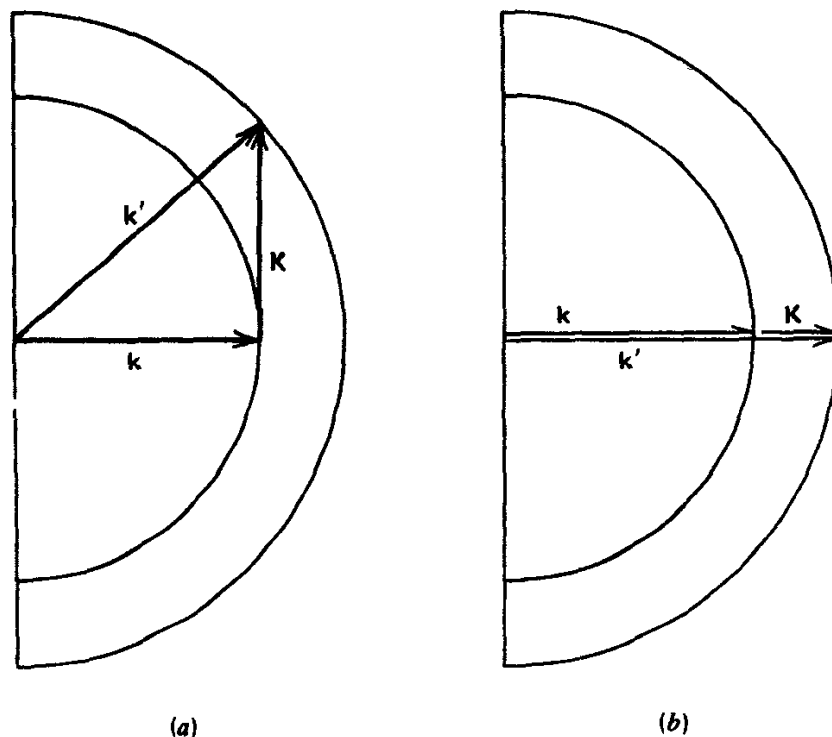


Figure 10.3. Acoustic-optic interaction in a uniaxial crystal: (a) noncollinear interaction; (b) collinear interaction.

where the last approximation is valid when $\Delta n = n_o - n_e \ll n_o$. Let us now assume that the incident beam has an angular spread $\Delta\theta$; then the acoustic wave number can vary over a range of

$$\Delta K = k_e \Delta\theta, \quad (10.1-20)$$

which corresponds to an acoustic bandwidth of

$$\Delta f = \frac{n_e v}{\lambda} \Delta\theta \approx \frac{n_o v}{\lambda} \Delta\theta \quad (10.1-21)$$

The maximum modulation bandwidth is determined by the condition that the diffracted beam does not overlap with the undiffracted beam, which requires that $\Delta\theta < \theta'$. Thus from Eq. (9.4-6) with $\lambda/\Lambda = (n_o^2 - n_e^2)^{1/2}$ and Eq. (10.1-21),

$$\Delta f < f_0. \quad (10.1-22)$$

Compared with (10.1-8), we find that birefringent acousto-optic modulators in the noncollinear interaction configuration offers no gain in bandwidth. However, the requirement on the angular spread of the acoustic beam

($\delta\phi \approx \delta\theta$) is eased. This offers the possibility of increasing the interaction length L without degrading the modulation bandwidth, and results in a higher diffraction efficiency η . The interaction configuration shown in Fig. 10.3(a) is frequently used as an acousto-optic beam deflector with the acoustic wave vector tangent to the normal surface of the diffracted mode (see Section 10.2).

Example: Collinear Acousto-optic Modulation. Referring to Fig. 10.3(b), we consider the acousto-optic interaction in which both the incident and diffracted beams are propagating collinearly along the y axis. The incident light beam is an extraordinary wave polarized along the c axis of the crystal. The diffracted light will be an ordinary wave polarized along the x axis. To conserve momentum, the acoustic wave must also propagate along the y axis with a frequency given by

$$f_0 = \frac{v}{\lambda}(n_o - n_e). \quad (10.1-23)$$

In this collinear acousto-optic interaction, the diffracted light can be separated from the undiffracted light by a polarizer. Let us now assume that the incident beam has an angular spread $\Delta\theta$. To maintain the diffraction direction along the y axis, the acoustic wave number must vary over a range ΔK such that

$$(K + \Delta K)^2 - K^2 = (k_e \Delta\theta)^2, \quad (10.1-24)$$

where $k_e = 2\pi n_e/\lambda$ is the wave vector of the incident light. This ΔK corresponds to a modulation bandwidth of

$$\Delta f = \frac{n_e^2 v^2}{2f_0 \lambda^2} (\Delta\theta)^2. \quad (10.1-25)$$

By using the relation (10.1-23) and $f\lambda = v$, the fractional bandwidth can be written

$$\frac{\Delta f}{f_0} = \frac{1}{2} \left(\frac{n_e \Delta\theta}{n_o - n_e} \right)^2. \quad (10.1-26)$$

From this it may appear as though the bandwidth could be large, provided the birefringence $n_o - n_e$ was small and $\Delta\theta \approx n_o - n_e$. However, when the birefringence is small, the angular spread of the acoustic beam becomes large. In fact the angular spread of the acoustic beam required is $\delta\phi =$

$2\Delta K/K$ and is given, according to Eqs. (10.1-24) and (10.1-23), by

$$\delta\phi = \left(\frac{k_e}{K}\right)^2 \Delta\theta^2 = \left(\frac{n_e \Delta\theta}{n_o - n_e}\right)^2. \quad (10.1-27)$$

Thus, from Eqs. (10.1-26) and (10.1-27),

$$\frac{\Delta f}{f_0} = \frac{1}{2}\delta\phi \approx \frac{\Lambda}{2L}. \quad (10.1-28)$$

The fractional bandwidth is inversely proportional to the interaction length L . It follows that it is difficult to obtain high efficiency and broad bandwidth, simultaneously, in collinear acousto-optic modulation.

10.2. ACOUSTO-OPTIC DEFLECTORS

One of the most important applications of acousto-optic interactions is in the deflection of optical beams. Basically, acousto-optic deflectors operate in the same way as Bragg diffraction modulators, the only difference being that the frequency rather than the amplitude of the sound wave is varied. The use of acousto-optic interaction offers the possibility of high-resolution beam deflection. Both random-access and continuously scanned deflectors can be obtained. The basic principle of operation is depicted in Fig. 10.4

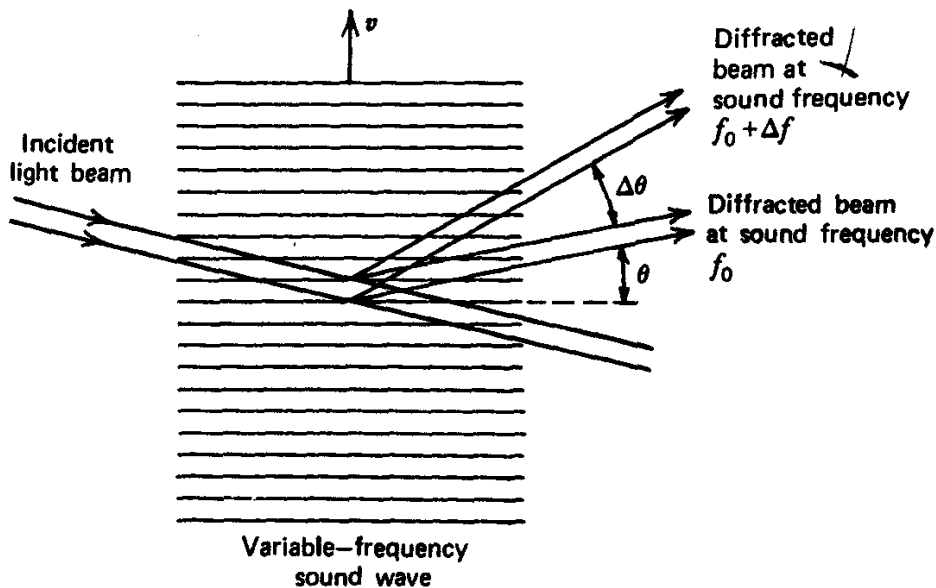


Figure 10.4. A change of frequency of the sound wave from f_0 to $f_0 + \Delta f$ causes a change $\Delta\theta$ in the direction of the diffracted beam, according to Eq. (10.2-1).

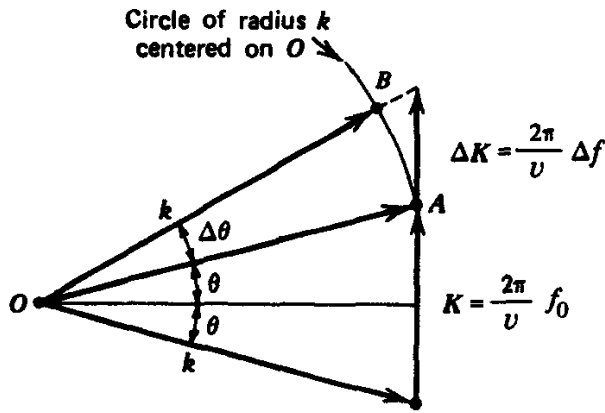


Figure 10.5. Momentum diagram, illustrating how the change in sound frequency from f_0 to $f_0 + \Delta f$ deflects the diffracted light beam from θ to $\theta + \Delta\theta$.

and can be understood by using Fig. 10.5. The important parameters for most applications are the number of resolution beam spots, the access time, and the efficiency.

We now consider the Bragg diffraction shown in Fig. 10.4. The angle of deflection at the Bragg condition is $2\theta_B = 2\sin^{-1}(\lambda f_0/2nv)$. The momentum-vector diagram corresponding to this diffraction is shown in Fig. 10.5. Now let the sound frequency change from f_0 to $f_0 + \Delta f$. Since $K = 2\pi f/v$, this causes a change of $\Delta K = 2\pi\Delta f/v$ in the magnitude of the sound wave vector as shown. Now the angle of incidence remains the same (θ_B), and the magnitude of the diffracted \mathbf{k} vector is virtually unchanged, so its tip is constrained to the circle locus shown in Fig. 10.5. Thus we can no longer close the momentum diagram, and momentum is no longer strictly conserved. The beam will be diffracted along the direction that least violates the momentum conservation.* This takes place along the direction OB , causing a deflection of the beam by $\Delta\theta$. Recalling that the angles θ and $\Delta\theta$ are all small and that $k \sin \theta = K$, we obtain

$$\Delta\theta = \frac{\Delta K}{k \cos \theta_B} = \frac{\lambda}{nv \cos \theta_B} \Delta f, \quad (10.2-1)$$

where θ_B is the Bragg diffraction angle at f_0 . The angle of deflection is thus proportional to the change in the sound frequency.

As in the case of electro-optic deflection, we are not interested so much in the absolute deflection $\Delta\theta$ as we are in the number of resolvable spots—that is, the factor by which $\Delta\theta$ exceeds the beam divergence angle. If we take the beam divergence angle as $\delta\theta \approx 2\lambda/\pi n\omega_0$ [Eq. (10.1-5)], where ω_0 is the

*That is, the direction that maximizes $\int \exp(i\Delta\mathbf{k} \cdot \mathbf{r}) d^3\mathbf{r}$, where $\Delta\mathbf{k} = \mathbf{k}' - \mathbf{k} - \mathbf{K}$ is the momentum mismatch and the integration is over the interaction region.

Gaussian-beam spot size, the number of resolvable spots is

$$\begin{aligned} N &= \frac{\Delta\theta}{\delta\theta} = \frac{\pi\omega_0}{2v \cos \theta_B} \Delta f \\ &= \tau \Delta f, \end{aligned} \quad (10.2-2)$$

where $\tau = \pi\omega_0/2v \cos \theta_B$ is approximately the time it takes the sound to cross the Gaussian-optical-beam spot and is usually called the access time of the deflector.

A common figure of merit for a deflector is the ratio of the total number of resolvable spots to the access time, expressed as a speed-capacity product, which, according to Eq. (10.2-2), is

$$\frac{N}{\tau} = \Delta f. \quad (10.2-3)$$

Thus, a high speed-capacity product is only available when the bandwidth Δf is large. It is therefore desirable to use high-frequency sound waves for beam deflectors, because large bandwidth Δf is only possible when the modulation frequency f_0 is high, according to Eq. (10.1-8).

In practice, the bandwidth Δf is limited by the availability of a broad-band transducer and by the Bragg-angle tolerance. The latter refers to the fact that the proper angle of incidence of the light for resonant Bragg diffraction is a function of the sound frequency ($\theta_B \approx \lambda f/2nv$). To operate a beam deflector over a bandwidth of Δf , it is important that the angle of incidence (angle between the incident-light wave vector \mathbf{k} and the sound wavefront) also cover a range of

$$\Delta\theta_B = \frac{\lambda}{2nv} \Delta f \quad (10.2-4)$$

in order to have a large number of resolvable spots. The incident light beam is usually well collimated (i.e., small $\delta\theta$). The sound wave must, consequently, have a finite angular spread $\delta\phi$ comparable to $\Delta\theta_B$ or even larger (i.e., $\Delta\theta_B \leq \delta\phi$). According to Eqs. (10.1-5) and (10.2-4), using $f_0\Lambda_0 = v$, we obtain

$$\frac{\Delta f}{f_0} \leq \frac{2n\Lambda_0^2}{\lambda L}, \quad (10.2-5)$$

where Λ_0 is the wavelength of sound at frequency f_0 . Thus large-bandwidth operation requires a small transducer length L . On the other hand, according to Eq. (10.1-12), a small interaction length L results in low efficiency. To overcome this difficulty, a beam-steering technique has been devised in which the sound beam is made to track the Bragg angle during the frequency change [6]. This can be done by constructing an array of acoustic transducers driven by electrical signals with a progressive phase shift between successive transducer elements (see Fig. 10.6). This arrangement removes the constraint (10.2-5) and greatly increases the operation bandwidth Δf and diffraction efficiency η by concentrating the acoustic power in the proper direction for Bragg diffraction at all frequencies within Δf .

To illustrate the performance of an acousto-optic beam deflector, we consider a deflection system using flint glass and a sound beam that can be varied in frequency from 80 to 120 MHz; thus, $\Delta f = 40$ MHz. Let the optical-beam diameter be 1 cm. From Table 9.3 we obtain $v = 3.1 \times 10^5$ cm/s; therefore the access time τ is 3.2×10^{-6} s, and the number of resolvable spots is $N = \tau\Delta f \approx 130$.

An improvement in bandwidth of an acousto-optic beam deflector has been demonstrated by using the phased array shown in Fig. 10.6 in a 3-cm-long PbMoO_4 crystal [8]. A laser beam ($\lambda = 5145$ Å) has been deflected through 2000 resolvable spots with an 8.5- μs access time. A

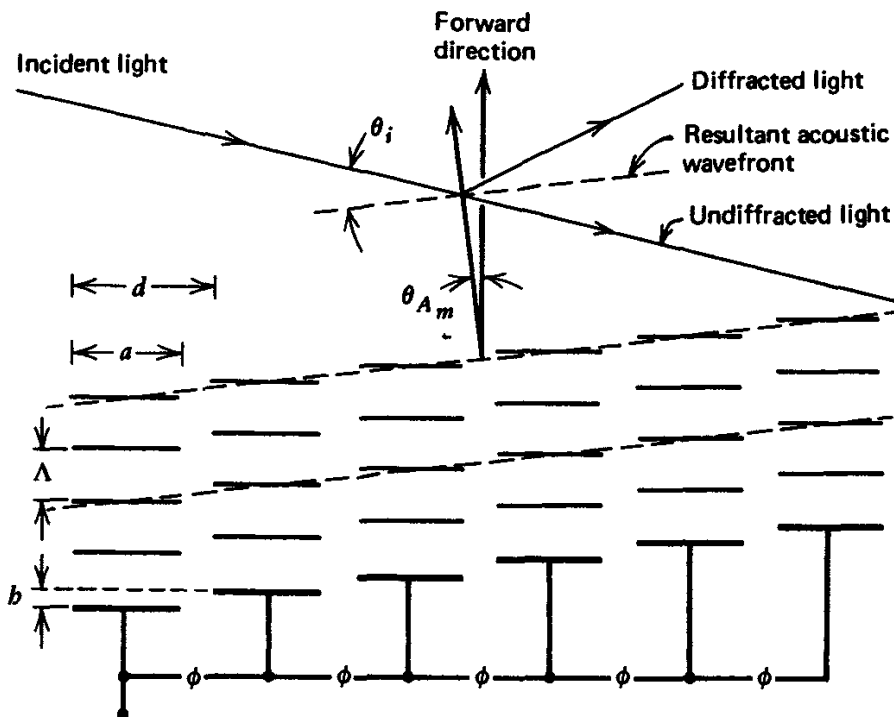


Figure 10.6. Acousto-optic Bragg diffraction of light from a phased acoustic-wave array [7].

bandwidth of 200 MHz was obtained. With 0.1 W of power 8% of the incident light energy is deflected.

A two-dimensional acousto-optic beam deflector using PbMoO_4 crystals has also been demonstrated [9], using two similar stages oriented orthogonally.

10.2.1. Birefringent Bragg Deflector

In the above derivation of the characteristics of the acousto-optic deflectors, we assume that the medium is isotropic. By using birefringent media, a significant improvement in the bandwidth and thus the number of resolvable spots of the beam deflector can be achieved. Referring to Fig. 10.7, we consider an acousto-optic interaction configuration in which the plane of

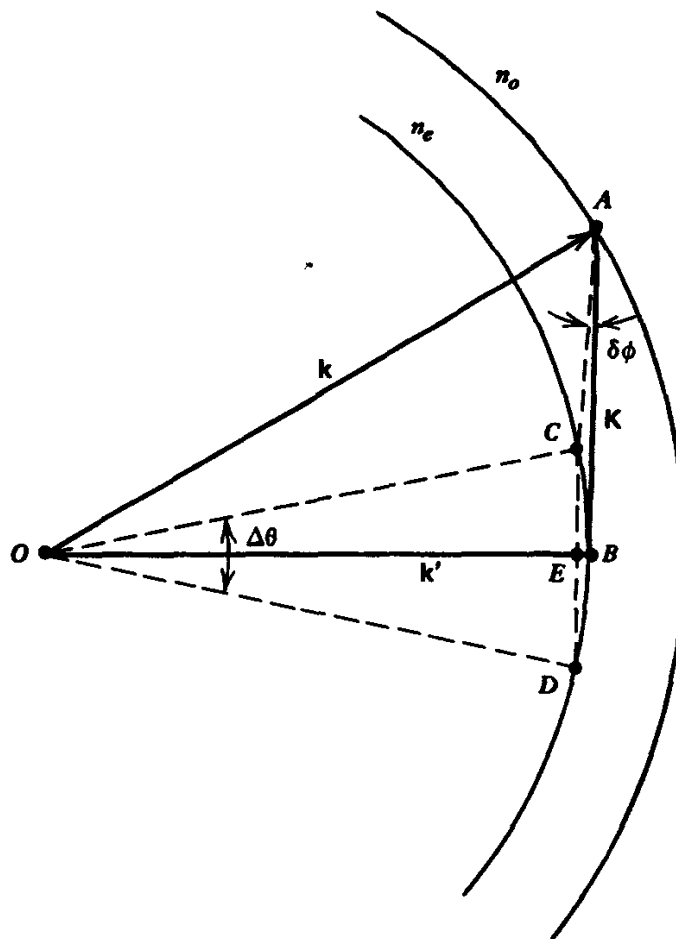


Figure 10.7. Interaction configuration of a birefringent acousto-optic beam deflector. The incident light is an ordinary wave with a wave vector $\mathbf{k} = OA$. The diffracted light is an extraordinary wave with wave vector \mathbf{k}' varied over an angle $\Delta\theta$. The acoustic wave vector \mathbf{K} must cover a range from AC to AD . The angular spread of the acoustic beam is $\delta\phi \approx BE/AB$. Note that the acoustic wave vector \mathbf{K} is normal to \mathbf{k}' .

scattering (i.e., the plane formed by \mathbf{k} and \mathbf{k}') is perpendicular to the c axis of a uniaxial crystal. The acoustic beam is launched in such a way that at the center frequency f_0 of operation the diffracted wave vector \mathbf{k}' is normal to the acoustic wave vector \mathbf{K}_0 . As described in the last chapter and the previous section, the Bragg condition can be satisfied over a broad frequency band without resorting to widely diverging (or steered) acoustic beams. From Fig. 9.6, we notice that the angle of incidence is nearly constant over a broad range of acoustic frequencies, whereas the angle of diffraction varies widely. Since the acoustic wave vector is approximately normal to the diffracted beam over the broad frequency range, the incident light must be the mode with the higher refractive index. For negative uniaxial crystals with $n_e < n_o$ (e.g., LiNbO_3), the incident light must be the ordinary wave, whereas the diffracted light must be the extraordinary wave. The wave vectors are given, respectively, by

$$k = \frac{2\pi n_o}{\lambda}, \quad k' = \frac{2\pi n_e}{\lambda} \quad (10.2-6)$$

The Bragg condition (conservation of momentum) requires that the acoustic frequency f_0 be given by

$$f_0 = \frac{v}{\lambda} (n_o^2 - n_e^2)^{1/2} = \frac{v}{\lambda} (2n \Delta n)^{1/2}, \quad (10.2-7)$$

where $n = \frac{1}{2}(n_e + n_o)$ is the average index of refraction, and $\Delta n = |n_o - n_e|$ is the birefringence of the material.

Let $\delta\phi$ be the angular spread of the acoustic beam required to deflect the light beam over an angular range of $\Delta\theta$ (see Fig. 10.7). This $\delta\phi$ is related to $\Delta\theta$ by

$$\delta\phi = \frac{k' - k' \cos \frac{1}{2}\Delta\theta}{K} = \frac{k'}{8K} (\Delta\theta)^2. \quad (10.2-8)$$

Substituting Eq. (10.1-5) for $\delta\phi$ in Eq. (10.2-8) and using Eq. (10.2-6) and $K = 2\pi/\Lambda$, we obtain

$$\Delta\theta = \left(\frac{8\lambda}{n_e L} \right)^{1/2}. \quad (10.2-9)$$

From Fig. 10.7, we note that the acoustic wave number must cover a range

ΔK in order to deflect the beam over an angle of $\Delta\theta$. This range is given by

$$\Delta K = k'\Delta\theta. \quad (10.2-10)$$

By using $K = 2\pi f/v$, Eq. (10.2-6), and Eq. (10.2-9), we obtain the following expression for the bandwidth Δf :

$$\Delta f = v \left(\frac{8n_e}{\lambda L} \right)^{1/2}. \quad (10.2-11)$$

If we recall that $v = f_0 \Lambda_0$, the fractional bandwidth can be written

$$\frac{\Delta f}{f_0} = \Lambda_0 \left(\frac{8n}{\lambda L} \right)^{1/2}, \quad (10.2-12)$$

where we have used n instead of n_e , since in most cases $n_o \approx n_e \approx n$. For comparison with the isotropic deflector, the ratio of the bandwidths, according to Eqs. (10.2-5) and (10.2-12), is

$$\frac{\Delta f_{\text{bi}}}{\Delta f_{\text{iso}}} = \frac{N_{\text{bi}}}{N_{\text{iso}}} > \frac{f_0}{v} \left(\frac{2\lambda L}{n} \right)^{1/2} = 2 \left(\frac{L}{\lambda} \Delta n \right)^{1/2}. \quad (10.2-13)$$

The last equality is obtained by using Eq. (10.2-7). According to Eq. (10.2-13), the bandwidth of a birefringent deflector is increased by a factor of $2(L\Delta n/\lambda)^{1/2}$ over that of the isotropic deflector. For a typical birefringent material with $\Delta n = 0.01$, a deflector with an interaction length $L = 1$ cm, and light with $\lambda = 1 \mu\text{m}$, this factor is 20.

The fractional bandwidth (10.2-12) of a birefringent deflector is always larger than that of the isotropic one [Eq. (10.2-5)]. In fact, the following relation exists between these two fractional bandwidths:

$$\left(\frac{\Delta f}{f_0} \right)_{\text{bi}} > 2 \left(\frac{\Delta f}{f_0} \right)_{\text{iso}}^{1/2}. \quad (10.2-14)$$

Since the fractional bandwidth is normally less than one, this means the fractional bandwidth of a birefringent deflector is larger than that of the corresponding isotropic one.

This improved performance using the interaction configuration shown in Fig. 10.7 in a birefringent crystal has been demonstrated experimentally [10]. An optical laser beam ($\lambda = 6328 \text{ \AA}$) has been continuously deflected through an angle of 4° by tuning the acoustic wave in a sapphire crystal from 1.28 to 1.83 GHz. A bandwidth Δf of 550 MHz was obtained. With a

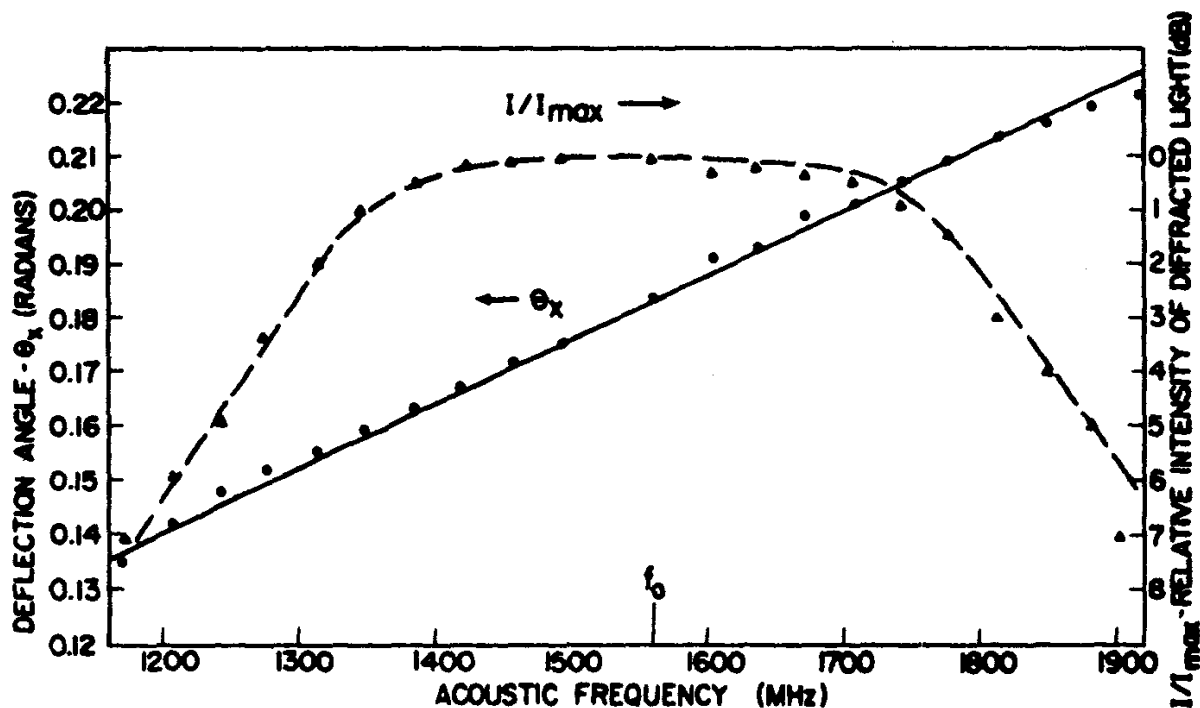


Figure 10.8. Results for deflection in x-cut sapphire. θ_x is the angle of deflection of the diffracted beam relative to the input beam. I/I_{\max} is the relative intensity of the diffracted beam, as explained in the text. f_0 is the acoustic frequency as calculated from Eq. (10.2-7). (After Lean et al. [10].)

typical access time of $2 \mu\text{s}$, the number of resolvable spots is approximately 1000. The experimental results are shown in Fig. 10.8.

10.2.2. Surface Acousto-optic Beam Deflectors

Bragg interactions have recently been demonstrated [11] between surface acoustic waves and optical guided waves (see Chapter 11) in thin-film dielectric waveguides. Since the diffraction efficiency η depends, according to Eq. (10.1-11), on the acoustic intensity I_a , the confinement of the acoustic power near the surface (to a depth $\sim \Lambda$) leads to low modulation or switching power. Figure 10.9 shows an experimental setup in which both the surface wave and the optical wave are guided in a single crystal of LiNbO_3 . The dielectric waveguide is produced by out-diffusion of Li from a layer of $\sim 10 \mu\text{m}$ near the surface, which raises the index of refraction. Figure 10.10 shows the deflected light spots as the acoustic frequency was varied in a beam deflector using three tilted-surface acoustic-wave transducers [13]. A random access time τ of $1.24 \mu\text{s}$ and a bandwidth of 358 MHz were obtained, which correspond to 400 resolvable spots.

The surface acousto-optic beam deflector is used as a key element in the RF spectrum analyzer (see Section 10.4).

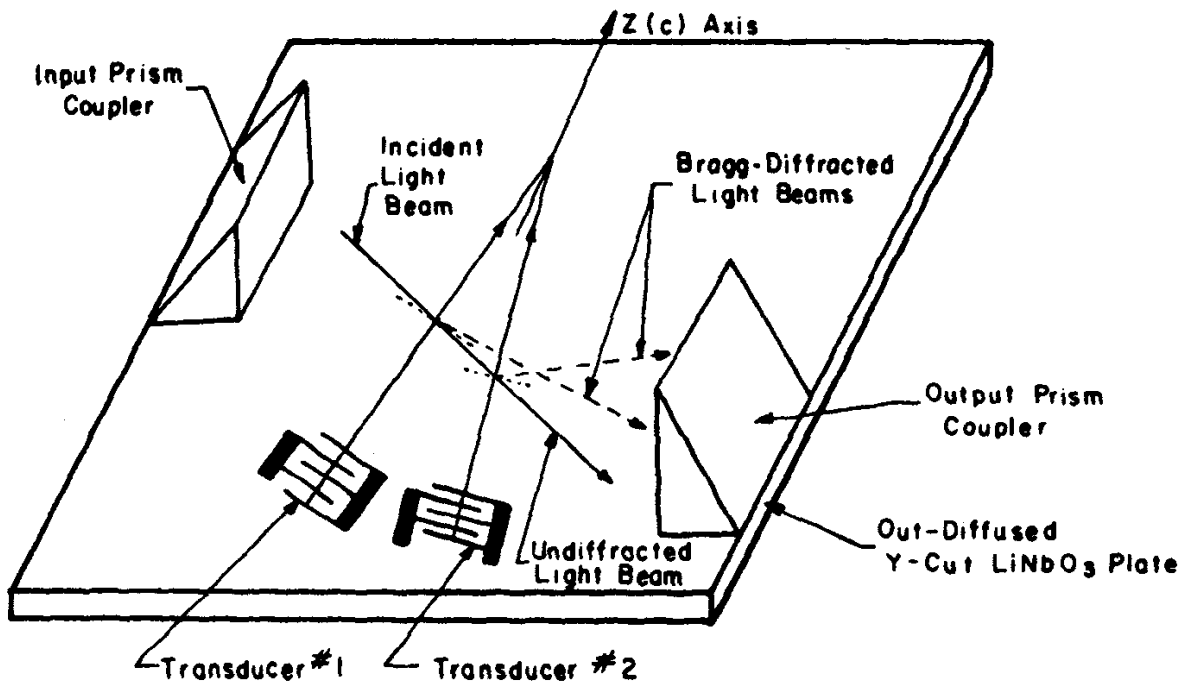


Figure 10.9. Guided-wave acousto-optic Bragg diffraction from two tilted surface acoustic waves [12].

10.3. ACOUSTO-OPTIC TUNABLE FILTERS (AOTF)

Another important application of the acousto-optic interaction is in the construction of a spectral tunable filter. Normally, an acousto-optic tunable filter employs the large-angle codirectional acousto-optic interaction. Strong acousto-optic interaction occurs only when the Bragg condition (conservation of momentum) is satisfied. If the incident light beam contains many spectral components, only one will satisfy the Bragg condition at a given acoustic frequency. In other words, only one spectral component will be diffracted at a given acoustic frequency. Therefore, by varying the acoustic frequency, the frequency (or wavelength) of the diffracted beam can also be varied. The fraction of power transferred from the incident beam to the diffracted beam in an interaction length L is given, according to Eq.

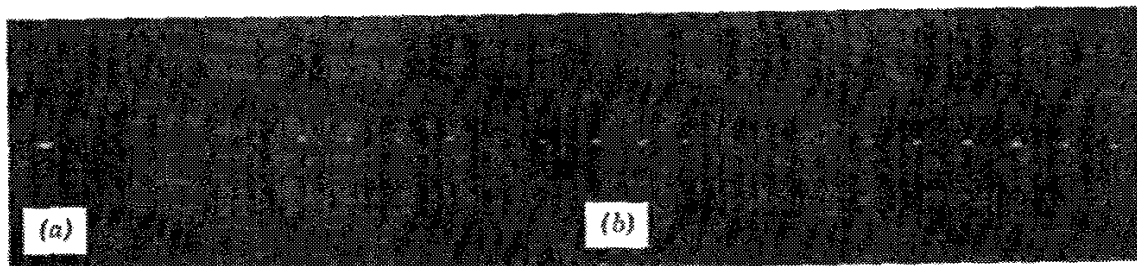


Figure 10.10. Far-field undeflected and deflected light spots: (a) undeflected light beam; (b) deflected light-beam positions as the acoustic frequency was varied from 155 to 410 MHz in 15-MHz steps. (After [13] copyright 1976 IEEE.)

(9.5-49), by

$$T = \frac{\sin^2 \left[\kappa_{12} L \sqrt{1 + (\Delta\beta/2\kappa_{12})^2} \right]}{1 + (\Delta\beta/2\kappa_{12})^2}, \quad (10.3-1)$$

where κ_{12} is the magnitude of the coupling constant (9.5-46), and $\Delta\beta$ is the momentum mismatch

$$\Delta\beta = \beta_1 - \beta_2 \pm K. \quad (10.3-2)$$

β_1 and β_2 are the components of the wave vectors of the incident and the diffracted beam, respectively, along the direction of propagation of the acoustic wave. Let θ_1 and θ_2 be the angles of the wave vectors measured from the wavefronts of the sound wave, such that

$$\beta_1 = \frac{\omega}{c} n_1 \sin \theta_1 = \frac{2\pi}{\lambda} n_1 \sin \theta_1, \quad (10.3-3)$$

$$\beta_2 = \frac{\omega}{c} n_2 \sin \theta_2 = \frac{2\pi}{\lambda} n_2 \sin \theta_2,$$

where n_1 and n_2 are the refractive indices associated with the incident and diffracted waves, respectively. The conservation of momentum (Bragg condition) $\Delta\beta = 0$ becomes

$$\frac{2\pi}{\lambda} (n_2 \sin \theta_2 - n_1 \sin \theta_1) = \pm \frac{2\pi}{v} f, \quad (10.3-4)$$

where f is the acoustic frequency and v is the velocity of sound in the medium.

From Eq. (10.3-4) it is seen that the wave number ($2\pi/\lambda$) of the diffracted light is proportional to the acoustic frequency f . An ideal acousto-optic tunable filter is normally operated at the condition when

$$\kappa_{12} L = \frac{1}{2}\pi, \quad (10.3-5)$$

so that the power conversion is 100% when the phase-matching condition $\Delta\beta = 0$ (10.3-4) is satisfied. Substituting Eq. (10.3-5) for κ_{12} in Eq. (10.3-1), the conversion efficiency (10.3-1) becomes

$$T = \frac{\sin^2 \left[\frac{1}{2}\pi \sqrt{1 + (\Delta\beta L/\pi)^2} \right]}{1 + (\Delta\beta L/\pi)^2}. \quad (10.3-6)$$

Thus the conversion efficiency drops to 50% when

$$\Delta\beta L = \pm 0.80\pi, \quad (10.3-7)$$

where L is the interaction length of the optical and acoustic fields. This corresponds to a bandwidth (full width at half maximum), according to Eqs. (10.3-4) and (10.3-7), of

$$\Delta\lambda_{1/2} = \frac{0.80\lambda^2}{|n_2 \sin \theta_2 - n_1 \sin \theta_1| L} \quad (10.3-8)$$

which, for the collinear case ($\theta_1 = \theta_2 = \frac{1}{2}\pi$), reduces to

$$\Delta\lambda_{1/2} = \frac{0.80\lambda^2}{|\Delta n| L} \quad (\text{collinear interaction}). \quad (10.3-9)$$

According to Eqs. (10.3-8) and (10.3-9), the bandpass width is inversely proportional to the interaction length L . The filter transmission T (or conversion efficiency) at a given acoustic frequency versus the normalized optical frequency deviation $\Delta\beta L$ is plotted in Fig. 10.11.

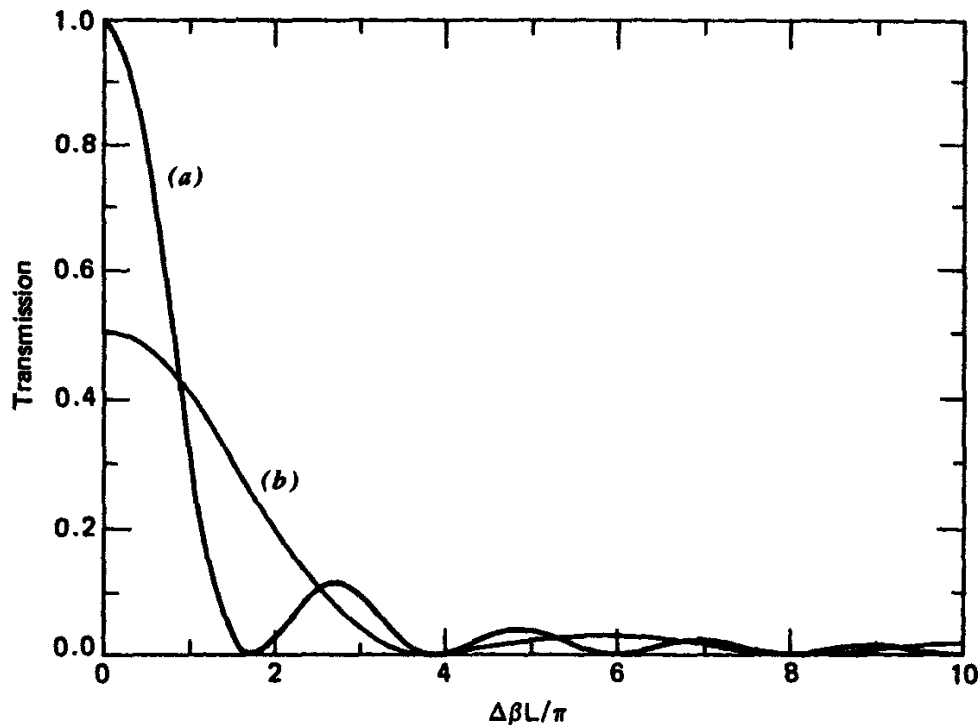


Figure 10.11. Calculated transmission of an acousto-optic tunable filter versus the normalized frequency deviation ($\Delta\beta L/\pi$): (a) peak transmission = 100% ($\alpha = 1$); (b) peak transmission = 50% ($\alpha = \frac{1}{2}$). The parameter α appears in Eq. (10.3-13).

An electronically tunable spectral filter based on the collinear acousto-optic interaction in an optically anisotropic medium has been proposed and demonstrated by Harris and his coworkers [14, 15]. One of the interaction configurations, which involves a shear wave, is briefly described in the example in Section 9.5-2. In their second experiment, the optical waves and the longitudinal acoustic wave are all propagating along the x axis of the LiNbO_3 crystal. The filter configuration is illustrated in Fig. 10.12(a). The incident light may be polarized along either the y or the z axis. Bragg diffraction into the orthogonal polarization occurs via the photoelastic constant p_{14} ($= p_{41}$) (see Problem 10.4). Spectral tuning from 7000 to 5500 Å has been obtained by changing the acoustic frequency from 750 to 1050 MHz [see Fig. 10.12(b)]. For a 1.8-cm-long LiNbO_3 crystal with the orientation shown in Fig. 10.12(a), the birefringence is $\Delta n = 0.09$. The bandpass width $\Delta\lambda_{1/2}$, according to Eq. (10.3-9), is about 2 Å at $\lambda = 6250$ Å. It should be noted that no secondary or higher-order passbands are present in the transmission spectrum, since the acoustic wave is sinusoidal. The acoustic intensity I_a required for a 100% power conversion (i.e., $\kappa_{12}L = \frac{1}{2}\pi$) is given, as in Eq. (10.1-9), by (see Problem 10.4)

$$I_a = \frac{\lambda^2}{2M_2L^2} \quad (10.3-10)$$

with

$$M_2 = \frac{n_o^3 n_e^3 p_{14}^2}{\rho v^3}. \quad (10.3-11)$$

If the acoustic intensity I_a is less than what is given by Eq. (10.3-10), the peak transmission is given, according to Eq. (10.3-1) (see Problem 10.4), by

$$T = \sin^2 \left(\frac{\pi}{\sqrt{2}} \frac{L}{\lambda} \sqrt{M_2 I_a} \right) \quad (10.3-12)$$

The acoustic intensity I_a is proportional to the electrical power applied to the transducer. There is, of course, usually a finite electrical-to-acoustical conversion power loss at the interface between the crystal and the transducer.

As a result of the crystal heating due to acoustic power dissipation, 100% power conversion is difficult to achieve in most tunable filters. Operation of an acousto-optic tunable filter under these circumstances results in a broadening of the passband width. This can be illustrated as follows: Let the

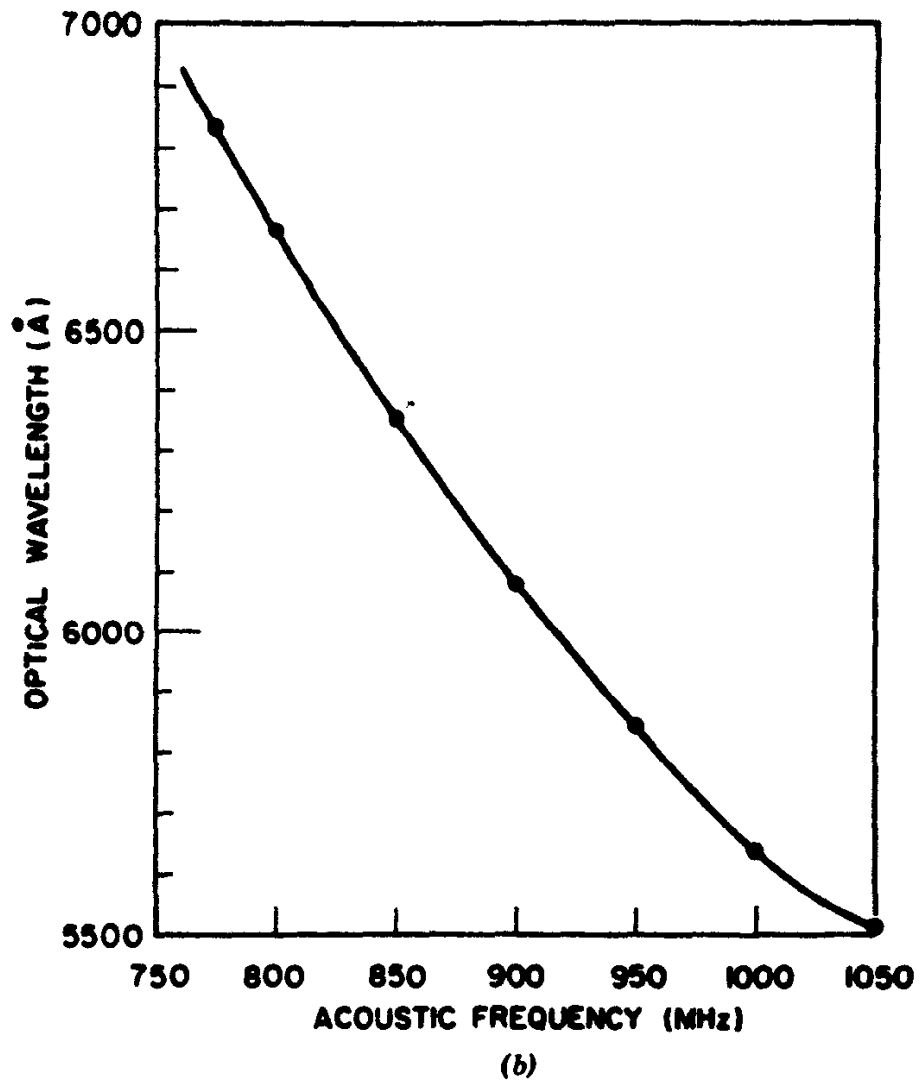
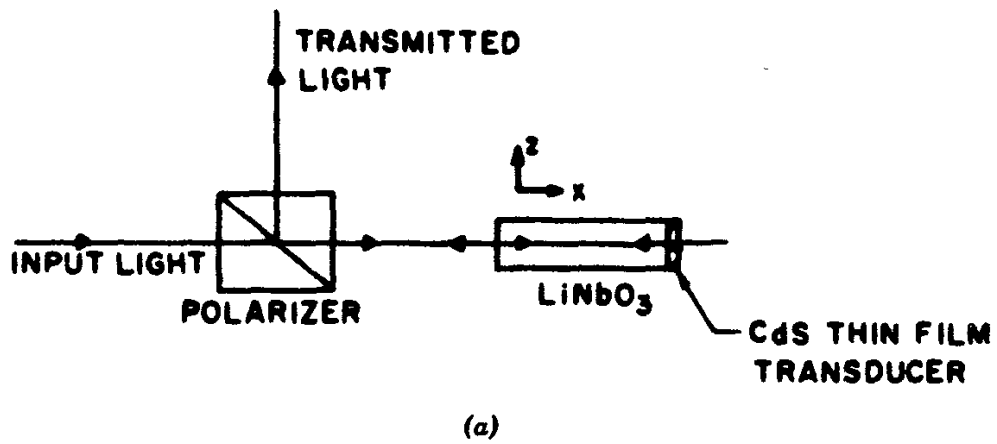


Figure 10.12. (a) Schematic drawing of an acousto-optic tunable filter based on a collinear interaction in a LiNbO_3 crystal. (b) The experimental tuning curve [15].

operation condition be such that $\kappa_{12}L = \frac{1}{2}\pi\alpha$ with α ranging from 0 to 1. The peak transmission for this case becomes $T = \sin^2(\frac{1}{2}\pi\alpha)$, which is less than 100% as long as $0 < \alpha < 1$. The transmission spectrum is given, according to Eq. (10.3-1), by

$$T = \frac{\sin^2 \left[\frac{1}{2}\pi\alpha \sqrt{1 + (\Delta\beta L/\pi)^2} \right]}{1 + (\Delta\beta L/\pi)^2}. \quad (10.3-13)$$

Therefore the first node ($T = 0$) occurs at

$$\Delta\beta = \frac{\pi}{L} \sqrt{\left(\frac{2}{\alpha}\right)^2 - 1}. \quad (10.3-14)$$

When the peak transmission is 100%, $\alpha = 1$. The first node appears at $\Delta\beta = \sqrt{3}\pi/L$. When the peak transmission is 50%, $\alpha = \frac{1}{2}$. The first node then appears at $\Delta\beta = \sqrt{15}\pi/L$, which corresponds to a broadening factor of more than 2. The sidelobe-to-peak transmission ratio is, however, decreased by a factor of $(\sin^2\frac{1}{2}\pi\alpha)/\alpha^2$. For $\alpha = \frac{1}{2}$, which corresponds to a peak transmission of 50%, the sidelobe-to-peak ratio is only half what it is when the peak transmission is 100% ($\alpha = 1$). This is, of course, at the expense of the broadening of the passband width $\Delta\lambda_{1/2}$. The bandwidth broadening and the sidelobe-to-peak ratio reduction are shown in Fig. 10.11(b).

10.3.1. Angular Aperture

The wave vectors describing the collinear acousto-optic interaction mentioned above are shown in Fig. 10.13. The loci of the optical wave vectors are concentric circles (in the xy plane) and for collinear interaction the tangents to the loci of incident- and diffracted-light wave vectors are parallel. Thus, to first order in the change of incidence angle, the momentum-matching condition (10.3-4) is still maintained. This leads to larger angular apertures of the collinear acousto-optic tunable filters which utilize wave vectors along the direction of the principal axes while maintaining a high resolving power (narrow bandwidth).

Let ψ be the angle of the incident light beam measured from the acoustic wave vector, that is, $\psi = \frac{1}{2}\pi - \theta_1$. Since $n_2 = n_1$, the angle of the diffracted light is approximately ψ . The phase-matching condition (10.3-2) can thus be written

$$\Delta\beta = \frac{2\pi}{\lambda} (n_2 - n_1) \cos \psi \pm K. \quad (10.3-15)$$

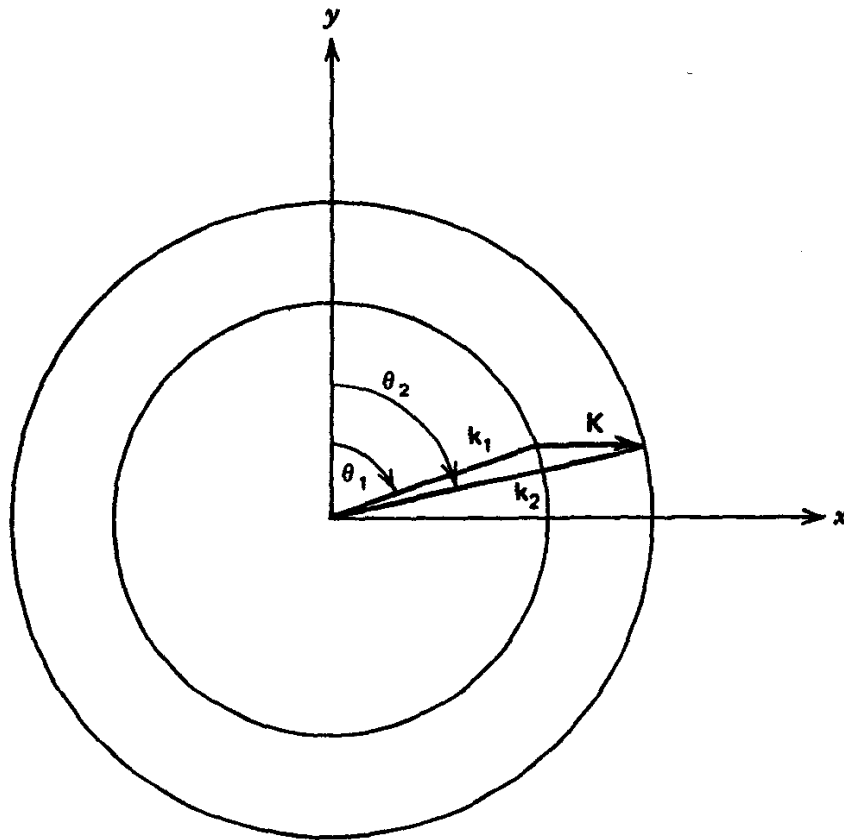


Figure 10.13. Wave-vector diagram for off-axis light in a collinear acousto-optic tunable filter. The interaction shown here is in the xy plane of a uniaxial crystal.

Let the normally incident light ($\psi = 0$ or $\theta_1 = \frac{1}{2}\pi$) be perfectly phase-matched ($\Delta\beta = 0$) at a given wavelength λ . If the incidence angle deviates from $\psi = 0$, phase-matching conditions are satisfied at another wavelength ($\lambda + \Delta\lambda$). This spectral shift is related to the internal angle of incidence ψ by the following equation:

$$\frac{1}{\lambda} = \frac{\cos \psi}{\lambda + \Delta\lambda}. \quad (10.3-16)$$

If ψ is small, the spectral shift $\Delta\lambda$ is much smaller than λ (i.e., $\Delta\lambda/\lambda \ll 1$), and we may expand $\cos \psi$ and obtain

$$\frac{\Delta\lambda}{\lambda} \approx -\frac{1}{2}\psi^2. \quad (10.3-17)$$

The angular aperture of a filter is defined as the angle of incidence when the spectral shift $\Delta\lambda$ is $\frac{1}{2}$ of the bandwidth $\Delta\lambda_{1/2}$. Thus, according to Eqs.

(10.3-9) and (10.3-17), the angular aperture $\psi_{1/2}$ is

$$\psi_{1/2} = \left(0.80 \frac{\lambda}{|\Delta n| L} \right)^{1/2} = \left(\frac{\Delta \lambda_{1/2}}{\lambda} \right)^{1/2} \quad (10.3-18)$$

The angle $\psi_{1/2}$ is the internal angle; the actual angle of incidence in air is larger due to Fresnel refraction. For $\psi_{1/2} \ll 1$, the external angle is approximately $n\psi_{1/2}$.

It is interesting to note that both the bandwidth $\Delta \lambda_{1/2}$ and the angular aperture are related to the number of acoustic wavelengths in the interaction length L (i.e., $N = L/\Lambda$). If we recall that the phase-matching condition

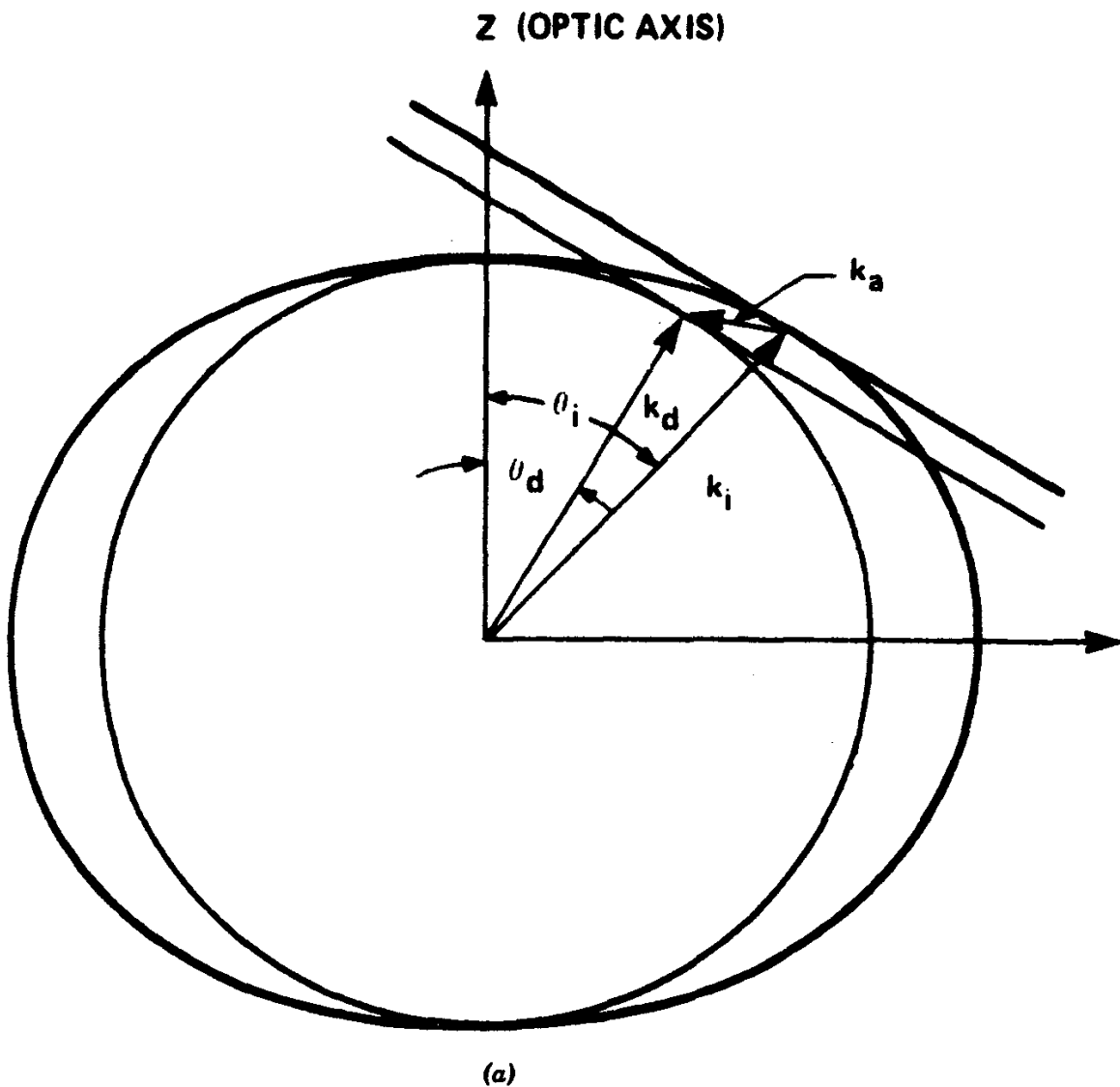


Figure 10.14. Noncollinear acousto-optic tunable filters: (a) wave-vector construction for the noncollinear acousto-optic interaction; (b) schematic of the TeO_2 acousto-optic tunable filter [16].

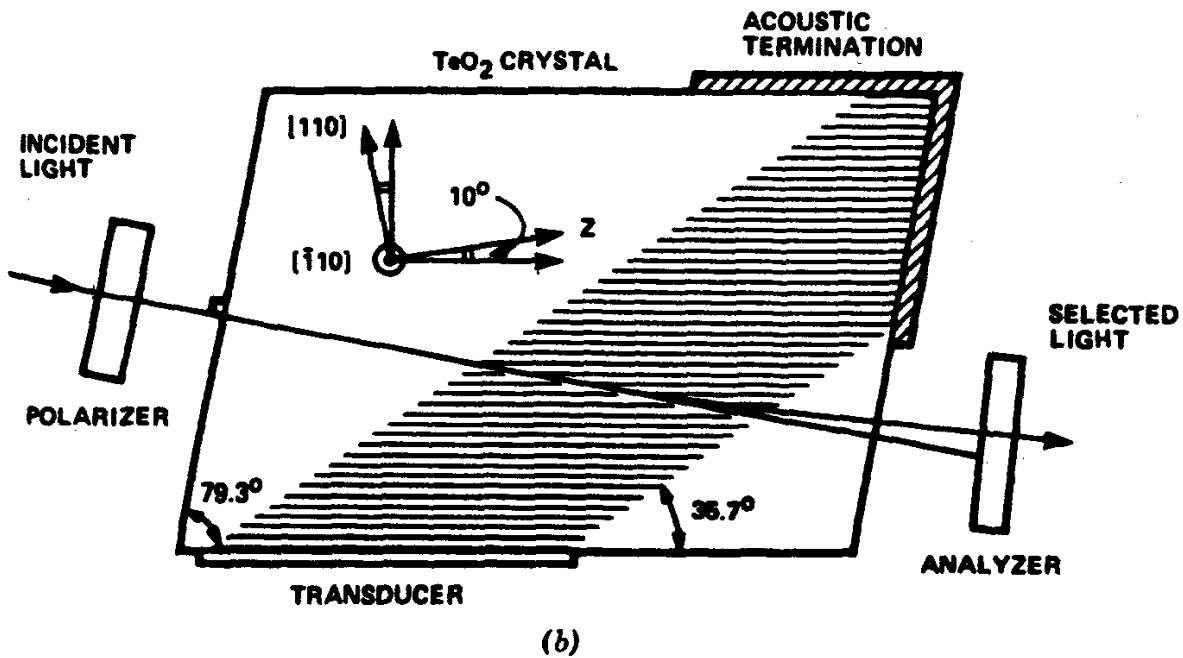


Figure 10.14. (Continued).

(10.3-4) is equivalent to $\Lambda = \lambda/|\Delta n|$, the expression (10.3-9) for the bandwidth can thus be written

$$\frac{\Delta\lambda_{1/2}}{\lambda} = \frac{0.80}{N}, \quad (10.3-19)$$

and the angular aperture can be written as

$$\psi_{1/2} = \left(\frac{0.80}{N} \right)^{1/2}. \quad (10.3-20)$$

According to Eq. (10.3-19), an acousto-optic filter acts essentially like a grating with a resolving power $(\lambda/\Delta\lambda_{1/2})$ proportional to the total number of grooves (acoustic wavelengths). The angular aperture $\psi_{1/2}$ of the collinear acousto-optic filter described above is much larger than that of a diffraction grating. A conventional diffraction grating has an angular aperture of the order of $1/N$.

Noncollinear acousto-optic interaction in anisotropic media can also be employed to make spectral tunable filters. These filters offer design flexibility and several important practical advantages, such as the freedom of choosing propagation directions for various applications and the freedom of choosing the operation acoustic frequency for a given crystal. Large angular aperture can still be obtained by operating in such a way that the tangents to the incident and diffracted light-wave vector loci are parallel. This is illustrated in Fig. 10.14(a). A TeO_2 noncollinear acousto-optic tunable filter

was constructed that had a bandwidth of 40 \AA at an $f/4 (\pm 7^\circ)$ aperture [16, 17]. Tuning from 7000 to 4500 \AA was obtained by changing the acoustic frequency from about 100 to 180 MHz . An infrared acousto-optic tunable spectral filter based on a noncollinear interaction in TeO_2 was recently reported that had a fractional bandwidth of 1% [18]. Spectral tuning from 2 to 5.2 \mu m was obtained by varying the acoustic frequency from about 20 to 52 MHz .

10.4. ACOUSTO-OPTIC SPECTRUM ANALYZER

Acousto-optic Bragg diffraction can also be used to analyze the power spectrum of an RF signal. In Section 10.2 we discussed the deflection of a light beam by varying the acoustic frequency in a Bragg diffraction. The diffraction efficiency is proportional to the power of the acoustic wave. Each angle of deflection $2\theta_B$ corresponds to an acoustic frequency according to the Bragg condition

$$2\theta_B = \frac{\lambda}{nv} f. \quad (10.4-1)$$

Referring to Fig. 10.15, we consider the case when the acoustic wave

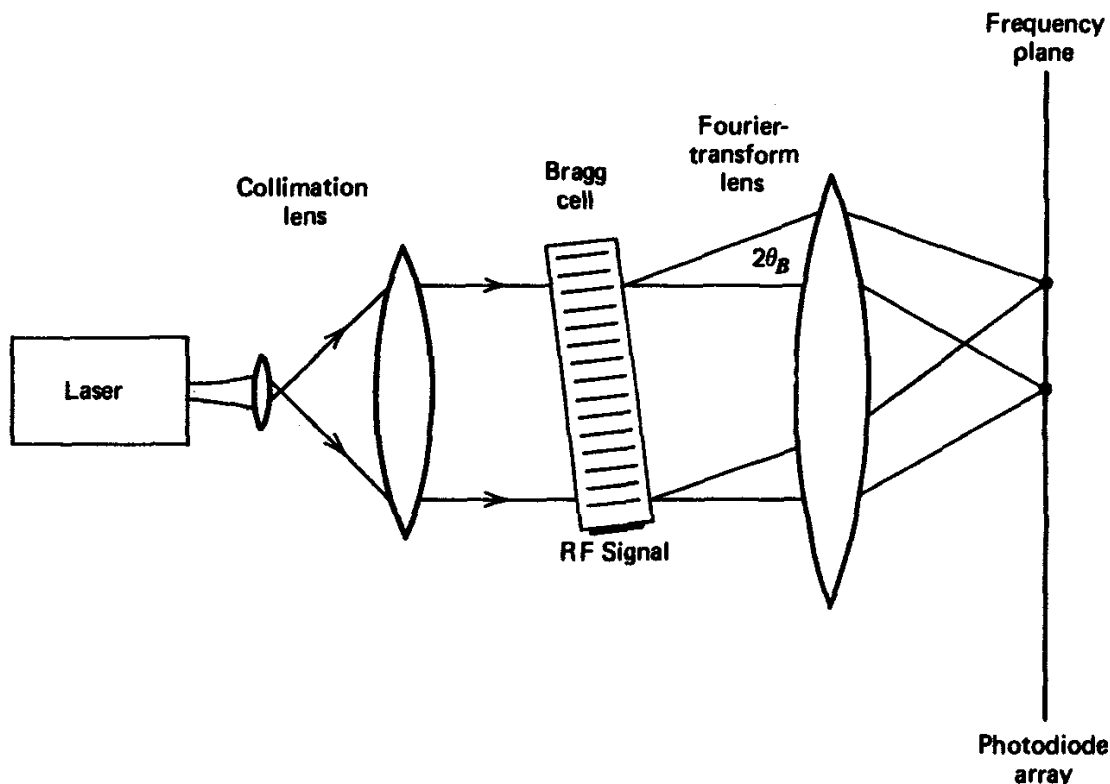


Figure 10.15. Basic acousto-optic spectrum analyzer.

consists of many frequency components. According to Eq. (10.4-1), each frequency component of the sound wave will deflect the light beam into a unique direction. The diffracted light thus consists of an angular distribution. By using a lens, each direction of the diffracted light will correspond to a spot in the focal plane. Since the diffraction efficiency is proportional to the power of the acoustic wave at each frequency, the optical intensity distribution in the focal plane is proportional to the power spectrum of the

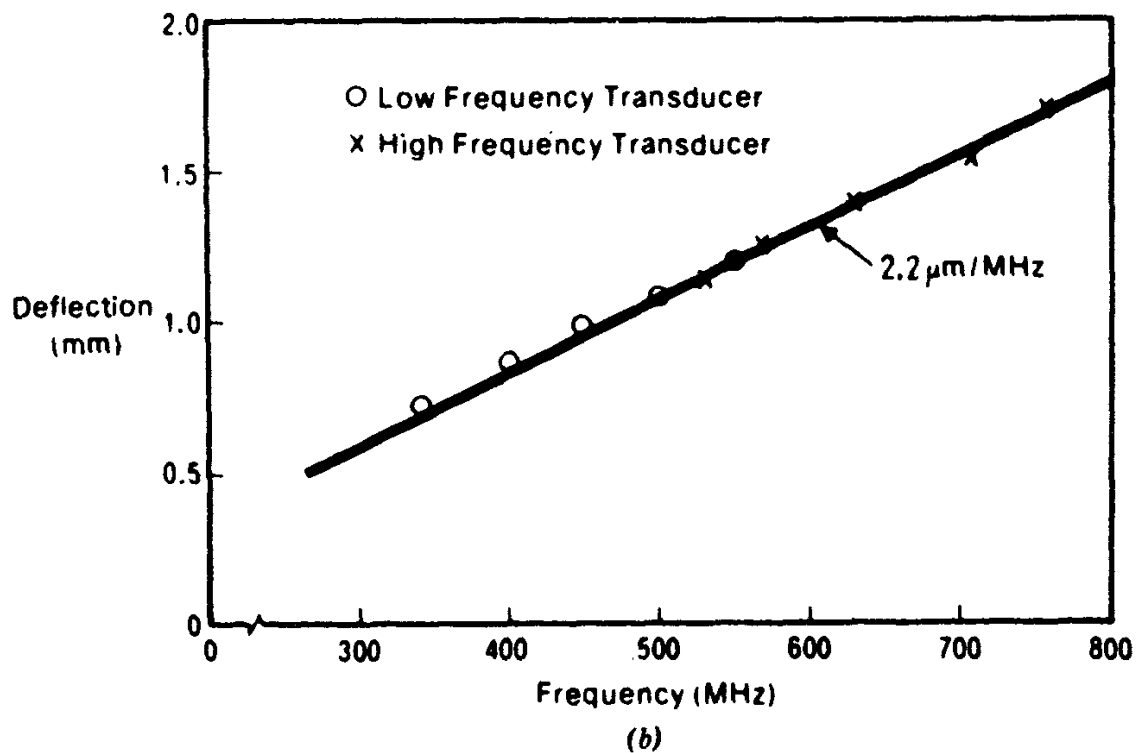
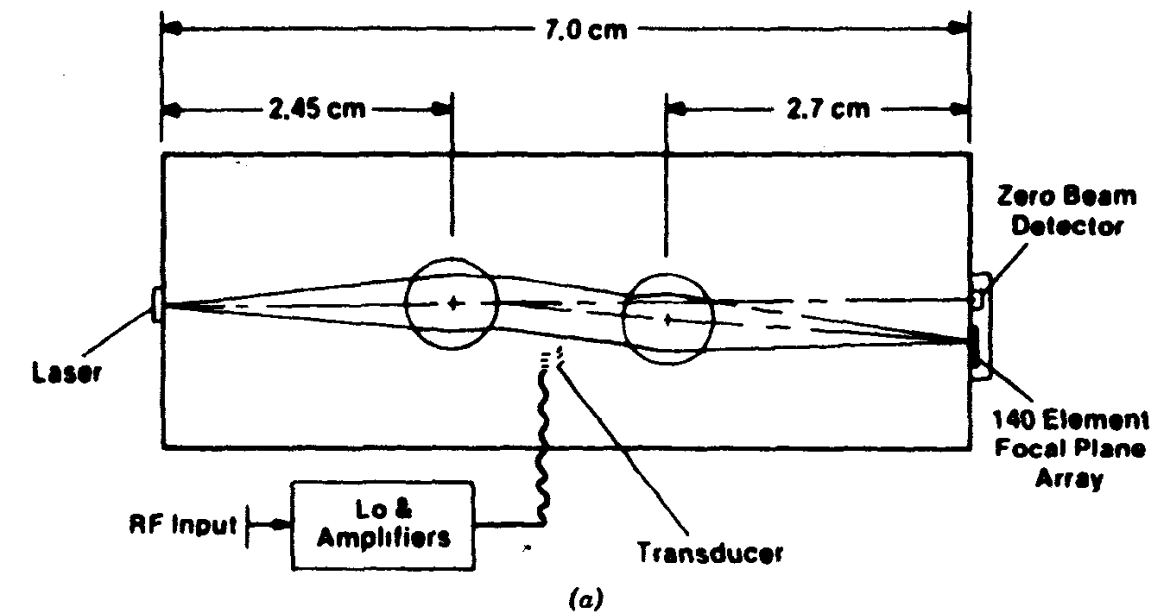


Figure 10.16. (a) Schematic of integrated optical RF spectrum analyzer. (b) Deflection of optical guided wave as a function of surface-acoustic-wave frequency [19].

RF signal. The optical intensity in the focal plane is usually sensed by a photodetector array. Since the acousto-optic spectrum analyzer is based on a simultaneous deflection of a laser beam into many directions, its operation characteristics, such as the RF signal bandwidth and the number of resolvable spots, are similar to those of beam deflectors.

An operational integrated optical RF spectrum analyzer using surface acousto-optic Bragg diffraction has been demonstrated recently by Mergerian [19] and his coworkers. A schematic drawing of this device is shown in Fig. 10.16(a). The measured deflection as a function of the RF frequency is shown in Fig. 10.16(b). The spectrum analyzer was fabricated on *x*-cut LiNbO₃ with the *c* axis parallel to the acoustic propagation. The optical wave is confined by the titanium-diffused thin film of 280-Å depth. The geodesic lenses are circularly symmetric aspherical depressions in the surface of the thin-film waveguide. The surface-acoustic-wave transducers are a two-element tilted array (see Fig. 10.9) designed to have a combined 400-MHz bandwidth centered at 600 MHz. The diffraction efficiency is about 5% with an RF power of 60 mW.

Spectral analysis traditionally relies on a heterodyne scanning of the output from a narrowband frequency-selective filter where the information about different frequencies arrives serially, and too slowly for many applications. The use of acousto-optic interaction for a spectrum analyzer offers means to process the signals in parallel and to display all the frequency components simultaneously in optical form. These techniques are very important in radar signal processing.

10.5. ACOUSTO-OPTIC SIGNAL CORRELATORS

The correlation between two signals is one of the most important quantities in radar signal processing. Acousto-optic interaction can be used to perform signal correlation. Referring to Fig. 10.17, we consider an acousto-optic correlator in which an input electrical signal (often a received radar echo signal) is impressed upon an acoustic wave via a transducer. The resulting strain field in the cell is given by

$$S(x, t) \propto S_1(x - vt) \exp[i(\Omega t - Kx)], \quad (10.5-1)$$

where Ω is the sound frequency, v is the sound velocity, and K is the wave number Ω/v . When a collimated light is directed into the cell at the Bragg

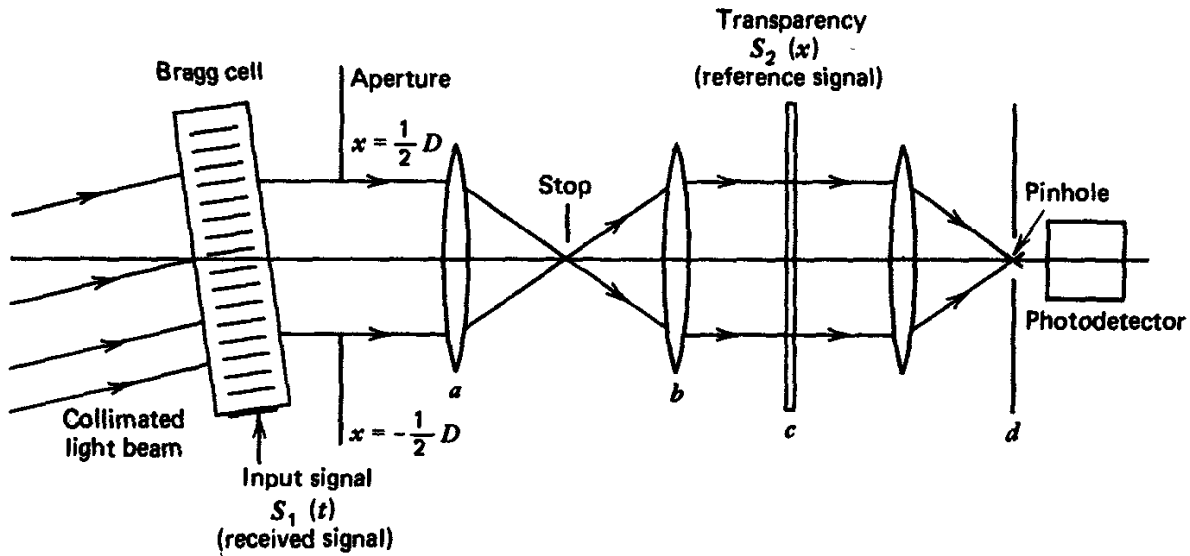


Figure 10.17. Schematic drawing of an acousto-optic signal correlator.

angle, the diffracted light, in the case of weak interaction, is given by

$$E_a(x) \propto S_1(x - vt) \exp[i(\omega + \Omega)t], \quad (10.5-2)$$

where ω is the frequency of the light. The first two lenses (a , b) plus the stop act as a filter which blocks the undiffracted light. The diffracted light (10.5-2) contains the information of the input signal $S_1(t)$. In fact, the input signal $S_1(t)$ is "written" across the light beam via the acousto-optic interaction. Every part of the signal is present in the processing aperture at one instant. This diffracted light beam is then transmitted through a transparency which contains the information of the reference signal $S_2(x)$. The light amplitude pattern to the immediate right of the transparency is given by

$$E_c \propto S_1(x - vt) S_2(x) \exp[i(\omega + \Omega)t]. \quad (10.5-3)$$

This light is then collected by a third lens, located so that the transparency is in its front focal plane. A small pinhole on the optical axis is situated in the rear focal plane. Because of the Fourier-transform properties of this third lens [20], the field in the aperture is given by

$$E_d \propto e^{i(\omega + \Omega)t} \int_{-\frac{1}{2}D}^{\frac{1}{2}D} S_1(x - vt) S_2(x) dx, \quad (10.5-4)$$

where D is the diameter of the aperture. A square law detector placed

immediately after the pinhole provides the output current

$$i(t) \propto \left| \int_{-\frac{1}{2}D}^{\frac{1}{2}D} S_1(x - vt) S_2(x) dx \right|^2. \quad (10.5-5)$$

Note that the output current is proportional to the finite cross correlation between S_1 and S_2 .

The correlation output (10.5-5) contains a considerable amount of information about the signal $S_1(t)$ which is normally the received echo in a radar or communication system. The reference $S_2(t)$ is generally supplied by the receiver and is normally the complex conjugate of $S_1(t)$. In this case the location of the correlation peak reveals the delay time between the signals and hence the range of the target. The width of the correlation peak is inversely proportional to the bandwidth $\Delta f_{1/2}$ of the signals correlated and is given by (see Problem 10.5)

$$\Delta t_{1/2} \approx \frac{1}{\Delta f_{1/2}}. \quad (10.5-6)$$

The signal-to-noise ratio (SNR) of the correlation peak can be expressed in terms of the signal-to-noise ratio (SNR_1) of the noisy input signal $S_1(t) + n(t)$, where $n(t)$ is the additive noise. It is given by [21]

$$\text{SNR} = (\Delta f_{1/2})T \cdot \text{SNR}_1, \quad (10.5-7)$$

where T is the length in time of signal correlated ($T = D/v$), and $\Delta f_{1/2}T$ is the time-bandwidth product of the correlator. This correlation gain ($\Delta f_{1/2}T$) in the signal-to-noise ratio over the original received signal is the

Table 10.2. Parameters of a Correlator

Acoustic mode	Longitudinal
Material	LiNbO ₃
Processing time T	10 μ s
Processing aperture D	5.5 cm
Bandwidth $\Delta f_{1/2}$	300 MHz
TB product $\Delta f_{1/2}T$	3000
Diffraction efficiency (modulation index)	5%
Signal-to-noise ratio	43 dB
Acoustic power	1.2 W
Signal power required	5 W

main reason for performing the correlation. In order to give the student a feel for correlator performance, parameters are given in Table 10.2 for a typical Bragg acousto-optical signal correlator [22].

PROBLEMS

- 10.1. *Raman–Nath acousto-optic modulators.* A light modulator operating in the Raman–Nath regime must have an interaction length L such that

$$\frac{2\pi\lambda L}{n\Lambda^2} < 1.$$

- (a) Show that the maximum allowable length is inversely proportional to the acoustic frequency and is given by

$$L_{\max} = \frac{nv^2}{2\pi\lambda f^2}.$$

- (b) For a longitudinal sound wave in fused quartz, the velocity is $v = 5.95 \times 10^5$ cm/s, and $n = 1.46$. Let the light be the 6328-Å line of a He–Ne laser. Show that the maximum allowable length for 10-MHz acoustic frequency is 13 cm.
- (c) Show that at 100 MHz the maximum allowable length becomes 1.3 mm. Use $M_2 = 1.51 \times 10^{-15}$ from Table 10.1 and Eq. (10.1-11) to find the acoustic intensity required for a 5% diffraction efficiency.
- 10.2. *Acoustic-beam spreading.* Consider an acoustical system with a bandwidth of $\Delta f = 100$ MHz. If the acoustic-beam spreading angle is sufficiently large to obtain diffraction over this bandwidth, the speed–capacity product is $N\tau^{-1} = 10^8$.
- (a) Show that for a typical acoustic velocity of 4×10^3 m/s, an optical beam of diameter 1 cm will permit a random-access time of 2.5 μ s to 250 positions.
- (b) Show that an optical beam of diameter 0.1 cm will give access to 25 positions at a rate of 0.25 μ s.
- (c) Let the wavelength of the light be 6328 Å, and take the refractive index of the medium to be 1.5. Show that the acoustic-beam spreading angle $\delta\phi$ must be comparable to or larger than 5×10^{-3} rad.

- (d) For an acoustic center frequency of 200 MHz, find the wavelength Λ and the interaction length which gives rise to a beam spread of 5×10^{-3} rad.
- 10.3. *Sapphire Bragg deflector.* Consider a birefringent Bragg beam deflector made of sapphire crystal with the interaction configuration shown in Fig. 10.7. Let the light source be a He-Ne laser of $\lambda = 6328 \text{ \AA}$. Take $n_o = 1.765$ and $n_e = 1.757$. Assume that the sound wave travels along the x axis of the crystal with a velocity of $5.85 \times 10^3 \text{ m/s}$.
- (a) Find the center frequency of the acoustic wave required for the polarization-change diffraction. Answer: $f_0 = 1.55 \text{ GHz}$.
- (b) Show that for an interaction length $L = 2.5 \text{ mm}$ the bandwidth is 350 MHz and the angular tuning range is 2° .
- (c) Let the optical beam diameter be 0.75 cm. Find the access time τ and the resolvable spots.
- 10.4. *Harris filter.* Consider the interaction of a longitudinal acoustic wave and an optical wave which are both propagating along the x axis of a LiNbO_3 crystal [see Fig. 10-12(a)].
- (a) Show that the strain field can be written

$$S = \begin{pmatrix} S_1 \\ 0 \\ 0 \\ 0 \\ 0 \\ 0 \end{pmatrix} \exp[i(\Omega t - Kx)],$$

where S_1 is the only nonvanishing strain component.

- (b) The point-group symmetry of LiNbO_3 crystal is 3m. From Table 9.1 and Eq. (9.1-3), show that the change in the optical impermeability induced by the strain field is

$$\Delta\eta = \begin{pmatrix} p_{11}S_1 & 0 & 0 \\ 0 & p_{12}S_1 & p_{14}S_1 \\ 0 & p_{14}S_1 & p_{13}S_1 \end{pmatrix} \exp[i(\Omega t - Kx)].$$

Therefore, the Bragg coupling between the y - and z -polarized waves occurs via the photoelastic coefficient p_{14} ($= p_{41}$).

- (c) Show that the acoustic frequency required is

$$f = \frac{v}{\lambda} |\Delta n|,$$

where $\Delta n = n_e - n_o$ is the birefringence of the crystal. For LiNbO_3 for the orientation shown, $v \approx 6.57 \times 10^3$ m/s and $\Delta n = 0.09$. find the acoustic frequency required for a passband at 6328 \AA . Answer: 934 MHz.

- (d) Find the bandwidth at 6328 \AA for a crystal of length 1.8 cm. Answer: 2 \AA.
- (e) Find the angular acceptance angle $\psi_{1/2}$ for a bandwidth of 2 \AA at $\lambda = 6328 \text{ \AA}$. Answer: 1° .

10.5. *Autocorrelation function and Wiener-Khintchine theorem.*

- (a) Show that the power spectrum (or spectral density) of a signal and the autocorrelation function form a Fourier-transform pair. In other words, let $\tilde{S}(\omega)$ be the Fourier transform of the signal $S(t)$. Show that

$$\int_{-\infty}^{\infty} S(t' + t)S^*(t') dt' = \frac{1}{2\pi} \int_{-\infty}^{\infty} e^{i\omega t} \tilde{S}^*(\omega) \tilde{S}(\omega) d\omega$$

This is known as the Wiener-Khintchine theorem.

- (b) Show that, according to (a), the width of the correlation peak is inversely proportional to the bandwidth of the signal and is given by Eq. (10.5-6).
- (c) Let the signal be a Gaussian pulse given by

$$S(t) = e^{-t^2/2\tau^2} e^{i\omega_0 t}.$$

Show that the autocorrelation function is given by

$$\Gamma(t) = \tau\sqrt{\pi} e^{-t^2/4\tau^2}$$

and the power spectrum is given by

$$|\tilde{S}(\omega)|^2 = \pi\tau^2 e^{-(\omega-\omega_0)^2\tau^2/2}.$$

Show that the width of the correlation peak and the power spectrum are given, respectively, by

$$\Delta t \approx \sqrt{2} \tau,$$

$$\Delta\omega \approx \frac{1}{\tau}.$$

REFERENCES

1. R. Adler, *IEEE Spectrum* 4 (5), 42 (1967).
2. L. Bergmann, *Der Ultraschall*, Hirzel, Stuttgart, 1954, Chapter 5.
3. E. I. Gordon, *Appl. Opt.* 5, 1629 (1966).
4. R. W. Dixon, *J. Appl. Phys.* 38, 3634 (1967).
5. A. Korpel, *Acousto-Optics*, Applied Solid State Science, R. Wolfe, Ed., Vol. 3, Academic Press, New York 1972.
6. A. Korpel et al., *Proc. IEEE* 54, 1429 (1966).
7. C. S. Tsai, *SPIE* 90, 69 (1976).
8. S. K. Yao and E. H. Young, *SPIE* 90, 23 (1976).
9. D. A. Pinnow, L. G. Van Uitert, A. W. Warner, and W. A. Bonner, *Appl. Phys. Lett.* 15, 83 (1969).
10. E. G. H. Lean, C. F. Quate, and H. J. Shaw, *Appl. Phys. Lett.* 10, 48 (1967).
11. L. Kuhn, M. L. Dakss, P. F. Heidrich, and B. A. Scott, *Appl. Phys. Lett.* 17, 265 (1970).
12. C. S. Tsai, Le T. Nguyen, S. K. Yao, and M. H. Alhaider, *Appl. Phys. Lett.* 26, 140 (1975).
13. C. S. Tsai, M. A. Alhaider, Le T. Nguyen, and B. Kim, *Proc. IEEE* 64, 318 (1976).
14. S. E. Harris and R. W. Wallace, *J. Opt. Soc. Am.* 59, 744 (1969).
15. S. E. Harris, S. T. K. Nieh, and D. K. Winslow, *Appl. Phys. Lett.* 15, 325 (1969).
16. I. C. Chang, *Appl. Phys. Lett.* 25, 370 (1974).
17. I. C. Chang, *SPIE* 90, 12 (1976).
18. M. Khoshnevisan, E. Sovero, P. R. Newman, and J. Tracy, *SPIE* 245, 63 (1980).
19. D. Mergerian et al., *Appl. Opt.* 19, 3033 (1980).
20. L. J. Cutrona et al., *IRE Trans. Inform. Theory* IT-6, 386 (1960).
21. R. A. Sprague, *SPIE* 90, 136 (1976).
22. W. T. Maloney, *IEEE Spectrum* 6, 40 (Oct. 1969).

11

Guided Waves and Integrated Optics

In this chapter we take up a number of topics that involve propagation of optical modes in dielectric structures (e.g., thin films and fibers) with dimensions comparable to the wavelength. As we know, a laser beam with a finite transverse dimension will diverge as it propagates in a homogeneous medium (see Chapter 2). This divergence disappears in guiding dielectric structures under the appropriate conditions. The optical modes in these dielectric waveguides correspond to confined propagation of electromagnetic radiation with a transverse dimension defined by the guide.

We derive first the fundamental properties of guided waves in a general dielectric structure. Optical modes are presented as the solution to an eigenvalue problem by solving Maxwell's equations subject to the boundary conditions imposed by the waveguide geometry. This approach is then applied to the slab dielectric waveguide. Both TE and TM modes of propagation are derived. The physics of confined propagation is explained in terms of the total internal reflection of plane waves from the dielectric interfaces.

This is followed by a formulation of the coupled-mode theory which will be employed to describe situations in which the normal power flow of the modes is perturbed by some agency. This formalism is applied in analyzing a number of important applications. These include (1) periodic (corrugated) optical waveguides and filters, (2) distributed-feedback lasers, (3) electro-optic mode coupling and directional couplers. Finally, wave-propagation characteristics in metal-clad waveguides, Bragg-reflection waveguides, and leaky waveguides are investigated and discussed.

11.1. GENERAL PROPERTIES OF DIELECTRIC WAVEGUIDES

The general requirement for a guide for electromagnetic radiation is that there be a flow of energy only along the guiding structure and not perpendicular to it. This means that the fields will be appreciable only in the

immediate neighborhood of the guiding structure. A dielectric cylinder of arbitrary cross section, such as is shown in Fig. 11.1, can serve as a waveguide provided its dielectric constant is large enough. For optical waves this means that the core of the guide must have a higher refractive index than its surroundings. Generally speaking, a beam propagating in a transversely inhomogeneous medium tends to bend toward the high-refractive-index region according to the ray equation (2.3-12). Thus the higher refractive index in the guiding region (core) has an effect similar to that of a converging lens. Under the appropriate conditions this converging effect due to higher core index may cancel out exactly the spreading due to diffraction. When this happens, a guided mode is supported by the dielectric structure.

We begin by considering a guide with an arbitrary cross section as illustrated in Fig. 11.1. The axis of the guide will be taken as the z axis, and the time variation of the modes is of the form $e^{i\omega t}$. Maxwell's equations can be written in the form

$$\nabla \times \mathbf{H} = i\omega\epsilon_0 n^2 \mathbf{E}, \quad (11.1-1)$$

$$\nabla \times \mathbf{E} = -i\omega\mu_0 \mathbf{H}, \quad (11.1-2)$$

where n is the refractive-index distribution of the dielectric structure and is a function of x and y only (i.e., $\partial n/\partial z = 0$). Since the whole dielectric structure is homogeneous along the z axis, solutions to the wave equations (11.1-1) and (11.1-2) can be taken as

$$\mathbf{E} = \mathcal{E}(x, y)\exp[i(\omega t - \beta z)], \quad (11.1-3a)$$

$$\mathbf{H} = \mathcal{H}(x, y)\exp[i(\omega t - \beta z)], \quad (11.1-3b)$$

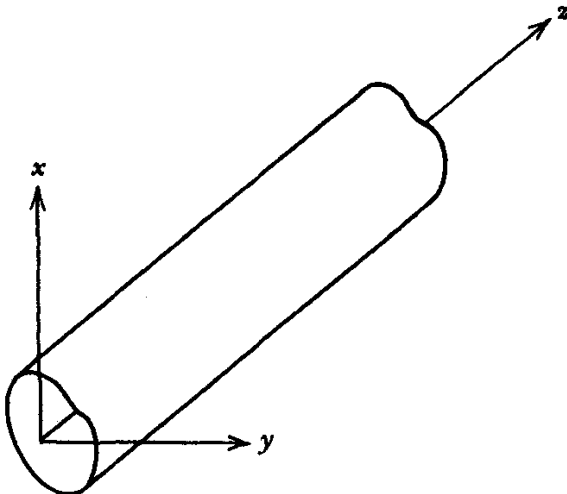


Figure 11.1. A section of a general cylindrical waveguide.

where β is the propagation constant to be determined from Maxwell's equations. We limit ourselves to dielectric structures which consist of piecewise homogeneous and isotropic materials, or materials with a small gradient in the distribution of the refractive index so that the wave equations reduce to (1.4-9). Substitution of Eq. (11.1-3a) for \mathbf{E} in Eq. (1.4-9) yields

$$\left\{ \nabla_t^2 + \left[\frac{\omega^2}{c^2} n^2(x, y) - \beta^2 \right] \right\} \mathcal{E}(x, y) = 0, \quad (11.1-4)$$

where $\nabla_t^2 = \nabla^2 - \partial^2/\partial z^2$ is the transverse Laplacian operator. Equation (11.1-4) governs the transverse behavior of the field. In the case of piecewise homogeneous dielectric structures, Eq. (11.1-4) holds separately in each homogeneous region. Therefore, the field must be solved for separately in each region, and then the tangential components of the field must be matched at each interface. Another important boundary condition for guided modes is that the field amplitudes are zero at infinity. The axial propagation constant β must be the same throughout the guide structure in order to satisfy the boundary conditions at all points on the interfaces of those homogeneous media.

The basic problem is that of finding the solution to the eigenvalue equation (11.1-4) subject to the continuity conditions on the tangential components of the fields at the dielectric interfaces and the boundary conditions at infinity. Given a refractive-index profile $n^2(x, y)$, there are in general an infinite number of eigenvalues β^2 , corresponding to an infinite number of modes. However, normally only a finite number of these modes are confined near the core and will propagate freely along the guide. One of the necessary conditions for a guided mode is that there is no transverse flow of energy. This requires that the fields fall off exponentially outside the guide structure. Consequently, the quantity $(\omega^2/c^2)n^2 - \beta^2$ must be negative in the region far away from the guiding region (core). In other words, the propagation constant β of a confined mode must be such that

$$\beta^2 > \frac{\omega^2}{c^2} n^2(\infty), \quad (11.1-5)$$

where $n^2(\infty)$ is the index of refraction at infinity ($\sqrt{x^2 + y^2} \rightarrow \infty$). On the other hand, if the fields vanish at infinity (i.e., $|E(\infty)|^2 = 0$), the continuity of the fields requires that the magnitude of the field $|E(x, y)|$ attain a maximum value at some point in the xy plane. Normally, $E(x, y)$ is a smooth function of space. The existence of a maximum requires that the

Laplacian of the field be negative. In other words, the propagation constant β of a confined mode must be such that

$$\beta^2 < \frac{\omega^2}{c^2} n^2(x, y) \quad (11.1-6)$$

in some region of the xy plane (usually the core). In particular, if n_c is the maximum value of the refractive-index profile $n(x, y)$, the propagation constant of a confined mode must always satisfy the following condition:

$$\beta^2 < \frac{\omega^2}{c^2} n_c^2. \quad (11.1-7)$$

In the region where the condition (11.1-6) is satisfied, the solutions to the wave equation (11.1-4) are oscillatory. These oscillatory solutions must be matched to the exponential solutions at the boundary of the dielectric interfaces. Therefore, not all the β 's satisfying the conditions (11.1-7) and (11.1-5) are legitimate eigenvalues of the confined modes. This will be illustrated further when we study the modes of a slab waveguide in the next section. In what follows we investigate some fundamental properties of waveguide modes.

11.1.1. Orthogonality of Modes

The waveguide modes supported by an arbitrary dielectric structure have an important and useful orthogonality property. Let $\mathbf{E}_1, \mathbf{H}_1$ and $\mathbf{E}_2, \mathbf{H}_2$ be the fields for two linearly independent solutions to Maxwell's equations (11.1-1) and (11.1-2). Since there is no source in the dielectric waveguide structure, the following relation holds:

$$\nabla \cdot (\mathbf{E}_1 \times \mathbf{H}_2 - \mathbf{E}_2 \times \mathbf{H}_1) = 0. \quad (11.1-8)$$

Equation (11.1-8) is known as the Lorentz reciprocity theorem and is valid provided ϵ and μ are symmetric tensors.

If we replace the operator ∇ by $\nabla_t + \mathbf{a}_z \partial/\partial z$ and assume that the fields $\mathbf{E}_1, \mathbf{H}_1, \mathbf{E}_2, \mathbf{H}_2$ are of the forms (11.1-3a) and (11.1-3b) with propagation constants β_1 and β_2 , respectively, then (11.1-8) reduces to

$$\nabla_t \cdot (\mathbf{E}_1 \times \mathbf{H}_2 - \mathbf{E}_2 \times \mathbf{H}_1) - i(\beta_1 + \beta_2) \mathbf{a}_z \cdot (\mathbf{E}_1 \times \mathbf{H}_2 - \mathbf{E}_2 \times \mathbf{H}_1) = 0, \quad (11.1-9)$$

where we recall that ∇_t is the transverse gradient operator and \mathbf{a}_z is a unit vector along the z axis. Using the two-dimensional form of the divergence theorem leads to

$$\begin{aligned} & \iint_S \nabla_t \cdot (\mathbf{E}_1 \times \mathbf{H}_2 - \mathbf{E}_2 \times \mathbf{H}_1) da \\ &= \oint_C (\mathbf{E}_1 \times \mathbf{H}_2 - \mathbf{E}_2 \times \mathbf{H}_1) \cdot \mathbf{n} dl \\ &= i(\beta_1 + \beta_2) \iint_S (\mathbf{E}_1 \times \mathbf{H}_2 - \mathbf{E}_2 \times \mathbf{H}_1) \cdot \mathbf{a}_z da, \quad (11.1-10) \end{aligned}$$

where S denotes an arbitrary surface in the xy plane, C denotes the boundary of the surface S , and \mathbf{n} is a unit vector normal to the curve C and \mathbf{a}_z . If we take S as the entire xy plane, then the contour integral in Eq. (11.1-10) vanishes, since the fields vanish at infinity. Thus we obtain

$$(\beta_1 + \beta_2) \iint (\mathbf{E}_1 \times \mathbf{H}_2 - \mathbf{E}_2 \times \mathbf{H}_1) \cdot \mathbf{a}_z da = 0. \quad (11.1-11)$$

Substitution of Eqs. (11.1-3a) and (11.1-3b) for \mathbf{E} and \mathbf{H} in Eq. (11.1-11) yields

$$(\beta_1 + \beta_2) \iint (\mathcal{E}_1 \times \mathcal{H}_2 - \mathcal{E}_2 \times \mathcal{H}_1) \cdot \mathbf{a}_z da = 0, \quad (11.1-12)$$

since the common exponential terms can be canceled. To show that each term in Eq. (11.1-12) vanishes separately, we consider the two solutions $\mathbf{E}_1, \mathbf{H}_1$ and $\mathbf{E}'_2, \mathbf{H}'_2$, where $\mathbf{E}'_2, \mathbf{H}'_2$ is the mirror transform of the mode $\mathbf{E}_2, \mathbf{H}_2$ with respect to the plane $z = 0$. Because of the symmetry of the structure, the transformed mode is also a solution to Maxwell's equations (11.1-1) and (11.1-2). This mirror transformation corresponds to a reversal in the direction of propagation, and the directions of the longitudinal electric field and the transverse magnetic field are also reversed; that is,

$$\begin{aligned} \mathbf{E}'_{2t} &= \mathcal{E}_{2t} \exp[i(\omega t + \beta_2 z)], \\ E'_{2z} &= -\mathcal{E}_{2z} \exp[i(\omega t + \beta_2 z)], \\ \mathbf{H}'_{2t} &= -\mathcal{H}_{2t} \exp[i(\omega t + \beta_2 z)], \\ H'_{2z} &= \mathcal{H}_{2z} \exp[i(\omega t + \beta_2 z)], \end{aligned} \quad (11.1-13)$$

where the subscript t indicates the transverse component. Since only the transverse components of the field contribute to the integral (11.1-11), (11.1-12), the equation corresponding to Eq. (11.1-12) for this case is

$$(\beta_1 - \beta_2) \iint (-\mathcal{E}_1 \times \mathcal{K}_2 - \mathcal{E}_2 \times \mathcal{K}_1) \cdot \mathbf{a}_z da = 0. \quad (11.1-14)$$

Addition and subtraction of Eqs. (11.1-12) and (11.1-14) yield

$$\iint (\mathcal{E}_1 \times \mathcal{K}_2) \cdot \mathbf{a}_z da = \iint (\mathcal{E}_2 \times \mathcal{K}_1) \cdot \mathbf{a}_z da = 0.$$

When there are no losses present (i.e., ϵ and μ are real tensors), a similar derivation leads to

$$\iint (\mathcal{E}_1 \times \mathcal{K}_2^*) \cdot \mathbf{a}_z da = \iint (\mathcal{E}_2^* \times \mathcal{K}_1) \cdot \mathbf{a}_z da = 0.$$

By including the time and z dependence, the orthogonality relation can be written

$$\iint \mathbf{E}_1 \times \mathbf{H}_2^* \cdot \mathbf{a}_z da = 0, \quad (11.1-16)$$

where \mathbf{H}_2^* is the complex conjugate of \mathbf{H}_2 . This latter relation shows that the power flow in a lossless dielectric waveguide is the sum of the power carried by each mode individually. If the power of each mode is normalized to 1 W, the orthonormalization of the modes can be written

$$\frac{1}{2} \iint (\mathbf{E}_l \times \mathbf{H}_m^*) \cdot \mathbf{a}_z da = \delta_{lm}, \quad (11.1-17)$$

where l, m are the mode subscripts, and δ_{lm} is the Kronecker delta. For transverse electric (TE) or transverse magnetic (TM) modes, the orthonormality (11.1-17) reduces to (see Problems 11.3 and 11.4)

$$\begin{aligned} \frac{\beta_m}{2\omega\mu} \iint \mathbf{E}_l \cdot \mathbf{E}_m^* da &= \delta_{lm} & (\text{TE}), \\ \frac{\beta_m}{2\omega} \iint \mathbf{H}_l \cdot \frac{1}{\epsilon} \mathbf{H}_m^* da &= \delta_{lm} & (\text{TM}). \end{aligned} \quad (11.1-18)$$

11.1.2. Energy Transport

In a lossless dielectric waveguide, each mode carries power and propagates along the guide independently of the presence of other modes. This is apparent from the orthogonality of the modes expressed by Eq. (11.1-17). The transport of power is given by the real part of the integral of the complex Poynting vector over the entire xy plane. Because of the orthogonality, we are able to treat the power transport of one mode at a time. For a given mode of propagation, the time-averaged power flow is given by

$$P = \frac{1}{2} \operatorname{Re} \int \int \mathbf{E} \times \mathbf{H}^* \cdot \mathbf{a}_z \, da. \quad (11.1-19a)$$

The field energy per unit length of the guide of the mode is given by

$$U = \frac{1}{4} \int \int (\mathbf{E} \cdot \epsilon \mathbf{E}^* + \mathbf{H} \cdot \mu \mathbf{H}^*) \, da, \quad (11.1-19b)$$

where we assume that ϵ and μ are real so that the integrand is also real. Since Maxwell's equations are linear, the power flow P and the energy density U are proportional. The constant of proportionality has the dimensions of velocity and is called the velocity of energy propagation:

$$v_e = \frac{P}{U}. \quad (11.1-20)$$

This energy velocity can be shown to equal the group velocity, which is defined as

$$v_g = \frac{\partial \omega}{\partial \beta}. \quad (11.1-21)$$

In a dielectric waveguide the propagation constant β for each mode is a function of ω . When a light pulse with a finite spread in frequency $\delta\omega$ is propagating in a guide, it is possible that the power of each spectral component is carried by only one mode. If $\delta\beta$ is the corresponding spread in the propagation constant of the mode, the velocity of the pulse is given by Eq. (11.1-21).

To prove that the energy velocity v_e and the group velocity v_g are equal, we start from Maxwell's equation by substituting $\nabla_t + \mathbf{a}_z \partial/\partial z$ for ∇ in Eqs. (11.1-1) and (11.1-2), or more generally, (6.7-10) and (6.7-11). Thus we

obtain

$$\nabla_t \times \mathbf{H} + \mathbf{a}_z \times \frac{\partial}{\partial z} \mathbf{H} = i\omega\epsilon\mathbf{E}, \quad (11.1-22)$$

$$\nabla_t \times \mathbf{E} + \mathbf{a}_z \times \frac{\partial}{\partial z} \mathbf{E} = -i\omega\mu\mathbf{H},$$

where we recall that \mathbf{a}_z is a unit vector along the guide. Since the z dependence of the mode is in the form of Eqs. (11.1-3a) and (11.1-3b), the equations (11.1-22) can be written

$$\nabla_t \times \mathbf{H} - i\beta\mathbf{a}_z \times \mathbf{H} = i\omega\epsilon\mathbf{E}, \quad (11.1-23)$$

$$\nabla_t \times \mathbf{E} - i\beta\mathbf{a}_z \times \mathbf{E} = -i\omega\mu\mathbf{H}.$$

Suppose now that β is changed by an infinitesimal amount $\delta\beta$. If $\delta\omega$, $\delta\mathbf{E}$, and $\delta\mathbf{H}$ are the corresponding changes in ω , \mathbf{E} , and \mathbf{H} , respectively, we may follow the derivation in Section 6.7 and obtain the following equation:

$$\nabla_t \cdot \mathbf{F} - 4i\delta\beta \operatorname{Re}[(\mathbf{E} \times \mathbf{H}^*) \cdot \mathbf{a}_z] = -2i\delta\omega[\mathbf{E} \cdot \epsilon\mathbf{E}^* + \mathbf{H} \cdot \mu\mathbf{H}^*], \quad (11.1-24)$$

where \mathbf{F} is given by

$$\mathbf{F} = \delta\mathbf{E} \times \mathbf{H}^* + \delta\mathbf{H}^* \times \mathbf{E} + \mathbf{H} \times \delta\mathbf{E}^* + \mathbf{E}^* \times \delta\mathbf{H}. \quad (11.1-25)$$

If we perform an integration over the entire xy plane on Eq. (11.1-24) and use the two-dimensional divergence theorem

$$\iint_S \nabla_t \cdot \mathbf{F} da = \oint_C \mathbf{F} \cdot \mathbf{n} dl, \quad (11.1-26)$$

we obtain

$$\oint_C \mathbf{F} \cdot \mathbf{n} dl - 8i\delta\beta P = -8i\delta\omega U, \quad (11.1-27)$$

where C is a contour at infinity and P, U are given by Eqs. (11.1-19a), (11.1-19b), respectively. The contour integral in Eq. (11.1-27) vanishes because the field amplitudes of the confined modes are zero at infinity. This leads to

$$\delta\beta P = \delta\omega U. \quad (11.1-28)$$

By using the definition of the group velocity and energy velocity, (11.1-28) can be written

$$v_e \delta\beta = \delta\omega = \left(\frac{\partial\omega}{\partial\beta} \right) \delta\beta = v_g \delta\beta. \quad (11.1-29)$$

Since $\delta\beta$ is an arbitrary infinitesimal number, we conclude that

$$v_e = v_g \quad (11.1-30)$$

for a guided mode in a dielectric structure.

To illustrate some of the features of the dielectric waveguide, we consider a planar waveguide of thickness t consisting of a nonpermeable dielectric with refractive index n_2 sandwiched between nonpermeable media with refractive indices n_1 on one side and n_3 on the other side. This simple structure is chosen because of the immense mathematical simplicity which results. A schematic drawing of the waveguide structure is shown in Fig. 11.2. Let the coordinate be chosen in such a way that the wave is propagating in the xz plane and the refractive index profile is given by

$$n(x, y) = \begin{cases} n_1 & 0 < x, \\ n_2 & -t < x < 0, \\ n_3 & x < -t. \end{cases} \quad (11.1-31)$$

Since no variation of n exists in the y dimension, we may put $\partial/\partial y = 0$ in

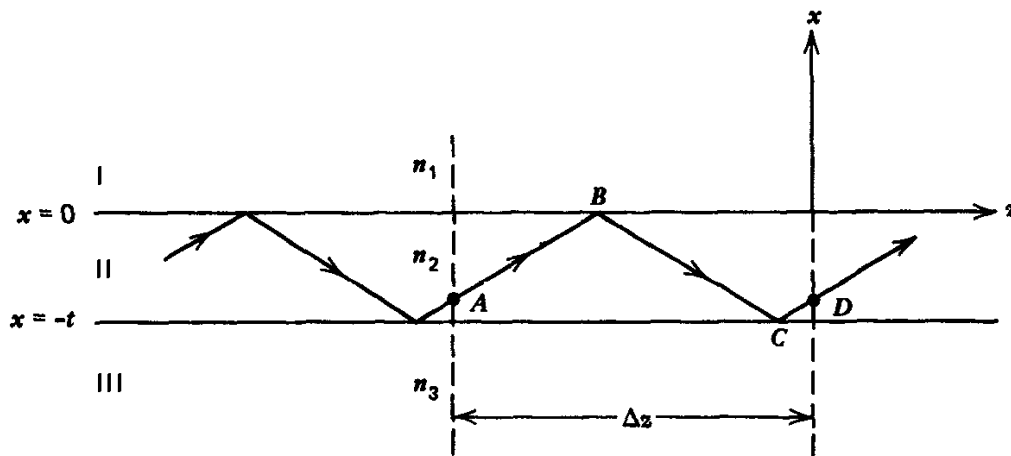


Figure 11.2. A slab dielectric waveguide with $\partial n/\partial y = 0$. The y axis is pointing out of the paper. $ABCD$ is a round-trip zigzag.

Eq. (11.1-4) and write it separately for regions I, II, and III. This leads to

$$\text{Region I:} \quad \frac{\partial^2}{\partial x^2} E(x, y) + (k_0^2 n_1^2 - \beta^2) E(x, y) = 0, \quad (11.1-32a)$$

$$\text{Region II:} \quad \frac{\partial^2}{\partial x^2} E(x, y) + (k_0^2 n_2^2 - \beta^2) E(x, y) = 0, \quad (11.1-32b)$$

$$\text{Region III:} \quad \frac{\partial^2}{\partial x^2} E(x, y) + (k_0^2 n_3^2 - \beta^2) E(x, y) = 0, \quad (11.1-32c)$$

where $k_0 = \omega/c$ and $E(x, y)$ is a Cartesian component of the mode function $\mathcal{E}(x, y)$ (11.1-3a).

Before embarking on a formal solution of Eq. (11.1-32), we may learn a great deal about the physical nature of the solutions by simple arguments. Let us consider the nature of the solutions as a function of the propagation constant β at a *fixed* frequency ω . Let us assume that $n_2 > n_3 > n_1$. For $\beta > k_0 n_2$, [that is, regime (a) in Fig. 11.3] it follows directly from Eq. (11.1-32) that $(1/E)(\partial^2 E/\partial x^2) > 0$ everywhere, and $E(x)$ is exponential in all three layers (I, II, III) of the waveguides. Because of the need to match both $E(x)$ and its derivatives at the two interfaces, the resulting field distribution is as shown in Fig. 11.3(a). The field increases without bound, at least on one side away from the waveguide, so that the solution is not physically realizable and thus does not correspond to a real wave.

For $k_0 n_3 < \beta < k_0 n_2$, as in parts (b) and (c), it follows from Eq. (11.1-32) that the solution is sinusoidal in region II, since $(1/E)(\partial^2 E/\partial x^2) < 0$, but is exponential in regions I and III. This makes it possible to have a solution $E(x)$ that satisfies the boundary conditions while *decaying* exponentially in regions I and III. Two such solutions are shown in Fig. 11.3(b) and (c). The energy carried by these modes is confined to the vicinity of the guiding layer II, and we will consequently refer to them as confined, or guided, modes. From the above discussion it follows that a necessary condition for their existence is that $k_0 n_1, k_0 n_3 < \beta < k_0 n_2$, so that confined modes are possible only when $n_2 > n_1, n_3$; that is, the inner layer possesses the highest index of refraction.

Mode solutions for $k_0 n_1 < \beta < k_0 n_3$, regime (d), correspond according to Eq. (11.1-32) to exponential behavior in region I and to sinusoidal behavior in regions II and III, as illustrated in Fig. 11.3(d). We will refer to these modes as substrate radiation modes. For $0 < \beta < k_0 n_1$, as in (e), the solution for $E(x)$ becomes sinusoidal in all three regions. These are the so-called radiation modes of the waveguides.

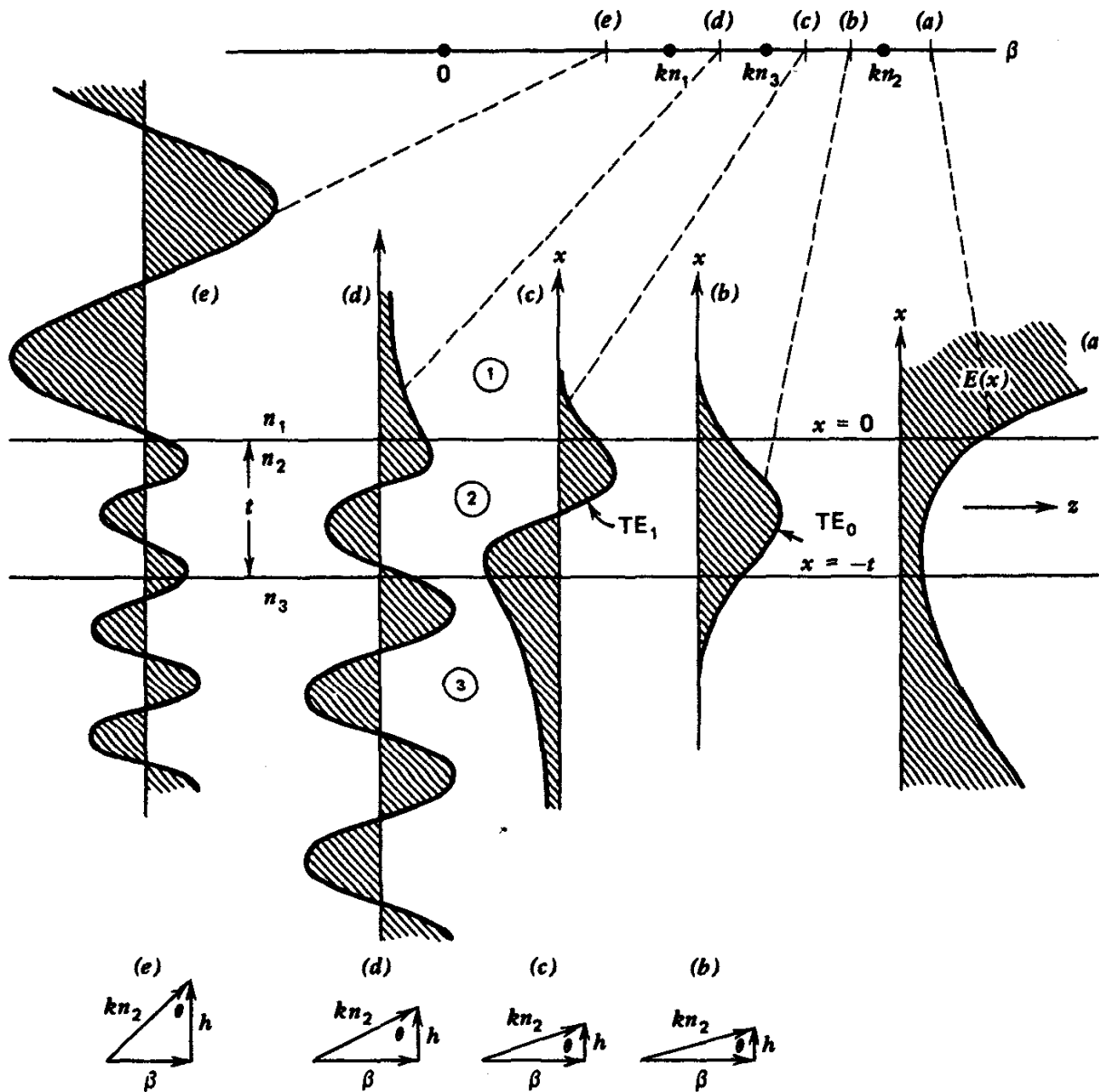


Figure 11.3. Top: the different regimes (a), (b), (c), (d), (e) of the propagation constant, β , of the waveguide shown in Fig. 11.2. Middle: the field distributions corresponding to the different values of β . Bottom: the propagation triangles corresponding to the different propagation regimes.

A solution of Eq. (11.1-32) subject to the boundary conditions at the interfaces (given in the next section) shows that while in regimes (d) and (c) β is a continuous variable, the values of allowed β in the propagation regime $k_0 n_3 < \beta < k_0 n_2$ are discrete. The number of confined modes depends on the width t , the frequency, and the indices of refraction n_1, n_2, n_3 . At a given wavelength the number of confined modes increases from 0 with increasing t . At some t , the mode TE_0 becomes confined. Further increases in t will allow TE_1 to exist as well, and so on.

A useful point of view is one of considering the wave propagation in the inner layer 2 as that of a plane wave propagating at some angle θ to the vertical x axis and undergoing a series of total internal reflections at the interfaces II–I and II–III. This is based on Eq. (11.1-32b). Assuming a solution in the form of $E \propto \sin(hx + \alpha) e^{-i\beta z}$, we obtain

$$\beta^2 + h^2 = k_0^2 n_2^2. \quad (11.1-33)$$

The resulting right triangles with sides β , h , and $k_0 n_2$ are shown in Fig. 11.3. Note that since the frequency is constant, $k_0 n_2 \equiv (\omega/c)n_2$ is the same for cases (b), (c), (d), and (e). The propagation can thus be considered formally as that of a plane wave directed along the hypotenuse with a *constant* propagation constant $k_0 n_2$. As β decreases, θ decreases until, at $\beta = k_0 n_3$, the wave ceases to be totally internally reflected at the interface III–II. This follows from the fact that the guiding condition $\beta > k_0 n_3$ leads, using $\beta = k_0 n_2 \sin \theta$, to $\theta > \sin^{-1}(n_3/n_2) = \theta_c$, where θ_c is the total-internal-reflection angle at the interface between layers II and III. Since $n_3 > n_1$, total reflection at the II–III interface guarantees total internal reflection at the I–II interface. The use of total internal reflection to derive the waveguide modes will be discussed in the latter part of the next section.

11.2. TE AND TM MODES IN AN ASYMMETRIC WAVEGUIDE

We now solve the wave equation (11.1-4) for the dielectric waveguide sketched in Fig. 11.2. We limit the derivation to the guided modes, which, according to Fig. 11.3, have propagation constant β such that

$$k_0 n_3 < \beta < k_0 n_2,$$

where $n_1 < n_3$. Taking $\partial/\partial y = 0$, Eq. (11.1-4) for the mode function becomes

$$\left[\frac{\partial^2}{\partial x^2} + (k_0 n_i^2 - \beta^2) \right] \mathcal{E} = 0, \quad i = 1, 2, 3, \quad (11.2-1)$$

where $i = 1, 2, 3$ corresponds to region I, II, III respectively. This guide can, in the general case, support a finite number of confined TE modes with field components E_y , H_x , and H_z , and TM modes with components H_y , E_x , and E_z .

11.2.1. TE Modes

The field component E_y of the TE mode can be taken in the form

$$E_y(x, y, z, t) = \mathcal{E}_y(x) e^{i(\omega t - \beta z)}. \quad (11.2-2)$$

The mode function $\mathcal{E}_y(x)$ is taken as

$$\mathcal{E}_y = \begin{cases} Ce^{-qx}, & 0 \leq x < \infty, \\ C \left[\cos hx - \frac{q}{h} \sin hx \right], & -t \leq x \leq 0, \\ C \left[\cos ht + \frac{q}{h} \sin ht \right] e^{p(x+t)}, & -\infty < x \leq -t. \end{cases} \quad (11.2-3)$$

Substitution of Eq. (11.2-3) into Eq. (11.2-1) leads to

$$\begin{aligned} h &= (n_2^2 k_0^2 - \beta^2)^{1/2}, \\ q &= (\beta^2 - n_1^2 k_0^2)^{1/2}, \\ p &= (\beta^2 - n_3^2 k_0^2)^{1/2}, \\ k_0 &\equiv \frac{\omega}{c}. \end{aligned} \quad (11.2-4)$$

The acceptable solutions for \mathcal{E}_y and $\mathcal{H}_z = (i/\omega\mu)(\partial\mathcal{E}_y/\partial x)$ should be continuous at both $x = 0$ and $x = -t$. The choice of coefficients in Eq. (11.2-3) is such as to make \mathcal{E}_y continuous at both interfaces as well as $\partial\mathcal{E}_y/\partial x$ at $x = 0$. By imposing the continuity requirement on $\partial\mathcal{E}_y/\partial x$ at $x = -t$, we get from Eq. (11.2-3)

$$h \sin ht - q \cos ht = p \left[\cos ht + \frac{q}{h} \sin ht \right],$$

or

$$\tan ht = \frac{p + q}{h(1 - pq/h^2)}. \quad (11.2-5)$$

Equation (11.2-5) is often called the mode condition meaning that the propagation constant β of a TE mode satisfies this condition. Given a set of refractive indices n_1 , n_2 , and n_3 of a plane waveguide, Eq. (11.2-5) in

general yields a finite number of solutions for β provided the thickness t is large enough. These modes are orthogonal according to the general proof given in Section 11.1.

The constant C appearing in Eq. (11.2-3) is arbitrary; yet for many applications, especially those in which the propagation and exchange of power involve more than one mode, it is advantageous to define C in such a way that it is simply related to total power in the mode. This point will become clear in Section 11.3. We choose C so that the field $\mathcal{E}_y(x)$ in Eq. (11.2-3) corresponds to a power flow of 1 W (per unit width in the y direction) in the mode. A mode for which $E_y = A\mathcal{E}_y(x)$ will thus correspond to a power flow of $|A|^2$ W/m. The normalization condition becomes

$$-\frac{1}{2} \int_{-\infty}^{\infty} E_y H_x^* dx = \frac{\beta_m}{2\omega\mu} \int_{-\infty}^{\infty} [\mathcal{E}_y^{(m)}(x)]^2 dx = 1, \quad (11.2-6)$$

where the symbol m refers to the m th confined TE mode [corresponding to the m th eigenvalue of Eq. (11.2-5)] and $H_x = -i(\omega\mu)^{-1} \partial E_y / \partial z$.

Using Eq. (11.2-3) in Eq. (11.2-6) leads, after substantial but straightforward calculation, to

$$C_m = 2h_m \left[\frac{\omega\mu}{|\beta_m| [t + (1/q_m) + (1/p_m)] (h_m^2 + q_m^2)} \right]^{1/2}. \quad (11.2-7)$$

The orthonormalization of the modes (11.1-17) becomes

$$\int_{-\infty}^{\infty} \mathcal{E}_y^{(l)} \mathcal{E}_y^{(m)} dx = \frac{2\omega\mu}{\beta_m} \delta_{l,m}. \quad (11.2-8)$$

11.2.2. TM Modes

The derivation of the confined TM modes is similar in principle to that of the TE modes. The field components are

$$\begin{aligned} H_y(x, z, t) &= \mathcal{H}_y(x) e^{i(\omega t - i\beta z)}, \\ E_x(x, z, t) &= \frac{i}{\omega\epsilon} \frac{\partial H_y}{\partial z} = \frac{\beta}{\omega\epsilon} \mathcal{H}_y(x) e^{i(\omega t - \beta z)}, \\ E_z(x, z, t) &= -\frac{i}{\omega\epsilon} \frac{\partial H_y}{\partial x}. \end{aligned} \quad (11.2-9)$$

The mode function $\mathcal{H}_y(x)$ is taken as

$$\mathcal{H}_y(x) = \begin{cases} -C \left[\frac{h}{\bar{q}} \cos ht + \sin ht \right] e^{p(x+t)}, & x < -t, \\ C \left[-\frac{h}{\bar{q}} \cos hx + \sin hx \right], & -t < x < 0, \\ -\frac{h}{\bar{q}} C e^{-qx}, & 0 < x. \end{cases} \quad (11.2-10)$$

The continuity of H_y and E_z at the two interfaces leads, in a manner similar to Eq. (11.2-5), to the eigenvalue equation

$$\tan ht = \frac{h(\bar{p} + \bar{q})}{h^2 - \bar{p}\bar{q}}, \quad (11.2-11)$$

where

$$\bar{p} \equiv \frac{n_2^2}{n_3^2} p, \quad \bar{q} = \frac{n_2^2}{n_1^2} q.$$

The normalization constant C is chosen so that the field represented by Eqs. (11.2-9) and (11.2-10) carries 1 W per unit width in the y direction:

$$\frac{1}{2} \int_{-\infty}^{\infty} H_y E_x^* dx = \frac{\beta}{2\omega} \int_{-\infty}^{\infty} \frac{\mathcal{H}_y^2(x)}{\epsilon(x)} dx = 1,$$

or, using $n^2(x) = \epsilon(x)/\epsilon_0$,

$$\int_{-\infty}^{\infty} \frac{[\mathcal{H}_y^{(m)}(x)]^2}{n^2(x)} dx = \frac{2\omega\epsilon_0}{\beta_m}. \quad (11.2-12)$$

Carrying out the integration using Eq. (11.2-10) gives

$$C_m = 2 \sqrt{\frac{\omega\epsilon_0}{\beta_m t_{\text{eff}}}},$$

$$t_{\text{eff}} \equiv \frac{\bar{q}^2 + h^2}{\bar{q}^2} \left(\frac{t}{n_2^2} + \frac{q^2 + h^2}{\bar{q}^2 + h^2} \frac{1}{n_1^2 q} + \frac{p^2 + h^2}{\bar{p}^2 + h^2} \frac{1}{n_3^2 p} \right). \quad (11.2-13)$$

The TM modes are also orthogonal. In fact, all the TE and TM modes are mutually orthogonal. The general orthonormality property is described by Eq. (11.1-17).

The general properties of the TE- and TM-mode solutions are illustrated in Fig. 11.4. In general, a mode becomes confined above a certain (cutoff) value of t/λ . At the cutoff value $p = 0$ and $\beta = n_3 k_0$, and the mode extends to $x = -\infty$. According to the mode conditions (11.2-5), (11.2-11), and (11.2-4), cutoff values of t/λ for TE and TM modes are given, respectively, by

$$\left(\frac{t}{\lambda}\right)_{\text{TE}} = \frac{1}{2\pi\sqrt{n_2^2 - n_3^2}} \left[m\pi + \tan^{-1} \left(\frac{n_3^2 - n_1^2}{n_2^2 - n_3^2} \right)^{1/2} \right], \quad (11.2-14)$$

$$\left(\frac{t}{\lambda}\right)_{\text{TM}} = \frac{1}{2\pi\sqrt{n_2^2 - n_3^2}} \left[m\pi + \tan^{-1} \frac{n_2^2}{n_1^2} \left(\frac{n_3^2 - n_1^2}{n_2^2 - n_3^2} \right)^{1/2} \right],$$

where m is an integer ($m = 0, 1, 2, 3, \dots$) which refers to the m th confined TE (or TM) mode. Note that the cutoff thickness of the TM_m mode is always larger than that of the TE_m mode, because $n_1 < n_2$. For values of t/λ slightly above the cutoff value, $p \geq 0$ and the mode is poorly confined.

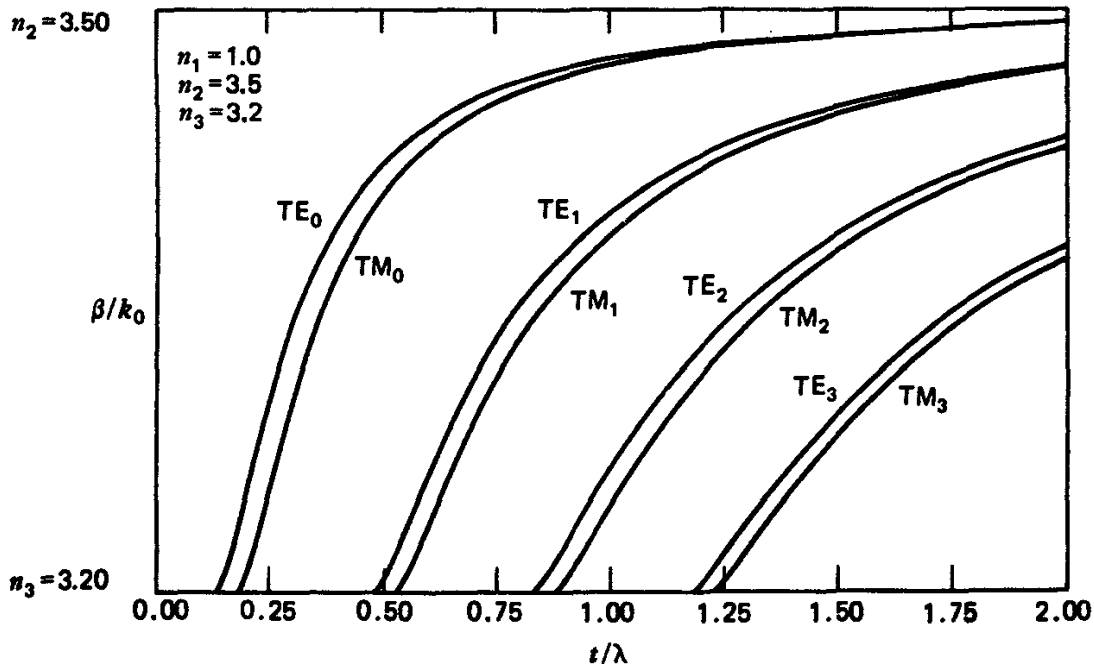


Figure 11.4. Dispersion curves for the confined modes of GaAs film on an AlGaAs substrate. $n_1 = 1.0$.

As the value of t/λ increases, so does the value of p , and the mode becomes increasingly confined to layer 2. This is reflected in the effective mode index $\beta\lambda/2\pi$, which at cutoff is equal to n_3 , and which for large t/λ approaches n_2 . In a symmetric waveguide ($n_1 = n_3$) the lowest-order modes, TE_0 and TM_0 , have no cutoff and are confined for all values of t/λ . The selective excitation of waveguide modes by means of prism couplers and a determination of their propagation constants β_m are described in [1].

The total number of confined modes that can be supported by a waveguide depends on the value of t/λ . Let us now consider what happens to the TE modes in a given waveguide (i.e., for fixed n_1, n_2, n_3 , and t) as the wavelength of the light decreases gradually, assuming that the medium remains transparent and the indices of refraction n_1, n_2 , and n_3 do not vary significantly. Since $k_0 = 2\pi/\lambda$, the effect of decreasing the wavelength is to increase the value of k_0 . At long wavelengths (low frequencies) such that

$$0 < \sqrt{n_2^2 - n_3^2} k_0 t < \tan^{-1} \left(\frac{n_3^2 - n_1^2}{n_2^2 - n_3^2} \right)^{1/2}, \quad (11.2-15)$$

t/λ is below the cutoff value and no confined mode exists in the waveguide. As the wavelength decreases so that

$$\tan^{-1} \left(\frac{n_3^2 - n_1^2}{n_2^2 - n_3^2} \right)^{1/2} < \sqrt{n_2^2 - n_3^2} k_0 t < \pi + \tan^{-1} \left(\frac{n_3^2 - n_1^2}{n_2^2 - n_3^2} \right)^{1/2}, \quad (11.2-16)$$

one solution to the mode condition (11.2-5) exists. The mode is designated as TE_0 and has a transverse h parameter falling within the range

$$0 < h_1 t < \pi, \quad (11.2-17)$$

so that it has no zero crossings in the interior of the guiding layer ($-t < x < 0$). When the wavelength decreases further so that the parameter $\sqrt{n_2^2 - n_3^2} k_0 t$ falls within the range

$$\pi + \tan^{-1} \left(\frac{n_3^2 - n_1^2}{n_2^2 - n_3^2} \right)^{1/2} < \sqrt{n_2^2 - n_3^2} k_0 t < 2\pi + \tan^{-1} \left(\frac{n_3^2 - n_1^2}{n_2^2 - n_3^2} \right)^{1/2}, \quad (11.2-18)$$

the mode condition (11.2-5) yields two solutions. One corresponds to a value of $ht < \pi$ and is thus that of the lowest-order TE_0 mode. In the second mode

$$\pi < h_2 t < 2\pi, \quad (11.2-19)$$

and consequently it has one zero crossing (i.e., point where $E_y = 0$) in the guiding region ($-t < x < 0$). This is the so-called TE_1 mode. Both of these modes correspond to the same frequency and can thus be excited simultaneously by the same input field. We notice, however, that the TE_0 mode has a larger value of p (i.e., $p_0 > p_1$), and is therefore more strongly confined to the guiding slab. It follows from Eq. (11.2-4) that $\beta_0 > \beta_1$, so that the phase velocity $v_0 = \omega/\beta_0$ of the TE_0 mode is smaller than that of the TE_1 mode. We can now generalize and state that the m th mode (TE or TM) satisfies

$$m\pi < h_m t < (m + 1)\pi \quad (11.2-20)$$

and has m zero crossings in the guiding layer ($-t < x < 0$). The general features of TM modes are similar to those of TE modes, except that the corresponding values of p are somewhat smaller, indicating a lesser degree of confinement. A larger fraction of the total TM-mode power thus propagates in the outer medium than for a TE mode of the same order. This point is taken up in Problem 11.5.

11.2.3. Ray-Optics Approach

The TE and TM modes of the slab waveguide discussed above can also be derived by ray-optics considerations. This is possible because such a waveguide consists of a piecewise homogeneous media with planar geometry. Wave propagation in each homogeneous region can be represented by a superposition of two plane waves. According to the discussion in Section 11.1, confined modes exist only in the region $n_3 k_0 < \beta < n_2 k_0$, where the plane waves experience total internal reflection at both the lower II–III and the upper II–I interfaces.

It looks as though the condition of total reflection at both interfaces were enough to assure a guided mode. However, it turns out that the total internal reflection is only a necessary condition. In other words, not all rays which are “trapped” by total reflection constitute a mode. A mode, by definition, must have a unique propagation constant and a well-defined field amplitude at each point in space and time. Consider the representation of a

mode $\mathcal{E}(x)\exp[i(\omega t - \beta z)]$ by a zigzagging plane wave of the form

$$\mathbf{E}(x, z, t) = \mathbf{E}_0 \exp[i(\omega t - \beta z - hx)], \quad (11.2-21)$$

where \mathbf{E}_0 is a constant and h is the transverse wave number. Let the plane wave travel a distance Δz in a time Δt in one zigzag $ABCD$ (see Fig. 11.2). If we follow the ray path $ABCD$ and add up the phase shifts due to propagation and total reflections at points B and C , we obtain a total phase shift of

$$\omega \Delta t - \beta \Delta z - 2ht + 2\phi_{21} + 2\phi_{23},$$

where $2\phi_{21}$ is the phase shift upon total reflection at point B , and $2\phi_{23}$ is the phase shift upon total reflection at point C . A mode of the form $\mathcal{E}(x)\exp[i(\omega t - \beta z)]$ propagating from point A to point D will gain a phase shift of $\omega \Delta t - \beta \Delta z$. Therefore, a totally reflecting zigzag ray will become a mode only when the extra transverse phase shift is an integral multiple of 2π , that is,

$$-2ht + 2\phi_{21} + 2\phi_{23} = -2m\pi, \quad (11.2-22)$$

where m is an integer. The minus sign in front of $2m\pi$ is inserted to make m correspond to the TE_m and TM_m modes of the waveguide. The phase shifts $2\phi_{21}$ and $2\phi_{23}$ for TE or TM waves can be expressed conveniently in terms of h , p , and q as

$$2\phi_{21} = \begin{cases} 2 \tan^{-1} \frac{q}{h} & (\text{TE}), \\ 2 \tan^{-1} \frac{n_2^2 q}{n_1^2 h} & (\text{TM}), \end{cases} \quad (11.2-23)$$

$$2\phi_{23} = \begin{cases} 2 \tan^{-1} \frac{p}{h} & (\text{TE}), \\ 2 \tan^{-1} \frac{n_2^2 p}{n_3^2 h} & (\text{TM}). \end{cases} \quad (11.2-24)$$

These phase shifts are confined between 0 and π . Therefore the fundamental mode corresponds to the situation when $2ht = 2\phi_{21} + 2\phi_{23}$, that is, $m = 0$. Higher-order modes involve larger ht . The integer m in Eq. (11.2-22), therefore, assumes only nonnegative values: $m = 0, 1, 2, 3, \dots$. The condi-

tion (11.2-22) is equivalent to the mode conditions (11.2-5) and (11.2-11) derived from the eigenvalue-problem approach.

Consider a specific example. A waveguide is formed by growing a 1.0- μm -thick GaAs film on an AlGaAs substrate. We have $n_1 = 1.0$, $n_2 = 3.50$, and $n_3 = 3.20$ at $\lambda = 1 \mu\text{m}$. There are three confined TE modes in this film according to Fig. 11.4, and the mode indices β/k_0 are 3.473, 3.394, and 3.264 for the mode orders $m = 0, 1$, and 2, respectively. These mode indices correspond to the ray incident angles θ_2 (defined by $\beta = n_2 k_0 \sin \theta_2$) of 82.9, 75.9, and 68.8° in that order. Note that all these angles are greater than the critical angle $\theta_c = 66.1^\circ$. The fundamental mode ($m = 0$) has always the largest mode index and angle of incidence; its mode index approaches n_2 . The highest-order mode has the lowest mode index, approaching n_3 , and the smallest angle of incidence, approaching the critical angle. Figure 11.5 shows the zigzag rays corresponding to the waveguide modes discussed above.

Ray optics offers a convenient way of obtaining the mode condition for a slab waveguide. However, in a more complicated waveguide structure which involves many layers or inhomogeneous layers, it is difficult to use. In addition, the ray optics approach only yields the mode condition. Nothing about the field distribution or the mode orthogonality is obtained.

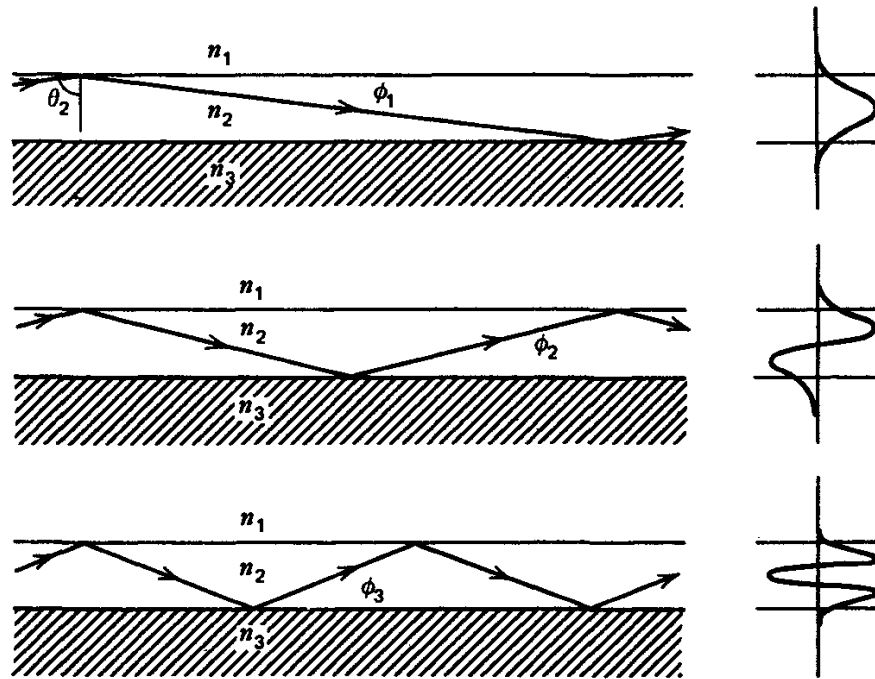


Figure 11.5. The three lowest-order TE modes of a slab waveguide and their corresponding zigzag rays. $\phi_3 > \phi_2 > \phi_1$ ($\phi = \frac{1}{2}\pi - \theta_2$).

11.3. DIELECTRIC PERTURBATION AND MODE COUPLING

In the preceding sections we derived some general properties of dielectric waveguide modes and, specifically, obtained solutions for the confined modes supported by a slab waveguide. The guided modes can actually be excited and propagate along the axis (z) of the dielectric waveguide independently of each other provided the dielectric function $\epsilon(x, y) = \epsilon_0 n^2(x, y)$ remains independent of z . In the case when there is a dielectric perturbation $\Delta\epsilon(x, y, z)$ due to waveguide imperfections, bending, surface corrugations, or the like, the eigenmodes are coupled with each other. In other words, if a pure mode is excited at the beginning of the waveguide, some of its power may be transferred to other modes. An increasingly large number of experiments and devices involve intentional coupling between such modes [2–5, 7]. Two typical examples involve TM \leftrightarrow TE mode conversion by the electro-optic [4, 5] or acousto-optic effect [2], or coupling of forward to backward modes by means of a corrugation in one of the waveguide interfaces. In this section we will use the coupled-mode theory developed in Chapter 6 to describe such mode coupling. Some of the important results are outlined as follows. The dielectric perturbation is represented by a small perturbing term $\Delta\epsilon(x, y, z)$ such that the dielectric tensor as a function of space can be written

$$\epsilon(x, y, z) = \epsilon_0(x, y) + \Delta\epsilon(x, y, z), \quad (11.3-1)$$

where $\epsilon_0(x, y)$ is the unperturbed dielectric function describing the waveguide structure. Wave propagation in such a perturbed waveguide can always be expressed in terms of a linear combination of the unperturbed eigenmodes:

$$\mathbf{E} = \sum A_m(z) \mathfrak{E}_m(x, y) \exp[i(\omega t - \beta_m z)], \quad (11.3-2)$$

where $A_m(z)$ are the mode amplitudes and are assumed to be functions of z . These eigenmodes $\mathfrak{E}_m(x, y) \exp[i(\omega t - \beta_m z)]$ satisfy the following wave equation:

$$\left[\frac{\partial^2}{\partial x^2} + \frac{\partial^2}{\partial y^2} + \omega^2 \mu \epsilon_0(x, y) - \beta_m^2 \right] \mathfrak{E}_m(x, y) = 0, \quad (11.3-3)$$

where we have neglected the term $\nabla(\nabla \cdot \mathbf{E})$, which is legitimate provided the variation of $\epsilon_0(x, y)$ over a wavelength is small. For the case of slab

waveguides, $\epsilon_0(x, y)$ is discontinuous at the dielectric interfaces, and $\nabla \cdot \mathbf{E}$ is zero for TE modes, since $\mathbf{E} \cdot \nabla \epsilon = 0$. Therefore Eq. (11.3-3) holds. For TM modes of the slab waveguide, Eq. (11.3-3) is not valid at the interfaces.

These modes are mutually orthogonal and satisfy the following orthonormality condition:

$$\langle m|k \rangle \equiv \int \mathcal{E}_m^* \cdot \mathcal{E}_k dx dy = \frac{2\omega\mu}{|\beta_m|} \delta_{km}. \quad (11.3-4)$$

This condition is always valid provided Eq. (11.3-3) is true.

Substitution of Eq. (11.3-2) into the wave equation (6.4-8) and using (11.3-4) leads to

$$\frac{d}{dz} A_k(z) = -\frac{i\omega}{4} \frac{\beta_k}{|\beta_k|} \sum_m \langle k|\Delta\epsilon|m \rangle A_m(z) e^{i(\beta_k - \beta_m)z}, \quad (11.3-5)$$

where $\langle k|\Delta\epsilon|m \rangle$ is defined as

$$\langle k|\Delta\epsilon|m \rangle = \int \mathcal{E}_k^* \cdot \Delta\epsilon \mathcal{E}_m dx dy. \quad (11.3-6)$$

Equation (11.3-5) describes the evolution of the mode amplitudes $A_k(z)$ as the wave propagates along the waveguide. It is a set of coupled differential equations and can be solved for a large variety of mode interactions [2]. Some important examples are considered in the following sections. A special case worth mentioning is when the dielectric perturbation $\Delta\epsilon = \Delta\epsilon(x, y)$ is a function of x and y only (i.e., $\partial\epsilon/\partial z = 0$). This is discussed below.

11.3.1. Uniform Dielectric Perturbation

The coupled-mode approach discussed above provides a way of investigating the coupling between the unperturbed modes due to the presence of the dielectric perturbation, especially when the perturbation is z -dependent. There are many practical situations where it is desirable or necessary to obtain the propagation constants and the modes of the whole waveguide structure including the dielectric perturbation $\Delta\epsilon(x, y)$. In the event that the wave equation is difficult to solve (or cannot be directly solved), perturbation theory provides a method of treating such problems. Often the perturbation $\Delta\epsilon(x, y)$ is chosen so that the unperturbed waveguide structure can be easily solved or has known solutions.

Let the unperturbed modes of propagation be

$$\mathbf{E}_m = \mathfrak{E}_m(x, y) \exp[i(\omega t - \beta_m z)], \quad m = 0, 1, 2, \dots,$$

whose transverse-mode functions \mathfrak{E}_m satisfy the unperturbed wave equation

$$[\nabla_t^2 + \omega^2 \mu \epsilon(x, y)] \mathfrak{E}_m(x, y) = \beta_m^2 \mathfrak{E}_m(x, y). \quad (11.3-7)$$

These modes form a complete orthogonal set, as discussed in Section 11.1, and obey the orthonormalization relation

$$\int \mathfrak{E}_m^* \cdot \mathfrak{E}_l dx dy = \frac{2\omega\mu}{\beta_m} \delta_{ml}. \quad (11.3-8)$$

We now consider the effect of a dielectric perturbation $\Delta\epsilon(x, y)$ which is small compared with $\epsilon(x, y)$. We assume that the application of such a small perturbation will only cause small changes in the mode functions and propagation constants. Let $\delta\mathfrak{E}_m$ and $\delta\beta_m^2$ be the changes in the mode functions and propagation constants, respectively. The true wave equation now takes the form

$$[\nabla_t^2 + \omega^2 \mu \epsilon + \omega^2 \mu \Delta\epsilon](\mathfrak{E}_m + \delta\mathfrak{E}_m) = (\beta_m^2 + \delta\beta_m^2)(\mathfrak{E}_m + \delta\mathfrak{E}_m). \quad (11.3-9)$$

If we neglect the second-order terms $\Delta\epsilon \delta\mathfrak{E}_m$ and $\delta\beta_m^2 \delta\mathfrak{E}_m$ and use Eq. (11.3-7), then Eq. (11.3-9) simplifies to

$$[\nabla_t^2 + \omega^2 \mu \epsilon] \delta\mathfrak{E}_m + \omega^2 \mu \Delta\epsilon \mathfrak{E}_m = \beta_m^2 \delta\mathfrak{E}_m + \delta\beta_m^2 \mathfrak{E}_m \quad (11.3-10)$$

To solve this we expand $\delta\mathfrak{E}_m$ in terms of the unperturbed mode functions:

$$\delta\mathfrak{E}_m(x, y) = \sum_l a_{ml} \mathfrak{E}_l(x, y), \quad (11.3-11)$$

where the a_{ml} 's are constants. Substituting Eq. (11.3-11) for $\delta\mathfrak{E}_m$ in Eq. (11.3-10) and using Eq. (11.3-7), we obtain

$$\sum_l a_{ml} (\beta_l^2 - \beta_m^2) \mathfrak{E}_l = (\delta\beta_m^2 - \omega^2 \mu \Delta\epsilon) \mathfrak{E}_m. \quad (11.3-12)$$

If we now scalar-multiply by \mathfrak{E}_m^* and integrate over the whole xy plane, we observe that the expression on the left vanishes because of the orthogonal

property (11.3-8). Thus we obtain the equation

$$\int \mathcal{E}_m^* \cdot (\delta\beta_m^2 - \omega^2\mu \Delta\epsilon) \mathcal{E}_m dx dy = 0. \quad (11.3-13)$$

Since $\delta\beta_m^2$ is a constant, this can be written

$$\delta\beta_m^2 = \frac{\int \mathcal{E}_m^* \cdot \omega^2\mu \Delta\epsilon(x, y) \mathcal{E}_m dx dy}{\int \mathcal{E}_m^* \cdot \mathcal{E}_m dx dy}. \quad (11.3-14)$$

This gives the first-order correction to the propagation constant β_m^2 . Using Eq. (11.3-8) and $\delta\beta_m^2 = 2\beta_m \delta\beta_m$, Eq. (11.3-14) can also be written

$$\delta\beta_m = \frac{\omega}{4} \int \mathcal{E}_m^* \cdot \Delta\epsilon(x, y) \mathcal{E}_m dx dy. \quad (11.3-15)$$

To obtain the correction $\delta\mathcal{E}_m$ for the mode function, we scalar-multiply each side of Eq. (11.3-12) by \mathcal{E}_l^* ($l \neq m$) and integrate over x and y . This leads to

$$a_{ml}(\beta_l^2 - \beta_m^2) \frac{2\omega\mu}{\beta_l} = - \int \mathcal{E}_l^* \cdot \omega^2\mu \Delta\epsilon(x, y) \mathcal{E}_m dx dy, \quad (11.3-16)$$

where we have utilized the orthonormalization properties (11.3-8) of the unperturbed modes. The coefficients in the expansion (11.3-11) for $\delta\mathcal{E}_m$ in terms of the set \mathcal{E}_l are thus given by

$$a_{ml} = \frac{\omega\beta_l}{2(\beta_m^2 - \beta_l^2)} \int \mathcal{E}_l^* \cdot \Delta\epsilon(x, y) \mathcal{E}_m dx dy, \quad l \neq m. \quad (11.3-17)$$

The value of a_{mm} is not given by this process; it is to be chosen so as to normalize the resultant mode function according to Eq. (11.3-8), and is given by (see Problem 11.7)

$$a_{mm} = -\frac{1}{4} \frac{\delta\beta_m^2}{\beta_m^2} = -\frac{1}{2} \frac{\delta\beta_m}{\beta_m} \quad (11.3-18)$$

Using Eq. (11.3-15) for $\delta\beta_m$, the coefficients a_{mm} can thus be written

$$a_{mm} = -\frac{\omega}{8\beta_m} \int \mathcal{E}_m^* \cdot \Delta\epsilon(x, y) \mathcal{E}_m dx dy. \quad (11.3-19)$$

It is convenient to use the "coupling coefficients" [similar to Eq. (6.4-17)]

$$\kappa_{lm} = \frac{\omega}{4} \int \mathcal{E}_l^* \cdot \Delta \epsilon(x, y) \mathcal{E}_m dx dy, \quad (11.3-20)$$

so that the expression for the first-order correction to the mode function can be written, according to Eqs. (11.3-17) and (11.3-11),

$$\delta \mathcal{E}_m = \sum_{l \neq m} \frac{2\beta_l}{\beta_m^2 - \beta_l^2} \kappa_{lm} \mathcal{E}_l - \frac{\kappa_{mm}}{2\beta_m} \mathcal{E}_m. \quad (11.3-21)$$

The correction to the propagation constant $\delta\beta_m$ (11.3-15) can thus be written

$$\delta\beta_m = \kappa_{mm}. \quad (11.3-22)$$

The results (11.3-21) and (11.3-15) will be used to evaluate the attenuation coefficients of the modes in a metal-clad waveguide (see Section 11.10).

11.4. PERIODIC WAVEGUIDE-BRAGG REFLECTION

Consider a periodic dielectric waveguide in which the periodicity is due to a corrugation of one of the interfaces as shown in Fig. 11.6. Such periodic waveguides are used for optical filtering [8] as well as in distributed-feedback lasers [9-11]. These two applications will be described further below.

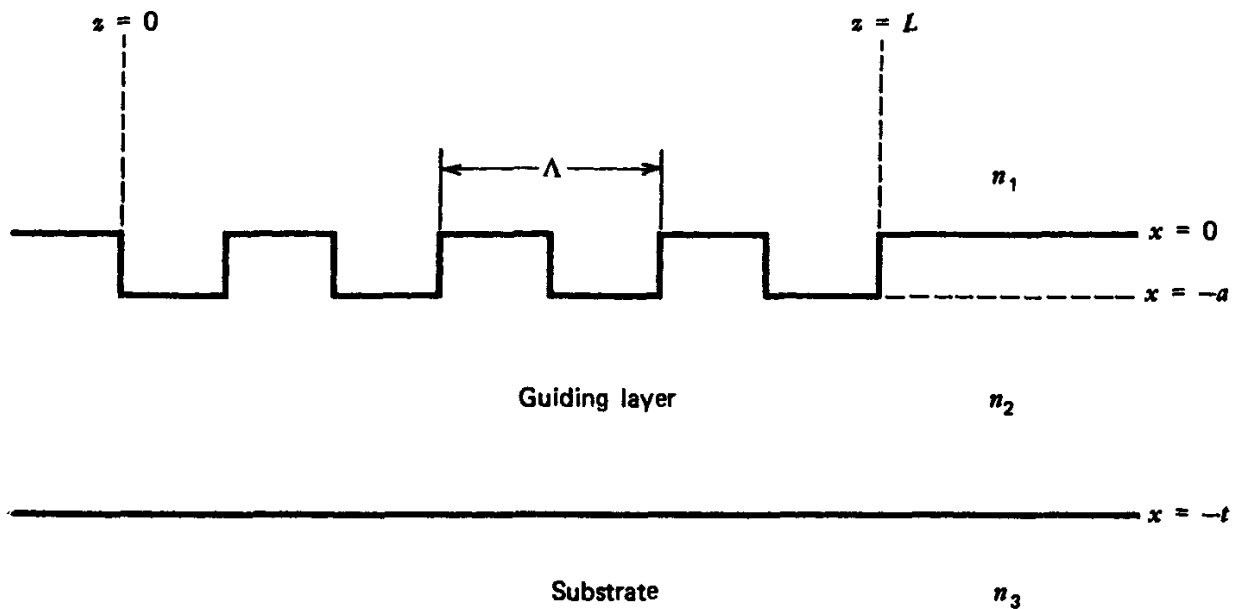


Figure 11.6. A corrugated periodic waveguide.

The corrugation is described by $\Delta\epsilon(x, y, z) = \epsilon_0 \Delta n^2(x, y, z)$. Since $\Delta n^2(x, y, z)$ is a scalar, it follows from Eq. (11.3-6) that the corrugation couples only TE to TE modes and TM to TM, but not TE to TM. According to the discussion in Chapter 6, we may consider the right side of Eq. (11.3-5) as a source term driving the k th mode. In order to have a continuous increase in the mode amplitude A_k , the right side must have a term which does not vary appreciably over a distance $z \gg \Lambda$, so that the integration does not average out to zero. This requires that

$$\beta_k - \beta_m = l \left(\frac{2\pi}{\Lambda} \right) \quad (11.4-1)$$

for some mode m with propagation constant β_m and some integer l . When this condition (11.4-1) is satisfied, the k th mode and the m th mode are resonantly coupled via the l th Fourier component of the periodic perturbation $\Delta\epsilon(x, y, z)$.

To be specific, let us assume that the period Λ of the perturbation $\Delta n^2(x, z)$ is so chosen that $l(\pi/\Lambda) = \beta_s$ for some integer l . The phase-matching condition (11.4-1) can thus be satisfied by the coupling between the mode β_s and its reflected mode which has a propagation constant of $-\beta_s$, since $\beta_s - (-\beta_s) = 2\beta_s = l(2\pi/\Lambda)$. To calculate the mode amplitudes from the coupled mode equations (6.4-33), we need to expand the perturbation $\Delta\epsilon(x, z)$ as a Fourier series. Let us consider the specific "square wave" corrugation of Fig. 11.6. In this case, the dielectric perturbation $\Delta\epsilon(x, z)$ can be written

$$\Delta\epsilon(x, z) = \Delta\epsilon(x) \frac{f(z) + 1}{2}, \quad (11.4-2)$$

where

$$\Delta\epsilon(x) = \begin{cases} \epsilon_0(n_1^2 - n_2^2), & -a \leq x \leq 0, \\ 0 & \text{otherwise,} \end{cases} \quad (11.4-3)$$

and $f(z)$ is the square-wave function defined by Eq. (6.5-8). By using the Fourier series (6.5-10) for $f(z)$, the dielectric perturbation $\Delta\epsilon(x, z)$ (11.4-2) becomes

$$\Delta\epsilon(x, z) = \Delta\epsilon(x) \left\{ \frac{1}{2} + \sum_{l \neq 0} \frac{i(1 - \cos l\pi)}{2l\pi} \exp \left[-il \left(\frac{2\pi}{\Lambda} \right) z \right] \right\} \quad (11.4-4)$$

$$= \sum_l \epsilon_l(x) \exp \left[-il \left(\frac{2\pi}{\lambda} \right) z \right], \quad (11.4-5)$$

where Eq. (11.4-5) is a more general form of expansion. For the square-wave corrugation, the l th Fourier component $\varepsilon_l(x)$ is given by

$$\varepsilon_l(x) = \begin{cases} \frac{i \Delta\varepsilon(x)}{l\pi} & l = \pm 1, \pm 3, \pm 5, \dots, \\ \frac{1}{2} \Delta\varepsilon(x) & l = 0, \\ 0 & l = \pm 2, \pm 4, \dots \end{cases} \quad (11.4-6)$$

The coupling between the forward mode (β_s) and the reflected mode ($-\beta_s$) is described by the contradirectional coupled mode equations (6.4-33), which now take the form

$$\begin{aligned} \frac{dA_s}{dz} &= -i\kappa B_s e^{i\Delta\beta z}, \\ \frac{dB_s}{dz} &= i\kappa^* A_s e^{-i\Delta\beta z}, \end{aligned} \quad (11.4-7)$$

where B_s is the amplitude of the reflected mode ($-\beta_s$), and $\Delta\beta$ and κ are given by

$$\Delta\beta = \beta_s - (-\beta_s) - l\left(\frac{2\pi}{\Lambda}\right) \quad (11.4-8)$$

and

$$\kappa = \frac{\omega}{4} \int_{-\infty}^{\infty} \varepsilon_l(x) |\mathfrak{E}_s(x)|^2 dx. \quad (11.4-9)$$

We note that the total power carried by both modes is conserved, since

$$\frac{d}{dz} [|A_s|^2 - |B_s|^2] = 0. \quad (11.4-10)$$

By using Eqs. (11.4-3) and (11.4-6), the coupling constant κ for odd l can be written

$$\kappa = \frac{i\omega\varepsilon_0(n_1^2 - n_2^2)}{4l\pi} \int_{-a}^0 |\mathfrak{E}_s(x)|^2 dx, \quad l = 1, 3, 5, \dots \quad (11.4-11)$$

In practice the period Λ is chosen so that, for some particular l , $\Delta\beta \approx 0$. We

note that for $\Delta\beta = 0$

$$\Lambda = l \frac{\lambda_0^{(s)}}{2}$$

where $\lambda_0^{(s)} = 2\pi/\beta_s$ is the guide wavelength of the s th mode.

We can now use the explicit expression of the field $\mathcal{E}_s(x)$ for the TE modes (11.2-3). The coupling constant κ now becomes

$$\kappa = \frac{i\omega\epsilon_0(n_1^2 - n_2^2)}{4l\pi} \int_{-a}^0 C_s^2 \left[\cos h_s x - \frac{q_s}{h_s} \sin h_s x \right]^2 dx. \quad (11.4-12)$$

Although the integral can be calculated exactly using Eqs. (11.2-3) and (11.2-5), an especially simple result follows if we consider that operation is sufficiently above propagation cutoff [$t(n_2 - n_3)/s\lambda \gg 1$] so that from Eqs. (11.2-4) and (11.2-5)

$$\beta_s \approx n_2 k_0,$$

$$h_s \rightarrow \frac{\pi s}{t}, \quad s = 1, 2, \dots = \text{transverse mode number}, \quad (11.4-13)$$

$$\frac{q_s}{h_s} \approx (n_2^2 - n_1^2)^{1/2} \left(\frac{2t}{s\lambda} \right).$$

The results can be verified using Eqs. (11.2-4) and (11.2-5). In addition, since $q_s \gg h_s$, we have from Eq. (11.2-7)

$$C_s^2 = \frac{4h_s^2 \omega \mu}{\beta_s t q_s^2} \quad (11.4-14)$$

in the well-confined regime, and for $h_s a \ll 1$ the integral of Eq. (11.4-11) becomes

$$\int_{-a}^0 [\mathcal{E}_s(x)]^2 dx = \frac{4\pi^2 s^2 \omega \mu}{3n_2 k_0} \left(\frac{a}{t} \right)^3 \left(1 + \frac{3}{q_s a} + \frac{3}{q_s^2 a^2} \right)$$

and the coupling constant can be written

$$\begin{aligned} \kappa_s \approx & -i \frac{2\pi^2 s^2}{3l\lambda} \frac{n_2^2 - n_1^2}{n_2} \left(\frac{a}{t} \right)^3 \\ & \times \left[1 + \frac{3}{2\pi} \frac{\lambda/a}{(n_2^2 - n_1^2)^{1/2}} + \frac{3}{4\pi^2} \frac{(\lambda/a)^2}{(n_2^2 - n_1^2)} \right]. \quad (11.4-15) \end{aligned}$$

The problem has thus been reduced to a pair of coupled differential equations (11.4-7) and an expression (11.4-15) for the coupling constant. Note that Eq. (11.4-15) is for TE modes only.

The general solution of the contradirectional coupled equations is given in Eq. (6.4-35). We now consider a waveguide with a corrugated section of length L as in Fig. 11.6. A wave with an amplitude $A(0)$ is incident from the left on the corrugated section. In this case, the boundary conditions are $A(z) = A(0)$ at $z = 0$ and $B(z) = 0$ at $z = L$. By substituting $A_1(z) = A(0)$ and $A_2(L) = 0$ in Eq. (6.4-35), we obtain the following expressions for the mode amplitudes:

$$A(z) = A(0) e^{i\frac{1}{2}\Delta\beta z} \left[\frac{s \cosh s(L-z) + i\frac{1}{2}\Delta\beta \sinh s(L-z)}{s \cosh sL + i\frac{1}{2}\Delta\beta \sinh sL} \right]$$

$$B(z) = A(0) e^{-i\frac{1}{2}\Delta\beta z} \left[\frac{-i\kappa^* \sinh s(L-z)}{s \cosh sL + i\frac{1}{2}\Delta\beta \sinh sL} \right], \quad (11.4-16)$$

where s and $\Delta\beta$ are given by

$$s = \sqrt{\kappa^* \kappa - \left(\frac{1}{2}\Delta\beta\right)^2}, \quad (11.4-17)$$

$$\Delta\beta = \beta_s - (-\beta_s) - i\frac{2\pi}{\Lambda}. \quad (11.4-18)$$

These expressions are formally identical to those for reflection from a periodic layered medium, except for the coupling constant. The fraction of power coupled to the backward-propagating mode $(-\beta_s)$, called the mode reflectivity, is defined as

$$R = \left| \frac{B(0)}{A(0)} \right|^2 \quad (11.4-19)$$

and is given, according to Eq. (11.4-16), by

$$R = \frac{\kappa^* \kappa \sinh^2 sL}{s^2 \cosh^2 sL + \left(\frac{1}{2}\Delta\beta\right)^2 \sinh^2 sL}. \quad (11.4-20)$$

This again is formally identical to the reflectivity of a periodic layered medium [Eq. (6.6-10)]. Under the phase-matching condition $\Delta\beta = 0$, the reflectivity R reaches its maximum value, according to Eq. (11.4-20):

$$R_{\max} = \tanh^2 |\kappa L|. \quad (11.4-21)$$

The mode amplitude in this case ($\Delta\beta = 0$) is given, according to Eq. (11.4-16), by

$$A(z) = A(0) \frac{\cosh|\kappa|(L-z)}{\cosh|\kappa|L},$$

$$B(z) = A(0) \frac{-i\kappa^* \sinh|\kappa|(L-z)}{\cosh|\kappa|L}. \quad (11.4-22)$$

The mode powers $|A(z)|^2$ and $|B(z)|^2$ for this case are shown as functions of z in Fig. 11.7. We note that the incident mode power drops off exponentially in the perturbation region. This situation is exactly the same as that of the reflection of light from a periodic layered medium (see Section 6.6 and Fig. 6.14). The exponential attenuation shown in Fig. 11.7 for the incident mode is a result of mode coupling with the backward-propagating mode. This decay in amplitude can also be explained in terms of the complex Bloch wave number when the incident wave satisfies the Bragg condition ($\Delta\beta = 0$). According to Eqs. (11.3-2), (11.4-16), and (11.4-18), we find that the z -dependent parts of the wave solutions in the periodic waveguide are

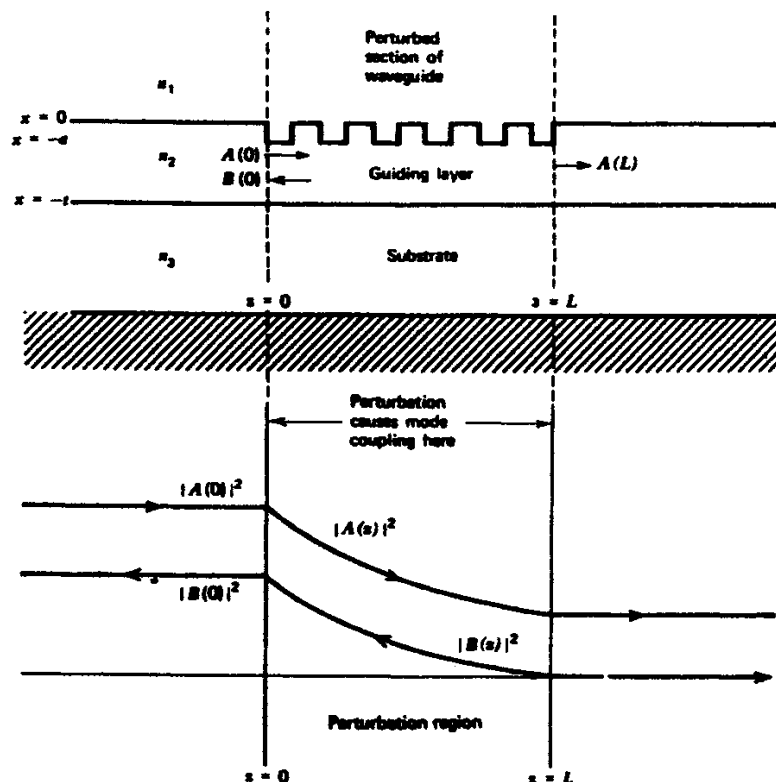


Figure 11.7. Top: a corrugated section of a dielectric waveguide. Bottom: the incident and reflected intensities inside the corrugated section.

exponentials with propagation constants

$$\beta' = l\frac{\pi}{\Lambda} \pm i\sqrt{\kappa^*\kappa - (\frac{1}{2}\Delta\beta)^2}. \quad (11.4-23)$$

These are precisely the Bloch wave numbers if the field (11.3-2) is written in Bloch form.

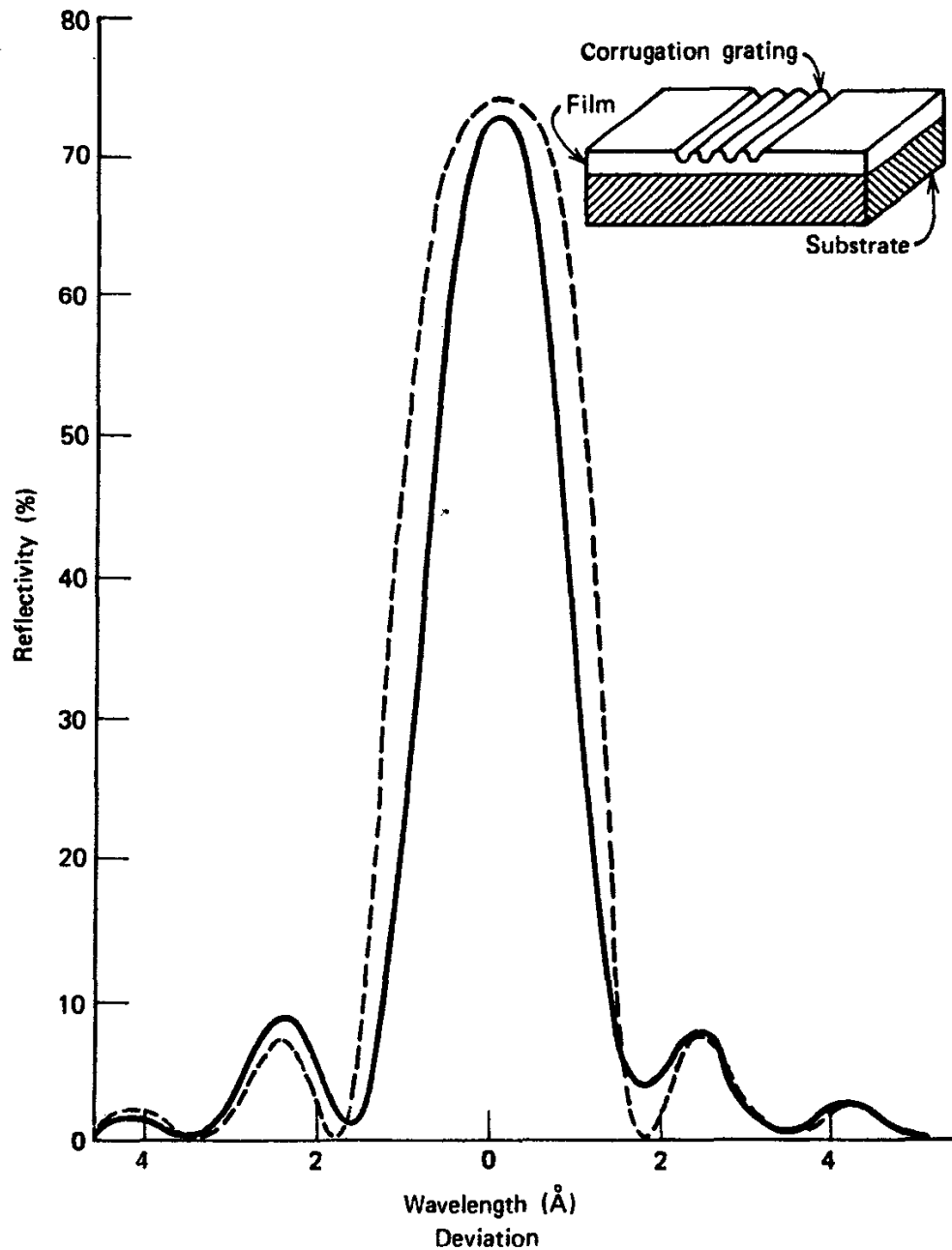


Figure 11.8. Illustration of a corrugation filter in a thin-film waveguide, plot (solid line) of reflectivity of filter versus wavelength deviation from the Bragg condition, and calculated response of filter (dashed line) $|B(0)/A(0)|^2$ using Eq. (11.4-20). (After [8]).

Let ω_0 be the frequency at which the phase-matching condition $\Delta\beta = 0$ is satisfied. Then $\Delta\beta$ can be written

$$\Delta\beta = \frac{2n}{c}(\omega - \omega_0), \quad (11.4-24)$$

where n is the mode index of the guided wave (i.e., $\beta_s = n\omega/c$). Thus the Bloch wave number β' can be written

$$\beta' = l\frac{\pi}{\Lambda} \pm i\sqrt{\kappa^*\kappa - \left(\frac{n}{c}\right)^2(\omega - \omega_0)^2}. \quad (11.4-25)$$

We note that for a range of frequencies such that $-2|\kappa| < \Delta\beta < 2|\kappa|$, β' has an imaginary part. This is the so-called “forbidden band” of the periodic waveguide shown in Fig. 11.6, and is formally identical to that of a periodic layered medium (see Section 6.6). Incident modes with frequencies in this region are evanescent in the corrugated section and are strongly reflected, provided the interaction length L is large enough. Thus a section of a corrugated waveguide acts as a band-rejection filter with a bandwidth given by $\Delta\beta = 4|\kappa|$, according to Eq. (11.4-23), or equivalently, according to Eq. (11.4-24),

$$\Delta\omega = \frac{2c}{n}|\kappa|. \quad (11.4-26)$$

A filter based on the Bragg reflection of a guided mode in a corrugated waveguide has been demonstrated experimentally. The measured results are shown in Fig. 11.8.

11.5. CODIRECTIONAL COUPLING IN A PERIODIC WAVEGUIDE

In the previous section we assumed that the period Λ is chosen so that $\beta_s = l\pi/\Lambda$ for some mode β_s and integer l . Under these conditions, the mode β_s is strongly coupled to its backward-propagating mode. The period is typically of the order of $\frac{1}{2}l\lambda_g$, where $\lambda_g = 2\pi/\beta_s$ is the guide wavelength of the s th mode. For efficient coupling, the integer l is chosen as small as possible, since the coupling constant κ decreases as $1/l$ according to Eq. (11.4-11). On the other hand, this period Λ is also limited by the fabrication technology. For example, the period required for the Bragg reflection of 1- μm radiation in a GaAs waveguide ($n \approx 3.3$) (see Fig. 11.4) is $l \times 1500 \text{ \AA}$. The integer l can be chosen as 3 for ease of fabrication.

In a multimode waveguide, if the period of surface corrugation is large enough so that $\beta_1 - \beta_2 \approx l(2\pi/\Lambda)$ for some pair of modes β_1 and β_2 propagating in the same direction and some integer l , these modes are strongly coupled provided the coupling constant is not zero. Let $A_1(z)$ and $A_2(z)$ be the mode amplitudes of the coupled modes. They are described, according to Eq. (11.3-5) or (6.4-27), by

$$\frac{d}{dz}A_1 = -i\kappa_{12}A_2e^{i\Delta\beta z}, \quad (11.5-1)$$

$$\frac{d}{dz}A_2 = -i\kappa_{12}^*A_1e^{-i\Delta\beta z},$$

where

$$\kappa_{12} = \frac{\omega}{4} \int_{-\infty}^{\infty} \mathfrak{E}_1^*(x) \cdot \epsilon_l(x) \mathfrak{E}_2(x) dx, \quad (11.5-2)$$

$$\Delta\beta = \beta_1 - \beta_2 - l\left(\frac{2\pi}{\Lambda}\right), \quad (11.5-3)$$

with $\epsilon_l(x)$ as the l th Fourier component of the dielectric perturbation (11.4-5) and is given by Eqs. (11.4-3) and (11.4-6) for a square-wave corrugation. We note that the total power carried by both modes is conserved, since

$$\frac{d}{dz}\{|A_1|^2 + |A_2|^2\} = 0. \quad (11.5-4)$$

Let $A_1(0)$ and $A_2(0)$ be the mode amplitudes at $z = 0$. The general solution to Eq. (11.5-1) is

$$A_1(z) = e^{i\frac{1}{2}\Delta\beta z} \left\{ \left[\cos sz - i\frac{\Delta\beta}{2s} \sin sz \right] A_1(0) - i\frac{\kappa_{12}}{s} \sin A_2(0) \right\}, \quad (11.5-5)$$

$$A_2(z) = e^{-i\frac{1}{2}\Delta\beta z} \left\{ -i\frac{\kappa_{12}^*}{s} \sin sz A_1(0) + \left[\cos sz + i\frac{\Delta\beta}{2s} \sin sz \right] A_2(0) \right\},$$

where

$$s^2 = |\kappa_{12}|^2 + \left(\frac{1}{2}\Delta\beta\right)^2. \quad (11.5-6)$$

By inspection of (11.5-5), we note that the fraction of power that is coupled from mode 2 to mode 1, or vice versa, in a distance z is

$$\frac{|\kappa_{12}|^2}{|\kappa_{12}|^2 + \left(\frac{1}{2}\Delta\beta\right)^2} \sin^2 sz, \quad (11.5-7)$$

which is a periodic function of z . We find that the power is exchanged back and forth between the modes provided the interaction length is large enough. The maximum fraction of power exchange is $|\kappa_{12}|^2 / [|\kappa_{12}|^2 + (\frac{1}{2}\Delta\beta)^2]$, which becomes small when $|\Delta\beta| \gg |\kappa_{12}|$. Complete power exchange occurs only when $\Delta\beta = 0$, that is, when the phase matches. Under the phase-matching condition $\Delta\beta = 0$ we have

$$A_1(z) = A_1(0)\cos \kappa z - i\frac{\kappa_{12}}{\kappa}A_2(0)\sin \kappa z, \quad (11.5-8)$$

$$A_2(z) = A_2(0)\cos \kappa z - i\frac{\kappa_{12}^*}{\kappa}A_1(0)\sin \kappa z,$$

where

$$\kappa = |\kappa_{12}|. \quad (11.5-9)$$

The power exchange in a codirectional mode coupling is similar to that of the coupled modes in a Šolc filter. The plot of the mode powers $A_1(z)$ and $A_2(z)$ in Fig. 6.11 also applies to this case.

The codirectional mode coupling is also frequency-dependent. Let n_1, n_2 be the mode index [i.e., $\beta_\alpha = n_\alpha(\omega/c)$, $\alpha = 1, 2$] associated with the coupled modes, and ω_0 be the frequency at which $\Delta\beta = 0$. Then $\Delta\beta$ can be written

$$\Delta\beta = \frac{(n_1 - n_2)(\omega - \omega_0)}{c}. \quad (11.5-10)$$

Strong coupling occurs only in the frequency region where $|\Delta\beta| < 2\kappa$, which translates into a frequency bandwidth of

$$\Delta\omega = \frac{4\kappa c}{|n_1 - n_2|}, \quad (11.5-11)$$

where κ is the magnitude of the coupling constant, c is the velocity of light, and $n_1 - n_2$ is the difference in the mode indices. If we compare this expression with that for the Bragg reflector [Eq. (11.4-22)], we find that the bandwidth of codirectional coupling is normally much larger, since $|n_1 - n_2|$ is usually small compared to n .

11.6. DISTRIBUTED-FEEDBACK LASERS

In the previous sections and Chapter 6, the dielectric perturbation $\Delta\epsilon(x, y, z)$ is assumed to be a real quantity, which describes most passive perturbations adequately. If a small gain is present in the medium, this gain can also be treated as a perturbation and can be included in $\Delta\epsilon(x, y, z)$ provided that $\Delta\epsilon(x, y, z)$ becomes a complex quantity. We now consider the electromagnetic propagation in a periodic medium which is described by a real dielectric function $\epsilon(x, y, z)$ and a complex periodic dielectric perturbation $\Delta\epsilon(x, y, z)$. We will show that laser oscillation can result without the need for end reflectors. The feedback is now provided by the continuous coherent backscattering from the periodic perturbation. In what follows we will give a general discussion which can be applied to both a bulk periodic medium (e.g., stratified medium) and a periodic waveguide.

The gain in a bulk medium is described by a complex dielectric constant $\epsilon_r + i\epsilon_i$ with a positive imaginary part $\epsilon_i > 0$, so that the propagation constant k' of a plane wave is given by

$$k'^2 = \omega^2\mu(\epsilon_r + i\epsilon_i) = k^2\left(1 + i\frac{\epsilon_i}{\epsilon_r}\right), \quad (11.6-1)$$

where k is given by

$$k^2 = \omega^2\mu\epsilon_r \quad (11.6-2)$$

and is the propagation constant of the wave in the absence of gain. If $\epsilon_i/\epsilon_r \ll 1$, Eq. (11.6-1) can be written

$$k' = k\left(1 + i\frac{\epsilon_i}{2\epsilon_r}\right) \quad (11.6-3)$$

If we now substitute this k' into Eq. (1.4-10), a plane wave propagating in the $+z$ direction becomes

$$\psi = Ae^{i(\omega t - k'z)} = Ae^{(k\epsilon_i/2\epsilon_r)z}e^{i(\omega t - kz)}. \quad (11.6-4)$$

It follows that the intensity of the wave increases according to the relation

$$I(z) = I_0 e^{gz}, \quad (11.6-5)$$

where the constant

$$g = \frac{k\varepsilon_i}{\varepsilon_r} \quad (11.6-6)$$

is the gain coefficient.

If gain is present in a periodic medium, the dielectric tensor (11.3-1) can now be written as

$$\varepsilon(x, y, z) = \varepsilon_0(x, y, z) + \Delta\varepsilon(x, y, z) + i\gamma(x, y, z), \quad (11.6-7)$$

where $\varepsilon_0(x, y, z)$ is the unperturbed dielectric tensor, $\Delta\varepsilon(x, y, z)$ is the dielectric perturbation (real), and $\gamma(x, y, z)$ is the perturbing term due to the presence of gain. Replacing $\Delta\varepsilon$ in Eq. (11.3-5) by $\Delta\varepsilon + i\gamma$, the coupled mode equation becomes

$$\begin{aligned} \frac{d}{dz} A_k(z) = & -\frac{i\omega}{4} \frac{\beta_k}{|\beta_k|} \sum_m \langle k|\Delta\varepsilon|m\rangle A_m(z) e^{i(\beta_k - \beta_m)z} \\ & + \frac{\omega}{4} \frac{\beta_k}{|\beta_k|} \sum_l \langle k|\gamma|l\rangle A_l(z) e^{i(\beta_k - \beta_l)z}, \end{aligned} \quad (11.6-8)$$

where $\langle k|\Delta\varepsilon|m\rangle$ is defined in Eq. (11.3-6) and $\langle k|\gamma|l\rangle$ is defined as

$$\langle k|\gamma|l\rangle = \int \mathfrak{E}_k^* \cdot \gamma \mathfrak{E}_l dx dy. \quad (11.6-9)$$

To see the effect of gain on the characteristics of contradirectional coupling, we consider a gain which is uniform in z , that is, $\gamma(x, y, z) = \gamma(x, y)$. By using Eq. (11.4-5) or (6.4-15), the coupled mode equation (11.6-8) can be written

$$\frac{d}{dz} A_k(z) = -i\frac{\omega}{4} \frac{\beta_k}{|\beta_k|} \sum_m \langle k|\varepsilon_l|m\rangle e^{i(\beta_k - \beta_m - 12\pi/\Lambda)z} + \frac{1}{2} g_k A_k(z), \quad (11.6-10)$$

where g_k is the gain coefficient for the k th mode and is given by

$$g_k = \frac{\omega}{2} \frac{\beta_k}{|\beta_k|} \int \mathfrak{E}_k^*(x, y) \cdot \gamma(x, y) \mathfrak{E}_k(x, y) dx dy. \quad (11.6-11)$$

We have neglected gain terms with $e^{i(\beta_k - \beta_l)z}$ dependence because they are fast-varying functions of z and give no net contribution to the mode amplitude $A_k(z)$.

We now consider the special case when $\beta_s = l(\pi/\Lambda)$, so that the s th mode is strongly coupled to its backward-propagating ($-\beta_s$) counterpart. Keeping only the slowly varying terms in Eq. (11.6-10), it becomes a pair of coupled equations

$$\begin{aligned}\frac{dA}{dz} &= -i\kappa B e^{i\Delta\beta z} + \frac{1}{2}gA, \\ \frac{dB}{dz} &= i\kappa^* A e^{-i\Delta\beta z} - \frac{1}{2}gB,\end{aligned}\tag{11.6-12}$$

where A, B are the mode amplitudes A_s, A_{-s} , respectively, κ is given by Eq. (11.4-9), $\Delta\beta$ is given by Eq. (11.4-8), and g is g_s (11.6-11). In the event when the coupling constant κ vanishes, the mode amplitudes become

$$\begin{aligned}A(z) &= A(0)e^{\frac{1}{2}gz}, \\ B(z) &= B(0)e^{-\frac{1}{2}gz},\end{aligned}\tag{11.6-13}$$

which agrees with Eq. (11.6-5). When κ is finite, Eq. (11.6-12) can be easily solved by defining $A'(z)$ and $B'(z)$ as

$$\begin{aligned}A(z) &= A'(z)e^{\frac{1}{2}gz}, \\ B(z) &= B'(z)e^{-\frac{1}{2}gz}.\end{aligned}\tag{11.6-14}$$

The equations (11.6-12) become

$$\begin{aligned}\frac{dA'}{dz} &= -i\kappa B' e^{i(\Delta\beta + ig)z}, \\ \frac{dB'}{dz} &= i\kappa^* A' e^{-i(\Delta\beta + ig)z}\end{aligned}\tag{11.6-15}$$

and are thus in a form identical to that of Eq. (11.4-7), provided we replace

$$\Delta\beta \rightarrow \Delta\beta + ig.\tag{11.6-16}$$

With this substitution we can then use Eq. (11.4-16) to write the solutions directly for the incident mode amplitude $A(z) = A'(z)e^{\frac{1}{2}gz}$ and the reflected

mode amplitude $B(z) = B'(z)e^{-\frac{1}{2}gz}$, within a section of length L , in the case of a single mode with amplitude $A(0)$ incident on the corrugated section at $z = 0$:

$$A(z) = A(0)e^{i\frac{1}{2}\Delta\beta z} \left[\frac{s \cosh s(L-z) + i\frac{1}{2}(\Delta\beta + ig)\sinh s(L-z)}{s \cosh sL + i\frac{1}{2}(\Delta\beta + ig)\sinh sL} \right],$$

$$B(z) = A(0)e^{-i\frac{1}{2}\Delta\beta z} \left[\frac{-i\kappa^* \sinh s(L-z)}{s \cosh sL + i\frac{1}{2}(\Delta\beta + ig)\sinh sL} \right], \quad (11.6-17)$$

where s and $\Delta\beta$ are given by

$$s = \sqrt{\kappa^* \kappa - \left[\frac{1}{2}(\Delta\beta + ig) \right]^2}, \quad (11.6-18)$$

$$\Delta\beta = \beta_s - (-\beta_s) - i\frac{2\pi}{\Lambda}. \quad (11.6-19)$$

The fact that s now is complex makes for a qualitative difference between the behavior of the passive periodic guide (11.4-16) and the periodic guide with gain (11.6-17). To demonstrate this difference consider the case when the condition

$$s \cosh sL + i\frac{1}{2}(\Delta\beta + ig)\sinh sL = 0 \quad (11.6-20)$$

is satisfied. It follows from Eq. (11.6-17) that both the reflection coefficient

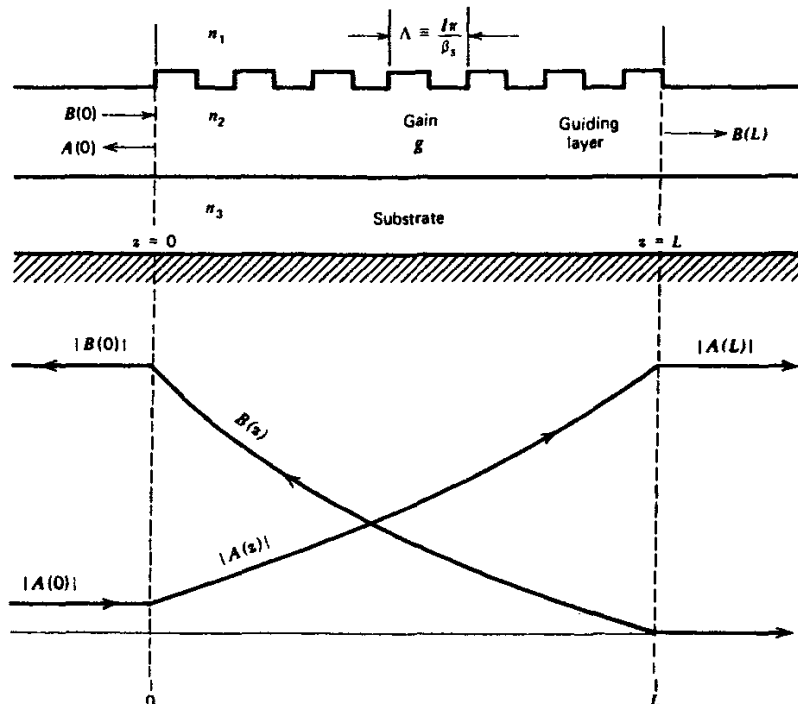


Figure 11.9. Incident and reflected mode amplitude inside an amplifying periodic waveguide.

$B(0)/A(0)$ and the transmission coefficient $A(L)/A(0)$ become infinite. The device acts as an oscillator, since it yields nonzero output field $B(0)$ and $A(L)$ with no input [$A(0) = 0$]. The condition (11.6-20) is thus the oscillation condition for a distributed-feedback laser [9]. For the case of $g = 0$, it follows from Eq. (11.4-16) or (11.4-20) that $|A(L)/A(0)| < 1$ and $|B(0)/A(0)| < 1$, as is appropriate for a passive device with no integral gain.

Under appropriate conditions and for sufficiently high gain constant g , so that Eq. (11.6-20) is nearly satisfied, the guide acts as a high-gain amplifier. The amplified output is available either in reflection with a gain

$$r = \frac{B(0)}{A(0)} = \frac{-i\kappa^* \sinh sL}{s \cosh sL + i\frac{1}{2}(\Delta\beta + ig)\sinh sL}, \quad (11.6-21)$$

or in transmission with a gain

$$t = \frac{A(L)}{A(0)} = \frac{se^{i\frac{1}{2}\Delta\beta L}}{s \cosh sL + i\frac{1}{2}(\Delta\beta + ig)\sinh sL}. \quad (11.6-22)$$

The behavior of the incident and reflected mode amplitudes for a high-gain case is sketched in Fig. 11.9. Note the qualitative difference between this case and the passive one depicted in Fig. 11.7.

The reflection gain $|B(0)/A(0)|^2$ and the transmission gain $|A(L)/A(0)|^2$ are plotted in Figs. 11.10 and 11.11, respectively, as a function of $\Delta\beta$ and g .

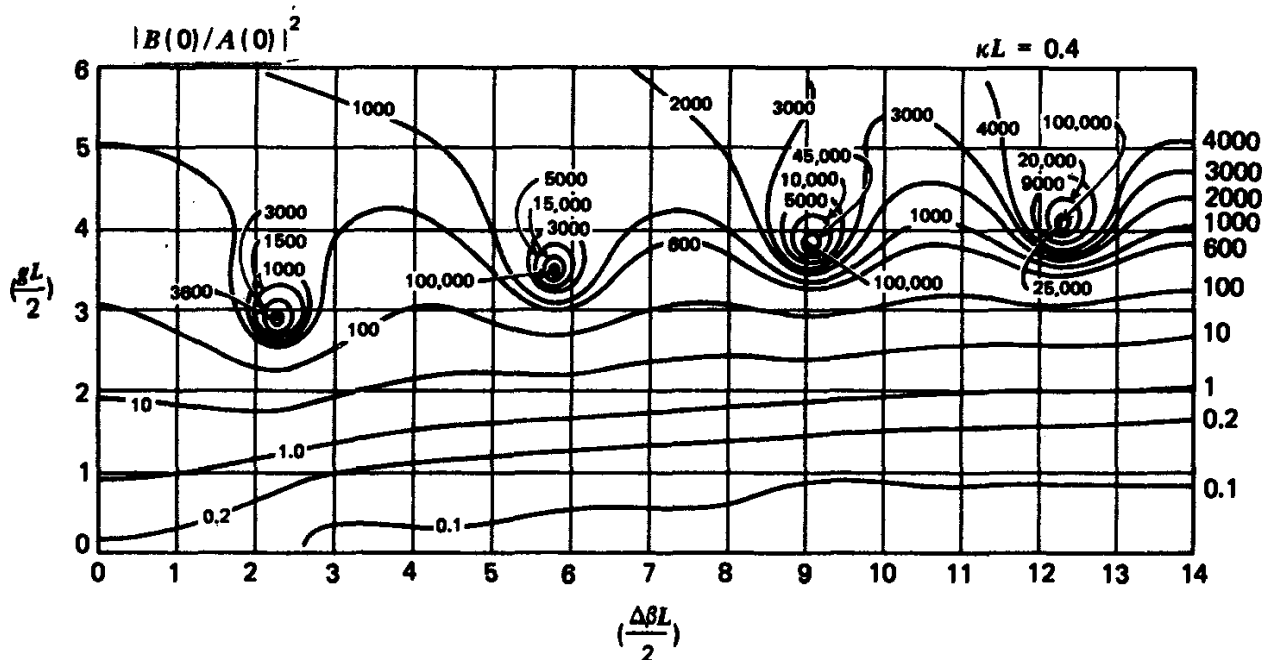


Figure 11.10. Reflection-gain contours in the $\Delta\beta L$ - gL plane. $\Delta\beta$ is defined in Eq. (11.4-18) and is proportional to the deviation of the frequency ω from the Bragg value $\omega_0 = \pi c/\Lambda n$.

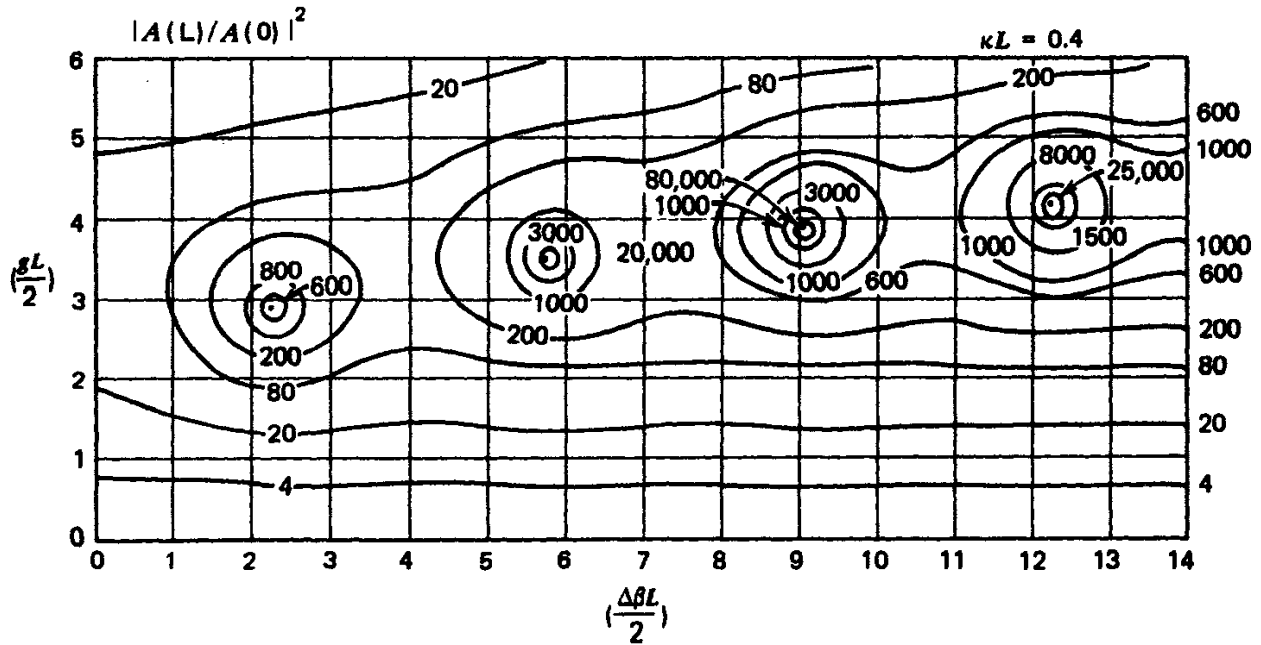


Figure 11.11. Transmission-gain contours in the $\Delta\beta L$ - gL plane.

Each plot contains four infinite-gain singularities at which the oscillation condition (11.6-20) is satisfied. These are four longitudinal laser modes. Higher orders exist at larger values of $\Delta\beta L$ but are not shown.

11.6.1. Oscillation Condition

The oscillation condition (11.6-20) can be written as

$$s - \frac{g - i\Delta\beta}{2} \tanh sL = 0. \quad (11.6-23)$$

This is a transcendental equation for the complex variable $\Delta\beta + ig$. In general, one has to resort to a numerical solution to obtain the threshold values of $\Delta\beta + ig$ for oscillation. In some limiting cases, however, we can obtain approximate solutions. In the high-gain $g \gg \kappa$ case we have from the definition $s^2 = \kappa^*\kappa - \frac{1}{4}(\Delta\beta + ig)^2$

$$s \approx \frac{g - i\Delta\beta}{2} + \frac{\kappa^*\kappa}{g - i\Delta\beta}. \quad (11.6-24)$$

By using this approximation, Eq. (11.6-23) can be written

$$1 - \tanh sL = - \frac{2\kappa^*\kappa}{(g - i\Delta\beta)^2}. \quad (11.6-25)$$

Since $g \gg \kappa$, $\tanh sL$ is near unity and therefore can be given approximately as

$$\tanh sL \simeq 1 - 2e^{-2sL}. \quad (11.6-26)$$

Thus, the oscillation condition (11.6-23) becomes

$$\frac{(g - i\Delta\beta)^2}{\kappa^*\kappa} e^{-2sL} = -1 \quad (11.6-27)$$

Equating the phases on both sides of (11.6-27) results in

$$-2 \tan^{-1} \left(\frac{\Delta\beta}{g} \right) + \Delta\beta L - \frac{2\kappa^*\kappa \Delta\beta L}{g^2 + (\Delta\beta)^2} = (2m + 1)\pi, \quad (11.6-28)$$

$$m = 0, \pm 1, \pm 2, \dots$$

For oscillation near the Bragg frequency ω_0 (i.e., the frequency at which $\Delta\beta = 0$) and in the limit $\Delta\beta \ll g$, the oscillation-mode frequencies are given by

$$(\Delta\beta)_m L \simeq (2m + 1)\pi, \quad (11.6-29)$$

and since $\Delta\beta = 2(\omega - \omega_0)n/c$ [see Eq. (11.4-24)],

$$\omega_m = \omega_0 + \left(m + \frac{1}{2}\right) \frac{\pi c}{nL}. \quad (11.6-30)$$

We note that no oscillation can take place exactly at the Bragg frequency ω_0 . Oscillations can also take place far away from the Bragg frequency according to Fig. 11.10. In these regimes $g \ll \Delta\beta$, and the mode frequencies are given by

$$(\Delta\beta)_{m'} L = 2m'\pi, \quad m' = \text{large integers}. \quad (11.6-31)$$

In either case, the mode-frequency spacing is

$$\omega_{m+1} - \omega_m = \frac{\pi c}{nL} \quad (11.6-32)$$

and is approximately the same as in a two-reflector resonator of length L . The threshold gain is obtained from the amplitude equality in (11.6-27)

$$\frac{\kappa^* \kappa e^{g_m L}}{g_m^2 + (\Delta\beta)_m^2} = 1, \quad (11.6-33)$$

indicating an increase in threshold gain with increasing mode number [i.e., increasing $(\Delta\beta)_m^2$]. This is also evident from the numerical gain plots (Figs. 11.10 and 11.11).

A diagram of a distributed-feedback laser using a GaAs–GaAlAs structure is shown in Fig. 11.12. The waveguiding layer as well as that providing the gain (active layer) is that of p -GaAs. The feedback is provided by corrugating the interface between the p -Ga_{0.93}Al_{0.07}As and p -Ga_{0.7}Al_{0.3}As, where the main index discontinuity responsible for the guiding occurs.

The increase in threshold gain with the longitudinal mode index m predicted by Eq. (11.6-33) and by the plots of Figs. 11.10 and 11.11 manifests itself in a high degree of mode discrimination in the distributed-feedback laser. This fact is displayed by the oscillation spectrum shown in Fig. 11.13, in which a single ($m = 0$) mode is evident.

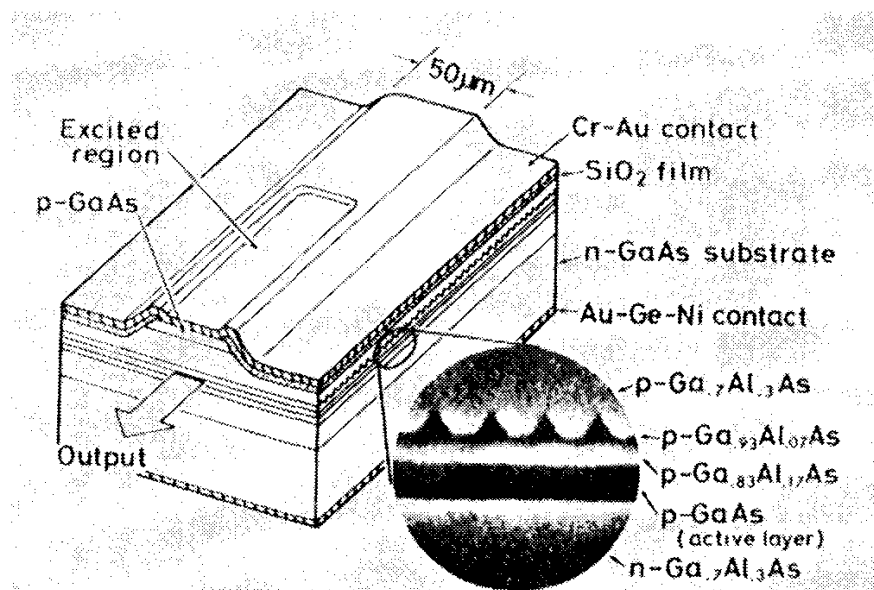


Figure 11.12. A GaAs–GaAlAs CW injection laser with a corrugated interface. The insert shows a scanning-electron-microscope photograph of the layered structure. The feedback is in third order ($l = 3$) and is provided by a corrugation with a period $\Lambda = 3\lambda_g/2 = 0.345 \mu\text{m}$. The thin ($0.2\text{-}\mu\text{m}$) p -Ga_{0.83}Al_{0.17}As layer provides a potential barrier which confines the injected electrons to the active (p -GaAs) layer, thus increasing the gain. (After [11].)

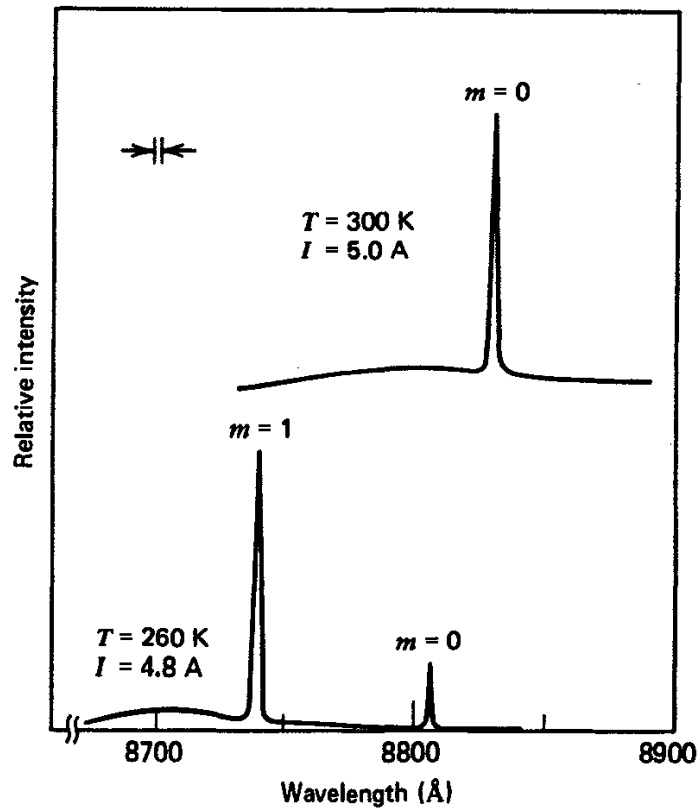


Figure 11.13. Oscillation spectrum of a distributed-feedback laser in a GaAs-GaAlAs double-heterostructure diode. m is the mode number. (After [11].)

11.7. ELECTRO-OPTIC MODULATION AND MODE COUPLING

One of the most important applications of thin-film waveguiding is in optical modulation and switching. The reason is twofold:

1. The confinement of the optical radiation to dimensions comparable to λ makes it possible to achieve the magnitude of electric fields that is necessary for modulation (see Section 8.1) with relatively small applied voltages. This leads to smaller modulation powers.
2. The absence of diffraction in a guided optical beam makes it possible to use longer modulation paths (see discussion in Section 8.3).

The main principle of electro-optic modulation in dielectric waveguides involves the diversion of all or part of the power from an input TE (or TM) mode to an output TM (or TE) mode which is caused by an applied dc (that is, “low”-frequency) field. To be specific, we consider next the case of TM \rightarrow TE mode conversion. This coupling is due to a perturbation in the dielectric function $\epsilon(x)$ induced by the applied electric field via the electro-

optic effect. Let $\Delta\epsilon$ be the change in the dielectric tensor $\epsilon(x)$ due to the presence of the dc electric field. According to the discussion in Section 6.4 or Section 11.3, when a pure TM mode \mathbf{E}_1 is excited at $z = 0$, the dielectric perturbation causes a perturbation polarization $\mathbf{P} = \Delta\epsilon \mathbf{E}_1$. This polarization, acting as a source, can excite a TE mode \mathbf{E}_2 , provided $\mathbf{E}_2 \cdot \Delta\epsilon \mathbf{E}_1$ does not vanish and $\beta_1^{\text{TM}} \approx \beta_2^{\text{TE}}$.

From the basic definition of the impermeability tensor $\eta = \epsilon_0 \epsilon^{-1}$ in Eq. (4.3-2), it follows that a change in the impermeability tensor is related to the corresponding change in the dielectric tensor by

$$\Delta\epsilon = -\frac{\epsilon \Delta\eta \epsilon}{\epsilon_0}. \quad (11.7-1)$$

Using Eq. (7.1-2), we thus relate $\Delta\epsilon$ to an applied dc electric field by

$$\Delta\epsilon = -\frac{\epsilon (rE^0) \epsilon}{\epsilon_0}, \quad (11.7-2)$$

where (rE^0) is the 3×3 matrix formed by the elements $r_{ijk} E_k^0$, r_{ijk} is the electro-optic tensor, E_k^0 is a component of the applied dc electric field, and summation over repeated indices (k) is assumed. For the case of slab waveguides made of isotropic materials, ϵ becomes a scalar $\epsilon_0 n^2(x)$, and the dielectric perturbation $\Delta\epsilon$ can be written

$$\Delta\epsilon = -\epsilon_0 n^4(x) (rE^0), \quad (11.7-3)$$

where E^0 is the dc applied electric field and may be a function of position.

We now consider the mode coupling between the TE_m and the TM_n mode, where m and n are the integer mode subscripts (see Fig. 11.4). Assume that there is no mode coupling to other modes and only these two modes are excited. Thus, the field can be represented by

$$\mathbf{E}(\mathbf{r}, t) = \left[A_m \mathfrak{E}_m^{\text{TE}}(x) e^{-i\beta_m^{\text{TE}} z} + B_n \mathfrak{E}_n^{\text{TM}}(x) e^{-i\beta_n^{\text{TM}} z} \right] e^{i\omega t}, \quad (11.7-4)$$

where $\mathfrak{E}_m^{\text{TE}}$ and $\mathfrak{E}_n^{\text{TM}}$ are the normal modes of the slab waveguide with propagation constants β_m^{TE} and β_n^{TM} , respectively. A_m and B_n are the mode amplitudes, which due to the coupling will be functions of z . According to the discussion in Sections 6.4, 11.3, and 11.5, these mode amplitudes are

described by

$$\frac{d}{dz}A_m = -i\kappa_{mn}B_n e^{i\Delta\beta z}, \quad (11.7-5)$$

$$\frac{d}{dz}B_n = -i\kappa_{mn}^*A_m e^{-i\Delta\beta z},$$

where

$$\Delta\beta = \beta_m^{\text{TE}} - \beta_n^{\text{TM}} - l\left(\frac{2\pi}{\Lambda}\right), \quad (11.7-6)$$

$$\kappa_{mn} = \frac{\omega}{4} \int_{-\infty}^{\infty} \mathfrak{E}_m^{*\text{TE}} \cdot \varepsilon_l(x) \mathfrak{E}_n^{\text{TM}}(x) dx,$$

with $\varepsilon_l(x)$ the l th Fourier expansion coefficient of the dielectric perturbation:

$$\Delta\varepsilon = \sum_l \varepsilon_l(x) \exp\left[-il\frac{2\pi}{\Lambda}z\right]. \quad (11.7-7)$$

Equation (11.7-3) is general enough to apply to a large variety of cases. The dependence of E^0 and r on x allows for coupling by electro-optic material in the guiding or bounding layers. The z dependence allows for situations where E^0 or r depends on the longitudinal position. To be specific, we consider first the case where the guiding layer $-t < x < 0$ is uniformly electro-optic and where E^0 is uniform over the same region, so that the integration in Eq. (11.7-6) is from $-t$ to 0. In that case, the overlap integral of Eq. (11.7-6) is maximum when the TE_m and TM_n are well confined and of the same order, so that $m = n$. In addition, according to Fig. 11.4, $\beta_m^{\text{TE}} \approx \beta_n^{\text{TM}}$ only when $m = n$. When the modes are well confined, $p, q \gg h$ and the mode index $\beta/(2\pi/\lambda)$ approaches n_2 (i.e., $\beta_m^{\text{TE}} \approx \beta_n^{\text{TM}} \rightarrow \beta \approx n_2 2\pi/\lambda$). Under these conditions, TE and TM modes have approximately the same field distribution. They differ in the direction of their electric-field vectors. The expressions (11.2-3), (11.2-9), and (11.2-10) for $\mathfrak{E}(x)$ in the guiding layer become

$$\mathfrak{E}_m^{\text{TE}}(x) \approx \mathfrak{y} \left(\frac{4\omega\mu}{t\beta_m^{\text{TE}}} \right)^{1/2} \sin \frac{m\pi x}{t}, \quad (11.7-8)$$

$$\mathfrak{E}_m^{\text{TM}}(x) \approx \mathfrak{x} \left(\frac{4\omega\mu}{t\beta_m^{\text{TM}}} \right)^{1/2} \sin \frac{m\pi x}{t},$$

where the z component of the TM wave is small compared with the x component (since $k \ll \beta$) and is neglected. In this case the coupling coefficient (11.7-6) becomes

$$\kappa = -\frac{1}{2}n_2^3k_0(rE^0)_{xy}, \quad (11.7-9)$$

where we have used $\beta_m^{\text{TM}} = \beta_m^{\text{TE}} = n_2k_0 = n_22\pi/\lambda$. The coupling is thus described, according to Eq. (11.7-5), by

$$\begin{aligned} \frac{dA_m}{dz} &= -i\kappa B_m e^{i(\beta_m^{\text{TE}} - \beta_m^{\text{TM}})z}, \\ \frac{dB_m}{dz} &= -i\kappa A_m e^{-i(\beta_m^{\text{TE}} - \beta_m^{\text{TM}})z}. \end{aligned} \quad (11.7-10)$$

Note that the above equations agree with the conservation of total power, that is,

$$\frac{d}{dz} (|A_m|^2 + |B_m|^2) = 0.$$

The equations (11.7-10) describe the codirectional coupling between two modes. The general solution is given by Eq. (6.4-30). For the phase-matched condition $\beta_m^{\text{TE}} = \beta_m^{\text{TM}}$ the solution of Eq. (11.7-10) in the case of a single input [$A_m(0) = A_0$, $B_m(0) = 0$ at $z = 0$] is, according to Eq. (6.4-30),

$$\begin{aligned} A_m &= A_0 \cos \kappa z, \\ B_m &= -iA_0 \sin \kappa z. \end{aligned} \quad (11.7-11)$$

Using Eq. (11.7-9), we can show that the field-length product E^0L for which $\kappa L = \frac{1}{2}\pi$ needed to effect a complete TM \leftrightarrow TE power transfer in a distance L is the same as that needed to go from “on” to “off” in the bulk modulator shown in Fig. 7.4. This result applies only in the limit of tight confinement. In general, the coupling coefficient κ is smaller than the value given by Eq. (11.7-9), and the E^0L product needed to achieve a complete power transfer is correspondingly larger.

When $\beta_m^{\text{TM}} \neq \beta_m^{\text{TE}}$, the solution of Eq. (11.7-10), subject to boundary conditions $A_m(0) = A_0$, $B_m(0) = 0$, is

$$\begin{aligned} A_m(z) &= A_0 e^{i\delta z} \left\{ \cos[(\kappa^2 + \delta^2)^{1/2} z] \right. \\ &\quad \left. - i \frac{\delta}{(\kappa^2 + \delta^2)^{1/2}} \sin[(\kappa^2 + \delta^2)^{1/2} z] \right\}, \quad (11.7-12) \\ B_m(z) &= -iA_0 e^{-i\delta z} \frac{\kappa}{(\kappa^2 + \delta^2)^{1/2}} \sin[(\kappa^2 + \delta^2)^{1/2} z], \end{aligned}$$

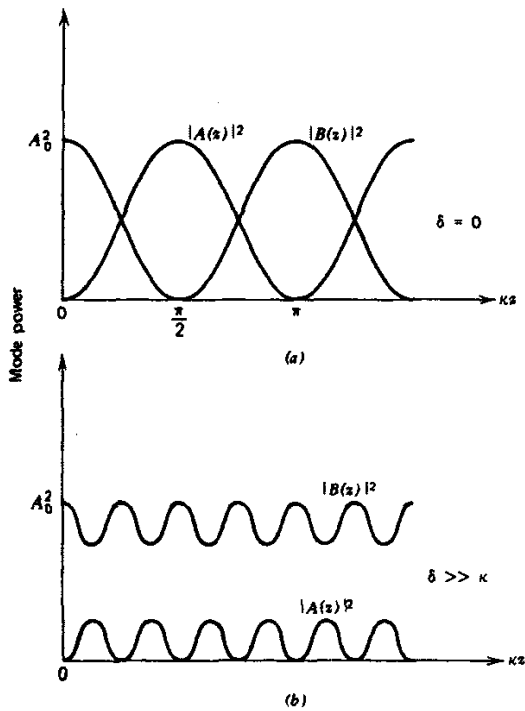


Figure 11.14. Power exchange between two coupled modes under (a) phase-matched conditions ($\beta_m^{\text{TM}} = \beta_m^{\text{TE}}$) as described by Eq. (11.7-11); (b) $\beta_m^{\text{TM}} \neq \beta_m^{\text{TE}}$, Eq. (11.7-12).

where

$$2\delta \equiv \beta_m^{\text{TE}} - \beta_m^{\text{TM}}. \quad (11.7-13)$$

The maximum fraction of the power that can be coupled from the input mode A_m to B_m is

$$\text{fraction of power exchanged} = \frac{\kappa^2}{\kappa^2 + \delta^2} \quad (11.7-14)$$

and becomes negligible once $\delta \gg \kappa$.

A plot of the mode power for the phase-matched ($\delta = 0$) and $\delta \neq 0$ cases is shown in Fig. 11.14.

11.7.1. Example: GaAs Thin-Film Modulator at $\lambda = 1 \mu\text{m}$

To appreciate the order of magnitude of the coupling, consider a case where the guiding layer is GaAs and $\lambda = 1 \mu\text{m}$. In this case (see Table 7.3)

$$n_2 \approx 3.5, n_2^3 r = 59 \times 10^{-12} \text{ m/V}.$$

Taking an applied field $E^{(0)} = 10^6$ V/m, we obtain from Eq. (11.7-9)

$$\kappa = 1.85 \text{ cm}^{-1},$$

$$L \equiv \frac{\pi}{2\kappa} = 0.85 \text{ cm}$$

for the coupling constant and the power-exchange distance, respectively.

An experimental setup used in one of the earliest demonstrations of electro-optic thin-film modulation is depicted in Fig. 11.15. The modulation scheme is identical to that illustrated in Fig. 8.4 and depends on an electro-optic induced phase retardation (8.1-30):

$$\begin{aligned} \Gamma &= (\beta_{\text{TM}} - \beta_{\text{TE}})L \\ &\approx \frac{2\pi n_2^3 r_{41} L}{\lambda t} V, \end{aligned} \quad (11.7-15)$$

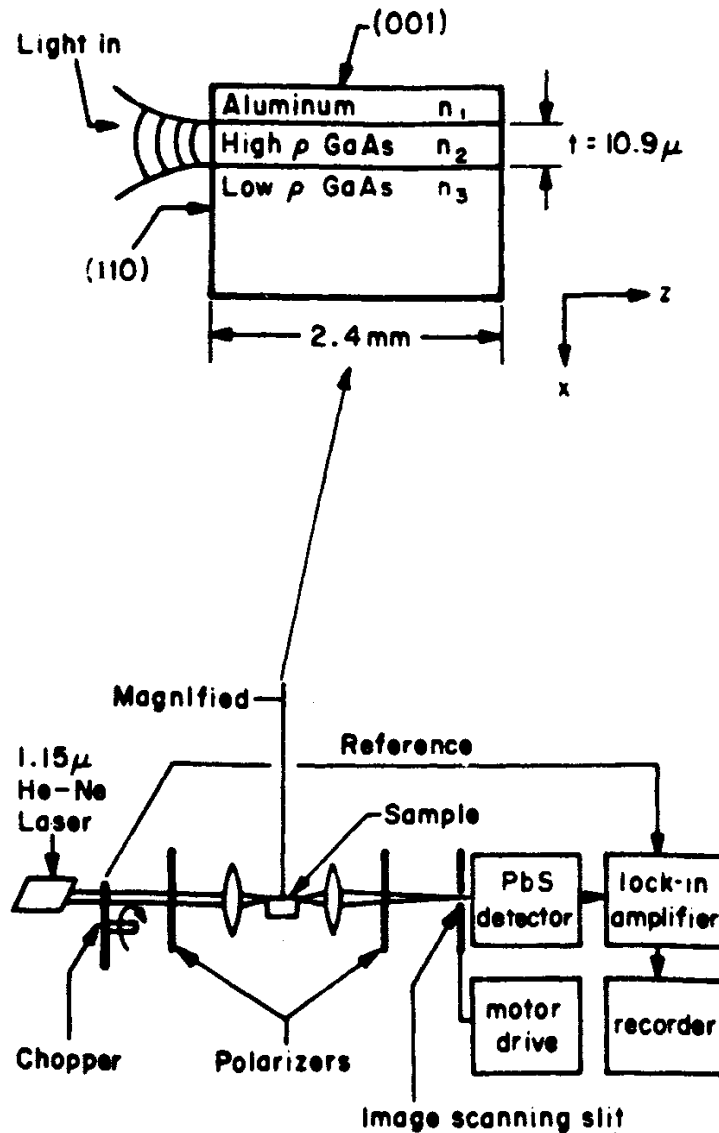


Figure 11.15. Electro-optic modulator in a GaAs epitaxial film. The modulation field is due to a reverse bias voltage applied to the metal–semiconductor junction [32].

where V is the applied voltage, and t and L are the height and length of the waveguide, respectively.

The ratio of the transmitted to the input intensities is given by Eq. (7.3-6) or equivalently by Eq. (11.7-11) [note that Γ of in Eq. (8.1-30) is the same as κ in Eq. (11.7-9)] as

$$\frac{I_0}{I_i} = \sin^2 \frac{1}{2} \Gamma. \quad (11.7-16)$$

An experimental transmission plot is shown in Fig. 11.16. There are cases when β^{TE} is very different from β^{TM} . For example, the modes of propagation in a waveguide made of anisotropic material (e.g., LiNbO_3) have different propagation constants depending on their polarization states, due to the natural birefringence of the guiding layer and the substrate. In these cases, a deliberate periodic variation of $E^0(z)$ or $r(z)$ with a period $2\pi/(\beta_m^{\text{TE}} - \beta_n^{\text{TM}})$ can be used, according to Eqs. (11.7-5) and (11.7-6), to

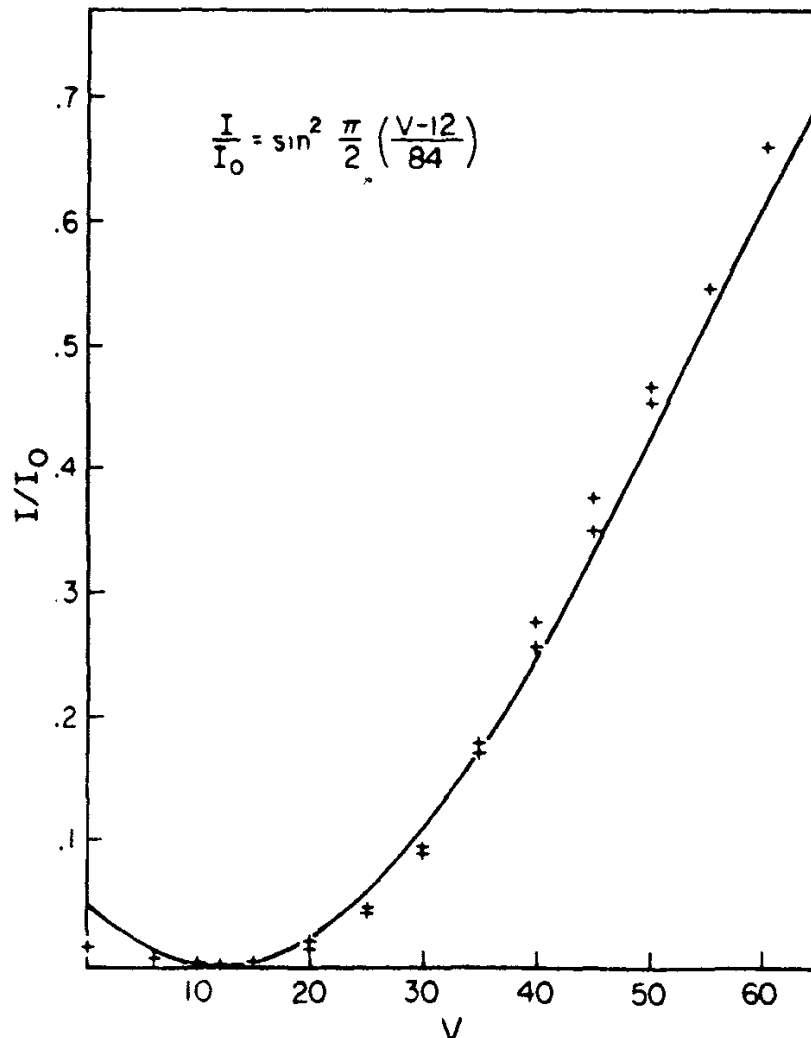


Figure 11.16. Transmittance of the waveguide, placed between crossed polarizers, as a function of the applied reverse voltage [32].

compensate for the mismatch factor $\exp[i(\beta_m^{\text{TE}} - \beta_n^{\text{TM}})z]$ in Eq. (11.7-5), thus leading again to a phase-matched operation. A complete electro-optic TE \leftrightarrow TM mode conversion in a Ti-diffused LiNbO₃ waveguide based on the periodic variation of the applied electric field has been reported recently [4, 5]. For a given electrode period Λ , complete mode power conversion is achievable only for the wavelength λ_0 such that the phase-match condition

$$\frac{2\pi}{\lambda_0} |n^{\text{TE}} - n^{\text{TM}}| = \frac{2\pi}{\Lambda}$$

is satisfied, where n^{TE} and n^{TM} are the mode indices for the TE and TM modes. Thus, this mode converter also acts as a filter. The polarization conversion in the waveguide is described by the codirectional coupled mode equations (11.7-5). Its transmission characteristics are very similar to those of a Šolc filter (Sections 5.3 and 6.5) or an acousto-optic tunable filter (Section 10.3). The fractional bandwidth, neglecting the modal dispersion (see Problem 11.8), is $\Delta\lambda/\lambda_0 = \Lambda/L = 1/N$, where N is the number of periods and L is the interaction length. Some details of this electro-optic TE \leftrightarrow TM mode converter are given in the following example.

11.7.2. Example: LiNbO₃ Waveguide Mode Converter-Filter

Referring to Fig. 11.17, we consider a Ti-diffused lithium niobate waveguide deposited with periodic electrodes. Assume that the thickness of the guiding layer t is much smaller than the period Λ . In practical situations, t is

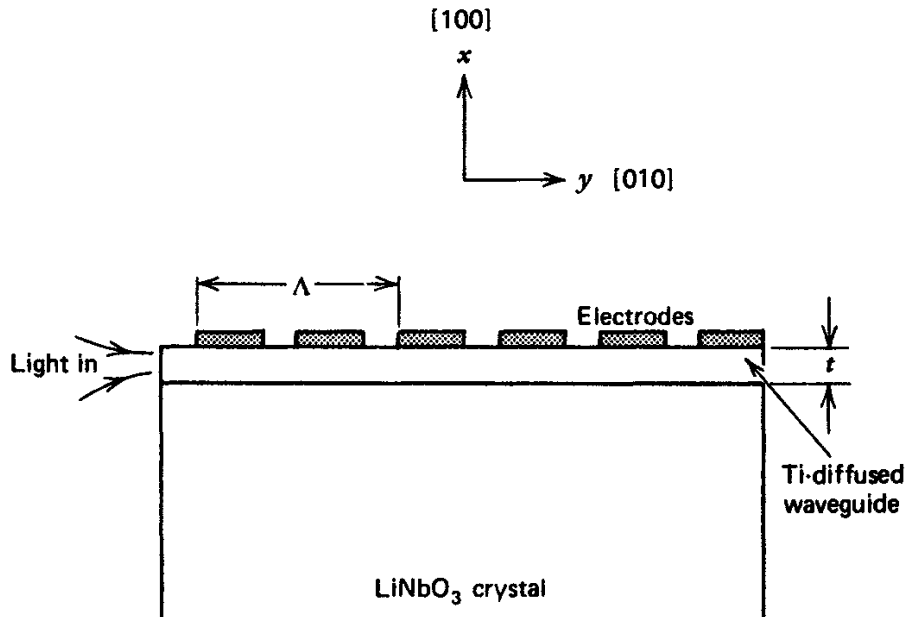


Figure 11.17. A schematic drawing of a LiNbO₃ electro-optic waveguide TM \leftrightarrow TE mode converter with periodic interdigital electrodes.

typically several hundred angstroms and Λ is of the order of several micrometers. Under these conditions, the electric field in the guiding layer due to the application of alternating plus and minus voltages on the electrodes can be given approximately by

$$\mathbf{E}^0 = \hat{x} \frac{V}{d} f(y), \quad (11.7-17)$$

where V is the magnitude of the voltage, d is the interelectrode gap, and $f(y)$ is the periodic square-wave function defined by Eq. (6.5-8). We have assumed that the x axis is perpendicular to the surface of the crystal and the wave is propagating along the y axis of the crystal. This periodic electric field (11.7-17) induces a periodic variation in the dielectric tensor via the electro-optic effect. LiNbO₃ has a point-group symmetry of $3m$. According to Table 7.1 and Eqs. (7.1-2) and (11.7-1), the xz component of the dielectric perturbation, $\Delta\epsilon_{xz}$, which causes the coupling between the TE (z -polarized) modes and TM ($\sim x$ -polarized) modes, is given by

$$\Delta\epsilon_{xz} = -\epsilon_0 n_e^2 n_o^2 r_{51} \frac{V}{d} f(y), \quad (11.7-18)$$

where n_e , n_o are the extraordinary and ordinary refractive indices of the guiding layer. In the well-confined case, the mode functions are given by Eq. (11.7-8) except that y must be replaced by z due to the new coordinate system used here. The propagation constants are given approximately by

$$\beta^{\text{TE}} \approx n_e \frac{2\pi}{\lambda}, \quad (11.7-19)$$

$$\beta^{\text{TM}} \approx n_o \frac{2\pi}{\lambda}.$$

The coupling constant κ_{mn} between the TE _{m} and TM _{n} modes due to the $l = 1$ Fourier expansion component of $\Delta\epsilon_{xz}$ is given, according to Eqs. (6.5-10), (11.4-5), (11.7-6), and (11.7-8), by

$$\kappa_{mn} = -\frac{i}{\lambda} (n_o n_e)^{3/2} r_{51} \frac{V}{d} \delta_{mn}, \quad (11.7-20)$$

where δ_{mn} is the Kronecker delta.

Taking $n^{\text{TE}} = n_e = 2.21$ and $n^{\text{TM}} = n_o = 2.30$ at $\lambda = 6328 \text{ \AA}$, we obtain from Eq. (11.7-6) the period Λ required for a phase-matched coupling:

$$\Lambda = 7.03 \text{ } \mu\text{m}.$$

Use $r_{51} = 28 \times 10^{-12}$ m/V from Table 7.2, $d = \Lambda/2 = 3.51 \mu\text{m}$, and $V = 20$ V, the coupling constant $\kappa = |\kappa_{mn}|$ is

$$\kappa = 28.8 \text{ m}^{-1}$$

Thus a complete conversion requires an interaction length of

$$L = \frac{\pi}{2\kappa} = 550 \mu\text{m}.$$

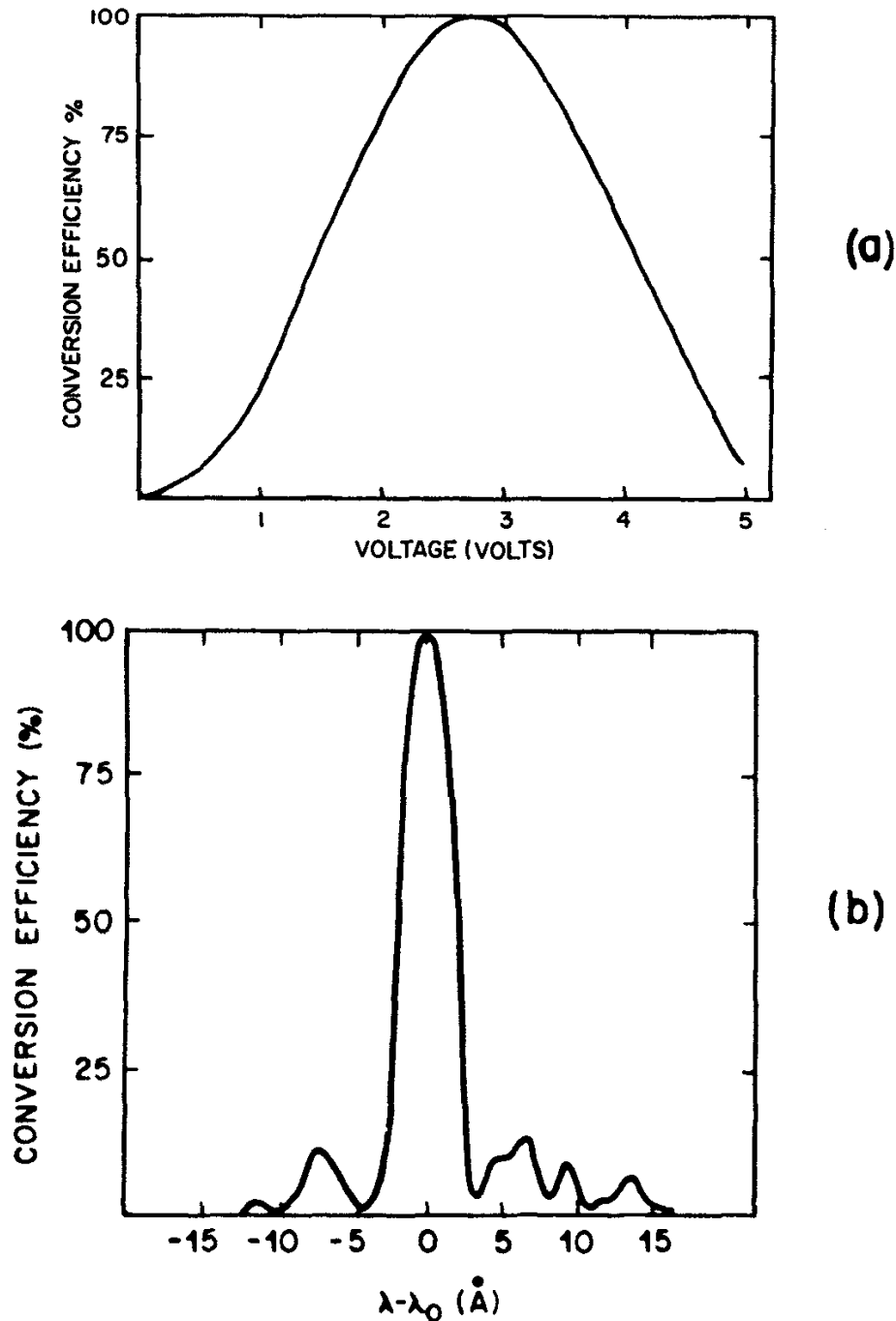


Figure 11.18. (a) Measured phase-matched ($\lambda = \lambda_0 = 0.6 \mu\text{m}$) TE \rightarrow TM conversion efficiency versus drive voltage and (b) measured wavelength response for fixed voltage ($V \approx 2.5$ V) for electrode length 6 mm [4, 5].

Note that since κ is directly proportional to the voltage V , a smaller applied voltage would require a longer interaction length L for complete conversion. The measured TE \leftrightarrow TM conversion efficiency for phase-matched coupling in a Ti-diffused channel waveguide of $L = 6$ mm is shown in Fig. 11.18(a) as a function of applied voltage V . Figure 11.18(b) shows the wavelength dependence of the mode conversion [4, 5].

Another form of electro-optic thin-film modulation utilizes two-dimensional Bragg diffraction of a waveguide mode from a spatially periodic modulation of the index of refraction. A periodic electric field set up by an interdigital electrode structure as in Fig. 11.19 gives rise to the periodic variation of the index of refraction. The situation is equivalent formally to that of Bragg scattering from a sound wave discussed in Chapter 9, where the index modulation was caused by the acoustic strain.

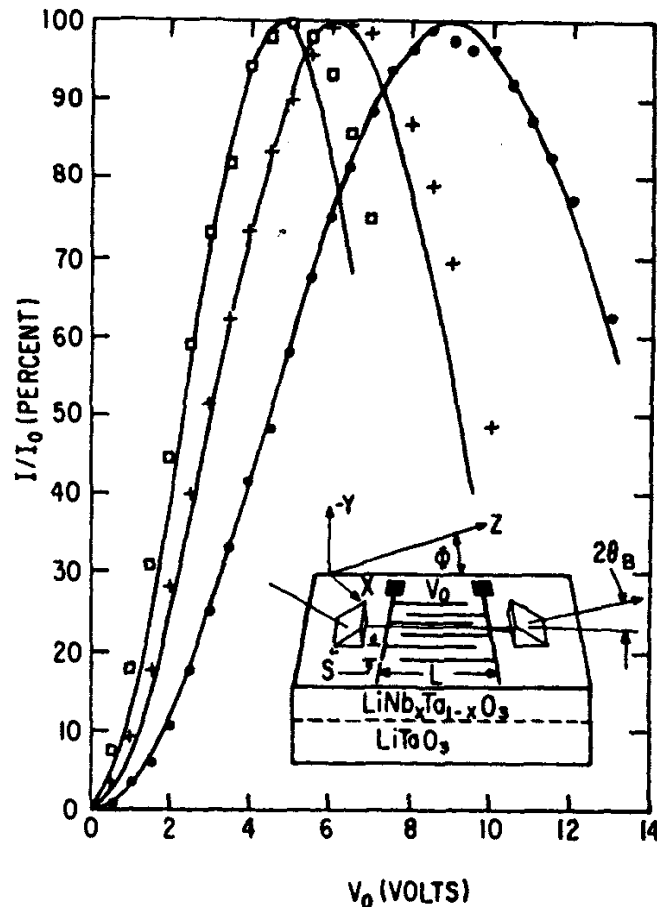


Figure 11.19. Schematic diagram of an electro-optic grating modulator in a $\text{LiNb}_x\text{Ta}_{1-x}\text{O}_3\text{-LiTaO}_3$ waveguide. The input mode, which is coupled into the waveguide via a prism, is deflected through an angle $2\theta_B$ when a voltage is applied to the interdigital electrode structure. $\Lambda = 7.6 \mu\text{m}$ and $l = 0.3$ cm. The curves show percentages of light diffracted as a function of voltage. Open squares: 4976 Å (He-Ne laser); crosses: 5598 Å (He-Ne laser); solid circles: 6328 Å (He-Ne laser). The solid curves are plots of $\sin^2(BV_0)$ normalized to the data at 75%. [After J. Hammer and W. Phillips, *Appl. Phys. Lett.*, 24, 545 (1974).]

A necessary condition for diffraction from a mode with a propagation vector β_i into a mode with β_d is, in analogy to Eq. (6.4-18),

$$\beta_d = \beta_i + \mathbf{a}_G \frac{2\pi}{\Lambda} m, \quad m = 1, 2, 3, \dots, \quad (11.7-21)$$

where Λ is the period of the spatial modulation and \mathbf{a}_G is a unit vector normal to the equiindex lines (that is, normal to the electrodes in Fig. 11.19). The vectors β_i and β_d are in the plane of the waveguide.

The momentum diagram corresponding to Eq. (11.7-21) is shown in Fig. 11.20 for the case of $m = 1$.

We take advantage of the formal equivalence of this case to that of Bragg diffraction from a sound wave to write the diffraction efficiency, as in Eq. (9.5-20), in the form

$$\frac{I_d}{I_i} = \sin^2\left(\frac{1}{2}kl \Delta n\right), \quad (11.7-22)$$

where Δn is the amplitude of the index modulation and is related to the appropriate Fourier component E_1 ($m = 1$ for first-order Bragg diffraction) of the low-frequency electric field by Eq. (7.2-9), that is

$$\Delta n = \frac{1}{2}n^3 r E_1, \quad (11.7-23)$$

where r is a suitable electro-optic tensor element which depends on the crystal orientation. Combining the last two equations leads to

$$\frac{I_d}{I_i} = \sin^2\left(\frac{\pi n^3 r l}{2\lambda} E_1\right). \quad (11.7-24)$$

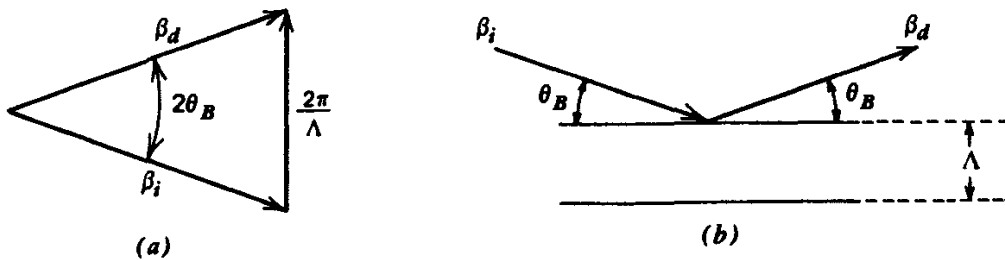


Figure 11.20. (a) A “momentum” diagram for diffraction of an input mode (β_i) into the direction β_d by setting up (electro-optically) an index grating with a period Λ . (b) A top view of the waveguide plane showing the direction of the incident (β_i) and diffracted (β_d) beams as well as the grating planes.

Since E_1 is proportional to the applied voltage V_0 , the diffraction efficiency (11.7-24) can be written as

$$\frac{I_d}{I_i} = \sin^2(BV_0) \quad (11.7-25)$$

with B inversely proportional to the optical wavelength λ .

The experimental transmission curves in Fig. 11.19 are in agreement with Eq. (11.7-25).

11.8. DIRECTIONAL COUPLING

We now consider the coupling between the modes of two parallel waveguides separated by a finite distance. Exchange of power between guided modes of adjacent waveguides is known as directional coupling. This phenomenon is similar to the electron motion in a two-atom molecule. Waveguide directional couplers perform a number of useful functions in thin-film devices, including power division, modulation, switching, frequency selection, and polarization selection.

Waveguide coupling can be treated by the coupled-mode theory. Consider the case of two cylindrical waveguides illustrated in Fig. 11.21. Let $\mathcal{E}_a(x, y)e^{i(\omega t - \beta_a z)}$ and $\mathcal{E}_b(x, y)e^{i(\omega t - \beta_b z)}$ be the modes of propagation of the individual waveguides when they are far apart. The electric field in the coupled-guide structure can be approximated by

$$\mathbf{E}(x, y, z, t) = A(z)\mathcal{E}_a(x, y)e^{i(\omega t - \beta_a z)} + B(z)\mathcal{E}_b(x, y)e^{i(\omega t - \beta_b z)} \quad (11.8-1)$$

provided the two waveguides are not too close to each other. In the absence of coupling—that is, if the distance between guides a and b is infinite— $A(z)$ and $B(z)$ do not depend on z and will be independent of each other, since each of the two terms on the right side of Eq. (11.8-1) satisfies the wave equation (11.1-4) separately.

Let $n^2(x, y)$ be the refractive-index distribution of the composite waveguide structure. To study the mode coupling, we decompose the refractive-index profile into three parts, and we get

$$n^2(x, y) = n_s^2(x, y) + \Delta n_a^2(x, y) + \Delta n_b^2(x, y), \quad (11.8-2)$$

where $n_s^2(x, y)$ represents the refractive-index distribution of the supporting

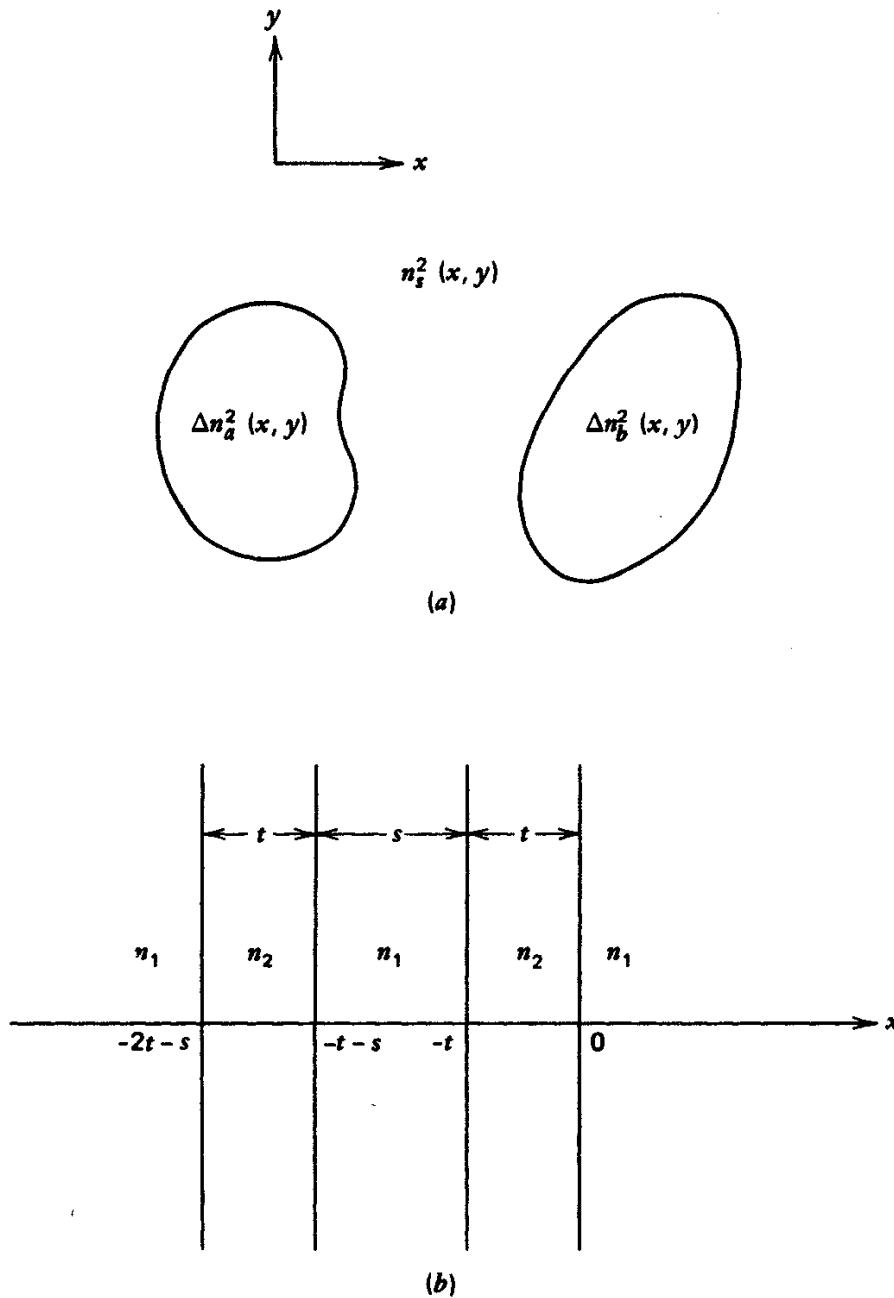


Figure 11.21. (a) A general waveguide structure consisting of two parallel cylindrical guides. (b) Two identical slab waveguides separated by a distance t . $\Delta n_b^2(x) = (n_2^2 - n_1^2)$ for $-t < x < 0$; $\Delta n_a^2(x) = (n_2^2 - n_1^2)$ for $-2t - s < x < -t - s$.

medium (cladding), $\Delta n_a^2(x, y)$ represents the presence of the waveguide a , and $\Delta n_b^2(x, y)$ represents the presence of the waveguide b . It is thus obvious that the individual waveguide modes $\mathcal{E}_\alpha(x, y)$ satisfy the equation

$$\left\{ \frac{\partial^2}{\partial x^2} + \frac{\partial^2}{\partial y^2} + \frac{\omega^2}{c^2} [n_s^2(x, y) + \Delta n_\alpha^2(x, y)] \right\} \mathcal{E}_\alpha(x, y) = \beta_\alpha^2 \mathcal{E}_\alpha(x, y),$$

$$\alpha = a, b. \quad (11.8-3)$$

The presence of waveguide b imposes a dielectric perturbation $\epsilon_0 \Delta n_b^2(x, y)$ on the propagation of the modes $\mathcal{E}_a(x, y)e^{i(\omega t - \beta_a z)}$ and vice versa. The total electric field (11.8-1) must obey the wave equation

$$\left\{ \frac{\partial^2}{\partial x^2} + \frac{\partial^2}{\partial y^2} + \frac{\partial^2}{\partial z^2} + \frac{\omega^2}{c^2} [n_s^2(x, y) + \Delta n_a^2(x, y) + \Delta n_b^2(x, y)] \right\} \mathbf{E} = 0. \quad (11.8-4)$$

To obtain the coupled equations for the mode amplitudes $A(z)$ and $B(z)$, we substitute Eq. (11.8-1) in Eq. (11.8-4) and use Eq. (11.8-3) and the assumption (6.4-10) of slow variation of mode amplitudes over z . These lead to

$$\begin{aligned} & -2i\beta_a \frac{dA}{dz} \mathcal{E}_a e^{i(\omega t - \beta_a z)} - 2i\beta_b \frac{dB}{dz} \mathcal{E}_b e^{i(\omega t - \beta_b z)} \\ & = -\frac{\omega^2}{c^2} \Delta n_b^2(x, y) A \mathcal{E}_a e^{i(\omega t - \beta_a z)} - \frac{\omega^2}{c^2} \Delta n_a^2(x, y) B \mathcal{E}_b e^{i(\omega t - \beta_b z)} \end{aligned} \quad (11.8-5)$$

We now take the scalar product of Eq. (11.8-5) with $\mathcal{E}_a^*(x, y)$ and $\mathcal{E}_b^*(x, y)$, respectively, and integrate over all x and y . The result, using the normalization condition (6.4-6), is

$$\begin{aligned} \frac{dA}{dz} &= -i\kappa_{ab} B e^{i(\beta_a - \beta_b)z} - i\kappa_{aa} A, \\ \frac{dB}{dz} &= -i\kappa_{ba} A e^{-i(\beta_a - \beta_b)z} - i\kappa_{bb} B, \end{aligned} \quad (11.8-6)$$

where

$$\kappa_{ab} = \frac{1}{4} \omega \epsilon_0 \int \mathcal{E}_a^* \cdot \Delta n_a^2(x, y) \mathcal{E}_b \, dx \, dy, \quad (11.8-7)$$

$$\kappa_{ba} = \frac{1}{4} \omega \epsilon_0 \int \mathcal{E}_b^* \cdot \Delta n_b^2(x, y) \mathcal{E}_a \, dx \, dy$$

and

$$\kappa_{aa} = \frac{1}{4} \omega \epsilon_0 \int \mathcal{E}_a^* \cdot \Delta n_b^2(x, y) \mathcal{E}_a \, dx \, dy, \quad (11.8-8)$$

$$\kappa_{bb} = \frac{1}{4} \omega \epsilon_0 \int \mathcal{E}_b^* \cdot \Delta n_a^2(x, y) \mathcal{E}_b \, dx \, dy.$$

In arriving at Eq. (11.8-6), we use the assumption that the waveguides are not too close, so that the overlap integral of the mode functions is small,

that is,

$$\int \mathcal{E}_a^* \cdot \mathcal{E}_b \, dx \, dy \ll \int \mathcal{E}_a^* \cdot \mathcal{E}_a \, dx \, dy. \quad (11.8-9)$$

The terms in κ_{aa} and κ_{bb} result from the dielectric perturbations to one of the waveguides due to the presence of the other waveguide, and represent only a small correction to the propagation constants β_a and β_b , respectively [see Eqs. (11.3-15) and (11.3-22)]. The terms in κ_{ab} and κ_{ba} represent the exchange coupling between the two guides. So if we take the total field as

$$\mathbf{E} = A(z) \mathcal{E}_a e^{i[\omega t - (\beta_a + \kappa_{aa})z]} + B(z) \mathcal{E}_b e^{i[\omega t - (\beta_b + \kappa_{bb})z]} \quad (11.8-10)$$

instead of Eq. (11.8-1), the equations (11.8-6) become

$$\frac{dA}{dz} = -i\kappa_{ab} B e^{i2\delta z}, \quad (11.8-11)$$

$$\frac{dB}{dz} = -i\kappa_{ba} A e^{-i2\delta z},$$

where

$$2\delta = (\beta_a + \kappa_{aa}) - (\beta_b + \kappa_{bb}). \quad (11.8-12)$$

The solution of Eq. (11.8-11) subject to a single input at guide a [i.e., $A(0) = A_0$, $B(0) = 0$] is given by Eq. (11.7-12). In terms of powers $P_a = A^*A$ and $P_b = B^*B$ in the two guides, the solution in the case $\kappa_{ab} = \kappa_{ba} = \kappa$ becomes

$$P_a(z) = P_0 - P_b(z), \quad (11.8-13)$$

$$P_b(z) = P_0 \frac{\kappa^2}{\kappa^2 + \delta^2} \sin^2 [(\kappa^2 + \delta^2)^{1/2} z],$$

where $P_0 = |A(0)|^2$ is the input power to guide a . Complete power transfer occurs in a distance $L = \pi/2\kappa$ provided $\delta = 0$, that is, the phase velocities in the two modes are equal. For $\delta \neq 0$, the maximum fraction of power that can be transferred is, from Eq. (11.8-13),

$$\frac{\kappa^2}{\kappa^2 + \delta^2}. \quad (11.8-14)$$

The coupling constant $\kappa = \kappa_{ab} = \kappa_{ba}$ is given by Eq. (11.8-7). It can be evaluated straightforwardly using the field expressions (11.2-3) and (11.2-10) for the case of two parallel slab dielectric waveguides. In the special case of

two identical slab waveguides, the coupling constant κ for the same TE modes of propagation is

$$\kappa = \frac{2h^2 p e^{-ps}}{\beta(t + 2/p)(h^2 + p^2)}, \quad (11.8-15)$$

where t is the guide width, s is the separation, and $p = q$ and h are given by Eq. (11.2-4). In the well-confined case, $t \gg 2/p$, and Eq. (11.8-15) simplifies to [13]

$$\kappa = \frac{2h^2 p e^{-ps}}{\beta t (h^2 + p^2)}. \quad (11.8-16)$$

A typical value of κ obtained at $\lambda = 1 \mu\text{m}$ with $t, s = 3 \mu\text{m}$ and $\Delta n = 5 \times 10^{-3}$ is $\kappa = 5 \text{ cm}^{-1}$, so that coupling distances are of the order of magnitude of $\kappa^{-1} = 2 \text{ mm}$.

A form of an electro-optic switch based on directional coupling [12] is as follows. The length L of the coupler is chosen so that for $\delta = 0$ (that is, the synchronous case) $\kappa L = \frac{1}{2}\pi$. From Eq. (11.8-13) it follows that all the input power to guide a exits from guide b at $z = L$. The switching is achieved by applying an electric field to guide a (or b) in such a way as to change its propagation constant until

$$\delta L = \frac{1}{2}(\beta_a - \beta_b)L = \frac{1}{2}\sqrt{3}\pi, \quad (11.8-17)$$

that is, $\delta = \sqrt{3}\kappa$. It follows from Eq. (11.8-13) that at this value of δ

$$P_a = P_0, \quad P_b = 0,$$

that is, the power reappears at the output of guide a . Control of δ can thus be used to achieve any division of the power between the outputs of guides a and b .

A switched directional coupler based on this principle has been demonstrated by using Ti-diffused strip guides in LiNbO_3 [17] and metal-gap strip guides in GaAs [15]. In these devices it is important that the interaction length L be an odd multiple of $\pi/2\kappa$. This insures complete conversion of optical power from guide a to guide b ("crossover") when the guides are phase-matched ($\Delta\beta = 0$). When the interaction length deviates from these ideal values, the crossover is not complete in these devices and crosstalk results [see Fig. 11.22(b)]. This crosstalk cannot be eliminated by an electrical adjustment. Thus low-crosstalk requirements impose stringent fabrication tolerances which may be difficult to meet.

To avoid the crosstalk problems due to fabrication errors in the interaction length L , alternating- $\Delta\beta$ couplers have been proposed [16]. In such a coupler configuration [see Fig. 11.22(c)] an electrical adjustment can be made for both the crossover and the straight-through states for just about any interaction length that is larger than $\pi/2\kappa$. Sectioned electrodes are deposited to provide voltages of alternating polarity along the waveguides to induce this alternating $\Delta\beta$. We now discuss the principle of operation of the simplest alternating- $\Delta\beta$ coupler structure as shown in Fig. 11.22(c).

To derive the output powers P_a and P_b , we need to solve the coupled mode equations (11.8-11) in the region $0 \leq z \leq \frac{1}{2}L$ and find the mode amplitudes $A(\frac{1}{2}L)$ and $B(\frac{1}{2}L)$. These two amplitudes are then used as the (boundary) input conditions for solving the coupled mode equation (11.8-11) in the region $\frac{1}{2}L \leq z \leq L$ with a reversed sign of $\Delta\beta$ (or δ). Because of the reversal of $\Delta\beta$, the propagation constants $\beta_a + \kappa_{aa}$ and $\beta_b + \kappa_{bb}$ of the two

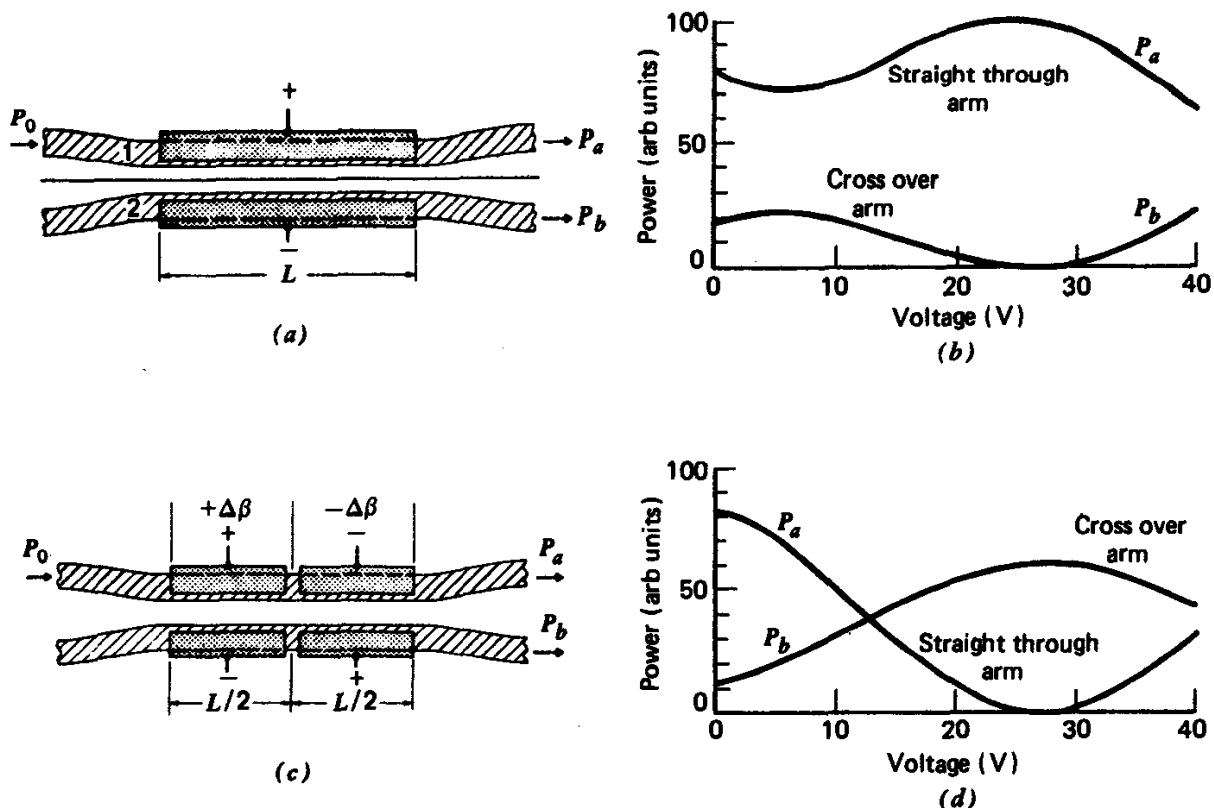


Figure 11.22. (a) Switched directional coupler consisting of two optical strip waveguides, with an interaction length L . (After [16]; copyright 1976 IEEE.) (b) Optical power coupled out of the switch in the straight-through arm and crossover arm waveguides as a function of voltage for (a). (c) Split-electrode configuration for a switched coupler with stepped $\Delta\beta$ reversal (alternating $\Delta\beta$ with two sections). (After [16]; copyright 1976 IEEE.) (d) Optical power P_a and P_b as a function of voltage for (c). (e) Switching diagram for a switched coupler with two sections of alternating $\Delta\beta$. The \otimes sign marks the cross-state conditions and the \ominus sign marks the bar-state conditions. (After [16]; copyright 1976 IEEE.)

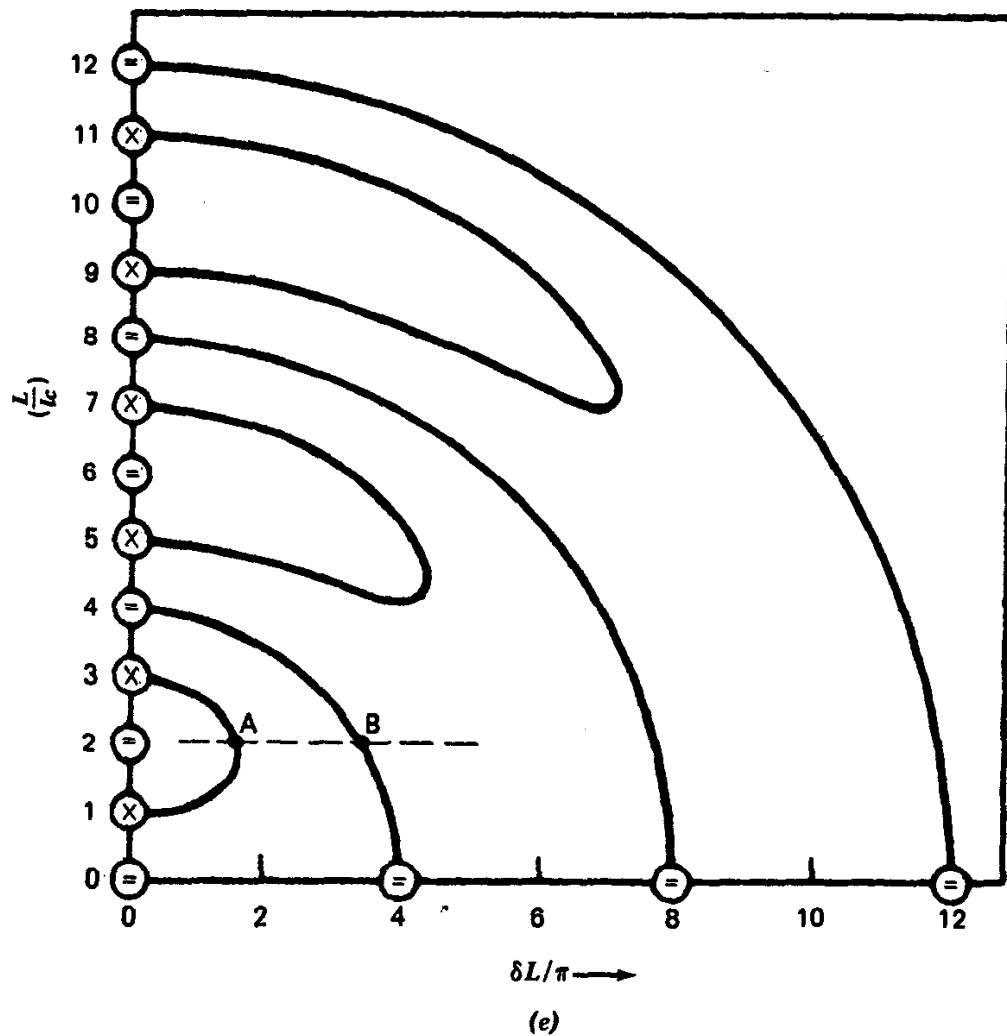


Figure 11.22. (Continued)

guides are no longer constant, since they now have different values in two adjacent sections. The mode amplitudes $A(z)$ and $B(z)$ defined in Eq. (11.8-10) must be redefined in the second section, $\frac{1}{2}L \leq z \leq L$. This is very inconvenient if the device has more than two sections. We then define two new mode amplitudes which are independent of the reversal of $\Delta\beta$:

$$A'(z) = A(z)e^{-i\delta z}, \quad (11.8-18)$$

$$B'(z) = B(z)e^{i\delta z},$$

where δ is given by Eq. (11.8-12). Using Eq. (11.8-18), the total electric field can be written

$$\mathbf{E} = [A'(z)\mathcal{E}_a + B'(z)\mathcal{E}_b]\exp[i(\omega t - \bar{\beta}z)], \quad (11.8-19)$$

where

$$\bar{\beta} = \frac{1}{2}(\beta_a + \kappa_{aa} + \beta_b + \kappa_{bb}). \quad (11.8-20)$$

We note, using Eq. (11.8-19), that these new mode amplitudes A' and B' are indeed independent of the reversal of $\Delta\beta$.

Using Eqs. (6.4-30) and (11.8-18), we may express $A'(\frac{1}{2}L)$ and $B'(\frac{1}{2}L)$ in terms of $A'(0)$ and $B'(0)$ as

$$\begin{pmatrix} A'(\frac{1}{2}L) \\ B'(\frac{1}{2}L) \end{pmatrix} = \begin{pmatrix} S & -iX \\ -iX^* & S^* \end{pmatrix} \begin{pmatrix} A'(0) \\ B'(0) \end{pmatrix}, \quad (11.8-21)$$

where

$$S = \cos \frac{1}{2}L\sqrt{\kappa^2 + \delta^2} - \frac{i\delta \sin \frac{1}{2}L\sqrt{\kappa^2 + \delta^2}}{\sqrt{\kappa^2 + \delta^2}}, \quad (11.8-22)$$

$$X = \frac{\kappa \sin \frac{1}{2}L\sqrt{\kappa^2 + \delta^2}}{\sqrt{\kappa^2 + \delta^2}}. \quad (11.8-23)$$

The factor S represents the straight-through coupling and the factor X the crossover coupling. In a similar way, $A'(L)$ and $B'(L)$ can be expressed in terms of $A'(\frac{1}{2}L)$ and $B'(\frac{1}{2}L)$ as

$$\begin{pmatrix} A'(L) \\ B'(L) \end{pmatrix} = \begin{pmatrix} S^* & -iX \\ -iX^* & S \end{pmatrix} \begin{pmatrix} A'(\frac{1}{2}L) \\ B'(\frac{1}{2}L) \end{pmatrix}, \quad (11.8-24)$$

where we have used the reversal of δ ($\delta = \frac{1}{2}\Delta\beta$) in the region $\frac{1}{2}L \leq z \leq L$. Substituting Eq. (11.8-21) into Eq. (11.8-24), we obtain

$$\begin{pmatrix} A'(L) \\ B'(L) \end{pmatrix} = \begin{pmatrix} S^*S - X^*X & -2iS^*X \\ -2iX^*S & S^*S - X^*X \end{pmatrix} \begin{pmatrix} A'(0) \\ B'(0) \end{pmatrix}. \quad (11.8-25)$$

If, again, we assume that there is a single input power of $P_0 = |A'(0)|^2$ into the guide, then $B'(0) = 0$. The optical-mode powers in the guides at $z = L$ are given, using Eqs. (11.8-25), (11.8-22), and (11.8-23), by

$$P_a(L) = P_0 \left[1 - \frac{2\kappa^2}{\kappa^2 + \delta^2} \sin^2 \frac{1}{2}L\sqrt{\kappa^2 + \delta^2} \right]^2, \quad (11.8-26)$$

$$P_b(L) = P_0 - P_a(L).$$

According to Eq. (11.8-26), complete power transfer from a to b occurs when

$$\frac{\kappa^2}{\kappa^2 + \delta^2} \sin^2 \frac{1}{2} L \sqrt{\kappa^2 + \delta^2} = \frac{1}{2}. \quad (11.8-27)$$

Defining the switching distance $l_c = \pi/2\kappa$ (l_c is the distance for a complete crossover of power when $\delta = 0$), we can rewrite this as

$$\frac{(L/l_c)^2}{(L/l_c)^2 + (2\delta L/\pi)^2} \sin^2 \left\{ \frac{\pi}{4} \sqrt{\left(\frac{L}{l_c}\right)^2 + \left(\frac{2\delta L}{\pi}\right)^2} \right\} = \sin^2 \left(\frac{\pi}{4} \right). \quad (11.8-27a)$$

A plot of the multibranch relation (11.8-27a) in the δL - L/l_c plane is shown in Fig. 11.22(e). The plot corresponds to the curves connecting the \otimes points on the ordinate. Each point on such a curve corresponds to a pair δL , L/l_c which results in complete power transfer. Corresponding plots are shown for the "through" (\ominus) loci.

It is now possible (e.g., for $1 \leq L/l_c \leq 3$) to switch from a complete "through" condition (\ominus) to a "cross" condition (\otimes) by changing $\delta L/\pi$ from the value indicated by B to A .

When $\delta = 0$, the crossover condition (11.8-27) reduces to $\kappa L = \frac{1}{2}\pi + n\pi$ ($n = 1, 2, \dots$). Equation (11.8-27) can be satisfied over a large range of L values provided δ is properly chosen. In fact, for κL in the range between $\frac{1}{2}\pi$ and $\frac{3}{2}\pi$, the condition can always be achieved by choosing a proper value for δ . This can be seen by plotting the left-hand side of Eq. (11.8-27) as a function of δ . At $\delta = 0$, the left-hand side is $\sin^2 \frac{1}{2} \kappa L$, which is greater than $\frac{1}{2}$ for $\frac{1}{2}\pi \leq \kappa L \leq \frac{3}{2}\pi$. For large values of δ , the left-hand side decays to zero as δ^{-2} . Since the left-hand side is a continuous function of δ , the solution must always exist for $\frac{1}{2}\pi \leq \kappa L \leq \frac{3}{2}\pi$.

Thus if δ is electrically tunable by the applied voltages, the alternating- $\Delta\beta$ configuration makes it possible to induce complete transfer of light from one guide to the other. An electro-optical switched directional coupler based on this principle has been demonstrated [17]. Figure 11.22(d) shows the output powers P_a and P_b as a function of the applied voltage.

A multiguide directional coupler such as that shown in Fig. 11.23(a) is described by a set of equations

$$\frac{dA_n}{dz} = -i\kappa A_{n-1} - i\kappa A_{n+1}, \quad (11.8-28)$$

which is an obvious extension of Eq. (11.8-11) to the multimode synchronous case ($\delta = 0$) when only adjacent modes couple to each other. The solution of Eq. (11.8-28) in the case of a single input, [i.e., $A_n(0) = 1, n = 0$; $A_n(0) = 0, n \neq 0$] is [14]

$$A_n(z) = (-i)^n J_n(2\kappa z), \quad (11.8-29)$$

where J_n is the Bessel function of order n .

A directional coupler based on this principle is shown in Fig. 11.23(a). The predicted Bessel-function distribution of the intensity at various propagation distances is shown in Fig. 11.23(b).

According to Eqs. (11.8-13) and (11.8-14), the fraction of power exchanged is small when $\delta \gg \kappa$. This occurs when the two waveguides are

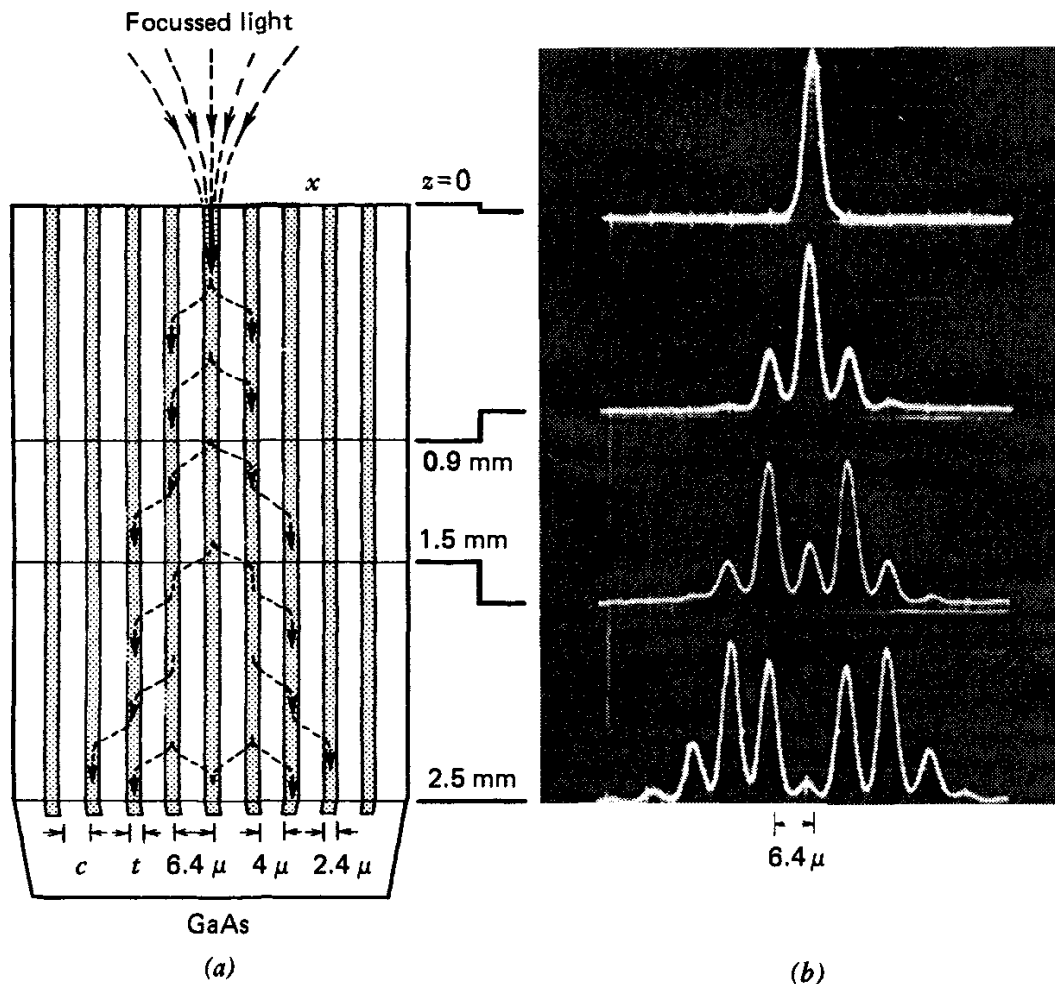


Figure 11.23. (a) Sketch of channel optical-waveguide directional coupler showing flow of light energy into adjacent channels. (b) Measured guided-light intensity profiles at various lengths. The profiles have been displayed relative to the sketch at the proper value of z . Intensity scale is arbitrary. The guides were produced by proton implantation into p^+ -GaAs crystal. (After [14].)

very different in dielectric constant and, therefore, the propagation constant. In this case a complete transfer of power is still possible, provided a periodic dielectric perturbation is introduced between the two guides. The period of this perturbation must be $2\pi/(\beta_a + \kappa_{aa} - \beta_b - \kappa_{bb})$ to compensate for the phase mismatch in the codirectional coupling and $2\pi/(\beta_a + \kappa_{aa} + \beta_b + \kappa_{bb})$ for the contradirectional coupling. These directional couplings via periodic perturbation are frequency-selective. For a given period Λ , maximum mode-power exchange is achievable only for a wavelength λ_0 such that the phase-matching condition

$$\frac{2\pi}{\lambda_0} |n_a \pm n_b| = \frac{2\pi}{\Lambda} \quad (11.8-30)$$

is satisfied, where n_a, n_b are the mode indices of propagation of waveguides a and b , respectively. The $+$ sign is for contradirectional coupling, whereas the $-$ sign is for the codirectional coupling. Because of the frequency selectivity, these directional couplings can be used for frequency multiplexing and demultiplexing (see Section 11.9). The fractional bandwidth of these couplings is of the order of $1/N$ (i.e., $\Delta\lambda/\lambda = 1/N$), where N is the number of periods, provided the modal dispersion can be neglected.

The periodic perturbation in the refractive index can be achieved by applying alternating voltages along the waveguides, provided the waveguides are made of electro-optic material. The use of electro-optic dielectric perturbation also gives a way of electrically switching the directional coupler.

11.9. FREQUENCY MULTIPLEXERS

Frequency multiplexing (sometimes referred to as color multiplexing or wavelength multiplexing) offers the possibility of greatly increasing the information capacity of an optical waveguide. In a frequency-multiplexed system, each information channel is assigned a range of frequencies (frequency band) for transmission. An important element of such a system is the frequency-selective coupler for combining and separating the channels. In this section we describe briefly several different types of frequency multiplexers for use in guided-wave optical communication. It should be noted that these types of couplers are reciprocal devices, and as such can combine, as well as separate optical-frequency channels.

11.9.1. Chirped Gratings

Consider a dielectric waveguide with a corrugated region of period Λ , and a guided optical beam of wavelength λ incident on the corrugated region at an

angle α [see Fig. 11.24(a)]. According to the discussion in Chapter 6, the beam will be deflected at an angle 2α , provided Bragg's condition

$$\lambda = 2n\Lambda \cos \alpha \quad (11.9-1)$$

is satisfied, where n is the mode index of the guided wave.

If the corrugated region consists of a grating with a variable period $\Lambda(z)$, then it follows that different locations in the corrugated waveguide will deflect different wavelengths, as shown in Fig. 11.24. A particular wavelength λ_1 will be reflected from that part of the chirped grating where the period Λ_1 satisfies the condition $\Lambda_1 = \lambda_1/(2n \cos \alpha)$, while a (different) wavelength λ_2 will be reflected from the portion of the grating where the period Λ_2 satisfies the condition $\Lambda_2 = \lambda_2/(2n \cos \alpha)$. These two wave-

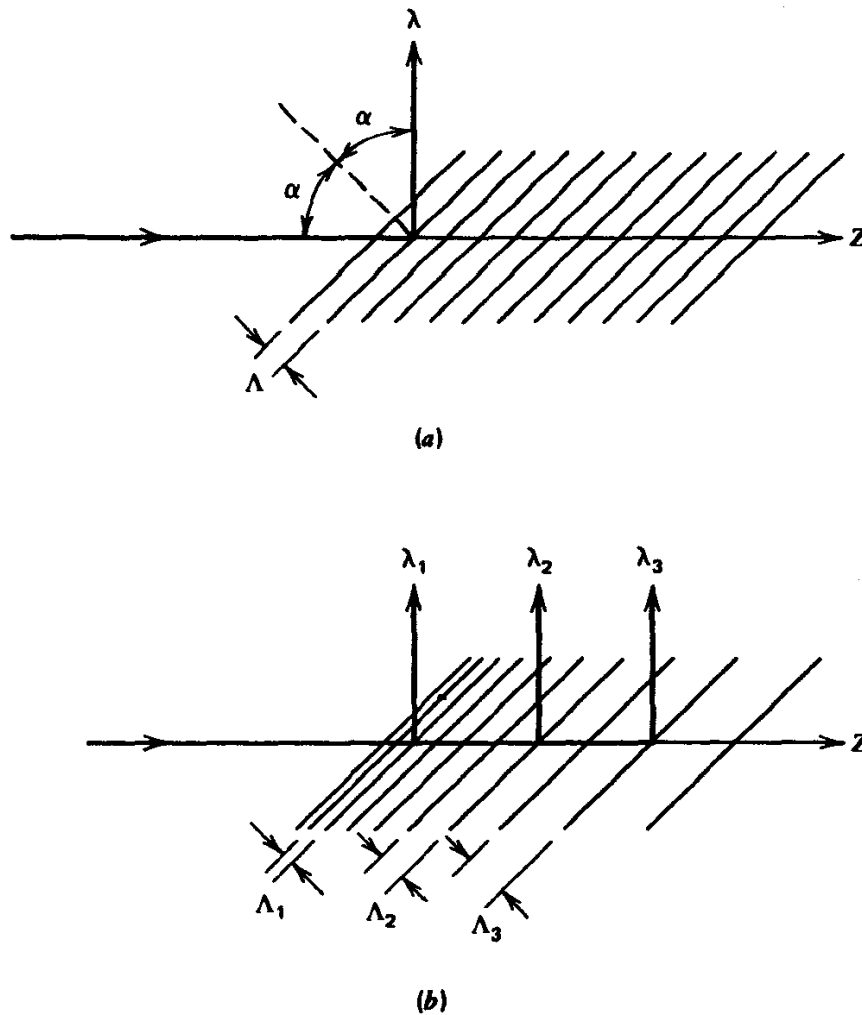
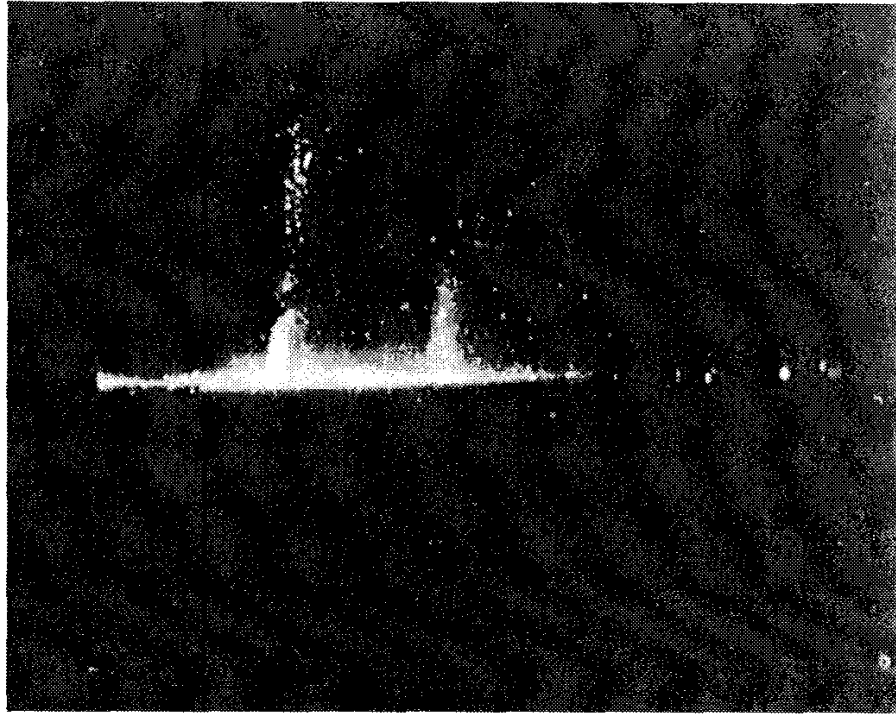
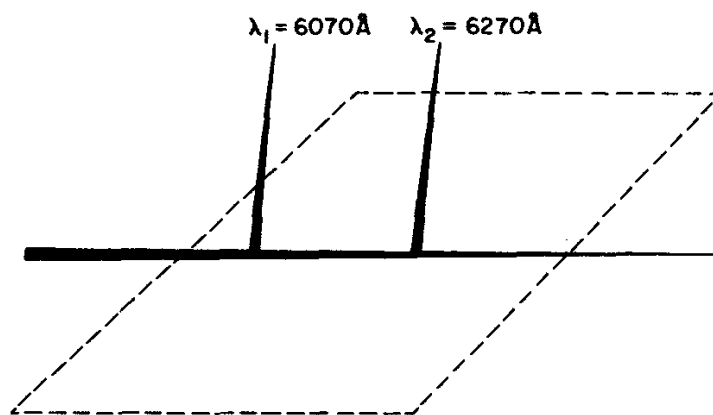


Figure 11.24. (a) Beamsplitting in a dielectric waveguide with a constant grating period Λ . (b) Beamsplitting and demultiplexing in a dielectric waveguide with chirped [variable period $\Lambda(z)$] grating.

lengths, which initially occupy the same beam, are thus demultiplexed, that is, separated spatially. The fraction of the light of wavelength λ_1 that is reflected depends on the length of the waveguide section for which the wavelength λ_1 falls within the “forbidden” propagation gap. It is thus a function of the chirp rate and of the coupling constant, which in a given waveguide depends on the corrugation height and profile.



(a)



(b)

Figure 11.25. (a) Double-exposure photograph showing the reflection of two different wavelengths from two different locations in a chirped-grating beamsplitter. (b) Schematic representation of the experiment shown in (a). The dashed lines outline the corrugated region, and the solid ones outline the laser beams.

A wavelength demultiplexer based on this idea has been demonstrated in a single-mode waveguide of thickness $0.95 \mu\text{m}$ [18, 19]. The period of the grating varies from 2930 to 3210 Å over a distance of 6.5 mm. The peak-to-trough height of the corrugations in the glass was approximately 500 Å. At an angle of incidence of 48° , the reflections at the two wavelengths 6070 and 6270 Å are separated spatially by 4 mm. The experimental observation of this demultiplexing is shown in Fig. 11.25.

11.9.2. Grating Directional Couplers

The directional coupling between two different waveguides can be made frequency-selective and highly efficient provided phase-matched coupling is achieved by a perturbation with a spatially periodic refractive index. Both codirectional and contradirectional couplings can occur, depending on the period of the grating. A codirectional coupling at wavelength λ_0 requires a grating period of $\Lambda = \lambda_0 / (n_a - n_b)$, while a contradirectional coupling at the same wavelength requires a grating period of $\Lambda = \lambda_0 / (n_a + n_b)$ according to Eq. (11.8-30), where n_a, n_b are the mode indices of guide a and b , respectively. Since the fractional bandwidth of strong coupling is on the order of $1/N$ (i.e., $\Delta\lambda/\Lambda \approx 1/N$), where N is the number of periods, it is obvious that the contradirectional coupler has the advantage of strong frequency selectivity (i.e., a narrow bandwidth) for short interaction length, but is more difficult to fabricate because of the short-period gratings required. A schematic drawing of a contradirectional coupler for use in guided-wave optical communication is shown in Fig. 11.26. For details about the spectral response and the design of grating directional couplers, interested readers are referred to [20, 21].

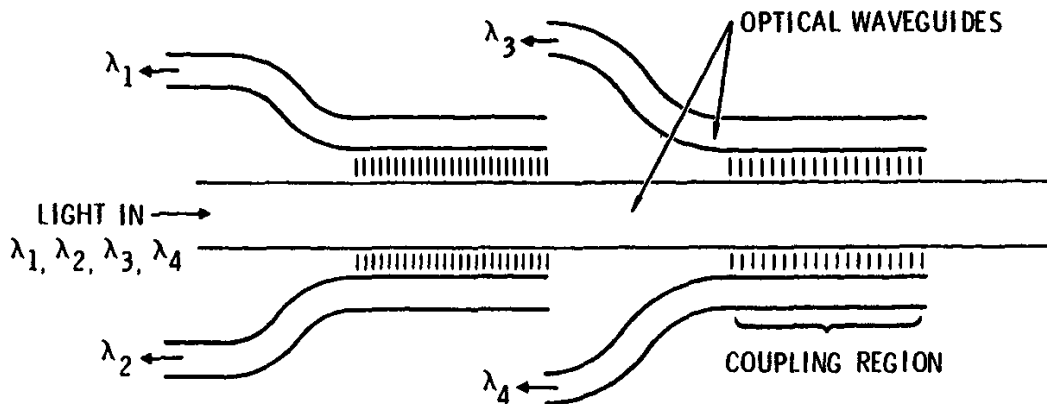


Figure 11.26. Frequency-selective couplers for use in optical-fiber communication.

11.10. OTHER PLANAR WAVEGUIDES

In the derivation of the TE and TM mode characteristics in Section 11.2, we assumed that the waveguides are made of dielectric materials with the refractive index of the guiding layer n_2 greater than those of the two bounding media (i.e., $n_2 > n_{1,3}$). This condition is necessary to achieve total internal reflections at the layer interfaces which are responsible for the confined propagation. In this section we consider two other planar waveguides in which this constraint is removed.

11.10.1. Metal-Clad Waveguides

Consider a slab waveguide structure as shown in Fig. 11.2 with the substrate (medium III) being metal. The refractive index n_3 of the metal substrate is a complex number. For example, the complex refractive indices of copper, gold, and silver at $\lambda = 6328 \text{ \AA}$ are, respectively, $n_3 = 0.16 - i3.37$, $0.16 - i3.21$, and $0.067 - i4.05$. Reflectivities from these metal surfaces are extremely high (almost 100%), especially at grazing incidence ($\theta \approx 90^\circ$), because of the large extinction coefficient (imaginary part) and the small real part of n_3 . In fact, if n_3 is a pure imaginary number, wave propagation in medium III is always evanescent. The reflectivity of light from such an ideal metal surface is always 100%, regardless of the angle of incidence and the state of polarization. Thus an ideal metal like this can provide the total reflection required for confined propagation. A medium with a pure imaginary refractive index has a negative dielectric constant and a zero optical conductivity. For copper, gold, and silver, $n_3^2 = -11.33 - i1.08$, $-10.28 - i1.03$, $-16.40 - i0.54$, respectively. Note that the imaginary part of n_3^2 , which is proportional to the optical conductivity σ , is small for all three.

For metal-clad waveguides with copper, gold, or silver as substrate, the mode characteristics may be derived approximately by neglecting the real part of the refractive index n_3 (or the imaginary part of n_3^2). In other words, we may assume that the metal substrate is a pure "dielectric" with a negative dielectric constant. In this approximation all the mode functions (11.2-3), (11.2-10) and mode conditions (11.2-5), (11.2-11) for TE and TM modes, respectively, can also be applied to the modes of these metal-clad waveguides. Since n_3^2 is negative, the field attenuation constant p in the metal substrate is large, according to Eq. (11.2-4). This means that the fraction of mode power inside the metal is very small. The modes are thus well confined, and the ohmic losses are expected to be small.

Since the metal substrate has a negative dielectric constant (i.e., $n_3^2 < 0$), total reflection always occurs at the interface between the guiding layer and

the metal substrate, regardless of the value of n_2 . Therefore, the refractive index of the guiding layer can be arbitrarily low, as long as $n_2 > n_1$. The propagation constant of the mode may have any value between $n_1 k_0$ and $n_2 k_0$, that is, $n_1 k_0 < \beta < n_2 k_0$. This range is much wider than with the usual dielectric waveguide. Thus metal-clad waveguides usually accommodate a large number of confined modes.

The field distribution and the propagation constant β of confined modes in metal-clad waveguide can be obtained by solving the mode conditions (11.2-5) for TE modes and (11.2-11) for TM modes. Since n_3^2 is complex, the propagation constants are in general complex. A waveguide mode with a complex propagation constant will attenuate as it propagates along the waveguide. Solving for the complex roots β_m of the transcendental equations (11.2-5) and (11.2-11) with complex n_3^2 is not an easy task. In metals with a small imaginary part of n^2 , the complex propagation constant can be obtained by the perturbation approach. A small imaginary part of n^2 corresponds to a small optical conductivity σ , and therefore small attenuation due to ohmic losses. In the perturbation approach, we first solve for the modes with a real n_3^2 and then use the small imaginary part of n_3^2 as a perturbation to calculate the small correction to the propagation constant β . Let the propagation constant be written

$$\beta_m = \beta_m^{(0)} - i\frac{1}{2}\alpha_m, \quad (11.10-1)$$

where $\beta_m^{(0)}$ is the propagation constant of the mode m with real n_3^2 and $-i\alpha_m/2$ is the correction term due to the imaginary part of n_3^2 . The power flow along the guide with a propagation constant (11.10-1) will be given by

$$P_m(z) = P_m(0)e^{-\alpha_m z}, \quad (11.10-2)$$

where $P_m^{(0)}$ is the power of mode m at $z = 0$. Let Δn_3^2 be the small dielectric perturbation due to the imaginary part of n_3^2 . The small correction $\delta\beta_m = -i\frac{1}{2}\alpha_m$ to the propagation constant is given, according to Eq. (11.3-15) by

$$\delta\beta_m = -i\frac{1}{2}\alpha_m = \frac{1}{4}\omega\epsilon_0 \int_{-\infty}^{\infty} \mathcal{E}_m^* \cdot \Delta n_3^2 \mathcal{E}_m dx, \quad (11.10-3)$$

where \mathcal{E}_m is the electric field of mode m given by Eqs. (11.2-3) and (11.2-10) with propagation constant $\beta_m^{(0)}$. By using Eq. (11.3-14), the correction to β_m^2 can be written

$$\delta\beta_m^2 = 2\beta_m \delta\beta_m = \left(\frac{\omega}{c}\right)^2 \Delta n_3^2 \Gamma_3, \quad (11.10-4)$$

where Γ_3 is the fraction of mode power flowing in the metal substrate (medium III) and is defined as

$$\Gamma_3 = \frac{\int_{-\infty}^{-t} |\mathcal{E}_m|^2 dx}{\int_{-\infty}^{\infty} |\mathcal{E}_m|^2 dx}. \quad (11.10-5)$$

According to the definition (11.10-5) and the expression (11.2-3) for the field, Γ_3 for the TE modes is given by (see Problem 11.5)

$$\Gamma_3^{\text{TE}} = \left(\frac{h^2}{h^2 + p^2} \right) \left(\frac{1/p}{t + 1/q + 1/p} \right). \quad (11.10-6)$$

Let $n_3 = n - i\kappa$, where n is the real part of n_3 and κ is the extinction coefficient of the metal; then $\Delta n_3^2 = -2in\kappa$. The correction term $\delta\beta_m$ can thus be written

$$\delta\beta_m = -i\frac{1}{2}\alpha_m = -i\frac{n\kappa}{\beta_m} \left(\frac{\omega}{c} \right)^2 \Gamma_3.$$

The attenuation coefficient α_m is thus given by

$$\alpha_m = \frac{2n\kappa}{\beta_m} \left(\frac{\omega}{c} \right)^2 \Gamma_3. \quad (11.10-7)$$

Note that Γ_3 depends also on the mode number m as well as on the polarization state. Generally speaking, TM waves have smaller β 's and also large Γ_3 's. Therefore, according to Eq. (11.10-7), TM modes are more lossy than TE modes (i.e., $\alpha_m^{\text{TM}} > \alpha_m^{\text{TE}}$). Higher-order modes (large m) have smaller β_m 's and also large Γ_3 's (i.e., they are less confined). Therefore, higher-order modes are more lossy than low-order modes. Table 11.1 shows the results of the calculation for silver-clad polystyrene waveguides [22]. Confined propagation of light in a silver-clad and in an aluminum-clad polystyrene waveguide has been observed and is shown in Fig. 11.27 [23].

The attenuation coefficient α_m may also be calculated directly from the rate of dissipation of energy in ohmic losses. According to Eq. (11.10-2), the attenuation coefficient may be defined as

$$\alpha_m = -\frac{1}{P_m} \frac{dP_m}{dz}, \quad (11.10-8)$$

where P_m is the power flow per unit length in y for the mode m , and

Table 11.1 Mode Indices of an Air–Polystyrene–Silver Waveguide Using a 1.81- μm -Thick polystyrene Film; and Losses in Air–Polystyrene–Silver Waveguides [23]

Mode	Mode index	
	Measured	Calculated
TE ₀	1.582	1.574
TE ₁	1.547	1.547
TE ₂	1.503	1.502
TE ₃	1.438	1.438
TE ₄	1.349	1.351
TE ₅	1.238	1.238
TE ₆	1.092	1.095

Mode	Mode index	
	Measured	Calculated
TM ₀	1.577	1.571
TM ₁	1.543	1.538
TM ₂	1.484	1.484
TM ₃	1.407	1.406
TM ₄	1.304	1.302
TM ₅	1.169	1.168
TM ₆	1.004	1.014

Thickness of Polystyrene Film (μm)	Loss (dB/cm)			
	TE ₀	TE ₁	TM ₀	TM ₁
1	13.609	51.77	136.46	313.92
2	1.85	7.60	19.03	62.94
2.5	1.03	4.03	9.92	33.58
3	0.63	2.32	5.91	20.21

$-dP_m/dz$ is the power dissipated in ohmic losses per unit length in y per unit length of the waveguide (in z). According to Ohm's law, there exists a current density $\mathbf{J} = \sigma\mathbf{E}$ in the metal. The time-average rate of dissipation of energy per unit volume in ohmic losses is $\frac{1}{2}\mathbf{J} \cdot \mathbf{E}^* = \frac{1}{2}\sigma|\mathbf{E}|^2$, so that $-dP_m/dz$ is given by

$$-\frac{dP_m}{dz} = \frac{1}{2} \int_{-\infty}^{\infty} \sigma |\mathbf{E}_m|^2 dx = \frac{1}{2} \int_{-\infty}^{\infty} \sigma |\mathcal{E}_m|^2 dx, \quad (11.10-9)$$

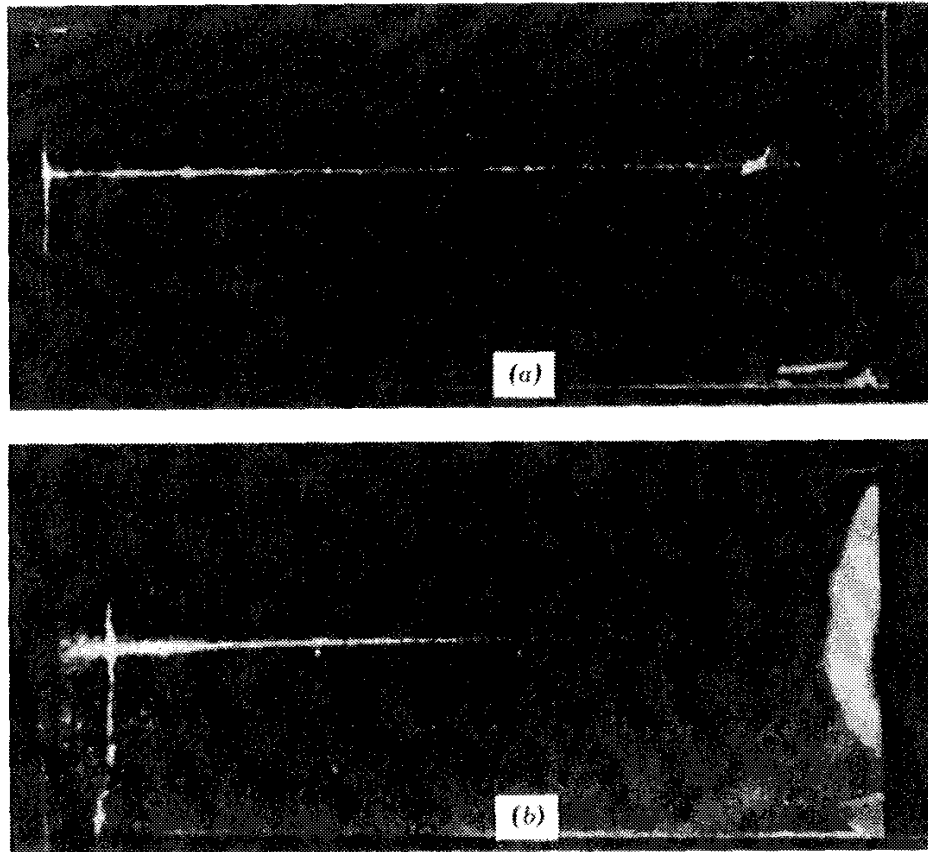


Figure 11.27. Photographs (a) and (b) show light-wave propagation in a silver-clad and in an aluminum-clad polystyrene waveguide. In such photographs, a short light path means a large loss in the waveguide [23].

where \mathcal{E}_m is the mode function of the guide. If \mathcal{E}_m is normalized to a mode power of $P_m = 1$ W/m, the attenuation coefficient α_m can be written, according to Eqs. (11.10-8) and (11.10-9),

$$\alpha_m = \frac{1}{2} \int_{-\infty}^{\infty} \sigma |\mathcal{E}_m|^2 dx. \quad (11.10-10)$$

This result is identical to Eq. (11.10-3) if we recall that $\Delta n_3^2 = -i\sigma/\epsilon_0\omega$.

Because of their discrimination against TM modes and higher-order modes, metal-clad waveguides can be used as mode filters or mode polarizers which transmit only low-order TE modes.

11.10.2. Bragg-Reflection Waveguides

Referring to Fig. 11.28, we consider a slab dielectric waveguide with a substrate made of a periodic layered medium consisting of thin layers of refractive indices n_1 and n_2 . The guiding layer has a refractive index of n_g

such that $n_a < n_g < n_{1,2}$, where n_a is the refractive index of the other bounding medium (for air, $n_a = 1$). The confined propagation may be considered formally as that of a plane wave zigzagging inside the core (n_g) and undergoing total internal reflection at the interface $x = -t$ with the low-index medium (n_a) and Bragg reflection at the interface $x = 0$ with the periodic layered medium. For high Bragg reflectivity it is necessary that the incidence angle satisfy the Bragg condition, or more exactly that the propagation condition inside the layered medium fall within one of the "forbidden" gaps (see Section 6.6).

To derive the mode characteristics, we assume that the periodic layered medium is semiinfinite, extending from $x = 0$ to $x = +\infty$. In the case of TE modes the only field components are E_y , H_x , and H_z . We take $E_y(x, z, t)$ in the form (11.2-2). The transverse function $\mathcal{E}_y(x)$ is taken as

$$\mathcal{E}_y(x) = \begin{cases} c_1 E_K(x) e^{-iKx}, & 0 \leq x, \\ c_2 \left\{ \cos[k_g(x+t)] + \frac{q_a}{k_g} \sin[k_g(x+t)] \right\}, & -t \leq x \leq 0, \\ c_2 e^{q_a(x+t)}, & x \leq -t, \end{cases} \quad (11.10-11)$$

where $c_{1,2}$ are constants $E_K(x) e^{-iKz}$ is the Bloch wave function of the electric field in the layered medium (see Section 6.2), and

$$q_a = (\beta^2 - n_a^2 k_0^2)^{1/2}, \quad (11.10-12)$$

$$k_g = (n_g^2 k_0^2 - \beta^2)^{1/2}.$$

The transverse function $\mathcal{E}_y(x)$ in the region between $x = 0$ and $x = -t$ is identical to that of a slab waveguide [Eq. (11.2-3)]. The new feature here is the Bloch wave in the semiinfinite periodic medium ($x \geq 0$). An explicit form of the Bloch wave in the regions with index n_1 is given by Eq. (6.2-25) (note: with z replaced by x).

The acceptable solutions for \mathcal{E}_y and $\mathcal{H}_z = (i/\omega\mu) (\partial\mathcal{E}_y/\partial x)$ are continuous at both $x = 0$ and $x = -t$. The particular choice of coefficients in Eq. (11.10-11) satisfies the continuity condition for \mathcal{E}_y and $\partial\mathcal{E}_y/\partial x$ at $x = -t$. By imposing the continuity condition on \mathcal{E}_y and $\partial\mathcal{E}_y/\partial x$ at $x = 0$, we get

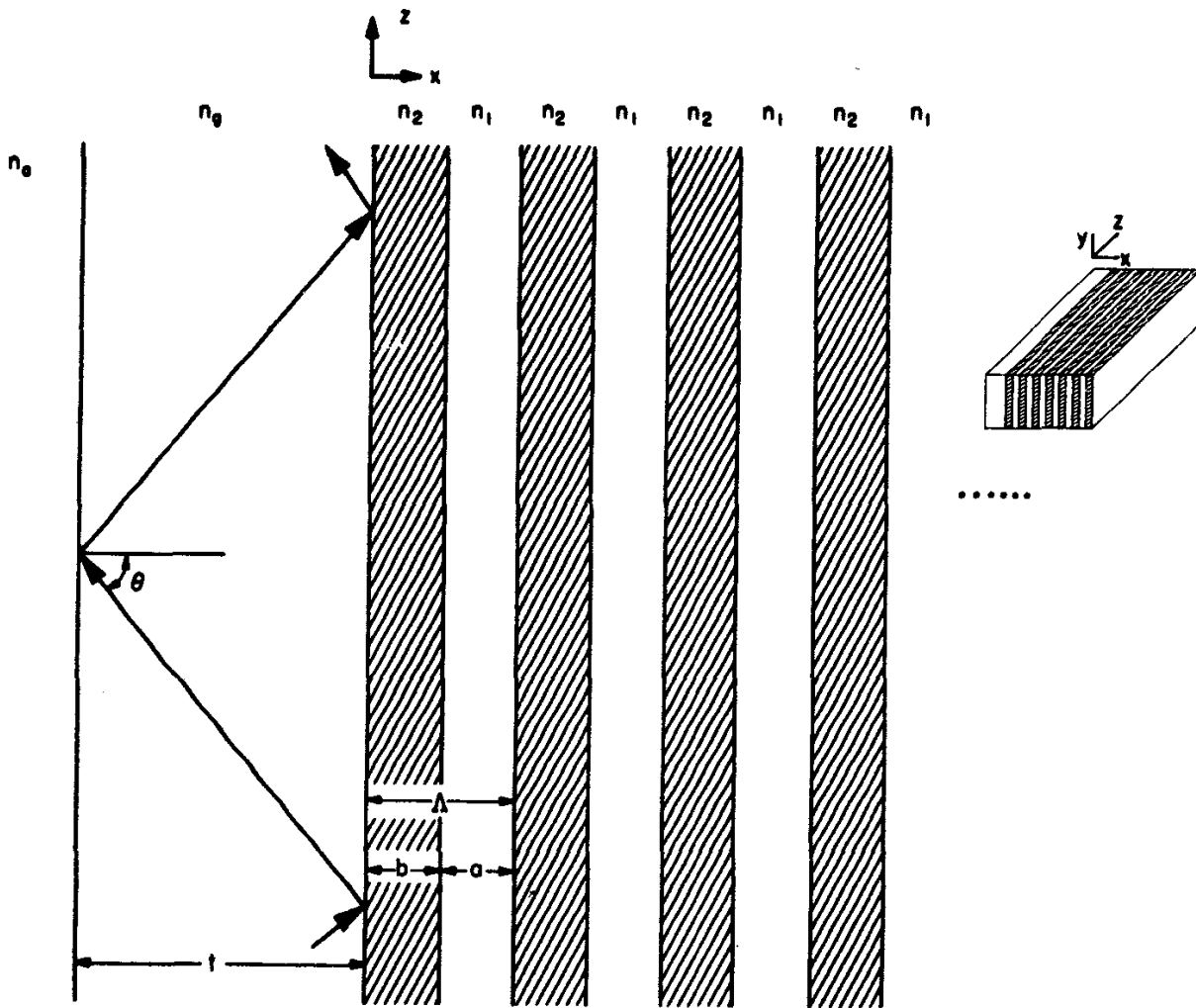


Figure 11.28. A Bragg-reflection (slab) dielectric waveguide ($\partial/\partial y = 0$).

from Eqs. (6.2-25) and (11.10-11)

$$c_1(a_0 + b_0) = c_2 \left[\cos k_g t + \frac{q_a}{k_g} \sin k_g t \right], \tag{11.10-13}$$

$$-ik_{1x}c_1(a_0 - b_0) = c_2[-k_g \sin k_g t + q_a \cos k_g t],$$

where a_0 and b_0 are given by Eq. (6.2-23), and

$$k_{1x} = (n_1^2 k_0^2 - \beta^2)^{1/2}. \tag{11.10-14}$$

By eliminating c_1, c_2 from Eq. (11.10-13) and using Eq. (6.2-23), a mode

condition for TE waves is obtained:

$$k_g \left(\frac{q_a \cos k_g t - k_g \sin k_g t}{q_a \sin k_g t + k_g \cos k_g t} \right) = ik_{1x} \left(\frac{e^{iK\Lambda} - A - B}{e^{iK\Lambda} - A + B} \right), \quad (11.10-15)$$

where A and B are given by Eq. (6.2-12), Λ is the period of the layered medium, and K is the Bloch wave number. The constants c_1 and c_2 are determined by Eq. (11.10-13) and the normalization condition (11.1-17) or (11.1-18).

Confined propagation modes result when the condition (11.10-15) is satisfied with real parameters β , q_a , and k_g , and when the propagation constant β is such that the light falls within one of the forbidden gaps. The latter condition insures that the Bloch wave number is complex:

$$K = \frac{m\pi}{\Lambda} - iK_i, \quad (11.10-16)$$

resulting in an evanescent oscillatory decay of the field amplitude in the layered medium ($x \geq 0$). A calculated field distribution of such a confined mode is shown in Fig. 11.29(b) [24]. Confined propagation of light in such a waveguide structure has been observed experimentally [25]. The measured transverse intensity distribution of a confined mode is shown in Fig. 11.30.

The above derivation assumes that the periodic layered medium is semiinfinite. Confined lossless propagation requires that the reflectivity at the interface between the guiding layer and the periodic medium be unity, which is only possible in an infinite structure. In practice, the number of periods is always finite. The reflectivity is somewhat less than unity. Thus the waveguide is slightly leaky. The attenuation coefficient α may be estimated roughly as follows: Let R be the reflectivity of light due to the Bragg reflection at the interface $x = 0$ ($R \leq 1$). If θ_g is the incidence angle of the ray in the guiding layer, the ray advances a distance of $2t \tan \theta_g$ in each round trip, zigzagging. Thus, in a section of length L , the number of round trips is $N' = L/(2t \tan \theta_g)$. The attenuation coefficient is thus given by

$$R^{N'} = e^{-\alpha L}. \quad (11.10-17)$$

Using $N' = L/2t \tan \theta_g$, $\beta = k_g \tan \theta_g$, the attenuation coefficient α can be written

$$\alpha = -\frac{\ln R}{2t \tan \theta_g} = -\frac{k_g}{2\beta t} \ln R. \quad (11.10-18)$$

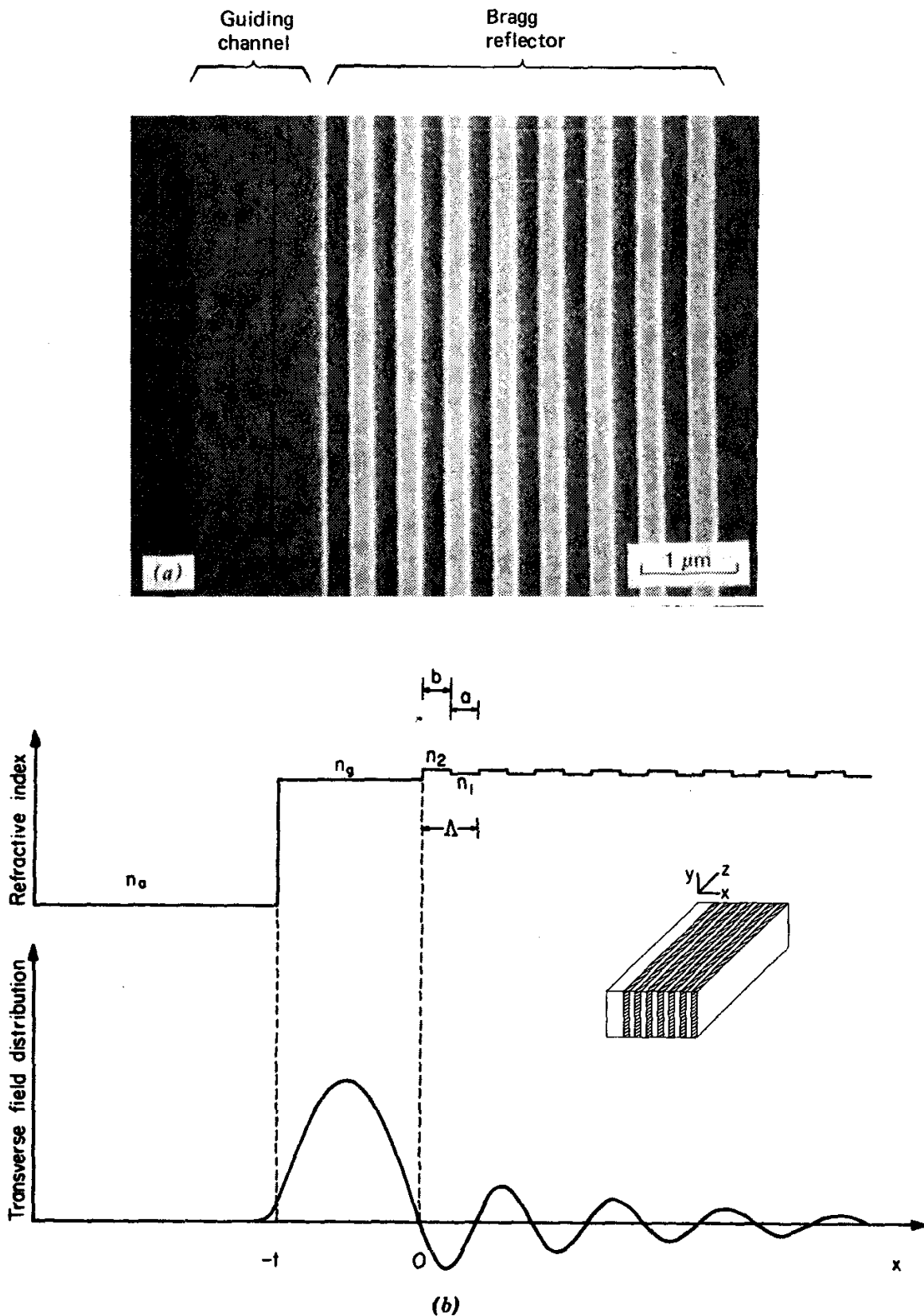


Figure 11.29. (a) A scanning electron micrograph of a cleaved section of a Bragg waveguide composed of alternating layers of GaAs and $\text{Al}_{0.20}\text{Ga}_{0.80}\text{As}$ [25]. (b) The refractive-index profile of a Bragg waveguide (top) and its calculated transverse field distribution (bottom). The indices of refraction are $n_a = 1$ (air), $n_g = 3.24$ ($\text{Al}_{0.38}\text{Ga}_{0.62}\text{As}$), $n_2 = 3.43$ (GaAs), and $n_1 = 3.35$ ($\text{Al}_{0.20}\text{Ga}_{0.80}\text{As}$) at a wavelength $\lambda = 1.15 \mu\text{m}$ [25].

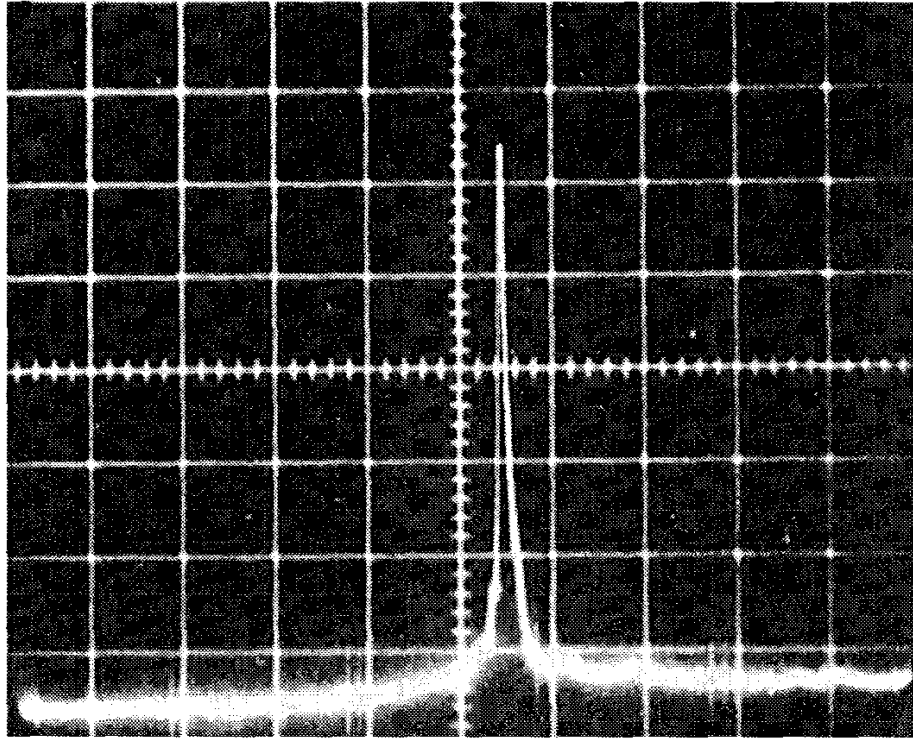


Figure 11.30. Measured transverse intensity distribution of a confined mode in a Bragg waveguide 2 mm long. The horizontal scale is about $10 \mu\text{m}$ per (big) division [25].

Note that α tends to zero when the reflectivity R approaches 100%. The reflectivity R of a Bragg reflector of finite number of layers is given by Eq. (6.6-10). If the incidence condition is such that the reflectivity achieves its maximum value $\tanh^2|\kappa|N\Lambda$ [see Eq. (6.6-11)], the attenuation coefficient α (11.10-18) can be given approximately, using $\ln(\tanh x) \approx -2e^{-2x}$ for large x , as

$$\alpha = \frac{2k_g}{\beta t} \exp(-2|\kappa|N\Lambda), \quad (11.10-19)$$

where κ is the coupling constant given by Eq. (6.6-5). Note that the attenuation coefficient α decreases exponentially as a function of the number of periods N .

11.11. LEAKY DIELECTRIC WAVEGUIDES

In Section 11.2 we derived the properties of TE and TM modes propagating in thin dielectric waveguides. It was shown that a thin dielectric slab is capable of supporting confined lossless propagation provided the index of

refraction of the inner layer (core) exceeds the refractive indices of the two bounding media, that is,

$$n_2 > n_{1,3}. \quad (11.11-1)$$

This condition is necessary to obtain an imaginary transverse propagation constant which corresponds to an evanescent decay of the mode field in the bounding media. There are many practical situations where it is desirable or necessary to guide power in a layer with a lower refractive index than exists in the two bounding media. A prime example of such a case is the waveguide laser in which the inner layer is molecular gas with $n_2 = 1$. In this situation, total reflections cannot be achieved at the interfaces. A wave fed into such a waveguide will thus proceed to lose power by “leaking” to the two bounding media, and will attenuate with z (the propagation direction).

A number of investigators [26] have recognized that the losses described above can, under certain circumstances, be quite small and the guides may thus be suitable for laser applications [27]. We note that the Fresnel reflectivity at the interfaces approaches unity when the angle of incidence reaches 90° . Thus the losses due to incomplete reflection from the dielectric interfaces are expected to be small when the rays are at grazing incidence. Recently, an increasing number of lasers—the so-called “waveguide lasers”—using “leaky” waveguides as the transmission medium have been demonstrated [28–30].

In what follows we will derive the TE mode characteristics and the attenuation coefficients for such modes. The ray-optics approach will also be used to derive the propagation constant and the attenuation coefficients for both TE and TM modes.

Referring to Fig. 11.31, we consider the TE wave propagation along the z direction. We take $E_y(x, z, t)$ in the form

$$E_y(x, z, t) = \mathcal{E}_y(x) \exp[i(\omega t - \beta z)]. \quad (11.11-2)$$

The transverse function $\mathcal{E}_y(x)$ is taken as

$$\mathcal{E}_y(x) = \begin{cases} C \exp(-ih_1 x), & 0 \leq x, \\ C \left[\cos h_2 x - i \frac{h_1}{h_2} \sin h_2 x \right], & -t \leq x \leq 0, \\ C \left[\cos h_2 t + i \frac{h_1}{h_2} \sin h_2 t \right] \exp[ih_3(x + t)], & x \leq -t \end{cases} \quad (11.11-3)$$

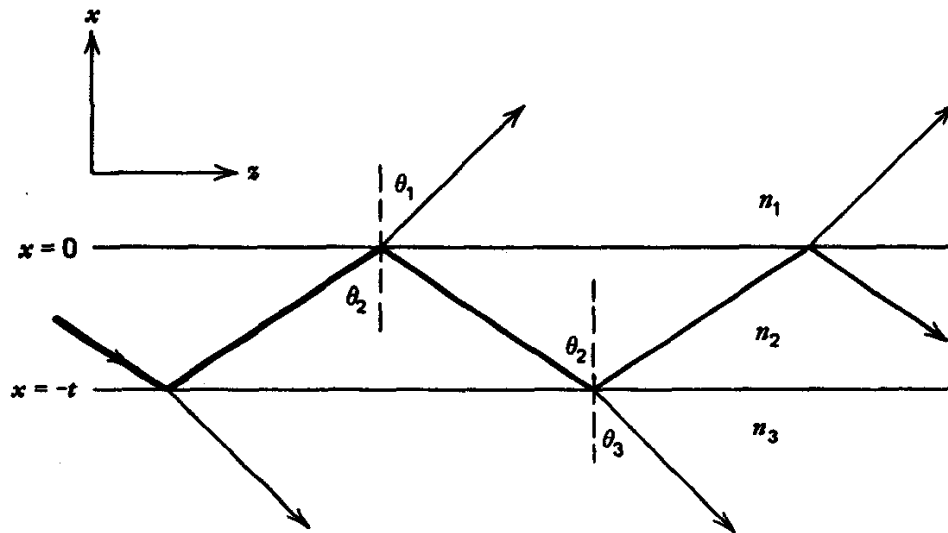


Figure 11.31. A leaky waveguide in which $n_2 < n_{1,3}$. θ_1 , θ_2 , and θ_3 are ray angles in media 1, 2, and 3, respectively.

where

$$h_i = (n_i^2 k_0^2 - \beta^2)^{1/2}, \quad i = 1, 2, 3, \quad (11.11-4)$$

$$k_0 = \frac{\omega}{c} = \frac{2\pi}{\lambda}.$$

The particular form (11.11-3) is chosen so that \mathcal{E}_y is continuous at $x = 0$ and $x = -t$ and H_z is continuous at $x = 0$. By imposing the continuity condition on H_z at $x = -t$ we get, from Eq. (11.11-3),

$$\tan h_2 t = i \frac{h_2 (h_1 + h_3)}{h_2^2 + h_1 h_3}. \quad (11.11-5)$$

We note here that the mode condition (11.11-5) can be obtained directly from Eq. (11.2-5) by substituting $q \rightarrow ih_1$, $h \rightarrow h_2$, $p \rightarrow ih_3$. This correspondence between the two sets of constants follows from comparing the form of the confined mode solution (11.2-3) with the leaky solution (11.11-3). The signs in front of h_1 and h_3 in the exponent of the solution (11.11-3) are chosen so that the solution represents outward propagating waves in the bounding media. This corresponds to the leakage of electromagnetic energy from the core to the bounding medium. Since the whole dielectric structure is passive (i.e., no gain or energy sources), the leakage of energy must correspond to a decrease of mode energy in the core as it propagates along z . Thus the propagation constant of a leaky mode must be a complex

number,

$$\beta = \beta^{(0)} - \frac{1}{2}i\alpha, \quad (11.11-6)$$

where $\alpha > 0$ is the mode power attenuation coefficient, and $\beta^{(0)}$ is a real number. In fact, the mode condition (11.11-5) derived from the electromagnetic analysis can never be satisfied by a real β within the range $0 \leq \beta^2 \leq n_2^2 k_0^2$. A complex propagation constant β (11.11-6) corresponds to an exponential decay in the mode power along z and a simultaneous exponential increase in wave intensity with $|x|$ in the bounding media, according to Eqs. (11.11-2), (11.11-3), and (11.11-4). Since the field amplitudes blow up at $|x| = \infty$, the mode field (11.11-3) with a complex β is not a legitimate solution of Maxwell's equations if the waveguide structure is infinite in extent. However, Eq. (11.11-3) does represent approximately the field near the core and inside the core in a practical waveguide structure of finite extent. The mode condition (11.11-5) can be solved together with Eq. (11.11-4) for h_1 , h_2 , and h_3 for the complex propagation constants β . An approximate solution can be obtained by the method of successive approximation (iteration) if the waveguide is "large" and the incidence angle θ_2 is near the grazing angle ($\theta_2 \approx \frac{1}{2}\pi$) so that $0 \approx h_2 \ll h_{1,3}$. In this case, the mode condition can be written approximately as

$$\tan h_2 t = ih_2 \left(\frac{1}{h_1} + \frac{1}{h_3} \right). \quad (11.11-7)$$

Since $h_2 \ll h_{1,3}$, the right-hand side of (11.11-7) is very small and can be neglected in the first approximation. This, the first approximate solution for h_2 is

$$h_2 = \frac{s\pi}{t}, \quad s = 1, 2, 3, \dots \quad (11.11-8)$$

For a large waveguide (i.e., large t), h_2 is indeed small provided the mode number s is small. Since $h_2 \approx 0$, the corresponding first approximations for β , h_1 , and h_3 are, according to Eq. (11.11-4),

$$\beta = n_2 k_0,$$

$$h_1 = k_0 (n_1^2 - n_2^2)^{1/2}, \quad (11.11-9)$$

$$h_3 = k_0 (n_3^2 - n_2^2)^{1/2}.$$

In the second iteration, we substitute h_1 , h_3 , and h_2 from Eqs. (11.11-9) and (11.11-8) into the right-hand side of Eq. (11.11-7). This leads to

$$\tan h_2 t = i \frac{s\pi}{t} \left[\frac{1}{k_0(n_1^2 - n_2^2)^{1/2}} + \frac{1}{k_0(n_3^2 - n_2^2)^{1/2}} \right]. \quad (11.11-10)$$

This equation can be regarded as an approximate expression for $h_2 t$, since the right-hand side is small:

$$h_2 \approx \frac{s\pi}{t} + i \frac{s\pi}{t^2} \left[\frac{1}{k_0(n_1^2 - n_2^2)^{1/2}} + \frac{1}{k_0(n_3^2 - n_2^2)^{1/2}} \right]. \quad (11.11-11)$$

Substituting Eq. (11.11-11) into Eq. (11.11-4) gives the second approximation for β :

$$\beta = n_2 k_0 \left[1 - \frac{1}{2} \left(\frac{s\pi}{n_2 k_0 t} \right)^2 \right] - i \left(\frac{s\pi}{k_0 t} \right)^2 \left[\frac{1}{t n_2 (n_3^2 - n_2^2)^{1/2}} + \frac{1}{t n_2 (n_1^2 - n_2^2)^{1/2}} \right]. \quad (11.11-12)$$

The attenuation coefficient for the TE_s mode is thus given by

$$\alpha_s^{\text{TE}} = 2 \left(\frac{s\pi}{k_0 t} \right)^2 \left[\frac{1}{t n_2 (n_3^2 - n_2^2)^{1/2}} + \frac{1}{t n_2 (n_1^2 - n_2^2)^{1/2}} \right], \quad s = 1, 2, 3, \dots, \quad (11.11-13)$$

or, equivalently, using $k_0 = 2\pi/\lambda$,

$$\alpha_s^{\text{TE}} = \frac{s^2}{2n_2 \lambda (t/\lambda)^3} \left[\frac{1}{(n_3^2 - n_2^2)^{1/2}} + \frac{1}{(n_1^2 - n_2^2)^{1/2}} \right], \quad s = 1, 2, 3, \dots \quad (11.11-14)$$

This result was obtained in [31]. We thus find that the attenuation coefficient decreases as t^{-3} . Since this attenuation is a result of the incomplete reflection at the dielectric interfaces (i.e., $R < 1$), the attenuation coefficient

for both TE and TM waves can be estimated by using the zigzagging-ray model.

11.11.1. Ray-Optics Approach

We now derive the attenuation coefficients and the propagation constant β using the ray-optics approach (see Section 11.2). Since the phase shifts ϕ_{21}, ϕ_{23} upon reflection from the dielectric interfaces are either 0 or π for the case when $n_2 < n_{1,3}$, the mode condition (11.2-22) becomes

$$h_2 t = n_2 k_0 \cos \theta_2 t = s\pi, \quad s = 1, 2, 3, \dots, \quad (11.11-15)$$

where θ_2 is the angle of incidence (see Fig. 11.31). Let R_{21} and R_{23} be the reflectivities at the dielectric interfaces $x = 0$ and $x = -t$, respectively. According to Eqs. (11.10-17) and (11.10-18), the attenuation coefficient α can be written

$$\alpha = -\frac{\ln(R_{21}R_{23})}{2t \tan \theta_2} = -\frac{h_2}{2\beta t} [\ln R_{21} + \ln R_{23}]. \quad (11.11-16)$$

Near grazing incidence ($\cos \theta_2 = 0$), these reflectivities can be written approximately as

$$R_{21} \approx \begin{cases} 1 - 4 \frac{n_2 \cos \theta_2}{n_1 \cos \theta_1} & \text{(TE),} \\ 1 - 4 \frac{n_1 \cos \theta_2}{n_2 \cos \theta_1} & \text{(TM),} \end{cases} \quad (11.11-17)$$

$$R_{23} \approx \begin{cases} 1 - 4 \frac{n_2 \cos \theta_2}{n_3 \cos \theta_3} & \text{(TE),} \\ 1 - 4 \frac{n_3 \cos \theta_2}{n_2 \cos \theta_3} & \text{(TM),} \end{cases} \quad (11.11-18)$$

where θ_1 and θ_3 are the ray angles (see Fig. 11.31) in media 1 and 3, respectively, and are given approximately, using Snell's law, by

$$\begin{aligned} \cos \theta_1 &\approx \left[1 - \left(\frac{n_2}{n_1} \right)^2 \right]^{1/2}, \\ \cos \theta_3 &\approx \left[1 - \left(\frac{n_2}{n_3} \right)^2 \right]^{1/2}. \end{aligned} \quad (11.11-19)$$

We now substitute Eqs. (11.11-17) and (11.11-18) for R_{21} and R_{23} , respectively, into Eq. (11.11-16) and use $\ln(1+x) \approx x$ for small x . The attenuation coefficients for TE and TM waves can thus be written, respectively,

$$\alpha^{\text{TE}} = \frac{2h_2}{\beta t} \left(\frac{n_2 \cos \theta_2}{n_1 \cos \theta_1} + \frac{n_2 \cos \theta_2}{n_3 \cos \theta_3} \right),$$

$$\alpha^{\text{TM}} = \frac{2h_2}{\beta t} \left(\frac{n_1 \cos \theta_2}{n_2 \cos \theta_1} + \frac{n_3 \cos \theta_2}{n_2 \cos \theta_3} \right). \quad (11.11-20)$$

Using Eq. (11.11-15), Eq. (11.11-19) and $\beta = n_2 k_0$ ($k_0 = 2\pi/\lambda$), we obtain the following expressions for the attenuation coefficients from Eq. (11.11-20):

$$\alpha_s^{\text{TE}} = \frac{s^2}{2n_2\lambda(t/\lambda)^3} \left[\frac{1}{(n_1^2 - n_2^2)^{1/2}} + \frac{1}{(n_3^2 - n_2^2)^{1/2}} \right], \quad (11.11-21)$$

$$\alpha_s^{\text{TM}} = \frac{s^2}{2n_2\lambda(t/\lambda)^3} \left[\frac{n_1^2}{n_2^2(n_1^2 - n_2^2)^{1/2}} + \frac{n_3^2}{n_2^2(n_3^2 - n_2^2)^{1/2}} \right]. \quad (11.11-22)$$

Note that the ray-optics result (11.11-21) is identical to Eq. (11.11-14), which is derived by using the electromagnetic-wave analysis. According to Eqs. (11.11-22) and (11.11-21), TM waves are more lossy than TE waves, since $n_2 < n_{1,3}$. This is directly related to the fact that the reflectivity for TM waves is always smaller than (or equal to) that of the TE waves (i.e., $R^{\text{TM}} \leq R^{\text{TE}}$). Higher-order modes (larger s) are more lossy, according to Eqs. (11.11-21) and (11.11-22), than lower-order modes. In the case when $n_1 < n_2 < n_3$, the expressions (11.11-21) and (11.11-22) are also valid, provided we exclude the pure imaginary term $(n_1^2 - n_2^2)^{-1/2}$ in the square brackets, which becomes a small correction term to the propagation constant. In the case of a symmetric leaky waveguide with $n_2 = 1$ and $n_1 = n_3 = n_0$, (11.11-21) and (11.11-22) become

$$\left. \begin{aligned} \alpha_s^{\text{TE}} &= \frac{s^2 \lambda^2}{t^3 (n_0^2 - 1)^{1/2}} \\ \alpha_s^{\text{TM}} &= \frac{s^2 \lambda^2 n_0^2}{t^3 (n_0^2 - 1)^{1/2}} \end{aligned} \right\} s = 1, 2, 3, \dots \quad (11.11-23)$$

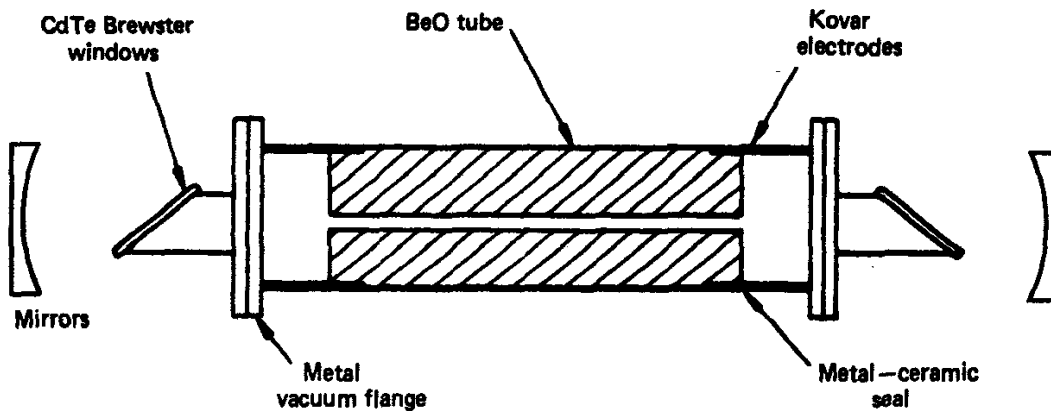


Figure 11.32. Construction details of a BeO capillary-bore laser. (After [30]; copyright 1973 IEEE.)

Some typical attenuation coefficients for the symmetric waveguide with $s = 1$, $n_0 = 2.0$, and $\lambda = 1 \mu\text{m}$ are

t (μm)	1	5	10	50
α^{TE} (cm^{-1})	5774	46.2	5.8	4.6×10^{-2}
α^{TM} (cm^{-1})	23094	184.8	23.1	1.85×10^{-1}

We thus find that for $t > 10\lambda$, $\alpha^{\text{TE}}\lambda \lesssim 6 \times 10^{-4}$. Such losses can easily be overcome by the gain of most laser media [28, 30].

A schematic drawing of a CO_2 10.6- μm waveguide laser, using the leaky mode described above, is shown in Fig. 11.32. The waveguiding is accomplished in a BeO capillary tube.

11.12. ELECTROMAGNETIC SURFACE WAVES (SURFACE PLASMONS)

In Section 6.9 we showed that electromagnetic surface waves can exist at the interface between a dielectric homogeneous medium and a periodic dielectric layered medium. These modes are in fact evanescent Bloch waves of the periodic medium. Both TE and TM waves can be supported, and many modes can exist at a given frequency ω . We now show that electromagnetic surface waves can also exist at the interface between two media, provided the dielectric constants of the media are opposite in sign (e.g., air and silver). Only a single TM mode exists at a given frequency. The amplitude of the wave decreases exponentially in the two directions normal to the interface. These modes are also called *surface plasmon* waves because of the

electron-plasma contribution to the negative dielectric constant of metals when the optical frequency is lower than the plasma frequency (i.e., $\omega < \omega_p$). In what follows we derive the propagation characteristics of the electromagnetic surface waves.

Referring to Fig. 11.33, we consider the wave propagation along the interface between a medium with a positive dielectric constant ($n_1^2 > 0$) and a medium with a negative dielectric constant ($n_3^2 < 0$). A typical example is the interface between air and silver, where $n_1^2 = 1$ and $n_3^2 = -16.40 - i0.54$ at $\lambda = 6328 \text{ \AA}$. If we neglect the small imaginary part ($-i0.54$), we may consider silver as a material with a negative dielectric constant. The presence of the imaginary part will cause attenuation in propagation along the interface. We will first solve for the surface modes by neglecting the imaginary part of the dielectric constant. The propagation attenuation coefficient will then be obtained by using perturbation theory or directly from the complex root of the mode condition.

The structure shown in Fig. 11.33 may be viewed as a special case of the waveguide structure shown in Fig. 11.2 with $t = 0$. Therefore, the field expressions (11.2-3), (11.2-10) and the mode conditions (11.2-5), (11.2-11) for TE and TM waves, respectively, can also be applied to the guide structure shown in Fig. 11.33. By putting $t = 0$ in Eq. (11.2-5), we obtain the mode condition for the TE surface waves:

$$p + q = 0, \quad (11.12-1)$$

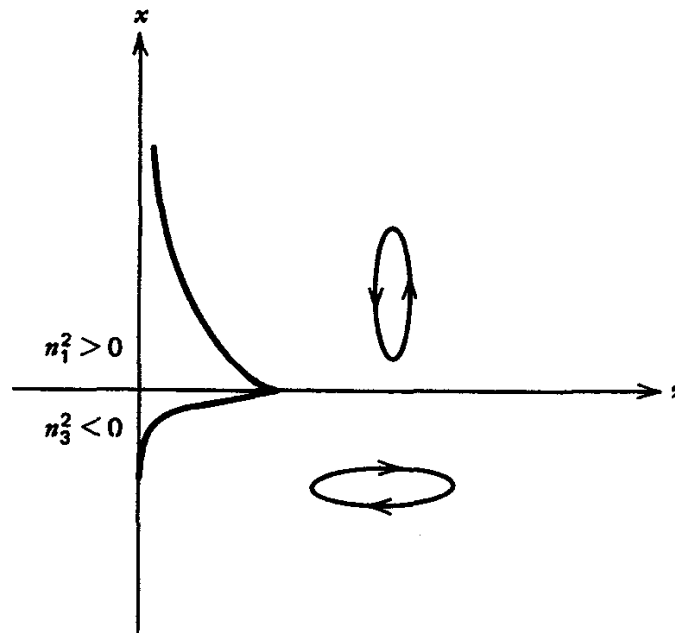


Figure 11.33. An electromagnetic surface wave at the interface between two media. The graph shows the field amplitudes H_y (or E_z) as functions of x , the distance normal to the interface. The two ellipses show the polarization states of the \mathbf{E} vector in the two media.

where p and q are the exponential attenuation constants in media 3 and 1, respectively. Since a confined mode requires that $p > 0$ and $q > 0$, Eq. (11.12-1) can never be satisfied. This proves that a TE surface mode cannot exist at the interface of two homogeneous media. For TM waves, the mode function $\mathcal{H}_y(x)$ can be written as

$$\mathcal{H}_y(x) = \begin{cases} Ce^{-qz}, & x \geq 0, \\ Ce^{px}, & x \leq 0, \end{cases} \quad (11.12-2)$$

where C is the constant of normalization. The mode condition can be obtained by insisting on the continuity of E_z at the interface $x = 0$, or directly from Eq. (11.2-11) by setting $t = 0$. The result is

$$\frac{p}{n_3^2} + \frac{q}{n_1^2} = 0. \quad (11.12-3)$$

Since $n_1^2 n_3^2 < 0$, the mode condition (11.12-3) for TM surface waves can be satisfied for confined propagation with $p > 0$ and $q > 0$. Using Eq. (11.2-4) for p and q , the mode condition (11.12-3) can be solved, and the propagation constant β is given by

$$\beta = \left(\frac{n_1^2 n_3^2}{n_1^2 + n_3^2} \right)^{1/2} \frac{\omega}{c}. \quad (11.12-4)$$

A confined propagating mode must have a real propagation constant. According to Eq. (11.12-4) and $n_1^2 n_3^2 < 0$, this requires that

$$n_1^2 + n_3^2 < 0, \quad (11.12-5)$$

that is, the sum of the dielectric constant of the media must be negative. The attenuation constants p and q are given, according to Eqs. (11.2-4) and (11.12-4), by

$$p^2 = \frac{-n_3^4}{n_1^2 + n_3^2} \left(\frac{\omega}{c} \right)^2, \quad (11.12-6)$$

$$q^2 = \frac{-n_1^4}{n_1^2 + n_3^2} \left(\frac{\omega}{c} \right)^2,$$

which are both positive according to Eq. (11.12-5). The electric field

components are given, according to Eqs. (11.2-9) and (11.12-2), by

$$E_x = \begin{cases} \frac{\beta}{\omega \epsilon_0} \frac{C}{n_1^2} e^{-qx} e^{i(\omega t - \beta z)}, & x \geq 0, \\ \frac{\beta}{\omega \epsilon_0} \frac{C}{n_3^2} e^{px} e^{i(\omega t - \beta z)}, & x \leq 0, \end{cases} \quad (11.12-7)$$

and

$$E_z = \begin{cases} \frac{iq}{\omega \epsilon_0} \frac{C}{n_1^2} e^{-qx} e^{i(\omega t - \beta z)}, & x \geq 0, \\ -\frac{ip}{\omega \epsilon_0} \frac{C}{n_3^2} e^{px} e^{i(\omega t - \beta z)}, & x \leq 0. \end{cases} \quad (11.12-8)$$

We note that the electric-field vector \mathbf{E} is elliptically polarized in the xz plane with the principal axes of the ellipses parallel to the coordinate axes. For propagation in the $+z$ direction ($\beta > 0$), the \mathbf{E} vector is right-hand elliptically polarized in the upper half space $x \geq 0$ and left-hand elliptically polarized in the lower half space $x \leq 0$. The ellipticities are β/q and $-\beta/p$ for the upper and the lower half space, respectively (see Fig. 11.33).

The normalization constant C is chosen so that the surface mode represented by Eqs. (11.12-2), (11.12-7), and (11.12-8) carries 1 W per unit width in the y direction. Using Eqs. (11.2-12) and (11.12-2), we obtain

$$C^2 = \frac{4\omega \epsilon_0}{\beta} \left(\frac{1}{qn_1^2} + \frac{1}{pn_3^2} \right)^{-1}. \quad (11.12-9)$$

11.12.1. Attenuation Coefficient

In the above derivation we assumed that both n_1^2 and n_3^2 are real numbers. In the case of an air-silver interface, for example, $n_1^2 = 1$ for air and n_3^2 has a small imaginary part for silver. In fact, for most metals, the dielectric constants $\epsilon_0 n^2$ are complex numbers in the optical frequency regions. Surface wave propagation at the interface between a metal and a dielectric medium suffers ohmic losses. The propagation therefore attenuates in the z -direction. This corresponds to a complex propagation constant

$$\beta = \beta^{(0)} - i\frac{1}{2}\alpha, \quad (11.12-10)$$

where α is the power attenuation coefficient (11.10-2), and $\beta^{(0)}$ is the real part of the propagation constant. The expression for the propagation constant β derived above [Eq. (11.12-4)] is in fact valid also when n_1^2 and n_3^2 are complex. We can thus obtain the attenuation coefficient α directly from Eq. (11.12-4); it is complex if n_1^2 and n_3^2 are complex. In the case of a dielectric-metal interface, n_1^2 is a real positive number and n_3^2 is a complex number $(n - i\kappa)^2$. The propagation constant of the surface wave is thus given, according to Eq. (11.12-4), by

$$\beta = \left[\frac{n_1^2 (n - i\kappa)^2}{n_1^2 + (n - i\kappa)^2} \right]^{1/2} \frac{\omega}{c}, \quad (11.12-11)$$

where κ is the extinction coefficient of the metal. In the spectral regimes of interest, $n \ll \kappa$. This corresponds to a small imaginary part of n_3^2 , since $n_3^2 = (n^2 - \kappa^2) - 2in\kappa$. In this case the propagation constant β can be written approximately as

$$\beta = \beta^{(0)} \left[1 - \frac{in\kappa n_1^2}{(n^2 - \kappa^2)(n_1^2 + n^2 - \kappa^2)} \right], \quad (11.12-12)$$

where

$$\beta^{(0)} = \left[\frac{n_1^2 (n^2 - \kappa^2)}{n_1^2 + (n^2 - \kappa^2)} \right]^{1/2} \frac{\omega}{c}. \quad (11.12-13)$$

Thus, the attenuation coefficient α can be written, according to Eqs. (11.12-10), (11.12-12), and (11.12-13),

$$\alpha = \frac{2n\kappa n_1^3}{\left[(n^2 - \kappa^2)(n_1^2 + n^2 - \kappa^2)^3 \right]^{1/2}} \frac{\omega}{c} \quad (11.12-14)$$

In the expressions (11.12-12) through (11.12-14) we keep factor $n^2 - \kappa^2$ because it is proportional to the real part of the dielectric constant of the metal. Thus in terms of the dielectric constants

$$\begin{aligned} \epsilon_1 &= \epsilon_0 n_1^2, \\ \epsilon_R - i\epsilon_I &= (n^2 - \kappa^2) - i2n\kappa, \end{aligned} \quad (11.12-15)$$

the propagation constant and the attenuation constant can be written, respectively, as

$$\beta^{(0)} = \left(\frac{\epsilon_1 \epsilon_R}{\epsilon_1 + \epsilon_R} \right)^{1/2} \frac{\omega}{c} \quad (11.12-16)$$

and

$$\alpha = \frac{\epsilon_I \epsilon_1^{3/2}}{[\epsilon_R (\epsilon_1 + \epsilon_R)^3]^{1/2}} \frac{\omega}{c}, \quad (11.12-17)$$

where ϵ_1 is the dielectric constant of the dielectric medium, and $\epsilon_R - i\epsilon_I$ is the complex dielectric constant of the metal. Note that $\epsilon_1 > 0$, $\epsilon_R < 0$, and $\epsilon_1 + \epsilon_R < 0$. ϵ_I is always greater than zero.

The attenuation coefficient can also be obtained from the ohmic-loss calculation and can be written [similarly to Eq. (11.10-10)] as

$$\alpha = \frac{1}{2} \int_{-\infty}^0 \sigma |\mathbf{E}|^2 dx, \quad (11.12-18)$$

where σ is the conductivity and is related to the complex dielectric constant by

$$\sigma = 2\omega\epsilon_0 n\kappa = \omega\epsilon_0 \epsilon_I. \quad (11.12-19)$$

Using the expressions (11.12-7) and (11.12-8) for the field \mathbf{E} , together with Eqs. (11.12-4) and (11.12-6), and carrying out the simple integration (11.12-18), we arrive at the same expression (11.12-14) for the attenuation coefficient α .

11.12.2. Example: Surface Waves at an Air–Silver Interface

At $\lambda = 6328 \text{ \AA}$ the complex refractive index of silver is $n - i\kappa = 0.067 - i4.05$. The surface mode at the interface between air and silver has a propagation constant, according to Eq. (11.12-13), of

$$\beta = 1.032 \frac{\omega}{c} = 10.25 \mu\text{m}^{-1}$$

and an attenuation coefficient, according to (11.12-14), of

$$\alpha = 0.0022 \frac{\omega}{c} = 220 \text{ cm}^{-1}.$$

The field attenuation constants p and q are

$$p = 4.18 \frac{\omega}{c} = \frac{26.26}{\lambda},$$

$$q = 0.25 \frac{\omega}{c} = \frac{1.60}{\lambda}.$$

Note that the field amplitude decreases to $e^{-26.26} = 4 \times 10^{-12}$ at a depth of $\lambda = 6328 \text{ \AA}$ in the silver. Thus the wave is essentially propagating in the air, while guided by the surface of the silver. This is also reflected in the phase velocity of the surface wave, which is $c/1.032$ and is very close to the velocity of light in air.

At $\lambda = 10 \text{ \mu m}$, $n - i\kappa = 10.8 - i60.7$ for silver, and the attenuation coefficient α becomes

$$\alpha = 0.6 \text{ cm}^{-1}.$$

If we put $n_1^2 = 1$ and neglect n^2 in the denominator in Eq. (11.12-14) since $n^2 \ll \kappa^2$, the attenuation coefficient α can be written

$$\alpha = \frac{4\pi n}{\kappa^3 \lambda}. \quad (11.12-20)$$

We note that α decreases as κ^{-3} . For metals like silver, gold, aluminum, and copper, the extinction coefficient κ becomes very large. Thus, according to Eq. (11.12-20), the attenuation coefficient α for the surface waves is expected to be smaller for these metals in the infrared spectral regimes.

PROBLEMS

11.1. *Lorentz reciprocity theorem.* Let $(\mathbf{E}_1, \mathbf{H}_1)$ and $(\mathbf{E}_2, \mathbf{H}_2)$ be two independent solutions of Maxwell's equations (11.1-1) and (11.1-2). Show that

$$\nabla \cdot (\mathbf{E}_1 \times \mathbf{H}_2 - \mathbf{E}_2 \times \mathbf{H}_1) = 0$$

provided ϵ and μ are Hermitian tensors (i.e., the medium is lossless).

11.2. *Mirror transform of a confined mode.* The dielectric waveguide structure with an index profile $n^2(x, y)$ is mirror-symmetric with respect to the plane $z = 0$.

(a) Let $\mathbf{E}_2, \mathbf{H}_2$ be the field vectors of a wave; show that the mirror-transformed field $\mathbf{E}'_2, \mathbf{H}'_2$ is given by Eq. (11.1-13).

(b) Show that

$$\frac{1}{2} \operatorname{Re}[\mathbf{E}'_2 \times \mathbf{H}'_2^*] \cdot \mathbf{a}_z = -\frac{1}{2} \operatorname{Re}[\mathbf{E}_2 \times \mathbf{H}_2^*] \cdot \mathbf{a}_z.$$

11.3. *Orthonormality relation for TE modes.* Let $(\mathbf{E}_l, \mathbf{H}_l)$ and $(\mathbf{E}_m, \mathbf{H}_m)$ be two arbitrary modes of the forms (11.1-3a) and (11.1-4b), and let I_{lm} be the integral

$$I_{lm} = \frac{1}{2} \iint (\mathbf{E}_l \times \mathbf{H}_m^*) \cdot \mathbf{a}_z da = \delta_{lm}.$$

(a) Show that

$$I_{lm} = \frac{\beta_m}{2\omega\mu} \iint \mathbf{E}_l \cdot \mathbf{E}_m^* da + \frac{i}{2\omega\mu} \iint (\mathbf{E}_l \cdot \nabla) E_{mz}^* da$$

by using Maxwell's equations (11.1-1) and (11.1-2) and $\nabla = \nabla_t + \mathbf{a}_z \partial/\partial z$. This shows that for TE waves with $E_z = 0$, the orthonormality relation (11.1-17) reduces to Eq. (11.1-18).

(b) Show, from (a) and integration by parts, that

$$2\delta_{lm} = I_{lm} + I_{ml}^* = \frac{\beta_l + \beta_m}{2\omega\mu} \iint \mathbf{E}_l \cdot \mathbf{E}_m^* da + \frac{i}{2\omega\mu} \iint (E_{lz} \nabla \cdot \mathbf{E}_m^* - E_{mz}^* \nabla \cdot \mathbf{E}_l) da.$$

Thus, either $\nabla \cdot \mathbf{E} = 0$ or $\mathbf{a}_z \cdot \mathbf{E} = 0$ is sufficient for the reduction of the orthonormality relations from Eq. (11.1-17) to Eq. (11.1-18).

(c) The wave equation (11.1-4) is valid provided $\nabla \cdot \mathbf{E} = 0$. Derive the orthogonality relation (11.1-18) directly from Eq. (11.1-4).

11.4. *Orthonormality relation for TM waves.* Follow the procedures in Problem 11.3 and use the same definition for I_{lm} .

(a) Show that

$$I_{lm} = \frac{\beta_m}{2\omega} \iint \mathbf{H}_l \cdot \frac{1}{\epsilon} \mathbf{H}_m^* da + \iint \frac{i}{2\omega\epsilon} (\mathbf{H}_l \cdot \nabla) H_{mz}^* da.$$

Thus for TM waves ($H_z = 0$), the orthonormality relation (11.1-17) reduces to Eq. (11.1-18).

- (b) Derive a relation similar to that of Problem 11.3(b). Show that $\mathbf{H} \cdot \nabla \epsilon = 0$ or $\mathbf{a}_z \cdot \mathbf{H} = 0$ is sufficient for the orthonormality relation (11.1-19).

11.5. *Mode confinement factor.* Let Γ_i be the fraction of power flowing in medium i ($i = 1, 2, 3$). In particular, Γ_2 is the fraction of mode power flowing in the guiding layer n_2 and is often called the mode confinement factor. If the mode is normalized to a power of 1 W, the Γ_i 's are defined as

$$\Gamma_i = \frac{1}{2} \operatorname{Re} \int_i (\mathbf{E} \times \mathbf{H}^*) \cdot \mathbf{a}_z dx, \quad i = 1, 2, 3,$$

where the integral is over the region occupied by medium i .

- (a) Show that for TE modes

$$\Gamma_1 = \frac{\frac{1}{q}}{t + \frac{1}{q} + \frac{1}{p}} \cdot \frac{h^2}{h^2 + q^2},$$

$$\Gamma_2 = \frac{t}{t + \frac{1}{q} + \frac{1}{p}} + \frac{\frac{1}{p}}{t + \frac{1}{q} + \frac{1}{p}} \cdot \frac{p^2}{h^2 + p^2}$$

$$+ \frac{\frac{1}{q}}{t + \frac{1}{q} + \frac{1}{p}} \cdot \frac{q^2}{h^2 + q^2},$$

$$\Gamma_3 = \frac{\frac{1}{p}}{t + \frac{1}{q} + \frac{1}{p}} \cdot \frac{h^2}{h^2 + p^2}.$$

[Note that $\Gamma_1 + \Gamma_2 + \Gamma_3 = 1$. This proves Eq. (11.2-7).]

(b) Show that for TM modes

$$\Gamma_1 = \frac{\frac{1}{q'}}{t' + \frac{1}{q'} + \frac{1}{p'}} \cdot \frac{h^2}{h^2 + q^2},$$

$$\Gamma_2 = \frac{t'}{t' + \frac{1}{q'} + \frac{1}{p'}} + \frac{\frac{1}{q'}}{t' + \frac{1}{q'} + \frac{1}{p'}} \cdot \frac{q^2}{h^2 + q^2}$$

$$+ \frac{\frac{1}{p'}}{t' + \frac{1}{q'} + \frac{1}{p'}} \cdot \frac{p^2}{h^2 + p^2},$$

$$\Gamma_3 = \frac{\frac{1}{p'}}{t' + \frac{1}{q'} + \frac{1}{p'}} \cdot \frac{h^2}{h^2 + p^2},$$

where

$$t' = \frac{t}{n_2^2},$$

$$\frac{1}{q'} = \frac{q^2 + h^2}{\bar{q}^2 + h^2} \cdot \frac{1}{n_1^2 q},$$

$$\frac{1}{p'} = \frac{p^2 + h^2}{\bar{p}^2 + h^2} \cdot \frac{1}{n_3^2 p}.$$

(c) Show that Γ_2 increases as β increases, and

$$\lim_{\beta \rightarrow n_2 k_0} \Gamma_2 = 1.$$

Thus, lower-order modes are more confined than higher-order modes, because lower-order modes have larger propagation

constants. [Hint: Use $h^2 + p^2 = (n_2^2 - n_3^2)k_0^2$ and $h^2 + q^2 = (n_2^2 - n_1^2)k_0^2$.]

- (d) Compare the mode confinement factor Γ_2 for TE_m and TM_m modes.
- (e) Show that in the limit of good confinement (i.e., $h \rightarrow 0$),

$$\frac{\Gamma_3^{TM}}{\Gamma_3^{TE}} = \frac{1 + \frac{p}{q} + pt}{1 + \frac{n_1^2}{n_3^2} \frac{p}{q} + \frac{n_2^2}{n_3^2} pt},$$

where $p = k_0(n_2^2 - n_3^2)^{1/2}$, $q = k_0(n_2^2 - n_1^2)^{1/2}$.

- (f) Show that for metal-clad waveguide ($n_3^2 < 0$),

$$\Gamma_3^{TM} > \Gamma_3^{TE}.$$

In other words, TM modes penetrate more into the metal than TE modes and are thus more lossy.

- 11.6. *Perturbed dielectric slab waveguide.* Let the dielectric perturbation to a slab waveguide be

$$\Delta n^2(x) = \begin{cases} \Delta n_1^2, & 0 \leq x, \\ \Delta n_2^2, & -t \leq x \leq 0, \\ \Delta n_3^2, & x \leq -t, \end{cases}$$

where Δn_1^2 , Δn_2^2 , and Δn_3^2 are constants (can be complex to include gain or loss).

- (a) Show that the correction to the propagation constant is

$$\delta\beta_m^2 = \left(\frac{\omega}{c}\right)^2 (\Gamma_1 \Delta n_1^2 + \Gamma_2 \Delta n_2^2 + \Gamma_3 \Delta n_3^2),$$

where

$$\Gamma_i = \frac{\int \mathcal{E}_m^* \cdot \mathcal{E}_m dx}{\int \mathcal{E}_m^* \cdot \mathcal{E}_m dx}, \quad i = 1, 2, 3,$$

with the integration \int_i performed over the medium i . These Γ 's represent the fraction of power flowing in the corresponding medium.

- (b) For a slab waveguide with a fixed thickness t , the propagation constants β_m^2 may be considered as functions of n_1^2 , n_2^2 , and n_3^2 . Thus $\delta\beta_m^2$ can be written

$$\delta\beta_m^2 = \frac{\partial\beta_m^2}{\partial n_1^2} \Delta n_1^2 + \frac{\partial\beta_m^2}{\partial n_2^2} \Delta n_2^2 + \frac{\partial\beta_m^2}{\partial n_3^2} \Delta n_3^2.$$

The function $\beta_m^2 = \beta_m^2(n_1^2, n_2^2, n_3^2)$ is given implicitly in the mode condition (11.2-5), (11.2-11). Show directly from Eq. (11.2-5) that

$$\frac{\partial\beta_m^2}{\partial n_i^2} = \left(\frac{\omega}{c}\right)^2 \Gamma_i, \quad i = 1, 2, 3.$$

- 11.7. Let the new mode of propagation be written

$$\mathcal{E}'_m = \mathcal{E}_m + a_{mm}\mathcal{E}_m + \delta\mathcal{E}_m,$$

where $a_{mm}\mathcal{E}_m$ is taken out of the expansion $\delta\mathcal{E}_m$ so that $\delta\mathcal{E}_m$ is now orthogonal to \mathcal{E}_m . If \mathcal{E}'_m is to be normalized as

$$\int \mathcal{E}'_m{}^* \cdot \mathcal{E}'_m dx dy = \frac{2\omega\mu}{\beta'_m},$$

where

$$\beta'_m{}^2 = \beta_m^2 + \delta\beta_m^2,$$

show that a_{mm} is given by

$$a_{mm} = -\frac{1}{4} \frac{\delta\beta_m^2}{\beta_m^2} = -\frac{1}{2} \frac{\delta\beta_m}{\beta_m}.$$

- 11.8. The transmission of a TE \leftrightarrow TM converter via periodic electro-optic interaction is given by Eqs. (6.5-19) and (6.5-20).

- (a) Show that half-maximum transmission occurs when

$$\Delta\beta L = 0.8\pi,$$

where $\Delta\beta$ is given by Eq. (11.7-6).

- (b) Show that the full width at half maximum in wavelengths, assuming no modal dispersion, is given by

$$\frac{\Delta\lambda_{1/2}}{\lambda_0} = \frac{0.8}{N}$$

- (c) Show that if the modal dispersion is included, the fractional bandwidth becomes

$$\frac{\Delta\lambda_{1/2}}{\lambda_0} = \frac{0.80}{N} \left| 1 - \frac{\lambda}{\Delta n} \frac{\partial \Delta n}{\partial \lambda} \right|^{-1},$$

where $\Delta n = n^{\text{TE}} - n^{\text{TM}}$.

11.9. *Surface plasmons.*

- (a) If the metal is viewed as a semiinfinite free-electron gas with a dielectric constant given by

$$\epsilon = \epsilon_0 \left(1 - \frac{\omega_p^2}{\omega^2} \right),$$

where ω_p is the plasma frequency, show that surface-plasmon modes exist only when

$$\omega^2 < \frac{1}{2}\omega_p^2.$$

Here we assume that $n_1^2 = 1$.

- (b) Show for the propagation constant β derived in Eq. (11.12-4) that

$$\beta > n_1 k_0,$$

provided $n_1^2 > 0$ and $n_1^2 + n_3^2 < 0$. Here $k_0 = \omega/c$.

- (c) Show that

$$\beta^2 = pq$$

and that the polarization states of the \mathbf{E} vector in the two media are mutually orthogonal.

- (d) Obtain an expression for the z component of the Poynting vector. Show that the Poynting power flows in the positive and

in the negative dielectric medium are opposite in direction. Thus a surface plasmon wave propagating along the silver surface along the $+z$ direction will have a negative Poynting power flow in the silver and a positive flow in the air.

- (e) The complex refractive index of gold at $\lambda = 10 \mu\text{m}$ is $n - i\kappa = 7.4 - i53.4$. Find the propagation constant $\beta^{(0)}$ and the attenuation coefficient α of the surface plasmon wave.

REFERENCES

1. P. K. Tien, R. Ulrich, and R. J. Martin, "Modes of propagating light in thin deposited semiconductor films," *Appl. Phys. Lett.* **14**, 291 (1969).
2. A. Yariv, "Coupled mode theory for guided wave optics," *IEEE J. Quant. Electron.* **9**, 919 (1973).
3. L. Kuhn, M. L. Dakss, P. F. Heidrich, and B. A. Scott, "Deflection of optical guided waves by a surface acoustic wave," *Appl. Phys. Lett.* **17**, 165 (1970).
4. R. C. Alferness, "Electro-optic waveguide TE \leftrightarrow TM mode converter with low drive voltage," *Opt. Lett.* **5**, 473 (1980).
5. R. C. Alferness, "Efficient waveguide electro-optic TE \leftrightarrow TM mode converter/waveguide filter," *Appl. Phys. Lett.* **36**, 513 (1980).
6. R. W. Dixon, "The photoelastic properties of selected materials and their relevance to acoustic light modulators and scanners," *J. Appl. Phys.* **38**, 5149 (1967).
7. H. Stoll and A. Yariv, "Coupled mode analysis of periodic dielectric waveguides," *Opt. Commun.* **8**, 5 (1973).
8. D. C. Flanders, H. Kogelnik, R. V. Schmidt, and C. V. Shank, "Grating filters for thin film optical waveguides," *Appl. Phys. Lett.* **24**, 194 (1974).
9. H. Kogelnik and C. V. Shank, "Coupled wave theory of distributed feedback lasers," *J. Appl. Phys.* **43**, 2328 (1972).
10. M. Nakamura, A. Yariv, H. W. Yen, S. Somekh, and H. L. Garvin, "Optically pumped GaAs surface laser with corrugation feedback," *Appl. Phys. Lett.* **22**, 515 (1973).
11. K. Aiki, M. Nakamura, J. Umeda, A. Yariv, A. Katzir, and H. W. Yen, "GaAs-GaAlAs distributed feedback laser with separate optical and carrier confinement," *Appl. Phys. Lett.* **27**, 145 (1975).
12. S. Somekh, Ph.D. Thesis, California Institute of Technology, 1973.
13. E. A. J. Marcatili, "Dielectric rectangular waveguides and directional couplers for integrated optics," *Bell Syst. Tech. J.* **48**, 2071 (1969).
14. S. Somekh, E. Garmire, A. Yariv, H. L. Garvin, and R. G. Hunsperger, "Channel optical waveguide directional couplers," *Appl. Phys. Lett.* **22**, 46 (1973).
15. J. C. Campbell, F. A. Blum, D. W. Shaw, and K. L. Lawley, "GaAs directional coupler switch," *Appl. Phys. Lett.* **27**, 202 (1975).
16. H. Kogelnik and R. V. Schmidt, "Switched directional couplers with alternating $\Delta\beta$," *IEEE J. Quant. Electron.* **QE-12**, 396 (1976).

17. R. V. Schmidt and H. Kogelnik, "Electro-optically switched coupler with stepped $\Delta\beta$ reversal coupler using Ti-diffused LiNbO₃ waveguide," *Appl. Phys. Lett.* **28**, 503 (1976).
18. A. C. Livanos, A. Katzir, A. Yariv, and C. S. Hong, "Chirped-grating demultiplexers in dielectric waveguides," *Appl. Phys. Lett.* **30**, 519 (1977).
19. A. Katzir, A. C. Livanos, J. B. Shellan, and A. Yariv, "Chirped gratings in integrated optics," *IEEE J. Quant. Electron.* **QE-13**, 296 (1977).
20. S. E. Miller, "Some theory and applications of periodically coupled waves," *Bell Syst. Tech. J.* **48**, 2189 (1969).
21. P. Yeh and H. F. Taylor, "Contradirectional frequency-selective couplers for guided-wave optics," *Appl. Opt.* **19**, 2848 (1980).
22. P. K. Tien, "Integrated optics and new wave phenomena," *Rev. Mod. Phys.* **49**, 361 (1977).
23. P. K. Tien, R. J. Martin, and S. Riva-Sanseverino, "Novel metal-clad optical components and method of forming high-index substrate for forming integrated optical circuits," *Appl. Phys. Lett.* **27**, 251 (1975).
24. P. Yeh and A. Yariv, "Bragg reflection waveguides," *Opt. Commun.* **19**, 427 (1976).
25. A. Y. Cho, A. Yariv, and P. Yeh, "Observation of confined propagation in Bragg waveguides," *Appl. Phys. Lett.* **30**, 471 (1977).
26. E. A. J. Marcatili and R. A. Schmeltzer, "Hollow metallic and dielectric waveguides for long distance optical transmission and lasers," *Bell. Syst. Tech. J.* **43**, 1783 (1974).
27. H. Steffen and F. K. Kneubuhl, "Dielectric tube resonators for infrared and submillimeter-wave lasers," *Phys. Lett.* **27A**, 612 (1968).
28. P. W. Smith, "A waveguide gas laser," *Appl. Phys. Lett.* **19**, 132 (1971).
29. T. J. Bridges, E. G. Burkhardt, and P. W. Smith, "CO₂ waveguide lasers," *Appl. Phys. Lett.* **20**, 403 (1972).
30. R. L. Abrams and W. B. Bridges, "Characteristics of sealed-off CO₂ waveguide lasers," *IEEE J. Quant. Electron.* **9**, 940 (1973).
31. D. B. Hall and C. Yeh, "Leaky waves in heteroepitaxial films," *J. Appl. Phys.* **44**, 2271 (1973).
32. D. Hall, A. Yariv, and E. Garmire, "Optical guiding and electro-optic modulation in GaAs epitaxial layers," *Opt. Commun.* **1**, 403 (1970).

Supplemental References

1. D. Marcuse, Ed., *Integrated Optics*, IEEE Press, New York, 1972 (a collection of reprints up to 1972 in integrated optics).
2. P. K. Tien, "Light waves in thin films and integrated optics," *Appl. Opt.* **10**, 2395 (1971).
3. E. Tamir, Ed., *Integrated Optics* Springer-Verlag, Berlin, 1975.
4. P. K. Tien, "Integrated optics and new wave phenomena in optical waveguides," *Rev. Mod. Phys.* **49**, 361 (1977).

12

Nonlinear Optics

12.1. INTRODUCTION

In this chapter and in the one following we consider some phenomena and applications which go under the name of nonlinear optics. This is the branch of optics which takes advantage of the nonlinear response of atoms and molecules to optical radiation fields.

In any real atomic system, polarization induced in the medium is not proportional to the optical electric field, but can be expressed in a Taylor series expansion as

$$P_i = \epsilon_0 \chi_{ij} E_j + 2d_{ijk} E_j E_k + 4\chi_{ijkl} E_j E_k E_l + \dots, \quad (12.1-1)$$

where P_i is the i th component of the instantaneous polarization and E_i is the i th component of the instantaneous field. Summations over repeated indices are assumed. χ_{ij} is the linear susceptibility, while d_{ijk} and χ_{ijkl} are the second-order and third-order nonlinear optical susceptibilities, respectively. In writing the response in the form (12.1-1), it is assumed that the system is lossless, so that the response is instantaneous. In that case it can be shown that the coefficients χ_{ij} , d_{ijk} , χ_{ijkl} are invariant under any reshuffling of their subscripts; for example, $\chi_{1231} = \chi_{2113}$.

The nonlinear optical response characterized by the parameters d_{ijk} and χ_{ijkl} gives rise to numerous interesting phenomena and applications. The second-order nonlinearity $P_i = 2d_{ijk} E_j E_k$ is responsible for second-harmonic generation [1] (frequency doubling), for sum- and difference-frequency generation, and for parametric amplification and oscillation. The third-order term $P_i = 4\chi_{ijkl} E_j E_k E_l$ figures in such diverse phenomena as third-harmonic generation [2], Raman and Brillouin scattering [3], self-focusing, and optical phase conjugation (see Chapter 13). In this chapter we will settle for a basic description of second-harmonic generation and of parametric amplification and oscillation (both second-order, nonlinear phenomena).

We will not concern ourselves in this chapter with the physical origins of the nonlinear coefficients d_{ijk} and χ_{ijkl} . We will take them as material parameters and merely explore the electromagnetic phenomena and applications made possible by nonlinearities. The reader interested in the basic physics can start with [4–7].

12.2. SECOND-ORDER NONLINEAR PHENOMENA — GENERAL METHODOLOGY

Consider the nonlinear coupling of two optical fields. The first, described in terms of its electric-field components, is given by

$$E_j^{\omega_1}(t) = \text{Re}(E_j^{\omega_1} e^{i\omega_1 t}) = \frac{1}{2}(E_j^{\omega_1} e^{i\omega_1 t} + \text{c.c.}) \quad (j = x, y, z), \quad (12.2-1)$$

while the second field at ω_2 is

$$E_k^{\omega_2}(t) = \text{Re}(E_k^{\omega_2} e^{i\omega_2 t}) \quad (k = x, y, z). \quad (12.2-2)$$

If the medium is nonlinear, then the presence of these field components can give rise to polarizations at frequencies $n\omega_1 + m\omega_2$, where n and m are any integers. Taking the polarization component at $\omega_3 = \omega_1 + \omega_2$ along the i direction as

$$P_i^{\omega_3 = \omega_1 + \omega_2}(t) = \text{Re}(P_i^{\omega_3} e^{i\omega_3 t}) \quad (12.2-3)$$

and limiting our attention to the second-order terms in Eq. (12.1-1)—that is,

$$P_i = 2d_{ijk} E_j E_k \quad (12.2-4)$$

—we obtain

$$\begin{aligned} P_i(t) &= 2d_{ijk} \left(\frac{1}{2} E_j^{\omega_1} e^{i\omega_1 t} + \frac{1}{2} E_j^{\omega_2} e^{i\omega_2 t} + \text{c.c.} \right) \\ &\quad \times \left(\frac{1}{2} E_k^{\omega_1} e^{i\omega_1 t} + \frac{1}{2} E_k^{\omega_2} e^{i\omega_2 t} + \text{c.c.} \right). \end{aligned} \quad (12.2-5)$$

Consider only the sum-frequency term

$$P_i^{\omega_1 + \omega_2}(t) = \frac{1}{2} \left[d_{ijk} E_j^{\omega_1} E_k^{\omega_2} e^{i(\omega_1 + \omega_2)t} + d_{ikj} E_k^{\omega_2} E_j^{\omega_1} e^{i(\omega_2 + \omega_1)t} + \text{c.c.} \right], \quad (12.2-6)$$

where we recall the convention of summation over repeated indices. In a lossless (instantaneous response) system, $d_{ikj} = d_{ijk}$ [8], so that

$$\begin{aligned} P_i^{\omega_1+\omega_2}(t) &= \frac{1}{2} P_i^{\omega_3-\omega_1+\omega_2} e^{i(\omega_1+\omega_2)t} + \text{c.c.} \\ &= d_{ijk} E_j^{\omega_1} E_k^{\omega_2} e^{i(\omega_1+\omega_2)t} + \text{c.c.}, \end{aligned}$$

or

$$P_i^{\omega_3-\omega_1+\omega_2} = 2d_{ijk} E_j^{\omega_1} E_k^{\omega_2}. \quad (12.2-7)$$

In lossy and consequently dispersive systems d_{ijk} will in general depend on ω_1 and ω_2 and whether the sum or their difference is considered. We may thus in general define the nonlinearity not in terms of the instantaneous optical fields as in Eq. (12.1-1), but in terms of their complex amplitudes

$$P_i^{\omega_3-\omega_1+\omega_2} = 2d_{ijk}(-\omega_3, \omega_1, \omega_2) E_j^{\omega_1} E_k^{\omega_2} \quad (12.2-8a)$$

and

$$P_i^{\omega_3-\omega_1-\omega_2} = 2d_{ijk}(-\omega_3, \omega_1, -\omega_2) E_j^{\omega_1} (E_k^{\omega_2})^*, \quad (12.2-8b)$$

where $d_{ijk}(-\omega_3, \omega_1, \omega_2)$ signifies that it is the coefficient relating the i th component of the complex amplitude $P_i^{\omega_3-\omega_1+\omega_2}$ to the product $E_j^{\omega_1} E_k^{\omega_2}$. Note that in general,

$$d_{ijk}(-\omega_3, \omega_1, \omega_2) \neq d_{ijk}(-\omega_3, \omega_2, \omega_1),$$

since the two coefficients relate to cases where the fields at ω_1 and ω_2 are along different directions, so that the resultant $P_i^{\omega_3-\omega_1+\omega_2}$ is not necessarily the same. On the other hand, we do have

$$d_{ijk}(-\omega_3, \omega_1, \omega_2) = d_{ikj}(-\omega_3, \omega_2, \omega_1). \quad (12.2-9)$$

Our primary interest will be in the case of transparent lossless crystals where the coefficients d_{ijk} do not depend on the frequencies involved or on whether their sum or difference is generated. In what follows we will drop all their frequency designations.

Only noncentrosymmetric crystals can possess a nonvanishing d_{ijk} tensor. This follows from the requirement that in a centrosymmetric crystal a reversal of the signs of $E_j^{\omega_1}$ and $E_k^{\omega_2}$ must cause a reversal in the sign of

$P_i^{\omega_3=\omega_1+\omega_2}$ and not affect the amplitude. Using Eq. (12.2-8), we get

$$-d_{ijk}E_j^{\omega_1}E_k^{\omega_2} = d_{ijk}(-E_j^{\omega_1})(-E_k^{\omega_2}),$$

so that $d_{ijk} \equiv 0$. Lack of inversion symmetry is also the prerequisite for linear electro-optic effect and piezoelectricity, so that all electro- and piezoelectric crystals can be expected to display second-order ($P \propto E^2$) nonlinear optical properties. The same argument can be used to show that all crystals as well as liquids and gases can display third-order optical nonlinearities.

The d_{ijk} coefficients are measured most often in second-harmonic-generation experiments where $\omega_1 = \omega_2 \equiv \omega$. In this case we have

$$P_i^{2\omega} = d_{ijk}E_j^\omega E_k^\omega. \quad (12.2-10)$$

Notice the factor-of-2 difference between Eqs. (12.2-10) and (12.2-8). This follows directly from Eq. (12.2-5). Since no physical significance can be attached to the interchange of j and k in Eq. (12.2-10), we can replace the subscripts kj and jk by the contracted indices according to Eq. (7.1-10):

$$xx = 1, \quad yy = 2, \quad zz = 3,$$

$$yz = zy = 4, \quad xz = zx = 5, \quad xy = yx = 6$$

The resulting d_{ij} components form a 3×6 matrix that operates on the E^2 column tensor to yield \mathbf{P} according to

$$\begin{pmatrix} P_x \\ P_y \\ P_z \end{pmatrix} = \begin{pmatrix} d_{11} & d_{12} & d_{13} & d_{14} & d_{15} & d_{16} \\ d_{21} & d_{22} & d_{23} & d_{24} & d_{25} & d_{26} \\ d_{31} & d_{32} & d_{33} & d_{34} & d_{35} & d_{36} \end{pmatrix} \begin{pmatrix} E_x^2 \\ E_y^2 \\ E_z^2 \\ 2E_z E_y \\ 2E_z E_x \\ 2E_x E_y \end{pmatrix}. \quad (12.2-11)$$

The contracted d_{ij} tensor obeys the same symmetry restrictions as the piezoelectric tensor and the electro-optic tensor, and in crystals of a given point-group symmetry it has the same form. The tensor forms are given in Table 12.1. In KH_2PO_4 (KDP), for example, which has a $\bar{4}2m$ point-group

Table 12.1. The Form of the Nonlinear Optical Tensor in Contracted Notation for all Crystal Classes

Centrosymmetric Classes					
Classes $\bar{1}$, $2/m$, mmm , $4/m$, $4mmm$, $\bar{3}$, $\bar{3}m$, $6/m$, $6mmm$, $m\bar{3}$, $m\bar{3}m$:					
$\begin{pmatrix} 0 & 0 & 0 & 0 & 0 & 0 \\ 0 & 0 & 0 & 0 & 0 & 0 \\ 0 & 0 & 0 & 0 & 0 & 0 \end{pmatrix}$					
Triclinic System					
Class 1— C_1 :					
$\begin{pmatrix} d_{11} & d_{12} & d_{13} & d_{14} & d_{15} & d_{16} \\ d_{21} & d_{22} & d_{23} & d_{24} & d_{25} & d_{26} \\ d_{31} & d_{32} & d_{33} & d_{34} & d_{35} & d_{36} \end{pmatrix}_{(18)}$					
Monoclinic System					
Class m — C_s :					
$m \perp x_3$	$\begin{pmatrix} d_{11} & d_{12} & d_{13} & 0 & 0 & d_{16} \\ d_{21} & d_{22} & d_{23} & 0 & 0 & d_{26} \\ 0 & 0 & 0 & d_{34} & d_{35} & 0 \end{pmatrix}_{(10)}$				
Class m — C_s :					
$m \perp x_2^a$	$\begin{pmatrix} d_{11} & d_{12} & d_{13} & 0 & d_{15} & 0 \\ 0 & 0 & 0 & d_{24} & 0 & d_{26} \\ d_{31} & d_{32} & d_{33} & 0 & d_{35} & 0 \end{pmatrix}_{(10)}$				
Class 2— C_2 :					
$2 \parallel x_3$	$\begin{pmatrix} 0 & 0 & 0 & d_{14} & d_{15} & 0 \\ 0 & 0 & 0 & d_{24} & d_{25} & 0 \\ d_{31} & d_{32} & d_{33} & 0 & 0 & d_{36} \end{pmatrix}_{(8)}$				
Class 2— C_2 :					
$2 \parallel x_2^a$	$\begin{pmatrix} 0 & 0 & 0 & d_{14} & 0 & d_{16} \\ d_{21} & d_{22} & d_{23} & 0 & d_{25} & 0 \\ 0 & 0 & 0 & d_{34} & 0 & d_{36} \end{pmatrix}_{(8)}$				
Orthorhombic System					
Class $mm2$ — C_{2v} :					
$\begin{pmatrix} 0 & 0 & 0 & 0 & d_{15} & 0 \\ 0 & 0 & 0 & d_{24} & 0 & 0 \\ d_{31} & d_{32} & d_{33} & 0 & 0 & 0 \end{pmatrix}_{(5)}$					
Class 222 — D_2 :					
$\begin{pmatrix} 0 & 0 & 0 & d_{14} & 0 & 0 \\ 0 & 0 & 0 & 0 & d_{25} & 0 \\ 0 & 0 & 0 & 0 & 0 & d_{36} \end{pmatrix}_{(3)}$					

Table 12.1. (Continued).

Tetragonal System

Class 4— C_4 :

$$\begin{pmatrix} 0 & 0 & 0 & d_{14} & d_{15} & 0 \\ 0 & 0 & 0 & d_{15} & -d_{14} & 0 \\ d_{31} & d_{31} & d_{33} & 0 & 0 & 0 \end{pmatrix}_{(4)}$$

Class $\bar{4}$ — S_4 :

$$\begin{pmatrix} 0 & 0 & 0 & d_{14} & d_{15} & 0 \\ 0 & 0 & 0 & -d_{15} & d_{14} & 0 \\ d_{31} & -d_{31} & 0 & 0 & 0 & d_{36} \end{pmatrix}_{(4)}$$

Class 4mm— C_{4v} :

$$\begin{pmatrix} 0 & 0 & 0 & 0 & d_{15} & 0 \\ 0 & 0 & 0 & d_{15} & 0 & 0 \\ d_{31} & d_{31} & d_{33} & 0 & 0 & 0 \end{pmatrix}_{(3)}$$

Class $\bar{4}2m$ — D_{2d} :

$$m \parallel x_1 \begin{pmatrix} 0 & 0 & 0 & d_{14} & 0 & 0 \\ 0 & 0 & 0 & 0 & d_{14} & 0 \\ 0 & 0 & 0 & 0 & 0 & d_{36} \end{pmatrix}_{(2)}$$

Class 422— D_4 :

$$\begin{pmatrix} 0 & 0 & 0 & d_{14} & 0 & 0 \\ 0 & 0 & 0 & 0 & -d_{14} & 0 \\ 0 & 0 & 0 & 0 & 0 & 0 \end{pmatrix}_{(1)}$$

Trigonal System

Class 3— C_3 :

$$\begin{pmatrix} d_{11} & -d_{11} & 0 & d_{14} & d_{15} & -d_{22} \\ -d_{22} & d_{22} & 0 & d_{15} & -d_{14} & -d_{11} \\ d_{31} & d_{31} & d_{33} & 0 & 0 & 0 \end{pmatrix}_{(6)}$$

Class 3m— C_{3v} :

$$m \perp x_1^a \begin{pmatrix} 0 & 0 & 0 & 0 & d_{15} & -d_{22} \\ -d_{22} & d_{22} & 0 & d_{15} & 0 & 0 \\ d_{31} & d_{31} & d_{33} & 0 & 0 & 0 \end{pmatrix}_{(4)}$$

Class 3m— C_{3v} :

$$m \perp x_2 \begin{pmatrix} d_{11} & -d_{11} & 0 & 0 & d_{15} & 0 \\ 0 & 0 & 0 & d_{15} & 0 & -d_{11} \\ d_{31} & d_{31} & d_{33} & 0 & 0 & 0 \end{pmatrix}_{(4)}$$

Table 12.1. (Continued).

Class 32— D_3 :

$$\begin{pmatrix} d_{11} & -d_{11} & 0 & d_{14} & 0 & 0 \\ 0 & 0 & 0 & 0 & -d_{14} & -d_{11} \\ 0 & 0 & 0 & 0 & 0 & 0 \end{pmatrix}_{(2)}$$

Hexagonal System

Class $\bar{6}$ — C_{3h} :

$$\begin{pmatrix} d_{11} & -d_{11} & 0 & 0 & 0 & -d_{22} \\ -d_{22} & d_{22} & 0 & 0 & 0 & -d_{11} \\ 0 & 0 & 0 & 0 & 0 & 0 \end{pmatrix}_{(2)}$$

Class 6— C_6 :^b

$$\begin{pmatrix} 0 & 0 & 0 & d_{14} & d_{15} & 0 \\ 0 & 0 & 0 & d_{15} & -d_{14} & 0 \\ d_{31} & d_{31} & d_{33} & 0 & 0 & 0 \end{pmatrix}_{(2)}$$

Class $\bar{6}m2$ — D_{3h} :

$$m \perp x_1^a \quad \begin{pmatrix} 0 & 0 & 0 & 0 & 0 & -d_{22} \\ -d_{22} & d_{22} & 0 & 0 & 0 & 0 \\ 0 & 0 & 0 & 0 & 0 & 0 \end{pmatrix}_{(1)}$$

Class $\bar{6}m2$ — D_{3h} :

$$m \perp x_2 \quad \begin{pmatrix} d_{11} & -d_{11} & 0 & 0 & 0 & 0 \\ 0 & 0 & 0 & 0 & 0 & -d_{11} \\ 0 & 0 & 0 & 0 & 0 & 0 \end{pmatrix}_{(1)}$$

Class 6mm— C_{6v} :

$$\begin{pmatrix} 0 & 0 & 0 & 0 & d_{15} & 0 \\ 0 & 0 & 0 & d_{15} & 0 & 0 \\ d_{31} & d_{31} & d_{33} & 0 & 0 & 0 \end{pmatrix}_{(3)}$$

Class 622— D_6 :

$$\begin{pmatrix} 0 & 0 & 0 & d_{14} & 0 & 0 \\ 0 & 0 & 0 & 0 & -d_{14} & 0 \\ 0 & 0 & 0 & 0 & 0 & 0 \end{pmatrix}_{(1)}$$

Cubic System

Class 23— T :

$$\begin{pmatrix} 0 & 0 & 0 & d_{14} & 0 & 0 \\ 0 & 0 & 0 & 0 & d_{14} & 0 \\ 0 & 0 & 0 & 0 & 0 & d_{14} \end{pmatrix}_{(1)}$$

Table 12.1. (Continued).

 Class $\bar{4}3m—T_d$:

$$\begin{pmatrix} 0 & 0 & 0 & d_{14} & 0 & 0 \\ 0 & 0 & 0 & 0 & d_{14} & 0 \\ 0 & 0 & 0 & 0 & 0 & d_{14} \end{pmatrix}_{(1)}$$

 Class 432— O :

$$\begin{pmatrix} 0 & 0 & 0 & 0 & 0 & 0 \\ 0 & 0 & 0 & 0 & 0 & 0 \\ 0 & 0 & 0 & 0 & 0 & 0 \end{pmatrix}_{(1)}$$

^aStandard orientation.

^bSame as class 4— C_4 .

 symmetry, the d_{ij} tensor is given by

$$d_{ij} = \begin{pmatrix} 0 & 0 & 0 & d_{14} & 0 & 0 \\ 0 & 0 & 0 & 0 & d_{14} & 0 \\ 0 & 0 & 0 & 0 & 0 & d_{36} \end{pmatrix} \quad (12.2-12)$$

and the components of the nonlinear polarization are

$$P_x = 2d_{14}E_zE_y,$$

$$P_y = 2d_{14}E_zE_x, \quad (12.2-13)$$

$$P_z = 2d_{36}E_xE_y.$$

A listing of some of the nonlinear coefficients of some important crystals is given in Table 12.2.

The nonlinear coefficients d_{ijk} defined in Eq. (12.1-1) gives rise to a linear electro-optic coefficients r_{ijk} according to †

$$d_{ijk} = -\frac{\epsilon_{ii}\epsilon_{jj}}{4\epsilon_0}r_{ijk}, \quad (12.2-14)$$

† The linear electro-optic effect may, in general, have contribution due to ionic motion which is not accounted by (12.2-14).

Table 12.2. The Nonlinear Optical Coefficients of a Number of Crystals [9]

Crystal	Point Group	λ (μm)	$d_{ijk}^{(2\omega)}$ ($\frac{1}{9} \times 10^{-22}$ MKS)	δ_{ijk} (10^9 MKS)
GaAs	$\bar{4}3m$	2.12	$d_{14} = 138$	$\delta_{14} = 1.9$
		10.6	107	
GaP	$\bar{4}3m$	1.064	$d_{14} = 80 \pm 14$	$\delta_{14} = 1.6$
		1.318	65	
		2.12	62	
		3.39	53	
		10.6	46	
GaSb	$\bar{4}3m$	10.6	$d_{14} = 311$	$\delta_{14} = 2.0$
InAs	$\bar{4}3m$	10.6	$d_{14} = 207$	$\delta_{14} = 2.3$
InSb	$\bar{4}3m$	28	$d_{14} = 462$	$\delta_{14} = 3.0$
β -ZnS	$\bar{4}3m$	10.6	$d_{14} = 24$	$\delta_{14} = 6.8$
ZnSe	$\bar{4}3m$	10.6	$d_{14} = 64$	$\delta_{14} = 9$
ZnTe	$\bar{4}3m$	10.6	$d_{14} = 72$	$\delta_{14} = 9$
CdTe	$\bar{4}3m$	28	$d_{14} = 48$	$\delta_{14} = 3.6$
CuBr	$\bar{4}3m$	1.064	$d_{14} = -8.29$	$\delta_{14} = -2.5$
		10.6	-6.2	
CuCl	$\bar{4}3m$	1.064	$d_{14} = -7.7$	$\delta_{14} = -3.7$
		10.6	$d_{14} = -5.3$	
CuI	$\bar{4}3m$	1.064	$d_{14} = -5.0$	$\delta_{14} = -0.7$
$\text{Bi}_4\text{Ge}_3\text{O}_{12}$	$\bar{4}3m$	1.064	$ d_{14} = 1.6$	$ \delta_{14} = 0.7$
CdSe	6mm	2.12	$d_{33} = 52$	$\delta_{33} = 5.7$
		10.6	44	
			$d_{31} = -23$	$\delta_{31} = -2.9$
			$ d_{15} = 25$	$ \delta_{15} = 3.2$
CdS	6mm	10.6	$d_{33} = 35$	$\delta_{33} = 8.0$
		1.06	80	
		10.6	$d_{31} = -21$	$\delta_{31} = -5.1$
			$ d_{15} = 23$	$ \delta_{15} = 5.5$
α -ZnS	6mm	10.6	$d_{33} = 29$	$\delta_{33} = 6.7$
			$d_{31} = -15$	$\delta_{31} = -3$
		1.06	$d_{33} = 35$	

Table 12.2. (Continued).

ZnO	6mm	1.06	$d_{33} = -7.2$ $d_{31} = 2.2$ $ d_{15} = 2.4$	$\delta_{33} = -4.5$ $\delta_{31} = 1.4$ $ \delta_{15} = 1.6$
BeO	6mm	1.064	$d_{33} = -0.26$ $d_{31} = -0.18$	$\delta_{33} = -0.52$ $\delta_{31} = -0.41$
SiC	6mm	1.064	$d_{33} = -18$ $d_{31} = 11$ $d_{15} = 10$	$\delta_{33} = -1.2$ $\delta_{31} = 0.85$ $\delta_{15} = 0.78$
AgI	6mm	1.318	$d_{33} = -21$ $d_{31} = 10$	$\delta_{33} = -7.1$ $\delta_{31} = 3.7$
GaSe	$\bar{6}m2$	10.6	$d_{22} = 64$	$\delta_{22} = 2.5$
LiIO ₃	6	1.064	$d_{31} = -5.7$ $d_{33} = -5.6$ $ d_{14} = 0.25$	$\delta_{31} = -7.3$ $\delta_{33} = -1.1$ $ \delta_{14} = 0.26$
LiKSO ₄	6	0.6943	$ d_{33} = 0.8$ $ d_{31} = 0.5$	
LiNbO ₃	3m	1.06	$d_{31} = -4.7$ $d_{33} = -27$ $d_{22} = 3.2$	$\delta_{31} = -1.1$ $\delta_{33} = -8.2$ $\delta_{22} = 0.72$
LiTaO ₃	3m	1.058	$d_{31} = -1.4$ $d_{33} = -21$ $d_{22} = 2.2$	$\delta_{31} = -0.44$ $\delta_{33} = -6.7$ $\delta_{22} = 0.73$
Ag ₃ SbS ₃ (pyrargyrite)	3m	10.6	$ d_{31} = 10.0$ $ d_{22} = 10.7$	$ \delta_{31} = 0.66$ $ \delta_{22} = 0.62$
Ag ₃ AsS ₃ (proustite)	3m	10.6	$ d_{31} = 14$	$ \delta_{31} = 1.0$
		10.6	$ d_{22} = 22$	$ \delta_{22} = 1.4$
Tourmaline	3m	1.06	$ d_{33} = 0.62$ $ d_{31} = 0.18$ $ d_{22} = 0.09$ $ d_{15} = 0.29$	$ \delta_{33} = 2.44$ $ \delta_{31} = 0.66$ $ \delta_{22} = 0.35$ $ \delta_{15} = 1.08$
α -Quartz (SiO ₂)	3m	1.064	$d_{11} = 0.4$ $d_{14} = -0.0036$	$\delta_{11} = 2.5$ $\delta_{14} = -0.02$
Te	3m	10.6	$ d_{11} = 733$	$ \delta_{11} = 1.1$
		28	$ d_{11} = 454$	

Table 12.2. (Continued).

Crystal	Point Group	λ (μm)	$d_{ijk}^{(2\omega)}$ ($\frac{1}{3} \times 10^{-22}$ MKS)	δ_{ijk} (10^9 MKS)
HgS	3m	10.6	$ d_{111} = 40$	$ \delta_{111} = 3.3$
		1.32	$ d_{111} = 56$	
Se	3m	10.6	$ d_{111} = 77$	$ \delta_{111} = 6$
AgGaSe ₂	$\bar{4}2\text{m}$	2.12	$ d_{36} = 54$	$ \delta_{36} = 4.0$
		10.6	$ d_{36} = 46$	
AgGaS ₂	$\bar{4}2\text{m}$	10.6	$d_{36} = 14$	$\delta_{36} = 3.0$
		1.064	$d_{36} = 23$	
AgInSe ₂	$\bar{4}2\text{m}$	10.6	$ d_{36} = 50$	$ \delta_{36} = 3.8$
CdGeAs ₂	$\bar{4}2\text{m}$	10.6	$ d_{36} = 280$	$ \delta_{36} = 2.9$
CdGeP ₂	$\bar{4}2\text{m}$	10.6	$ d_{36} = 129$	$ \delta_{36} = 2.8$
CuInS ₂	$\bar{4}2\text{m}$	10.6	$ d_{36} = 8.8$	$ \delta_{36} = 0.87$
CuGaS ₂	$\bar{4}2\text{m}$	10.6	$ d_{36} = 11 \pm 4$	$ \delta_{36} = 1.5$
CuGaSe ₂	$\bar{4}2\text{m}$	10.6	$ d_{36} = 35$	$ \delta_{36} = 2.3$
ZnSiAs ₂	$\bar{4}2\text{m}$	10.6	$ d_{36} = 87$	$ \delta_{36} = 1.8$
ZnGeP ₂	$\bar{4}2\text{m}$	10.6	$d_{14} = 88$	$\delta_{14} = 2.3$
KH ₂ PO ₄ (KDP)	$\bar{4}2\text{m}$	1.318	$d_{36} = 0.48$	$\delta_{36} = 4.5$
		0.6328	0.57	
		0.6943	0.56	
		1.06	0.50	
		1.15	0.49	
NH ₄ H ₂ PO ₄ (ADP)	$\bar{4}2\text{m}$	1.064	$ d_{36} = 0.61$	$ \delta_{36} = 5.1$
		0.6328	0.69	
		0.6943	0.68	
		1.318	0.57	
KD ₂ PO ₄	$\bar{4}2\text{m}$	0.6943	$ d_{36} = 0.42$	$ \delta_{36} = 3.8$
ND ₄ D ₂ PO ₄	$\bar{4}2\text{m}$	0.6943	$ d_{36} = 0.61$	$ \delta_{36} = 5.0 \pm 0.8$
RbH ₂ PO ₄	$\bar{4}2\text{m}$	1.0642	$ d_{36} = 0.4$	$ \delta_{36} = 3.4$
			$ d_{14} = 0.6$	$ \delta_{14} = 4.5$
		0.6943	$ d_{36} = 0.5$ $ d_{14} = 0.9$	
BaTiO ₃	4mm	1.058	$d_{33} = -7.03$	$\delta_{33} = -1.5$
			$d_{31} = -18$	$\delta_{31} = -3.4$
			$d_{15} = -18$	$\delta_{15} = -3.2$

Table 12.2. (Continued).

PbTiO ₃	4mm	1.064	$ d_{15} = 41.7 \pm 0.6$ $ d_{31} = 47.1 \pm 0.3$ $ d_{33} = 9.3 \pm 0.2$	$ \delta_{15} = 3.32$ $ \delta_{31} = 3.78$ $ d_{33} = 0.76$
Sr _{0.5} Ba _{0.5} Nb ₂ O ₆ (SBN)	4mm	1.064	$ d_{31} = 5.3 \pm 0.5$ $ d_{33} = 14.1$ $ d_{15} = 7.5$	$ \delta_{31} = 1.1$ $ \delta_{33} = 3.43$ $ \delta_{15} = 1.67$
TeO ₂	422	1.064	$ d_{14} = 0.50$	$ \delta_{14} = 0.10$
CdGa ₂ S ₄	$\bar{4}$	1.064	$ d_{36} = 32 \pm 0.2$	$\delta_{14} = 5.2 \pm 0.6$
InPS ₄	$\bar{4}$	1.064	$ d_{36} = 22 \pm 0.3$ $ d_{31} = 28 \pm 0.6$	$ \delta_{36} = 3.8$ $ \delta_{31} = 5.0$
Ba ₂ NaNb ₅ O ₁₅	4	1.064	$d_{31} = -16$ $d_{32} = -16$ $d_{33} = -22$ $d_{15} = -16$ $d_{24} = -15$	$\delta_{31} = -3.7$ $\delta_{32} = -3.7$ $\delta_{33} = -6.3$ $\delta_{15} = -3.7$ $\delta_{24} = -3.5$
KNbO ₃	4	1.064	$ d_{31} = 12$ $ d_{32} = 14$ $ d_{33} = 22$ $ d_{15} = 13$ $ d_{24} = 14$	$ \delta_{31} = 3.4$ $ \delta_{32} = 3.5$ $ \delta_{33} = 7.1$ $ \delta_{15} = 3.5$ $ \delta_{24} = 3.3$
Li(COOH) · H ₂ O	4	1.064	$ d_{31} = 0.12$ $d_{32} = -1.4$ $d_{33} = 2.1$	$ \delta_{31} = 2.0$ $\delta_{32} = -12$ $\delta_{33} = 16$
α -HIO ₃	222	1.064	$ d_{14} = 6.6$	$ \delta_{14} = 5.2$

where ijk are the principal coordinate subscripts. The proof of this relation is left for the student as an exercise (see Problem 12.1).

The third-order nonlinear susceptibility χ_{ijkl} is related to the quadratic electro-optic coefficients s_{ijkl} (7.1-2) by

$$\chi_{ijkl} = -\frac{\epsilon_{ii}\epsilon_{jj}}{12\epsilon_0} s_{ijkl}, \quad (12.2-15)$$

where the tensor components are again defined in the principal coordinate system (see Problem 12.2).

12.3. ELECTROMAGNETIC FORMULATION OF NONLINEAR INTERACTION

We start with Maxwell's equations in a form which includes the polarization \mathbf{P} explicitly:

$$\begin{aligned}\nabla \times \mathbf{H} &= \mathbf{J} + \frac{\partial \mathbf{D}}{\partial t} = \mathbf{J} + \frac{\partial}{\partial t}(\epsilon_0 \mathbf{E} + \mathbf{P}), \\ \nabla \times \mathbf{E} &= -\frac{\partial}{\partial t}(\mu_0 \mathbf{H}).\end{aligned}\tag{12.3-1}$$

The polarization \mathbf{P} is made up of a linear and a nonlinear term:

$$\mathbf{P} = \epsilon_0 \chi_L \mathbf{E} + \mathbf{P}_{NL},\tag{12.3-2}$$

where

$$(P_{NL})_i = 2d'_{ijk} E_j E_k,\tag{12.3-3}$$

and where the tensor aspect of χ_L is ignored.

The first of the equations (12.3-1) can be written as

$$\nabla \times \mathbf{H} = \sigma \mathbf{E} + \frac{\partial}{\partial t} \epsilon \mathbf{E} + \frac{\partial \mathbf{P}_{NL}}{\partial t}.\tag{12.3-4}$$

The primed designation d'_{ijk} is to remind us that i, j , and k , the Cartesian directions, are not necessarily the same as the crystal x, y, z axes, in which case d'_{ijk} is the transformed d_{ijk} . The symbol σ represents the conductivity (losses), and $\epsilon = \epsilon_0(1 + \chi_L)$. After taking the curl of both sides of the second of the equations (12.3-1), replacing $\nabla \times \mathbf{H}$ by Eq. (12.3-4), and using $\nabla \times \nabla \times \mathbf{E} = \nabla \nabla \cdot \mathbf{E} - \nabla^2 \mathbf{E}$, we get

$$\nabla^2 \mathbf{E} = \mu_0 \sigma \frac{\partial \mathbf{E}}{\partial t} + \mu_0 \epsilon \frac{\partial^2 \mathbf{E}}{\partial t^2} + \mu_0 \frac{\partial^2}{\partial t^2} \mathbf{P}_{NL},\tag{12.3-5}$$

where $\nabla \cdot \mathbf{E} = 0$.

At this point we specialize the problem to one dimension by taking $\partial/\partial y = \partial/\partial x = 0$ and assuming propagation along z . We also limit the consideration to three frequencies ω_1, ω_2 , and ω_3 and take the corresponding fields to be in the form of traveling plane waves

$$\begin{aligned}E_i^{(\omega_1)}(z, t) &= \frac{1}{2} [E_{1i}(z) e^{i(\omega_1 t - k_1 z)} + \text{c.c.}], \\ E_k^{(\omega_2)}(z, t) &= \frac{1}{2} [E_{2k}(z) e^{i(\omega_2 t - k_2 z)} + \text{c.c.}], \\ E_j^{(\omega_3)}(z, t) &= \frac{1}{2} [E_{3j}(z) e^{i(\omega_3 t - k_3 z)} + \text{c.c.}],\end{aligned}\tag{12.3-6}$$

where i, j, k refer to Cartesian coordinates and can each take on values x and y . Note that for $\mathbf{P}_{\text{NL}} = 0$ the solution of Eq. (12.3-5) is given by Eq. (12.3-6) with $E_{1i}(z)$, $E_{2k}(z)$, and $E_{3j}(z)$ independent of z .

The i component of the nonlinear polarization at $\omega_1 = \omega_3 - \omega_2$, for example, is given according to Eqs. (12.3-3) and (12.3-6) as

$$\left[P_{\text{NL}}^{(\omega_1)}(z, t) \right]_i = d'_{ijk} E_{3j}(z) E_{2k}^*(z) e^{i[(\omega_3 - \omega_2)t - (k_3 - k_2)z]} + \text{c.c.} \quad (12.3-7)$$

Returning to the wave equation (12.3-5) and taking the i th component (for $\partial/\partial x = \partial/\partial y = 0$) yields

$$\nabla^2 E_i^{(\omega_1)}(z, t) = \frac{\partial^2}{\partial z^2} E_i^{(\omega_1)}(z, t) = \frac{1}{2} \frac{\partial^2}{\partial z^2} \left[E_{1i}(z) e^{i(\omega_1 t - k_1 z)} + \text{c.c.} \right]. \quad (12.3-8)$$

By carrying out the indicated differentiation and assuming that the variation of the complex field amplitudes with z is small enough so that

$$\frac{dE_{1i}}{dz} k_1 \gg \frac{d^2 E_{1i}}{dz^2},$$

we get from Eq. (12.3-8)

$$\nabla^2 E_i^{(\omega_1)}(z, t) = -\frac{1}{2} \left[k_1^2 E_{1i}(z) + 2ik_1 \frac{dE_{1i}(z)}{dz} \right] e^{i(\omega_1 t - k_1 z)} + \text{c.c.} \quad (12.3-9)$$

with similar expressions for $\nabla^2 E_j^{(\omega_3)}(z, t)$ and $\nabla^2 E_k^{(\omega_2)}(z, t)$. Using equation (12.3-5), we may write the wave equation for $E_i^{(\omega_1)}(z, t)$ as

$$\begin{aligned} & \left[\frac{k_1^2}{2} E_{1i} + ik_1 \frac{dE_{1i}}{dz} \right] e^{i(\omega_1 t - k_1 z)} + \text{c.c.} \\ & = \left[(-i\omega_1 \mu_0 \sigma + \omega_1^2 \mu_0 \epsilon) \frac{1}{2} E_{1i} e^{i(\omega_1 t - k_1 z)} + \text{c.c.} \right] - \mu_0 \frac{\partial^2}{\partial t^2} \left[P_{\text{NL}}(z, t) \right]_i, \end{aligned} \quad (12.3-10)$$

where we have used $\partial/\partial t = i\omega_1$. We have also assumed that when the number of interacting frequencies is finite, Eq. (12.3-5) must be satisfied separately by each frequency component.

Replacing $[P_{\text{NL}}(z, t)]_i$ in the last equation by Eq. (12.3-7), and recognizing that $\omega_1^2 \mu_0 \epsilon = k_1^2$, we obtain

$$ik_1 \frac{dE_{1i}}{dz} e^{-ik_1 z} = -\frac{i\omega_1 \sigma \mu_0}{2} E_{1i} e^{-ik_1 z} + \mu_0 \omega_1^2 d'_{ijk} E_{3j} E_{2k}^* e^{-i(k_3 - k_2)z},$$

or after dividing by $ik_1 e^{-ik_1 z}$ (and allowing σ to be a function of frequency),

$$\frac{dE_{1i}}{dz} = -\frac{\sigma_1}{2} \sqrt{\frac{\mu_0}{\epsilon_1}} E_{1i} - i\omega_1 \sqrt{\frac{\mu_0}{\epsilon_1}} d'_{ijk} E_{3j} E_{2k}^* e^{-i(k_3 - k_2 - k_1)z},$$

and similarly,

$$\frac{dE_{2k}^*}{dz} = -\frac{\sigma_2}{2} \sqrt{\frac{\mu_0}{\epsilon_2}} E_{2k}^* + i\omega_2 \sqrt{\frac{\mu_0}{\epsilon_2}} d'_{kij} E_{1i} E_{3j}^* e^{-i(k_1 - k_3 + k_2)z},$$

$$\frac{dE_{3j}}{dz} = -\frac{\sigma_3}{2} \sqrt{\frac{\mu_0}{\epsilon_3}} E_{3j} - i\omega_3 \sqrt{\frac{\mu_0}{\epsilon_3}} d'_{jik} E_{1i} E_{2k} e^{-i(k_1 + k_2 - k_3)z}.$$

(12.3-11)

These equations constitute the main result of this section. We will apply them in the following sections to some specific cases.

12.4. OPTICAL SECOND-HARMONIC GENERATION

The second-harmonic-generation experiment that ushered in the field of nonlinear optics was performed by Franken, Hill, Peters, and Weinreich [1] in 1961. A sketch of the original experiment is shown in Fig. 12.1. A ruby-laser beam at 6943 Å was focused on the front surface of a crystalline quartz plate. The emergent radiation was examined with a spectrometer and was found to contain radiation at twice the input frequency (i.e., at $\lambda = 3471.5$ Å). The conversion efficiency in this first experiment was $\sim 10^{-8}$. The utilization of more efficient materials, higher-intensity lasers, and phase-matching techniques has resulted, in the last few years, in conversion efficiencies approaching unity. These factors will be discussed later in the section.

Consider next Eq. (12.3-11) for second-harmonic generation (SHG). This is the limiting case of the three-frequency interaction where two of the frequencies, ω_1 and ω_2 , are equal, and $\omega_3 = 2\omega_1$. We consequently need to

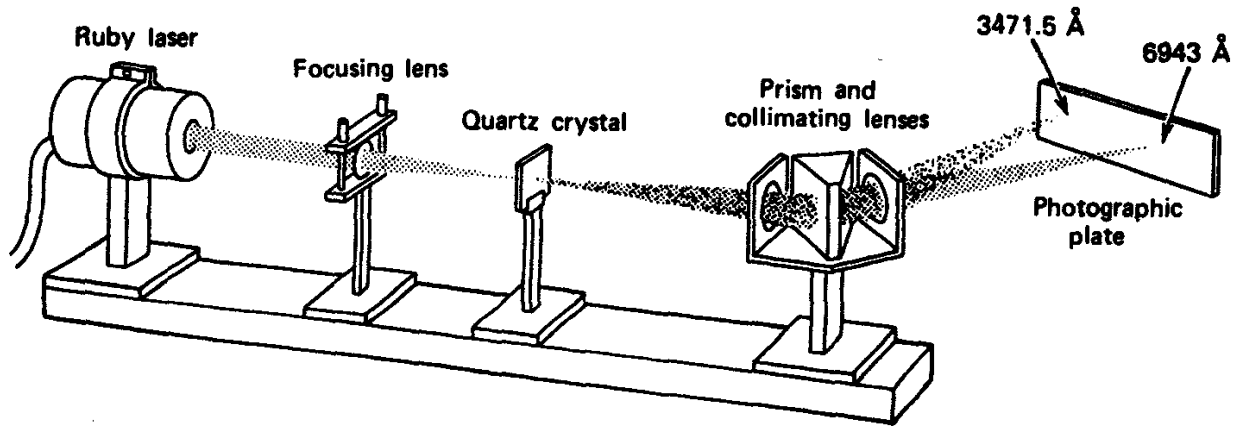


Figure 12.1. Arrangement used in the first experimental demonstration of second-harmonic generation [1]. A ruby-laser beam at $\lambda = 0.694 \mu\text{m}$ is focused on a quartz crystal, causing the generation of a (weak) beam at $\frac{1}{2}\lambda = 0.347 \mu\text{m}$. The two beams are then separated by a prism and detected on a photographic plate.

consider only two equations of (12.3-11), the first (or second) and the last. To further simplify the analysis, and yet retain its validity for the majority of the experimental situations, we assume that the amount of power lost from the input (ω_1) beam [by conversion to ($2\omega_1$)] is negligible, so that $dE_{1i}/dz \approx 0$ and we need consider only the last of the equations (12.3-11). If the medium is transparent at ω_3 , then $\sigma_3 = 0$ and we have

$$\frac{dE_{3j}}{dz} = -i\omega\sqrt{\frac{\mu_0}{\epsilon}} d'_{jik} E_{1i} E_{1k} e^{i\Delta k z}, \quad (12.4-1a)$$

where

$$\omega = \omega_1 = \frac{1}{2}\omega_3, \quad \epsilon = \epsilon_3,$$

and

$$\Delta k = k_3^{(j)} - k_1^{(i)} - k_1^{(k)}, \quad (12.4-1b)$$

and where $k_1^{(i)}$ is the propagation constant for the beam at ω_1 , which is polarized along the i direction.

We now assume that i, j , and k can take on values x and y which are chosen to be along the polarization direction of the eigenmodes of propagation in the crystal. The wave at ω_1 in general is a linear superposition of these two eigenmodes and thus has both x and y components. The superscripts on k indicate that the magnitude of the propagation constant depends on the polarization state of the beam. Note that a factor of $\frac{1}{2}$ is included on the right-hand side of Eq. (12.4-1a) because of the degeneracy $\omega_2 = \omega_1$ [see Eqs. (12.2-10) and (12.2-8)].

The solution of Eq. (12.4-1) for $E_{3j}(0) = 0$ (i.e., no second-harmonic input) and for a crystal of length L is

$$E_{3j}(L) = -i\omega\sqrt{\frac{\mu_0}{\epsilon}} d'_{jik} E_{1i} E_{1k} \frac{e^{i\Delta k L} - 1}{i\Delta k}, \quad (12.4-2)$$

where we recall that summation over repeated indices ($i, k = x, y$) is assumed. There are, in general, four terms on the right side of Eq. (12.4-2). We now consider the case when the right side is dominated by the two cross terms d'_{jik} and d'_{jki} ($i \neq k$), due to either phase matching or larger nonlinear coefficients. Thus, using the permutation symmetry of the tensor d'_{ijk} , we obtain from Eq. (12.4-2)

$$E_{3j}^*(L) E_{3j}(L) = \frac{4\mu_0}{\epsilon} \omega^2 (d'_{ijk})^2 E_{1i}^2 E_{1k}^2 L^2 \frac{\sin^2 \frac{1}{2} \Delta k L}{(\frac{1}{2} \Delta k L)^2}, \quad (12.4-3)$$

where $i = x, k = y$ (or $i = y, k = x$) and there is *no* summation over repeated indices. The factor 4 is a result of the squaring of 2 (two crossed terms). To obtain an expression for the second-harmonic power output $P^{(2\omega)}$ we use the relation (1.4-21):

$$\frac{P^{(2\omega)}}{\text{area}} = \frac{1}{2} \sqrt{\frac{\epsilon}{\mu_0}} E_{3j} E_{3j}^*.$$

Using this last expression in Eq. (12.4-3) results in

$$\frac{P_j^{(2\omega)}}{\text{area}} = 2\sqrt{\frac{\mu_0}{\epsilon}} \omega^2 (d'_{ijk})^2 E_{1i}^2 E_{1k}^2 L^2 \frac{\sin^2 \frac{1}{2} \Delta k L}{(\frac{1}{2} \Delta k L)^2},$$

or in terms of intensities,

$$\frac{P_j^{(2\omega)}}{A} = 8 \left(\frac{\mu_0}{\epsilon} \right)^{3/2} \frac{\omega^2 d_{ijk}'^2 L^2}{n^3} \frac{P_i^{(\omega)} P_k^{(\omega)}}{A^2} \frac{\sin^2 \frac{1}{2} \Delta k L}{(\frac{1}{2} \Delta k L)^2}, \quad (12.4-4)$$

where $P_i^{(\omega)}$ and $P_k^{(\omega)}$ are the mode powers of the wave at ω ($i \neq k$). For the case $P_i^{(\omega)} = P_k^{(\omega)} \equiv \frac{1}{2} P^{(\omega)}$, Eq. (12.4-4) becomes

$$\frac{P^{(2\omega)}}{P^{(\omega)}} = 2 \left(\frac{\mu_0}{\epsilon_0} \right)^{3/2} \frac{\omega^2 (d'_{ijk})^2 L^2}{n^3} \left(\frac{P^{(\omega)}}{\text{area}} \right) \frac{\sin^2 \frac{1}{2} \Delta k L}{(\frac{1}{2} \Delta k L)^2}, \quad (12.4-5)$$

where we have taken $\epsilon_1 \approx \epsilon_3 = \epsilon_0 n^2$. If we were to use the direct term (xx or yy) when the wave at ω is polarized along x or y , we would arrive at the same results (12.4-3) and (12.4-5).

12.4.1. Phase-Matching in Second-Harmonic Generation

According to Eq. (12.4-5), a prerequisite for efficient second-harmonic generation is that $\Delta k = 0$ —or, using $\omega_3 = 2\omega$, $\omega_1 = \omega_2 = \omega$,

$$k^{(2\omega)} = 2k^{(\omega)}, \quad (12.4-6)$$

where we assume that $k_1^{(i)} = k_1^{(k)} = k^{(\omega)}$.

If $\Delta k \neq 0$, the second-harmonic wave generated at some plane (e.g., z_1), having propagated to some other plane (z_2), is not in phase with the second-harmonic wave generated at z_2 . This results in the interference described by the factor

$$\frac{\sin^2 \frac{1}{2} \Delta k L}{(\frac{1}{2} \Delta k L)^2}$$

in Eq. (12.4-5). Two adjacent peaks of this spatial interference pattern are separated by the so-called “coherence length,”

$$l_c = \frac{2\pi}{\Delta k} = \frac{2\pi}{k^{(2\omega)} - 2k^{(\omega)}} \quad (12.4-7)$$

The coherence length l_c is thus a measure of the *maximum crystal length that is useful in producing the second-harmonic power*. Under ordinary circumstances it may be no larger than 10^{-2} cm. This is because the index of refraction n normally increases with ω , so Δk is given by

$$\Delta k = k^{(2\omega)} - 2k^{(\omega)} = \frac{2\omega}{c}(n^{2\omega} - n^\omega), \quad (12.4-8)$$

where we have used the relation $k^{(\omega)} = \omega n^\omega / c$. The coherence length is thus

$$l_c = \frac{\pi c}{\omega(n^{2\omega} - n^\omega)} = \frac{\lambda}{2(n^{2\omega} - n^\omega)}, \quad (12.4-9)$$

where λ is the free-space wavelength of the fundamental beam. If we take a typical value of $\lambda = 1 \mu\text{m}$ and $n(2\omega) - n(\omega) \approx 10^{-2}$, we get $l_c \approx 100 \mu\text{m}$. If l_c were to increase from $100 \mu\text{m}$ to 2cm , as an example, according to Eq. (12.4-4) the second-harmonic power would go up by a factor of 4×10^4 .

The technique that is used widely [10, 11] to satisfy the *phase-matching* requirement, $\Delta k = 0$, takes advantage of the natural birefringence of anisotropic crystals, which was discussed in Chapter 4. Using the relation $k^{(\omega)} = \omega\sqrt{\mu\epsilon_0}n^\omega$, Eq. (12.4-6) becomes

$$n^{2\omega} = n^\omega, \quad (12.4-10)$$

so the indices of refraction at the fundamental and second-harmonic frequencies must be equal. In normally dispersive materials the index of the ordinary wave or the extraordinary wave along a given direction increases with ω , as can be seen from Table 12.3. This makes it impossible to satisfy Eq. (12.4-10) when both the ω and 2ω beams are of the same type—that is, when both are extraordinary or ordinary. We can, however, under certain circumstances, satisfy Eq. (12.4-10) by using two waves of different type: one extraordinary and one ordinary. To illustrate the point, consider the dependence of the index of refraction of the extraordinary wave in a uniaxial crystal on the angle θ between the propagation direction and the

Table 12.3. Index-of-Refraction Dispersion Data on KH_2PO_4 ^a

Wavelength, μm	Index	
	n_o (ordinary ray)	n_e (extraordinary ray)
0.2000	1.622630	1.563913
0.3000	1.545570	1.498153
0.4000	1.524481	1.480244
0.5000	1.514928	1.472486
0.6000	1.509274	1.468267
0.7000	1.505235	1.465601
0.8000	1.501924	1.463708
0.9000	1.498930	1.462234
1.0000	1.496044	1.460993
1.1000	1.493147	1.459884
1.2000	1.490169	1.458845
1.3000	1.487064	1.457838
1.4000	1.483803	1.456838
1.5000	1.480363	1.455829
1.6000	1.476729	1.454797
1.7000	1.472890	1.453735
1.8000	1.468834	1.452636
1.9000	1.464555	1.451495
2.0000	1.460044	1.450308

crystal optic (z) axis. It is given by Eq. (4.6-4) as

$$\frac{1}{n_e^2(\theta)} = \frac{\cos^2\theta}{n_o^2} + \frac{\sin^2\theta}{n_e^2}. \quad (12.4-11)$$

If $n_e^{2\omega} < n_o^\omega$, there exists an angle θ_m at which $n_e^{2\omega}(\theta_m) = n_o^\omega$; so if the fundamental beam (at ω) is launched along θ_m as an ordinary ray, the second-harmonic beam will be generated along the *same direction* as an extraordinary ray. The situation is illustrated by Fig. 12.2. The angle θ_m is determined by the intersection of the sphere (shown as a circle in the figure) corresponding to the index surface of the ordinary beam at ω with the index ellipsoid (12.4-11) of the extraordinary ray that gives $n_e^{2\omega}(\theta)$. The angle θ_m for negative uniaxial crystals—that is, crystals in which $n_e^\omega < n_o^\omega$ —is that satisfying $n_e^{2\omega}(\theta_m) = n_o^\omega$, or, using Eq. (12.4-11),

$$\frac{\cos^2\theta_m}{(n_o^{2\omega})^2} + \frac{\sin^2\theta_m}{(n_e^{2\omega})^2} = \frac{1}{(n_o^\omega)^2}. \quad (12.4-12)$$

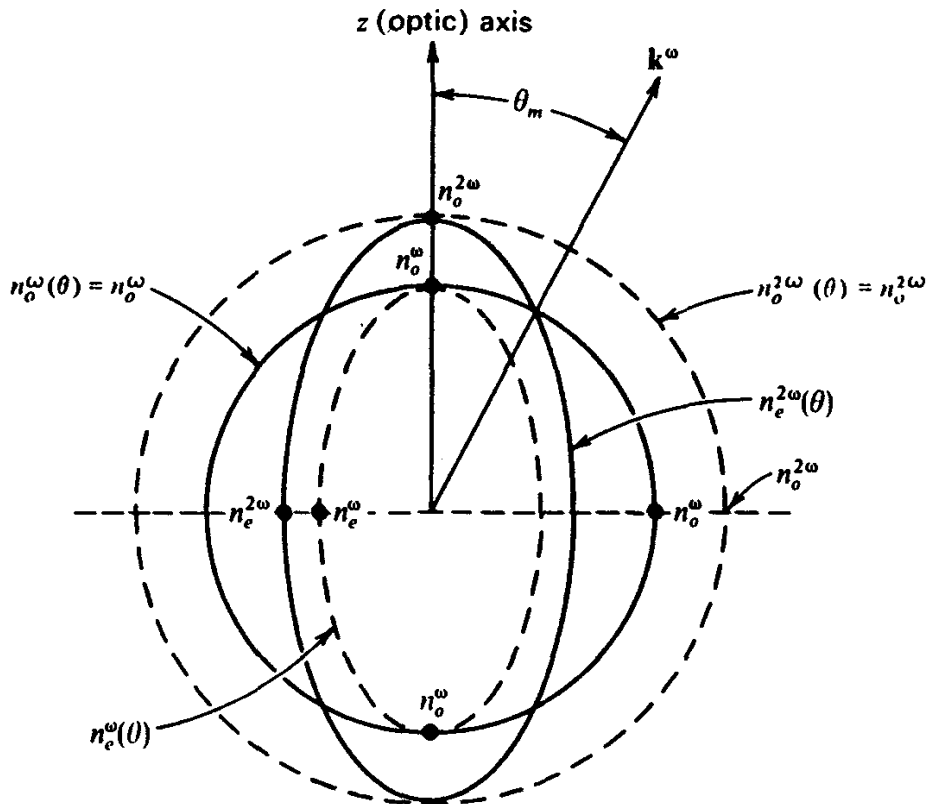


Figure 12.2. Normal (index) surfaces for the ordinary and extraordinary rays in a negative ($n_e < n_o$) uniaxial crystal. If $n_e^{2\omega} < n_o^\omega$, the condition $n_e^{2\omega}(\theta) = n_o^\omega$ is satisfied at $\theta = \theta_m$. The eccentricities shown are exaggerated.

Solving for θ_m ,

$$\sin^2 \theta_m = \frac{(n_o^\omega)^{-2} - (n_o^{2\omega})^{-2}}{(n_e^{2\omega})^{-2} - (n_o^{2\omega})^{-2}}. \quad (12.4-13)$$

12.4.2. Example: Second-Harmonic Generation in KH_2PO_4 (KDP)

Using a fundamental beam derived from a ruby laser ($\lambda = 6943 \text{ \AA}$) and a KDP crystal, the indices of refraction are obtained by extrapolating the data of Table 12.3:

$$n_e = 1.466, \quad n_e^{2\omega} = 1.487, \quad n_o = 1.506, \quad n_o^{2\omega} = 1.534.$$

The matching angle θ_m is then, according to Eq. (12.4-13), $\theta_m = 50.4^\circ$.

Another mode of index matching in KDP is one in which the components i and k of the input beam at ω do not both belong to ordinary rays, but one (e.g., k) is an extraordinary ray. The 2ω beam remains an extraordinary ray. Here the index-matching condition, $\Delta k = 0$, can be written as

$$n_{je}^{2\omega}(\theta) = \frac{1}{2} [n_{io}^{(\omega)} + n_{ke}^{(\omega)}(\theta)], \quad (12.4-14)$$

where j, i, k refer to the axes of the coordinate system that are chosen as the reference frame. The index-matching angle, θ_m for this case, is given by

$$\left[\frac{\cos^2 \theta_m}{(n_o^{2\omega})^2} + \frac{\sin^2 \theta_m}{(n_e^{2\omega})^2} \right]^{-1/2} = \frac{1}{2} \left\{ n_o^\omega + \left[\frac{\cos^2 \theta_m}{(n_o^\omega)^2} + \frac{\sin^2 \theta_m}{(n_e^\omega)^2} \right]^{-1/2} \right\}, \quad (12.4-15)$$

which is a reexpression of Eq. (12.4-14) with $n_{je}^{2\omega}(\theta)$ and $n_{ke}^\omega(\theta)$ replaced by their explicit expressions using Eq. (12.4-11).

In an SHG experiment the need to satisfy the index-matching condition (12.4-15) plus the restrictions imposed by the form of the nonlinear optical tensor limit the degrees of freedom that are available in choosing the directions of polarization. In KDP, as an example, the nonlinear polarization is, according to Eq. (12.1-13),

$$\begin{aligned} P_x^{2\omega} &= 2d_{14} E_z^\omega E_y^\omega, \\ P_y^{2\omega} &= 2d_{14} E_z^\omega E_x^\omega \\ P_z^{2\omega} &= 2d_{36} E_x^\omega E_y^\omega. \end{aligned} \quad (12.4-16)$$

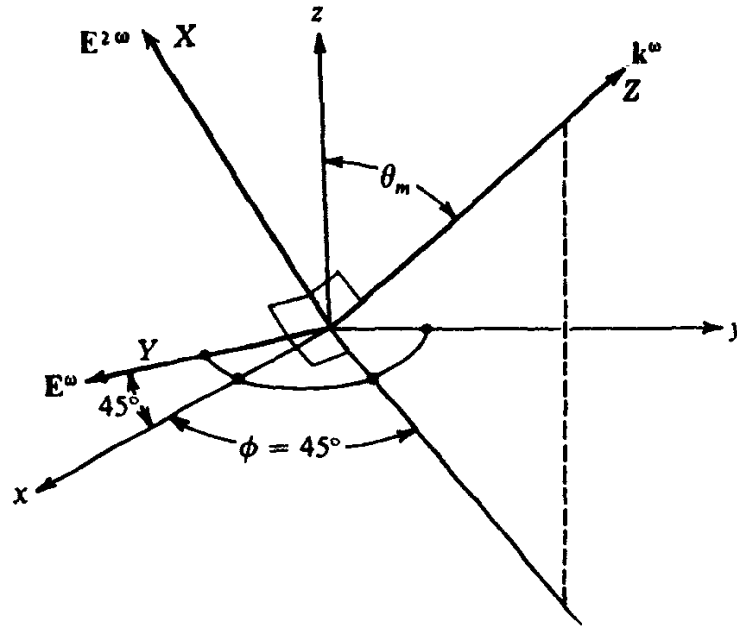


Figure 12.3. Second-harmonic generation in KDP. E^ω is at 45° to the x and y axes. The direction of propagation k^ω is at angle θ_m to the optic (z) axis. (All vectors dotted on passing through the arc are in the xy plane.)

In the index-matching scheme that leads to Eq. (12.4-13), the fundamental beam is an ordinary ray, and consequently $E_z^\omega = 0$.^{*} This dictates that the second-harmonic polarization is given by the last equation of (12.4-16) and has a z component only. The component of P_z normal to the direction of propagation is equal to $2d_{36}E_x^\omega E_y^\omega \sin \theta_m$ and is thus maximum for $E_x^\omega = E_y^\omega = E^\omega / \sqrt{2}$, which occurs when the azimuthal angle for E^ω is $\frac{1}{4}\pi$, as shown in Fig. 12.3.

According to Eq. (12.4-4) the penalty for deviating from the index-matching condition at a fixed L is a reduction of the second-harmonic power output by the factor

$$\frac{P^{(2\omega)}}{P_{\max}^{(2\omega)}} = \frac{\sin^2 \frac{1}{2} \Delta k L}{(\frac{1}{2} \Delta k L)^2}. \quad (12.4-17)$$

This equation can be checked most easily by varying the angle $\sigma = \theta - \theta_m$ between the index-matching direction and the direction of propagation. For small values of σ we can approximate $\Delta k(\theta) = k_e^{2\omega}(\theta) - 2k_o^\omega$ by

$$\Delta k(\theta) = 2\beta\sigma,$$

^{*}Here we ignore the fact that, strictly speaking, D_z and not E_z is zero. For $n_e = n_o$, D_z and E_z are nearly parallel.

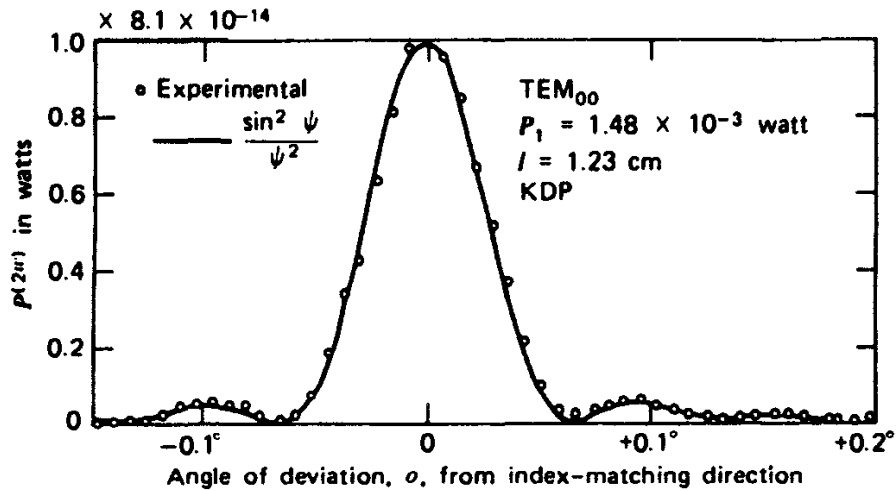


Figure 12.4. Variation of second-harmonic power with σ , the angle between the fundamental beam and the phase-matching direction. (After [13].)

where β is a constant that depends on n_o^ω , $n_o^{2\omega}$, and $n_e^{2\omega}$. The factor $\frac{1}{2}\Delta k L$ in Eq. (12.4-17) is thus equal to $\beta\sigma L \equiv \psi$. A plot of the second-harmonic power output as a function of σ is shown in Fig. 12.4. The figure also contains the theoretical $(\sin^2\psi)/\psi^2$ curve.

12.5. SECOND-HARMONIC GENERATION WITH A DEPLETED INPUT

In the treatment of second-harmonic generation leading to Eq. (12.4-4) it was assumed that the input intensity at ω was not affected by the interaction. This limits the validity of the result to situations where the fraction of the power converted from ω to 2ω is small. In this section we will lift this restriction.

We return to Eq. (12.3-11) and define the new field variables A_l by

$$A_l = \sqrt{\frac{n_l}{\omega_l}} E_l, \quad l = 1, 2, 3, \quad (12.5-1)$$

so that the intensity at ω_l is

$$I_l = \frac{P_l}{A} = \frac{1}{2} \sqrt{\frac{\epsilon_0}{\mu_0}} n_l |E_l|^2 = \frac{1}{2} \sqrt{\frac{\epsilon_0}{\mu_0}} \omega_l |A_l|^2. \quad (12.5-2)$$

Since a photon's energy is $\hbar\omega_l$, it follows that $|A_l|^2$ is proportional to the

photon flux at ω_l , the proportionality constant being independent of frequency.

Equation (12.3-11) can now be written as

$$\begin{aligned}\frac{dA_1}{dz} &= -\frac{1}{2}\alpha_1 A_1 - i\kappa A_2^* A_3 e^{-i\Delta k z}, \\ \frac{dA_2^*}{dz} &= -\frac{1}{2}\alpha_2 A_2^* + i\kappa A_1 A_3^* e^{i\Delta k z}, \\ \frac{dA_3}{dz} &= -\frac{1}{2}\alpha_3 A_3 - i\kappa A_1 A_2 e^{i\Delta k z},\end{aligned}\quad (12.5-3)$$

where 1, 2, 3 are the polarization directions of \mathbf{E}_1 , \mathbf{E}_2 , \mathbf{E}_3 , and

$$\begin{aligned}\Delta k &\equiv k_3 - (k_1 + k_2), \\ \kappa &\equiv d'_{123} \sqrt{\frac{\mu_0 \omega_1 \omega_2 \omega_3}{\epsilon_0 n_1 n_2 n_3}}, \\ \alpha_l &\equiv \sigma_l \sqrt{\frac{\mu_0}{\epsilon_l}}, \quad l = 1, 2, 3.\end{aligned}\quad (12.5-4)$$

The advantage of using the A_l instead of E_l is now apparent, since unlike Eq. (12.3-11), the relations (12.5-3) involve a single coupling parameter κ .

In the case of second-harmonic generation, there is no A_2 field and a similar derivation leads to

$$\begin{aligned}\frac{dA_1}{dz} &= -i\kappa A_3 A_1^* e^{-i\Delta k z}, \\ \frac{dA_3}{dz} &= -i\frac{1}{2}\kappa A_1^2 e^{i\Delta k z}.\end{aligned}\quad (12.5-5)$$

Note that a factor of $\frac{1}{2}$ is included because of the degeneracy $\omega_2 = \omega_1$ [see Eqs (12.2-10) and (12.2-8)]. In the phase-matched case ($\Delta k = 0$) if we choose $A_1(0)$ as a real number, then $A_1(z)$ is also real, these equations become

$$\frac{dA_1}{dz} = -\kappa A_3' A_1, \quad \frac{dA_3'}{dz} = \frac{1}{2}\kappa A_1^2, \quad (12.5-6)$$

where $A_3 \equiv -iA_3'$. It follows that

$$\frac{d}{dz} (A_1^2 + 2A_3'^2) = 0,$$

so that, assuming no input at ω_3 ,

$$A_1^2 + 2A_3'^2 = A_1^2(0),$$

or, from Eq. (12.5-6),

$$\frac{dA_3'}{dz} = \frac{1}{2}\kappa[A_1^2(0) - 2A_3'^2]$$

and

$$A_3'(z) = \frac{1}{\sqrt{2}}A_1(0)\tanh\left[\frac{A_1(0)}{\sqrt{2}}\kappa z\right]. \quad (12.5-7)$$

The conversion efficiency is

$$\frac{P^{(2\omega)}}{P^{(\omega)}} = \frac{2|A_3'(z)|^2}{|A_1(0)|^2} = \tanh^2\left[\frac{A_1(0)}{\sqrt{2}}\kappa z\right]. \quad (12.5-8)$$

Note that as $\kappa A_1(0)z \rightarrow \infty$, $A_3'(z) \rightarrow (1/\sqrt{2})A_1(0)$, so that all the input photons can be converted into half as many output photons (at twice the frequency) and *no more*.

A plot of the conversion efficiency of the no-depletion approximation (12.4-5) and that given by Eq. (12.5-8) is shown in Fig. 12.5.

12.6. SECOND-HARMONIC GENERATION WITH GAUSSIAN BEAMS

The analysis of second-harmonic generation in Sections 12.4 and 12.5 is based on a plane-wave model. In practice one uses Gaussian beams and one needs to investigate the effect of the diffraction of such beams on nonlinear processes such as second-harmonic generation.

The inverse dependence of the conversion efficiency as given by Eq. (12.4-5) on the beam cross-sectional area requires that the beam be focused onto the nonlinear crystal. A typical situation is sketched in Fig. 12.6. Here $z_0 \equiv \pi n \omega_0^2 / \lambda$, according to Eq. (2.2-11), is the distance in which the beam cross-sectional area doubles relative to its value at the waist. If the crystal length L is much shorter than z_0 , the beam cross section remains essentially a constant within the crystal, and we can use the plane-wave result (12.4-3):

$$|E^{(2\omega)}|^2 = \frac{4\mu_0}{\epsilon} \omega^2 (d'_{ijk})^2 |E^{(\omega)}|^4 L^2 \frac{\sin^2 \frac{1}{2} \Delta k L}{(\frac{1}{2} \Delta k L)^2}, \quad (12.6-1)$$

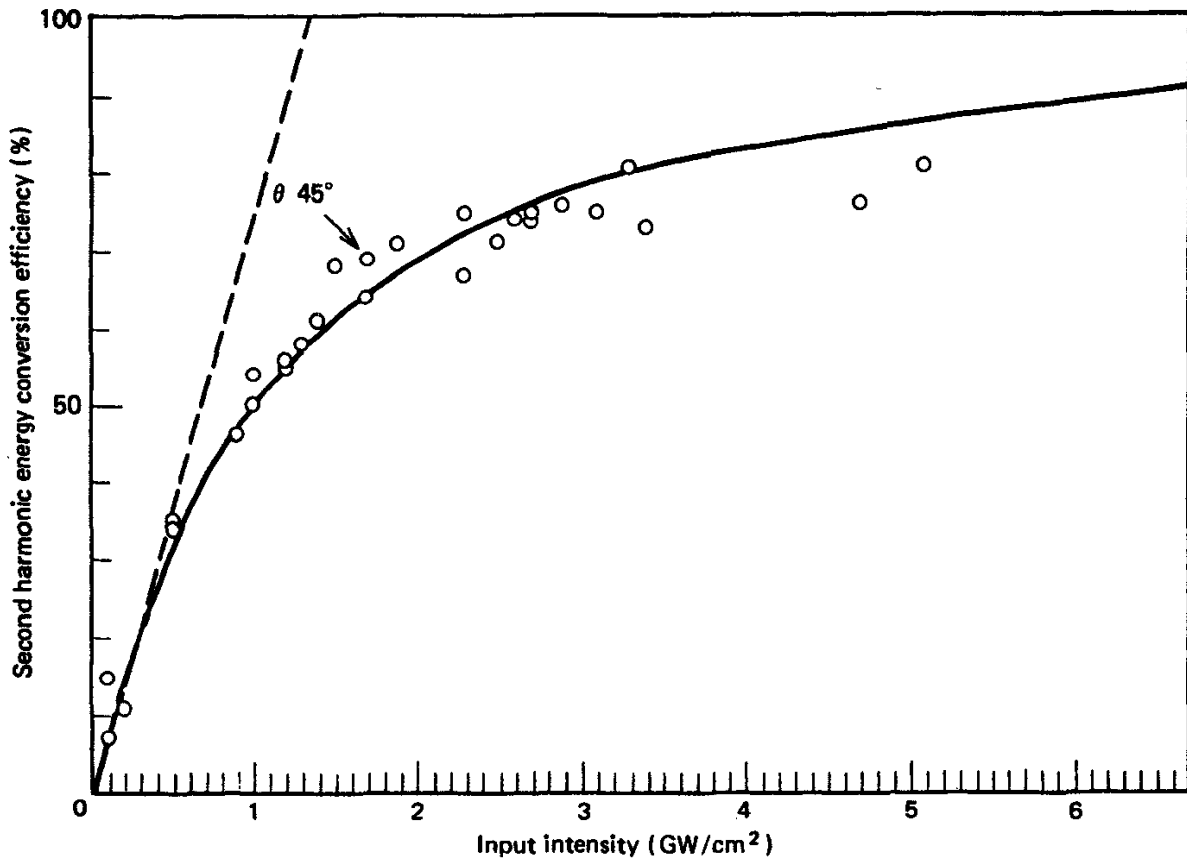


Figure 12.5. Second-harmonic energy-conversion efficiency from $\lambda = 1.054$ to $0.527 \mu\text{m}$ in a 12-mm-thick KDP crystal. Dashed curve: "nondepletion approximation" (12.4-5); solid curve: "exact" solution (12.5-8). The circles are experimental results [15].

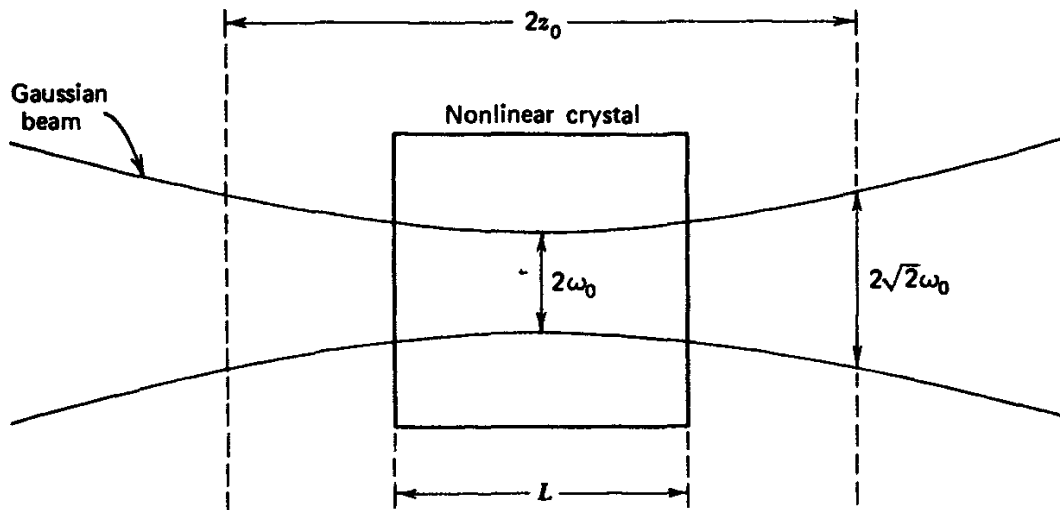


Figure 12.6. Gaussian beam focused inside a nonlinear optical crystal.

where

$$E^{(\omega)}(r) \approx E_0 e^{-r^2/\omega_0^2}. \quad (12.6-2)$$

Using

$$P^{(\omega)} = \frac{1}{2} \sqrt{\frac{\epsilon}{\mu_0}} \int_{\text{cross section}} |E^{(\omega)}|^2 dx dy \approx \sqrt{\frac{\epsilon}{\mu_0}} E_0^2 \frac{1}{4} \pi \omega_0^2$$

as well as (12.6-2), we obtain, by integrating (12.6-1),

$$\frac{P^{(2\omega)}}{P^{(\omega)}} = 8 \left(\frac{\mu_0}{\epsilon_0} \right)^{3/2} \frac{\omega^2 d^2 L^2}{n^3} \frac{P^{(\omega)}}{\pi \omega_0^2} \frac{\sin^2 \frac{1}{2} \Delta k L}{\left(\frac{1}{2} \Delta k L \right)^2} \quad (12.6-3)$$

where we have taken $n^\omega \approx n^{2\omega}$ and $d'_{ijk} \equiv d$. Equation (12.6-3) is identical to Eq. (12.4-5) except that area = $\frac{1}{4} \pi \omega_0^2$ and it now applies to a Gaussian beam. The L^2 dependence of the conversion efficiency will tempt us to use long crystals. But, according to Fig. 12.6, once $L > 2z_0$, the increase of the beam cross section will reduce the conversion efficiency. We thus expect the maximum conversion efficiency to result when $L \approx 2z_0$ and to be given by Eq. (12.6-3) when we put $L = 2z_0 = 2(\pi \omega_0^2 n / \lambda)$. We will refer to this condition as confocal focusing. The result is

$$\left. \frac{P^{(2\omega)}}{P^{(\omega)}} \right|_{\text{confocal focusing}} = \frac{8}{\pi c} \left(\frac{\mu_0}{\epsilon_0} \right)^{3/2} \frac{\omega^3 d^2 L}{n^2} P^{(\omega)} \frac{\sin^2 \frac{1}{2} \Delta k L}{\left(\frac{1}{2} \Delta k L \right)^2}. \quad (12.6-4)$$

An exact analysis [14] shows that optimum conversion results when $L = 5.68z_0$ and the resulting power is approximately 1.2 times that given by Eq. (12.6-4).*

By comparing Eq. (12.6-4) with the plane-wave solution (12.4-5), we find that under optimum focusing conditions the conversion efficiency increases as the crystal length L , rather than as L^2 .

*Recent experiments [15] on second-harmonic generation with pulsed high-intensity beams have achieved conversion efficiencies of $> 80\%$ at $\lambda = 1.06 \mu\text{m}$.

12.6.1. Example: Optimum Focusing

Consider second-harmonic conversion under confocal focusing conditions. In KH_2PO_4 from $\lambda = 1$ to $0.5 \mu\text{m}$. Using $L = 1 \text{ cm}$, $d = d_{36} \sin \theta = 3.6 \times 10^{-24} \text{ MKS}$, $n = 1.5$, we obtain from Eq. (12.6-4)

$$\frac{P^{(2\omega)}}{P^{(\omega)}} = 1.75 \times 10^{-4} P^{(\omega)}.$$

12.7. PARAMETRIC AMPLIFICATION

The second-order optical nonlinearity which is responsible for second-harmonic generation can also be used to amplify weak optical signals. The basic configuration involves an input "signal" at ω_1 that is incident on a nonlinear optical crystal together with an intense pump wave at ω_3 , where $\omega_3 > \omega_1$ [16–18]. The amplification of the ω_1 wave is accompanied by the generation of an "idler" wave at $\omega_2 = \omega_3 - \omega_1$.

12.7.1. The Basic Equations of Parametric Amplification

In the nondepleted-pump approximation we take $A_3(z) = A_3(0)$ and write the first two equations of (12.5-3) as

$$\begin{aligned} \frac{dA_1}{dz} &= -\frac{1}{2}\alpha_1 A_1 - i\frac{1}{2}gA_2^* e^{-i\Delta k z}, \\ \frac{dA_2^*}{dz} &= -\frac{1}{2}\alpha_2 A_2^* + i\frac{1}{2}gA_1 e^{i\Delta k z}, \end{aligned} \quad (12.7-1)$$

where

$$\begin{aligned} \Delta k &= k_3 - k_1 - k_2, \\ g &= 2\kappa A_3(0) = 2\sqrt{\frac{\mu_0}{\epsilon_0} \frac{\omega_1 \omega_2}{n_1 n_2}} d' E_3(0). \end{aligned} \quad (12.7-2)$$

Let us consider the general case in which both "signal" and "idler" waves with (complex) amplitudes $A_1(0)$ and $A_2(0)$, respectively, are present

at the input. The solution of Eq. (12.7-1) with $\alpha_i = 0$ (no losses) is

$$A_1(z) e^{i\frac{1}{2}\Delta k z} = A_1(0) \left[\cosh bz + i \frac{\Delta k}{2b} \sinh bz \right] - i \frac{g}{2b} A_2^*(0) \sinh bz \quad (12.7-3)$$

$$A_2^*(z) e^{-i\frac{1}{2}\Delta k z} = A_2^*(0) \left[\cosh bz - i \frac{\Delta k}{2b} \sinh bz \right] + i \frac{g}{2b} A_1(0) \sinh bz \quad (12.7-4)$$

where

$$b = \frac{1}{2} \sqrt{g^2 - (\Delta k)^2}, \quad (12.7-5)$$

$$\Delta k = k_3 - k_1 - k_2. \quad (12.7-6)$$

In the simple case of a parametric amplifier we have a single input, for example $A_1(0)$. Putting $A_2(0) = 0$ and considering for simplicity the phase-matched case $\Delta k = 0$, we obtain from Eqs. (12.7-3), (12.7-4), and (12.7-5)

$$A_1(z) = A_1(0) \cosh \frac{1}{2}gz, \\ A_2^*(z) = iA_1(0) \sinh \frac{1}{2}gz. \quad (12.7-7)$$

The increase in power of the “signal” (ω_1) and “idler” (ω_2) waves is at the expense of the pump (ω_3) wave. As a matter of fact we can show, using Eq. (12.5-3) with $\alpha_i = 0$, that

$$-\frac{d}{dz}(A_3 A_3^*) = \frac{d}{dz}(A_1 A_1^*) = \frac{d}{dz}(A_2 A_2^*). \quad (12.7-8)$$

Since $A_i A_i^*$ is proportional to the photon flux at ω_i , equation (12.7-8) is a statement of the fact that for each photon added to the “signal” wave (ω_1) one photon is added to the “idler” wave (ω_2) and one photon is removed from the pump wave (ω_3). Since $\omega_3 = \omega_1 + \omega_2$, energy is conserved. Relation (12.7-8) can be extended by integration to the whole interaction volume in which case the changes in total power between the input and output

planes are related by

$$-\Delta\left(\frac{P_3}{\omega_3}\right) = \Delta\left(\frac{P_1}{\omega_1}\right) = \Delta\left(\frac{P_2}{\omega_2}\right) \quad (12.7-9)$$

where P represents beam power. Equation (12.7-9) is known as the Manley-Rowe relation [19].

Numerical Example—Parametric Amplification. To obtain an appreciation for the magnitude of the gain available in parametric amplification, consider the case of a LiNbO_3 crystal pumped by a traveling pump. Using the data

$$\nu_1 = \nu_2 = 3 \times 10^{14} \text{ Hz} \quad (\lambda_1 = \lambda_2 = 1 \mu\text{m}),$$

$$\nu_3 = 6 \times 10^{14} \text{ Hz},$$

$$d_{31} \approx 0.5 \times 10^{-22} \quad (\text{see Table 12.2}),$$

$$n_1 = n_2 \approx 2.2,$$

$$\frac{P_3}{\text{area}} = 5 \times 10^6 \text{ W/cm}^2 \quad (E_3 = 4.13 \times 10^6 \text{ V/m})$$

in Eq. (12.7-2) gives

$$g = 1.34 \text{ cm}^{-1}.$$

This shows that even at high densities of pump power the amount of parametric gain is modest. It is for this reason that the effect is used primarily to obtain oscillation rather than as a means for amplification.

12.8. PARAMETRIC OSCILLATION

In the last section it was shown that a pump wave at ω_3 can provide, via interaction in a nonlinear crystal, simultaneous amplification for optical waves at ω_1 and ω_2 such that $\omega_3 = \omega_1 + \omega_2$. If the nonlinear crystal is placed within an optical resonator that provides resonances for the signal or idler waves (or both), the parametric gain will, at some threshold pumping intensity, cause simultaneous oscillation at both the signal and idler frequencies. The threshold for this oscillation corresponds to the point at which the parametric gain just balances the losses of the signal and idler

waves [16–18]. This is the physical basis of the optical parametric oscillator. Its practical importance derives from its ability to convert the power output of a pump laser to a coherent output at the “signal” and “idler” frequencies—which, as will be shown below, can be tuned continuously over large ranges.

A doubly resonant parametric oscillator, that is, one where both the “signal” and “idler” modes resonate (possess high Q), is shown in Fig. 12.7.

Before embarking on a rigorous analysis of parametric oscillation, we will consider an extremely simple point of view that is helpful in illustrating the basic nature of the interaction. We start with Eq. (12.7-1) and take the fields $A_1(z)$ and $A_2(z)$ as those of the parametric oscillator sketched in Fig. 12.7. The distributed-loss constants α_1 and α_2 now account for the mirror losses. This is possible when the loss per pass is small. We then have

$$\alpha_i l = 1 - R_i \quad (i = 1, 2), \quad (12.8-1)$$

where l is the length of the resonator. In a steady-state oscillation $dA_1/dz = dA_2/dz = 0$ and Eq. (12.7-1) become

$$\begin{aligned} -\frac{1}{2}\alpha_1 A_1 - i\frac{1}{2}gA_2^* &= 0, \\ i\frac{1}{2}gA_1 - \frac{1}{2}\alpha_2 A_2^* &= 0. \end{aligned} \quad (12.8-2)$$

Nontrivial solutions for A_1 and A_2 thus exist if the determinant of the coefficients in Eq. (12.8-2) vanishes, that is, when

$$g^2 = \alpha_1 \alpha_2. \quad (12.8-3)$$

We will now consider the same problem in a more rigorous fashion.

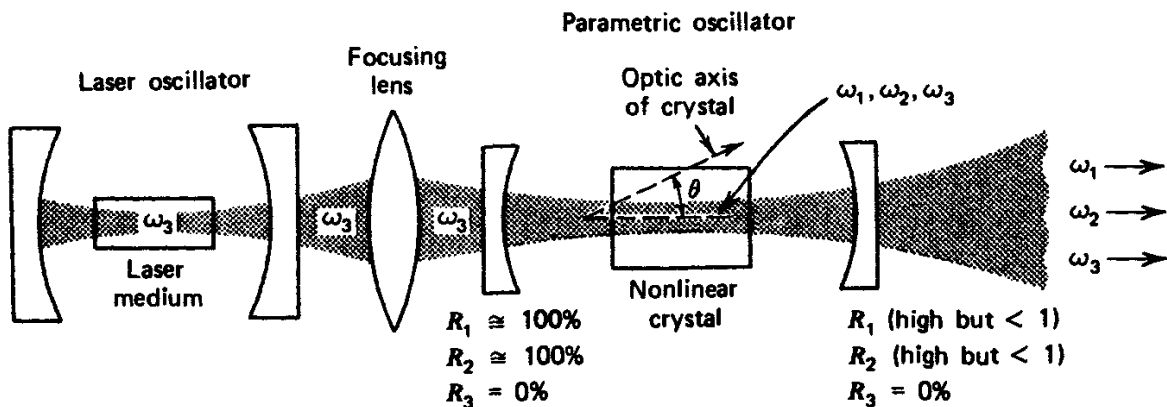


Figure 12.7. Schematic diagram of an optical parametric oscillator in which the laser output at ω_3 is used as the pump. The resulting gain gives rise to oscillations at ω_1 and ω_2 (where $\omega_3 = \omega_1 + \omega_2$) in an optical cavity that contains the nonlinear crystal and resonates at ω_1 and ω_2 .

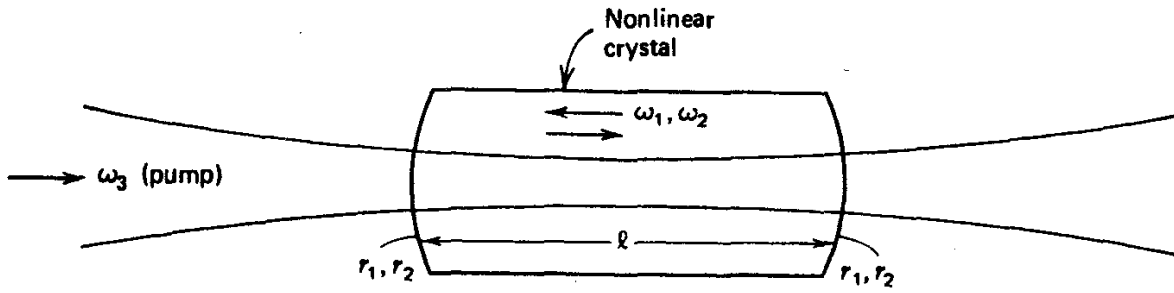


Figure 12.8. A crystal parametric oscillator.

12.8.1. Self-Consistent Analysis of Parametric Oscillation

In this section we derive the equations governing steady-state oscillation in parametric oscillators, employing a self-consistent approach.

The basic model is shown in Fig. 12.8. We assume, for simplicity, a nonlinear crystal shaped as an optical resonator whose curved ends present reflectances* r_1 and r_2 , respectively, to the signal and idler fields while being transparent to the pump field. The combined idler-signal field at an arbitrary plane z will be described by the column vector

$$\tilde{A}(z) = \begin{pmatrix} A_1(z)e^{-ik_1z} \\ A_2^*(z)e^{ik_2z} \end{pmatrix}, \quad (12.8-4)$$

where $k_i = (\omega_i/c)n_i$. The propagation of $\tilde{A}(z)$ through a nonlinear crystal of length l is described, according to Eqs. (12.7-3) and (12.7-4) by

$$\begin{aligned} &\tilde{A}(l) \\ &= \begin{pmatrix} e^{-i(k_1 + \frac{1}{2}\Delta k)l} \left[\cosh bl + \frac{i\Delta k}{2b} \sinh bl \right] - ie^{-i(k_1 + \frac{1}{2}\Delta k)l} \frac{g}{2b} \sinh bl \\ ie^{i(k_2 + \frac{1}{2}\Delta k)l} \frac{g}{2b} \sinh bl e^{i(k_2 + \frac{1}{2}\Delta k)l} \left[\cosh bl - \frac{i\Delta k}{2b} \sinh bl \right] \end{pmatrix} \tilde{A}(0) \end{aligned} \quad (12.8-5)$$

We now require that the vector $\tilde{A}(z)$ reproduce itself after one complete round trip inside the resonator. Using Fig. 12.9, this condition is

$$\tilde{A}_e = \tilde{A}_a. \quad (12.8-6)$$

*The complex field reflection coefficients are r_1 and r_2 . They are related to the mirror reflectivities by $|r_i|^2 = R_i$.

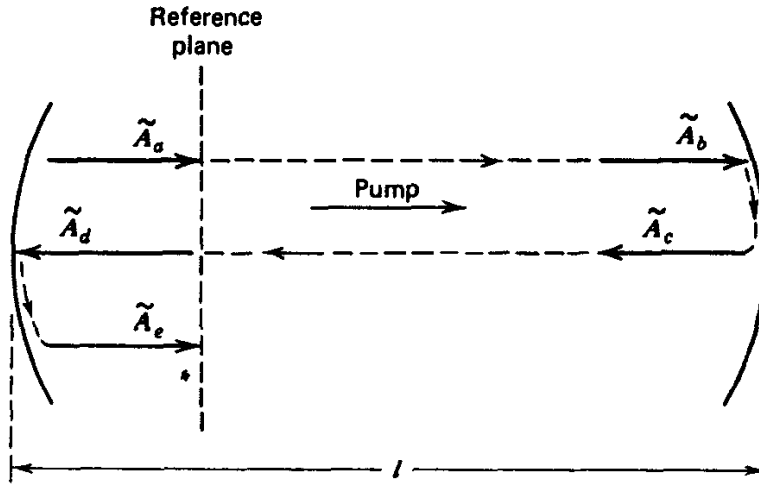


Figure 12.9. The round-trip propagation of the idler-signal “vector” \tilde{A} used in deriving the oscillation condition (15.8-12).

\tilde{A}_e is obtained from \tilde{A}_a by multiplying the latter by four matrices: one accounting for reflection at the left mirror, one for propagation from right to left (for which there is no parametric gain), one for reflection at the right mirror, and one, given by Eq. (12.8-5), for the pass from left to right. Assuming a phase-matched $\Delta k = 0$ operation, a complete round trip is thus described by

$$\begin{aligned} \tilde{A}_e &= \begin{pmatrix} r_1 & 0 \\ 0 & r_2^* \end{pmatrix} \begin{pmatrix} e^{-ik_1 l} & 0 \\ 0 & e^{ik_2 l} \end{pmatrix} \begin{pmatrix} r_1 & 0 \\ 0 & r_2^* \end{pmatrix} \\ &\quad \times \begin{pmatrix} e^{-ik_1 l} \cosh \frac{1}{2} gl & -ie^{-ik_1 l} \sinh \frac{1}{2} gl \\ ie^{ik_2 l} \sinh \frac{1}{2} gl & e^{ik_2 l} \cosh \frac{1}{2} gl \end{pmatrix} \tilde{A}_a, \end{aligned} \quad (12.8-7)$$

or

$$\tilde{A}_e = \tilde{M} \tilde{A}_a, \quad (12.8-8)$$

where

$$\tilde{M} = \begin{pmatrix} r_1^2 e^{-i2k_1 l} \cosh \frac{1}{2} gl & -ir_1^2 e^{-i2k_1 l} \sinh \frac{1}{2} gl \\ i(r_2^*)^2 e^{i2k_2 l} \sinh \frac{1}{2} gl & (r_2^*)^2 e^{i2k_2 l} \cosh \frac{1}{2} gl \end{pmatrix}. \quad (12.8-9)$$

The self-consistency condition (12.8-6) can now be written as

$$\tilde{A}_a = \tilde{M} \tilde{A}_a, \quad (12.8-10)$$

so that for a nontrivial \tilde{A}_a

$$\det|\tilde{M} - \tilde{I}| = 0, \quad (12.8-11)$$

or, using Eq. (12.8-9),

$$\begin{aligned} & [r_1^2 e^{-i2k_1 l} \cosh \frac{1}{2} g l - 1] [(r_2^*)^2 e^{i2k_2 l} \cosh \frac{1}{2} g l - 1] \\ & = r_1^2 (r_2^*)^2 e^{i2(k_2 - k_1)l} \sinh^2 \frac{1}{2} g l \end{aligned} \quad (12.8-12)$$

This is the *oscillation condition* of the parametric oscillator.

An inspection of Eq. (12.8-12) reveals that the minimum threshold gain g_l will result when each of the two factors on the left side is a *real positive* number. For this to happen the following relations must hold:

$$\begin{aligned} -\phi_1 + 2k_1 l &= 2m\pi, \\ -\phi_2 + 2k_2 l &= 2s\pi, \end{aligned} \quad (12.8-13)$$

where m and s are two integers and

$$(r_{1,2})^2 = R_{1,2} e^{i\phi_{1,2}}. \quad (12.8-14)$$

The conditions (12.8-13) are equivalent to stating that the “signal” (ω_1) and “idler” (ω_2) oscillation frequencies must correspond to two longitudinal modes of the optical resonator.

We will next use Eq. (12.8-12) to derive the threshold conditions for two important classes of parametric oscillators.

12.8.2. The Doubly Resonant Parametric Oscillator

In this case the configuration provides high- Q resonances to both ω_1 and ω_2 . Using Eq. (12.8-13) in Eq. (12.8-12) leads to

$$(R_1 + R_2) \cosh \frac{1}{2} g l - R_1 R_2 = 1. \quad (12.8-15)$$

For high-reflectivity mirrors, $R_1, R_2 \approx 1$, $\cosh \frac{1}{2} g l \approx 1 + \frac{1}{8} g^2 l^2$, and Eq. (12.8-15) becomes

$$g_l l = 2\sqrt{(1 - R_1)(1 - R_2)}. \quad (12.8-16)$$

Using Eq. (12.7-2) and expressing the pump field E_3 in terms of the intensity

$$I_3 = \frac{1}{2} \sqrt{\frac{\epsilon_0 n_3^2}{\mu_0}} E_3^2,$$

Eq. (12.8-16) becomes

$$I_{3t} = \left(\frac{\epsilon_0}{\mu_0} \right)^{3/2} \frac{n_1 n_2 n_3 (1 - R_1)(1 - R_2)}{2 \omega_1 \omega_2 l^2 d^2}. \quad (12.8-17)$$

12.8.3 Example: Parametric-Oscillation Threshold

Let us estimate the threshold pump requirement of a parametric oscillator of the kind shown in Fig. 12.3 that utilizes a LiNbO_3 crystal. We use the following set of parameters:

$$1 - R_1 = 1 - R_2 = 2 \times 10^{-2}$$

(i.e., the total loss per pass at ω_1 and ω_2 is 2%),

$$\lambda_1 = \lambda_2 = 1 \mu\text{m}$$

$$l = 1 \text{ cm} \quad (\text{crystal length}),$$

$$n_1 = n_2 = n_3 = 2.2,$$

$$d_{31}(\text{LiNbO}_3) = 5 \times 10^{-23} \text{ MKS.}$$

Substitution in Eq. (12.8-17) yields

$$I_{3t} = 4.5 \times 10^3 \text{ W/cm}^2.$$

This is an easily achievable intensity even on a continuous basis, so that the example helps us appreciate the attractiveness of optical parametric oscillation as a means for generating coherent optical radiation at new optical frequencies.

12.9. FREQUENCY TUNING IN PARAMETRIC OSCILLATION

Unlike the laser, the parametric oscillator does not depend on resonant transitions and consequently can be tuned over wide frequency regions. The pair of "idler" (ω_1) and "signal" (ω_2) frequencies that oscillate is that for

which the phase-matching condition

$$\omega_3 n_3 = \omega_1 n_1 + \omega_2 n_2 \quad (12.9-1)$$

and the energy-conservation condition

$$\omega_3 = \omega_1 + \omega_2 \quad (12.9-2)$$

are satisfied simultaneously. The relation (12.9-1) is, of course, just another way of writing $k_3 = k_1 + k_2$ for collinear interaction.

In a crystal the indices n_1 , n_2 , and n_3 depend in general on the crystal orientation (for extraordinary rays), temperature, electric field, and pressure. The control of any of these variables can be used, in view of Eq. (12.9-1), for tuning the output frequencies, ω_1 and ω_2 , of the parametric oscillator.

To be specific, let us take up the problem of angle tuning. Consider a parametric oscillator pumped by an extraordinary pump wave at ω_3 . The frequencies ω_1 and ω_2 correspond to ordinary waves. At some crystal orientation θ_0 (the angle between the crystal c axis and the axis of the resonator) oscillation takes place at ω_{10} and ω_{20} where the indices of refraction are n_{10} and n_{20} , respectively. At $\theta = \theta_0$ we have, according to Eq. (12.9-1),

$$\omega_3 n_{30}(\theta_0) = \omega_{10} n_{10} + \omega_{20} n_{20},$$

We now rotate the crystal by $\Delta\theta$. This causes the index n_3 to change so that the need to satisfy the phase matching condition (12.9-1) causes ω_1 and ω_2 to change slightly. The new oscillation takes place with the following changes relative to oscillation at θ_0 .

$$\omega_3 \rightarrow \omega_3 \quad (\text{pump frequency is unchanged}),$$

$$n_{30} \rightarrow n_{30} + \Delta n_3,$$

$$n_{10} \rightarrow n_{10} + \Delta n_1,$$

$$n_{20} \rightarrow n_{20} + \Delta n_2,$$

$$\omega_{10} \rightarrow \omega_{10} + \Delta\omega_1,$$

$$\omega_{20} \rightarrow \omega_{20} + \Delta\omega_2,$$

$$\Delta\omega_2 = -\Delta\omega_1$$

Since Eq. (12.9-1) needs to be satisfied at the new set of frequencies, we have

$$\omega_3(n_{30} + \Delta n_3) = (\omega_{10} + \Delta\omega_1)(n_{10} + \Delta n_1) + (\omega_{20} - \Delta\omega_1)(n_{20} + \Delta n_2).$$

Neglecting second order terms $\Delta n \Delta\omega$ and using Eq. (12.9-2), we obtain

$$\Delta\omega_1|_{\theta-\theta_0} = \frac{\omega_3 \Delta n_3 - \omega_{10} \Delta n_1 - \omega_{20} \Delta n_2}{n_{10} - n_{20}}. \quad (12.9-3)$$

Since the pump is extraordinary, n_3 is a function of θ . The indices n_1 and n_2 of the ordinary rays depend on frequency but not θ . We can thus write

$$\begin{aligned} \Delta n_1 &= \left. \frac{\partial n_1}{\partial \omega} \right|_{\omega_{10}} \Delta\omega_1, \\ \Delta n_2 &= \left. \frac{\partial n_2}{\partial \omega} \right|_{\omega_{20}} \Delta\omega_2, \end{aligned} \quad (12.9-4)$$

and

$$\Delta n_3 = \left. \frac{\partial n_3}{\partial \theta} \right|_{\theta_0} \Delta\theta. \quad (12.9-5)$$

These relations as well as $\Delta\omega_2 = -\Delta\omega_1$ can be used in Eq. (12.9-3) to yield

$$\frac{\partial \omega_1}{\partial \theta} = \frac{\omega_3 \frac{\partial n_3}{\partial \theta}}{(n_{10} - n_{20}) + \left[\omega_{10} \frac{\partial n_1}{\partial \omega} - \omega_{20} \frac{\partial n_2}{\partial \omega} \right]} \quad (12.9-6)$$

for the rate of change of the oscillation frequency with respect to the crystal orientation. Using Eq. (4.6-4) and the relation $d(1/x^2) = -(2/x^3) dx$, we obtain

$$\frac{\partial n_3}{\partial \theta} = -\frac{n_3^3}{2} (\sin 2\theta) \left[\left(\frac{1}{n_e^{\omega_3}} \right)^2 - \left(\frac{1}{n_o^{\omega_3}} \right)^2 \right]$$

that, when substituted in (12.9-6) gives

$$\frac{\partial \omega_1}{\partial \theta} = \frac{-\frac{1}{2} \omega_3 n_3^3 \left[\left(\frac{1}{n_e^{\omega_3}} \right)^2 - \left(\frac{1}{n_o^{\omega_3}} \right)^2 \right] \sin 2\theta}{(n_{10} - n_{20}) + \left(\omega_{10} \frac{\partial n_1}{\partial \omega} - \omega_{20} \frac{\partial n_2}{\partial \omega} \right)}. \quad (12.9-7)$$

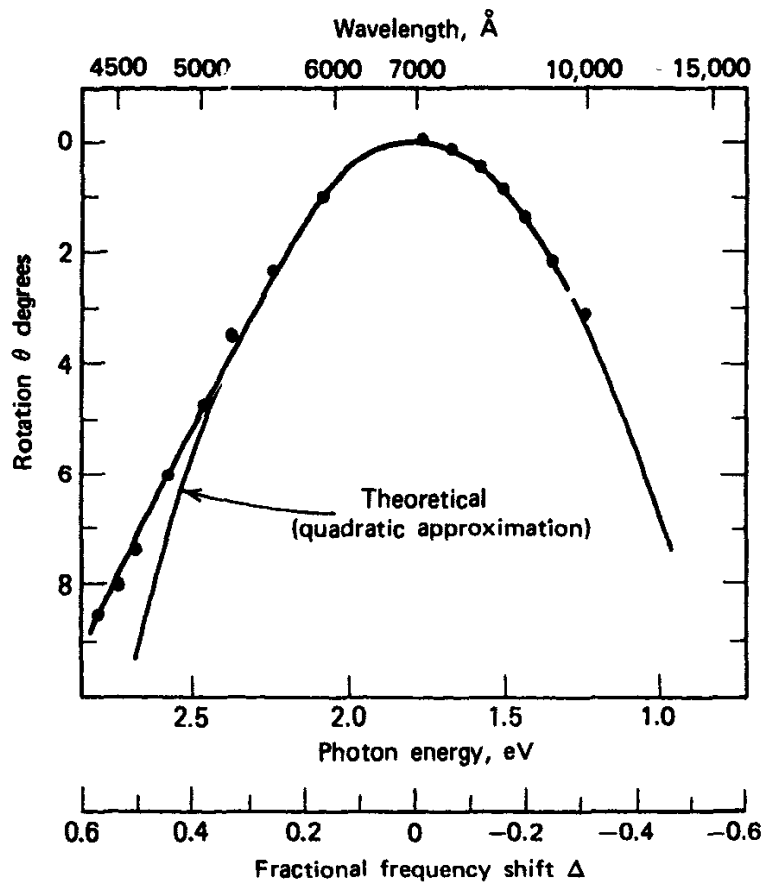


Figure 12.10. Dependence of the signal frequency ω_1 on the angle between the pump propagation direction and the optic axis of the ADP crystal. The angle θ is measured with respect to the angle for which $\omega_1 = \frac{1}{2}\omega_3$. $\Delta \equiv (\omega_1 - \frac{1}{2}\omega_3) / \frac{1}{2}\omega_3$. (After [20].)

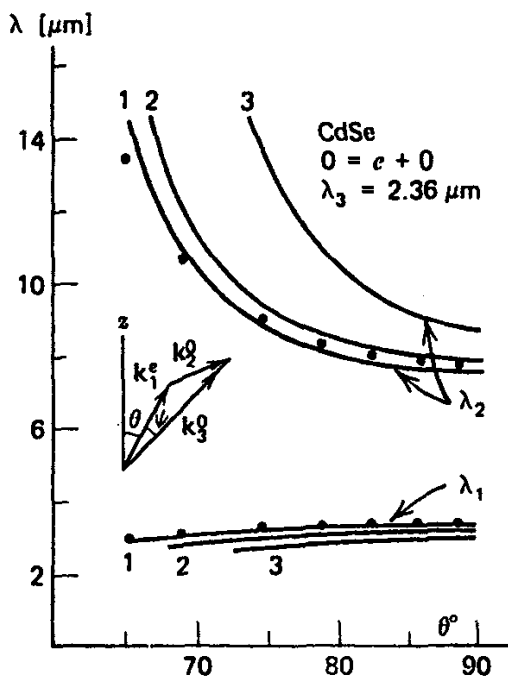


Figure 12.11. Angle-tuning curves for CdSe with $\lambda_3 = 2.36 \mu\text{m}$: 1, collinear interaction, $\psi = 0$; 2, 3, noncollinear interaction, $\psi = 0.5, 1^\circ$; k_3, k_1, k_2 , wave vectors of pump, signal, idler frequencies; θ , angle between signal wave vector and CdSe optic axis; ψ , angle between pumping wave vector and signal 1. (After [21].)

An experimental curve showing the dependence of the signal and idler frequencies on θ in $\text{NH}_4\text{H}_2\text{PO}_4$ (ADP) is shown in Fig. 12.10. Also shown is a theoretical curve based on a quadratic approximation of Eq. (12.9-7), which was plotted using the dispersion (i.e., n versus ω) data on ADP. An angular-tuning curve of a CdSe oscillator [21] is shown in Fig. 12.11.

Reasoning similar to that used to derive the angle-tuning expression (12.9-7) can be applied to determine the dependence of the oscillation frequency on any other physical variable.

12.10. FREQUENCY UPCONVERSION

Parametric interactions in a crystal can be used to convert a signal from a "low" frequency ω_1 to a "high" frequency ω_3 by mixing it with a strong laser beam at ω_2 , where

$$\omega_1 + \omega_2 = \omega_3. \quad (12.10-1)$$

Using a quantum-mechanical point of view [3, 22–25], we can consider the basic process taking place in frequency upconversion as one in which a "signal" (ω_1) photon and a pump (ω_2) photon are annihilated while, simultaneously, one photon at ω_3 is generated. Since a photon energy is $\hbar\omega$, the conservation of energy dictates that $\omega_3 = \omega_1 + \omega_2$, and the conservation of momentum leads to the relationship

$$\mathbf{k}_3 = \mathbf{k}_1 + \mathbf{k}_2, \quad (12.10-2)$$

between the wave vectors at the three frequencies. This point of view also suggests that the number of output photons at ω_3 cannot exceed the input number at ω_1 .

The experimental situation is demonstrated by Fig. 12.12. The ω_1 and ω_2 beams are combined in a partially transmissive mirror (or prism), so that they traverse together (in near parallelism) the length, l , of a crystal possessing nonlinear optical characteristics.

The analysis of frequency upconversion starts with Eq. (12.5-3). Assuming negligible depletion of the pump wave (A_2) and no losses ($\alpha = 0$) at ω_1 and ω_2 , we can write the first and third of these equations as

$$\frac{dA_1}{dz} = -i\frac{1}{2}gA_3, \quad \frac{dA_3}{dz} = -i\frac{1}{2}gA_1, \quad (12.10-3)$$

where, using Eq. (12.5-4) and (12.5-1) and choosing without loss of general-

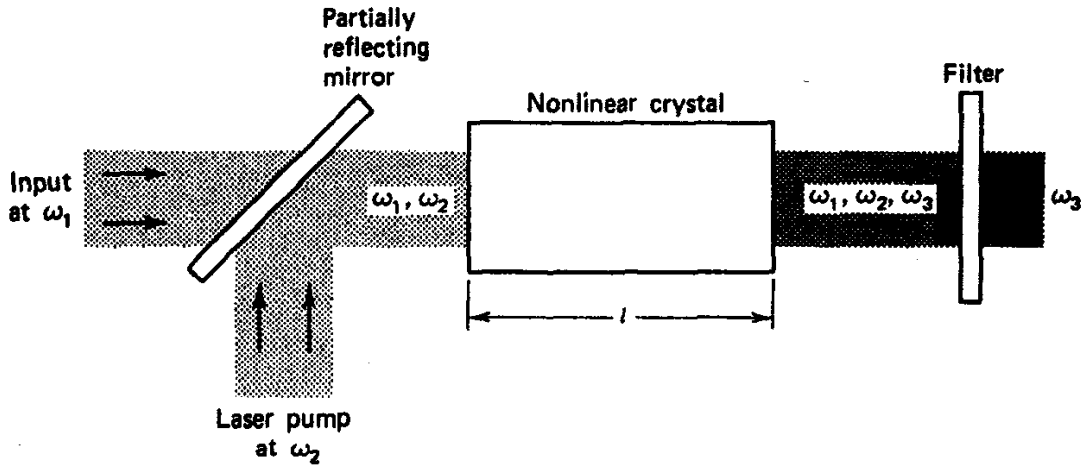


Figure 12.12. Parametric upconversion in which a signal at ω_1 and a strong laser beam at ω_2 combine in a nonlinear crystal to generate a beam at the sum frequency $\omega_3 = \omega_1 + \omega_2$.

ity the pump phase as zero so that $A_2(0) = A_2^*(0)$,

$$g \equiv 2\sqrt{\frac{\omega_1\omega_3}{n_1n_3} \frac{\mu_0}{\epsilon_0}} dE_2, \quad (12.10-4)$$

where E_2 is the amplitude of the electric field of the pump laser. Taking the input waves with (complex) amplitudes $A_1(0)$ and $A_3(0)$, the general solution of Eq. (12.10-3) is

$$\begin{aligned} A_1(z) &= A_1(0)\cos \frac{1}{2}gz - iA_3(0)\sin \frac{1}{2}gz \\ A_3(z) &= A_3(0)\cos \frac{1}{2}gz - iA_1(0)\sin \frac{1}{2}gz. \end{aligned} \quad (12.10-5)$$

In the case of a single (low-frequency) input at ω_1 , we have $A_3(0) = 0$. In this case,

$$\begin{aligned} |A_1(z)|^2 &= |A_1(0)|^2 \cos^2 \frac{1}{2}gz, \\ |A_3(z)|^2 &= |A_1(0)|^2 \sin^2 \frac{1}{2}gz; \end{aligned} \quad (12.10-6)$$

therefore,

$$|A_1(z)|^2 + |A_3(z)|^2 = |A_1(0)|^2.$$

In the discussion following (12.5-2) we pointed out that $|A_i(z)|^2$ is proportional to the photon flux (photons per square meter per second) at ω_i . If we

rewrite Eq. (12.10-6) in terms of powers, we obtain

$$P_1(z) = P_1(0)\cos^2\frac{1}{2}gz,$$

$$P_3(z) = \frac{\omega_3}{\omega_1}P_1(0)\sin^2\frac{1}{2}gz. \quad (12.10-7)$$

In a crystal of length l , the conversion efficiency is thus

$$\frac{P_3(l)}{P_1(0)} = \frac{\omega_3}{\omega_1} \sin^2\frac{1}{2}gl \quad (12.10-8)$$

and can have a maximum value of ω_3/ω_1 , corresponding to the case in which all the input (ω_1) photons are converted to ω_3 photons.

In most practical situations the conversion efficiency is small (see the following numerical example), so using $\sin x \approx x$ for $x \ll 1$, we get

$$\frac{P_3(l)}{P_1(0)} = \frac{\omega_3}{\omega_1} \left(\frac{g^2 l^2}{4} \right),$$

which, by the use of Eqs. (12.10-4) and (12.5-2), can be written as

$$\frac{P_3(l)}{P_1(0)} \approx \frac{2\omega_3^2 l^2 d^2}{n_1 n_2 n_3} \left(\frac{\mu_0}{\epsilon_0} \right)^{3/2} \frac{P_2}{A}, \quad (12.10-9)$$

where A is the cross-sectional area of the interaction region.

Numerical Example—Frequency Upconversion. The main practical interest in parametric frequency upconversion stems from the fact that it offers a means of detecting infrared radiation (a region where detectors either are inefficient, are very slow, or require cooling to cryogenic temperatures) by converting the frequency into the visible or near-visible part of the spectrum. The radiation can then be detected by means of efficient and fast detectors such as photomultipliers or photodiodes [23–26].

As an example of this application, consider the problem of upconverting a 10.6- μm signal, originating in a CO_2 laser, to 0.96 μm by mixing it with the 1.06- μm output of an Nd^{3+} -YAG laser. The nonlinear crystal chosen for this application has to have low losses at 1.06 and 10.6 μm , as well as at 0.96 μm . In addition, its birefringence has to be such as to make phase matching possible. The crystal proustite (Ag_3AsS_3) [26], listed in Table 12.2,

meets these requirements. Using the data

$$\frac{P_{1.06 \mu\text{m}}}{A} = 10^4 \text{ W/cm}^2 = 10^8 \text{ W/m}^2,$$

$$l = 1 \text{ cm},$$

$$n_1 \approx n_2 \approx n_3 = 2.6,$$

and

$$d_{\text{eff}} = 1.1 \times 10^{-22}$$

(taken conservatively as a little less than half the value given in Table 12.2 for d_{22}), we obtain from Eq. (12.10-9)

$$\frac{P_{A=0.96 \mu\text{m}}}{P_{A=10.6 \mu\text{m}}} = 3 \times 10^{-3},$$

indicating a useful amount of conversion efficiency. Actual experiments in LiIO_3 [27], using a ruby $0.6943\text{-}\mu\text{m}$ pump, result in photon-conversion efficiencies near 100% at $3.39 \mu\text{m}$.

One of the more important aspects of sum-frequency generation has been in mixing together the output of various lasers to achieve radiation with a wavelength in the vicinity of $16 \mu\text{m}$, needed in uranium isotope separation schemes which are based on UF_6 .

PROBLEMS

12.1. *Relation between d_{ijk} and r_{ijk} .* Let the total electric field be

$$E_j = E_j^{\text{dc}} + \left(\frac{1}{2} E_j^\omega e^{i\omega t} + \text{c.c.} \right).$$

(a) Show that, according to (12.1-1)

$$P_i^\omega = \varepsilon_0 \chi_{ij} E_j^\omega + 4d_{ijk} E_k^{\text{dc}} E_j^\omega$$

(b) Show that the above relation can also be derived from

$$P_i^\omega = \varepsilon_0 \chi_{ij} E_j^\omega + \lim_{\substack{\omega_1 \rightarrow \omega \\ \omega_2 \rightarrow 0}} \{ P_i^{\omega_3 = \omega_1 + \omega_2} + P_i^{\omega_3 = \omega_1 - \omega_2} \},$$

where $P_i^{\omega_3 = \omega_1 \pm \omega_2}$ are given by Eq. (12.2-8).

- (c) If we write $P_i^\omega = (\epsilon_{ij} + \Delta\epsilon_{ij})E_j^\omega$, where $\Delta\epsilon_{ij}$ is $4d_{ijk}E_k^{\text{dc}}$, and use

$$\Delta\eta_{ij} = [\epsilon_0(\epsilon + \Delta\epsilon)^{-1}]_{ij} - [\epsilon_0\epsilon^{-1}]_{ij} = r_{ijk}E_k^{\text{dc}},$$

show that

$$d_{ijk} = -\frac{1}{4\epsilon_0}\epsilon_{i\alpha}r_{\alpha\beta k}\epsilon_{\beta j},$$

where summation over repeated indices α, β is assumed.

- (d) In the principal coordinate system, the relation becomes

$$d_{ijk} = -\frac{\epsilon_{ii}\epsilon_{jj}}{4\epsilon_0}r_{ijk}.$$

12.2. Relation between χ_{ijkl} and s_{ijkl} .

- (a) Show that

$$P_i^\omega = (\epsilon_0\chi_{ij} + 4d_{ijk}E_k^{\text{dc}} + 12\chi_{ijkl}E_k^{\text{dc}}E_l^{\text{dc}})E_j^\omega.$$

- (b) Show that

$$\chi_{ijkl} = -\frac{1}{12\epsilon_0}\epsilon_{i\alpha}s_{\alpha\beta kl}\epsilon_{\beta j}.$$

- (c) Show that in the principal coordinates

$$\chi_{ijkl} = -\frac{\epsilon_{ii}\epsilon_{jj}}{12\epsilon_0}s_{ijkl}.$$

- (d) Show that in an isotropic medium

$$\chi_{xyxy} = \chi_{yxyx} = \frac{\epsilon_0}{12}nK\lambda,$$

where n is the index of refraction, K is the Kerr constant, and λ is the vacuum wavelength. Estimate the third-order susceptibility χ_{yxyx} of CS_2 at $\lambda = 1 \mu\text{m}$ using the Kerr constant listed in Table 7.6.

12.3. *Symmetry properties of nonlinear susceptibilities.* The nonlinear susceptibilities defined by Eq. (12.1-1) can be written as

$$2d_{ijk} = \frac{1}{2!} \left(\frac{\partial^2 P_i}{\partial E_j \partial E_k} \right), \quad 4\chi_{ijkl} = \frac{1}{3!} \left(\frac{\partial^3 P_i}{\partial E_j \partial E_k \partial E_l} \right).$$

(a) Show that the indices $ijkl$ are permutable, that is,

$$d_{ijk} = d_{ikj},$$

$$\chi_{ijkl} = \chi_{ikjl} = \chi_{iklj} = \chi_{ilkj} = \chi_{iljk} = \chi_{iljk}.$$

(b) Show that if we define $D_i = \epsilon_{ij} E_j$, then

$$\epsilon_{ij} = \epsilon_0 (\delta_{ij} + \chi_{ij}) + 2d_{ijk} E_k + 4\chi_{ijkl} E_k E_l.$$

(c) Since $\epsilon_{ij} = \epsilon_{ji}$, show that d_{ijk} and χ_{ijkl} are symmetric with respect to any permutation of their indices.

REFERENCES

1. P. A. Franken, A. E. Hill, C. W. Peters, and G. Weinreich, *Phys. Rev. Lett.* **7**, 118 (1961).
2. P. D. Maker, R. N. Terhune, and C. M. Savage, in *Proceedings Third Conference on Quantum Electronics, Paris, 1963*, P. Grivet and N. Bloembergen, Eds., Columbia University Press, New York, 1964, p. 1559.
3. See, for example, A. Yariv, *Quantum Electronics*, 2d Ed., Wiley, New York, 1975, Chapter 18.
4. N. Bloembergen, *Nonlinear Optics*, Benjamin, New York, 1965.
5. J. A. Armstrong, N. Bloembergen, J. Ducuing, and P. S. Pershan, "Interactions between light waves in a nonlinear dielectric," *Phys. Rev.* **127**, 1918-1939 (1962).
6. N. Bloembergen and P. S. Pershan, "Light waves at the boundary of nonlinear media," *Phys. Rev.* **128**, 606-622 (1962).
7. N. Bloembergen and Y. R. Shen, "Quantum-theoretical comparison of nonlinear susceptibilities in parametric media, lasers, and Raman lasers," *Phys. Rev.* **133**, A37-A49 (1964).
8. D. A. Kleinman, "Nonlinear dielectric polarization in optical media," *Phys. Rev.* **126**, 1977 (1962).
9. S. K. Kurtz, J. Jerphagnon, and M. M. Choy, *Nonlinear Dielectric Susceptibilities* (Landolt-Bornstein), New Series, K.-H. Hellwege, Ed., Vol. 11, Springer-Verlag, Berlin, 1979.
10. P. D. Maker, R. W. Terhune, M. Nisenoff, and C. M. Savage, "Effects of dispersion and focusing on the production of optical harmonics," *Phys. Rev. Lett.* **8**, 21 (1962).
11. J. A. Giordmaine, "Mixing of light beams in crystals," *Phys. Rev. Lett.* **8**, 19 (1962).

12. F. Zernike, Jr., "Refractive indices of ammonium dihydrogen phosphate and potassium dihydrogen phosphate between 2000 Å and 1.5 μm," *J. Opt. Soc. Am.* **54**, 1215 (1964).
13. A. Ashkin, G. D. Boyd, and J. M. Dziedzic, "Observation of continuous second harmonic generation with gas lasers," *Phys. Rev. Lett.* **11**, 14 (1963).
14. G. D. Boyd and D. A. Kleinman, "Parametric interaction of focused Gaussian light beams," *J. Appl. Phys.* **39**, 3597 (1968).
15. W. Seka, S. D. Jacobs, J. E. Rizzo, R. Boni, and R. S. Craxton, "Demonstration of high efficiency harmonic conversion of high power Nd-Glass laser radiation", *Opt. Comm.* **34**, 469 (1980).
16. Parametric amplification was first demonstrated by C. C. Wang and G. W. Racette, "Measurement of parametric gain accompanying optical difference frequency generation," *Appl. Phys. Lett.* **6**, 169 (1965).
17. The first demonstration of optical parametric oscillation is that of J. A. Giordmaine and R. C. Miller, "Tunable optical parametric oscillation in LiNbO₃ at optical frequencies," *Phys. Rev. Lett.* **14**, 973 (1965).
18. Some of the early theoretical analyses of optical parametric oscillation are attributable to R. H. Kingston, "Parametric amplification and oscillation at optical frequencies," *Proc. IRE* **50**, 472 (1962), and N. M. Kroll, "Parametric amplification in spatially extended media and applications to the design of tunable oscillators at optical frequencies," *Phys. Rev.* **127**, 1207 (1962).
19. J. M. Manley and H. E. Rowe, "General energy relations in nonlinear reactances," *Proc. IRE* **47**, 2115 (1959).
20. D. Magde and M. Mahr, "Study in ammonium dihydrogen phosphate of spontaneous parametric interaction tunable from 4400 Å to 16000 Å," *Phys. Rev. Lett.* **18**, 905 (1967).
21. A. A. Davydov, L. A. Kulevskii, A. M. Prokhorov, A. D. Savel'ev, V. V. Smirnov, and A. V. Shirkov, "A tunable infrared parametric oscillator in a CdSe crystal," *Opt. Comm.* **9**, 234 (1973); also R. L. Herbst and R. L. Byer, "Efficient parametric mixing in CdSe," *Appl. Phys. Lett.* **19**, 527 (1971); R. L. Herbst and R. L. Byer, "Single resonant CdSe infrared parametric oscillator," *Appl. Phys. Lett.* **21**, 189 (1972).
22. W. H. Louisell, A. Yariv, and A. E. Siegman, "Quantum fluctuations and noise in parametric processes," *Phys. Rev.* **124**, 1646 (1961).
23. F. M. Johnson and J. A. Durado, "Frequency up-conversion," *Laser Focus* **3**, 31 (1967).
24. J. E. Midwinter and J. Warner, "Up-conversion of near infrared to visible radiation in lithium-meta-niobate," *J. Appl. Phys.* **38**, 519 (1967).
25. J. Warner, "Photomultiplier Detection of 10.6 μm Radiation using optical up-conversion in proustite," *Appl. Phys. Lett.* **12**, 222 (1968).
26. K. F. Hulme, O. Jones, P. H. Davies, and M. V. Hobden, "Synthetic proustite (Ag₃AsS₃): A new material for optical mixing," *Appl. Phys. Lett.* **10**, 133 (1967).
27. T. R. Gurski, "High quantum efficiency infrared up-conversion," *Appl. Phys. Lett.* **23**, 273 (1973).

13

Phase-Conjugate Optics

13.1. INTRODUCTION

Phase-conjugate optics is the name given to a new area in coherent optics [1, 2]. This area involves the use of *nonlinear optical techniques for real-time processing of electromagnetic fields*. The name is due to the fact that all the applications demonstrated or proposed to date involve phase reversal of an incoming electromagnetic wave.

There exist numerous practical and scientific implications of phase-conjugate optics. These include image transmission, pulse compression, image processing (including convolution and correlation), and real-time holography. We will illustrate this point by describing, before embarking on the detailed theory, two such applications: propagation through a distorting medium and image transmission of images in a multimode fiber.

13.2. PROPAGATION THROUGH A DISTORTING MEDIUM

Consider as an example the problem of an optical beam

$$\begin{aligned} E_1(\mathbf{r}, t) &= \text{Re}[\psi(\mathbf{r}) e^{i(\omega t - kz)}] \\ &= \text{Re}[A_1(\mathbf{r}) e^{i\omega t}] \end{aligned} \quad (13.2-1)$$

propagating through a linear lossless distorting medium essentially in the z direction (from left to right). The dependence of ψ on \mathbf{r} reflects spatial modulation by information, the effects of distortion, and diffraction. If in some region of space near z_0 we somehow generate a field $E_2(\mathbf{r}, t)$ which is described locally by

$$\begin{aligned} E_2(\mathbf{r}, t) &= \text{Re}[\psi^*(\mathbf{r}) e^{i(\omega t + kz)}] \\ &= \text{Re}[A_2(\mathbf{r}) e^{i\omega t}], \end{aligned} \quad (13.2-2)$$

then

$$A_2(\mathbf{r}) = A_1^*(\mathbf{r}) \quad \text{for all } z < z_0.$$

The field $E_2(\mathbf{r}, t)$ will be called in this book the *complex conjugate* of $E_1(\mathbf{r}, t)$. We note that to get E_2 from E_1 we take the complex conjugate of the *spatial part only*, leaving the factor $e^{i\omega t}$ intact. (This is equivalent to leaving the spatial part alone but reversing the sign of t . That is, the field E_2 is related to E_1 by "time reversal.")

To appreciate the practical consequences of conjugation, consider a field E_1 propagating from left to right through a distorting medium as shown in Fig. 13.1. The electric permittivity (dielectric constant) of the composite medium is $\epsilon(\mathbf{r})$, which is a real quantity accounting for the presence of passive linear components such as lenses, wedges, and/or distorting media. The scalar forward-propagating ($+z$) beam is taken as

$$E_1(\mathbf{r}, t) = \text{Re}[\psi_1(\mathbf{r})e^{+i(\omega t - kz)}]. \quad (13.2-3)$$

The scalar wave equation obeyed by this wave is taken as

$$\nabla^2 \psi_1 + [\omega^2 \mu \epsilon(\mathbf{r}) - k^2] \psi_1 - 2ik \frac{\partial \psi_1}{\partial z} = 0. \quad (13.2-4)$$

This form is valid as long as the fractional variation of $\epsilon(\mathbf{r})$ in one optical wavelength is small compared to unity.

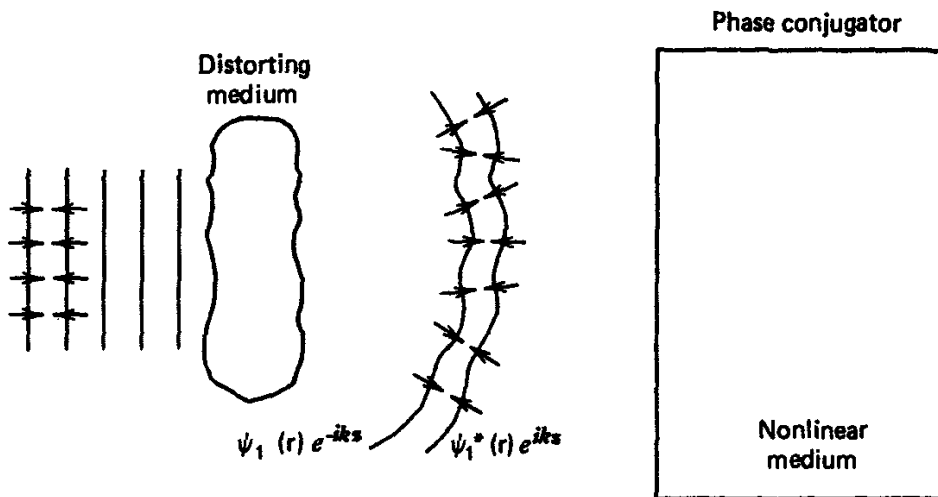


Figure 13.1. Complex conjugation of an input field $\psi_1(\mathbf{r})e^{-iks}$.

Let us next, as a purely mathematical operation, consider the complex conjugate of Eq. (13.2-4):

$$\nabla^2 \psi_1^* + [\omega^2 \mu \epsilon(\mathbf{r}) - k^2] \psi_1^* + 2ik \frac{\partial \psi_1^*}{\partial z} = 0. \quad (13.2-5)$$

This is also the wave equation obeyed by a wave propagating in the $-z$ direction of the form

$$E_2(\mathbf{r}, t) = \text{Re}[\psi_2(\mathbf{r})e^{i(\omega t + kz)}], \quad (13.2-6)$$

provided we put

$$\psi_2(\mathbf{r}) = a\psi_1^*(\mathbf{r}), \quad (13.2-7)$$

where a is any constant. What we have shown is that a wave E_2 , whose complex amplitude is everywhere the complex conjugate of E_1 , satisfies the same wave equation as that obeyed by E_1 . (This is true for an arbitrary wave in any lossless medium with a real ϵ ; see Problem 13.7.)

The practical corollary of the formal proof given above is the following: consider a complex monochromatic beam E_1 which propagates from some plane A to another plane B through a medium $\epsilon(\mathbf{r})$. If in the vicinity of B we generate, by some means, a wave E_2 whose complex amplitude over an area which contains the incident beam is the complex conjugate of that of E_1 (within a multiplicative constant), then E_2 will propagate backwards and *remain everywhere the complex conjugate of E_1 . Its wavefronts everywhere thus coincide with those of E_1 .*

This aspect of phase conjugation was demonstrated in some of the earlier experiments [3, 4].

13.3. IMAGE TRANSMISSION IN FIBERS

The second fundamental illustration of the potential area of application of phase conjugation is in long-distance image transmission in optical waveguides [5, 6]. The problem of phase conjugation in an optical waveguide, say a fiber, is illustrated in Fig. 13.2. Let the incident field at the input plane of the guide be

$$f_1(x, y, z = 0, t) = \sum_{m=0}^N \sum_{n=0}^N A_{mn} E_{mn}(x, y) e^{i\omega t}, \quad (13.3-1)$$

where E_{mn} is the spatial mode function m, n of the particular waveguide used. The summation is over the discrete spectrum of guided modes, whose number is taken as N^2 . The output field at the fiber's end is obtained by propagating each mode a distance L and then summing:

$$f_2(x, y, L, t) = \sum_m \sum_n A_{mn} E_{mn}(x, y) \exp[i(\omega t - \beta_{mn} L)], \quad (13.3-2)$$

where β_{mn} is the propagation constant of mode m, n and where we have neglected the possibility of mode-dependent losses. In general, the picture field (13.3-2) is different from the input field (13.3-1), due to the phase factors $\beta_{mn} L$. In practice, this corresponds to a scrambling of spatial information. If, however, we can generate a complex conjugate of the output field (13.3-2),

$$f_3(x, y, L, t) = \sum_m \sum_n A_{mn}^* E_{mn}^*(x, y) \exp[i(\omega t + \beta_{mn} L)], \quad (13.3-3)$$

and launch it into a section of length L of a fiber identical in length and all other characteristics to the first one, the result will be an output field

$$\begin{aligned} f_4(x, y, 2L, t) &= \sum_m \sum_n A_{mn}^* E_{mn}^*(x, y) \exp[i(\omega t + \beta_{mn} L - \beta_{mn} L)] \\ &= \sum_m \sum_n A_{mn} E_{mn}(x, y) e^{i\omega t}. \end{aligned} \quad (13.3-4)$$

Except for the complex conjugation, the field f_4 at $z = 2L$ is the same as the input field f_1 , and the spatial information carried by the wave has thus been recovered.

The practical realization of this scheme requires two sections of identical near-perfect fibers which have negligible intermodal scattering and negligible loss for all the modes. A similar scheme using a single section of fiber

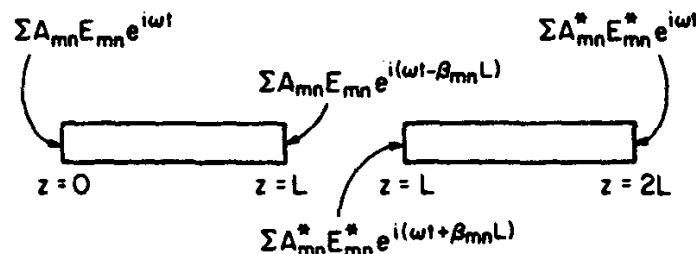


Figure 13.2. Compensation (and restoration for image loss) by modal dispersion in a dielectric waveguide using phase conjugation.

was demonstrated experimentally [13]. In this scheme, the phase conjugate signal was generated via the degenerate four wave mixing (see next section) in a barium titanate (BaTiO_3) crystal and then retraversed the same fiber. This results in a reconstruction of the input image.

13.4. THEORY OF PHASE CONJUGATION BY FOUR-WAVE MIXING [7]

In this section we present the basic theory of phase conjugation by four-wave mixing. Here we depend on the third-order nonlinearity, which according to Eq. (12.1-1) can be represented as

$$P_i = 4\chi_{ijkl}E_jE_kE_l. \quad (13.4-1)$$

Using methods identical to those leading to Eq. (12.2-7) (the details are left as a problem), we find that the complex amplitude of the induced polarization at the frequency $\omega_1 = \omega_2 + \omega_3 - \omega_4$ is related to the electric-field amplitudes according to

$$\begin{aligned} P_i(\omega_1 = \omega_2 + \omega_3 - \omega_4) & \\ & = 6\chi_{ijkl}(-\omega_1, \omega_2, \omega_3, -\omega_4)E_j(\omega_2)E_k(\omega_3)E_l^*(\omega_4) \end{aligned} \quad (13.4-2)$$

In the case of a material medium with an instantaneous polarization response, the element χ_{ijkl} in Eq. (13.4-2) is numerically equal to that in Eq. (13.4-1). The factor 6 results from the number of different ways in which the combination $E_j(\omega_2)E_k(\omega_3)E_l^*(\omega_4)$ arises in Eq. (13.4-1). Unlike the second-order coefficient d_{ijk} , which is nonvanishing only in noncentrosymmetric crystals, symmetry allows the coefficient χ_{ijkl} to be nonvanishing in any medium, including isotropic materials (gases, liquids, glasses) as well as cubic crystals. The form of the χ_{ijkl} tensor, however, is dictated by the point-group symmetry of the medium. A tabulation of its form in different symmetries is given in Hellwarth [8]. That reference includes an extensive discussion of the various physical phenomena which result in third-order optical nonlinearities. A short listing of χ_{yxxy} in some common materials is included in Table 13.1.

The basic experimental arrangement of four-wave mixing is illustrated in Fig. 13.3. The nonlinear medium is pumped by two intense counter propagating plane wave beams E_1 and E_2 of frequency ω . In what follows we use

Table 13.1. $\chi_{xyyx}(-\omega, \omega, \omega, -\omega)$ of Some Materials at $\lambda = 694 \text{ nm}^a$

Material	n	$\chi_{xyyx}(-\omega, \omega, \omega, -\omega)$ (10^{-34} MKS)
CS ₂	1.612	441
CCl ₄	1.454	6.2
Fused quartz	1.455	1.5
YAG	1.829	7.41
Benzene	1.493	68.9
LSO glass	1.505	2.26
ED-4 glass	1.557	2.8
SF-7 glass	1.631	9.8
BK-7 glass	1.513	2.26
LaSF-7 glass	1.91	12.4

^aFrom Hellwarth [8].

the subscripts to label the wave and not to indicate its polarization. The polarizations are assumed fixed. The waves are taken as

$$E_{1,2} = A_{1,2}(\mathbf{r}) e^{i(\omega t - \mathbf{k}_{1,2} \cdot \mathbf{r})}. \quad (13.4-3)$$

The medium supports two other waves which are propagating essentially in opposition to each other along some arbitrary direction z . Their complex amplitudes are $A_1(\mathbf{r})$ and $A_2(\mathbf{r})$. The waves E_3 and E_4 are not, in general, plane waves, and we consider E_4 as some kind of input wave and E_3 as the output. We find that if the frequency ω_4 of wave 4 is $\omega_4 = \omega$ (i.e., the same as that of the pump waves 1 and 2), then wave 3 will be generated with $\omega_3 = \omega$ and its complex amplitude everywhere will be the complex conjugate of that of E_4 . The direction of propagation of wave 4 is arbitrary. The four

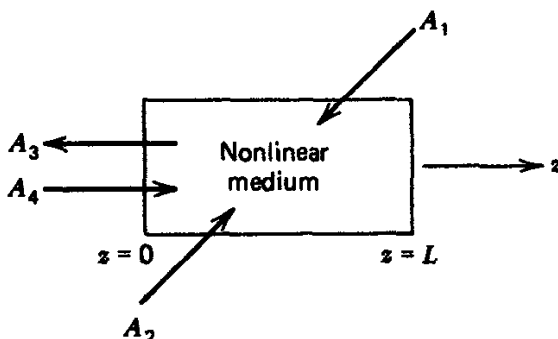


Figure 13.3. The basic experimental arrangement for phase conjugation by four-wave mixing.

waves are assumed to be polarized along a given set of directions, and we henceforth treat the interaction using scalar symbols.

The four waves 1, 2, 3, 4 are coupled by means of the nonlinear polarization (13.4-2). Consider, as an example, the nonlinear polarization term due to the mixing of waves 1, 2, and 4:

$$\begin{aligned} P_{\text{NL}}^{(\omega-\omega+\omega-\omega)}(\mathbf{r}, t) &= \frac{1}{2}\chi^{(3)}A_1A_2A_4^*e^{i[(\omega+\omega-\omega)t-(\mathbf{k}_1+\mathbf{k}_2)\cdot\mathbf{r}+kz]} \\ &= \frac{1}{2}\chi^{(3)}A_1A_2A_4^*e^{i(\omega t+kz)}, \end{aligned} \quad (13.4-4)$$

since $\mathbf{k}_1 + \mathbf{k}_2 = 0$. Note by comparison with Eq. (13.4-2) that $\chi^{(3)} \equiv 6\chi_{ijkl}$. Equation (13.4-4) corresponds to a polarization wave with a frequency ω and a wave vector $\mathbf{k} = -\hat{\mathbf{e}}_2k$ and will thus excite a wave E_3 of the form

$$E_3 = A_3(z)e^{i(\omega t+kz)}.$$

Once generated, this new wave E_3 will mix with waves A_1, A_2 to generate a polarization

$$P_{\text{NL}}^{(\omega-\omega+\omega-\omega)}(z, t) = \frac{1}{2}\chi^{(3)}A_1A_2A_3^*e^{i(\omega t-kz)}, \quad (13.4-5)$$

which has the same frequency and propagation vector as E_4 , so that it will interact strongly with this wave. This is how the interaction and power exchange of waves 3 and 4 is mediated via the pump waves 1 and 2. In treating this interaction mathematically we will assume that the intensities of the pump waves E_1 and E_2 are so strong as to be little affected by the power exchange, so that A_1 and A_2 will be taken as constants. We will also assume that $|A_1| = |A_2|$, so that the slowing down (optical Kerr effect) of each pump wave by the other is the same, and thus can be neglected. We thus need to consider only the propagation of waves E_3 and E_4 .

We start with the basic coupling equation (12.3-10) of a wave to a nonlinear polarization. In the case of the backward wave E_3 , we replace k_1 in (12.3-10) by $-k$, assume no losses ($\sigma = 0$), and recalling that $k^2 = \omega^2\mu_0\epsilon$, obtain

$$-ik\frac{dA_3}{dz}e^{i(\omega t+kz)} = -\mu_0\frac{\partial^2}{\partial t^2}[P_{\text{NL}}^{(\omega)}(z, t)]. \quad (13.4-6)$$

Using Eq. (13.4-4) for P_{NL} leads to

$$\frac{dA_3}{dz} = i\frac{\omega}{2}\sqrt{\frac{\mu_0}{\epsilon}}\chi^{(3)}A_1A_2A_4^*, \quad (13.4-7)$$

and similarly,

$$\frac{dA_4^*}{dz} = i \frac{\omega}{2} \sqrt{\frac{\mu_0}{\epsilon}} \chi^{(3)} A_1^* A_2^* A_3,$$

where we have used $k = \omega \sqrt{\mu_0 \epsilon}$. The last two equations can be rewritten as

$$\begin{aligned} \frac{dA_3}{dz} &= i \kappa^* A_4^*, \\ \frac{dA_4^*}{dz} &= i \kappa A_3, \end{aligned} \quad (13.4-8)$$

where

$$\kappa^* = \frac{\omega}{2} \sqrt{\frac{\mu_0}{\epsilon}} \chi^{(3)} A_1 A_2.$$

Most of the research literature in phase conjugate optics uses the CGS system of units. Our derivation is based on MKS units. The equations (13.4-8), which are the basic starting point for describing many applications, remain unchanged in CGS units (esu) except that the definition of the coupling constant is

$$(\kappa^*)_{\text{esu}} = \frac{2\pi\omega}{cn} \chi^{(3)} A_1 A_2, \quad (13.4-9)$$

where, of course, all the physical quantities $\chi^{(3)}$, $A_{1,2}$, c must be expressed in esu. To be able to move back and forth between the two systems of units, it is useful to remind ourselves that

$$1 \text{ statvolt/cm} = 2.99793 \times 10^4 \text{ V/m}$$

and

$$\chi_{\text{MKS}}^{(3)} = \frac{4\pi\epsilon_0}{9 \times 10^8} \chi_{\text{esu}}^{(3)} = \frac{\chi^{(3)} \text{esu}}{8.1 \times 10^{18}}. \quad (13.4-10)$$

If we specify the complex amplitudes $A_3(L)$ and $A_4(0)$ of the two weak waves at their respective input planes ($z = L$, $z = 0$), the solution of Eq. (13.4-8) is

$$\begin{aligned} A_3(z) &= \frac{\cos|\kappa|z}{\cos|\kappa|L} A_3(L) + i \frac{\kappa^* \sin|\kappa|(z-L)}{|\kappa| \cos|\kappa|L} A_4^*(0), \\ A_4^*(z) &= i \frac{|\kappa| \sin|\kappa|z}{\kappa^* \cos|\kappa|L} A_3(L) + \frac{\cos|\kappa|(z-L)}{\cos|\kappa|L} A_4^*(0). \end{aligned} \quad (13.4-11)$$

Most of the experimental situations involve a single input $A_4(0)$ at $z = 0$. In this case the reflected wave at the input ($z = 0$) is

$$A_3(0) = -i \left(\frac{\kappa^*}{|\kappa|} \tan |\kappa|L \right) A_4^*(0), \quad (13.4-12)$$

while at the output ($z = L$)

$$A_4^*(L) = \frac{A_4^*(0)}{\cos |\kappa|L}. \quad (13.4-13)$$

First we note that the reflected wave $A_3(0)$ is proportional to $A_4^*(0)$, that is, to the complex conjugate of the input wave $A_4(0)$. It follows directly from the linearity of the equations (13.4-8) that if the input field E_4 is not a plane wave but possesses complex wavefronts (but still a monochromatic field), so that

$$E_4 = \text{Re}[\psi(\mathbf{r}) e^{i(\omega t - kz)}]$$

[where $\psi(\mathbf{r})$ is some complex function], then the reflected field E_3 is of the form

$$E_3(\mathbf{r})_{z < 0} = \text{Re} \left[-i \left(\frac{\kappa^*}{|\kappa|} \tan |\kappa|L \right) \psi^*(\mathbf{r}) e^{i(\omega t + kz)} \right], \quad (13.4-14)$$

so that the analysis of the equations (13.4-8) applies not only to plane-wave inputs but to waves with arbitrary wavefronts.

We have thus established that the four-wave mixing geometry of Fig. 13.3 performs the function of phase conjugation demanded of the magical mirror of Fig. 13.1 and that the reflected wave E_3 will unravel in its backward propagation any distortion suffered by the incident wave E_4 . This compensation feature was demonstrated in experiments by Woerdman [9] and by Stepanov et al. [10] in 1971.

Although our main purpose was to demonstrate phase conjugation, the formal solution leading to Eq. (13.4-12) reveals some new features. We note that for

$$\frac{1}{4}\pi < |\kappa|L < \frac{3}{4}\pi \quad (13.4-15)$$

we have

$$|A_3(0)| > |A_4(0)|$$

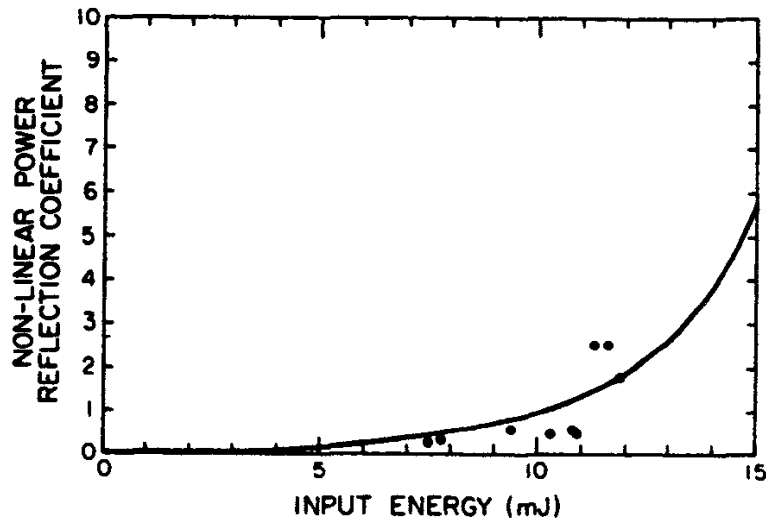


Figure 13.4. Plot of nonlinear power reflection coefficient versus pump energy (in mJ): [●] data; solid line, least-squares fit to $R = \tan^2 \alpha \epsilon_p$.

and the phase-conjugate mirror acts as a reflection amplifier. The power gain of the amplifier is

$$\left| \frac{A_3(0)}{A_4(0)} \right|^2 = \tan^2 |\kappa| L. \quad (13.4-16)$$

Some early measurements of reflection gain (up to 300%) in a carbon disulfide cell using a Q-switched ruby laser radiation ($\lambda = 0.6943 \mu\text{m}$) are shown in Fig. 13.4. The experimental apparatus is sketched in Fig. 13.5.

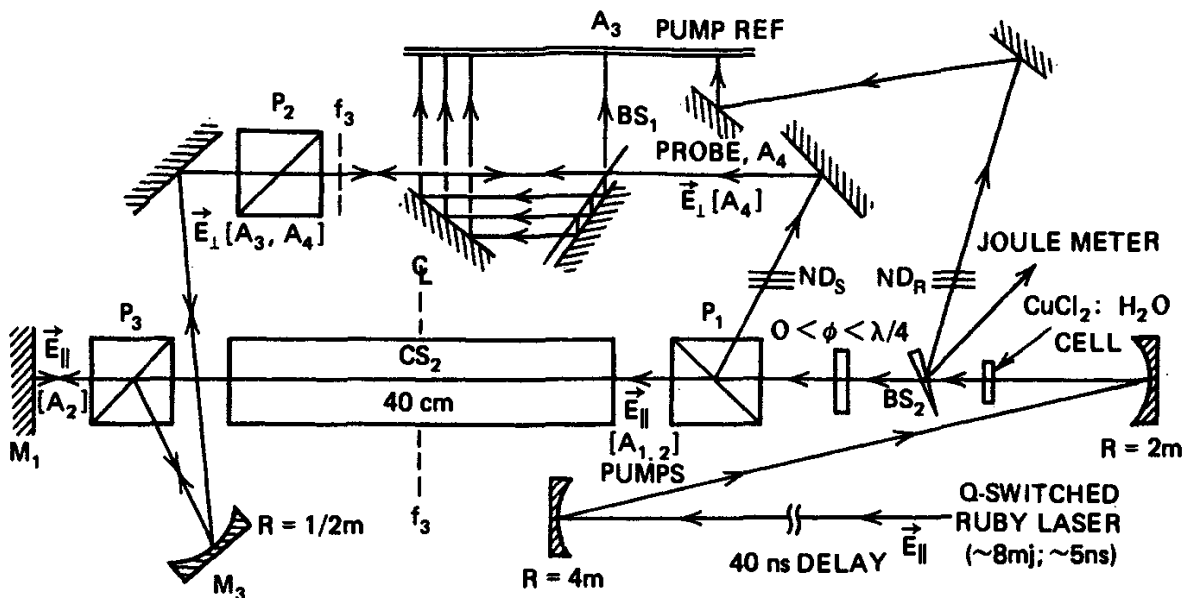


Figure 13.5. Experimental apparatus for measurement of the nonlinear reflection coefficient (all mirrors are totally reflecting).

It also follows from Eq. (13.4-13) that for a single input $A_4(0)$ the transmitted wave $A_4(L)$ is given by

$$A_4(L) = \frac{1}{\cos|\kappa|L} A_4(0) \quad (13.4-17)$$

and is thus always bigger than $A_4(0)$, that is, the device functions as a transmission amplifier for all values of κ at any pumping level.

A quantum-mechanical analysis of the four-wave interaction reveals that the amplification of the forward wave A_4 and the generation of the backward wave A_3 is at the expense of the pump waves A_1 and A_2 . For each photon added to A_3 , one photon must be added to A_4 while, simultaneously, a photon is subtracted from each of A_1 and A_2 .

The field distribution inside the medium under the high-amplification condition $\frac{1}{4}\pi < |\kappa|L < \frac{1}{2}\pi$ is shown in Fig. 13.6.

If the pump intensity (i.e., the product $|A_1 A_2|$) is increased until $|\kappa|L = \frac{1}{2}\pi$, then according to Eqs. (13.4-16) and (13.4-17)

$$\left| \frac{A_3(0)}{A_4(0)} \right| = \infty, \quad \frac{A_4(L)}{A_4(0)} = \infty,$$

which can be interpreted as a situation where a vanishingly small input $A_4(0)$ gives rise to finite outputs $A_4(L)$ and $A_3(0)$ from both sides of the interaction volume. A device which emits radiation without an input is by definition an oscillator. We thus established theoretically the possibility of mirrorless oscillation, which is reminiscent of the distributed-feedback (DFB) laser described in Chapter 11. The analogy to the DFB laser is quite

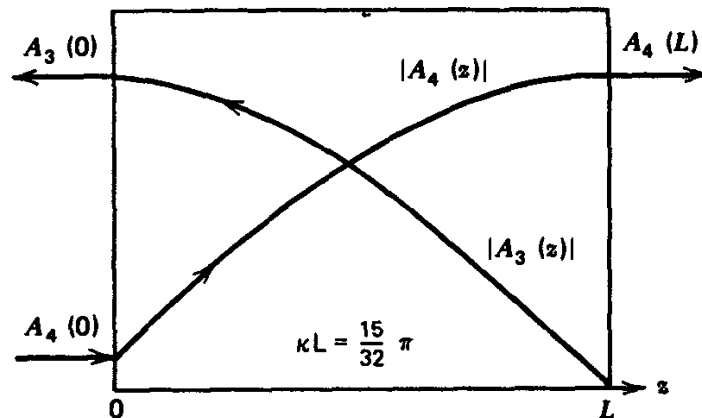


Figure 13.6. The field distribution inside the nonlinear medium under high-amplification conditions.

revealing. In the latter the coupling between the forward and backward waves was provided by a spatial periodic perturbation of the medium with a period equal to some half odd integer times the wavelength of oscillation in the medium. In the four-wave oscillator waves A_2 and A_4 set up an index (or loss) grating which reflects A_1 into the direction of A_3 , while simultaneously A_3 and A_1 set up a grating which diffracts A_2 into the direction of A_4 . It is easy to show that the Bragg conditions are satisfied automatically in both sets of gratings if the geometry of Fig. 13.3 is employed. The intensity distribution inside the nonlinear medium under oscillation conditions is plotted in Fig. 13.7.

An experimental setup in which oscillation was observed is shown in Fig. 13.8. We note that the pump waves A_1 and A_2 , the latter produced by reflection of A_1 from mirror M_1 , are polarized orthogonally to the oscillation waves. This is made possible by the existence in CS_2 , as well as in all isotropic media, of a nonvanishing tensor component χ_{1221} .

13.4.1. A Numerical Estimate of κ

For most practical situations we need, according to the equations (13.4-11), a pumping intensity large enough so that $\kappa L \sim 1$. Many of the phase-conjugation experiments to date have been performed in CS_2 , so it is interesting to calculate the expected magnitude of the coupling constant κ in this material. We use

$$\begin{aligned}\chi_{yxxxy}(-\omega, \omega, \omega, -\omega) &\approx 3.57 \times 10^{-13} \text{ esu} \\ &= 4.41 \times 10^{-32} \text{ MKS.}\end{aligned}$$

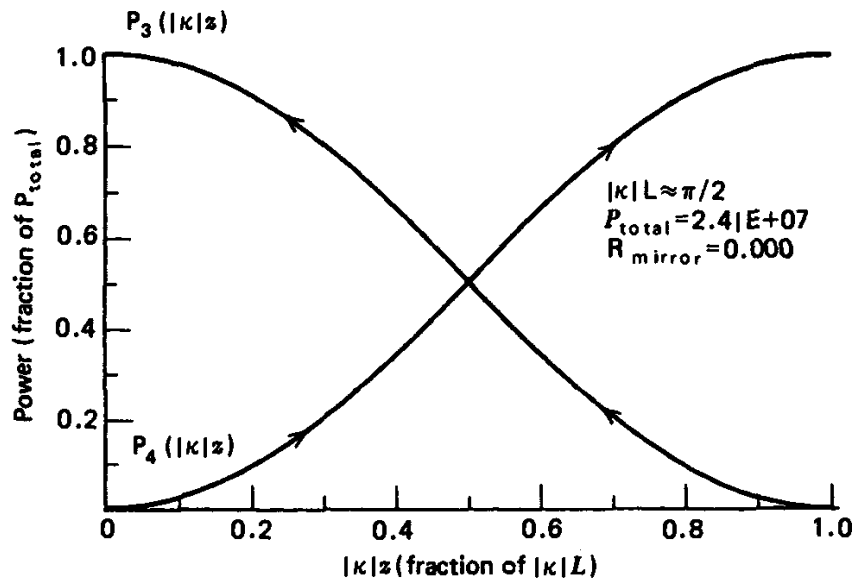


Figure 13.7. Intensity distributions of the input power P_4 and the conjugate-field power P_3 as a function of $|\kappa|z$ near the oscillation condition ($|\kappa|L = \frac{1}{2}\pi$). (After [1].)

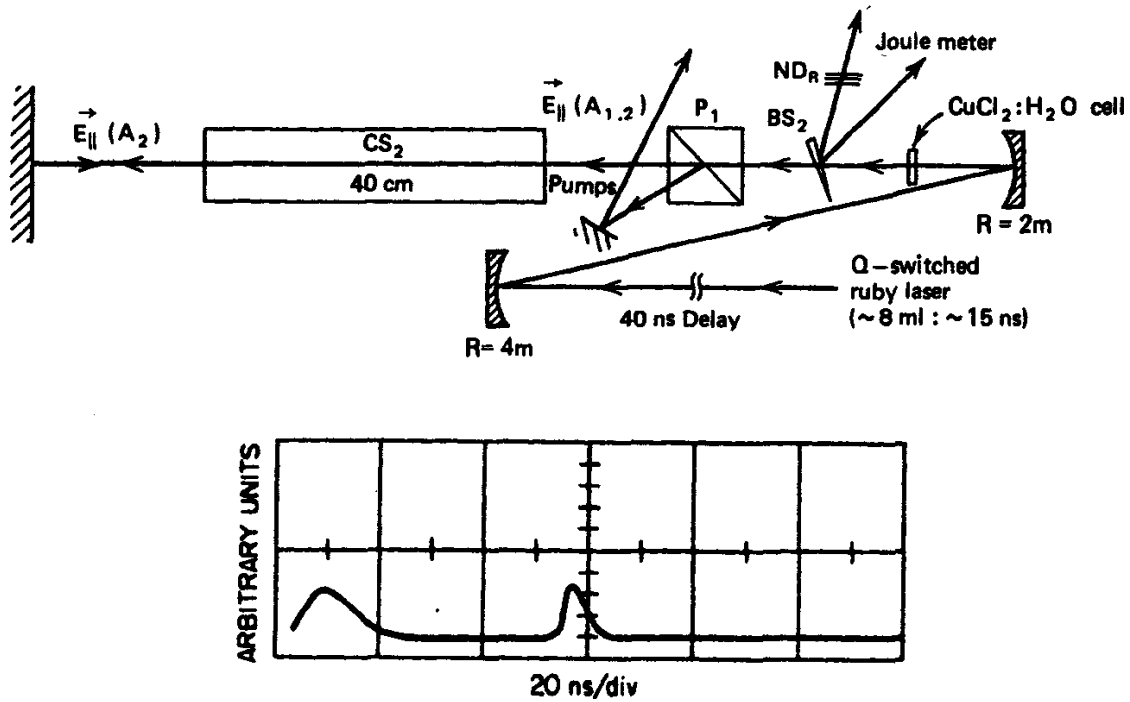


Figure 13.8. The experimental arrangement used in observing oscillation by four wave mixing. (After [1].)

(Here we have used $\chi_{\text{MKS}}^{(3)} = \chi_{\text{esu}}^{(3)}/8.1 \times 10^{18}$.) Using Eq. (13.4-9) and

$$A_1 = A_2 = \sqrt{\frac{2I}{\epsilon_0 n c}},$$

we obtain

$$\kappa_{\text{MKS}} = \frac{2\pi}{n\epsilon_0\lambda} \sqrt{\frac{\mu}{\epsilon}} \chi^{(3)} I_1 = 2.68 \times 10^{14} \frac{\chi^{(3)}}{n^2\lambda} I_1.$$

Using

$$\chi_{\text{CS}_2}^{(3)} = 6\chi_{yxxy}(-\omega, \omega, \omega, -\omega) = 2.03 \times 10^{-31} \text{ MKS},$$

$$\lambda = 10^{-6} \text{ m}, \quad n = 1.62,$$

we obtain

$$\kappa(\text{m}^{-1}) = 0.21 I_1 (\text{MW}/\text{cm}^2).$$

To get values of $\kappa L \sim 1$ with, say, $L = 10$ cm requires intensities in the range of tens of megawatts per cm^2 , which are available only from pulsed lasers. The requisite intensities can be reduced by orders of magnitude if one takes advantage of the large values of $\chi^{(3)}$ which result when the applied

frequency is near some transition frequency in the medium. Such resonantly enhanced four-wave mixing experiments in atomic sodium vapor have been reported [11].

For a more detailed description of this field, including such applications as image processing, frequency filtering, and pulse narrowing, the reader is referred to [12, 14].

PROBLEMS

- 13.1. Consider a medium whose permittivity depends on the field intensity according to

$$\epsilon(\mathbf{r}) = \epsilon_0(\mathbf{r}) + \epsilon_2(\mathbf{r})|E|^2,$$

where E is the total complex amplitude of the monochromatic field at point \mathbf{r} . Show that the wave equation

$$\nabla^2 E - \frac{\mu}{c^2} [\epsilon_0(\mathbf{r}) + \epsilon_2(\mathbf{r})|E|^2] \frac{\partial^2 E}{\partial t^2} = 0$$

is satisfied by

$$E = [\psi(\mathbf{r}) e^{-ikz} + a f(\mathbf{r}) e^{ikz}] e^{i\omega t} + \text{c.c.}$$

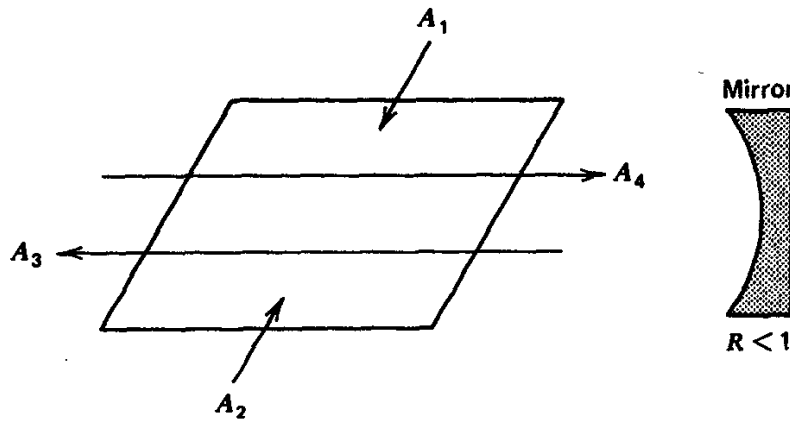
provided

$$f(\mathbf{r}) = \psi^*(\mathbf{r}),$$

$$|a| = 1.$$

This is true for any lossless medium as long as ϵ is real. In the proof we discard spatially nonsynchronous terms with $e^{\pm i3kz}$ dependence. If you have completed the proof you have succeeded in showing that a phase-conjugate wave can compensate by backward propagation not only for static index inhomogeneities [$\epsilon_0(\mathbf{r})$], but also for intensity-dependent distortions [$\epsilon_2|E|^2$].

- 13.2. Consider the experimental arrangement of the accompanying figure. Show that the threshold condition for oscillation in a direction



normal to the plane of the mirror is

$$|\kappa|L = \tan^{-1} \frac{1}{r},$$

where $R = |r|^2$ is the reflectance of the mirror.

- 13.3. Show that if the nonlinear medium used in the experimental arrangement of Fig. 13.3 is lossy, then the coupled mode equations (13.4-8) become

$$\begin{aligned} \frac{dA_3}{dz} &= i\kappa^* e^{-\alpha L/2} A_4^* + \frac{\alpha}{2} A_3, \\ \frac{dA_4^*}{dz} &= i\kappa e^{-\alpha L/2} A_3 - \frac{\alpha}{2} A_4^*, \end{aligned}$$

where α is the intensity absorption coefficient and

$$\kappa = \frac{\omega}{2} \sqrt{\frac{\mu_0}{\epsilon}} \chi^{(3)} A_1^*(L) A_2^*(0).$$

Solve these equations subject to the boundary conditions $A_3(L) = 0$ and a given $A_4(0)$. Show that the reflection coefficient is

$$r = \frac{A_3(0)}{A_4^*(0)} = \frac{-2i\kappa^* e^{-\alpha L/2} \tan(\kappa_{\text{eff}} L)}{\alpha \tan(\kappa_{\text{eff}} L) + 2\kappa_{\text{eff}}}$$

with

$$\kappa_{\text{eff}} = \sqrt{|\kappa|^2 e^{-\alpha L} - \left(\frac{\alpha}{2}\right)^2}$$

- 13.4. Solve the coupling equations (13.4-8) for the case when the frequency of the weak input wave A_4 is not the same as that of the pump waves (i.e., $\omega_1 = \omega_2$, $\omega_4 \neq \omega_1$). Plot the frequency response

$$|r| = \left| \frac{A_3(\omega + \delta)}{A_4^*(\omega - \delta)} \right|$$

as a function of the frequency offset δ . Here ω is the pump frequency and $\omega - \delta$ is the input frequency. [Caution: Watch for the phase factor $\mathbf{k}_1 + \mathbf{k}_2 - (\mathbf{k}_3 + \mathbf{k}_4)$ in

$$(\mathbf{k}_1 + \mathbf{k}_2) \cdot \mathbf{r} + (k_{3z} + k_{4z})z,$$

which for $\delta \neq 0$ is no longer zero.]

- 13.5. Show, using reasoning similar to that leading to Eq. (12.2-7), that for the case of an atom in which the induced polarization is a single-valued function of the electric field (instantaneous response), $\chi_{ijkl}(-\omega_1, \omega_2, \omega_3, -\omega_4)$ of Eq. (13.4-2) is the same as χ_{ijkl} of Eq. (13.4-1).
- 13.6. Show that the resonant frequencies of a laser resonator in which one of the reflectors has been replaced by a phase-conjugate mirror do not depend on the distance between reflectors.
- 13.7. *Conjugate waves.* Consider the electric-field vector of a monochromatic radiation

$$\mathbf{E}_1(\mathbf{r}, t) = \mathbf{E}(\mathbf{r})e^{i\omega t},$$

where the amplitude function $\mathbf{E}(\mathbf{r})$ satisfies the equation

$$\nabla \times (\nabla \times \mathbf{E}) - \omega^2 \mu \epsilon \mathbf{E} = 0.$$

- (a) Show that the conjugate wave

$$\mathbf{E}_2(\mathbf{r}, t) = \mathbf{E}^*(\mathbf{r})e^{i\omega t}$$

also obeys the same equation provided $\mu \epsilon$ is a real quantity (i.e., in a lossless medium).

- (b) Let

$$\mathbf{E}(\mathbf{r}) = \mathbf{A}(\mathbf{r})e^{i\phi(\mathbf{r})},$$

where A and ϕ are real functions of \mathbf{r} . Show that the wavefronts (surfaces of constant phase) of the waves \mathbf{E}_1 and \mathbf{E}_2 are given by

$$\begin{aligned}\phi(\mathbf{r}) + \omega t &= C_1, \\ -\phi(\mathbf{r}) + \omega t &= C_2,\end{aligned}$$

where C_1 and C_2 are constants. Since C_1 and C_2 are arbitrary, these wavefronts can be simply represented at any instant t by

$$\phi(\mathbf{r}) = \text{constant}.$$

In other words, $\mathbf{E}_1(\mathbf{r}, t)$ and $\mathbf{E}_2(\mathbf{r}, t)$ have exactly the same wavefronts in the entire space \mathbf{r} .

- (c) We now consider the propagation of a wavefront across space during a time interval $(t, t + dt)$. Show that the wavefront displacements for the waves E_1 and E_2 are given, respectively, by

$$d\mathbf{r}_1 \cdot \nabla\phi(\mathbf{r}) + \omega dt = 0$$

and

$$-d\mathbf{r}_2 \cdot \nabla\phi(\mathbf{r}) + \omega dt = 0.$$

This shows that the motion of the wavefront of the conjugate wave is opposite to that of the original wave.

- (d) Let

$$\mathbf{E}(\mathbf{r}) = \int \mathbf{B}(\mathbf{k}) e^{i\mathbf{k} \cdot \mathbf{r}} d^3k.$$

Show that each Fourier component of the conjugate wave is propagating exactly opposite to the corresponding component of the original wave.

- 13.8. *Polarization states of conjugate waves.* Let

$$\mathbf{E}_1(z, t) = \mathbf{E} e^{i(\omega t - kz)},$$

$$\mathbf{E}_2(z, t) = \mathbf{E}^* e^{i(\omega t + kz)},$$

$$\mathbf{E}_3(z, t) = \mathbf{E} e^{i(\omega t + kz)},$$

where \mathbf{E} is a complex constant and k is the propagation constant.

- (a) Show that if \mathbf{E}_1 is linearly polarized, so are \mathbf{E}_2 and \mathbf{E}_3 .
- (b) Show that if \mathbf{E}_1 is right-hand circularly polarized, so is its conjugate wave \mathbf{E}_2 . The wave \mathbf{E}_3 is now left-handed circularly polarized. The physical implications are: The spin of a photon is reversed upon reflection from a conjugator-mirror, whereas the helicity (spin component along the propagation direction) remains unchanged.

13.9. *Self-induced index modulation.* Consider the propagation of an intense optical beam in a medium possessing a strong Kerr effect.

- (a) Show that the complex amplitude of the polarization can be written

$$P_i^\omega = \epsilon_0 \chi_{ij} E_j^\omega + 3\chi_{ijkl} E_k^{\omega*} E_l^\omega E_j^\omega,$$

where E_j^ω is the complex amplitude of the electric field.

- (b) Assume that the electric field is polarized along the x direction. Show that the index of refraction associated with the beam can be written

$$n = n_0 + \frac{1}{2} n_2 \mathbf{E}^* \cdot \mathbf{E}$$

and show that

$$n_2 = \frac{3\chi_{1111}}{\epsilon_0 n_0}.$$

This n_2 is responsible for the self-focusing of laser beams in certain media.

REFERENCES

1. See, for example, A. Yariv, "Phase conjugate optics and real time holography," *IEEE J. Quant. Electron.* **QE-14**, 650 (1978).
2. See, for example, C. R. Giuliano, "Applications of optical phase conjugation," *Physics Today*, April 1981, p. 27.
3. B. Y. Zeldovich, V. I. Popovichev, V. V. Ragulskii, and F. S. Faisullov, "Connection between the wave fronts of the reflected and exciting light in stimulated Mandel'shtam-Brillouin scattering," *JETP Lett. (USA)* **15**, 109 (1972).
4. O. Y. Nosach, V. I. Popovichev, V. V. Ragulskii, and F. S. Faisullov, "Cancellation of Phase Distortions in an Amplifying medium with a "Brillouin Mirror"" *JETP Lett. (USA)* **16**, 435 (1972).
5. A. Yariv, "Three-dimensional pictorial transmission in optical fibers," *Appl. Phys. Lett.* **28**, 88 (1976).

6. A. Yariv, "On transmission and recovery of three-dimensional image information in optical waveguides," *J. Opt. Soc. Am.* **66**, 301 (1976).
7. R. W. Hellwarth, "Generation of time reversal wavefronts by nonlinear refraction," *J. Opt. Soc. Am.* **67**, 1 (1977).
8. R. W. Hellwarth, "Third-order optical susceptibilities of liquids and solids," *Proc. Quant. Electr.* **5**, Pergamon Press, 1977, pp. 1-68.
9. J. P. Woerdman, "Formation of a transient free carrier hologram in Si," *Opt. Commun.* **2**, 212 (1970).
10. B. I. Stepanov, E. V. Ivakin, and A. S. Rubanov, "Recording two-dimensional and three-dimensional dynamic holograms in transparent substances," *Sov. Phys.—Dokl.* **16**, 46 (July 1971).
11. P. F. Liao, D. M. Bloom, and N. P. Economou, "CW optical wave front configuration by saturated absorption in atomic sodium vapor," *Appl. Phys. Lett.* **32**, 813 (1978).
12. R. Fisher, Ed., *Phase Conjugate Optics*, Academic Press, New York, 1983.
13. G. J. Dunning and R. C. Lind, "Demonstration of image transmission through fibers by optical phase conjugation," *Opt. Lett.*, **7**, 558 (1982).
14. D. M. Pepper, "Nonlinear optical phase conjugation," *Optical Engineering* **21**, 156 (1982). This special issue also contains many papers on optical phase conjugation.

Author Index

- Abeles, F., 219
Abrams, R. L., 503
Adhav, R. S., 275
Adler, R., 365, 404
Aiki, K., 502
Alferness, R. C., 502
Alhaider, M. A., 404
Allen, S. D., 317
Armstrong, J. A., 547
Arnaud, J. A., 53
Ashkin, A., 548
Azzam, R. M. A., 68
- Bashara, N. M., 68
Bergmann, L., 404
Bhagavantam, S., 275
Blinov, L. M., 275
Bloembergen, N., 547
Bloom, D. M., 53, 567
Blum, F. A., 502
Boni, R., 548
Bonner, W. A., 404
Born, M., 21, 68, 96, 120, 219
Boyd, G. D., 548
Bridges, T. J., 503
Bridges, W. B., 503
Burkhardt, E. G., 503
Byer, R. L., 548
- Campbell, J. C., 502
Chang, I. C., 404
Chen, P. C., 219
Cho, A. Y., 219, 503
Choy, M. M., 547
Cohen, L. G., 53
Condon, E. U., 96, 120
Cook, W. R., Jr., 275
- Craxton, R. S., 548
Cutrona, L. J., 404
- Dakss, M. L., 404, 502
Damon, R. W., 365
Davies, P. H., 548
Davydov, A. A., 548
DelGaudio, A. M., 53
Dixon, R. W., 365, 372, 404, 502
Drude, P., 53
Ducuing, J., 547
Duguay, M. A., 317
Dunning, G. J., 567
Durado, J. A., 548
Dziedzic, J. M., 548
- Economou, N. P., 567
Evans, J. W., 154
- Faisullov, F. S., 566
Feldman, A., 317
Fisher, R., 567
Flanders, D. C., 502
Fork, R. L., 317
Fowler, V. J., 317
Fowles, G. R., 120
Franken, P. A., 518, 547
- Garmire, E., 317, 502, 503
Garvin, H. L., 502
Gibbs, H. M., 316
Giordmaine, J. A., 547, 548
Gires, F., 291, 309, 317
Giuliano, C. R., 566
Gordon, E. I., 365, 372, 404
Grivet, P., 547
Gurski, T. R., 548

- Hall, D., 503
Hall, D. B., 503
Hammer, J., 457
Hansen, J. W., 317
Harris, S. E., 390, 404
Heidrich, P. F., 404, 502
Hellwarth, R. W., 553, 567
Hellwege, K.-H., 275, 365, 547
Herbst, R. L., 548
Hill, A. E., 518, 547
Hobden, M. V., 548
Hong, C. S., 154, 219, 503
Hulme, K. F., 548
Hunsperger, R. G., 502
- Illegems, M., 219
Ippen, E. P., 365
Ivakin, E. V., 567
- Jackson, J. D., 21
Jacobs, S. D., 548
Jaffe, H., 275
Jerphagnon, J., 547
Johnson, F. M., 548
Jones, O., 548
Jones, R. C., 62, 121, 154
- Kaminow, I. P., 316
Katzir, A., 502, 503
Kawakami, S., 53
Kerr, J., 221
Khoshnevisan, M., 404
Kim, B., 404
Kingston, R. H., 548
Kittel, C., 365
Kleinman, D. A., 547, 548
Kneubuhl, F. K., 503
Kogelnik, H., 53, 502, 503
Korpel, A., 365, 404
Kossel, D., 209, 219
Kroll, N. M., 548
Kuhn, L., 404, 502
Kulevskii, L. A., 548
Kurtz, S. K., 547
- Landau, L. D., 21
Lawley, K. L., 502
Lean, E. G. H., 365, 404
Li, T., 53
Liao, P. F., 567
- Lifshitz, E. M., 21
Lin, C., 53
Lind, R. C., 567
Livanos, A. C., 503
Louisell, W. H., 548
Lyot, B., 154
- McMachon, D. H., 365
Magde, D., 548
Mahr, M., 548
Maker, P. D., 547
Maloney, W. T., 365, 404
Manley, J. M., 548
Marburger, J. H., 317
Marcatili, E. A. J., 53, 502, 503
Marcuse, D., 53, 503
Martin, R. J., 502, 503
Mason, W. P., 365
Mergerian, D., 404
Midwinter, J. E., 548
Mikulyak, R. M., 219
Miller, R. C., 548
Miller, S. E., 53, 503
Mollenauer, L. F., 53
Mumford, B. B., 317
Munster, C., 101, 120
- Nakamura, M., 502
Namba, C. S., 316
Newman, P. R., 404
Ng, W., 219
Nguyen, Le T., 404
Nieh, S. T. K., 404
Nisenoff, M., 547
Nishizawa, J., 53
Nosach, O. Y., 566
- Odishaw, H., 120
Öhman, Y., 154
- Pepper, D. M., 567
Pershan, P. S., 547
Personick, S. D., 53
Peters, C. W., 518, 547
Phillips, W., 457
Pinnow, D. A., 154, 404
Pisarevskii, Yu. V., 275
Pockels, F., 221
Popovichev, V. I., 566
Presby, H. M., 53

- Prokhorov, A. M., 548
- Quate, C. F., 404
- Racette, G. W., 548
Ragulskii, V. V., 566
Rigrod, W., 53
Riva-Sanseverino, S., 503
Rizzo, J. E., 548
Rowe, H. E., 548
Rubanov, A. S., 567
- Salzmann, E., 365
Sapriel, J., 365
Savage, C. M., 547
Savel'ev, A. D., 548
Schlafer, J., 317
Schmeltzer, R. A., 503
Schmidt, R. V., 502, 503
Scott, B. A., 404, 502
Seka, W., 548
Shaldin, Yu. V., 275
Shank, C. V., 317, 502
Sharpless, W. M., 316
Shaw, D. W., 502
Shaw, H. J., 404
Shellan, J. B., 503
Shen, Y. R., 547
Shirkov, A. V., 548
Shurcliff, W. A., 68
Siegman, A. E., 548
Smirnov, V. V., 548
Smith, P. W., 317, 503
Šolc, I., 154
Somekh, S., 502
Sonin, A. S., 275
Sovero, E., 404
Sprague, R. A., 404
Steffen, H., 503
Stepanov, B. I., 557, 567
Stoll, H., 502
Szivessy, G., 101, 120
- Tamir, E., 503
- Tarry, H. A., 154
Taylor, D. W., 53
Taylor, H. F., 503
Terhune, R. N., 547
Tien, P. K., 502, 503
Tomlinson, W. J., 317
Tournois, P., 291, 309, 317
Tracy, J., 404
Tregubov, G. A., 275
Tsai, C. S., 404
Turner, E. H., 317
- Ulrich, R., 502
Umeda, J., 502
- van der Ziel, J. P., 219
Van Uitert, L. G., 404
Vasilevskaya, A. S., 275
- Wahlstrom, E. E., 68
Wallace, R. W., 404
Wang, C. C., 548
Warner, A. W., 404
Warner, J., 548
Weinreich, G., 518, 547
Weismann, D., 365
West, E. A., 154
Winslow, D. K., 404
Woerdman, J. P., 557, 567
Wolf, E., 21, 53, 68, 120, 219, 365
Wolfe, R., 365, 404
- Yao, S. K., 404
Yariv, A., 53, 154, 219, 317, 502, 503, 547,
548, 566, 567
Yeh, C., 503
Yeh, P., 53, 154, 219, 503
Yen, H. W., 502
Yen, R., 317
Young, E. H., 404
- Zeldovich, B. Y., 566
Zernike, F., Jr., 548

Subject Index

- ABCD Law, 29, 33
- Absorption coefficient, 116, 563
- Access time, 381
- Acoustic intensity, 343, 352, 368, 390
- Acoustic resonance, 265
- Acoustic waves, 318, 320, 351
- Acousto-optic deflectors, 379
 - surface, 386
- Acousto-optic devices, 366
- Acousto-optic effect, 318
 - in germanium, 328
 - in LiNbO_3 , 363
 - in water, 320
- Acousto-optic interaction, 329
 - in LiNbO_3 , 351
 - particle picture, 332
- Acousto-optic materials, tables of, 324, 345, 346, 374
- Acousto-optic modulation, 366
 - collinear, 378
 - noncollinear, 373
 - in uniaxial crystals, 373
- Acousto-optic modulators, 366
 - bandwidth, 368
 - birefringent, 373
 - efficiency, 371
 - Raman-Nath, 367, 401
- Acousto-optics, 318
 - surface, 358, 364
- Acousto-optic signal correlators, 398
- Acousto-optic spectrum analyzers, 396
- Acousto-optic tunable filters, 387
 - angular aperture, 392, 394
 - bandwidth, 389, 395
 - LiNbO_3 , 391
 - TeO_2 , 395
 - transmission, 389, 392
- ADA, *see* $\text{NH}_4\text{H}_2\text{AsO}_4$
- Adiabatic following, 145
- ADP, *see* $\text{NH}_4\text{H}_2\text{PO}_4$
- AD*P, *see* $\text{NH}_4\text{D}_2\text{PO}_4$
- Ag_3AsS_3 , *see* Proustite
- AgAuTe_4 , 224
- AgCl , index of refraction, 12
- AgGaS_2 , 94, 224
 - electro-optic coefficients, 232
 - index of refraction, 232
 - nonlinear optical susceptibility, 514
 - optical rotatory power, 95
- AgGaSe_2 , nonlinear optical susceptibility, 514
- $\beta\text{-Ag}_2\text{Hgl}_4$, 224
- AgI , nonlinear optical susceptibility, 513
- AgInSe_2 , nonlinear optical susceptibility, 514
- AgIO_4 , 224
- Ag_3SbS_3 , *see* Pyrargyrite
- Airy formula, 219
- Al_2BeO_4 (Alexandrite), 224
- Alexandrite, 224
- AlF_3 , 225
- $\text{Al}_x\text{Ga}_{1-x}\text{As}$, 157, 177, 208, 211, 213, 420, 424, 446
- Al_2O_3 , *see* Sapphire
- Al_2SiO_5 , 224
- Aluminum, 495
- Ampere's law, 2
- Amplification, 443, 504
 - parametric, 531, 533
 - reflection, 443, 558
 - transmission, 444, 557, 559
- Amplitude modulation, 241, 251, 288
 - acousto-optic, 366
 - electro-optic, 241

- Amplitude modulation (*Continued*)
 index, 254
- Amplitude modulators, 242, 285
 acousto-optic, 366
 electro-optic, 241
 Fabry-Perot, 289, 290
 GaSe, 256
- Analyzer, 128, 130, 256
- Angle tuning, 539, 541
- Angular aperture:
 of AOTF, 392, 394
 of Lyot-Öhman filter, 153
- Angular beam spread, 29, 369
- Angular frequency, 6, 10
- Angular momentum, 57, 59
 of circularly polarized light, 57, 59, 66
 of electromagnetic fields, 19
 of elliptically polarized light, 66, 67
- Anisometric molecules, 266
- Anisotropic media, 54, 69
 classification of, 82
 electromagnetic propagation in, 69
 twisted, 143
 wave propagation in, 104
- Antisymmetric tensor, 97, 116
- AOTF, *see* Acousto-optic tunable filters
- AsI₃, 225
- As-S glass (As₂S₃):
 acousto-optic properties, 346, 374
 index of refraction, 12, 346, 374
 strain-optic coefficients, 324
- Asymmetric waveguides, 416
- Attenuation coefficient:
 Bragg reflection waveguides, 480, 482
 in leaky waveguides, 486, 488
 in metal-clad waveguides, 475
 of surface plasmon, 492, 493
- Autocorrelation function, 403
- BaAl₂O₄, 225
- BaF₂, index of refraction, 12
- Ba₂NaNb₅O₁₅, nonlinear optical susceptibility, 515
- Ba_xSr_{1-x}Nb₂O₆, *see* Strolian barium niobate
- Band edges, 161, 171
- Bandgap, 163, 164, 174, 198, 201
- Band structure, 169, 193
- Bandwidth, 292, 392, 400, 438
 of acousto-optic modulators, 368
 of AOTF, 389, 395
 of Bragg reflectors, 197, 198, 436
 of directional couplers, 472
 of electro-optic modulators, 294
 of Lyot-Öhman filters, 151
 modulation, 370, 377, 378, 383
 of Solc filter, 138, 142
- Barium titanate (BaTiO₃), 224, 225, 553
 electro-optic effect in, 263
 index of refraction, 85, 233, 261
 linear electro-optic coefficients, 233
 nonlinear optical susceptibility, 514
 quadratic electro-optic coefficients, 261
- BaTiO₃, *see* Barium titanate
- Beam deflectors:
 acousto-optic, 379
 electro-optic, 309
- Beam radius of curvature, 28, 31
- Beam spot size, 28, 31, 37, 42, 51
- Beam spreading, 29
 acoustic, 355, 369, 383, 401
- Beam waist, 36
- Bending, 425
- Benzene:
 index of refraction, 262
 Kerr constant, 262, 554
 third-order nonlinear susceptibility, 554
- BeO, 489
 index of refraction, 85
 nonlinear optical susceptibility, 513
- Beryl, index of refraction, 85
- Beryllium oxide, *see* BeO
- Bessel function, 244, 468
 differential equation, 467
 identity, 244, 357, 361
- BGO, *see* Bi₁₂GeO₂₀
- Bias retardation, 243
- Biaxial crystal, 82, 83, 84, 85
 light propagation in, 89, 114
 normal surface of, 91
- Bi₄Ge₃O₁₂:
 index of refraction, 12
 nonlinear optical susceptibility, 512
- Bi₁₂GeO₂₀ (BGO), 225
 acousto-optic properties, 375
 electro-optic coefficients, 231
 index of refraction, 231, 375
- Bi₁₂SiO₂₀ (BSO), 225
 acousto-optic properties, 375
 electro-optic coefficients, 231

- index of refraction, 231
- Birefringence, 121, 153, 269
 - electrically induced, 238, 241, 282
 - of liquid crystals, 268
- Birefringent Bragg deflectors, 383
- Birefringent filters, *see* Polarization interference filters
- Birefringent optical systems, 121
- Birefringent plate, 129, 131
- Bistability, 299
- Bistable electro-optic devices, 298, 302
- Bistable Fabry-Perot, resonators, 298, 300, 303, 314
- Bloch modes, 159
- Bloch theorem, 156
- Bloch wave number, 159, 161, 169
 - in periodic waveguides, 435
- Bloch waves, 155, 169
 - evanescent, 171, 209, 478
 - near Bragg condition, 160
 - in periodic layered media, 156, 171
- Bloch wave vector, 156
- BN, 225
- B₂O₃, 225
- Bond charge, 221
- Boundary conditions, 3, 407
- Bragg condition, 157, 161, 185, 215, 334, 349, 354, 388
- Bragg deflectors:
 - birefringent, 383
 - sapphire, 402
- Bragg diffraction:
 - acousto-optic, 330
 - in anisotropic media, 333, 334
 - codirectional, 349, 350
 - contradirectional, 350, 352
 - coupled-mode analysis, 337
 - electro-optic, 457
 - large angle, 338, 339, 347
 - small angle, 338, 339, 340
 - in uniaxial crystals, 335
- Bragg reflection, 174
 - exchange, 193
 - in periodic waveguides, 429
 - reflectivity of, 176
- Bragg-reflection waveguides, 477
 - attenuation in, 480, 482
 - GaAs-AlGaAs, 481
 - mode condition, 480
- Bragg reflectors, 176, 189, 218
 - coupled mode theory, 194
 - GaAs-AlGaAs, 177, 180
 - reflectivity of, 176, 197
 - reflectivity spectrum, 178, 179, 180, 198
 - transmissivity of, 218
- Bragg regime, 356, 367
- Brewster's angle, 172, 196
- Brillouin scattering, 504
- Brillouin zone, 194
- BSO, *see* Bi₁₂SiO₂₀
- CaCO₃ (Calcite), 225
- CaCl₂, 224
- Cadmium sulfide, *see* CdS
- CaF₂, index of refraction, 12
- Calcite, 69, 121, 132, 153, 225
 - index of refraction, 85
- Carbon disulfide, *see* CS₂
- CCl₄:
 - index of refraction, 262, 554
 - Kerr constant, 262
 - third-order nonlinear susceptibility, 554
- CDA, *see* CsH₂AsO₂
- CdF₂, index of refraction, 12
- CdGa₂S₄, 224
 - nonlinear optical susceptibility, 515
- CdGeAs₂, nonlinear optical susceptibility, 514
- CdGeP₂, nonlinear optical susceptibility, 514
- CdInS₂, nonlinear optical susceptibility, 514
- CdMoO₄, strain-optic coefficients, 327
- CdS, 153, 225
 - acousto-optic properties, 346, 374
 - birefringence dispersion, 153
 - electro-optic coefficients, 231
 - index of refraction, 12, 231, 346, 374
 - nonlinear optical susceptibility, 512
 - strain-optic coefficients, 326
- CdSe, 225, 541
 - electro-optic coefficients, 231
 - index of refraction, 12, 231
 - nonlinear optical susceptibility, 512
 - parametric oscillator, 541, 542
- CdTe, 225, 273, 279, 283
 - electro-optic coefficients, 230
 - index of refraction, 12, 85, 230
 - nonlinear optical susceptibility, 512
 - strain-optic coefficients, 324

- Centrosymmetric crystals, 223, 506, 508
 Chebyshev's identity, 134
 Chirped grating, 469, 470, 471
 Cholesteric-nematic phase transition, 270
 Cholesteric phase, 267, 268
 Cinnabar, 94
 Clipper, optical, 303
 Codirectional coupling, 186, 436, 472
 Bragg, 349, 350
 Coherence length, 521
 CO₂ laser, 489, 544
 Collinear relationship, §1
 Color multiplexing, 469
 Column vector, 165
 Complex amplitude, 6
 Complex beam parameter $q(z)$, 33, 36, 38
 Complex conjugate, 550, 551
 Complex-function formalism, 6
 Conductivity, optical, 494, 516
 Confined modes, 407
 mirror transform of, 409, 495
 confinement factor, 497
 Confocal beam parameter, 37, 297
 Conical refraction, 91, 92, 93, 115
 cone angle, 92, 93, 115
 Conjugate waves, 21, 550, 564
 polarization states of, 565
 Conjugation, 549
 Conservation of charge, 18
 Conservation of energy, 5
 in acousto-optic interaction, 332
 in anisotropic media, 119
 in mode coupling, 187, 188, 217
 Conservation laws, 5
 Conservation of momentum, in acousto-optic interaction, 332, 361, 388
 Constitutive equations, 2
 Continuity equation, 5, 18
 Contracted indices, 222, 319, 507
 Contradirectional coupling, 187, 353, 431, 472
 Bragg, 350, 352
 Convolution, 549
 Copper, 473, 495
 Correlation, 549
 Corrugation, surface, 425
 Coulomb's law, 2
 Coupled mode equations, 106, 185
 analysis of wave propagation in anisotropic media, 104
 co-directional coupling, 186
 contra-directional coupling, 187
 Coupled mode theory, 177
 of Bragg reflectors, 194
 of Solc filters, 189
 Coupling coefficient, 183, 429
 for plane waves, 186
 Coupling constant, 183, 186
 of acousto-optic interaction, 340, 352
 of four wave mixing in CS₂, 560
 of modes in Bragg reflectors, 195
 of modes in directional couplers, 463
 of modes due to periodic corrugation, 431, 432, 455
 of modes in Solc filters, 192
 Correlation gain, 400
 Correlators:
 acousto-optic, 398
 properties of, 400
 Crossover, 463, 466
 Crosstalk, 463
 Crystals:
 biaxial, 82, 83
 isotropic, 82, 83
 negative, 84, 85
 positive, 84, 85
 refractive index of some, 85
 uniaxial, 84
 CS₂, 546
 four wave mixing in, 558
 index of refraction, 262, 554
 Kerr constant, 262
 third-order nonlinear susceptibility, 554
 Verdet constant, 104
 CsBr, index of refraction, 12
 CsCuCl₃, 225
 CsH₂AsO₄ (CDA):
 electro-optic coefficients, 233
 index of refraction, 233
 CsI, index of refraction, 12
 CuBr:
 index of refraction, 12
 nonlinear optical susceptibility, 512
 CuCl, 283
 index of refraction, 12
 nonlinear optical susceptibility, 512
 CuGaS₂, nonlinear optical susceptibility, 514
 CuGaSe₂, nonlinear optical susceptibility, 514
 CuI:
 index of refraction, 12

- nonlinear optical susceptibility, 512
- CuInS₂, nonlinear optical susceptibility, 514
- Curie temperature, 225, 232, 233, 261, 263, 266
- Cutoff wavelength, for TE and TM modes, 420

- Dextrorotatory substance, 94
- Diamond:
 - index of refraction, 12, 85
 - Verdet constant, 104
- Dichroic polarizers, 116
- Dielectric constant, 2
 - complex, 473, 494
 - negative, 473, 490
 - principal, 72, 77
- Dielectric perturbation, 105, 177, 191, 337
 - uniform, 426
 - in waveguides, 425
- Dielectric tensor, 2, 69
 - of anisotropic medium, 69
 - antisymmetric part of, 97, 116
 - Hermitian, 71, 116
 - symmetric, 71
- Dielectric waveguides, 405
 - energy transport in, 411
 - general properties of, 405
 - modes of, 416
 - orthogonality of modes, 408
 - perturbed, 499
 - planar, 413
- Differential gain, 299, 302, 314
- Diffraction efficiency:
 - of acousto-optic modulators, 368, 371
 - of electro-optic grating, 358, 359
 - of large-angle Bragg diffraction, 351, 353
 - of Raman-Nath diffraction, 358
 - of small-angle Bragg diffraction, 342, 344, 347
 - of surface acousto-optics, 362, 363
- Directional couplers, 459
 - alternating- $\Delta\beta$, 464
 - frequency selective, 472
 - grating, 472
- Directional coupling, 459
 - electro-optic, 463
- Director, 268
- Dirac delta function, 181, 361
- Dispersion, 11
 - anomalous, 17
 - group velocity, 17, 44, 306
 - modal, 43, 44
 - normal, 17
 - relation, 156, 162, 163, 169
- Dispersive medium, 11, 14, 304
- Distorting medium, 549
- Distortionless propagation, 50
- Distributed feedback lasers, 439, 559
 - GaAs-AlGaAs, 446
 - mode coupling in, 440
 - oscillation condition, 444
- Doppler frequency shift, 331
- Double refraction, 88
 - circular, 94
 - graphic method of finding angles of refraction, 89
 - in uniaxial crystals, 90
- Dynamical condition, for Bragg coupling, 184
- Dynamic scattering, 270

- Effective photo-elastic coefficient, 343
- Effective strain component, 343
- Efficiency, of acousto-optic modulators, 371
- Eigen phase velocity, 72
- Eigen polarization, 72, 113
- Eigenmodes, 76
- Eigenwaves, 72
 - displacement vector of, 118
 - fast and slow, 121, 122
- Eikonal, 32
 - equation of geometrical optics, 32
- Elasto-optic coefficient, 265, 321
 - in contracted notations, 321
 - see also* Photo-elastic coefficient
- Electric charge density, 2
- Electric current density, 2
- Electric displacement, 1
- Electric field vector, 1
- Electric susceptibility tensor, 70
- Electromagnetic field, 1
- Electromagnetic propagation:
 - in anisotropic media, 69
 - in nonlinear media, 516
 - in periodic media, 155
 - see also* Wave propagation
- Electromagnetic surface wave, 209, 489
 - in air-silver interface, 494

- Electromagnetic surface wave (*Continued*)
 field distribution, 212, 490
 in GaAs-AlGaAs layered media, 213, 214
- Electro-optic Bragg diffraction, 457
- Electro-optic coefficients:
 in contracted notation for all crystal classes, 227
 and crystal symmetry, 270
 definition, 221
 linear, 221, 226
 physical properties of, 264
 quadratic, 221, 257
 quadratic, of isotropic media, 274
 table of linear, 230
 table of quadratic, 261
- Electro-optic crystals:
 tables of, 230, 261
 wave propagation in, 245
- Electro-optic devices, 276
 bistable, 298
- Electro-optic effect, 220
 in BaTiO₃, 263
 in KDP, 226
 in LiNbO₃, 237
 linear, 223
 in liquid crystals, 266
 quadratic, 256
 in uniaxial crystals, 272
- Electro-optic modulator, 276
 bistable, 302
 Fabry-Perot, 288
 field-of-view of, 312
 geometrical consideration, 297
 GaAs thin film, 451, 452
 grating, 457
 LiTaO₃, 282
 using cubic crystals, 283
- Electro-optic modulation, 238
 in dielectric waveguides, 447, 452, 457
 longitudinal, 277
 transverse, 281
- Electro-optics, 220
- Electro-optic tunable filters, 143
- Electro-optic tunable retardation plate, 273
- Ellipticity, 60, 100
 angle, 62
 of eigenmodes in gyrotropic media, 100, 119
 of surface plasmon, 492
- Energy density, 6, 80, 203
 of electric field, in anisotropic media, 77
 time-averaged, 8, 13, 204
- Energy flow, 6
 in anisotropic media, 76, 79
 time-averaged, 8, 13
 velocity of, 80
- Energy velocity, 79, 114
 averaged, 203
 in dielectric waveguides, 411
 in periodic media, 201, 203
- Envelope function, 15
- Equation of motion:
 for \vec{D} vector, 110, 112, 245
 for \vec{E} vector, 108
- Etalon:
 Fabry-Perot, 289, 299
 Gires-Tournois, 291
- Evanescent Bloch wave, 163, 171, 209
- Extinction coefficient, 473, 493
- Extraordinary ray, 86, 523, 524
 index of refraction, 87
 polarization, 87
- Fabry-Perot:
 asymmetric, 291, 309
 bistable devices, 299, 300
 cavity, 288, 291
 electro-optic modulators, 288
- Faraday rotation, 103
- Faraday's law of induction, 2
- Feldspar, 85
- γ -Fe₂O₃, 224
- Field of view, 154
 of cubic electro-optic modulators, 312
 of iso-index filters, 154
- Figure of merit, 343, 372
- Filters:
 iso-index, 153
 Lyot, 121
 Lyot-Öhman, 132, 150
 polarization interference, 131
 Šolc, 121, 132, 133, 139, 141, 153, 187, 218, 336
- Finesse:
 of Fabry-Perot etalon, 290
 of Lyot-Öhman filters, 151
- Fine structure, 147
- Floquet theorem, 156

- Fluorite:
 index of refraction, 85
 Verdet constant, 104
- Forbidden bands, 159, 161, 162, 163, 164, 176, 200, 436
 of one dimensional periodic media, 171, 172, 173, 210, 214
- Form birefringence, 203
 of GaAs-AlAs layered media, 208
- Fourier expansion, 158, 183, 449
 of square wave function, 191
- Fourier spectrum, 14
- Fourier transform, 399
- Four wave mixing, 553
 oscillator, 561
- Free spectral range, 151
- Frequency chirp, 50, 303
- Frequency doubling, 504
- Frequency multiplexers, 469
 chirped grating for, 469
 grating directional coupler, 472
- Frequency spread, 13
- Frequency tuning:
 in parametric oscillation, 538
- Frequency up-conversion, 542
 for infrared detection, 544
 in LiIO_3 , 545
- Fresnel, 94, 359
 equation of wave normal, 75, 98, 114
 reflection, 122, 147, 172, 362
 transmission coefficients, 363
- Fused silica (Fused quartz):
 acousto-optic properties, 345, 346, 374
 index of refraction, 12, 345
 strain-optic coefficients, 324
- Fused quartz, *see* Fused silica
- GaAs, 175, 177, 208, 211, 213, 225, 273, 279, 283, 313, 420, 424, 436
 acousto-optic properties, 346, 374
 electro-optic coefficients, 230
 electro-optic directional couplers, 468
 index of refraction, 12, 85, 230, 346, 374
 injection lasers, 446
 nonlinear optical susceptibility, 512
 strain-optic coefficients, 324
 thin-film modulators, 451, 452
- GaP:
 acousto-optic properties, 346, 374
 electro-optic coefficients, 230
 index of refraction, 12, 230, 346, 374
 nonlinear optical susceptibility, 512
 strain-optic coefficients, 324
- GaS, 225
- $\alpha\text{-Ga}_2\text{S}_3$, 224
- GaSb:
 index of refraction, 12
 nonlinear optical susceptibility, 512
- GaSe, 225, 273
 amplitude modulators, 256
 nonlinear optical susceptibility, 513
- Gauss' divergence theorem, 2
- Gaussian beam, 10, 297
 angular spread, 29
 complex beam radius $q(z)$, 33, 36, 38
 focusing, 36
 high-order modes in homogeneous medium, 37
 in homogeneous medium, 25
 in lens-like medium, 29
 modulation, 314
 in quadratic index media, 38
 radius of curvature, 27, 28, 31, 36
 spot size, 27, 28, 31, 36, 51
 transformation of, 33
 transformation by a lens, 50
- Ge, 225
 acousto-optic effect in, 328
 index of refraction, 12
 strain-optic coefficients, 324
- Ge_3N_4 , 225
- GeO_2 , 224
- Geodesic lenses, 398
- Ge-Se-As glass:
 acousto-optic properties, 375
 index of refraction, 375
 strain-optic coefficients, 324
- Gires-Tournois etalon, 291, 309
- Glan prism, 115
- Glass (clear lead):
 acousto-optic properties, 375
 index of refraction, 375
- Glass (crown), Verdet constant, 104
- Glass (flint): 382
 acousto-optic properties, 345
 index of refraction, 345
 third-order nonlinear susceptibility, 554
 Verdet constant, 104

- Glass (yellow lead):
 acousto-optic properties, 375
 index of refraction, 375
 Gold, 473, 495
 Graded-index fiber, 29
 Grating directional couplers, 472
 Grating pair, 309
 Gratings, 323
 Group velocity, 13, 16, 17, 21
 dispersion, 17, 21, 306, 315
 of extraordinary wave in uniaxial
 crystals, 114
 of guided waves, 411
 of light in anisotropic media, 79, 80, 114
 of light in periodic media, 201
 Guest-host effect, 270
 Guided waves, 405
 Gypsum, index of refraction, 85
 Gyration:
 tensor, 98, 102, 116
 vector, 97, 103
 Gyrotropic media, 119
- Half-wave plate, 116, 125, 127, 148
 Half-wave voltage, 241, 279, 280, 283
 Harmonic oscillators, 38, 41
 damped, 264
 Harris filter, 402
 Helical molecule, 97
 Helmholtz equation, 23
 He-Ne laser, 301, 457
 Hermite-Gaussian functions, 39
 Hermite polynomial, 38, 41
 Hermitian conjugate, 124, 149
 Hermitian tensor, 71, 97, 116
 He-Se laser, 457
 Heterodyne scanning, 398
 α -HgS, nonlinear optical susceptibility,
 514
 α -HIO₃ (alpha iodic acid):
 acousto-optic properties, 345
 electro-optic coefficients, 234
 index of refraction, 234, 345
 nonlinear optical susceptibility, 515
 Holography, 549
 H₂S, 225
 Huygens principle, 359
 Hydrodynamical equation of motion,
 18
 Hysteresis, 299, 301
- Ice, index of refraction, 85
 Idler wave, 531, 532
 Image processing, 549
 Image transmission, 549
 in fibers, 551
 Impedance, of space, 13
 Imperfection, 425
 Impermeability tensor, 78
 transverse, 79
 InAs, 225, 279, 283
 index of refraction, 12
 nonlinear optical susceptibility, 512
 Index ellipsoid, 77, 85, 220
 method of, 78
 Index matching, *see* Phase matching
 Index modulation, self-induced, 566
 Index of refraction, 11
 of anisotropic media, 82, 85
 complex, 473, 493
 of eigenwaves, 72, 75
 extraordinary, 87
 of isotropic medium, 11
 of metals, 473, 494, 495
 of some crystals, 85
 of some optical materials, 12
 ordinary, 86, 87
 principal, 77
 InP, index of refraction, 12
 InPS₄, nonlinear optical susceptibility, 515
 InSb:
 index of refraction, 12
 nonlinear optical susceptibility, 512
 Integrated optics, 405
 Intensity transmission, 127
 Ion lattice, 221
 Intraatomic field, 223
 Inversion symmetry, 223
 Iso-index:
 crystals, 153
 filters, 153
 Isotope separation, 545
 Isotropic crystal, 82, 83
- Jones, 62
 calculus, 121
 matrix formulation, 121
 vector, 62, 64, 65
 vector representation, 62
- KBr, index of refraction, 12

- KCl, index of refraction, 12
 KCuF₄, 224
 KDA, *see* KH₂AsO₄
 KDP, *see* KH₂PO₄
 KD*P, *see* KD₂PO₄
 KD₂PO₄ (KD*P), 265
 electro-optic coefficients, 233
 index of refraction, 233
 nonlinear optical susceptibility, 514
 temperature dependence of r_{63} , 267
 wavelength dependence of r_{63} , 266
 Kerr constant, 262
 of some substances, 262
 Kerr effect, 221, 309
 in isotropic media, 257
 Kerr media, 29
 KH₂PO₄ (KDP), 69, 224, 235, 237, 240,
 244, 265, 276, 295, 301, 310, 507
 acousto-optic properties, 346, 374
 beam deflector, 311
 dispersion data, 522
 electro-optic effect in, 226
 frequency dependence of r_{63} , 266
 index of refraction, 85, 233, 261, 346,
 374
 linear electro-optic coefficients, 233
 nonlinear optical susceptibility, 514
 quadratic electro-optic coefficients, 261
 rotation of principal axes, 235, 237
 second harmonic generation in, 524
 strain-optic coefficients, 327
 temperature dependence of r_{63} , 267
 wavelength dependence of r_{63} , 266
 KI, index of refraction, 12
 Kinematic condition:
 for Bragg coupling, 184
 for refraction, 88
 KIO₃, 224
 electro-optic coefficients, 234
 index of refraction, 234
 KLiSO₄, 225
 KNa(C₄H₄O₆)·4H₂O (Rochelle salt),
 224
 KNbO₃, 224
 electro-optic coefficients, 234
 index of refraction, 234
 nonlinear optical susceptibility, 515
 K(Nb_{0.37}Ta_{0.63})O₃, 224
 index of refraction, 261
 quadratic electro-optic coefficients, 261
 KOH, 224
 KTa_xNb_{1-x}O₃, 224, 225
 electro-optic coefficients, 233
 index of refraction, 233
 KTaO₃:
 index of refraction, 261
 quadratic electro-optic coefficients, 261
 KTN, *see* KTa_xNb_{1-x}O₃
 Kronecker delta, 181, 455
 KRS-5:
 acousto-optic properties, 345, 376
 index of refraction, 345, 376
 strain-optic coefficients, 325
 KRS-6, strain-optic coefficients, 325

 Laser beams, propagation of, 22
 Laser oscillator, 35
 Laser pulse, 13
 Lattice deformation, 264
 Lattice resonance, 265
 Lattice translation, 169
 Lattice vector, 155
 Layered media, 165, 210
 GaAs-AlGaAs, 180, 208, 213
 Lead molybdate, 382, 383
 acousto-optic beam deflector, 382
 acousto-optic properties, 345, 346, 375
 Bragg scattering, 344
 index of refraction, 345, 346
 strain-optic coefficients, 327
 Leaky dielectric waveguides, 482
 attenuation coefficients, 486, 488
 Lens-like media, 23, 38
 fundamental Gaussian beams in, 29
 Gaussian beam modes in, 38
 rays in, 31
 Levorotatory substance, 94
 Li(COOH)·H₂O, nonlinear optical suscepti-
 bility, 515
 LiF:
 acousto-optic properties, 345
 index of refraction, 12, 345
 LiFe₃O₈, 225
 Light valves, 147
 LiIO₃:
 electro-optic coefficients, 232
 frequency up-conversion in, 545
 index of refraction, 232
 nonlinear optical susceptibility, 513
 LiKSO₄, nonlinear optical susceptibility, 513

- Limiter, optical, 303
 LiNbO₃, 251, 255, 283, 288, 292, 303, 352, 373, 383, 386, 402, 453
 acousto-optic effect in, 363
 acousto-optic properties, 345, 346, 374
 acousto-optic tunable filter, 390, 391
 Bragg diffraction in, 335, 457
 collinear acousto-optic interaction, 351
 contradirectional collinear acousto-optic interaction, 353
 electro-optic coefficients, 232
 electro-optic directional coupler, 463
 electro-optic effect in, 237
 electro-optic phase modulator, 250
 index of refraction, 85, 232, 346, 374
 longitudinal modulator, 277
 nonlinear optical susceptibility, 513
 parametric amplification, 533
 parametric oscillation in, 538
 phase modulator, 250
 spectrum analyzer, 298
 strain-optic coefficients, 326
 waveguide mode converter, 454
 LiTaO₃, 148, 225, 283, 288
 acousto-optic properties, 346, 374
 electro-optic coefficients, 232
 electro-optic modulator, 282
 index of refraction, 232, 346, 374
 nonlinear optical susceptibility, 513
 strain-optic coefficients, 326
 Li₂O₂, 225
 Liquid crystal, 69
 cholesteric, 267, 270
 director of, 267
 electro-optic effects in, 266
 nematic, 267, 269, 270
 twisted nematic, 143, 145, 270
 smectic, 267, 268
 Lithium niobate, *see* LiNbO₃
 Lithium tantalate, *see* LiTaO₃
 Lorentz force, 18, 103
 Lorentz reciprocity theorem, 76, 408, 495
 Lucite:
 acousto-optic properties, 376
 index of refraction, 376
 strain-optic coefficients, 324
 Lyot filters, 121
 Lyot-Öhman filters, 132, 150
 angular aperture, 153
 bandwidth, 151
 iso-index, 153
 Magnetic field vector, 1
 Magnetic induction, 1
 Magnetic monopole, 2, 19
 charge density, 19
 Magneto-gyration coefficient, 103
 Magneto-optic effect, 103
 Material dispersion, 48
 Material equations, 2
 Matrix:
 ABCD, 29, 33
 Jones, 121
 refractive index, 111
 rotation, 124
 unimodular, 134
 unit cell translation, 168
 unitary, 124
 wave, 108
 4 x 4, 147
 Maxwell's equations, 1, 156, 406
 in momentum space, 72, 80
 Maxwell's stress tensor, 18
 MBBA, 267
 Metal-clad waveguides, 473
 attenuation in, 475
 mode indices of, 476
 MgF₂ :
 index of refraction, 12
 strain-optic coefficients, 327
 MgO, 225
 index of refraction, 12
 MgO₂, 225
 Mica, 85, 115, 224
 index of refraction, 85
 Minimum spot size, 28
 Mirrorless oscillation, 559
 Mirror transform, 409, 495
 MnSe₂, 225
 Modal dispersion, 43, 44
 Modal scrambling, 552
 Mode condition:
 Bragg waveguide, 480
 TE, 417, 484
 TM, 419
 Mode confinement factor, 497
 Mode coupling, 425
 in dielectric waveguides, 425, 447
 Mode discrimination, 446
 Mode filter, 477

- Mode index, 424, 438, 454, 476
 Mode polarizer, 477
 Mode reflectivity, 433
 Modulation:
 amplitude, 241, 288
 depth, 255, 281, 283, 288, 290, 295
 high frequency, 293
 index, 244, 249, 250, 251, 256, 280, 357
 phase, 243, 247
 Modulators:
 acousto-optic, 366
 electro-optic amplitude, 242
 electro-optic phase, 244
 GaAs thin-film, 451, 452
 GaSe amplitude, 256
 LiNbO₃ phase, 250
 traveling wave, 296
 Molecular beam epitaxy, 157, 177, 180, 208
 Momentum density, electromagnetic field, 18
 Monochromatic radiation, 22
 NaCl:
 index of refraction, 12, 85
 strain-optic coefficients, 324
 Verdet constant, 104
 NaF:
 index of refraction, 12
 strain-optic coefficients, 325
 NaIO₄, 224
 NaNO₂, 85
 NaNO₃, 225
 index of refraction, 85
 Narrowband filters, 127, 143
 ND₄D₂PO₄, nonlinear optical susceptibility, 514
 Nd-YAG laser, 544
 Nematic phase, 267, 268
 NH₄D₂PO₄ (AD*P), 265
 electro-optic coefficients, 233
 index of refraction, 233
 wavelength dependence of r_{63} , 266
 NH₄H₂PO₄ (ADP), 132, 244, 265, 541
 acousto-optic properties, 346, 374
 frequency dependence of r_{63} , 266
 index of refraction, 85, 233, 261, 346, 374
 linear electro-optic coefficients, 233
 nonlinear optical susceptibility, 514
 quadratic electro-optic coefficients, 261
 strain-optic coefficients, 327
 wavelength dependence of r_{63} , 266
 NiAs, 225
 Nitrobenzene, Kerr constant, 262
 Nitrotoluene, Kerr constant, 262
 Nonlinear interaction, 516
 Nonlinear optical materials, table of, 512
 Nonlinear optics, 504
 Nonlinear susceptibility tensor, 264, 504
 in contracted notation, 508
 second order, 504
 symmetry properties, 547
 third order, 504
 Nonlinearity, 298, 505
 Normal modes of propagation, 38, 72, 181
 in anisotropic media, 72
 in gyrotropic media, 99, 108, 112
 in optically active media, 95, 108, 109
 in periodic media, 156
 unperturbed, 105
 Normal surface, 73
 Number of resolvable spots, 311, 381, 386
 Off-axis effect, 151
 Ohmic losses, 476, 492, 494
 Ohm's law, 476
 Optical activity, 94
 electromagnetic theory, 96
 Fresnel theory, 94
 Optical bistability, 298, 301, 303
 Optical clipper, 303
 Optical differential amplifier, 303
 Optical indicatrix, 77
 Optical limiter, 303
 Optical rotatory power, 94, 96, 98
 of some materials, 95
 specific, 96
 Optical switches, 303
 Optic axes, 73, 74, 82
 Ordinary ray, 86, 87, 523, 524
 Orientational effect, of liquid crystal, 269
 Orthogonality, 76, 410
 Orthogonal relation, 181
 of eigenmodes, 76
 of normal modes, 181, 410
 of waveguide modes, 410
 Orthogonal triad, 75
 Orthonormality relation, 106, 426, 427

- Orthonormality relation (*Continued*)
 for TE modes, 410, 496
 for TM modes, 410, 496
- Oscillation:
 parametric, 504, 533
 spectrum, 447
 via four wave mixing, 559
- Parabolic approximation, 182
- Parametric amplification, 531
 basic equations of, 531
 in LiNbO_3 , 533
- Parametric oscillation, 533
 frequency tuning in, 538
 oscillation condition, 537
 self-consistent analysis, 535
 threshold, 537, 538
- Parametric oscillator, 537
- PbF_2 , index of refraction, 12
- $\text{Pb}_4\text{Ge}_3\text{O}_{11}$, 225
- PbHPO_4 , 224
- PbMoO_4 , *see* Lead molybdate
- PbNO_3 :
 acousto-optic properties, 376
 index of refraction, 376
- PbSb_2S_4 , 225
- PbSiO_3 , 224
- PbTiO_3 , nonlinear optical susceptibility, 515
- Periodic layered media, 165
- Periodic media, 136, 155
 one-dimensional, 156
 primitive vectors, 156
 translational invariance, 156
- Periodic perturbation, 136, 177, 323, 560
- Periodic square wave function, 191
 Fourier expansion of, 216
- Periodic waveguides, 429
 co-directional coupling in, 436
 contra-directional coupling, 431
- Permeability tensor, 2
- Permittivity tensor, 2, 70
- Permutation symmetry, 222, 319
- Phase, 6, 31
 surface of constant, 10, 32
- Phase compensator, 283
- Phase conjugate mirror, 558, 563
- Phase conjugate optics, 549
- Phase conjugate oscillator, 559
- Phase conjugate resonator, 562, 563
- Phase conjugation, 553
- Phase grating, 356
- Phase matching, 136, 184, 469
 longitudinal, 184
 in second harmonic generation, 521
- Phase modulation, 243, 247, 290
 index, 244, 249
 self-, 309
- Phase modulator, 244, 291
 KDP, 244
 LiNbO_3 , 250
- Phase retardation, 123
 electro-optic, 239, 280, 285, 287
- Phase shift, 147, 292
 due to electro-optic effect, 276, 277
 upon total reflection, 423
- Phase transition, 266
- Phase velocity, 10, 17, 114, 188, 201
 of Bloch wave, 202
 of extraordinary wave in uniaxial crystals, 114
 of light, 10, 17
 of light in anisotropic media, 79, 80
 mismatch, 296
 of sound, 329, 345, 346, 374
- Phonon, 332
- Phosphorus, Verdet constant, 104
- Photo-elastic:
 coefficients, 318
 effect, 318
 materials, table of, 324
- Photon, 57, 59
 angular momentum, 57, 59, 66
 flux, 527
- Piezoelectric coefficients, 265
- Piezoelectric effect, 507
- Planar dielectric waveguides, 413
- Plane waves, 10
 in anisotropic media, 72
 electromagnetic, 11
 monochromatic, 8
- Plasma frequency, 501
- PLZT:
 index of refraction, 231, 261
 linear electro-optic coefficients, 231
 quadratic electro-optic coefficients, 261
- Pockels effect, 221
- Point groups, 224
- Polarizability, 264
- Polarization, 54

- ellipse, 56, 57, 58, 60, 101
 - of monochromatic plane waves, 55
 - sense of revolution, 57, 59
- Polarization interference filters, 131
- Polarization state, 55, 62, 65
 - complex number representation, 61
 - converter (or transformer), 122
 - in electro-optic crystals, 240
 - equation of motion for, 110
 - of extraordinary ray, 87
 - Jones vector representation, 62, 65
 - in optically active media, 107
 - within Solc folded filters, 137
- Polarized light, 54
 - circularly, elliptical, linearly, 57
 - left-handed circularly, 57, 59, 60
 - right-handed circularly, 57, 59, 60
- Polarizers, 64, 128, 149
 - dichroic, 116
 - Glan prism, 115
 - Jones matrix of, 125
 - prism, 115
 - sheet, 125
- Polystyrene:
 - acousto-optic properties, 345, 376
 - index of refraction, 345, 376
 - strain-optic coefficients, 324
- Power exchange, 451
- Power flow:
 - conservation of, 119, 342, 431
 - in dielectric waveguides, 411
- Power limiting, 302
- Poynting's theorem, 5
- Poynting's vector, 6, 80, 203
 - of Bloch waves, 204
 - of guided waves, 411
 - of plane waves, 13
 - of surface plasmon, 501
 - time-averaged, 8, 13, 204
- Primitive vectors, 156
- Principal dielectric axes, 70
 - transformation, 226
- Projection operator, 149
- Propagation axes, 246
 - in cubic crystal, 273
- Propagation constant, 407
 - of surface plasmon, 491, 493
- Proustite (Ag_3AsS_3), 225, 544
 - electro-optic coefficients, 232
 - index of refraction, 85, 232
 - nonlinear optical susceptibility, 513
 - strain-optic coefficients, 326
- Pulse:
 - broadening, 48, 51
 - compression, 304, 549
 - distortion, 17
 - Gaussian, 20, 45, 306, 403
 - Lorentzian, 20
 - propagation, 13
 - shaping, 302, 314
 - spreading, 17, 43
 - square wave, 20
 - width, 47, 308
- Pyrrargyrite, nonlinear optical susceptibility, 513
- Quadratic electro-optic coefficients:
 - in contracted notation, 258
 - table of, 261
- Quadratic electro-optic effect, 256
- Quadratic index:
 - glass fibers, 43, 49
 - see also* Graded-index fibers
 - media, 38
- Quarter-wave:
 - plate, 116, 126, 128, 148, 242
 - stack, 173, 217
- Quartz, 69, 84, 94, 121, 132, 149, 153, 225, 401
 - acousto-optic properties, 345, 346, 374
 - index of refraction, 85, 345, 346, 374, 554
 - left-, right-handed, 94
 - nonlinear optical susceptibility, 513
 - optical rotatory power, 95
 - second harmonic generation in, 518, 519
 - strain-optic coefficients, 326
 - third-order nonlinear susceptibility, 554
- Raman-Nath:
 - acousto-optic modulators, 401
 - diffraction, 354
 - regime, 356, 367
- Raman scattering, 504
- Radiation modes, 414
 - substrate, 414
- Ray, 31
 - equation, 32
 - extraordinary, 86, 87
 - integral, 32

- Ray (*Continued*)
 in lenslike media, 31
 matrix, 33, 34, 35
 ordinary, 86, 87
 parameter, 33
 paraxial, 32
 trajectory, 32
 zigzag, 423, 478
- Ray equation, 32
 for lens-like media, 33
- Ray optics approach:
 for leaky dielectric waveguides, 487
 for slab waveguide modes, 422
- Rayleigh waves, 358
- RbH₂PO₄ (RDP), 265
 nonlinear optical susceptibility, 514
 temperature dependence of r_{63} , 267
- RDP, *see* RbH₂PO₄
- Real time holography, 549
- Reciprocal lattice vectors, 158
- Reciprocity, *see* Lorentz reciprocity theorem
- Reflection:
 amplifier, 558
 gain, 443
- Reflection coefficient, 219
- Reflectivity:
 near grazing incidence, 487
 of Bragg reflectors, 176, 197, 198
- Refractive-index matrix, 111, 246
- Resolving power, 395
- Retardation plate, 122
 electro-optic tunable, 273
 half-wave, 125
 quarter-wave, 126
see also Wave plate
- RF spectrum analyzers, 396, 397
- Rochelle salt, 224
- Rotation, 217
 coordinate, 226
 Faraday, 103
 optical, 94
- Ruby laser, 518, 519, 545
- Rutile (TiO₂):
 acousto-optic properties, 345
 index of refraction, 85
 strain-optic coefficients, 327
- S (sulphur), 225
- Sapphire (Al₂O₃), 225
- acousto-optic beam deflectors, 386
- acousto-optic properties, 345, 346, 374
- Bragg deflectors, 385
- index of refraction, 12, 345, 346, 374
- strain-optic coefficients, 326
- SBN, *see* Strontian barium niobate
- SbSI, 224
 index of refraction, 85
- Scalar wave, 14
 equation, 22, 550
- Se (selenium), 94, 225
 nonlinear optical susceptibility, 514
 optical rotatory power, 95
- Second harmonic generation, 518
 conversion efficiency, 520, 529
 with a depleted input, 526
 with Gaussian beams, 528
 in KDP crystal, 524, 529
 phase matching in, 521
 in quartz, 518
- Self-induced index modulation, 566
- SF-4:
 acousto-optic properties, 346, 374
 index of refraction, 346, 374
- Shear wave, 328
- Si, 225
 index of refraction, 12
 strain-optic coefficients, 325
- SiC:
 index of refraction, 12
 nonlinear optical susceptibility, 513
- Signal-to-noise ratio (SNR), 400
- Signal wave, 531, 532
- Silver, 473, 494
- Silver thiogallate, *see* AgGaS₂
- β -Si₃N₄, 225
- SiO₂, *see* Quartz
- Slab dielectric waveguide, 413, 422, 499
- Smectic phase, 267, 268
- Snell's law, for ordinary wave, 88
- SnO₂, strain-optic coefficients, 326
- Sodium chlorate, 94
- Sodium chloride, *see* NaCl
- Sodium nitrate, *see* NaNO₃
- Sodium vapor, 562
- Softening, of phonon mode, 266
- Solc filters, 121, 132, 153, 187, 218, 336
 bandwidth, 138, 142
 coupled mode theory of, 189
 fan-type, 139, 141

- folded-type, 132, 133
- power exchange in, 194
- transmission spectrum, 139, 143, 148
- transmissivity, 135, 142, 193
- Soleil-Babinet compensator, 302
- Sound velocity, 329, 345, 346, 374
- Sound waves, 318, 320, 328, 337
- Space harmonics, 201
- Specific rotatory power, 96
- Spectrum analyzers, acousto-optic, 396, 397
- Speed-capacity product, 381
- Spot size, 27, 28, 31, 36, 42
 - of Hermite-Gaussian modes in quadratic index media, 42
 - minimum, 28
- Square wave corrugation, 430
- Square wave function, 191
- Square wave media, 215
- $\text{Sr}_{.5}\text{Ba}_{.5}\text{Nb}_2\text{O}_6$, *see* Strontian barium niobate
- SrTeO_3 , 224
- SrTiO_3 , 225
 - quadratic electro-optic coefficients, 261
 - index of refraction, 12, 261
- Stokes' Theorem, 4
- Straight-through coupling, 466
- Strain field, 320, 328
- Strain-optic coefficients, 319
 - table of, 324
- Strain-optic tensor, 318
- Strain tensor, 318
- Strontian barium niobate (SBN):
 - acousto-optic properties, 375
 - electro-optic coefficients, 233
 - index of refraction, 233, 375
 - nonlinear optical susceptibility, 515
 - strain-optic coefficients, 327
- Strychnine sulfate, 94
- Sugar, 94
- Surface:
 - of constant frequency in \vec{k} -space, 74, 206
 - of constant phase, 10, 32
- Surface acousto-optics, 358, 364
- Surface charge density, 4
- Surface current density, 4
- Surface plasmon, 489, 501
 - at an air-silver interface, 494
 - attenuation coefficient, 492, 493
- Surface states, 209
- Surface waves:
 - acoustic, 358, 387
 - electromagnetic, 209, 489, 494
- Susceptibility:
 - linear, 504
 - nonlinear, 504
 - symmetry property, 547
- Switching distance, 467
- Taylor series, 14, 504
- Te (tellurium), 94, 225
 - acousto-optic properties, 346, 374
 - index of refraction, 346, 374
 - nonlinear optical susceptibility, 513
 - optical rotatory power, 95
- TE modes, 405, 416, 473
 - of leaky waveguides, 483
 - mode condition of, 417
 - orthonormality relation for, 410, 496
 - of slab waveguides, 416, 417
- TeO_2 , 224
 - acousto-optic properties, 345, 375
 - acousto-optic tunable filters, 395
 - index of refraction, 345
 - nonlinear optical susceptibility, 515
 - optical rotatory power, 95
 - strain-optic coefficients, 327
- TE-TM, mode conversion, 425, 447, 500
 - in Ti-diffused LiNbO_3 waveguides, 454
- TE waves, 166
- Thin lens, 34
- Third harmonic generation, 504
- Threshold gain, 446
- Time-averaging, of sinusoidal products, 7
- Time-bandwidth product, 400
- Time reversal, 550
- TiO_2 , 224
 - acousto-optic properties, 346, 374
 - index of refraction, 12, 85, 345, 346, 374
 - strain-optic coefficients, 327
 - see also* Rutile
- TM modes, 405, 416, 473
 - mode condition, 419
 - of slab waveguides, 416, 418
 - orthonormality relation of, 410, 496
- TM waves, 168, 491
- Topaz, index of refraction, 85
- Total internal reflection, 416
 - phase shift, 423

- Total internal reflection (*Continued*)
in slab waveguides, 422
- Tourmaline:
index of refraction, 85
nonlinear optical susceptibility, 513
- Transition temperature, 225, 232, 233,
261, 263, 266
- Transit time limitation, 294, 313
- Translational symmetry, 155
- Translation matrix, 168
- Transmission:
amplifier, 559
gain, 443
intensity, 127
- Transmission coefficient, 219
- Transmission spectrum:
of fan Solc filter, 143
of folded Solc filter, 139
- Transmissivity, 135
of folded Solc filters, 135, 193
of fan Solc filters, 142
- Transverse electric modes, *see* TE modes
- Transverse electric (TE) waves, 166
- Transverse magnetic modes, *see* TM modes
- Transverse magnetic (TM) waves, 168, 491
- Transverse wave, 12
- Traveling wave modulators, 296
- Turpentine, 94
- Twisted anisotropic media, 143
linear, 144, 270
- Twisted nematic liquid crystals, 143, 145,
154
- Twist effect, of liquid crystal, 270
- UF_6 , 545
- Uncertainty Relation, Heisenberg's, 20
- Undulation, 358
- Uniaxial crystals, 82, 83
electro-optic effect in, 272
light propagation in, 84
negative, 84, 206
positive, 84
- Unimodular matrix, 134, 175
- Unitary matrix, 124
- Unit cell, 165, 166
- Variation of constants, method of, 182
- Verdet constant, 103
of some materials, 104
- Viscosity, 269
- Volume grating, via acousto-optic effect,
323
- Water (H_2O):
acousto-optic effect in, 320, 344
acousto-optic properties, 345, 346, 374
index of refraction, 345, 346, 374
Kerr constant, 262
strain-optic coefficients, 324
Verdet constant, 104
- Wave equations, 8, 10, 407
for electric field, 9
for magnetic field, 10
- Wave matrix, 108
- Wave packet, 14, 80
minimum, 20
- Wave plate, 121
Jones matrix of, 124
half-, 116, 125, 127, 148
polarization state transformation by, 149
quarter-, 116, 126, 128, 148
retardation, 122
- Wave propagation, 12
in anisotropic media, 71
in biaxial crystals, 89
through distorting media, 549
in electro-optic crystals, 245
in gyrotropic media, 94, 104
in uniaxial crystals, 84
see also Electromagnetic propagation
- Wavefront, 28, 32, 309, 551
- Wavefront correction, 551
- Waveguide laser, 483, 489
- Waveguides:
Bragg reflection, 477, 481
dielectric, 405
leaky dielectric, 482
metal-clad, 473
slab, 413, 422, 499
- Wavelength, 11
- Wavelength multiplexing, 469
- Wave vector, 10
- Wiener-Khintchine theorem, 403
- Wurtzite, 326
- Xylene:
acousto-optic properties, 376
index of refraction, 376
- YAG, *see* $Y_3Al_5O_{12}$

- YAlO₃, index of refraction, 85
- Y₃Al₅O₁₂ (YAG):
acousto-optic properties, 346, 374
index of refraction, 346, 374, 554
strain-optic coefficients, 325
third-order nonlinear susceptibility, 554
- Y₃Fe₅O₁₂ (YIG):
acousto-optic properties, 346, 374
index of refraction, 346, 374
strain-optic coefficients, 325
- YIG, *see* Y₃Fe₅O₁₂
- Zero crossing, 422
- Zinc blende, 286
- Zircon, *see* ZrSiO₄
- ZnGeP₂, nonlinear optical susceptibility, 514
- ZnO, 225
electro-optic coefficients, 231
index of refraction, 231
nonlinear optical susceptibility, 513
- α-Zns(wurtzite), 225
electro-optic coefficients, 231
index of refraction, 85, 231
nonlinear optical susceptibility, 512
strain-optic coefficients, 326
- β-ZnS(sphalerite), 279
acousto-optic properties, 346, 374
electro-optic coefficients, 230
index of refraction, 12, 230, 346, 374
nonlinear optical susceptibility, 512
strain-optic coefficients, 325
- ZnSe:
electro-optic coefficients, 230
index of refraction, 12, 230
nonlinear optical susceptibility, 512
- ZnSiAs₂, nonlinear optical susceptibility, 514
- ZnTe, 225
electro-optic coefficients, 230
index of refraction, 12, 230
nonlinear optical susceptibility, 512
- ZrSiO₄, index of refraction, 85